Kent Academic Repository

Ley, Nathan Benjamin (2015) *Investigations Into Fragment Ligand Binding Using Quantitative STD and WaterLOGSY NMR Spectroscopy.* **Doctor of Philosophy (PhD) thesis, University of Kent, University of Kent.**

Investigations Into Fragment Ligand Binding Using Quantitative STD and WaterLOGSY NMR Spectroscopy

Nathan Benjamin Ley

PhD Biochemistry 2015

A thesis submitted to the University of Kent for the degree of PhD in Biochemistry at the School of Biosciences, Faculty of Sciences

University of Kent

<u>Declaration</u>

No part of this thesis has been submitted in support of an application for any degree or

qualification of the University of Kent or any other university or institute of learning

Nathan Benjamin Ley

August 2015

Acknowledgements

"Anticipation is the greater part of pleasure"

Angela Carter, *The Bloody Chamber*

Contents

Table of contents

Abbreviations

^{1}H	proton (magnetic nuclei: 100% natural abundance)
^{13}C	carbon isotope-13 (magnetic nuclei: 1.11% natural abundance)
^{15}N	nitrogen isotope-15 (magnetic nuclei: 0.36% natural abundance)
^{31}P	phosphorus isotope-31 (magnetic nuclei: 100% natural abundance)
1D	one-dimensional
2D	two-dimensional
3D	three-dimensional
τ_c	correlation time
ADP	adenosine di-phosphate
ATP	adenosine tri-phosphate
B_0	applied magnetic field
COSY	correlation spectroscopy
CSP	chemical shift perturbation
D_2O	deuterium oxide
DMSO	di-methylsulfoxide
DNA	deoxyribonucleic acid
ESI-TOF	electrospray ionization time-of-flight
FBDD	fragment-based drug discovery
FW	formula weight
GDP	guanosine di-phosphate
GTP	guanosine tri-phosphate
GEM	group epitope mapping
GlcNAc	*N*-acetyl-D-glucosamine
Hsp90	heat shock protein 90
HSQC	heteronuclear single quantum coherence
Hz	hertz
IC_{50}	half maximal inhibitory concentration
INPHARMA	inter-ligand NOE for pharmacophore mapping
ITC	isothermal titration calorimetry
K_D	dissociation constant
kDa	kilo Dalton
k_{off}	off rate
k_{on}	on rate
LC-MS	liquid chromatography mass spectrometry
LE	ligand efficiency
logP	partition coefficient
MHz	mega Hertz
MS	mass spectrometry
NADP	nicotinamide adenine dinucleotide phosphate
NMR	nuclear magnetic resonance
NOE	nuclear Overhauser effect
NOESY	nuclear Overhauser effect spectroscopy
PPM	parts per million
PDB	protein data bank file

SALMON	solvent accessibility, ligand binding, and mapping of ligand orientation by NMR spectroscopy
SPR	surface plasmon resonance
STD	saturation transfer difference
STD-AF	STD amplification factor
TOCSY	total correlation spectroscopy
TM	melting temperature
TMS	tetramethylsilane
TSP	Trimethylsilyl propionate
T_1	longitudinal/spin-lattice relaxation time constants
T_2	transverse/spin-spin relaxation
WaterLOGSY	water-ligand observed via gradient spectroscopy
WGA	wheat germ agglutinin

Abstract

Ligand-observed NMR spectroscopy is frequently employed in early-stage drug discovery, often as an initial screen to narrow the field of potential drug-like molecules. However, its use is limited to this early stage. More information regarding binding mode can be extracted from these experiments via quantification, and this should help extend the remit of these experiments beyond simple screening functions.

Initially, it was shown that the amount of signal that could be produced from an STD NMR experiment could be dramatically increased by careful consideration of the selective saturation pulse. By systematically shortening the Gaussian pulse and positioning it at specific offset positions, it was shown that these dramatic increases in signal are genuine and need not result in false positives.

Quantitative STD NMR spectroscopy as applied to Hsp90 and a series of small fragment ligands provided evidence to suggest that the precise inter-atomic distances between a protein and ligand within a crystal structure correlate with both initial rates of STD build up, and T1-adjusted STD values. This precise correlation has implications for chemotype clustering and initial binding mode selection, something which should be useful in the absence of a crystal structure.

Taking the same quantitative principles and applying to LOGSY experiments elucidated another, discrete property of protein-ligand binding. Examining the 'LOGSY difference' signal for protons of a ligand allows us to see what protons are in close proximity to conserved, bound water at the protein-ligand binding interface. This is fundamentally different to the information gained from STD experiments.

Applying the insights to a protein of a different nature, Ras, it was shown that quantitative STD can be applied to proteins of both different size and structure. Furthermore, more evidence was acquired to suggest that conserved, bound water in the binding site really is responsible for generating LOGSY signal. In the absence of these molecules, as in Ras, proximity of a proton to an exchangeable tends to dominate. In addition we were able to show that these quantitative methods can be used together to help eliminate incorrect computationally generated docking poses.

The work presented in this thesis provides evidence for the advantages of STD and LOGSY NMR spectroscopy in fragment-based drug discovery. The information that can be extracted from relatively simple ligand-observed NMR experiments should be used to provide more evidence at an earlier stage of the drug discovery process, hopefully reducing late-stage attrition and helping us get to the therapeutic drug molecules we need a little more quickly.

Chapter 1

Introduction

1.1   A basic introduction to NMR spectroscopy

NMR spectroscopy probes the fundamental property of nuclear spin. 'NMR active' nuclei - with a spin ½ - include naturally abundant nuclei such as ^{1}H and ^{31}P, as well as more rare isotopes such as ^{15}N and ^{13}C. This is fortunate since these are the nuclei that comprise the vast majority of biochemically interesting atoms in molecules of interest, from small organic molecules through to large macromolecular protein complexes.

These nuclei are NMR active because when placed within an external magnetic field the spin of the nucleus induces a magnetic moment, μ. This magnetic moment aligns in the magnetic field either with or against the field, and precesses with a frequency related to the strength of this applied external field (B_0). A magnet of strength 14.1 T causes hydrogen nuclei (protons) to precess – or resonate - with a frequency of approximately 600 MHz.

However despite all protons resonating with approximately the same frequency, there are small differences in the frequencies of different proton environments. This is due to differences in the local environment around each proton nucleus. Different individual proton resonances dictate that each type of proton appears at a different 'chemical shift', and this is observed on a typical 1D ^{1}H NMR spectrum, as illustrated in figure 1.1.
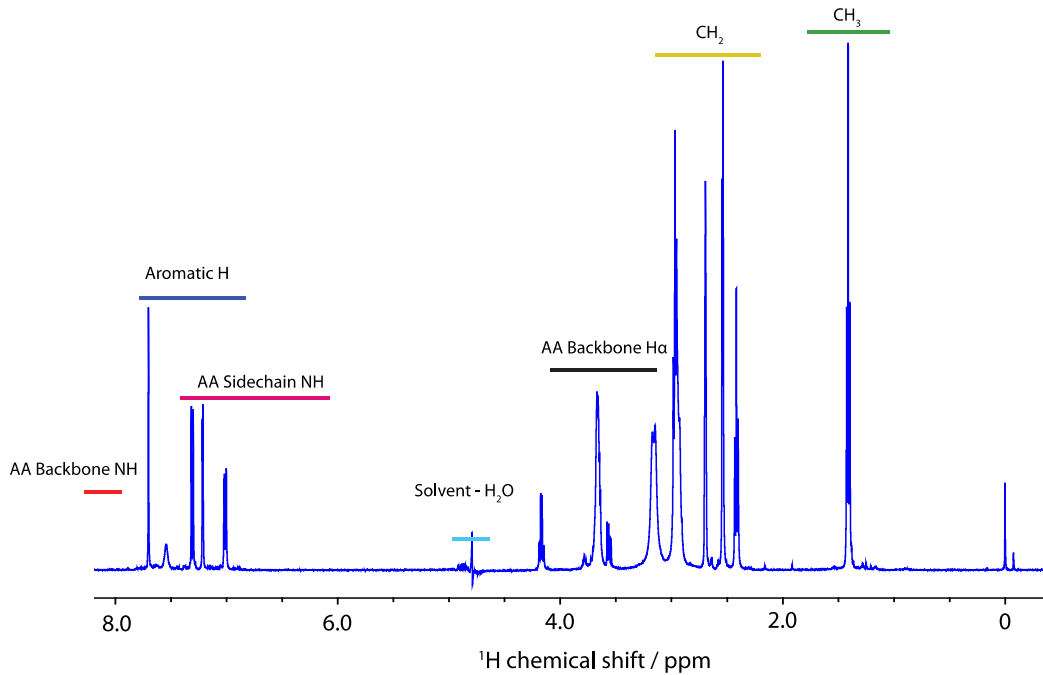
Figure 1.1: 1D ^{1}H proton NMR spectrum of a typical small molecule with different proton groups.

A chemical shift describes the extent of de-shielding that a particular nucleus undergoes, which is dependent on the electronegativity of neighboring atoms. For example, a proton directly bonded to an electronegative atom such as nitrogen experiences a significantly de-shielded electron cloud, and appears with a higher chemical shift value, relative to the reference. In contrast, non-electronegative atoms surround protons of methyl groups - that is non-electron withdrawing atoms - resulting in minimal de-shielding of its nucleus, and a lower chemical shift, relative to the reference.

In simple, small organic molecules there are several different proton environments, whereas in proteins there will be several thousand different proton environments. For structural studies of larger proteins this spectral overlap necessitates extending NMR

experiments into 2 and 3 dimensions, isotopic labeling, and deuteration of proteins. However, these issues are circumvented by the approach of study taken in this thesis.

1.1.2 Nuclear Overhauser Effect

The Nuclear Overhauser Effect (NOE) is a fundamental concept in NMR spectroscopy that rests at the heart of ligand-observed NMR experiments that comprise this chapter. The NOE is the transfer of spin polarisation (or magnetisation) from one nuclear spin population (*S*) to that of another population (*I*) via cross-relaxation, assuming *I* is the spin that is measured and *S* is the spin whose resonance is saturated (Anderson and Freeman, 1962, Neuhaus and Williamson, 1989). For an NOE to be observed atoms must be close enough together in space that they are dipole-dipole coupled appreciably, rather than being spin-spin coupled.

The NOE occurs through space rather than through bonds. As a result the NOE can inform upon which atoms are within close proximity of each other. For an NOE to be observed protons must be within 6 Å of each other in space. The intensity of an NOE is related to distance as shown by equation 1.

$$NOE \propto \frac{1}{r^6}$$
(Equation 1)

Intensity is proportional to the inverse of the inter-proton distance, raised to the sixth power. This is a major boon for certain NMR experiments, as it allows us to examine inter-proton interactions through space.
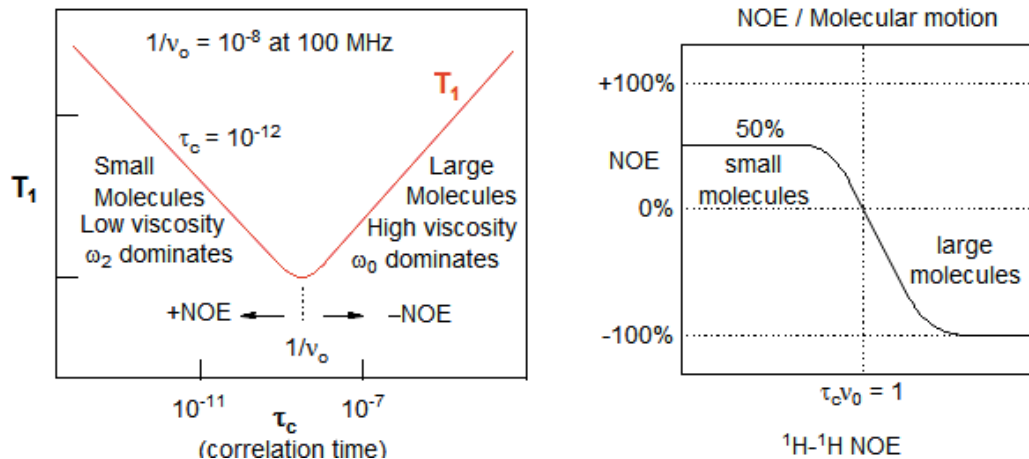
Figure 1.2: The relationship between NOE intensity, sign and correlation time

The NOE possesses a 'sign' that is either positive or negative, and relates to tumbling time. This is shown in figure 1.2. The size and sign of the NOE depends on the tumbling time of the protein as well the distance between nuclei. As correlation time increases (i.e. tumbling rate decreases) the NOEs tend towards -100% as omega tau increases. The NOE can appear non-existent at null points in circumstances when omega-tau = 1.

However limitations do still remain. Spin diffusion by cross relaxation across multiple spins in a large molecule can affect every spin until steady state, something which is needs to be taken into account.

Through the Nuclear Overhauser Effect SpectroscopY (NOESY) experiment, the limit of the NOE enables secondary and tertiary structure of proteins to be

determined, when used in conjunction with other structural experiments including TOtal Correlation SpectroscopY (TOCSY) and COrrelation SpectroscopY (COSY).

1.2 The STD Experiment

Saturation transfer difference NMR (STD NMR) is a powerful ligand-observed NMR experiment that identifies when ligands bind to a protein (Mayer and Meyer, 1999, Mayer and Meyer, 2001, Meyer and Peters, 2003). It was developed by Mayer and Meyer in 1999 and was proposed as a method for screening compound libraries in order to identify binding activity to proteins. STD NMR is presented as a simple and easy way in which the ligand binding epitope may be observed, by associating greater STD signals with parts of the ligand that bind. Central tenets of the method are illustrated with a sample of *N*-acetylglucosamine (GlcNAc) binding to wheat germ agglutinin, a protein-ligand setup that not coincidentally forms the basis of investigations reported in chapter 2.

The technique works via selective saturation of nuclei in a protein, followed by transfer of magnetisation onto bound ligands via spin diffusion, as shown in figure 1.4.

1.2.1 Basics of STD NMR
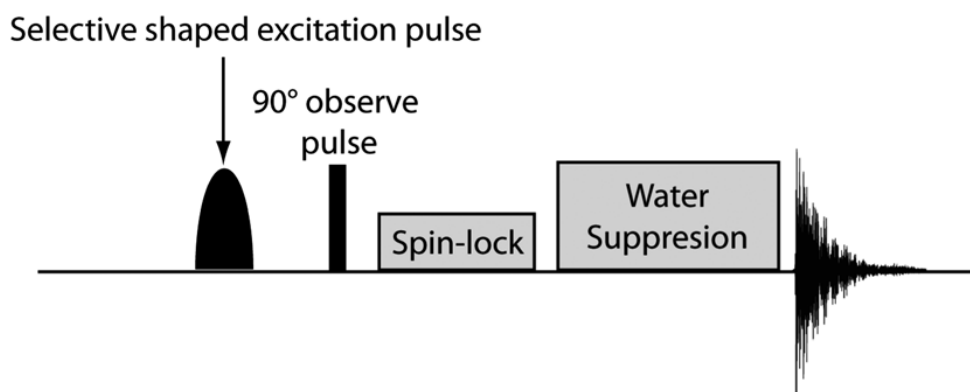
Figure 1.3: ¹H STD NMR pulse sequence highlighting the shaped excitation pulse that drives saturation of the protein. Pulse sequence components responsible for spin-locking – in order to reduce protein background signal – and water suppression are also shown

The experiment is composed of two parts, and the spectra from the on resonance experiment is subtracted from the off resonance spectrum, hence a difference spectrum. To begin with an off resonance spectrum is acquired. This involves proceeding through the pulse sequence in Figure 1.3 with both a selective shaped pulse and an ordinary 90° hard pulse. In the off resonance experiment, selective saturation is deliberately placed well away from any proton resonance in the system, at say -30 ppm. The net result of the off resonance experiment is a simple 1D ^{1}H NMR spectrum of the ligands in the system (As they are present in a large excess), as
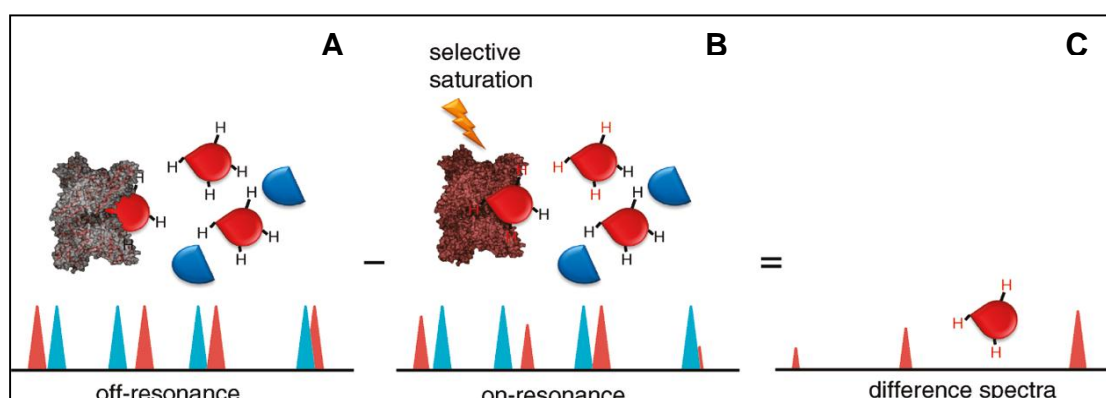
Figure 1.4: (A) The off resonance experiment acquires a 1D spectrum of the ligand, whereas (B) the on resonance spectrum gives a 1D spectrum of the ligand with small attenuations of peaks of the ligand involved at the binding interface. Subtraction of spectra from each other provides the STD difference spectrum (C).

acquired via the square-wave hard pulse, and shown in fig. 1.4A.

Following this, as part of the on resonance experiment, the selective saturation is placed within the upfield region of the protein chemical shift envelope. This causes NMR excitation of methyl groups within the protein, which is subsequently transferred through the protein by spin-diffusion and onto any ligand at the binding interface. In combination with the off-resonance spectrum acquired with a hard pulse, this negative NOE transfer manifests itself as a small reduction in the intensity of peaks belonging to the bound ligand (fig. 1.4B). This attenuation is small, but subtraction of on resonance spectra from corresponding off spectra provides the useful 'STD difference' spectrum (fig. 1.4C). Signals of non-binding ligands will give the same spectrum with both 'on' and 'off' resonance pulses, such that after subtraction all signals are cancelled out and there is no 'difference' signal.

1.2.2 Nature of the selective pulse

Selective pulses in STD NMR are typically applied as a Gaussian pulse train, and must be positioned very carefully so as to avoid accidental excitation of protein and/or ligand where appropriate. Rectangular hard pulses are rarely employed for selective excitation due to possessing an unfavourable excitation profile including unwanted side bands that are responsible for unwanted excitation of signals beyond the desired width. The Gaussian envelope is given by:

$$S(t) = \exp[-a(t - t_0)^2] \qquad \text{(Equation 2)}$$

S is the intensity of the pulse, a is the pulse duration (and hence pulse width), t is the time and t_0 is the centre of the pulse envelope. Fourier transform of the Gaussian

envelope gives a Gaussian function that reduces side bands, and this makes Gaussian pulses favourable over other types of pulse.

At the same time as wanting to reduce accidental excitation beyond specified limits, obtaining maximum signal from a single is also an important consideration in order to avoid experimental inefficiencies. Both factors must be taken into account when choosing pulse type, pulse length, and position of application(Cutting et al., 2007). This concept forms the basis of chapter 2.

1.2.3   The advantages of STD NMR

STD has a number of advantages over the protein-observed NMR experiments discussed thus far. One of the main advantages is the reduced requirement for large quantities of protein and ligand. In addition, there is no need for any isotopic enrichment of any kind (^{15}N or ^{13}C), something that is extremely costly when producing large quantities of protein target. Another advantage is the ease and versatility of the experiment, which can be acquired in a few minutes compared to the timescales required for protein-observed experiments. Furthermore, if one wanted to extend the STD experiment to two dimensions, that is now easily possible(Wagstaff et al., 2010).

In terms of experimental setup the limit on protein target size is also lifted. Whereas protein-observed experiments may wish to keep a cap on protein size (to below, say, 30 kDa(Barile and Pellecchia, 2014)) in order to aid resolution and assignment (due to relaxation dependent line broadening), with STD larger protein size is positively

encouraged in order to aid efficient spin diffusion through the protein. However as a result the protein should not be below 10 kDa(Meyer and Peters, 2003). Furthermore, STD is an extremely versatile technique and is applicable to investigations involving membrane proteins and other large macromolecules such as virus coat proteins.

1.2.4   Group epitope mapping (GEM)

The tentative ability to establish binding mode from simple 1D STD data is a promising avenue, and forms the basis of investigations in chapter 3, wherein I shall go into much more detail. In simple terms; the regions of the ligand in closer proximity to the protein receptor *tend* to receive more saturation than more distant parts of the ligand, and this can be used to infer binding mode(Mayer and Meyer, 2001). However this is not routinely carried out with confidence and there is dramatic scope to improve its implementation. Of course, there are caveats too.

1.2.5   Ligands binding too weakly or tightly

Ligands binding to a protein target can be considered as an association between protein [P] and ligand [L], given as follows:

$$P + L \rightleftharpoons PL \qquad\qquad \text{(Equation 3)}$$

k_{on} and k_{off} are the rate constants for the association and dissociation events respectively. As per textbook theory, the dissociation constant may then be described as:

$$K_D = \frac{[P][L]}{[PL]} = \frac{k_{off}}{k_{on}} \qquad\qquad \text{(Equation 4)}$$

Assuming a diffusion-controlled on rate of $10^7 \, \text{s}^{-1} \, \text{M}^{-1}$, k_{off} can be calculated for fixed dissociation constants i.e. K_D 1 mM = 10,000 s^{-1}, 1 µM = 10 s^{-1} and 1 nM = 0.01 s^{-1}.

However k_{on} is not constant, and can vary between 10^4 and 10^{11} s^{-1} leading to large variations in k_{off}. Off rates generally tend to be larger for small ligands, something that has implications for NMR binding experiments.

Fast exchange on the chemical shift time scale is defined as $k_{off} > \omega$, intermediate exchange as $k_{off} = \omega$, and slow exchange as $k_{off} < \omega$. Fast exchange in NMR is therefore associated with chemical shift differences between the bound and unbound states. In fast exchange, the rate of exchange (Hz) is greater than the chemical shift difference (Hz).

At faster k_{off} values signals appear at the chemical shift value corresponding to the weighted average of the chemical shifts of the signals from the bound and free ligand.

A drawback of ligand-observed NMR techniques STD is the lower limit on binding affinity. Slow exchange between bound and unbound states of a ligand – the case when K_D drops below 0.1 µM, evidently driven by slow k_{off} values – means that saturation is not effectively transferred to the free ligand state in solution. This false negative scenario is a limitation of the experiment and precludes STD NMR from being useful much further beyond fragment ligand screening stage in the drug discovery process.

In STD experiments it is the ligand that is observed. As with all ligand-observed screening experiments, 'fast exchange' between ligand and receptor is assumed, and

considered necessary for the experiment to be useful. To this end, experiments are

carried out with at least a 10 times excess of ligand over protein.

It is estimated that for an STD experiment to be useful(Mayer and Meyer, 1999) the

K_D must be $10^{-8} < K_D < 10^{-3}$ M. Weak binders leave more than half of receptor sites

unoccupied, which causes STD signal to be too weak. On the other hand, strong

binders spend too great a proportion of time in the bound state, resulting in a

decreased exchange rate constant. This causes free ligand magnetisation to relax back

to equilibrium quicker than the receptor is able to bind to new ligand to saturate.

Consequently the population of free saturated ligand is too low, and the STD signal

disappears.
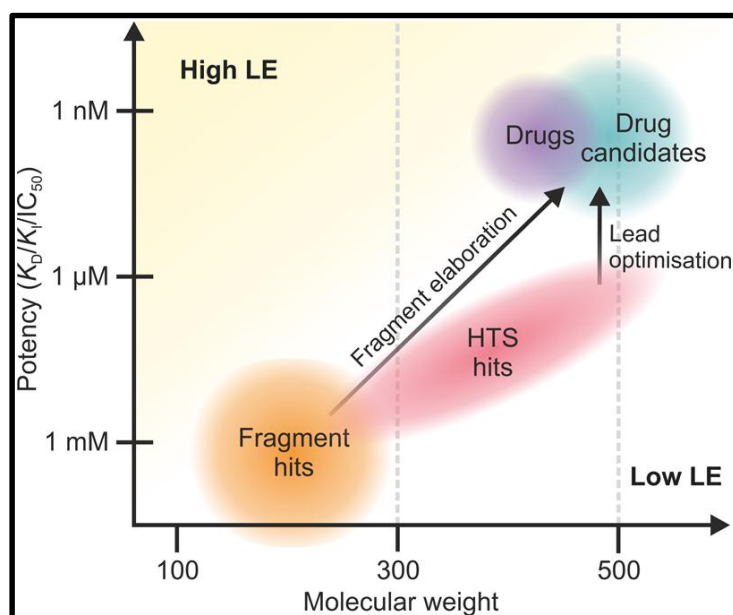
Figure 1.5: A schematic of the FBDD process. As fragment hits are elaborated upon there is an increase in both mass and potency (Figure adapted from(Scott et al., 2012))

The K_D of fragments to be investigated in this thesis are validated fragment hits and

are known binders. Where dissociation constants are unknown, either the equivalent

values as calculated by T_m analysis or the IC50 values are known.

As fragment hits are elaborated upon according to input from both structural biology and medicinal chemistry, there is usually a simultaneous increase in both mass and potency(Scott et al., 2012). This is to be expected, but it does mean that quantitative STD NMR ceases to be useful from a fairly early stage of the fragment-based drug discovery (FBDD) process.

This early screening stage is important enough such that any reforms using pre-existing techniques are a massive advantage. Perhaps if we can be more informed about our fragment hits from an earlier stage in the FBDD process before moving forward – without having to spend too much extra time or money – the chances of late-stage attrition are surely reduced.

1.2.6 What is meant by 'quantitative' NMR?

For the purposes of this thesis, 'quantitative' refers various aspects of biomolecular NMR spectroscopy. In chapter 2 we refer the 'quantification' of STD amplification factors based on peak heights and intensities of one-dimensional STD NMR spectra. In chapter 3 and 4 'quantitative' refers to this same principle, but with the extension of calculating initial rates of STD build up from this data, and the act of dividing amplification factors by T_1.

In other contexts 'quantitative', with respect to STD NMR, can have other meanings, most notably it can refer to the 'Complete Relaxation and Conformational Exchange Matrix' (CORCEMA-ST) algorithms. This program is able to predict the *expected*

STD intensities for a given protein-ligand complex. In order to do this, it requires myriad inputs including PDBs of the protein, ligand, and bound protein-ligand structures, knowledge of the ligand T1 values, information on the protein/ligand correlation times, as well as the concentrations of the NMR sample. Given this requirement for so much data pre-analysis, and how difficult the program is to use, this analysis had no involvement with CORCEMA-ST analysis, and we preferred to focus on a simpler, non-computational, more pragmatic approach to quantitative STD analysis. (Jayalakshmi and Krishna, 2004, Krishna and Jayalakshmi, 2006)

Quantitative STD may also refer to a method very closely related to this analysis, that of calculation of protein-ligand binding affinities via STD initial growth rates. Here, the dissociation constant is determined by single-ligand titration experiments. Competition experiments with a ligand of known affinity allows indirect determination of K_D (Angulo et al., 2010).

At this juncture it must be stressed that 'quantitative STD' in this thesis refers not to any of these contexts.

1.3   Water-Ligand Observed via Gradient SpectroscopY (WaterLOGSY)

Water-Ligand Observed via Gradient SpectroscopY (WaterLOGSY) is an alternative ligand-observed NMR screening technique. It was developed around the turn of the millennium by Dalvit et al(Dalvit et al., 2001, Dalvit et al., 2000) as another primary method for screening compound libraries for compounds that bind to proteins.

Their method built upon the previous observation that water molecules were often found to be conserved in several x-ray structures at the protein-ligand interface(Poornima and Dean, 1995). Water molecules in protein cavities were determined to possess residence times between a few ns to several hundred μs(Dalvit et al., 2001, Otting and Wuethrich, 1989), a long time relative to the effective correlation time where intermolecular water-proton NOEs change sign, but short compared to the chemical shift timescale where a separate resonance for bound water would be observed (ms). This led to the development of saturating the protein in a protein-ligand complex, via selective saturation of the water signal, thereby retaining the sign of the starting magnetisation.

Instead of selectively saturating the protein, bulk water is targeted, and magnetisation is transferred from protein to ligand. For free ligands in solution magnetisation is also transferred directly via the bulk water. The relay processes involved in magnetisation transfer to free and bound ligand are shown in fig. 1.6.
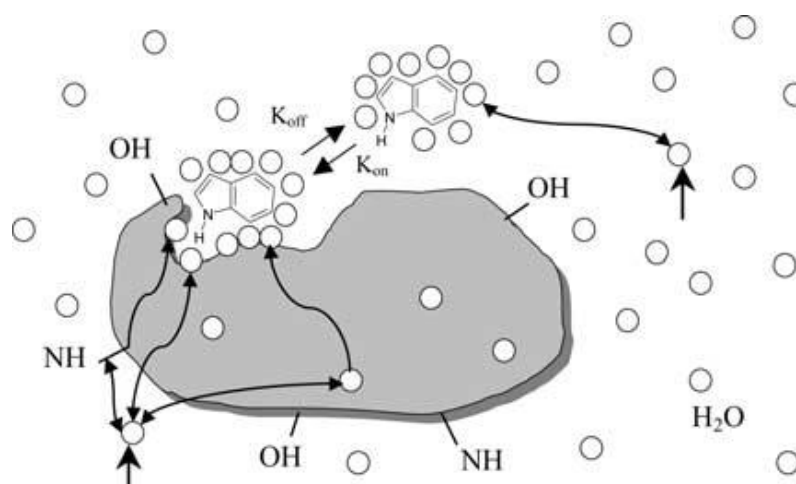
Figure 1.6: The WaterLOGSY principle. The ligand is shown in both free and bound states, with the protein possessing cavities in the binding site. Solid arrows represent excitation of bulk water molecules (circles) with the various magnetisation transfer pathways illustrated as curves lines. Figure taken from (Dalvit et al., 2001)

Selectively excited bound water at the binding interface, followed by NOE mixing, allows for effective magnetisation transfer to the protein whilst conserving the negative sign of the NOE. The other mechanism of magnetisation transfer (which also conserves the sign of the NOE) via the protein is mediated by chemical exchange with labile protons such as those of carboxyl, amino, hydroxyl and other groups(Liepinsh and Otting, 1996, Dalvit et al., 2001). Both these processes act together to transfer magnetisation from bulk water to protein and subsequently to the bound ligand.

On the other hand, free ligand that only interacts with bulk water experiences a positive NOE from the water, and this is due to these water molecules experiencing a much faster tumbling time. A ligand bound to the protein takes on the tumbling correlation time of the protein, which is significantly slower. Opposite sign NOEs cause NMR signals of opposite sign, and this in turn allows us to distinguish between those ligands that bind, and those that do not.

1.4   Fragment-based drug discovery

Fragment-based drug discovery (FBDD) describes the creation of a drug compound via building up from small, weakly binding molecules and successive modifications to improve potency and ligand efficiency. Small molecular weight fragments that bind weakly, but form high quality interactions with a protein target, are selected to optimise into larger, more potent molecules(Jencks, 1981, Scott et al., 2012). Initial fragment molecules tend to conform to the Rule of Three(Congreve et al., 2003), a standard rule of thumb for determining optimal fragment ligand properties: a molecular weight of less than 300 Da, a calculated logP of $\leq$ 3, three or fewer hydrogen bond donors, and up to three hydrogen bond acceptors.

Using an appropriate fragment library, compounds are screened using one of several biophysical techniques to detect weak non-covalent interactions, after which fragment 'elaboration' occurs in which validated hits undergo cycles of synthesis into larger compounds with input from structural biology, medicinal chemistry and computational chemistry. This eventually produces a potent compound.

1.4.1   Other Techniques in FBDD

Several biophysical techniques are used by FBDD users during the early stages of development. X-ray crystallography is the generally considered to be the most powerful primary screening technique by FBDD practitioners. This generates three-dimensional structures of protein-ligand complexes at atomic resolution. These structures are considered very important for validating hits, as well as for establishing

initial binding modes. However this is dependent on access to synchrotrons, as well as high quality crystals, which may not always be possible.

Native mass spectrometry (MS) is extremely versatile. Protein/fragment mixtures undergo electrospray ionization (ESI) and fragment binding can be observed as a corresponding increase in the mass of the target. This way, fragments can be screened in large cocktails, and a gauge on affinity gained from the relative abundance of different protein-ligand species(Vivat Hannah et al., 2010). However the requirement for relatively large amount of target limits the utility of this technique.

Another technique is surface plasmon resonance (SPR), in which the protein target is covalently bound to the gold surface of an SPR chip, and solutions of individual ligands are then passed over it. If a fragment binds to the target, an increase in mass is detected, and from the resulting association/dissociation curve the binding kinetics and affinity can be calculated(Navratilova and Hopkins, 2010). This provides information for k_{on} and k_{off}, rather than simply K_D and so might be more suited for follow up studies rather than initial screening.

Typically a range of techniques is employed in order to ensure results are validated. There is a distinct lack of correlation between fragment hits obtained via different techniques, in fact it is possible to run a fragment screen using two different methods on an identical library and arrive at a dramatically different set of hits(Wielens et al., 2013).

1.4.2   Other NMR Techniques in FBDD

The principal NMR method employed in FBDD – other than ligand-observed experiments – is chemical shift perturbation mapping (CSP). Here, two 2D Heteronuclear single quantum coherence spectroscopy (HSQC) experiments are run in the absence and presence of a ligand. In a ^{15}N HSQC spectrum each peak is representative of an amide proton, thus representing a particular amino acid. Any shift of a particular amide proton upon ligand binding is indicative of ligand binding. In contrast to ligand-observed NMR, this is very much protein-observed. The method relies on chemical shifts of amide peaks of the protein target being acutely sensitive to changes in local environment.

It also depends upon isotopic enrichment of protein (^{15}N) since the natural abundance of this spin ½, NMR-active nucleus, is only 0.368%. This process can be tricky and costly, and is a clear limitation.

CSPs can be used as an initial screen on a library of ligands in order to identify binders but is more likely to be employed as a secondary method in order to give more information. Both the interface and the kinetics of binding can be identified by titration of increasing quantities of ligand(Medek et al., 2000). Given fast exchange between protein and ligand, incrementally increasing the ligand concentration produces a trajectory of CSPs for certain amide peaks, these can then be fitted to determine the dissociation constant(Williamson, 2013).

1.4.3 The fruits of FBDD

In 2011 a phase 3 randomised clinical trial of 675 patients with untreated metastatic melanoma taking the drug vemurafenib – who possessed the BRAF V600E mutation – showed improved rates of overall survival (OS) and progression-free survival (PFS) over the previous standard therapy, dacarbazine(Chapman et al., 2011). Later that year the FDA approved the drug, and it became the first drug to be approved that had been produced with fragment-based principles.

The discovery of vemurafenib began with an initial screen of 20,000 compounds between 150 and 350 Daltons binding to various kinases by *in vitro* phosphorylation measurement. Of these, 238 compounds were found to bind to three kinases and subsequently > 100 bound crystal structures were solved(Tsai et al., 2008). Using a structure-guided approach the potent, selective inhibitor was subsequently found to inhibit BRAF V600E with an IC_{50} of 13 nM.

Whilst this significant milestone for FBDD was passed in 2011, the future holds the prospect of much greater reward. In phase 3 trials currently is the BACE inhibitor MK-8931 and a trial involving 1500 patients with Alzheimer's disease set to be completed in 2018. In phase 2 trials are many FBDD-derived compounds for a variety of disease indications (including multiple myeloma, non-Hodgkin's lymphoma, non-small cell lung cancer, and gastrointestinal stromal tumour), among them are compounds that inhibit: CDKs 1, 2, 4 and 5(Wyatt et al., 2008), VEGF(Albert et al., 2006), JAK2(Howard et al., 2009) and Hsp90(Murray et al., 2010, Woodhead et al., 2010).

1.5   The story of AT13387

1.5.1   FBDD as applied to Hsp90

Of most relevance to the studies presented in this thesis is the discovery of Hsp90 inhibitor AT13387. Hsp90 has proven to be perfectly suited to fragment-based approaches in the past(Barker et al., 2009), and several compounds are now in the clinic. However it's the approach taken by Astex that is the most interesting, and forms the launchpad for my investigations.

1.5.2   The Astex approach

A combination of NMR and x-ray crystallography was applied to Hsp90(Murray et al., 2010). Hsp90 is a molecular chaperone involved in the stabilisation and function of other proteins in the cell(Bukau et al., 2006). Several of the proteins stabilized by Hsp90 are implicated in cancer progression(Workman et al., 2007), hence the clear attraction of Hsp90 as a target for chemotherapeutic agents. Typical Hsp90 function depends on the conversion of ATP to ADP via the N-terminal ATPase domain(Pearl and Prodromou, 2006). This nucleotide-binding site has been fully characterised crystallographically(Prodromou et al., 1997) and inhibition of this site has been shown to cause the down-regulation of the proteins that bind to Hsp90(Vilenchik et al., 2004).

1600 compounds were screened against the N-terminal domain of Hsp90. Fragments were screened in cocktails of four using the WaterLOGSY experiment, and any cocktails that contained a fragment that showed either a 'medium' or 'strong' positive LOGSY signal were taken and examined further in competition mode. Adding ADP

to the mixture, which under the experimental conditions binds weakly to Hsp90, enabled this. Any reduction in the LOGSY signal of ADP is indicative of displacement by a fragment in the mixture, allowing definitive identification of a fragment that binds in the nucleotide-binding site, also eliminating any false positives. Adding 5 mM Mg^{2+} to the mixture increases the affinity of ADP for the binding site, and so doing this acts as a second competition experiment, giving further information on the affinity of the fragment for the site. Extremely weak binders are displaced(Murray et al., 2010).

125 compounds progressed from NMR to x-ray crystallographic screening, using both co-crystallisation and soaking experiments. Of these compounds, 26 were capable of providing crystal structures and isothermal titration calorimetry was then used to determine their dissociation constants. Four key examples are shown in figure 1.7.
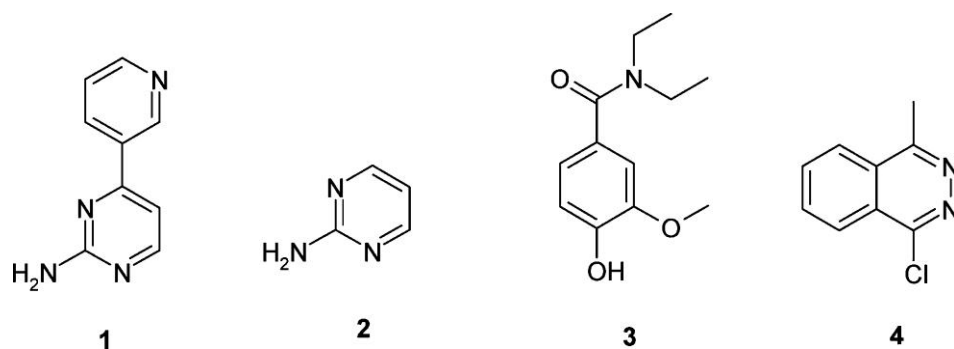
Figure 1.7: Structures of four validated hits for Hsp90 identified by fragment screening.

Of particular note are fragments 1 and 3, both of which feature heavily in this thesis. Crystallographic analysis of the 26 ligand-protein complex structures sheds light on binding mode and the nature of possible interactions.

1.5.2.1   Optimising the interactions of fragment 1 – The aminopyrimidine route

The binding interactions between Hsp90 and fragment 1 – as in fig. 1.8 - were shown to be sub-optimal by virtue of the bond twisting between the two aromatic rings as well as the poor filling of the proximal lipophilic pocket (made up of the side chains Met98, Leu107, Phe138, Val150 and Val 186). Both of these were areas that would clearly need to be addressed in any subsequent fragment elaboration in order to improve the hydrophobic fit.
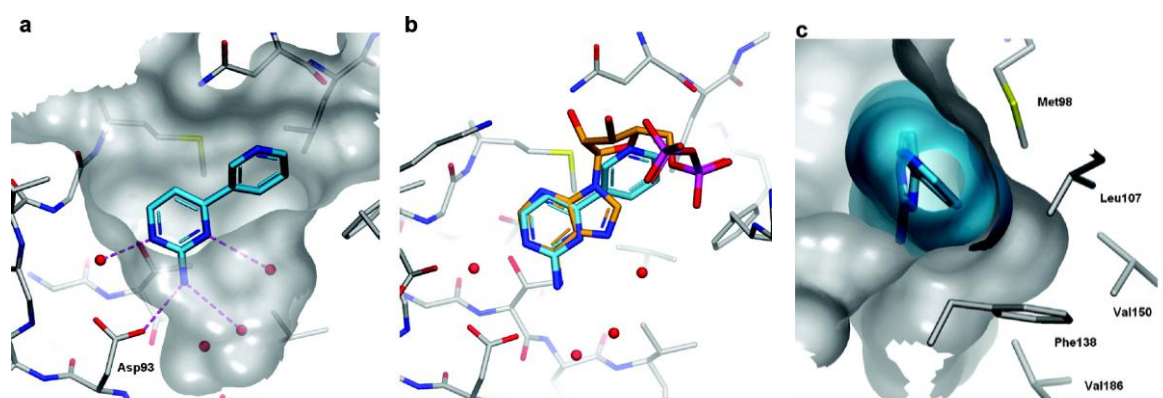
Figure 1.8: Analysis of the binding mode of aminopyrimidine fragments to Hsp90. A) the crystal structure of Hsp90 and compound 1 shown with key hydrogen bonds to conserved water molecules and Asp93 at the bottom of the binding site. B) Overlays of compound 1 and ADP highlighting the conserved nature of the binding interactions. C) 'proximal lipophilic pocket' of Hsp90 shown by the bulge as poorly occupied by compound 1.

Optimisation of fragment 1 began with virtual screening of close analogues, which resulted in the identification of compound 5, a simple chloro analogue (as in figure 1.9), which gave an improvement in affinity of 100 times as measured by ITC. From this it was then deemed worthy to synthesize analogues of compound 5 by substituting groups at positions R2 and R6 of the phenyl ring in an attempt to both stabilize the twist in the bond observed in fig. 1.8 as well as fill the proximal lipophilic pocket. These changes are shown in figure 1.9.
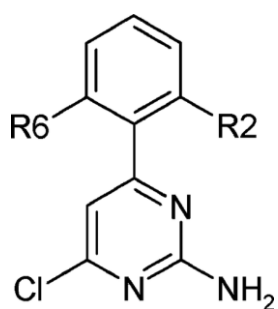
Compound	R2	R6	ITC (µM)	LE	Cell IC50 (µM)
1			250	0.38	
5	H	H	2	0.56	
6	OMe	H	0.35	0.55	
7	OMe	OMe	0.068	0.54	7.9
8	Cl	OMe	0.036	0.6	6.4
9	Cl	H	0.083	0.64	18

Figure 1.9: Compounds 1, 5, and a list of analogues of compound 5 (at positions 2 and 6) and their associated potencies

The result was compounds 6-9. Compound 9 clearly has the greatest ligand efficiency whilst all four compounds possess dissociation constants lower than 0.1 µM. Compound 9 was selected as the molecule for the next iteration, with alterations at positions 4 and 5, in order to introduce more lipophilic interactions with the protein as well as aid solubility.

The resulting compounds are shown below in figure 1.10, with compound 14 showing the most promise in terms of the combination of IC$_{50}$, LE (ligand efficiency: see equation 5) and K$_D$, and was deemed a potential lead molecule from the aminopyrimidine series.

Compound	R4	R5	ITC (µM)	LE	Cell IC50 (µM)
10	Cl	H	0.012	0.68	4.1
11	H	OMe	0.048	0.59	7.9
12	Cl	OMe	0.0063	0.62	1.8
13	OMe	H	0.028	0.61	
14	Cl	Morpholine	0.0048	0.45	1.9
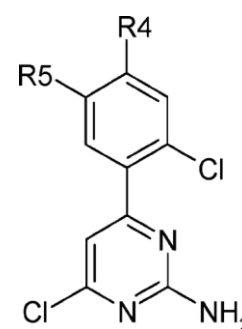
Figure 1.10: Compounds 10-14. SAR at positions 4 and 5 based on compound 9 (pictured)
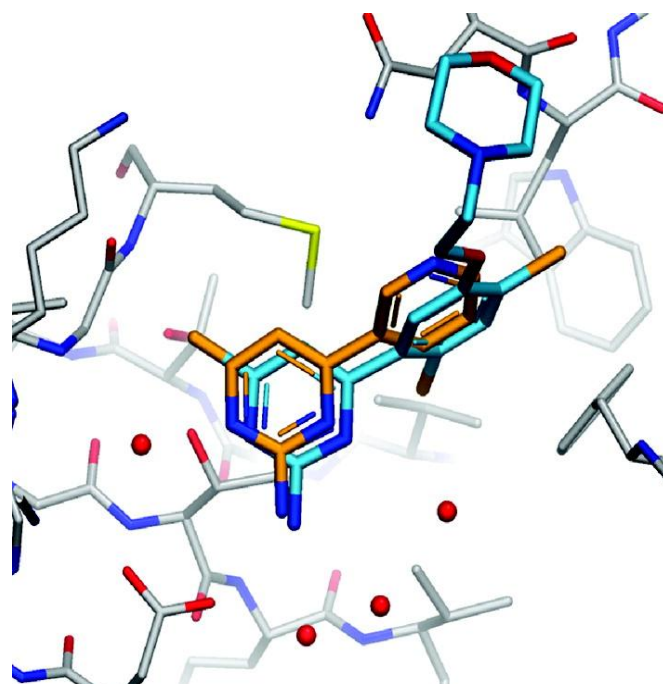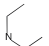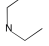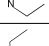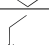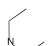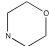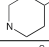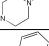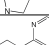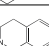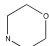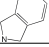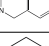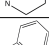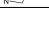
Figure 1.11: Crystallographic overlays of compound 1 (orange) and compound 14 (cyan). Despite various modifications the original binding mode is still clearly conserved

1.5.2.2   Optimising the interactions of fragment 3 – The phenol route

Starting with compound 3 as a scaffold, several changes at position 1 led to the synthesis of chloro, ethyl and isopropyl and tert-butyl analogues (15-18). Compounds 18 and 17 exhibited a reduction in K_D by a factor of 100, as shown in fig. 1.12.

Compound	Formula	R1	R2	ITC (µM)	LE	Cell IC50 (µM)
3	4-OH	OMe	(structure)	790	0.26	
15	4-OH	Cl	(structure)	1130	0.27	
16	4-OH	Et	(structure)	45	0.37	
17	4-OH	iPr	(structure)	7	0.41	
18	4-OH	tBu	(structure)	8.6	0.38	
19	2-OH	iPr	(structure)	51	0.34	
20	2-OH	tBu	(structure)	134	0.29	
21	4-OH	tBu	(structure)	1.1	0.43	22
22	4-OH	tBu	(structure)	2.3	0.38	
23	4-OH	tBu	(structure)	2.5	0.35	
24	4-OH	tBu	(structure)	0.25	0.41	
25	4-OH	tBu	(structure)	2.5	0.31	8.3
26	4-OH	tBu	(structure)	0.4	0.38	7.9
27	4-OH	iPr	(structure)	0.47	0.48	71
28	4-OH	iPr	(structure)	0.068	0.47	17
29	4-OH	iPr	(structure)	0.128	0.43	15
30	2,4-OH	iPr	(structure)	0.011	0.57	0.14
31	2,4-OH	iPr	(structure)	0.00054	0.57	0.031
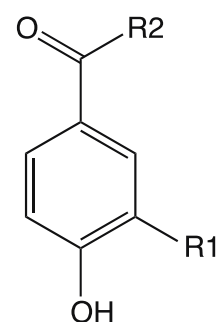
4-OH formula
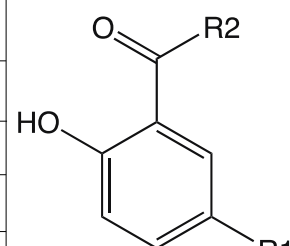
2-OH formula
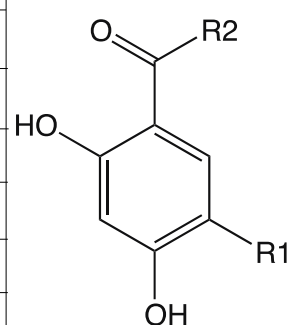
2,4-OH formula

Figure 1.12: Optimisation of the phenol series using compound 3 as a base (pictured)

Next it was decided to shift the 4-OH group to a 2-OH group position due to the fact that the binding natural product (radicicol) possesses hydroxyl groups at both positions, and its 2-OH group forms a hydrogen bond with the Asp 93 side chain.

Compounds 19 and 20 based on the 2-OH formula were synthesized but a large reduction in potency was observed compared to compounds 17 and 18.

After this compound 18 – with a K_D of 8.6 μM – had its diethylamide group replaced with a number of other amides, and compounds 21- 26 were synthesized. This was done in order to stabilize the twisted torsion angle between the phenyl ring and carbonyl group (which is essential for indirect hydrogen bonding with Asp93, as in fig. 1.13).
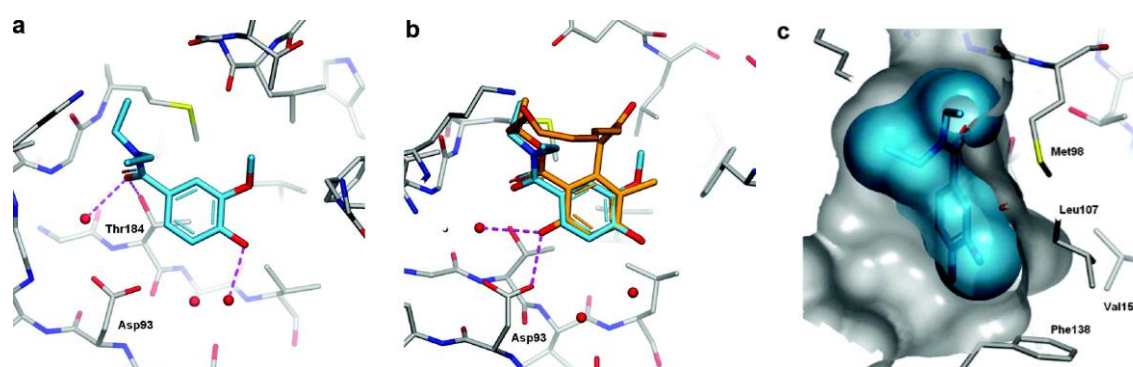
Figure 1.13: Compound 3 bound to Hsp90. A) Hydrogen bonds to two conserved water molecules. B) Compound 3 superimposed with radicicol, illustrating the importance of the additional hydroxyl group in radicicol, which makes a direct hydrogen bond with Asp93 as well as a conserved water molecules, hinting that conversion of the phenol to a resorcinol may be beneficial. C) As with the aminopyrimidine series better filling of the proximal lipophilic pocket was also required, and this was achieved by replacing the methoxy group with other larger substituents

Of the new tertiary amides compound 24 was the most promising, exhibiting an increase in affinity of several hundred-times, to a K_D of 0.25 μM. Three new compounds 27 – 29 were synthesized on the basis of altering compounds 21, 24 and 26 respectively by substituting tert-butyl group to an isopropyl group. This change increased affinity for all three compounds, reduced lipophilicity, and provided better filling of the pocket as dictated in fig 1.13C.

The final change was to incorporate the extra hydroxyl group that is present in the Hsp90 binding natural product, Radicicol(Schulte et al., 1998). This change to the fragment to add the 2'OH is shown in the final two fragments in fig 1.12. This 2,4-OH configuration led to compounds 30 and 31 from compounds 27 and 28 respectively. The extra hydroxyl group at position 2 gave increases in affinity to 0.011 µM and 0.00054 µM from 0.47 µM and 0.128 µM respectively. Compound 31 in particular gave excellent improvements in ligand efficiency and cell activity, and the three overall group changes from fragment 3 are highlighted in figure 1.14.
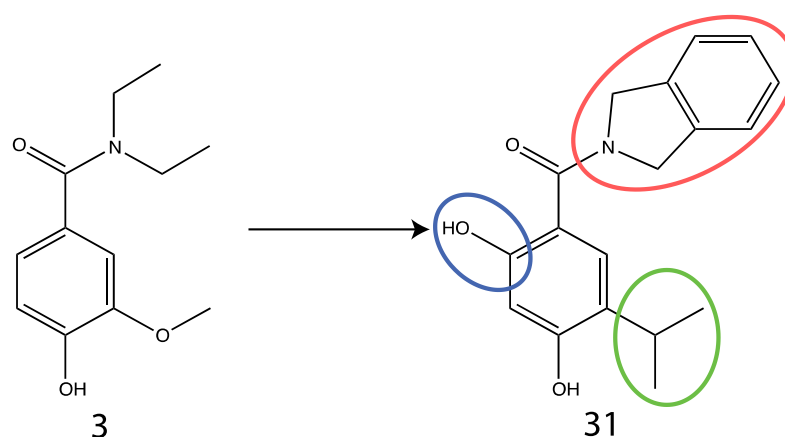
Figure 1.14: Conversion of compound 3 to compound 31 via modification at the three groups indicated. These changes result in a lead molecule that's over 1,000,000 times more potent than the starting phenol.

1.5.2.3 In summary

Following this FBDD campaign two compounds are determined to be lead compounds, via a process that can be deemed the most efficient fragment to lead campaigns ever reported(Verdonk and Rees, 2008). Optimisation of small molecular weight fragments in two lead campaigns - from both aminopyrimidines and phenols – allowed for the optimisation of lead compounds around 300 Da in mass. This is suggested to be optimal as it allows for further tuning, as functional groups may now

be added to the compound that improve non-potency related properties, without the fear that the compound would edge out of 'drug-like space'.

A clinical candidate for Hsp90 – AT13387 – was subsequently developed as an extension to this FBDD process(Woodhead et al., 2010) that ultimately built on the resorcinol lead. This compound is now in phase II trials for a range of different cancers.

Important FBDD concepts are beautifully illustrated here. Firstly, small fragments that bind very weakly – at K_{DS} greater than 100 μM – are perfect starting points. Fragment 3 of the phenol series possessed a K_D of 790 μM, and in many drug screening programmes would be dismissed instantly. FBDD however takes into consideration more than potency, and a compound that binds extremely weakly could easily offer high quality interactions that act as an attractive structural scaffold that may have otherwise been missed but is now available for modification. Another key point in this example is the use of ligand efficiency as a metric:

$$LE = \frac{-\Delta G}{HAC} = \frac{-RT\ln(K_d)}{HAC}$$
(Equation 5)

LE, ligand efficiency; HAC, heavy atom count; ΔG, gibbs free energy; K_D, dissociation constant

Ligand efficiency, as in the example of the discovery of AT13387, is used to monitor the potency of compounds during lead identification and to assess whether or not any increase in potency is worth it in terms of heavy atoms added. Ligand efficiency is clearly useful as used in this example, but it is not the only parameter worth monitoring.

As part of my investigations I shall be taking some of the fragments in this Hsp90 story mentioned thus far, and will use both protein and ligands to probe the parameters of the STD experiment.

1.6   Aims and overview

Ligand-observed NMR is the term given for NMR experiments between a protein target and a ligand in which the signals of the ligand are the only ones that matter. This category comprises a number of experiments, of which two we focus on in this investigation: STD and LOGSY. If these ligand-observed NMR experiments can be expanded to provide more information on protein ligand binding than simply giving a 'yes' or 'no' answer for a hit - such as unambiguously defining the binding epitope, describing a binding site interaction, or combining with computational models to eliminate incorrect solutions - the remit of these relatively simple experiments is improved forever. This would extend the applicability of ligand-observed NMR from being a pure NMR discipline into one in which non-specialists may routinely employ, hopefully enabling cross-pollination into different fields of biochemical research.

Chapter 2

Optimising selective excitation pulses to maximize saturation transfer difference NMR spectroscopy

2.1 Introduction

Saturation transfer difference NMR (STD NMR) is a powerful ligand-observed NMR experiment used for identifying small ligand molecules that interact with a particular protein (Biet and Peters, 2001, Mayer and Meyer, 1999, Mayer and Meyer, 2001, Meyer and Peters, 2003). This chapter focuses on optimising the basic STD experiment via modification of the selective Gaussian pulse, in order to achieve significantly enhanced signal and consequently STD amplification factors. The work described in this chapter was published in 2014 as a journal article(Ley et al., 2014) (see appendix item A).

2.1.1 The STD Experiment

STD NMR is a popular, powerful experiment. It's extensively used in industry and academia to screen and identify small-molecule ligands that bind to target biomolecules in drug discovery contexts (Jhoti et al., 2007, Lepre et al., 2004, Moore et al., 2004, Pellecchia et al., 2008, Sillerud and Larson, 2006, Stockman and Dalvit, 2002, Wishart, 2005). In more recent times, STD NMR has been used to help cast light upon investigations into the binding mode of samples containing a single ligand and protein as a secondary screen (Begley et al., 2010a, DiCara et al., 2007, Kemper et al., 2010a, Wagstaff et al., 2010). In light of these contexts, it is important to obtain results that optimise all avenues to achieve maximum signal.
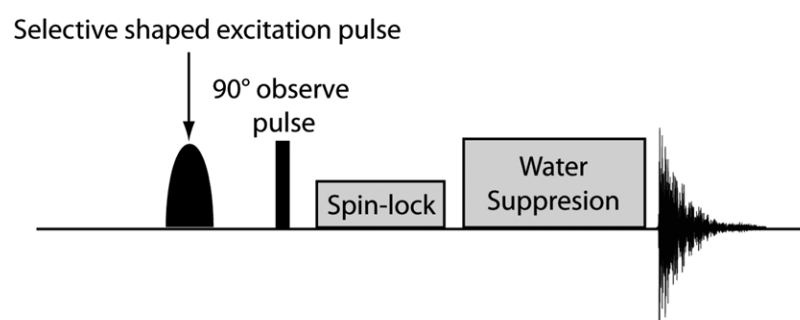
Figure 2.1: **^{1}H STD NMR pulse sequence highlighting the shaped excitation pulse that drives saturation of the protein. Pulse sequence components responsible for spin-locking – in order to reduce protein background signal – and water suppression are also shown**

^{1}H STD NMR experiments begin with selective saturation of the protein by virtue of a specific, shaped excitation pulse, illustrated in fig. 2.1

The shaped pulse is placed within the spectral envelope of the protein − typically between 0 ppm and -1 ppm − and saturates the protein ^{1}H via excitation of upfield methyl protons and subsequent efficient spin diffusion through the protein.

Protons of any ligand involved in an interaction with the protein also experience this saturation via intermolecular NOE transfer at the binding interface, so long as magnetisation transfer occurs before the ligand dissociates from the protein. This is measured in a ^{1}H NMR ligand spectrum as the difference between two datasets: one where the protein is saturated ('on' resonance or I) and another when the protein is not saturated ('off' resonance or I_0). The STD difference spectrum I_{STD} is defined as (I-I_0). Any signal in an STD difference spectrum is indicative of a bound ligand, and is sufficient for qualitatively stating 'yes' or 'no' as to whether or not a fragment molecule binds.

2.1.2   Typical conditions for STD NMR

In order to ensure that selective saturation targets only methyl resonances of the protein and avoids indirectly saturating the ligand directly, the position of 'on' resonance saturation is typically chosen to be between 0 ppm and -1 ppm, whilst the position of 'off' resonance saturation is specifically placed distant from both ligand and protein envelope (ca. −30 ppm).

For experimental setups involving large proteins, virus-like particles, or cells the 'off' resonance saturation position must be much further downfield or upfield, say ± 300 ppm. This is in order to prevent accidental excitation of the protein, a scenario made possible by the large protein molecular weight(Rademacher et al., 2008).

The protein is typically saturated by the repetition of a shaped excitation pulse that is usually between 20 to 50 ms in length and for a total duration of between 1 to 10 seconds. The pulse is shaped in nature (for example Gaussian(Freeman, 1998) or E-burp(Cutting et al., 2007)) in order to limit its excitation profile beyond certain bounds and prevent accidental excitation of the ligand. Gaussian and E-burp pulses are preferred to hard pulses in STD NMR due to the near absence of side lobes and low excitation at large offset positions from the pulse(Cutting et al., 2007, Freeman, 1998, Meyer and Peters, 2003).

It is crucial that selective pulses are applied to sufficiently saturate the protein as optimally as possible, whilst preventing accidental excitation of the ligand protons. In this chapter, we examine the process of rationally placing selective Gaussian pulses of differing length at different offset positions so as to maximize STD signal whilst minimising accidental excitation of the ligand.

2.1.3   Our Model System – WGA/GlcNAc

This chapter focuses on a model system: wheat-germ agglutinin (WGA) and *N*-acetyl-D-glucosamine. This protein-ligand system was selected due to its availability and ubiquity. It also provides a simple methyl peak to follow as the largest signal and most upfield resonance.
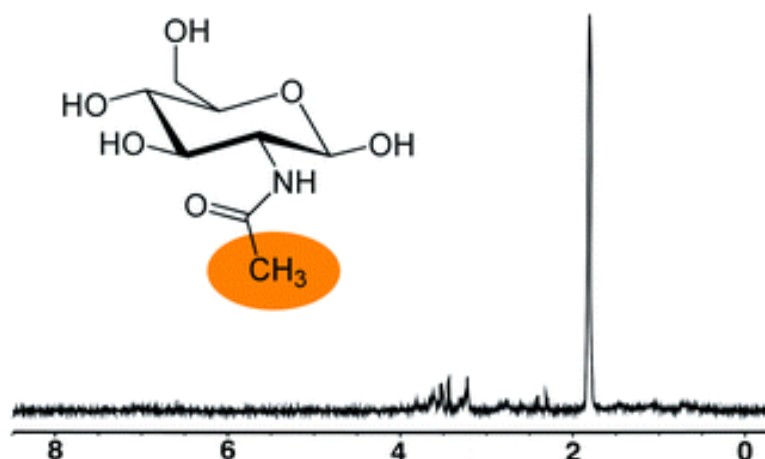
Figure 2.2: The GlcNAc ligand with methyl group highlighted. Alongside is a typical STD spectrum with the large peak representing that of the methyl group.
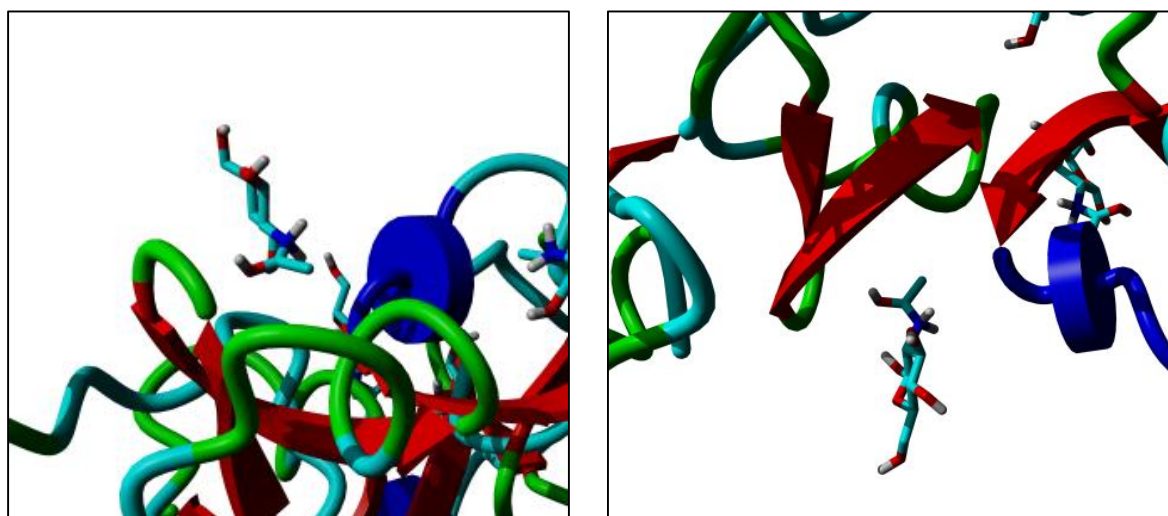
Figure 2.3: Two of the four unique binding sites of WGA with bound ligand. GlcNAc can be seen positioned with the methyl group orientated towards the protein. Figures taken from PDB 2UVO(Schwefel et al., 2010)

WGA is a lectin found in the seeds of *Triticum vulgaris.* It specifically binds GlcNAc as well as *N*-acetylneuraminic acid and is known to inhibit fungal growth via an interaction with fungal cell wall components(Mirelman et al., 1975). WGA forms a 36 kDa homodimer with a two-fold symmetry axis(Wright, 1980, Wright,

1989, Harata et al., 1995). Each polypeptide chain forms four domains of 43 residues each (A-D). There exist eight functional carbohydrate-binding sites per WGA dimer, hence four unique sites per monomer unit. A binding site for GlcNAc is formed via a cluster of three conserved aromatic residues of which the second stacks against the sugar ring(Wright and Kellogg, 1996). Polar residues from adjacent domains then compliment this binding.

Binding sites are not identical and the sites involving domains A and D possess an inherently lower affinity for GlcNAc than binding sites involving B and C domains(Wright and Kellogg, 1996). As a result of this heterogeneity in binding affinity it is impossible to quantify the effects of GlcNAc binding by NMR, however it is worth noting that in all instances of binding the methyl group is usually orientated towards the protein, which explains the disproportionately large STD signal for the group, of which we take advantage.

2.2   Materials and Methods

2.2.1   Sample production and preparation

Wheat-germ agglutinin (WGA) protein from *Triticum vulgaris* and *N*-acetyl-D-glucosamine (GlcNAc) were purchased from Sigma-Aldrich. Samples were prepared as 20 μM WGA and 1 mM GlcNAc in deuterium oxide and pH corrected to 7.4 in a buffer of 10 mM sodium phosphate and 10 mM sodium chloride. This ensured a ligand-to-protein ratio of 50:1 for all experiments.

In addition 1 mM Raffinose pentahydrate was added in excess to a sample containing WGA and GlcNAc as a negative STD control experiment for the spectra shown in fig. 2.4.

Excitation profiles constructed as shown in figs. 2.9 and 2.10 were generated from a sample of 100% deuterium oxide (D_2O), and ligand-only negative control experiments in figs. 2.11 and 2.12 were prepared in identical manner as usual STD samples, simply without the protein.

2.2.2   NMR experiments

All experiments were run at 283 K using a Bruker AV3 600 MHz NMR spectrometer equipped with a QCI-F cryoprobe. A standard Bruker STD sequence was used and water suppression was achieved using a standard Bruker 3-9-19 WATERGATE sequence. Datasets were processed and analysed with Bruker Topspin 3.2 and ^{1}H spectra were referenced to 4,4-dimethyl-4-silapentane-1-sulphonic acid (DSS).

Shaped pulses were generated and optimised using Bruker Shape Tool. STD NMR datasets were obtained over 512 interleaved scans (256 'on' scans and 256 'off' scans) for 2.5, 5, 10, 25 or 50 ms Gaussian shaped pulses, with variable 'on' saturation positions but with 'off' saturation constantly set to -30 ppm.

The resonance for the methyl GlcNAc protons was measured for absolute intensity using MestReNova (Mnova) and used to calculate STD amplification factors (STD_{AF}) from the STD difference spectra $[I_{STD} = (I - I_0)]$ and the control spectra (I_0) as has been previously described using the equation(Meyer and Peters, 2003):

$$STD_{AF} = \left(\frac{I_{STD}}{I_0}\right) \times Ligand\ Excess \qquad \text{(Equation 6)}$$

Practical excitation profiles – using both single shaped pulses as well as Gaussian trains - for the various Gaussian pulses are designed to show the excitation limits for the various length pulses used. Although spectrometer software enables us to evaluate shaped pulses for excitation and width, we deemed it prudent to determine these ourselves. Profiles for single shaped pulses were acquired for 2.5, 5, 10, 25 and 50 ms Gaussian pulses (fig. 2.9) whereas excitation profiles for pulse trains were acquired for 2.5 and 5 ms Gaussian pulses (fig. 2.10). Pulse trains used were the same as those used to produce standard STD NMR data. The usual approach for providing saturation for STD is to loop the selective pulse without an inter-pulse delay. A 2 second saturation period uses 400 5 ms pulses or 800 2.5 ms pulses. Measuring the residual ^{1}H resonance (HDO) in deuterium oxide provides a single resonance to measure with a narrow half peak height below 0.003 ppm (2 Hz). Sweeping the

carrier frequency in a pulse-acquire experiment containing the shaped pulse of interest and measuring the resulting intensity produced the excitation profiles.

The negative control experiment shown in figs. 2.11 and 2.12 is designed to measure virtual STD amplification factors for the GlcNAc methyl resonance in the absence of protein at a range of 'on'-resonance offset positions, such that any accidental excitation will clearly manifest itself as a non-zero STD_{AF} value. *'I' and 'I$_0$'* experiments should in theory produce the same result in the absence of protein. Since $I_{STD} = (I - I_0)$, the difference spectrum should be blank and produce an STD_{AF} value of zero. However, if a difference spectrum is obtained then this must be because $I_{STD} > 0$. If $I \neq I_0$, and there is no protein present, then there must be accidental excitation of the ligand.

In combination, both negative controls should allow identification of offset values at which we can definitively say we have caused accidental excitation. It should also help identify the maximum allowable percentage excitation at which a false-positive spectrum can still be avoided

2.3   Results

2.3.1   Standard STD NMR spectrum for WGA/GlcNAc/Raffinose

The bedrock of all analysis within this chapter centres on the binding of GlcNAc to WGA, and the monitoring of this process via STD NMR. Below shows a typical STD NMR spectrum for GlcNAc binding to WGA
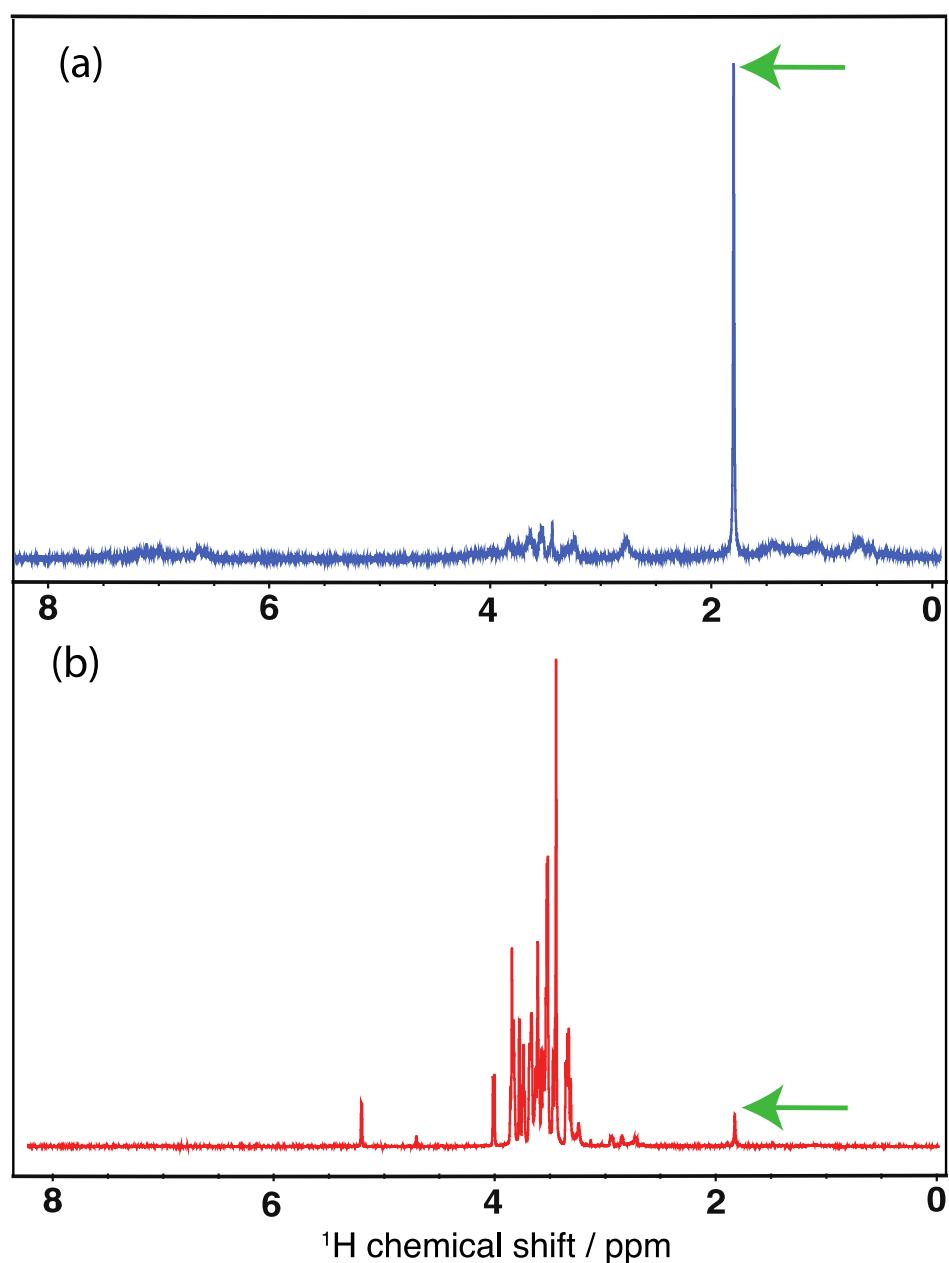
Figure 2.4: ^{1}H STD NMR difference (a) and control (b) spectra obtained over 256 scans with a 10 ms Gaussian pulse for WGA/GlcNAc/Raffinose. The GlcNAc ^{1}H methyl resonance is highlighted by the arrows

In fig. 2.4 the signal relating to the methyl protons of GlcNAc is clearly evident at 1.8 ppm relative to DSS. The protons of the methyl group clearly appear with the greatest intensity in the STD spectrum, and these provide the perfect signal to monitor the effects of changing both the Gaussian pulse length and 'on' saturation position, by virtue of being the most upfield observable signal of the ligand.

2.3.2 Effect of altering the 'on' resonance position and the Gaussian pulse length

2.5 ms Gaussian Pulse (GlcNac / WGA)
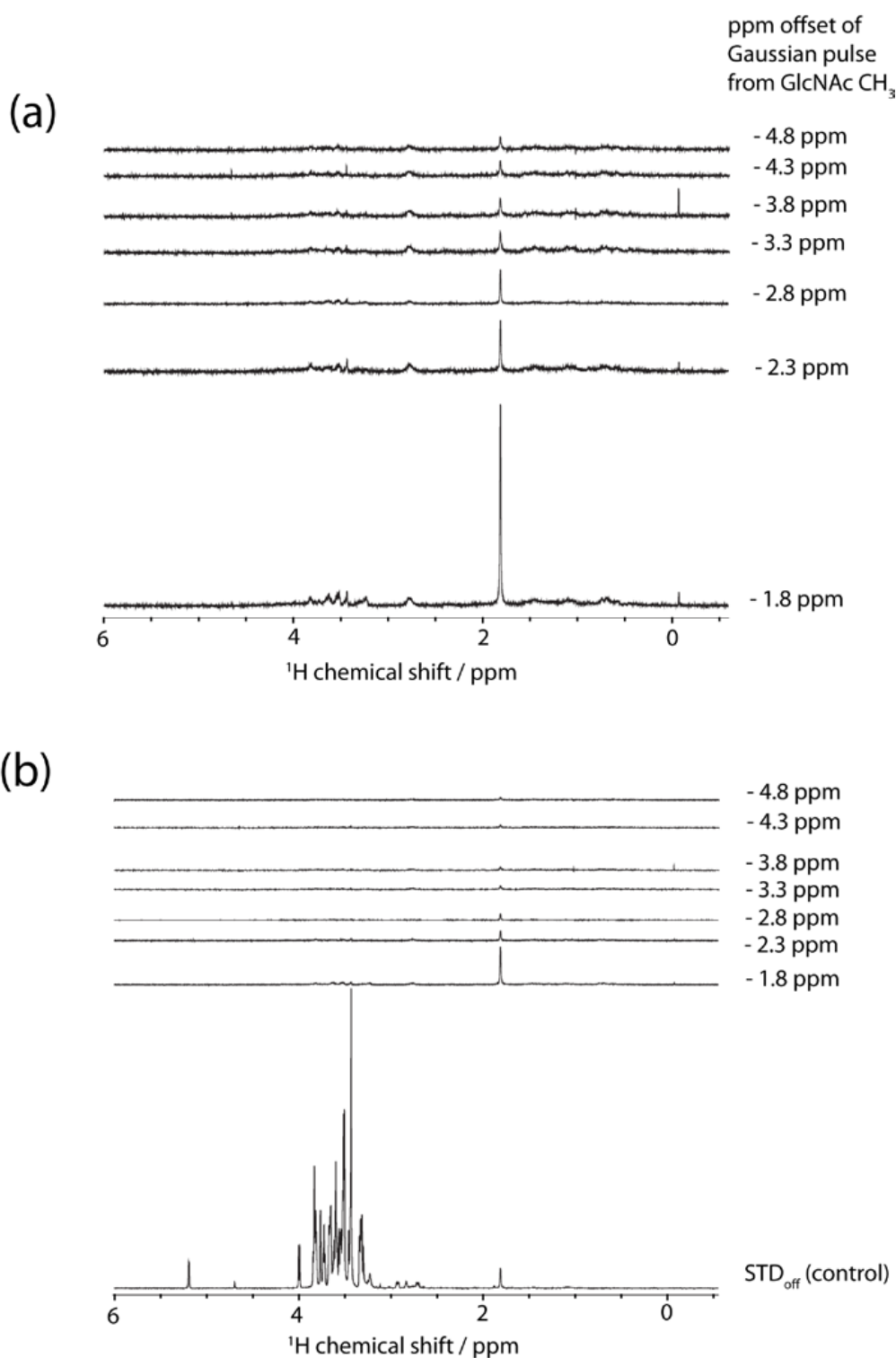
Figure 2.5: ^{1}H STD NMR spectra of WGA/GlcNAc over a range of 'on' saturation offset positions for a 2.5 ms Gaussian pulse. Expanded STD$_{diff}$ datasets are shown in (a) and datasets scaled to the STD$_{control}$ are shown in (b)
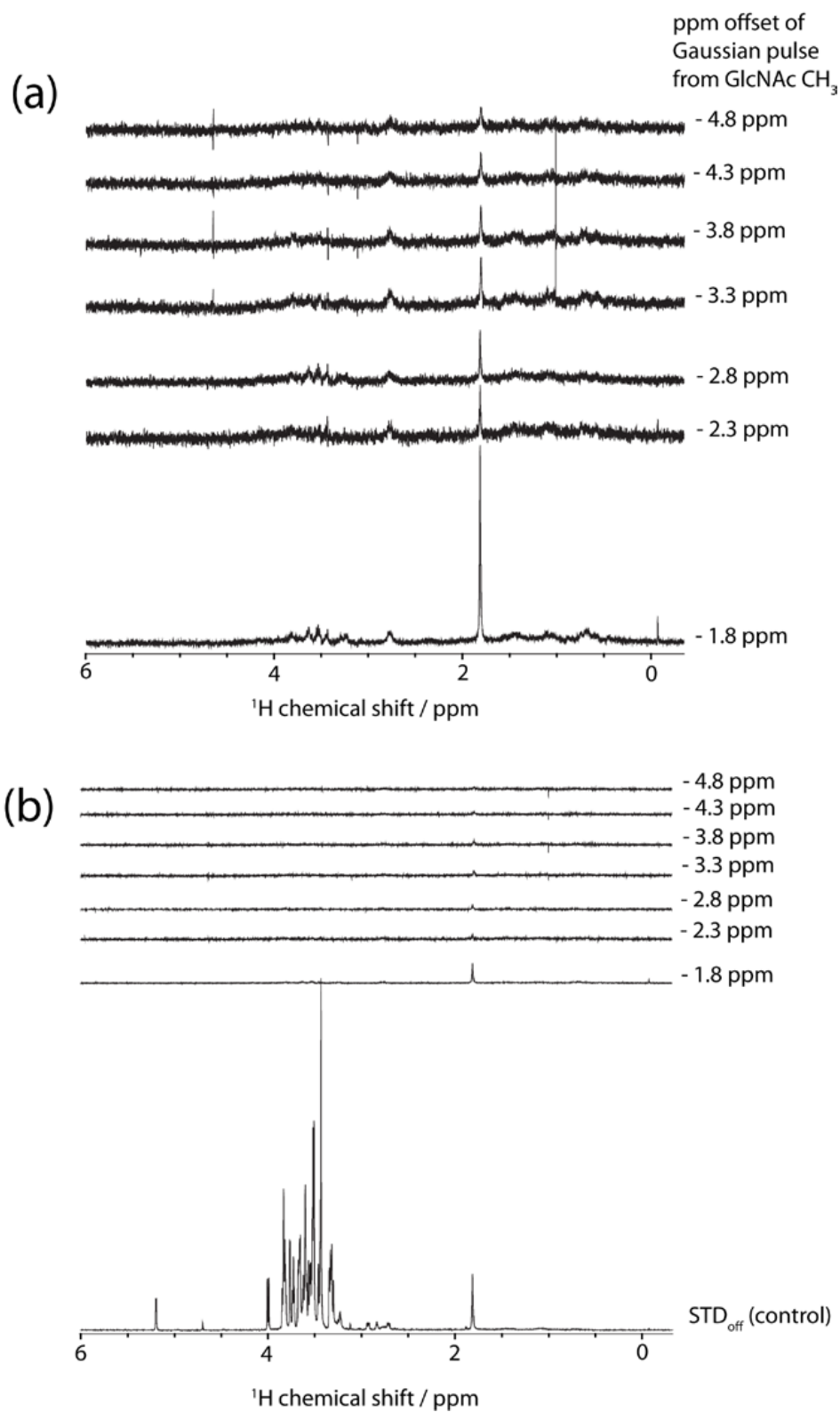
Figure 2.6: ^{1}H STD NMR spectra of WGA/GlcNAc over a range of 'on' saturation offset positions for a 5 ms Gaussian pulse. Expanded STD$_{diff}$ datasets are shown in (a) and datasets scaled to the STD$_{control}$ are shown in (b)

57

10.0 ms Gaussian Pulse (GlcNac / WGA)
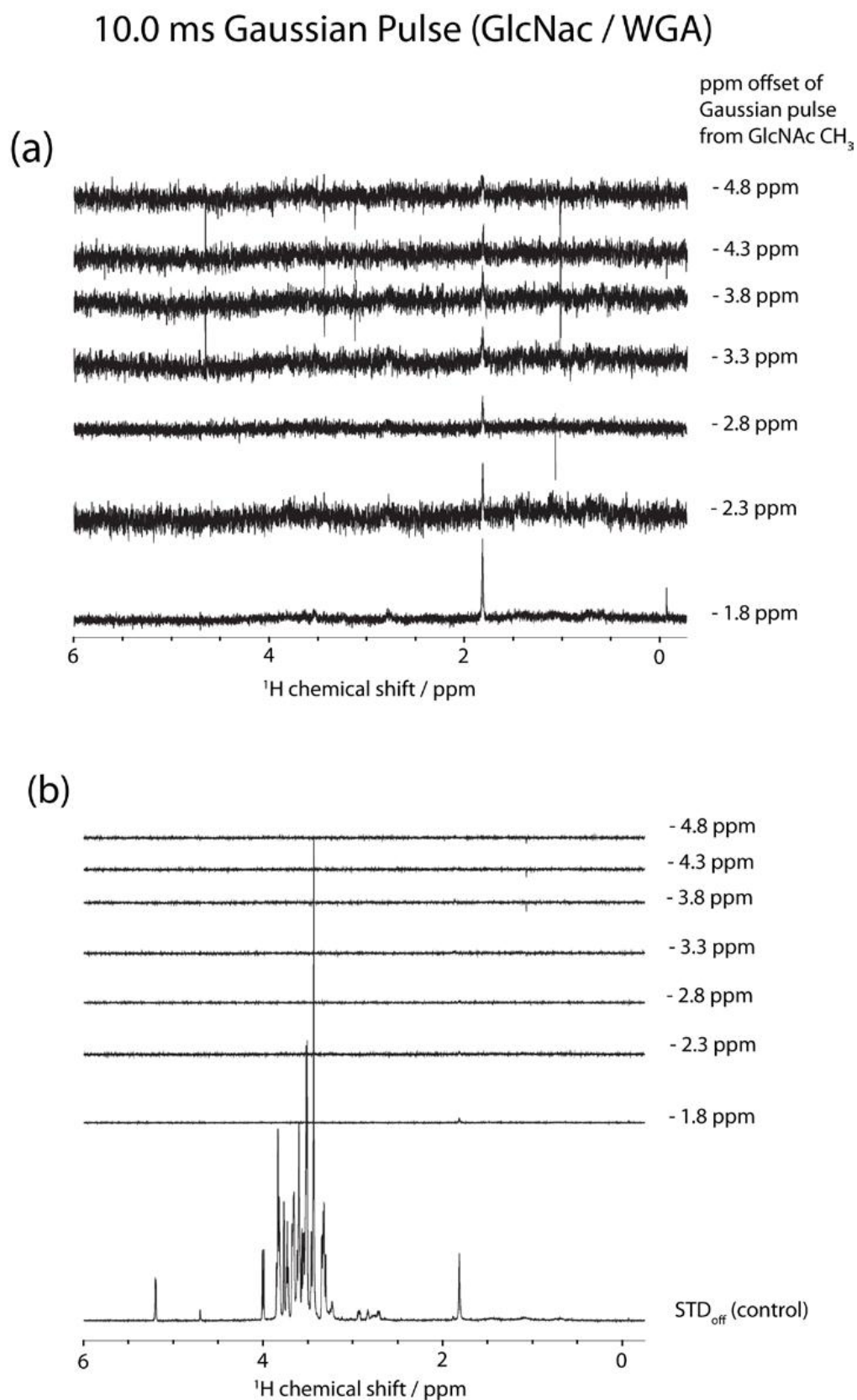
Figure 2.7: ¹H STD NMR spectra of WGA/GlcNAc over a range of 'on' saturation offset positions for a 10 ms Gaussian pulse. Expanded STD$_{diff}$ datasets are shown in (a) and datasets scaled to the STD$_{control}$ are shown in (b)

The various spectra in figs. 2.5-2.7 illustrate the effect of altering the 'on' resonance position with respect to the upfield GlcNAc resonance - as well as altering the Gaussian pulse length – on STD amplification factor. Taking the absolute intensity – or peak height - for the GlcNAc resonance allows calculation of the STD amplification factor at each variation. All the data extracted from these spectra is summarized neatly below in fig. 2.8.
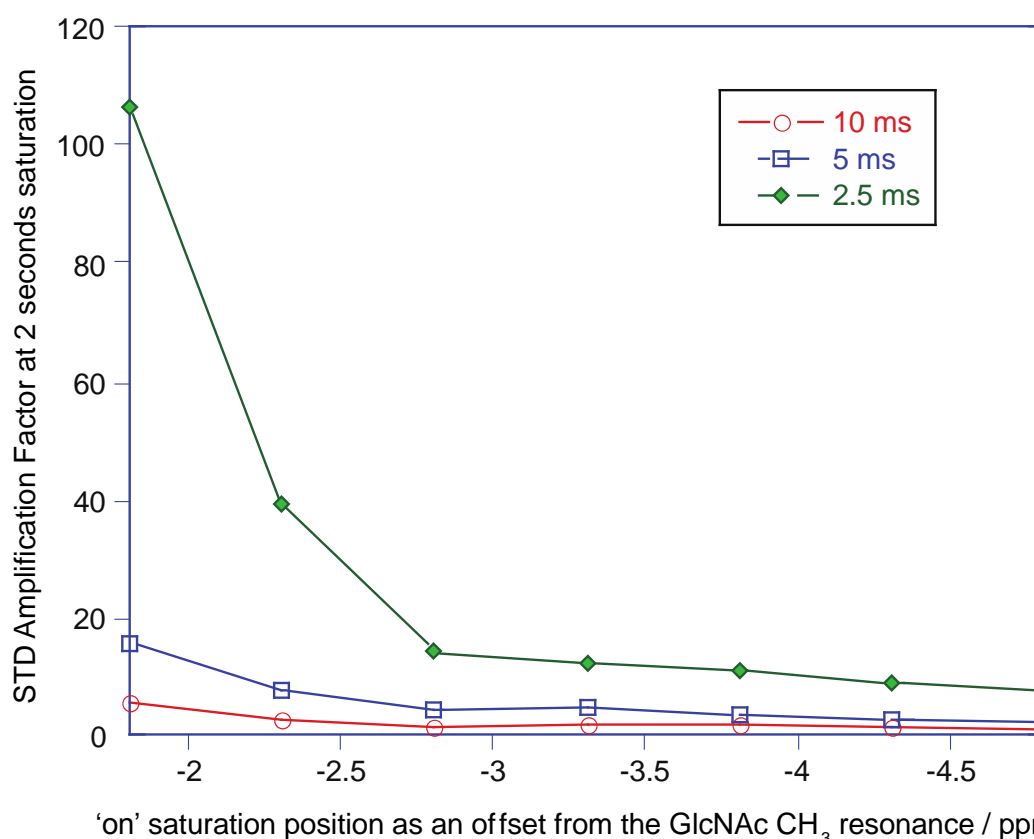
Figure 2.8: GlcNAc methyl ^{1}H STD amplification factors in the presence of WGA for 2.5, 5 and 10 ms Gaussian pulses over a range of 'on' saturation points. The 'on' resonance position is shows as a ppm offset (600 MHz ^{1}H) from the ligand resonance; i.e. an offset of -1.8 ppm is at 0 ppm.

Shortening the length of the Gaussian pulse in fig. 2.8 clearly suggests that a 2.5 ms Gaussian pulse placed at -1.8 ppm (1080 Hz) upfield from the ligand resonance seems to provide the optimum STD signal. This gives an amplification factor seven times greater than the equivalent 5 ms Gaussian pulse, and nineteen times greater than an equivalent 10 ms Gaussian. The calculated amplification factors for the 2.5 ms

Gaussian pulse exceed the 5 ms and 10 ms counterparts across the entirety of the range of 'on' resonance saturation positions.

2.3.3 Practical NMR Gaussian excitation profiles
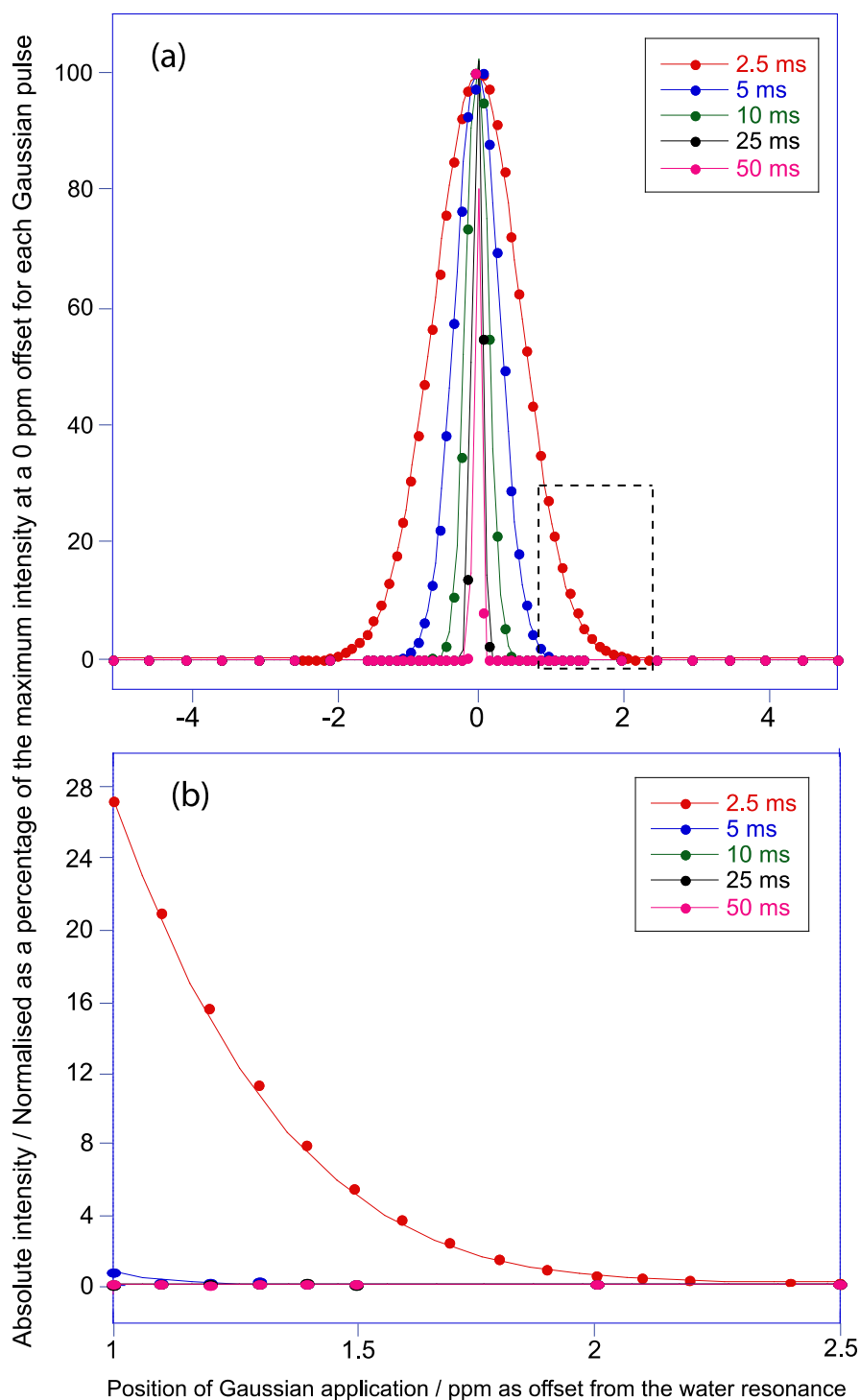
Figure 2.9: Excitation profiles for a single Gaussian pulse of variable length. The profiles were created by delivering a single Gaussian pulse at one of the fixed saturation times, at 14.1 T (600 MHz ^{1}H). Each profile was acquired by measuring the intensity of the ^{1}HDO resonance in deuterium oxide (D_2O) with a 0.1 ppm resolution between data points over a ±5 ppm offset window.

The excitation profiles generated in fig. 2.9 illustrate that shorter length Gaussian pulses have a broader range of excitation, with the 2.5 ms pulse exciting over a significantly wider range. As fig. 2.9 shows, the 2.5 ms Gaussian pulse excites up to ~2.5 ppm upfield and downfield from the position of application. To verify these results, it's prudent to also examine the intensity of the water signal across a range of offset positions for a train of Gaussian pulses, rather than just a shaped pulse.
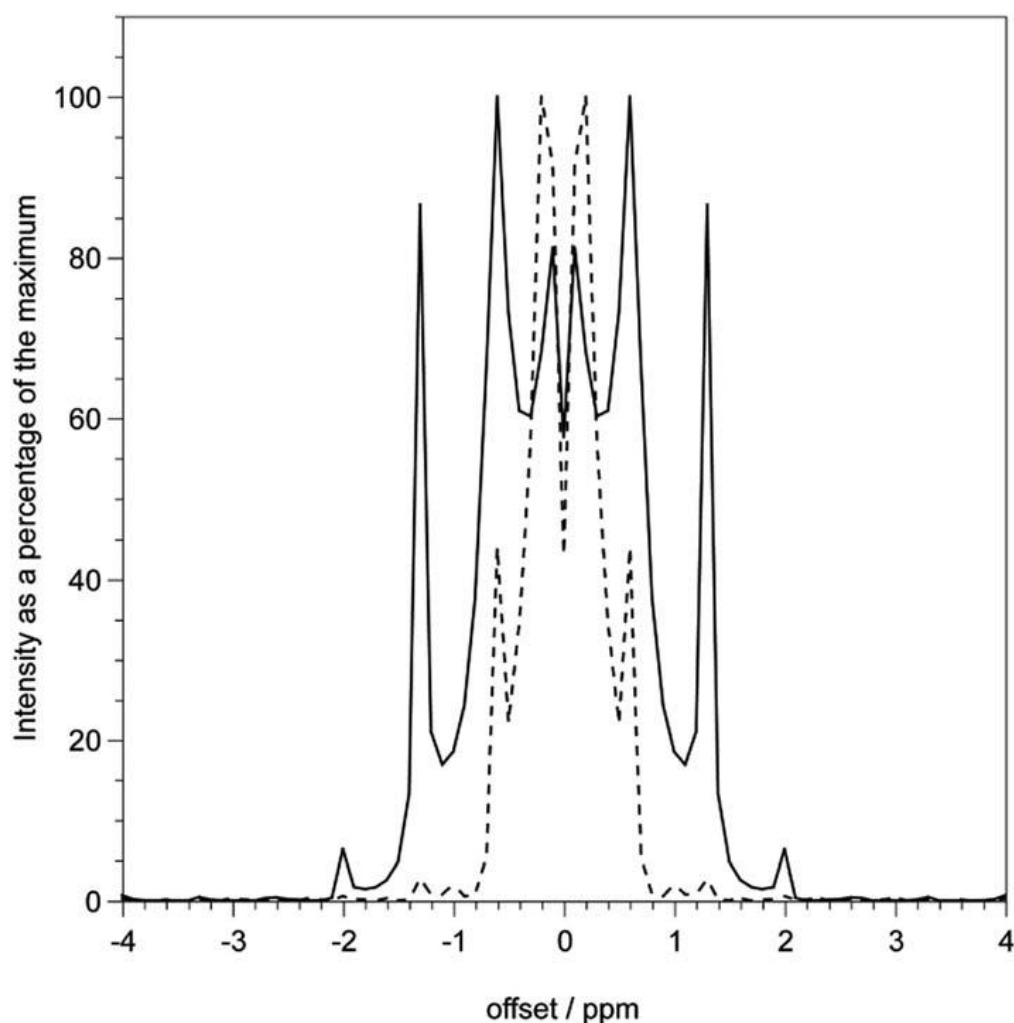
Figure 2.10: Excitation profiles for 2.5 ms (solid line) and 5 ms (dotted line) Gaussian pulses delivered as a train of pulses – for 2 seconds in total - at 14.1 T (600 MHz ^{1}H). Each profile was acquired by measuring the intensity of the ^{1}HDO resonance in deuterium oxide (D$_2$O) with a 0.1 ppm resolution between data points over a ±4 ppm offset window.

The excitation profiles generated in fig. 2.9 illustrate the same principle as those in fig. 2.10. The same expected result – that a shortening of the Gaussian pulse length creates a wider excitation profile – is clearly observed. In addition, fig. 2.10 shows that a profile obtained from a 2 second train of pulses is significantly different to that obtained from a single Gaussian pulse. Again, the pulse train profiles confirm that a 2 ppm offset is sufficient for a 5 ms Gaussian pulse, but that a 2.5 ms pulse should be placed at least 2.5 ppm from the nearest ligand resonance.

2.3.4 Negative controls: STD experiments in the absence of protein

The final experiments examine a full STD experiment on an identical experimental setup as figs. 2.5-2.8 but in the absence of protein. Any STD amplification factor in this control experiment must be indicative of direct excitation of the ligand by the 2.5 ms Gaussian pulse
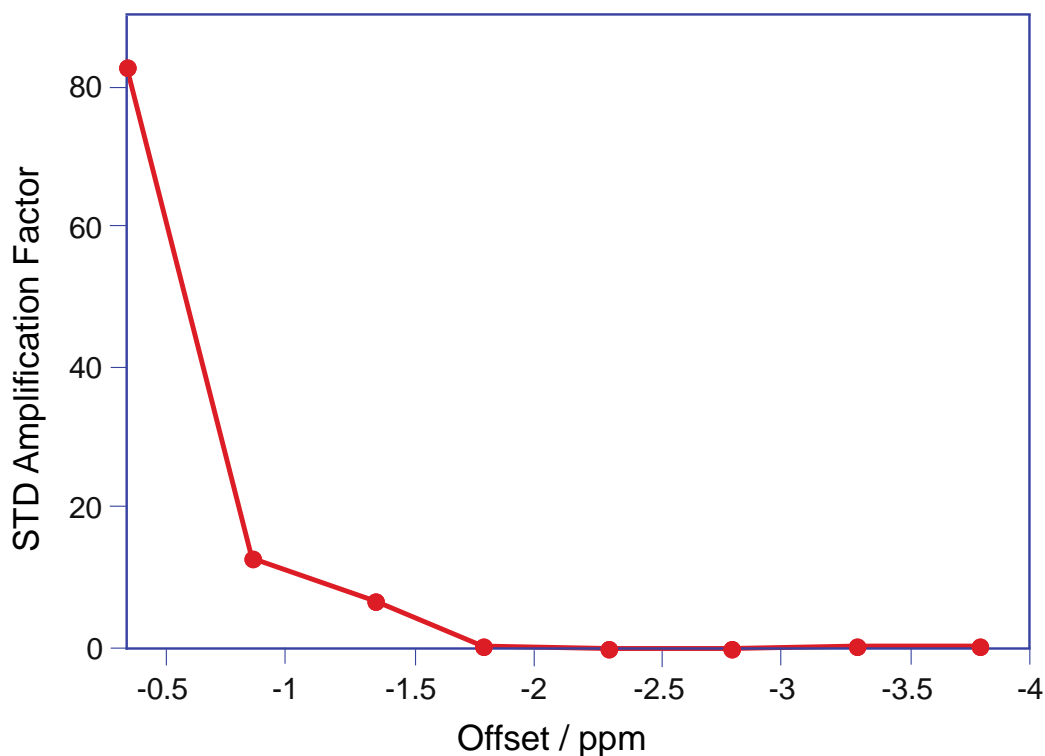
Figure 2.11: Calculated STD NMR amplification factors acquired using a 2.5 ms Gaussian pulse over a range of 'on' saturation points for 1 mM GlcNAc as a control in the absence of WGA protein

The STD amplification factor values fall to zero when the 2.5 ms pulse is placed at offsets greater than or equal to 1.8 ppm. This result corroborates that of fig. 2.10 in which the 1.8 ppm position provides a valley in the excitation profile in between two offsets of 1.4 and 2 ppm.

This result is illustrated more elegantly below in fig. 2.12. The relative intensities of the methyl CH_3 signal from STD spectra that generated the data in fig. 2.11 are shown as spectral overlays below.
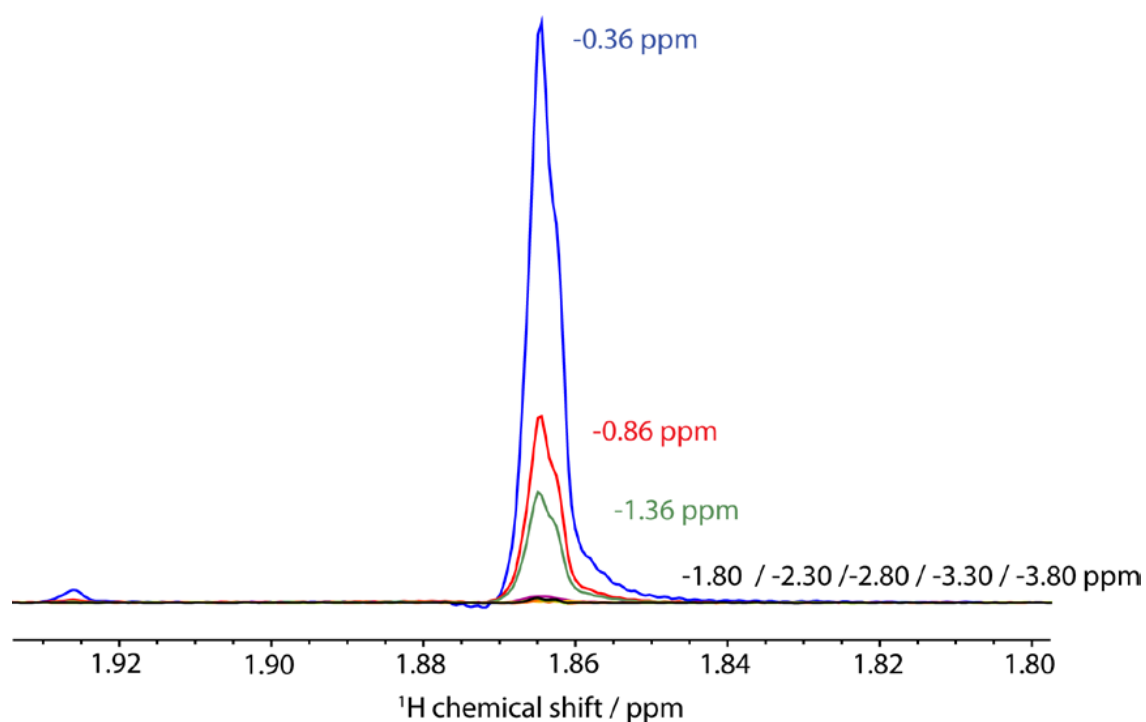
Figure 2.12: ^{1}H NMR difference spectra of the GlcNAc CH₃ resonance generated with different 'on' saturation offsets for a 2.5 ms Gaussian pulse to identify perturbation of the ligand resonance. Offset of the 'on' saturation pulse is indicated by the ppm values shown

As can be clearly seen, STD signal caused by direct excitation of the ligand falls away dramatically at offsets of 1.8 ppm or greater.

2.4   Discussion

2.4.1   Initial observations of altering the length and position of the Gaussian pulse

Spectra such as that exhibited in fig. 2.4 are representative of all data acquired and processed in this chapter, and involved in creation of subsequent spectra. Qualitatively, figures 2.5 – 2.7 show that the STD signal to noise ratio increases as the pulse length shortens, for all offset positions. The STD signal to noise ratio of the GlcNAc peak also increases as the offset position is gradually moved closer towards the ligand, for all Gaussian pulse lengths.

These results are best illustrated in fig. 2.8 that shows how the 2.5 ms Gaussian pulse placed at -1.8 ppm upfield (1080 Hz) from the ligand resonance provides the maximum STD signal, with an amplification factor seven times greater than a 5 ms pulse, and 19 times greater than a 10 ms pulse at the same offset position. These results are generally unsurprising, as it has been previously noted that STD spectra display a dependence on the power level of the shaped pulse(Cutting et al., 2007). It's clear that the STD signal acquired using the 2.5 ms pulse surpass that acquired with the 5 ms and 10 ms pulses over the whole 'on'-resonance range, but more intriguing is how the measured amplification factors with the 2.5 ms pulse increase dramatically as it is applied at offset positions less than 2.8 ppm (1680 Hz) upfield from the GlcNAc methyl resonance.

The increase that is observed with the 2.5 ms pulse - at very close offset positions - upon first glance may instantly be attributed to accidental excitation of the ligand in either the bound or unbound state. This would clearly be undesirable and can be tested

in two ways: obtaining practical NMR Gaussian excitation profiles, and acquiring virtual STD spectra for GlcNAc in the absence of protein. Any direct excitation would clearly manifest itself here.

2.4.2 Practical NMR Gaussian excitation profiles as a negative control

The excitation profiles produced with a Gaussian pulse train confirm that an offset of 2 ppm is sufficient for a 5 ms Gaussian pulse but that a 2.5 ms pulse should be placed at least 2.5 ppm from the nearest ligand resonance in order to prevent accidental excitation. The appearance of these profiles are markedly different to those produced using a single pulse.

The profile created with a single 2.5 ms Gaussian pulse reaches an outer limit of approximately 2.2 ppm in both directions, which tallies with that created with a pulse train. Similarly the limit of the 5 ms pulse in both directions is ~1.4 ppm achieved with both pulse types. On this basis the profiles are comparable, but the profiles created with a pulse train show that the smooth Gaussian distribution obtained using a single pulse hides a multitude of differences. The 2.5 ms pulse train provides the profile with significant sidebands at offsets of 0.6, 1.4 and 2 ppm. Sidebands caused by pulse combs are well-known phenomena and are due to perturbation of magnetic trajectories between on and off resonance positions(Freeman, 1998).

2.4.3 STD experiments in the absence of protein

In the absence of protein, calculated STD amplification factors > 1 are evidently present, proving that accidental excitation of the ligand directly is possible. This is perhaps not surprising at an offset of 0 ppm. This calculated STD amplification factor

value falls sharply across the range we calculated with a 2.5 ms Gaussian pulse, and reaches a value of zero by the time the offset is moved beyond 1.8 ppm. Figure 12 displays the STD spectral data used in calculation of fig. 2.11 as overlays. As can be seen, there are only three offset positions that produce non-zero STD values.

Despite the 2.5 ms Gaussian side band (as seen in fig. 2.10) at an offset of 1.4 ppm delivering over 85% of the maximum excitation intensity, the equivalent point in in the negative control experiment in fig. 2.11 provided only a modest STD amplification factor of less than 10. Conversely the sideband at a 0.6 ppm offset is responsible for a significantly greater STD amplification factor. In combination these data suggest that although Gaussian pulse trains generate significant side bands, their effect on saturation and ability to provide accidental excitation in STD could be limited. The excitation sideband at 2 ppm in fig. 2.10 provides no control amplification in fig. 2.11 and suggests the small side band does not cause significant excitation of the ligand. The 1.8 ppm and 2 ppm offsets in fig. 2.10 correlate to 1.5% and 6.4% of the maximum excitation for a Gaussian pulse train respectively. Since both of these offsets provide zero STD amplification factor in the control experiment, they must be below the lower excitation limit where false positive data could occur in a 256 scan STD NMR experiment.

2.4.4 The trade-off between bullishness and discretion

Typically selective saturation is positioned to be applied around 0 ppm in order to excite protons of upshifted methyl groups within the protein. It is not unreasonable to suggest that efficiency of protein excitation has a direct influence protein saturation and hence STD signal of ligand. Optimal positioning of shaped excitation pulses with

respect to protein methyl protons clearly boosts efficiency. This is something that should be striven for by anyone conducting an STD experiment, and is shown clearly in fig. 2.8 as the shaped pulse offset position is reduced, with respect to the nearest ligand resonance. This will be different for different ligands, but ligand methyl groups are typically most upshifted and hence usually the benchmark against which STD experiments should be optimised. In the unlikely case of a mixture of ligands with solely aromatic protons, much less caution can be exercised and significant gains are to be had by applying the offset position at a value above zero.

The particular protein target used in STD experiments has an effect on optimisation of a shaped pulse, and larger proteins possessing greater numbers of upshifted methyl protons are amenable to shaped pulses with far *larger* offsets, by virtue of dipolar line broadening extending the protein excitation envelope.

As a result of these factors, fig. 2.8 should be considered as data specific to the WGA/GlcNAc system, and STD optimisation should be tailored for each new protein-ligand system, something which is especially important when moving towards more quantitative STD NMR experiments(Angulo and Nieto, 2011, Kemper et al., 2010a).

2.4.5   Conclusions

This chapter provides compelling evidence that Gaussian shaped excitation pulses can comfortably be shorter than 50 ms in length, and rationally placed in order to minimise direct excitation of the ligand. The approach illustrated here at 14.1 T with 256 'on' scans and 256 'off' scans shows how a 2.5 ms Gaussian pulse can be placed as close as -1.8 ppm upfield from the nearest ligand resonance to provide the maximum saturation of the protein and deliver optimal STD amplification factors: up to nineteen times greater amplification factors than that obtained with a 10 ms pulse train. In light of the control experiments and if one wishes to exercise severe caution, it is suggested that the optimal signal is obtained with a 2.5 ms Gaussian pulse placed at 2.5 ppm away from the nearest ligand resonance.

Broadly speaking, ^{1}H STD NMR can be optimised by using shorter-length Gaussian shaped pulses that are rationally placed at relatively short offset distances from the closest ligand resonance. Our examples have measured STD amplification factor values over a range of offset positions in the presence and absence of protein to identify the optimum offset position for each pulse length.

The increased efficiency in saturating the protein with shorter length pulses is due to exciting a larger population of upshifted methyl groups in the protein. Our work in this chapter certainly suggests that the widespread use of 20 ms and 50 ms Gaussian pulses in STD NMR in current practice is disadvantageous, and that the application of shorter-length pulses should certainly be considered, given appropriate checks on direct ligand excitation with negative controls.

This approach described in this chapter could equally be applied to E-burp or other pulse schemes. Optimisation of any STD shaped pulse can dramatically improve the sensitivity of STD NMR data, and should be considered as part of any protein-ligand system setup.

Chapter 3

Initial investigations into quantitative STD NMR spectroscopy with Heat Shock Protein 90 and fragment ligands

3.1 Introduction

This chapter explores the concept of quantitative STD NMR (qSTD) and assesses its accuracy and application with respect to two fragment ligands of the therapeutic target Hsp90. The ability to infer information pertaining to a ligand binding mode simply from a series of 1D NMR experiments is an exciting prospect. Here it is shown that correlations are observed between experimental STD intensities and intermolecular proton-proton contacts between the ligand and protein. Hsp90 and its fragment ligands are an ideal model system to use for the investigations in this chapter as Hsp90 is an extremely well characterised protein, structures in both free and bound form are readily available, and it's a setup that has previously been extensively explored by NMR.

3.1.1 STD NMR as a screening tool

The uses of STD NMR in a screening context are varied. To this day, basic STD experiments are used to evaluate the quality and suitability NMR fragment screening libraries(Doak et al., 2013). It's also used for identifying compounds binding to virus particles(Benie et al., 2003), and also for screening mixtures to characterise peptides binding to membrane proteins(Meinecke and Meyer, 2001).In these scenarios STD NMR is typically used in conjunction with a series of complementary techniques – such as affinity chromatography, isothermal titration calorimetry (ITC), Surface Plasmon resonance (SPR) and x-ray crystallography.

3.1.2 STD NMR for Group Epitope Mapping (GEM)

The STD NMR experiment is a powerful experiment despite its principal functionality as a screening tool in industrial and academic research, it is often employed to infer the binding mode through a process called "Group Epitope Mapping"(Mayer and Meyer, 2001, Mayer and James, 2004). Group epitope mapping enables the qualitative identification of parts of a ligand that are in closer contact with a protein receptor than other parts of the ligand. Historically, this has been utilised to investigate binding epitopes of carbohydrate ligands to receptors.

All this has been made possible since the inception of the 'build-up curve' and the 'amplification factor'(Mayer and Meyer, 2001, Mayer and James, 2004). As shown in fig. 3.1, a build up curve is achieved by plotting amplification factor against the total saturation time of the experiment. An amplification factor is a reflection on the size of an STD signal relative to that same signal in a reference spectrum (calculations shown in methods section). This is calculated for each individual proton of a ligand at a range of saturation times. The rate of the build up of this curve - gradient or initial rate - gives a distinct value that may be compared against those for other neighboring protons of the ligand.
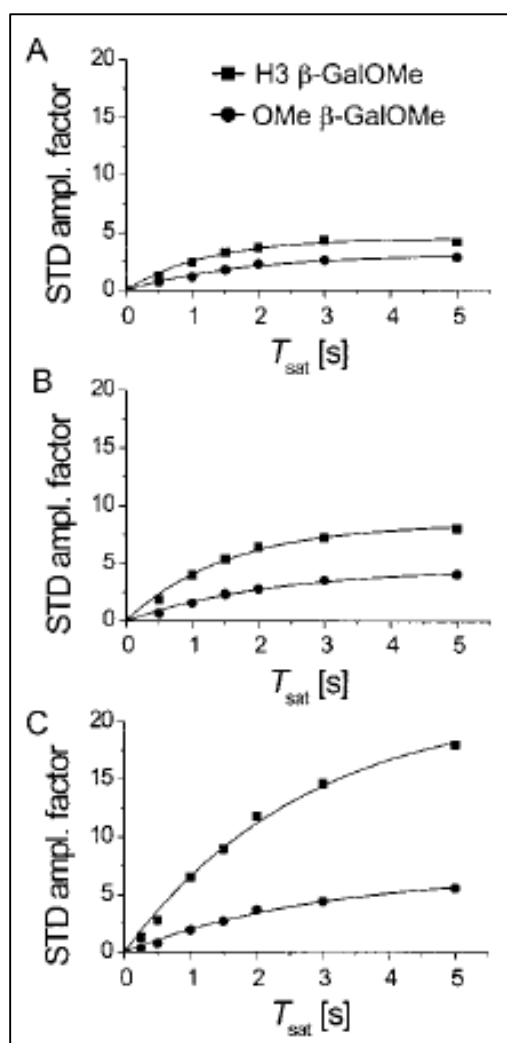
Figure 3.1: STD amplification factor as a function of STD saturation time (s), illustrated for 2 protons of β-GalOMe binding to *Ricinus communis* agglutinin I. Three different ligand concentrations (A) 0.5 mM, (B) 1 mM and (C) 4 mM were examined in the presence of 40 µM protein (Figure taken from Mayer & Meyer(Mayer and Meyer, 2001))

Careful analysis of the H3 proton in fig. 3.1 suggests a faster buildup than the OMe protons. This appears to be true across all concentrations, with the magnitude of signal reaching a maximum with the highest ligand ratio (100:1). This leads to the conclusion that the H3 proton is in receipt of greater saturation transfer from the

protein, and is most likely orientated closer to the binding site than the OMe group in the ligand.

3.1.3 Quantitative STD NMR of Hsp90

Despite the increasing use of quantitative STD methods to solve pressing biological problems - such as elucidating the protein-peptide interactions of integrin αvβ6(Wagstaff et al., 2010), or analysing a complex between Ferredoxin-NADP$^+$ reductase with its coenzyme(Antonini et al., 2014) - Heat Shock Protein 90 (Hsp90) remains an under-explored, fertile field to be ploughed with these tools. Given the advance of Hsp90 inhibitor lead compounds to late-stage clinical trials(Woodhead et al., 2010) there is now wider access to this well-characterised protein, along with access to more industrial data and information(Murray et al., 2010). As a result it feels both appropriate and timely to probe this protein further.
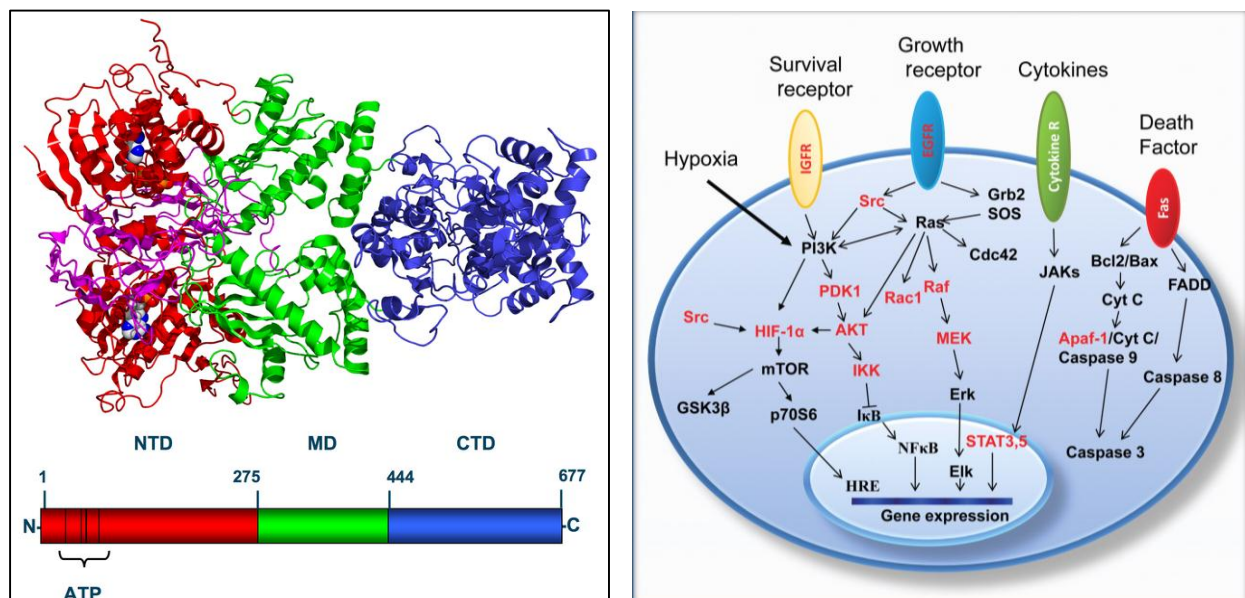
Figure 3.2: Domain structure and cellular roles of Hsp90. Proteins highlighted in red indicate those that are known to be stabilized by Hsp90 (Ali et al., 2006, Moser et al., 2009)

Hsp90 is relatively large for a globular protein. It's found in bacteria and all branches of eukarya, but it is absent in archaea. Cytoplasmic Hsp90 is essential for viability under all conditions in eukaryotes (Chen et al., 2006, Prodromou et al., 1997).

The overall structure of Hsp90 contains a mixture of α-helices, β-sheets, and random coils. Such is its nature as a cytoplasmic protein, the protein is globular, largely non-polar on the inside and polar on the exterior. Hsp90 contains nine helices and eight anti-parallel beta sheets, which join together to form numerous α/β sandwiches. 3_{10} helices comprise almost 11% of the protein's constitution, much higher than the average of 4% found in other proteins (Goetz et al., 2003).

Hsp90 is a molecular chaperone that assists in the stabilization, folding, transport and maintenance of other proteins in the cell (Bukau et al., 2006). It possesses an N-terminal ATP-binding domain (25 kDa), a middle domain (12 kDa), and a c-terminal domain (40 kDa).

The region of the protein near the N-terminus has a high-affinity ATP-binding site. ATP binds to a large cleft in the side of protein, which is 15 Å deep (see figure 3.3). This cleft has a high affinity for ATP, and in the presence of a suitable protein substrate, Hsp90 cleaves the ATP into ADP and P_i.

Several of the proteins stabilized by Hsp90 are implicated in cancer progression, such as RAF and MEK (Workman et al., 2007), and are known to drive aberrant cell division and cell survival. Its multi-functional role as the fulcrum of various

intracellular signalling pathways therefore makes it an attractive target for direct inhibition.

Ordinary Hsp90 function depends on the conversion of ATP to ADP via the N-terminal ATPase domain(Pearl and Prodromou, 2006). This nucleotide-binding site has been fully characterised crystallographically(Prodromou et al., 1997) and inhibition of this site has been shown to cause the down-regulation of the proteins that
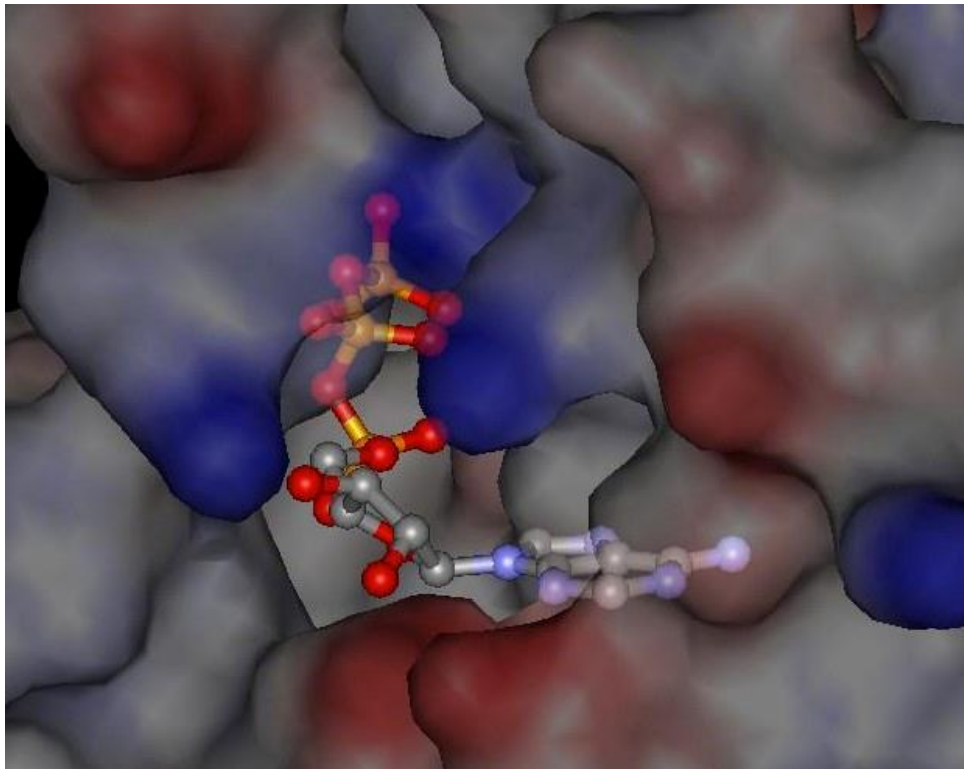
Figure 3.3: The crystal structure of the ATP binding site of Hsp90. ATP is shown as a ball and stick model, and negatively charged regions of the are shown in red (positive regions shown in blue). Figure taken from (Ali et al., 2006)

bind to Hsp90(Vilenchik et al., 2004). This was subsequently explored and elaborated upon by the Astex FBDD platform, and ultimately led to the development of AT13387 and late stage clinical trials.

The N-terminal domain of the protein possesses a mass of 24.5 kDa. STD NMR spectroscopy is generally suited to scenarios wherein the protein receptor in question has a large mass. A large molecular weight ensures efficient spin diffusion, by virtue of the large rotational correlation time (τ_c), ensuring optimal saturation transfer between the protein and ligand.

3.2 Materials and Methods

3.2.1 Protein Production and purification

Hsp90 (N-terminal domain) protein was provided by Astex Pharmaceuticals after having been expressed and purified, as set out in the accompanying paper(Murray et al., 2010). Hsp90α was cloned into a pET28 vector and then expressed in BL21 (DE3). The protein was purified using a Ni^{2+} affinity column, thrombin tag-cleaved, and then purified by gel filtration.

The amino acid sequence for the Human Hsp90 protein (post thrombin cleavage) was encoded by the plasmid as follows:

GSHMDQPMEEEEVETFAFQAEIAQLMSLIINTFYSNKEIFLRELISNSSDALDKI
RYESLTDPSKLDSGKELHINLIPNKQDRTLTIVDTGIGMTKADLINNLGTIAKS
GTKAFMEALQAGADISMIGQFGVGFYSAYLVAEKVTVITKHNDDEQYAWES
SAGGSFTVRTDTGEPMGRGTKVILHLKEDQTEYLEERRIKEIVKKHSQFIGYPI
TLFVE

3.2.2 Identification of the protein by Mass Spectrometry

In order to confirm the identity of the N-terminal domain Hsp90 construct, the protein underwent electrospray time-of-flight (ESI-TOF) mass spectrometry at Astex Pharmaceuticals using an Agilent 1200 LC and Bruker MicroTOF mass spectrometer, internally calibrated using Agilent low concentration Tunemix.

3.2.3 Fragment Ligands

Astex Pharmaceuticals provided a range of fragment ligands. The focus of analysis for this chapter uses the following six selected fragments to investigate Hsp90 fragment binding.

Fragment A (PDB 2XDK)
FW: 172.19
K_D: 250 µM (ITC)

Fragment B (PDB 2XDL)
FW: 223.27
K_D: 790 µM (ITC)

Fragment C
FW: 158.2

Fragment D
FW: 145.16
IC50: > 1000 µM

Fragment E
FW: 159.19

Fragment F
FW: 172.23
K_D: 100 µM (TM)
IC50: 91 µM
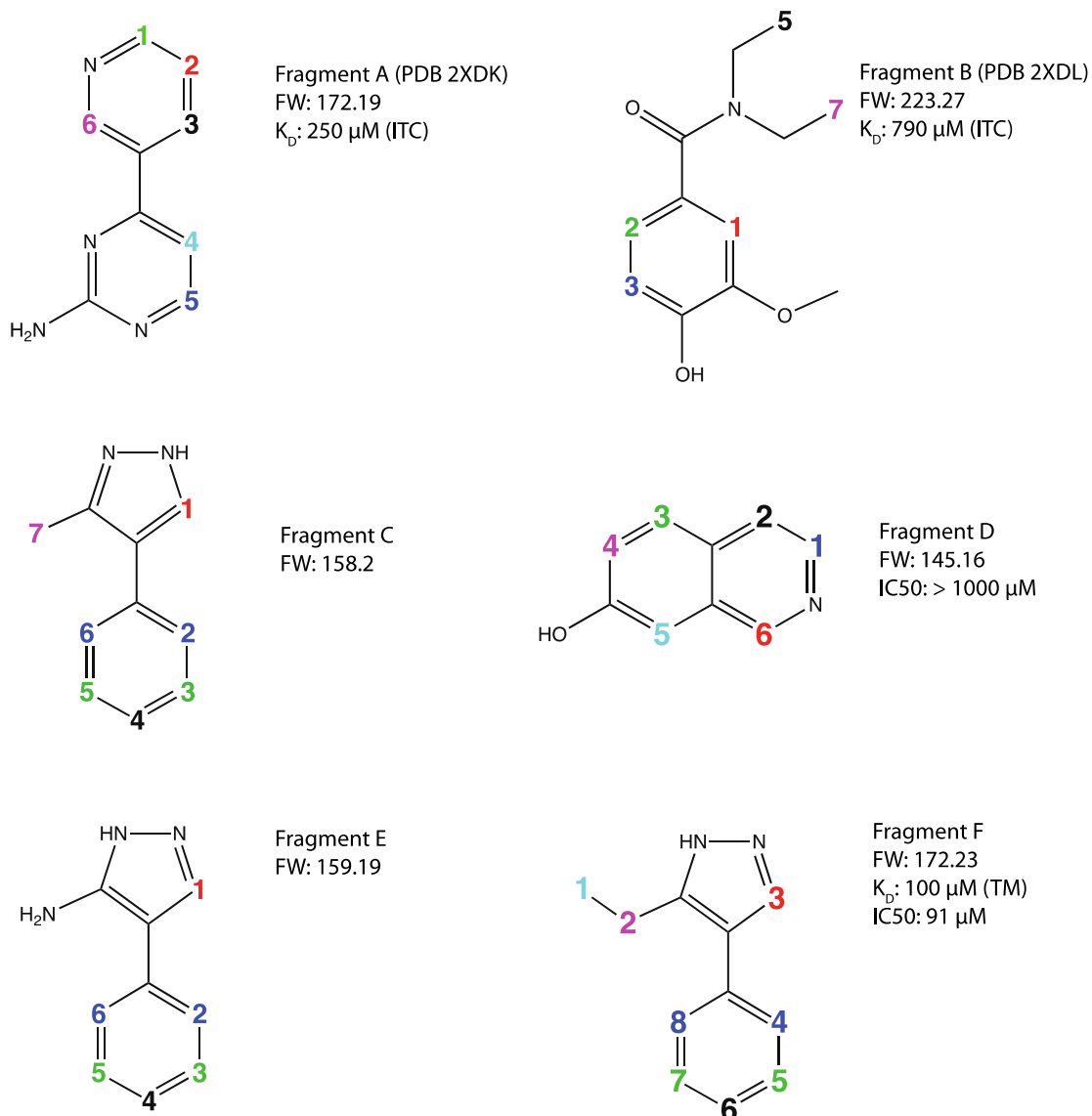
Figure 3.4: Fragment ligands were provided as freeze-dried compounds that were subsequently diluted into 100 mM DMSO stocks. Numbers denote protons or proton groups. Fragments A and B are available as PDB structures at rscb.org

3.2.4 NMR Experimental Setup

3.2.4.1 Sample Preparation

Samples for STD NMR were prepared as 12 μM Hsp90 protein and 1.2 mM fragment ligand (DMSO final 2%) in 20 mM Tris, 100 mM NaCl, 1 mM DTT, and 15% D_2O at pH 7.2. The ratio of ligand to protein for all NMR experiments was 100:1, unless otherwise specified. All experiments were carried out at 5 °C in order to optimise the efficiency of binding and achieve improved signal-to-noise.

Samples for inversion recovery were prepared in exactly the same way for each individual ligand in the absence of protein.

3.2.4.2 STD NMR

STD NMR experiments were performed at 500 MHz using a Bruker DRX500 spectrometer equipped with a TXI cryoprobe, using a standard Bruker STD sequence. STD NMR datasets were obtained over 128 scans (64 scans 'on' and 64 scans 'off' saturation) with a 40 ms Gaussian shaped pulse (positioned at -3 ppm) and an extended relaxation delay of 7 seconds. Water suppression was achieved using a standard Bruker 3-9-19 WATERGATE sequence. Spectra were acquired with 16384 data points and a spectral width of 12 ppm.

Datasets were processed and analysed using Bruker Topspin 3.2 and absolute intensities quantified using MestReNova (Mnova). Intensities were used to calculate STD amplification factors (STD_{AF}) from the STD difference spectra $[I_{STD} = (I - I_0)]$

and the control spectra (I_0) as has been previously described using the equation(Meyer and Peters, 2003):

$$STD_{AF} = \left(\frac{I_{STD}}{I_0}\right) \times Ligand\ Excess \qquad \text{(Equation 6)}$$

Repeating the same STD experiment for a range of saturation times - between 0.5 and 5 seconds – enables the calculation of initial rates as laid out previously(Begley et al., 2010). Buildup curves for all individual protons were fit to equation 7 by plotting STD_{AF} against saturation time (t) using KaleidaGraph software:

$$STD_{AF} = STD_{AFMax}(1 - e^{-k_{STD}t}) \qquad \text{(Equation 7)}$$

The initial rate (STD_{Fit}) is then determined by multiplying together the two KaleidaGraph output values for k_{STD} and STD_{AFMax}, as this product is the first derivative of equation 7:

$$STD_{Fit} = k_{STD}(SAF_{AFMax}) \qquad \text{(Equation 8)}$$

The rate can also be determined by manually inputting a given pair of [x, y] co-ordinates and a measured value for STD_{AFMax} into equation 7 in order to solve for k_{STD}. The initial rate (STD_{FIT}) is again then calculated by multiplying with k_{STD}. In addition there was an 'error' associated with each of these values in KaleidaGraph, which were multiplied and used to calculate % error for each rate. These were used to determine the upper and lower bounds of the estimate for rate.

3.2.4.3 Inversion Recovery for Longitudinal Relaxation Time constant (T_1)

Inversion recovery experiments were performed at 500 MHz using a Bruker DRX500 spectrometer equipped with a TXI cryoprobe. Spectra were acquired with 8 scans, 32768 data points, and a spectral width of 20 ppm. Datasets were processed and analysed with Bruker Topspin 3.2. For each individual sample a series of 15 consecutive experiments were set up, with delay times (τ) each of 0.2, 0.4, 0.6, 0.8, 1, 1.2, 1.4, 1.6, 1.8, 2, 2.2, 2.4, 2.6, 2.8 and 3 seconds. Each delay time results in a differing integral value (a broad range from negative to positive), which when plotted against delay time allows the data to be fit to equation 9 using KaleidaGraph:

$$M_t = M_0(1 - 2e^{-\frac{\tau}{T1}}) \qquad \text{(Equation 9)}$$

The equation is then solved for T_1, or given by KaleidaGraph. This T_1 value extracted for each proton is unique, and is a reflection of the type of chemical environment a proton experiences.

Calculating the T_1 values allows for the second prong of this analysis, analyzing STD group epitope mapping considering relaxation of the ligand (GEM-CRL)(Kemper et al., 2010b, Kemper et al., 2010a). This depends upon acquiring a single set of STD values at a fixed saturation time, and then dividing each value by the T_1 for each proton. This normalises the data and corrects for differences in longitudinal relaxation. In theory this information should be as useful as an initial rate. As part of this analysis all comparisons and association between experimental data and the binding site structure will include both initial rates and T_1-adjusted data.

3.2.5 Correlation of Experimental STD NMR data with Hsp90 structural data

Building on from calculated STD initial rates (STD_{FIT}), it is suggested in the same study that "Normalised STD_{FIT} values were taken as measures of distance-dependent saturation transfer efficiency and used to estimate relative distance between protein [*Sic*] and all resolvable protons on a given ligand when bound"(Begley et al., 2010). This gives an expectation that initial rates of STD buildup could be used in a fully quantitative way.

However, in practice almost all studies normalise initial rates to the maximum STD_{Fit}, and express others as a percentage of this.
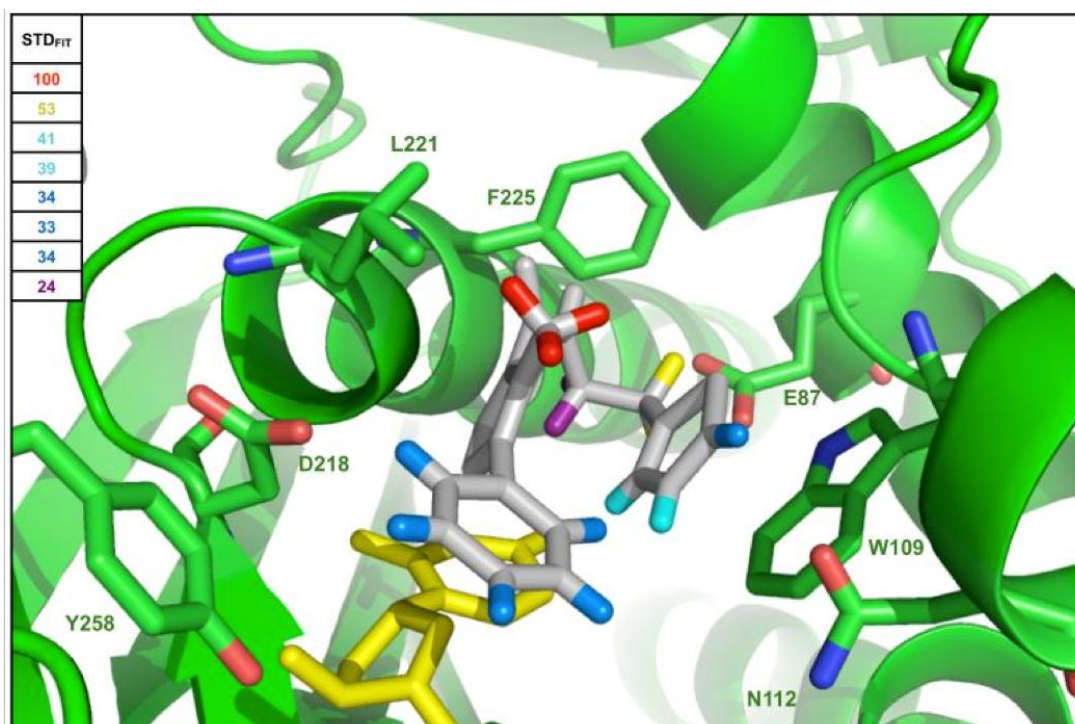
Figure 3.5: An AutoDock conformation of a ligand bound to protein. Relative STD_{Fit} values for protons of the ligand (normalised to 100) are colour coded. Figure adapted from(Begley et al., 2010)

Initial rates are usually utilized as a qualitative tool, an augmentation for other information, as exemplified by recent studies(Tanoli et al., 2013). In this particular instance in fig. 3.5 *STD_Fit* is used to corroborate an AutoDock pose in order to assess its general suitability(Begley et al., 2010). However, the approach herein is followed to gain more precise information. To begin with we take distance information from two publicly available PDB structures: 2XDK and 2XDL (Fragments   A and B) and probe deeper. All subsequent structural data comes from in-house Astex PDB files that are unpublished. All inter-proton distances discussed and explored in this thesis are listed in appendix B.

The restraint measurements taken for comparison were the inter-proton distances between each individual proton of the ligand and all protons of side chains in the binding site, within 6Å. Each individual distance (r) was then processed as $\frac{1}{r^6}$ as NOE transfer is dependent to the reciprocal of the 6th power of distance. This lends greater weight to the saturation transfer pathways that are in close proximity(Neuhaus and Williamson, 1989). These were summated for each individual ligand proton to give an overall value for the sum of distances that might contribute saturation transfer.

Donor methyl groups were treated by 'sum averaging': for example if the individual distances between the three protons of a methyl group and a ligand proton were 6 Å, 5 Å and 4 Å respectively, then this would be averaged to 5 Å and therefore treated as $\frac{1}{(5)^6}$.

In the case of methyl, methylene, or symmetrical recipient protons of the ligand, all saturation transfer signal is driven through multiple equivalent protons that appear at one frequency, yet there are multiple intermolecular proton-proton distances to deal with as given by the crystal structure. In this instance, any initial rate or T_1-adjusted STD value is processed as usual, and the final value is then divided according to the proportions. For example, if one proton of a CH_2 group possesses twice as many intermolecular pathways (as the sum of all $1/\mathring{A}^6$) than the other, the experimental STD value (or rate) is divided in a ratio of 2:1 between them for the purposes of correlation.

More accurately this can be expressed as: $(STD \times f)$ where STD is an initial rate or T_1-adjusted STD value, and f represents the fraction of the total cumulative distances that a particular proton provides (as the sum of $1/\mathring{A}^6$), from all protons in the group. f is a different fractional value for each proton, but all add up to 1. The merits of this approach shall be discussed later.

3.3 Results

3.3.1 Identification of the protein by Mass Spectrometry
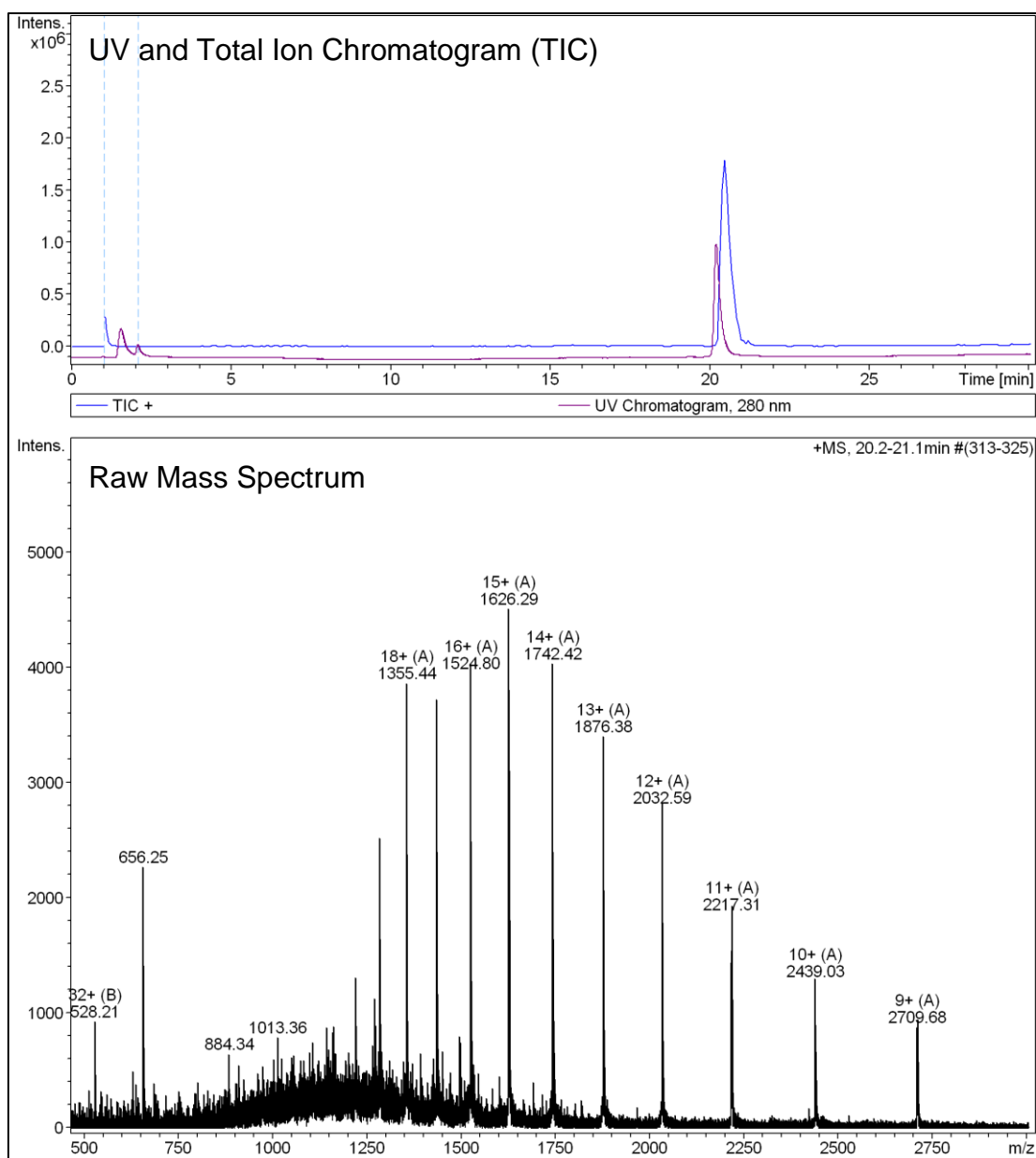
Figure 3.6: Hsp90 LC-MS and accompanying spectrum for Hsp90

The UV chromatogram output from the LC-MS yielded a single peak containing a single protein species with an elution time of 20.5 minutes.
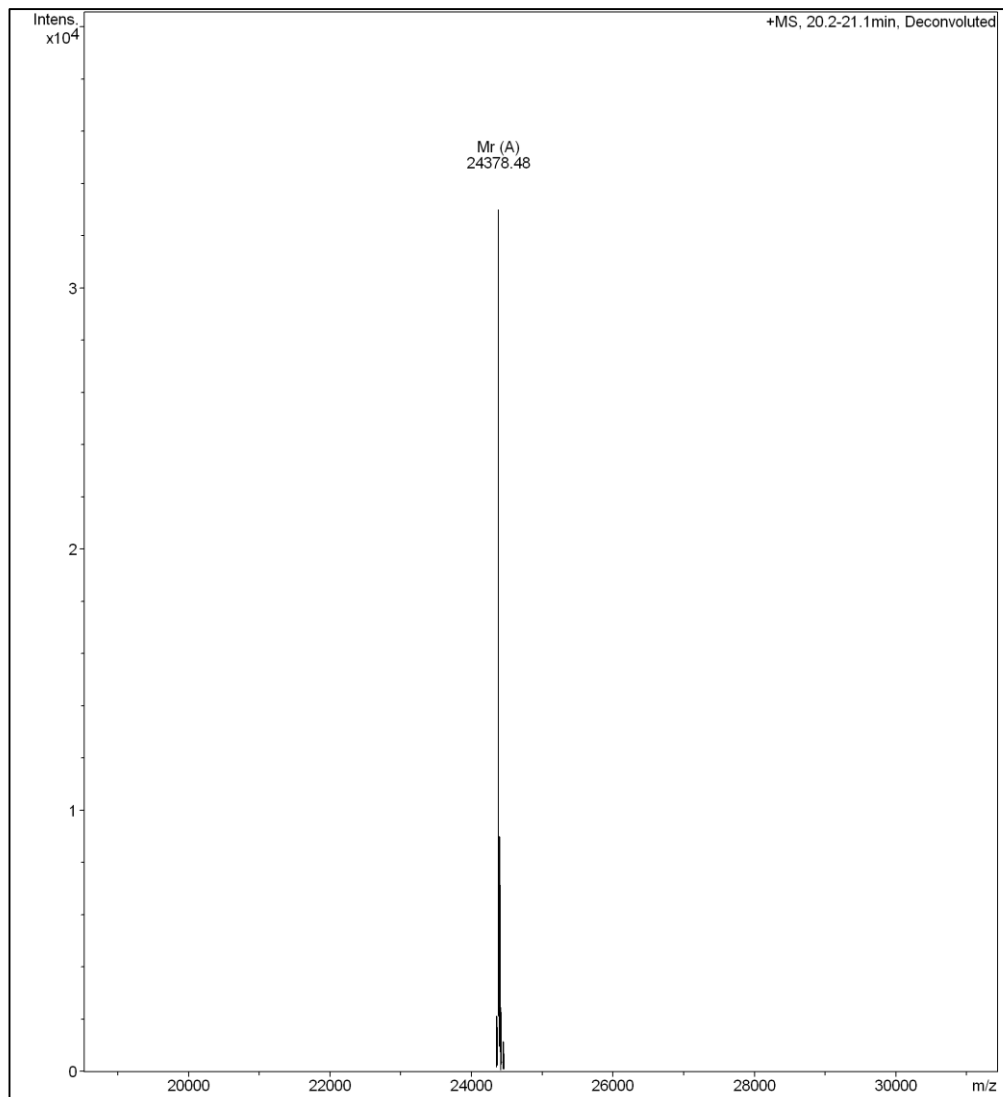
GSHMDQPMEEEEVETFAFQAEIAQLMSLIINTFYSNKEIFLRELISNSSDA
LDKIRYESLTDPSKLDSGKELHINLIPNKQDRTLTIVDTGIGMTKADLINNL
GTIAKSGTKAFMEALQAGADISMIGQFGVGFYSAYLVAEKVTVITKHND
DEQYAWESSAGGSFTVRTDTGEPMGRGTKVILHLKEDQTEYLEERRIKEI
VKKHSQFIGYPITLFVE

**Figure 3.7: Deconvoluted mass spectrum showing the singly-charged species
of Hsp90 with sequence data below**

The distribution of multiply charged species in fig. 3.6 is consistent with the singly
charged species (shown in fig. 3.7). However the final mass is 147 Da short of the
expected mass (24508.7 Da). Given the protein sequence this is likely due to N-

terminal cleavage of the GS dipeptide (mass 144 Da, a legacy of thrombin cleavage. Protein sequence begins at the first D residue). An alternative and less likely explanation is that is could be the result of a missing C-terminal glutamic acid residue.

Neither of these modifications is likely to alter protein folding and neither of these residues is considered to play a role in the binding site.

3.3.2 Initial Rate of STD buildup as shown for Fragment A

Consecutive STD experiments (as in fig. 3.8) with different saturation periods (0 – 5 seconds) were applied to Fragment A.
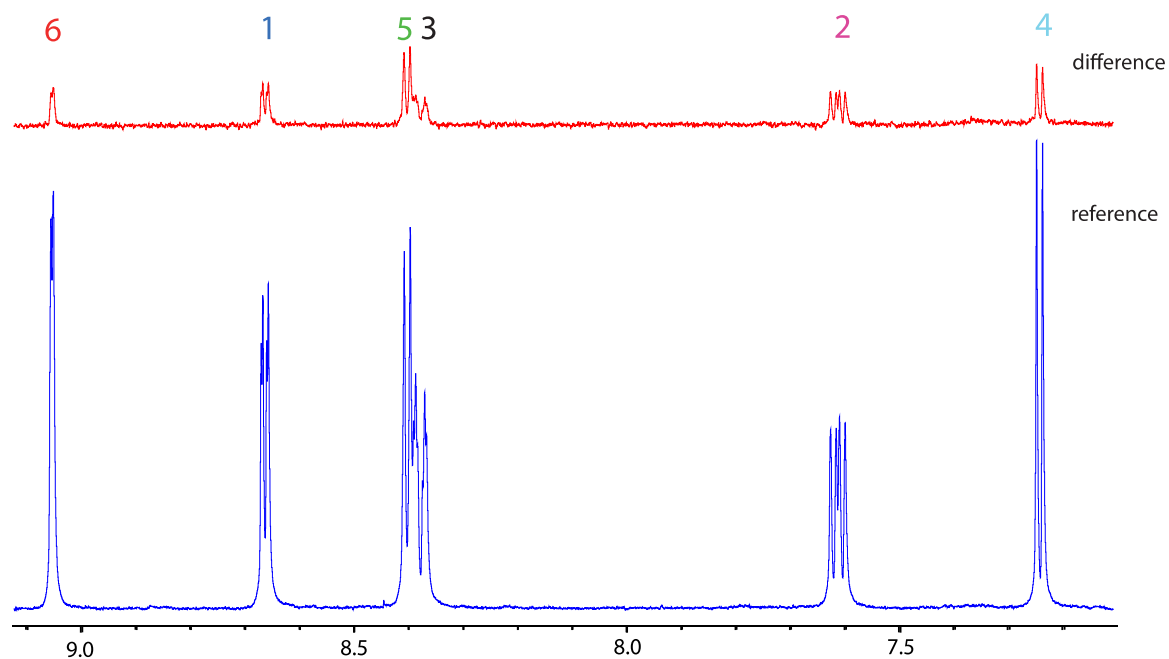
Figure 3.8: An example of an STD reference and difference spectrum for fragment A bound to Hsp90, in this instance acquired at a saturation time of 5 seconds. The absolute intensities of each peak are measured and applied to the STD amplification factor formula

The data were fit to give values for initial rates (fig. 3.9A)

Proton	Initial Rate / STD-AF s^{-1}
6	3.918 ± 0.534
1	5.99 ± 0.456
5	11.115 ± 1.34
3	7.284 ± 0.614
2	10.846 ± 0.797
4	8.655 ± 0.897
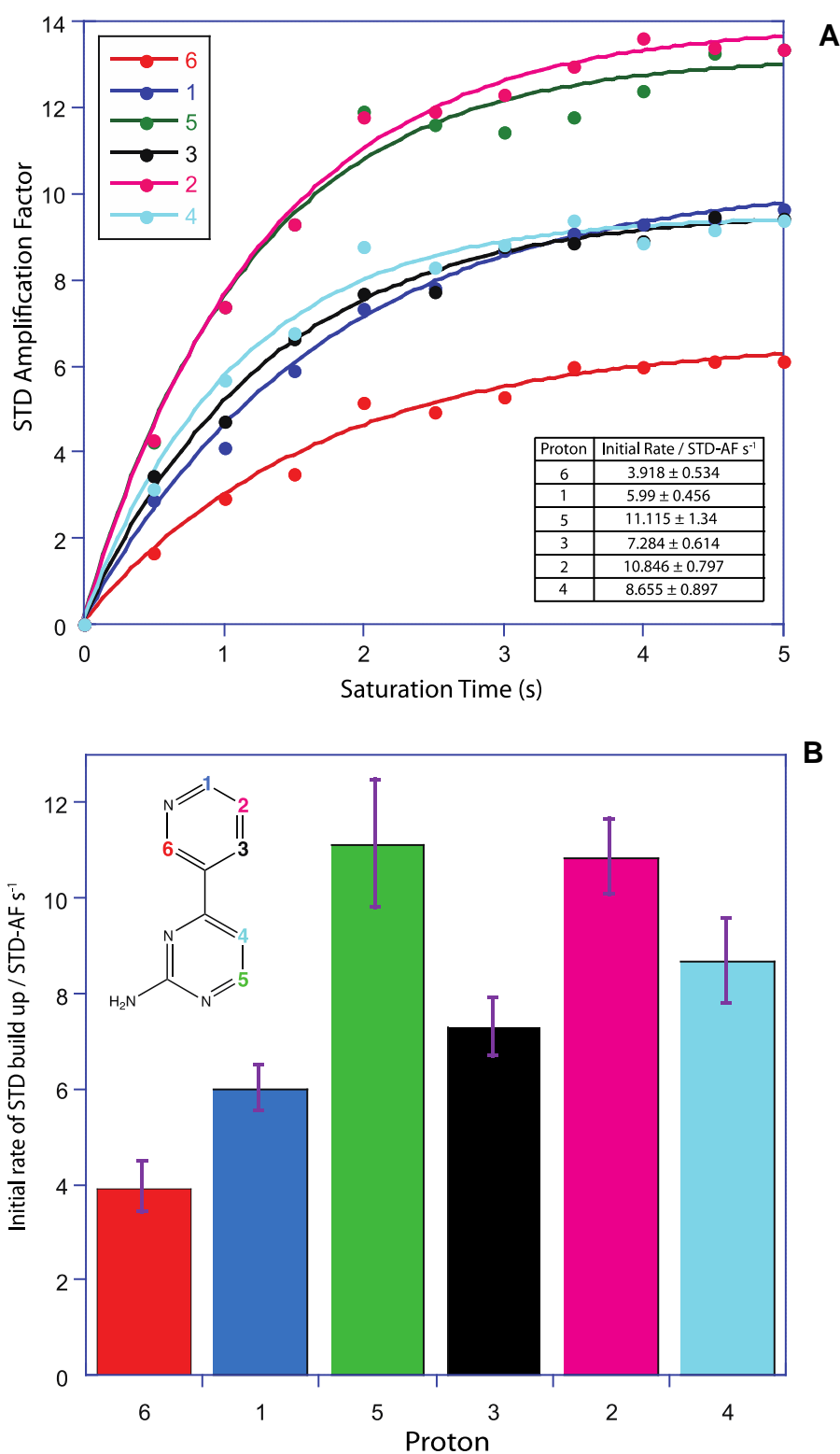
Figure 3.9: Data acquired for each proton were processed as amplification factors (A) and fit to the curves to give the initial rates in (B). Protons 5 and 2 clearly have the steepest initial rates, whilst proton 6 clearly receives the least. Rates and errors as calculated by Kaleidagraph.

The STD values are typically normalised as a percentage of the maximum value. For

Fragment A, this can be seen as illustrated in fig. 3.10.
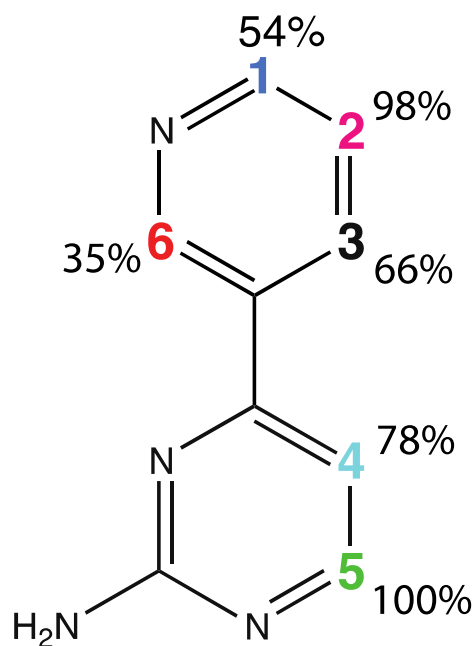
Figure 3.10: Initial STD rates normalised in percentage terms.

More interesting is to quantify all the individual interactions. As is clearly observable,

there is a general positive correlation between the structure and the experiment (fig.

3.11).

3.3.3 Correlating Initial Rate of STD buildup with structural data
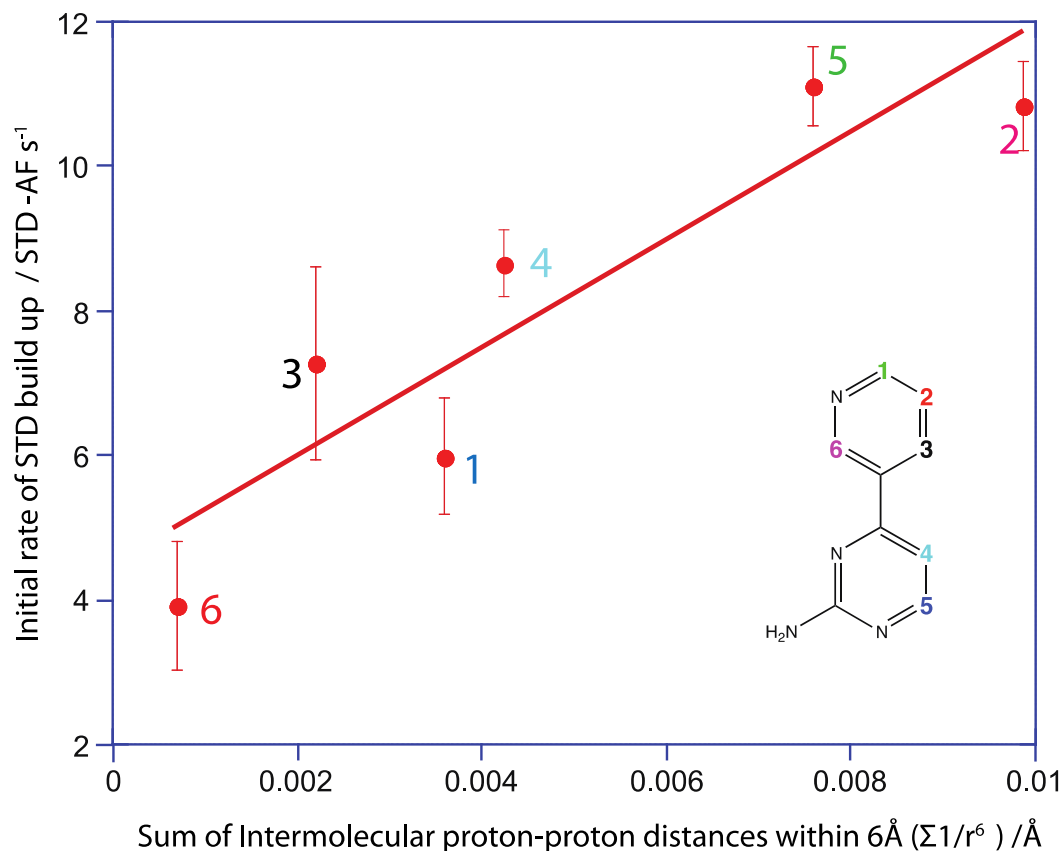
Figure 3.11: The initial rate of STD build up for the 6 individual protons of Fragment A plotted against the sum of the intermolecular proton-proton distances, as derived from the crystal structure (methodology explained in section 3.2.5, three dimensional structure in fig. 3.32).

A positive correlation may be observed between the sum of the intermolecular proton-proton distances and the initial rate of STD build up. This is an interesting result, and appears to be the first time anyone has ever tried correlating the two variables to this degree of accuracy.

Given a reasonably high-resolution crystal structure, we are thus able to show that experimental STD NMR data has a direct relationship with the structure of the binding site.

3.3.4 Inversion Recovery for Longitudinal Relaxation Time constant (T_1) and its application in the GEM-CRL method

The inversion recovery experiment was performed for Fragment A with the data recorded below.

Proton	$T_1 (s)$	Error
6	1.7972	0.0057
1	1.9002	0.0051
5	1.8892	0.0037
3	1.6039	0.0058
2	1.5824	0.0055
4	1.3428	0.0069
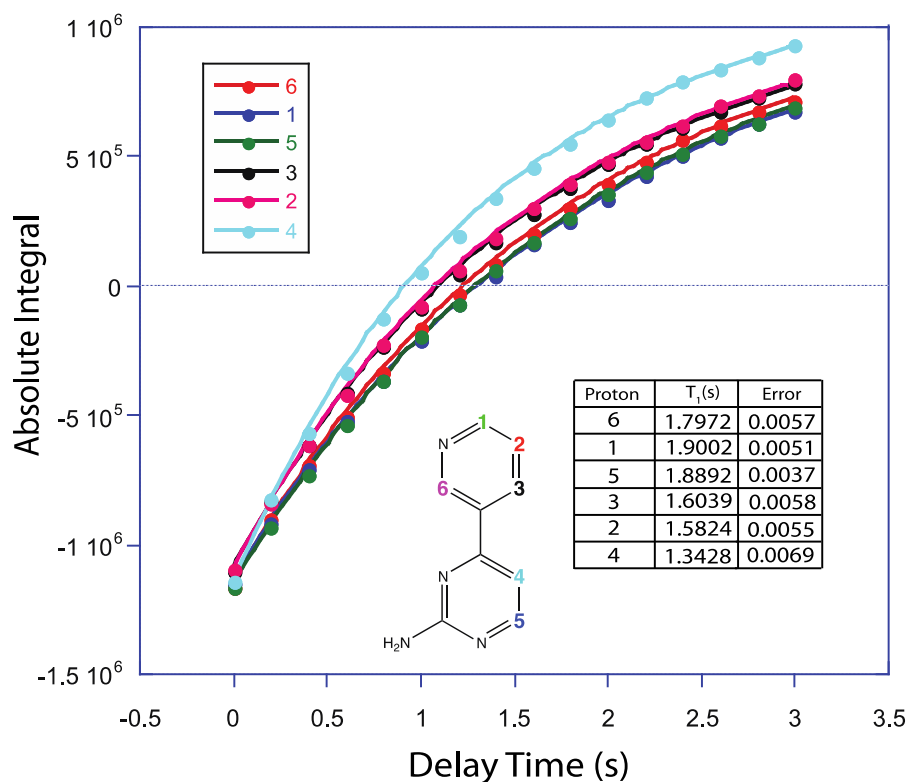
Figure 3.12: ^{1}H Inversion recovery data for Fragment A. All T_1 values are similar, as is to be expected for all aromatic protons. The small differences in T_1 can be observed in the rate of the curves

After obtaining the experimentally determined T_1 values, it is now possible to assess STD data without having to consider the rate of build up over a series of saturation times. The T_1 values are fairly similar, but they are subtly different enough to cause distortions in the STD signal recorded at a given saturation time. A proton with a

shorter T_1 decays faster during the sequence and inadvertently reduces the STD intensity. This manifests itself most clearly at longer saturation times.

Figure 3.13 shows the effect of modulating STD amplification factors for protons according to their respective T_1 values, by dividing STD amplification factor by the experimentally derived value.
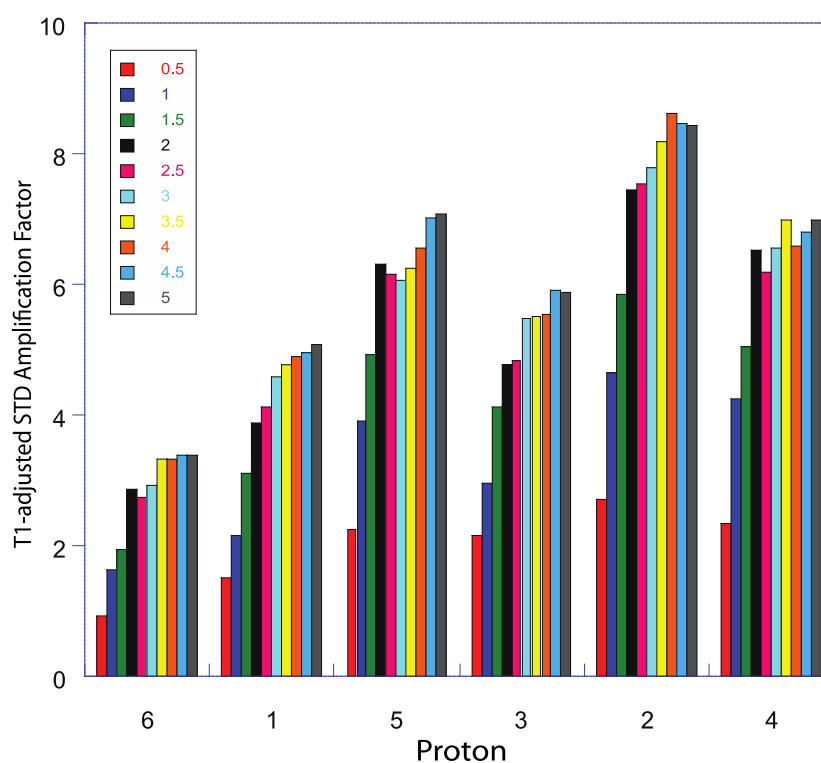
Figure 3.13: ^{1}H T_1 -adjusted STD amplification factors for each proton of the ligand, across all saturation times

Within each proton grouping, STD buildup is observed as the saturation time increases, and for each saturation time, the patterns across the amplification factors remain consistent.

Now it is prudent to analyse this T_1-adjusted data in the same way as we did for the STD initial rates previously, in the context of the structural data.
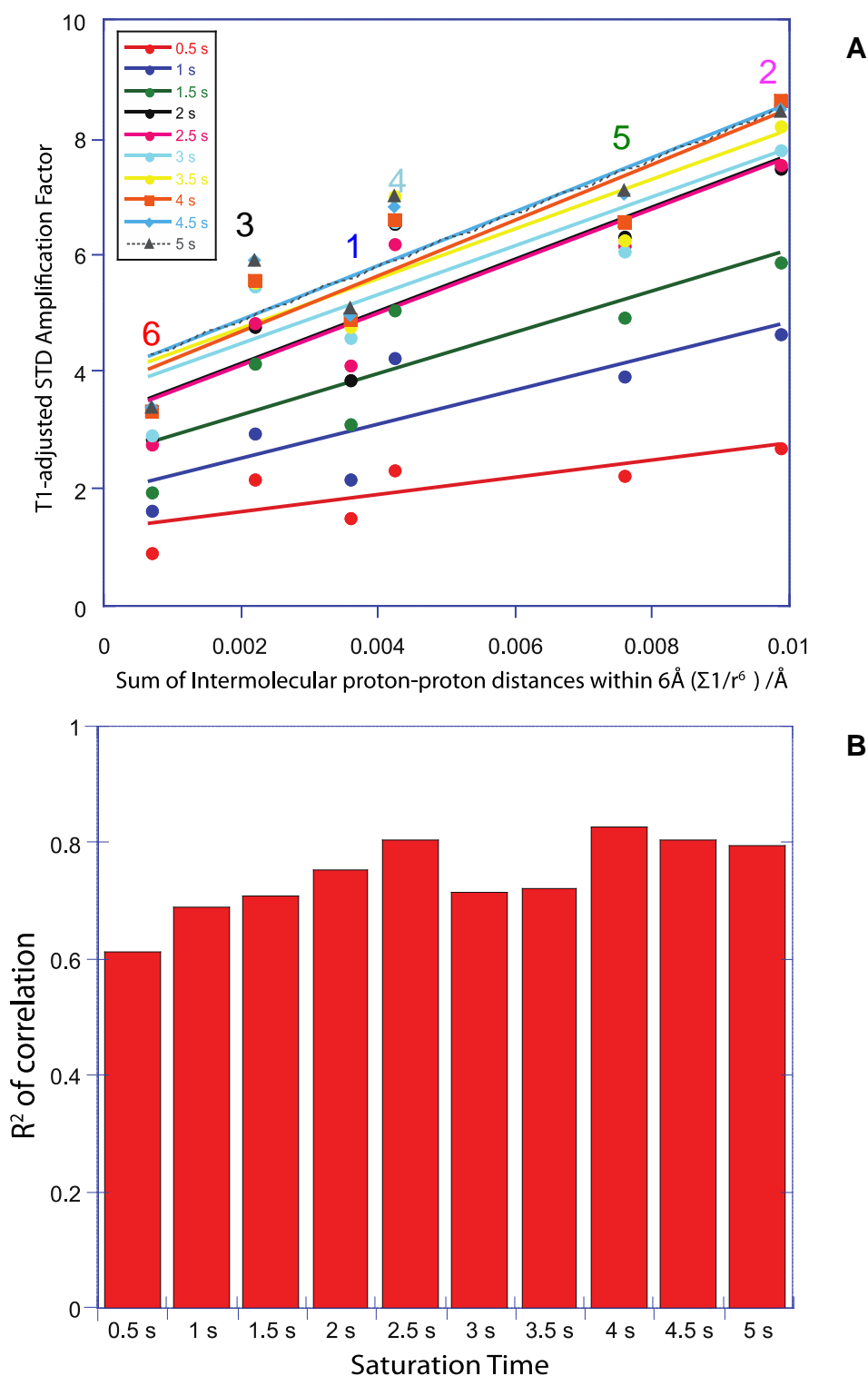
Figure 3.14: (A) STD amplification factor – adjusted for T_1 – plotted against the sum of the intermolecular proton-proton distances for each individual proton (as derived from PDB 2XDK), at each of the ten saturation times. The same positive correlation between the two variables may be observed, and this is maintained across all of the saturation periods, as shown in (B) by the consistent R^2 value.

Fig. 3.14A shows the correlation between the sum of the intermolecular proton-proton distances for a given proton, and the T_1-adjusted STD.

To support these findings, the same analysis was carried out for five further fragments (B − F) known to bind to Hsp90. From this, it was suspected that similar trends might be observed. First though, I will walk through the case of fragment B, in order to explain how we dealt with ligands that possess methyl and methylene groups

3.3.5 Fragment B

STD spectra were acquired for the usual set of saturation times (0.5 s − 5 s). Fig 3.15A and 3.14B are example spectra acquired with five seconds saturation.
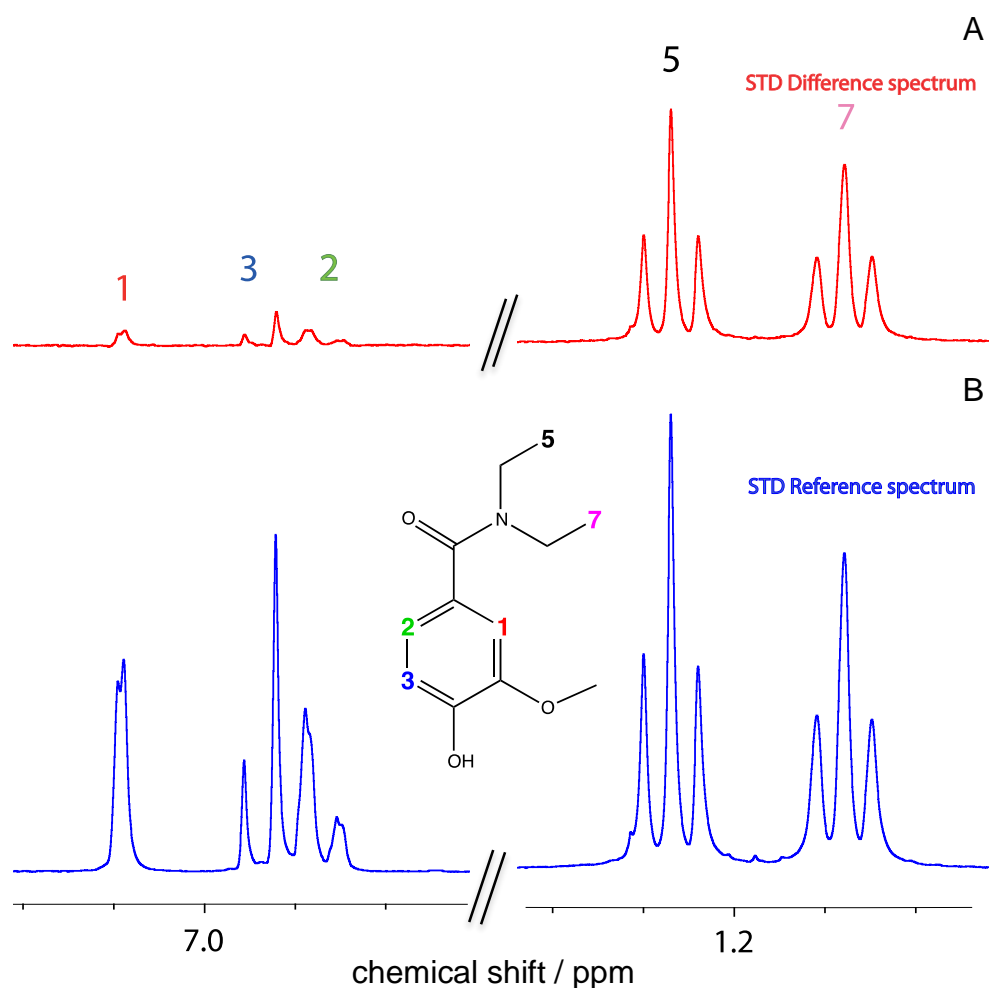
Figure 3.15: STD difference (A) and reference (B) spectra for fragment B binding to Hsp90

As with fragment A the STD build up curve is constructed by plotting the amplification factor of each proton at each saturation time, enabling the calculation of initial rates.

Proton	Initial Rate / STD-AF s^{-1}
1	4.65 ± 0.505
3	6.557 ± 0.416
2	6.555 ± 0.545
5	61.67 ± 2.158
7	73.28 ± 4.706
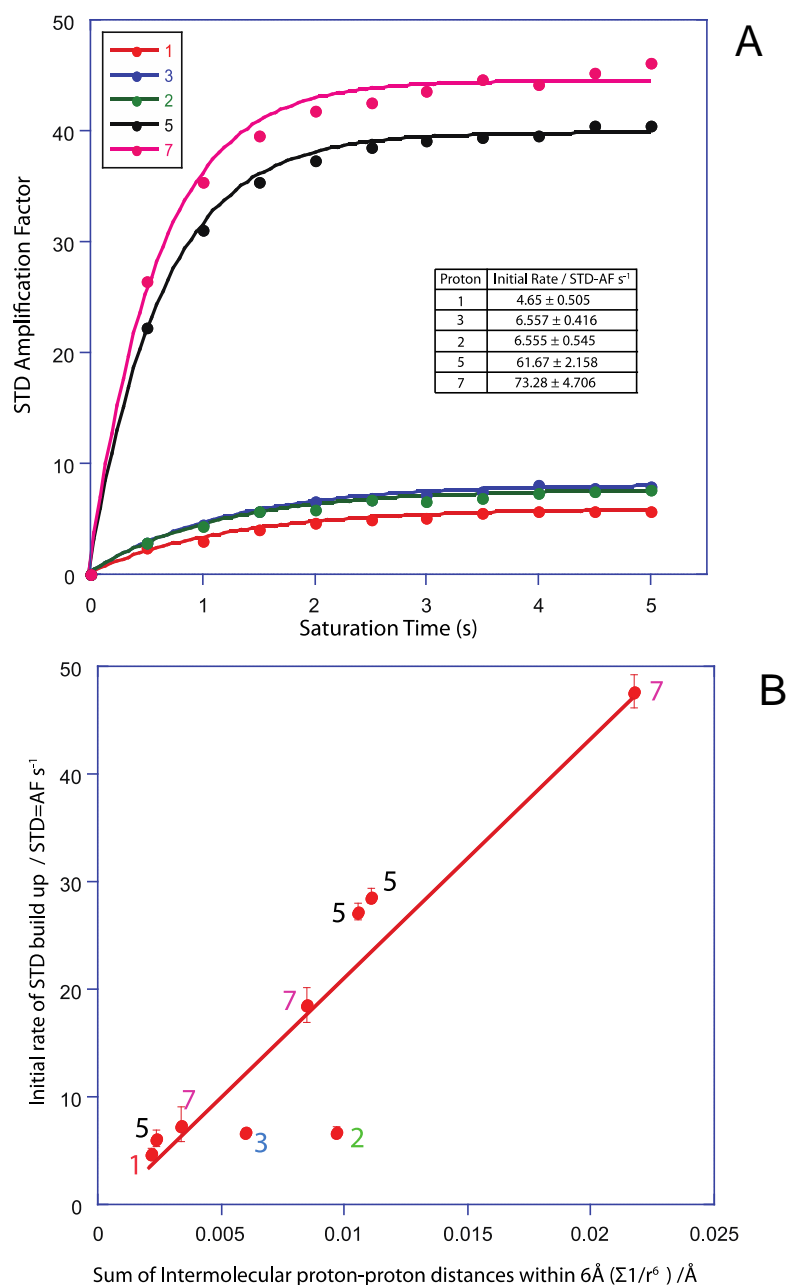
Figure 3.16: STD buildup curves for fragment B in the presence of Hsp90 (A), and (B) correlation of STD initial rates with the sum of the intermolecular proton-proton contacts

Quantitative STD with a fragment such as fragment B necessitates some additional treatment. For the correlation of the intermolecular structure as in fig 3.16 it was essential to split the initial rate for proton groups 7 and 5. These protons belong to

methyl groups and as such comprise three protons. This is reflected in the significantly steeper initial rates for these groups. In order to deal with cases such as these, the initial rate was divided into three values, in proportion with the intermolecular distance values for each individual proton as derived from the crystal structure. In this particular example it is worth noting that the similarity of the initial rates for proton groups 5 and 7 could be due to amide bond rotamer exchange, which may be distorting the rate values.

The same division treatment applies to T_1-adjusted STD values. The T_1 for the whole group is used to divide the STD for the whole group, the final values which is then divided in the appropriate proportions. This is explained in the methods section.

It may also come to your attention that two proton groups, the methylene proton groups of the ethylamide, do not feature in the analysis. The reason for this is because the STD signal for these groups is not sufficiently strong to measure, and also happens to fall in a chemical shift range that is obscured by biological buffers.

In terms of the T_1-adjusted STD method the same principles as fragment A may be applied to fragment B. The inversion recovery curve is shown below

Proton	T_1(s)	Error
1	1.1486	0.0037
3	1.3442	0.0055
2	1.309	0.0063
5	0.6335	0.0042
7	0.6135	0.0032
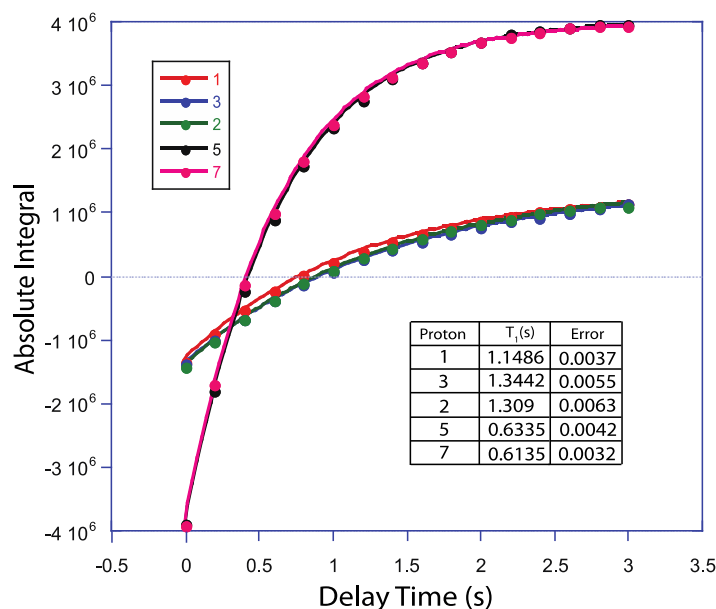
Figure 3.17: Inversion recovery curves for fragment B

As with before, the T_1 values derived from inversion recovery experiments can be used as a factor to divide STD amplification factor values at all saturation times. These T_1-adjusted STD values can then also be plotted against intermolecular structure.
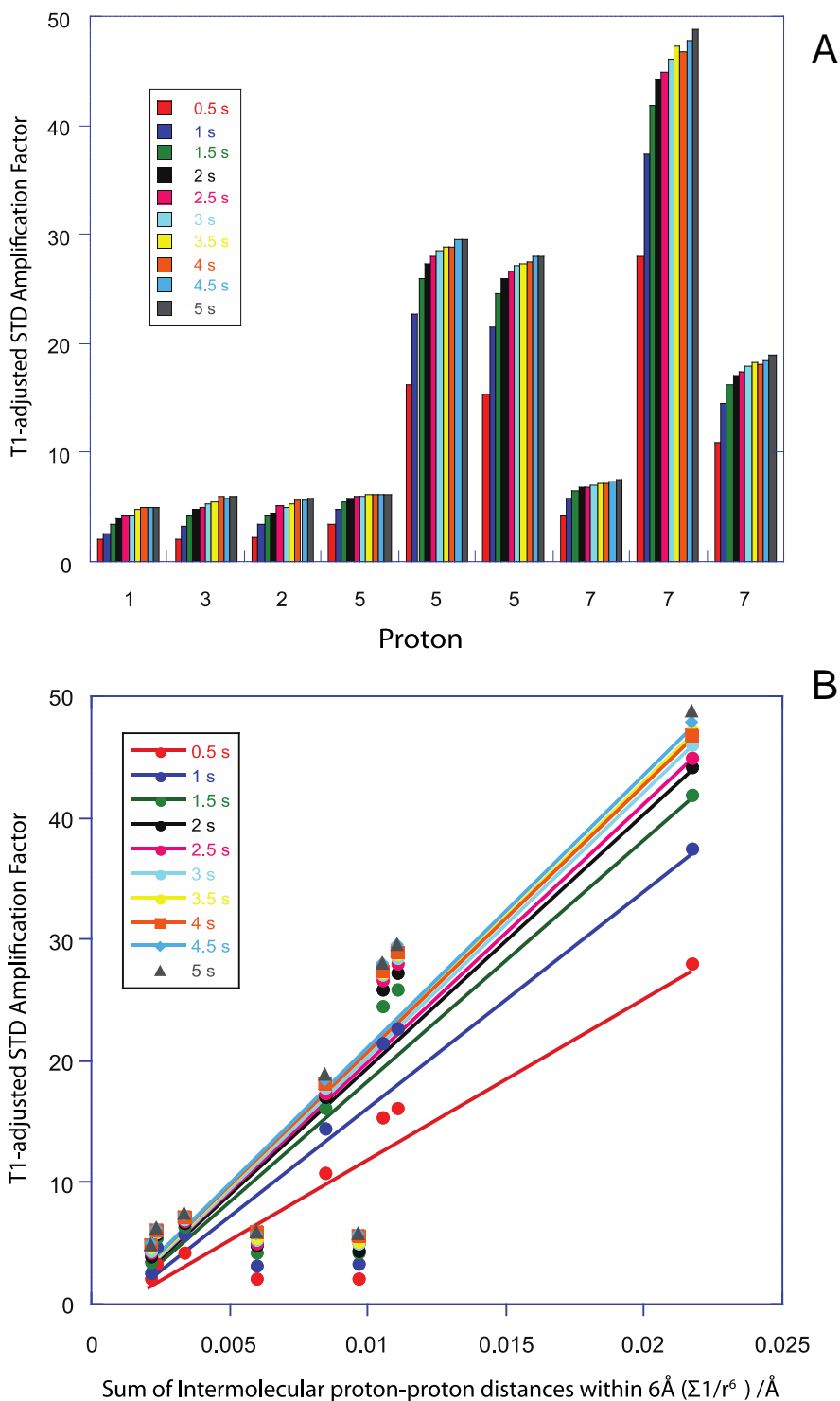
Figure 3.18: (A) T$_1$-adjusted STD amplification factors for all protons of fragment B. (B) these values plotted against intermolecular structure to provide a similar correlation as initial rate

3.3.6 Fragment C
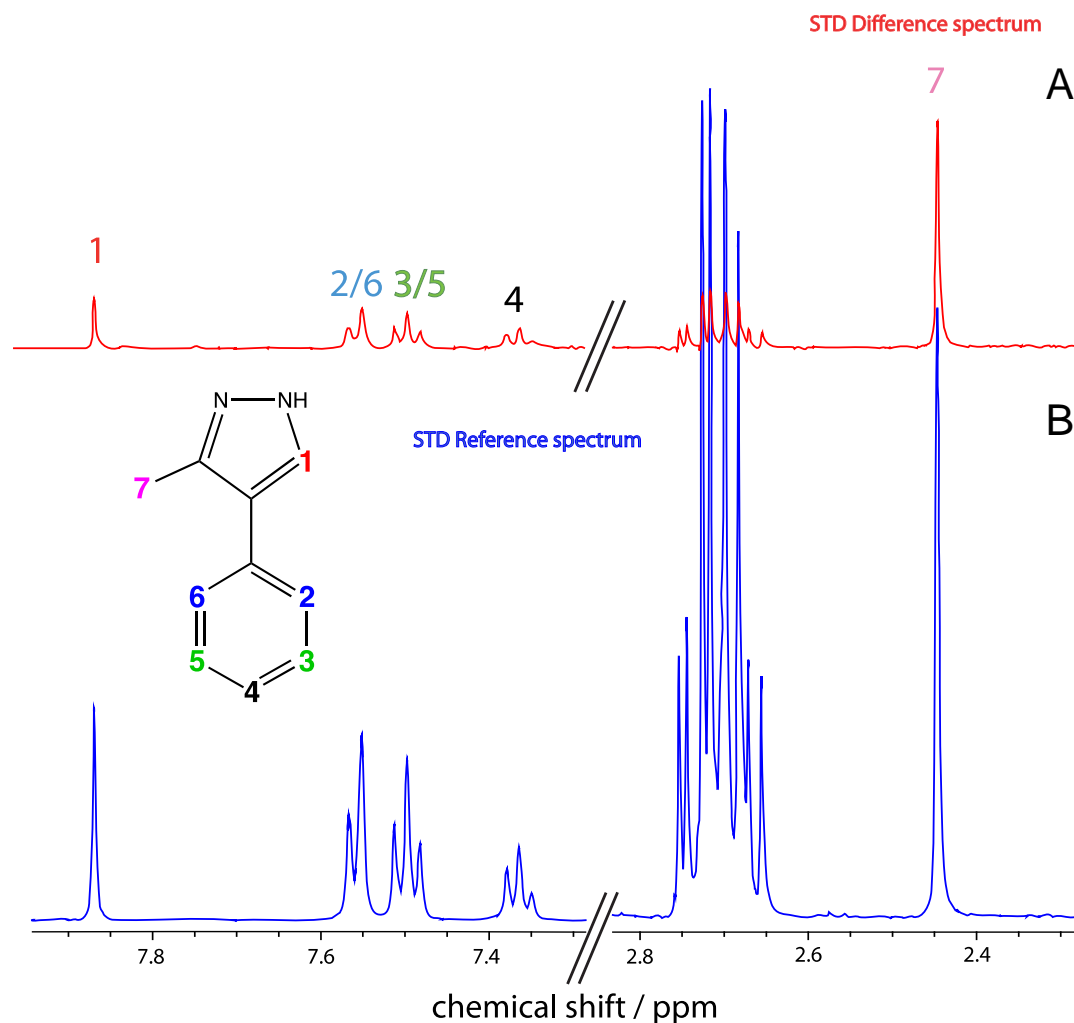
Figure 3.19: Example STD difference (A) and reference (B) spectra for fragment C binding to Hsp90. Resonances between 2.6-2.8 ppm are signals from components of the buffer such as DTT
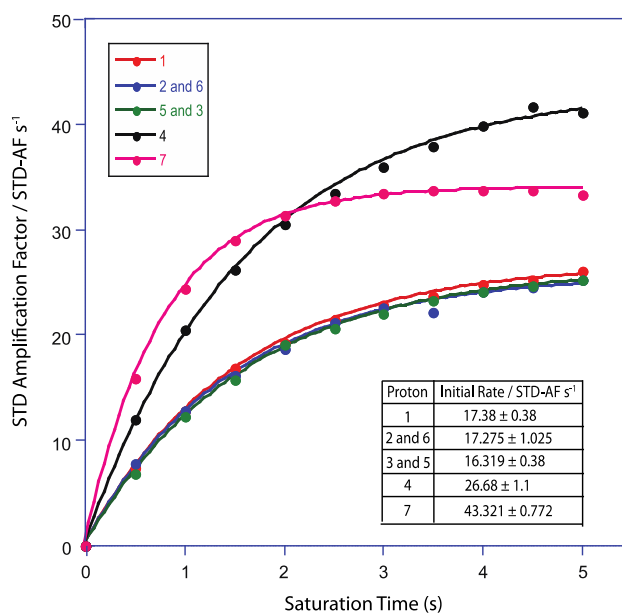
Figure 3.20: STD build up curves for fragment C binding to Hsp90

Fig 3.21A shows how there is a strong positive correlation between the initial rates of STD build up and the sum of the intermolecular proton-proton contacts. Inversion recovery data enabled calculation of accurate T_1 values that were then used to modulate STD values at each fixed saturation time. As fig 3.21D shows, these T_1-adjusted STD values also correlate very well with intermolecular structure, at all saturation times.
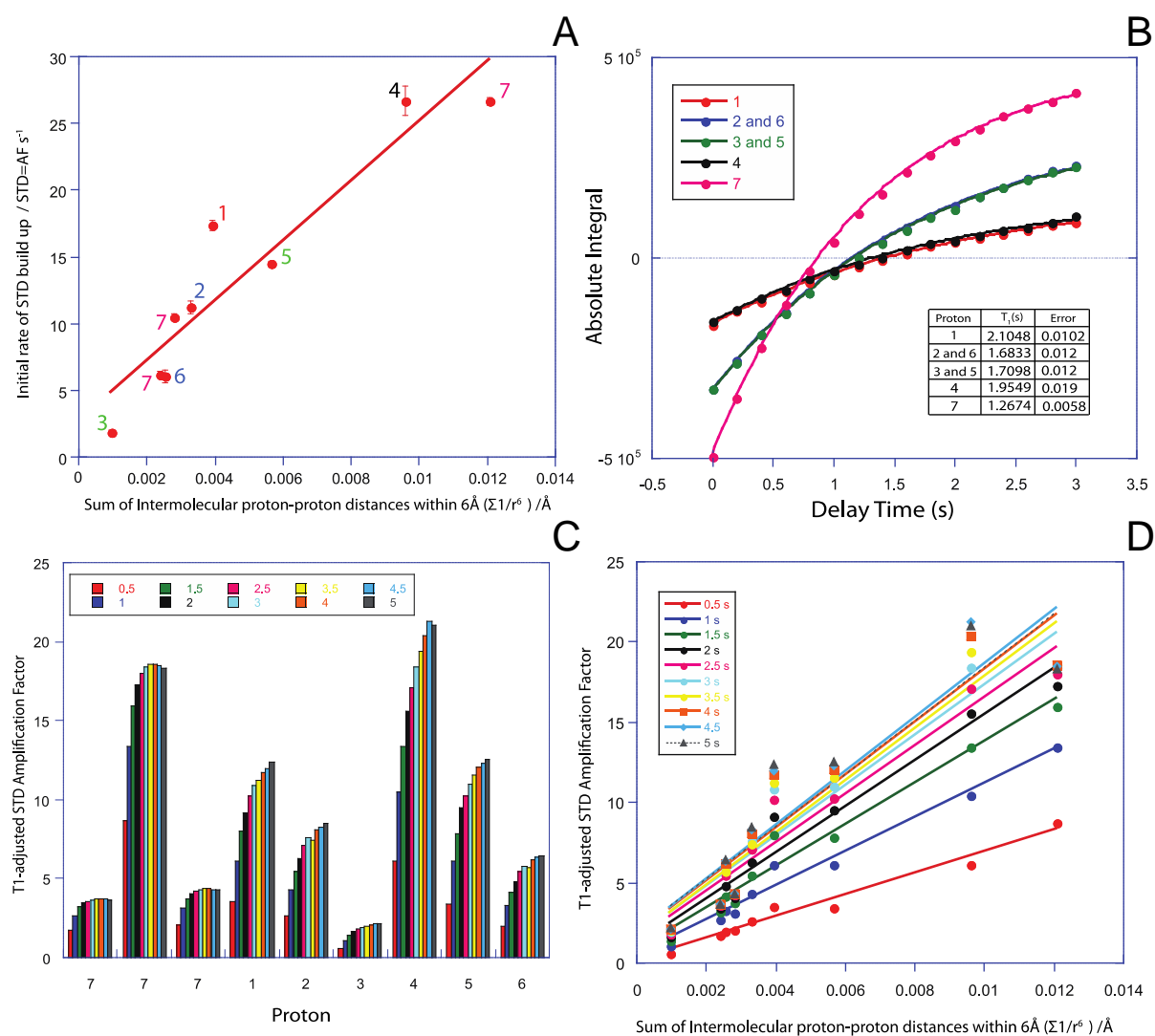
Figure 3.21: (A) Correlation of STD initial rates for fragment C with Hsp90 structure. (B) Inversion recovery curves for fragment C and associated T_1 values. (C) T_1-adjusted STD values at each fixed saturation time, and (D) these values correlated against intermolecular structure

3.3.7 Fragment D
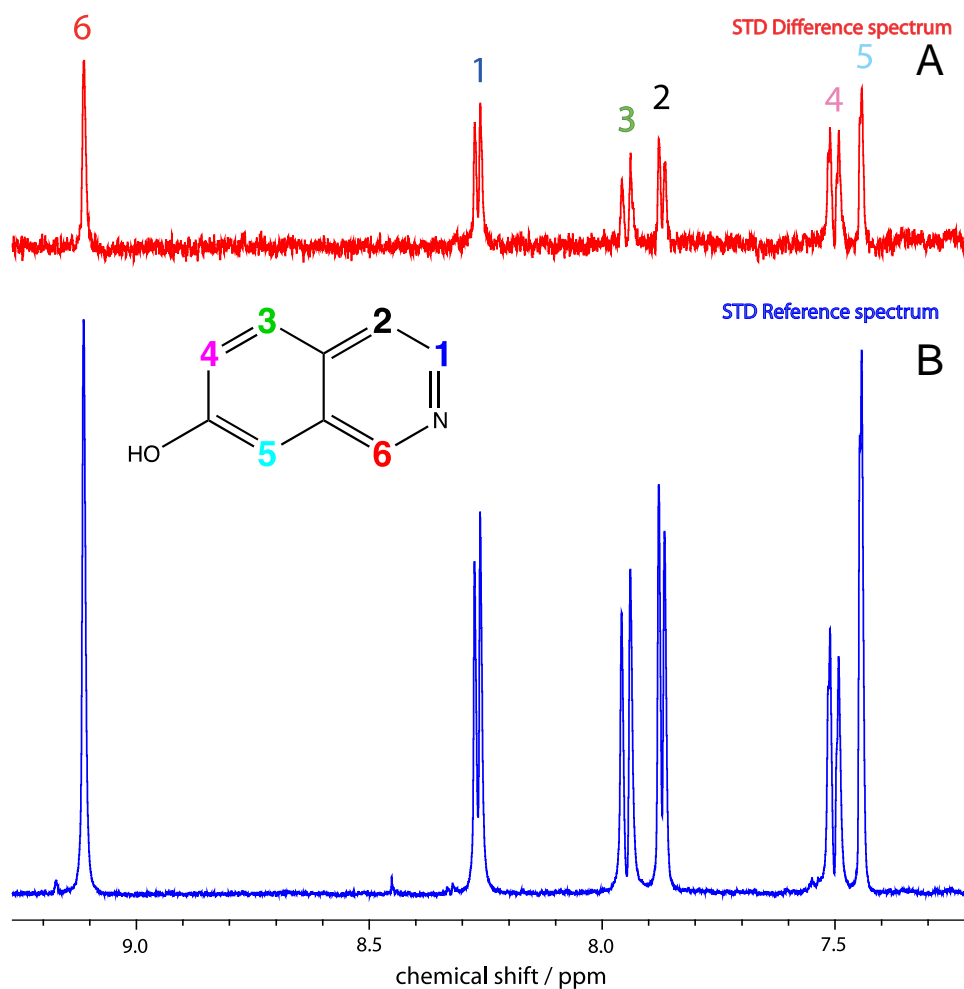
Figure 3.22: Example STD difference (A) and reference (B) spectra for fragment D binding to Hsp90

Proton	Initial Rate / STD-AF s⁻¹
6	9.46 ± 0.458
1	9.23 ± 0.85
3	7.38 ± 1.002
2	7.34 ± 0.45
4	11.42 ± 1.61
5	8.096 ± 0.685
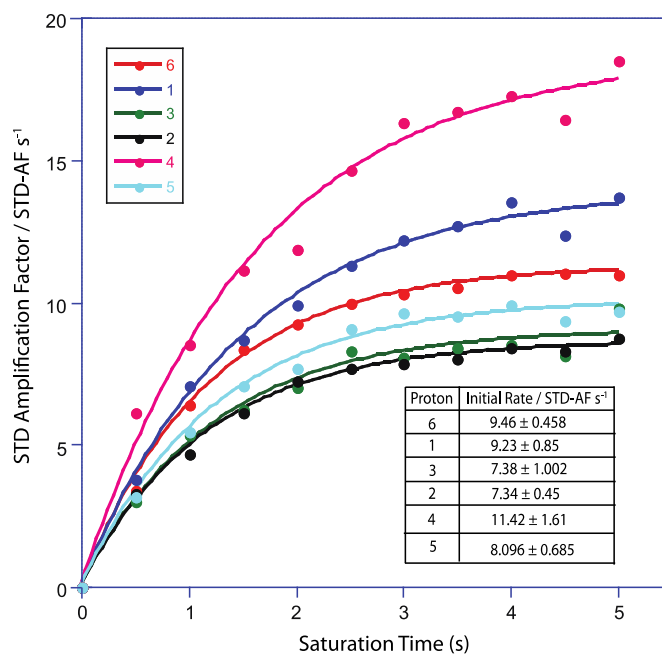
Figure 3.23: STD build up curves for fragment D binding to Hsp90

STD build up curves for fragment D in the presence of Hsp90 are reasonable, with a fairly large degree of error caused by the points at 2 and 4.5 seconds (visible in fig. 3.23). Nonetheless, a reliable positive correlation is still observed with structure in fig 3.24A. Again, accurate inversion recovery experiments yielded reliable T_1 results, which when used to divide STD amplification factors result in a good correlation.
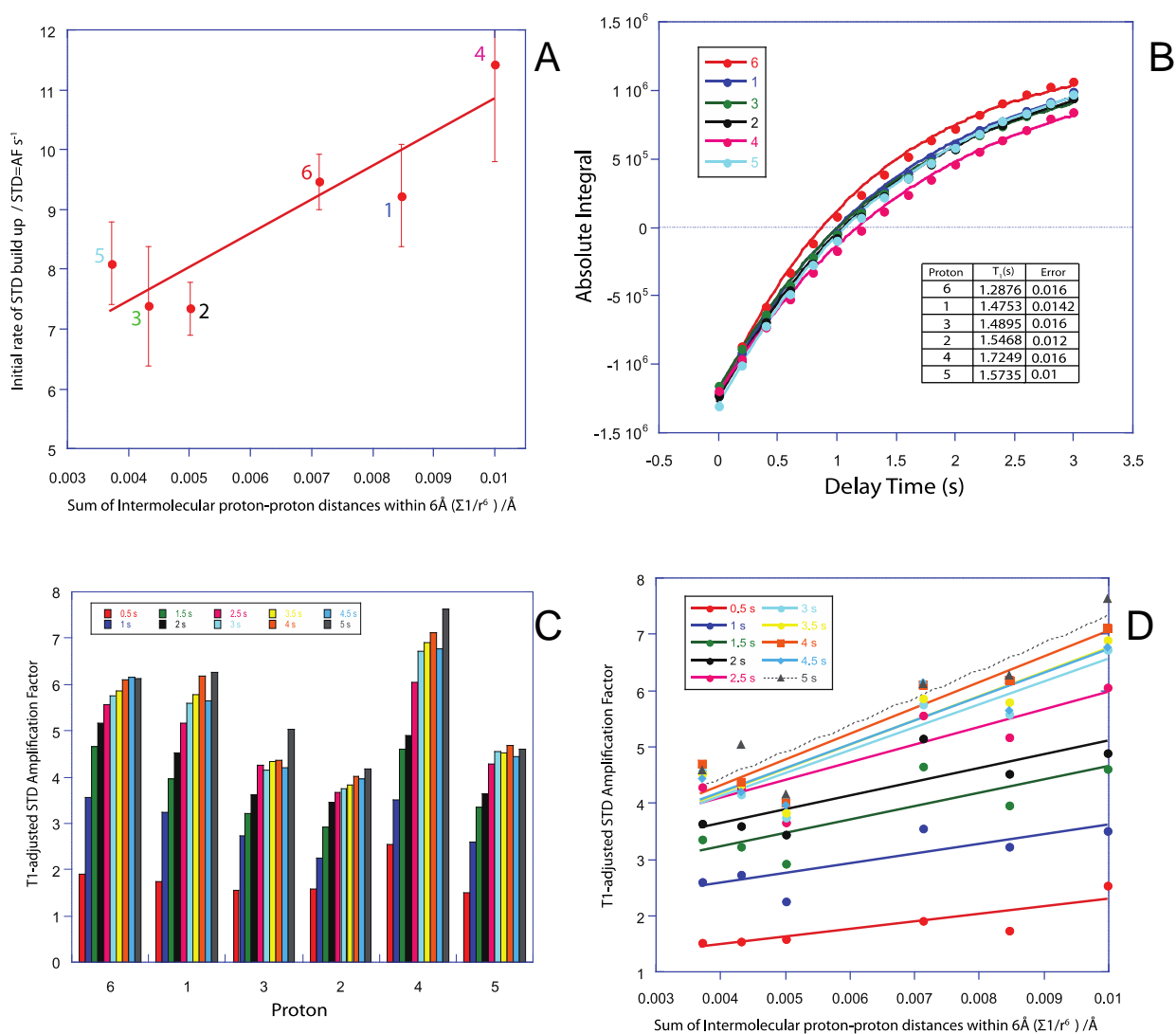
Figure 3.24: (A) Correlation of STD initial rates for fragment D with Hsp90 structure. (B) Inversion recovery curves for fragment D and associated T_1 values. (C) T_1-adjusted STD values at each fixed saturation time, and (D) these values correlated against intermolecular structure

3.3.8 Fragment E
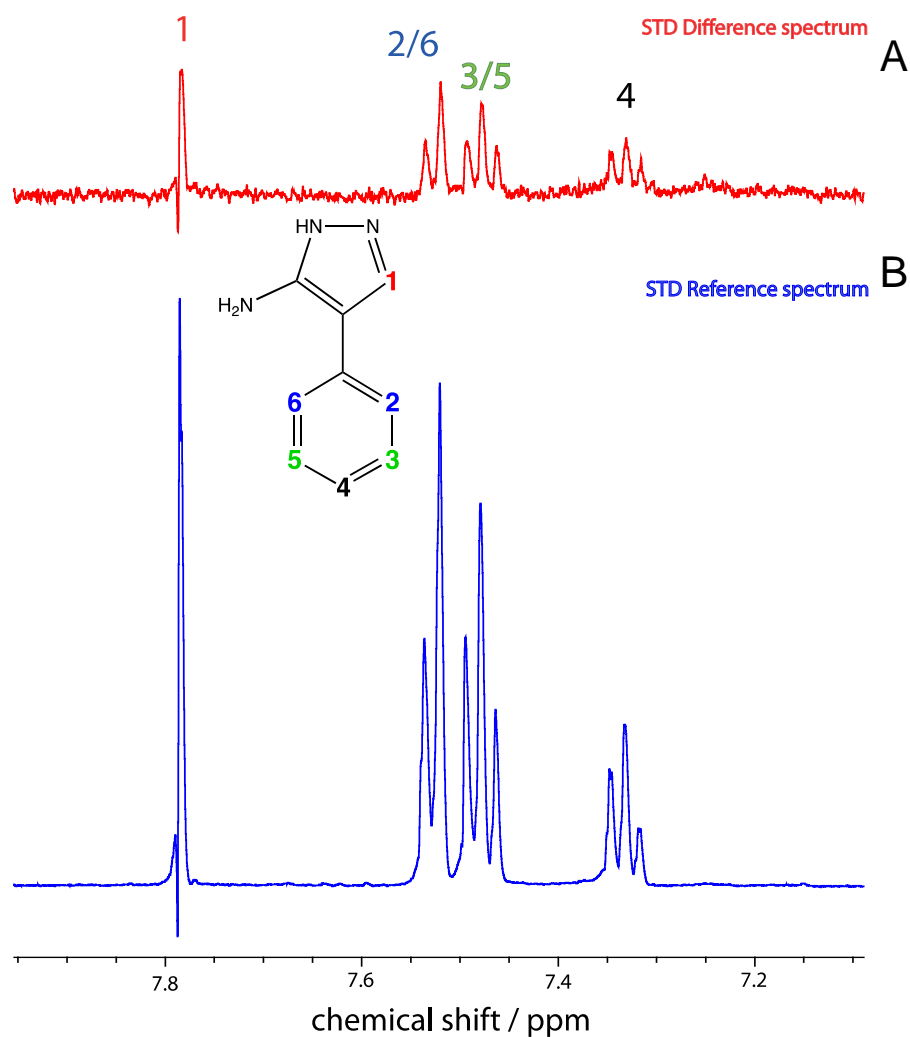
Figure 3.25: Example STD difference (A) and reference (B) spectra for fragment E binding to Hsp90

Proton	Initial Rate / STD-AF s^{-1}
1	3.178 ± 0.777
2 and 6	3.514 ± 0.542
3 and 5	3.34 ± 0.542
4	6.02 ± 1.188
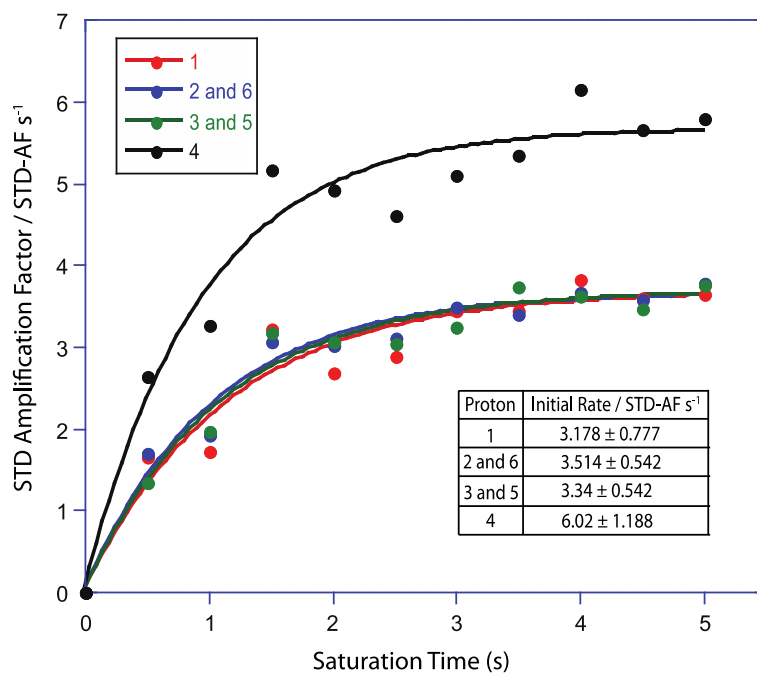
Figure 3.26: STD build up curves for fragment E binding to Hsp90

STD build up curves for fragment E are reasonable (see fig. 3.26), as are the initial rates derived herein. Again a good correlation is made between these rates and intermolecular structure (fig 3.27A). A similar trend may be observed with T_1-adjusted STD data in figure 3.26D.
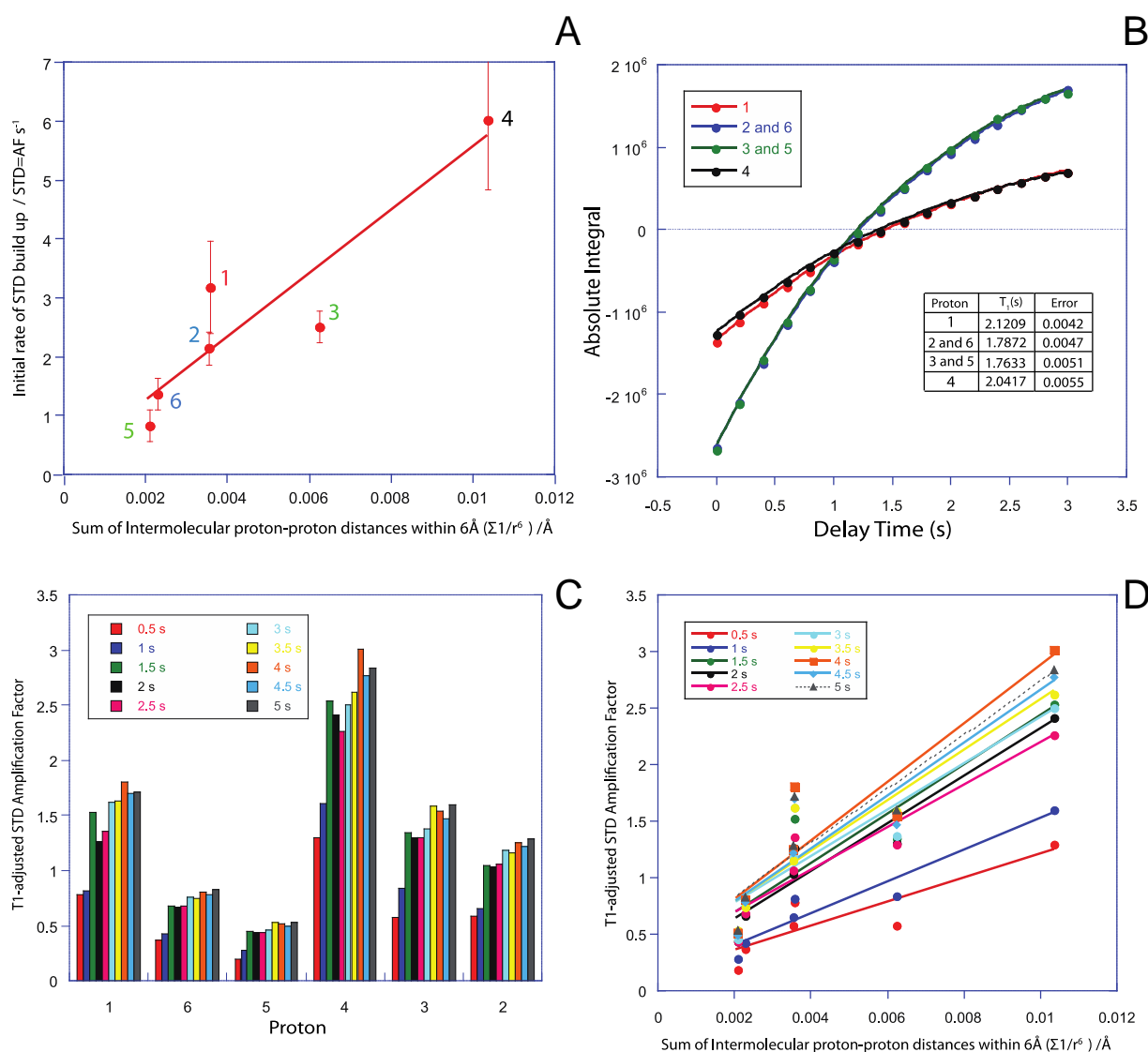
Figure 3.27: (A) Correlation of STD initial rates for fragment E with Hsp90 structure. (B) Inversion recovery curves for fragment E and associated T_1 values. (C) T_1-adjusted STD values at each fixed saturation time, and (D) these values correlated against intermolecular structure

3.3.9 Fragment F
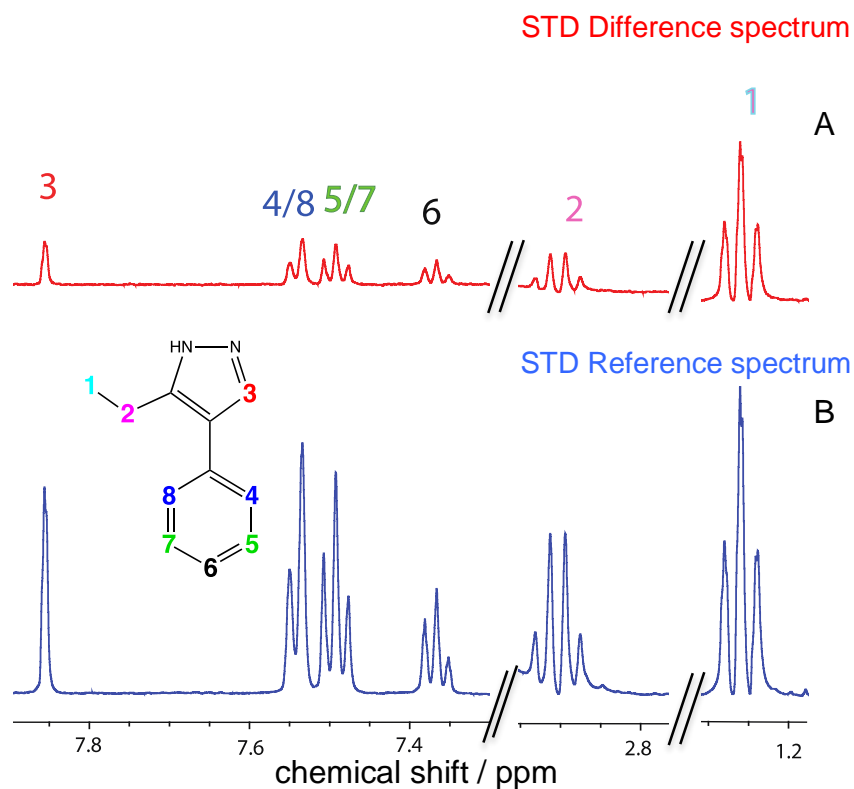
Figure 3.28: Example STD difference (A) and reference (B) spectra for fragment F binding to Hsp90
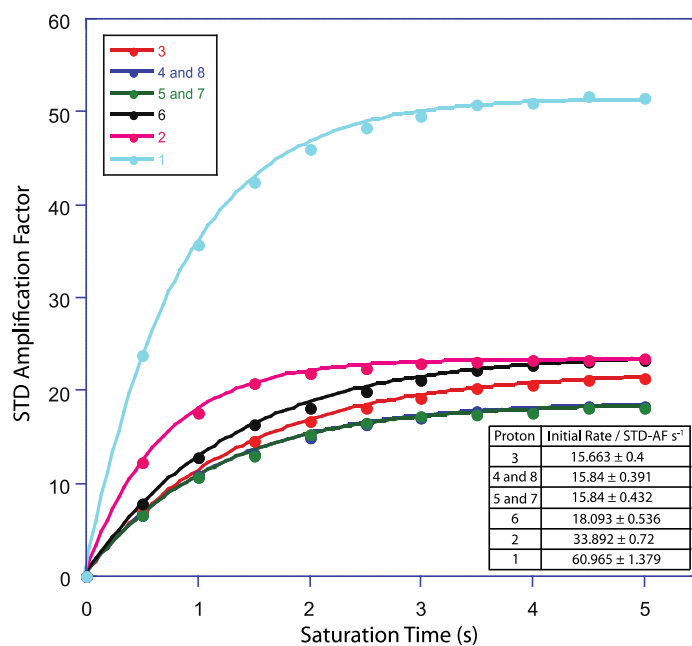
Figure 3.29: STD build up curves for fragment F binding to Hsp90

STD build up curves in fig. 3.29 show a set of very smooth fits and this is reflected in the initial rates with very small associated error. Correlation between initial rates and structure is broadly positive, bar one data point of proton group 2. Inversion recovery curves in fig 3.30B are good and give a varied range of T_1 values. Correlation of T_1-adjusted STD values with intermolecular structure is similar if not slightly weaker than that caused by initial rates (fig 3.30D).
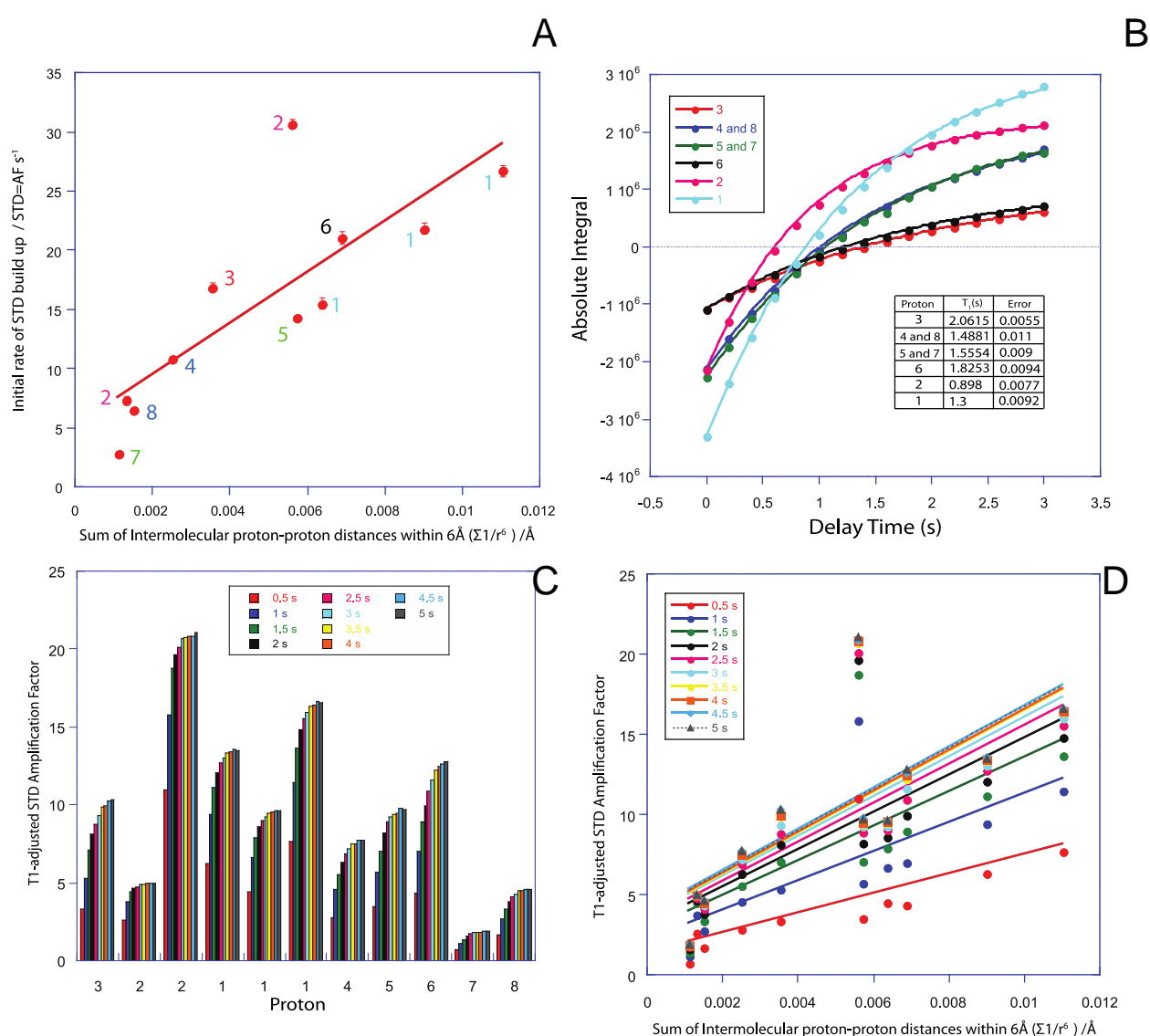
Figure 3.30: (A) Correlation of STD initial rates for fragment F with Hsp90 structure. (B) Inversion recovery curves for fragment F and associated T_1 values. (C) T_1-adjusted STD values at each fixed saturation time, and (D) these values correlated against intermolecular structure

3.4 Discussion

3.4.1 Initial observations based on fragment A

3.4.1.1 Initial rate of STD buildup

The curiosity piqued by the ease with which STD NMR data for Fragment A could be quantified - and used to produce six unique initial rate values for six unique protons - led to pursuing if there were any correlations with the crystal structure.

The buildups and initial rates in fig. 3.9A and 3.9B allow for a unique comparison with the crystal structure in fig 3.11. Plotting initial STD rates against the sum of intermolecular proton-proton contacts, using restraints measured from the crystal structure. This plot suggests there is a definite correlation between the rate of saturation transfer and the position of protons in the ligand, relative to amino acid side chains that comprise that binding site. The correlation is made on the basis of 6 protons, but it is clear and unambiguous.

Alternatively, it is possible to simply compare against the single shortest intermolecular proton-proton distance. In this instance, as shown by fig. 3.31, the correlation is very similar, and emphasizes the importance and distance dependence of NOE transfer.
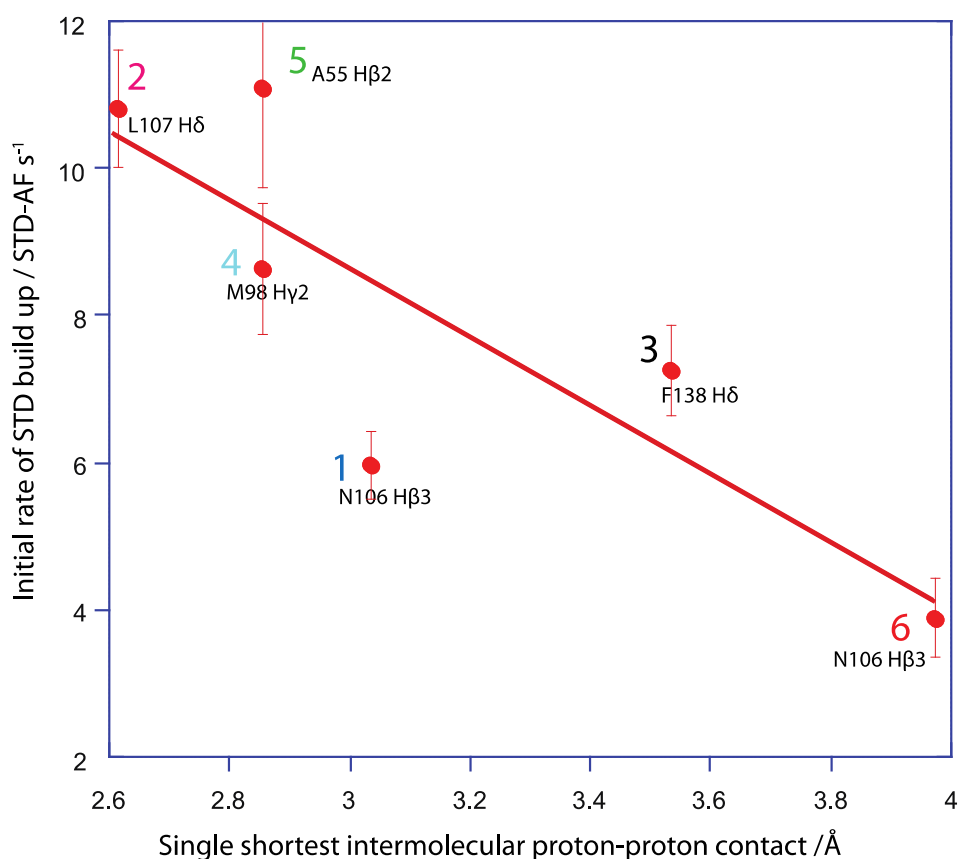
Figure 3.31: Correlating initial rate data with the single-shortest intermolecular proton-proton contact. The nearest amino acid residue is highlighted for each proton

The graph in fig. 3.31 provides a simple correlation without scouring restraints from the crystal structure. As expected, it is a mirror image of fig 3.11, and illustrates the significance of the single closest magnetisation transfer pathway.

The STD values are typically normalised as a percentage of the maximum value. For Fragment A, this can be seen as illustrated in fig. 3.32.
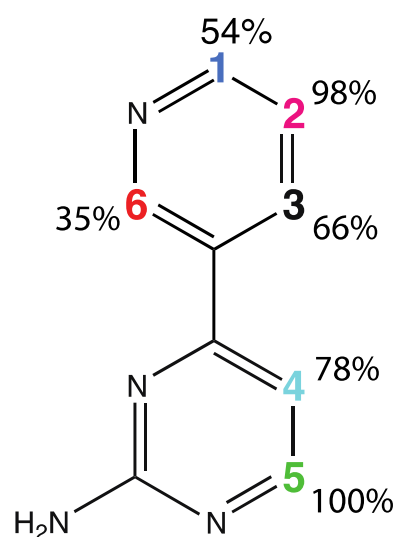
Figure 3.32: Initial STD rates normalised in percentage terms.

Presenting the information in this manner is not very informative regarding fragment orientation, due to the relatively small number of unique protons. However, the data does suggest the side of the fragment containing proton 6 is not the primary contact side. However, even suggesting this is not particularly insightful, because the Hsp90 ADP binding site is a 15 Å deep pocket(Prodromou et al., 1997, Schulte et al., 1998), allowing for many different orientations of a small fragment.

Quantifying all the individual interactions, as our analysis has focused on, is much more informative for small fragments binding to a protein such as Hsp90.

3.4.1.2 ^{1}H T_1-adjusted STD data

Similar conclusions exist for the T_1-adjusted STD data as apply to initial rate data. This can be evidenced by the correlations with intermolecular structure in figs. 3.14A, 3.18B, 3.21D, 3.24D, 3.27D and 3.30D (for fragments A − F respectively). The

correlation between the T_1-adjusted STD - at any given saturation time period – and the distance restraints is consistently equally as good as that between the restraints and the initial rate.

3.4.2 Observations across the 5 subsequent fragments

Generally speaking, the same patterns for fragment A are observed across the full spectrum of fragments that were examined. This is what provides the most weight to any conclusions: the patterns are repeated in subsequent investigations with fragments B - F.

Intense STD signals were observed from protons at the tip of the phenyl rings of fragments C, E and F (protons 4, 4 and 6 respectively). Conversely the single proton adjacent to the nitrogen atom in the pyrazole ring consistently received less saturation transfer (protons 1, 1 and 3 respectively). This cannot be circumstantial, but must relate to binding mode similarities and the precise shape of the binding site environment in which these protons find themselves.

3.4.3 Examining experimental STD data in the context of overall structure

The novel aspect of this work is the comparison of experimental STD NMR data directly up against atomic-resolution structural data, and so it is appropriate to look at the structural context in which some of these fragments exist. Fragment A is shown below:
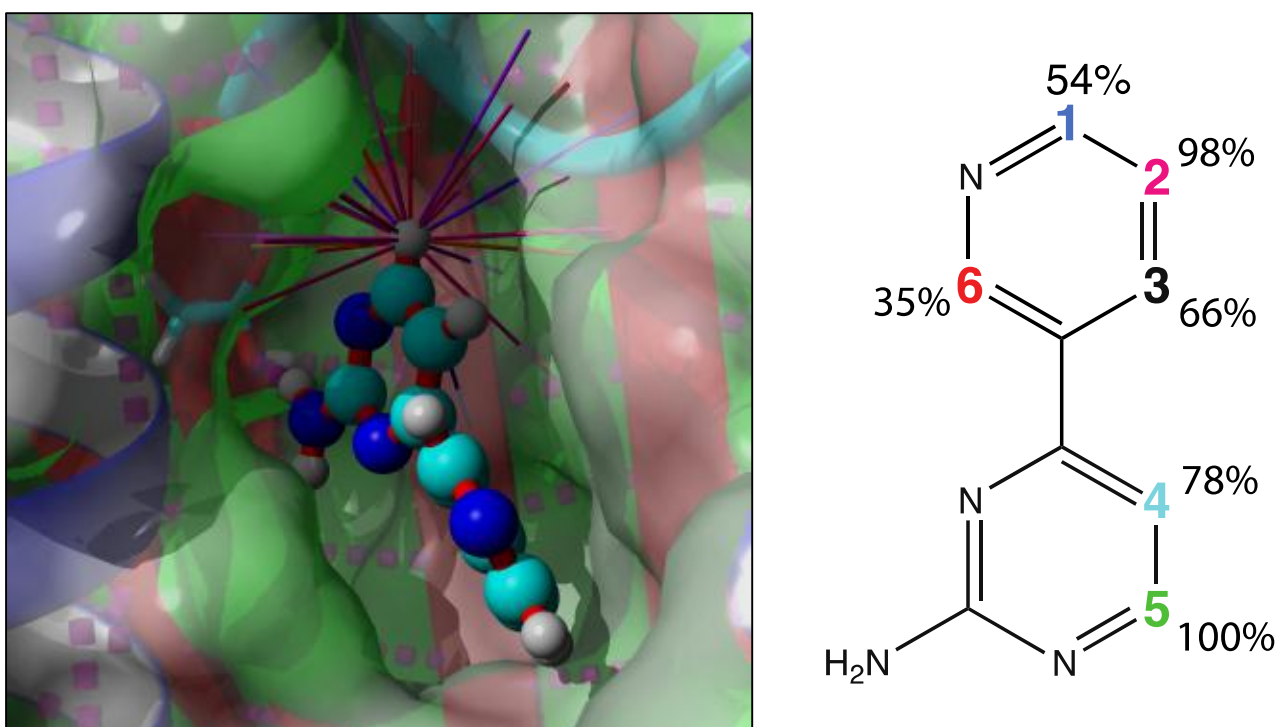
Figure 3.33: Fragment A bound in the Hsp90 crystal structure, with the relative degrees of saturation of individual protons on the right. Lines emanating from proton 5 represent inter-proton distances between it and atoms of the protein within 6 A.

For fragments, the Hsp90 binding site is particularly large (15Å deep(Prodromou et al., 1997)), and so it is not possible to simply say something such as "one half of the ligand protrudes whilst the other is buried". As shown in fig. 3.33, protons 2 and 5 receive the largest saturation transfer, yet exist at opposing ends of the binding site;

orientation would not be possible to deduce on this basis. Therefore, the experimental

STD data is not capable of inferring ligand orientation on its own.

 It's a similar story with the pyrazoles (fragments C, E and F) that were analysed.

Overlays of the ligands of the crystal structures are shown below. The protons within

the red circles are more "STD dominant" in terms of the saturation transfer they

receive, as derived from the experimental STD data.

Again, looking at the surface image (fig 3.33) it may seem counter-intuitive that two

protons from opposite ends of the ligand can be "STD dominant". Closer analysis of

the amino acid side chains involved in these saturation transfer pathways makes it

clearer.
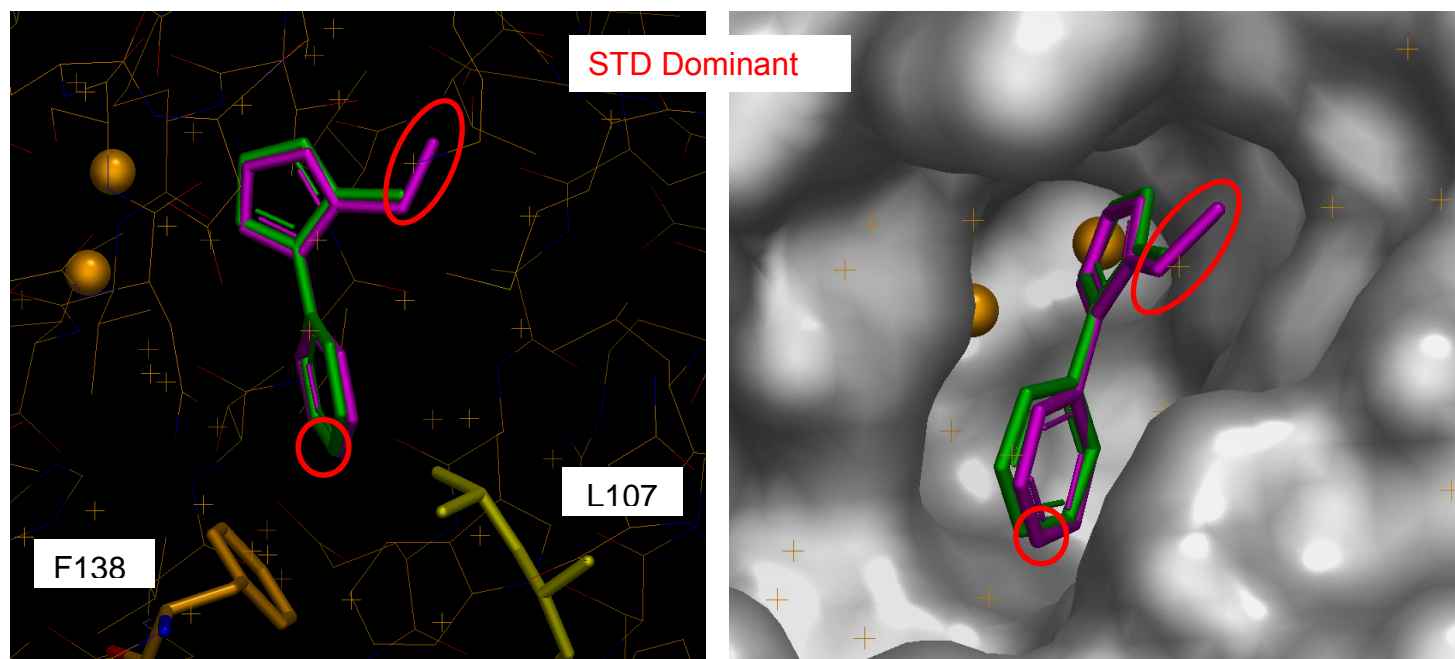
Figure 3.34: Overlays of crystal structures of bound Fragments D and F to Hsp90. (A) with side chains F138 and L107 as highlighted sticks, and (B) showing a 'surface' image of the structure

In the case of the proton at the tip of the phenyl ring (at the bottom in fig. 3.34A and

3.34B), these have the shortest intermolecular pathways to L107 and F138 for

saturation transfer (highlighted in fig. 3.34A and 3.34B). Methionine 98 (not shown) provides the main STD pathway for the circled protons at the top of the molecule (methyl group).

However, an observation of fragments C, E and F overlaid as in fig. 3.35 did open the possibility that if these two fragments bind in an identical mode; we could confirm this through similar STD build up patterns. This would effectively achieve a "binding mode clustering", approach from qSTD experiments?

3.4.4 Binding mode clustering

Fragments C, E and F are all of the same chemotype; pyrazoles.
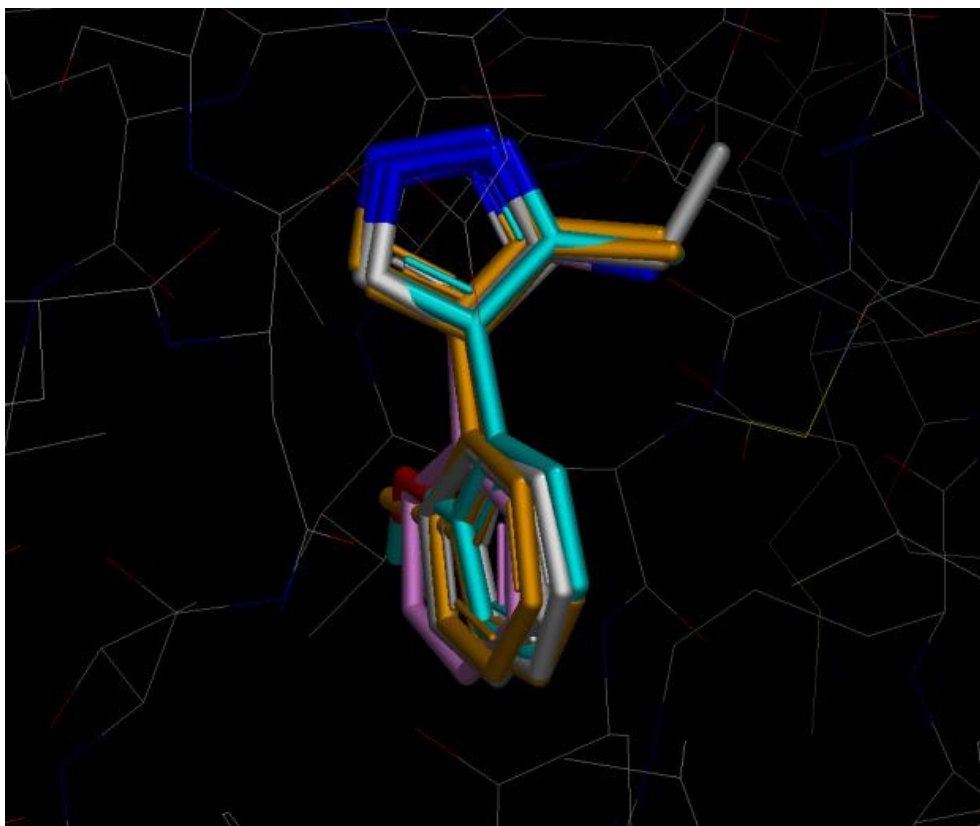
Figure 3.35: Overlay of the crystal structures of bound pyrazole fragment ligands C, E and F to Hsp90

When fragments of a particular chemotype from a screening library are known to bind to a protein, there is a very high probability that they bind in a similar mode. In the screening library from which these fragments were selected there were multiple chemotypes including phenols (such as fragment B) and aminopyrimidines (such as fragment A). The pyrazoles were interesting to analyse simply because there were so many of them that bound with a reasonable K_D, and with good solubilities.

As fig. 3.35 shows, all pyrazoles in this analysis bind with the same mode. Assuming the STD analysis thus far is correct, one would expect to see equivalent protons within the pyrazole chemotype "light up", or receive comparable saturation transfer. This is indeed the case with these fragments.

This is a useful approach, particularly if specific screening hits cannot be validated by crystallography.

With a set of initial rates from buildups, or T_1-adjuted STD values, I am suggesting that you can say - with confidence - whether or not the binding mode of a particular fragment falls into line with binding mode of the others within the chemotype.

Conversely, this also means that any 'rogue' binding mode should be easy to identify from its own STD pattern. A case in point is the additional fragment G (yellow in fig. 3.36) that binds in the same mode with respect to the pyrazole group, but the phenyl ring is clearly displaced relative to the other fragments. This should manifest itself as either a reduction or an increase in the STD to the tip of the ring, relative to the other fragments. This gives a powerful insight into binding mode from relatively primitive

data. In practice this particular fragment could not be tested due to not being soluble in aqueous buffer.
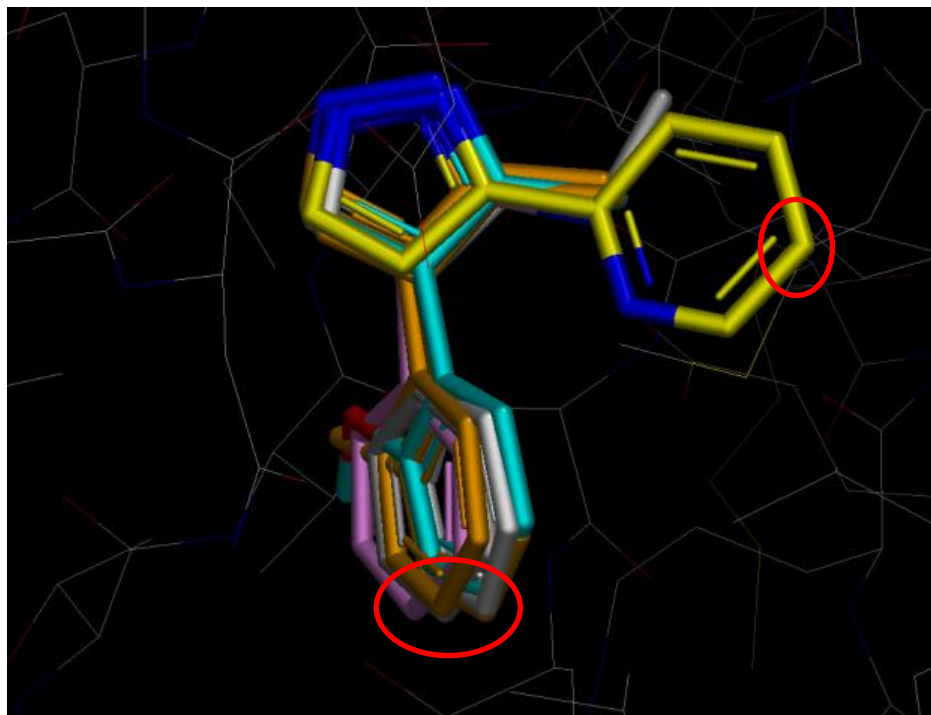
Figure 3.36: Additional fragment G overlaid with the other pyrazoles. 'Equivalent' protons at the tip of the phenyl ring (circled red) should have different STD properties

3.4.5 Caveats and situations in which the method may not be applicable

3.4.5.1 Dealing with experimental data of methyl, methylene or symmetrical protons

In assessing the reliability and validity of these results (particularly with respect to fragments B, D, E and F) it is of course prudent to ask questions about the treatment of the experimental data - whether that be initial rates or T_1-adjusted STD values - for the protons of the methyl & methylene groups, as well as the protons that are symmetrical or equivalent in the spectrum.

It is clear that the most reliable data shown thus far relate to Fragments A and D. This is simply because these data represent a straightforward case of one proton versus one distance measurement. The results of fragments A and D require no alternative treatment whereas fragment B, C, E and F do. Fragments B and F possess methyl groups wherein the 'information' for three protons is driven through one chemical shift. As explained earlier, for these we take a 'sum averaging' approach and divide data to take into account multiple proton contributions. Fragments C, E and F possess symmetrical protons where the information for two protons is encoded in one chemical shift, and a similar division takes place. This must be done for the sake of a reasonable correlation.

Even if you wish to exclude 're-constructed' points (that is to say, initial rate or T_1-adjusted STD data points in a correlation that have been created by division of an experimental value, as with methyl or symmetrical protons), the points made about binding mode clustering still hold.

Finally, it is also worth mentioning that there is considerable doubt surrounding the validity of simply taking proton-proton measurements from a crystal structure. The crystal structures in question are all solved to a resolution of 2 Å or better. However this relates to the position of all non-hydrogen atoms fit to the electron density. The position of protons – added internally by Astex – is unlikely to be perfect despite the virtues of stereochemistry. This, allied with the knowledge that a crystal structure is a merely snapshot in time of a protein-ligand complex (and not to mention, represents the complex at an extremely cold temperature, hence no dynamics), suggests that all results should be treated with caution.

However, it cannot be ignored that the power of these findings is that they are repeatable across a range of fragments, and indeed across multiple proteins, as we will see later on.

3.4.6 INPHARMA

The INPHARMA method is another ligand-observed NMR tool considered to be useful and informative regarding protein-ligand binding modes(Dias and Ciulli). INPHARMA can help determine the relative binding orientation of two ligands that compete to bind to the same binding pocket on a particular protein(Orts et al., 2009, Sanchez-Pedregal et al., 2005). If the orientation of one ligand is known, this infers upon the binding mode of the other competitive ligand by intermolecular NOE transfer to the other, mediated by the protein. Inter-ligand NOEs by INPHARMA depend upon running a NOESY experiment with a long mixing time.
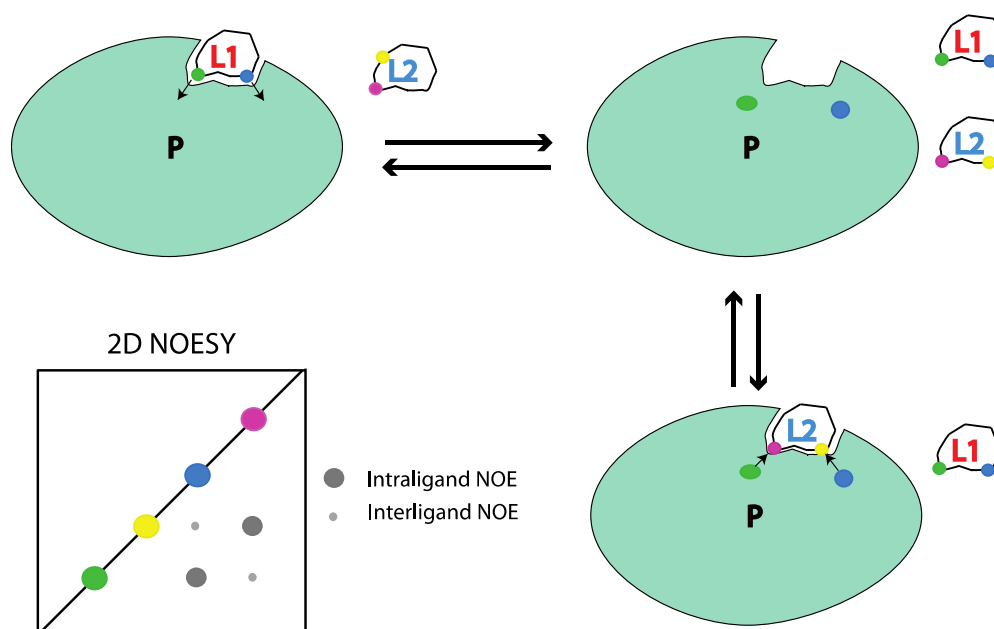
Figure 3.37: NOESY experiments are run with pairs of competitively binding ligands. INPHARMA inter-ligand NOEs are observed as small NOEs between competing ligands. This occurs between regions of ligands that bind in the same part of a protein pocket

The experimental rationale is illustrated in figure 3.37. We decided to test out the INPHARMA principle using two fragment ligands used to investigate binding to Hsp90, fragments A and B, and use it as a method against which we could directly compare STD NMR.

After trialing a series of conditions only two sets of experimental conditions yielded a single INPHARMA NOE, and in both cases the same NOE. The samples were prepared as typical STD experiments (see earlier in this chapter) and NOESY experiments acquired with 16 scans (5 hours) and 2048 x 256 data points at 275K. In one case the sample was prepared in 90% H_2O and 10% D_2O, and the other prepared in 100% D_2O. In both instances the NOESY experiment was run with a 1 second mixing time.

A suspected INPHARMA NOE between fragments A and B is shown below in figure 3.38.
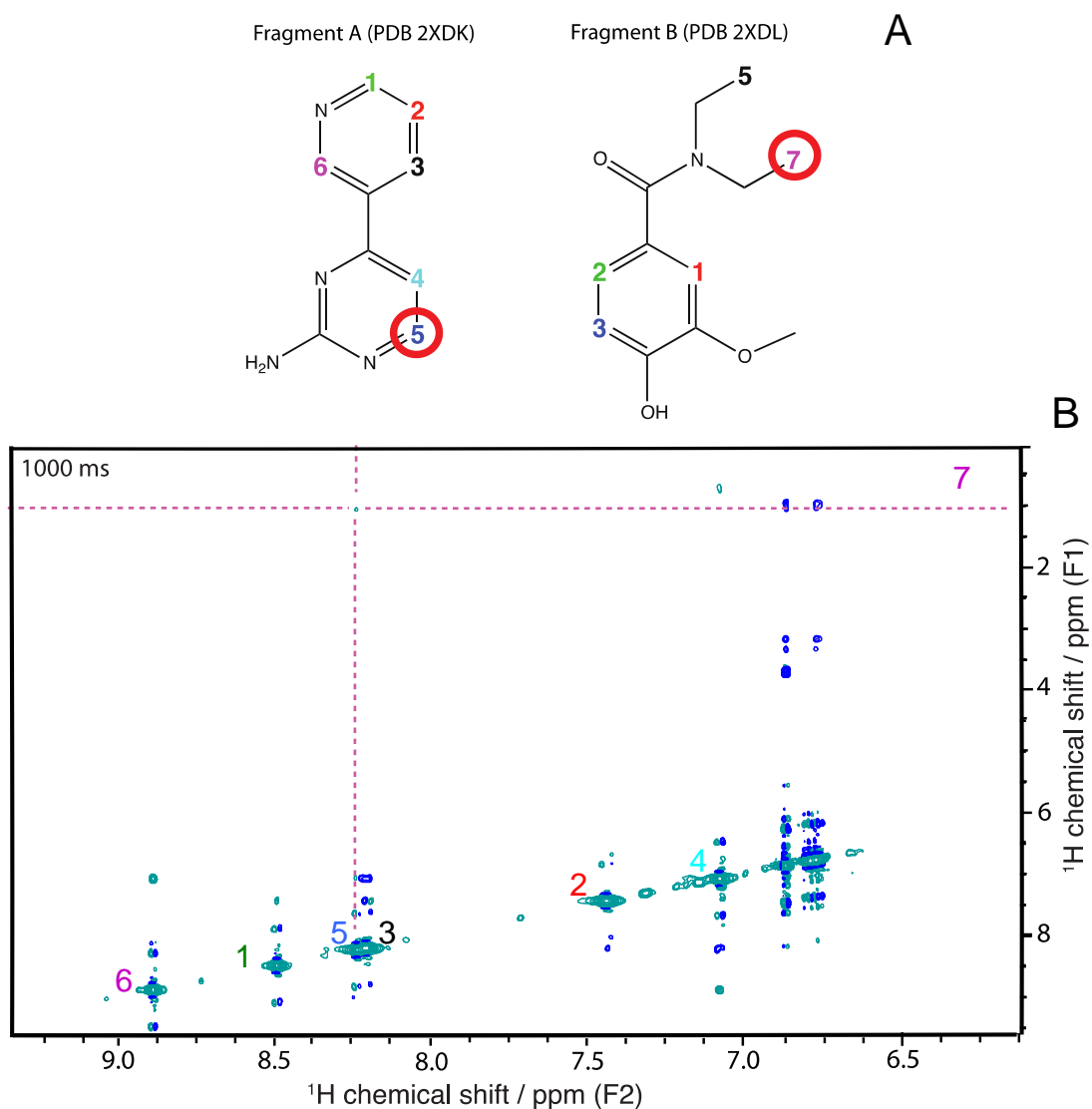
Figure 3.38: NOESY experiment for Hsp90 in the presence of two competitive binding fragment ligands. Fragment ligands are shown (A) and INPHARMA NOE shown in (B) between circled protons as highlighted

The majority of NOEs are clearly intra-molecular, but at ~(8.25, 1) ppm a small cross peak is observed. This is observed to be between protons 5 and 7, of fragments A and B respectively. No other intermolecular NOEs could be seen under any conditions.

The plausibility of this INPHARMA NOE was assessed by overlay of the bound ligands to examine relative binding modes, as seen in figure 3.39.
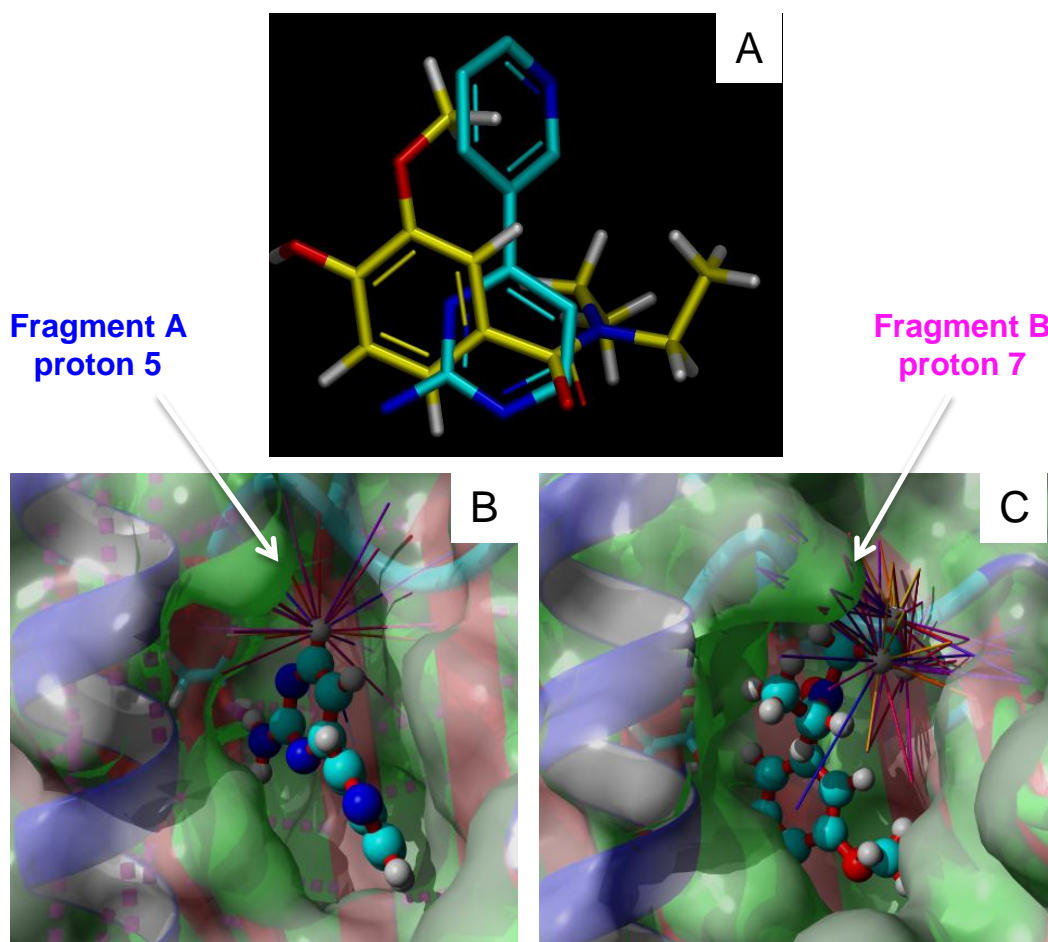
Figure 3.39: (A) fragments A (cyan) and B (yellow) overlaid according to the bound crystal structures with Hsp90. Fragments A (B) and B (C) bound to Hsp90 with intermolecular contacts with the protein shown

The closest protein side chain to both of these protons is Methionine 98, so an INPHARMA NOE between these two protons is certainly plausible, as agreed by the overlays in fig. 3.39A. However, the relative binding modes would expect to produce many more intermolecular NOEs than just the one.

After correspondence with members of the structural and computational group at EMBL (Heidelberg) they too suggest that more INPHARMA NOEs should be observable. However they state that their attempts with ligand binding to Hsp90 also proved fruitless, and attributed this to the fact that although their ligands bound with micromolar dissociation constants, the k_{off} was too low in their case.

I would suggest that this is a severe limitation of the method, and along with the knowledge that single NOESY INPHARMA experiments are routinely known to take 24 hours, this surely reduces the efficiency of the method and reduces the extent to which one may apply the method to other protein-ligand problems. On this basis, quantitative STD appears in a relatively favourable light, in terms of how much information may be weaned from experiment and how efficient the methods are.

Alternative methods exist to try and maximize the INPHARMA NOE signals. Recently hyperpolarization techniques have been developed to overcome the inherently low sensitivity of a two-step NOE transfer(Lee et al., 2012). The "hyperpolarized binding pocket NOE" technique involves hyperpolarizing one ligand, dissolving it in heated D_2O and then immediately injecting it into a pre-prepared sample of protein and partner ligand. This could well be one option to attempt, but it

seems a rather large amount of effort to go to, especially in light of how easy it is to

acquire seemingly superior information from simple quantitative STD experiments.

Chapter 4

Quantifying data from Water-Ligand Observed via Gradient SpectroscopY (WaterLOGSY)

4.1 Introduction

This chapter investigates the **W**ater-**L**igand **O**bserved via **G**radient **S**pectroscop**Y** (WaterLOGSY) experiment and attempts to quantify LOGSY data using a similar process as was done for the quantitative STD experiments, based on initial rates of LOGSY signal build up. LOGSY is predominantly used as a screening tool in FBDD, but this chapter illustrates attempts to obtain more useful information from the experiment, and interpret any subsequent findings.

4.1.1 WaterLOGSY

As described in the main introduction, WaterLOGSY(Dalvit et al., 2000) is another ligand-observed NMR screening technique. In this experiment selective saturation is targeted at bulk water, and the water magnetisation is transferred to the ligand via the protein.

In this chapter we deal with ligands that are all validated hits for Hsp90 and are certain that all bind to the target protein. As a result, we are less preoccupied with the binary question of whether or not something binds, but are more interested in other properties of these binding events, that will become evident.

4.1.2 Current uses for the WaterLOGSY experiment

LOGSY was used as the primary screening tool in the development of the Hsp90 inhibitor AT13387(Murray et al., 2010). Here, 1600 compounds from a fragment library were screened in cocktails of four. Compounds were defined as having a 'medium' or 'strong'

LOGSY signal if the largest aromatic signal in a particular LOGSY difference spectrum (generated as explained below) was greater than > 10% (medium) or > 20% (strong) of the same signal in a 1D spectrum. Compounds passing either of these barriers then underwent LOGSY in competition mode wherein they were individually screened in the presence of ADP – known to bind weakly to the ATP-ase domain of Hsp90 – and displacement of the ADP LOGSY signal was monitored. Ultimately 1600 compounds were reduced to only 125, simply on the basis of the WaterLOGSY experiment.

Another example of LOGSY as a screening tool is a study that took a library of 2000 compounds to screen against the key Alzheimer's disease target β-secretase (BACE-1)(Geschwindner et al., 2007). Again LOGSY was used as the initial step to narrow the field down before compounds were characterised by BIAcore (SPR). A relatively low overall hit rate of 0.5% was reported for compounds that bound with modest affinities in the low millimolar range.

There are several examples involving LOGSY in the scientific literature, but as yet the experiment has not been considered in any real quantitative terms. Armed with the Hsp90 protein and a series of fragment ligands, we are in a position to speculatively explore the possibilities of quantifying data from LOGSY experiments, using the same exact samples that we scrutinized by STD NMR.

4.1.3 Effect of ligand ratio and how to generate "difference' spectra

At high concentrations of ligand the free ligand becomes dominant. This needs to be corrected by running an identical parallel experiment in the absence of protein. The maximum differences in signal are attained with high concentrations of ligand, but without the control sample this would not be obvious (see fig. 4.1). This forms the basis of all experiments in this chapter.
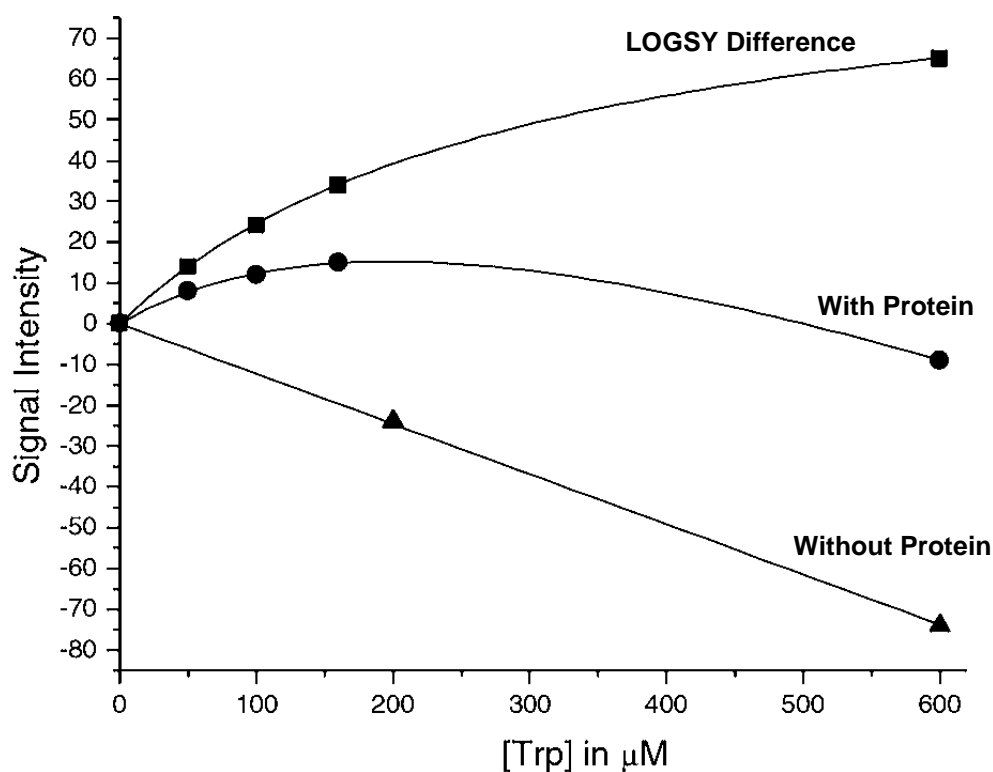
Figure 4.1: LOGSY signal intensity for one proton - for a fixed protein concentration (10 μM) - as a function of ligand concentration. Figure adapted from(Dalvit et al., 2001)

Fig. 4.1 illustrates that differences in signal intensity between samples with and without protein provide the biggest and most equitable signal. If examined in isolation without considering any control spectrum, any single signal in a LOGSY spectrum could appear vanishingly small or even negative. This is why it is essential to run a ligand-only control in parallel and analyse the difference between this and the 'with protein' sample.

4.1.4 Quantification of LOGSY NMR signal magnitude –

4.1.4.1.SALMON – **S**olvent **A**ccessibility, **L**igand binding, and **M**apping of ligand

Orientation by **N**MR spectroscopy(Ludwig et al., 2008)

Before our analysis that forms the basis of this chapter, researchers had previously set up an

interesting LOGSY experiment between a ligand (1 mM CB1954) and a protein (NQO2).
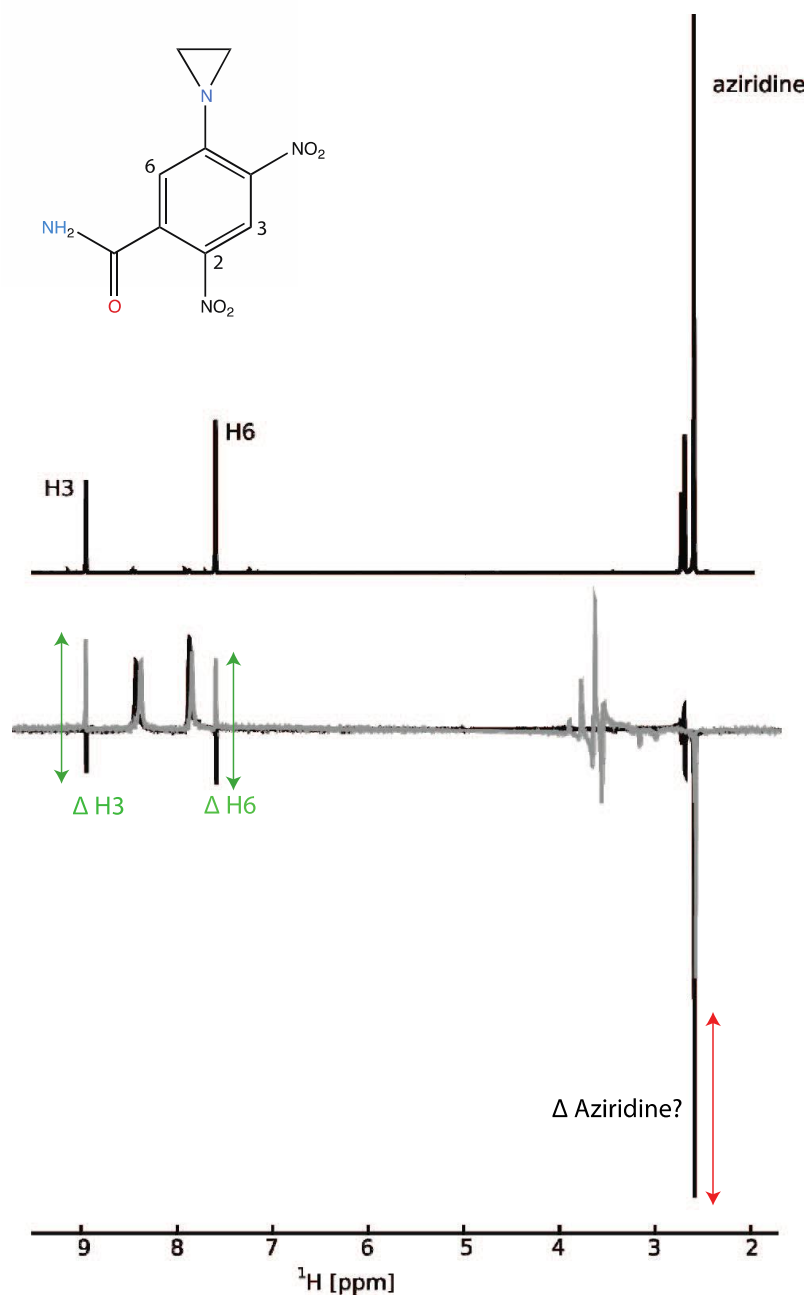
Figure 4.2: 1D spectrum (top) of ligand CB1954 and LOGSY spectra (bottom) of both free ligand (black) and bound ligand (grey). Arrows illustrate differences in signal intensity caused by the presence of the protein. Figure adapted from Ludwig et al(Ludwig et al., 2008)

Two spectra were acquired – on both LOGSY sample and ligand-only reference sample – at 800 MHz with a NOESY mixing time of 1.2 s.

Their publication suggests that the change in sign of the H3 and H6 signals is typical of binding, and they are intrigued by the fact that the signal of the aziridine group protons does not change sign. They attribute this fact to the aziridine group protruding from the protein and being more accessible to bulk water. However, I believe they are missing a key aspect of this data; indicated by the red arrow in fig. 4.2: whilst the H3 and H6 protons appear to qualitatively change sign, there is a difference in their signals that can actually be measured and fully quantified. On this basis, the same treatment can be applied to the aziridine signal, despite the fact that both signals are qualitatively negative. The aziridine signal does not change sign, but is clearly reduced, and this change can be measured. This one key difference between the approaches of the SALMON methodology and how we approach the matter; we aim to quantify signals absolutely and observe any possible trends.

It is also worth noting that the authors concluded by suggesting that simple interpretation of which signals change in sign is sufficient to determine binding epitopes for ligands with solvent-accessible protons: "With the help of a protein structure, the solvent accessibility can be translated into orientation of the ligand". We aim to test the validity of this statement in this chapter.

Furthermore the analysis does not provide an explanation of how to deal with proton groups. For the purposes of the ligand CB1954, this does not matter – since only the aziridine group possesses more than one proton – but as in the quantitative STD chapter it's a probable scenario and addressed in the methods.

4.1.4.2.Increasing the NOE mixing time of a LOGSY experiment

Increasing the NOE mixing period of a LOGSY experiment is known to cause increases in signal magnitude. This idea is illustrated in fig. 4.3 for three protons of a ligand binding to protein.
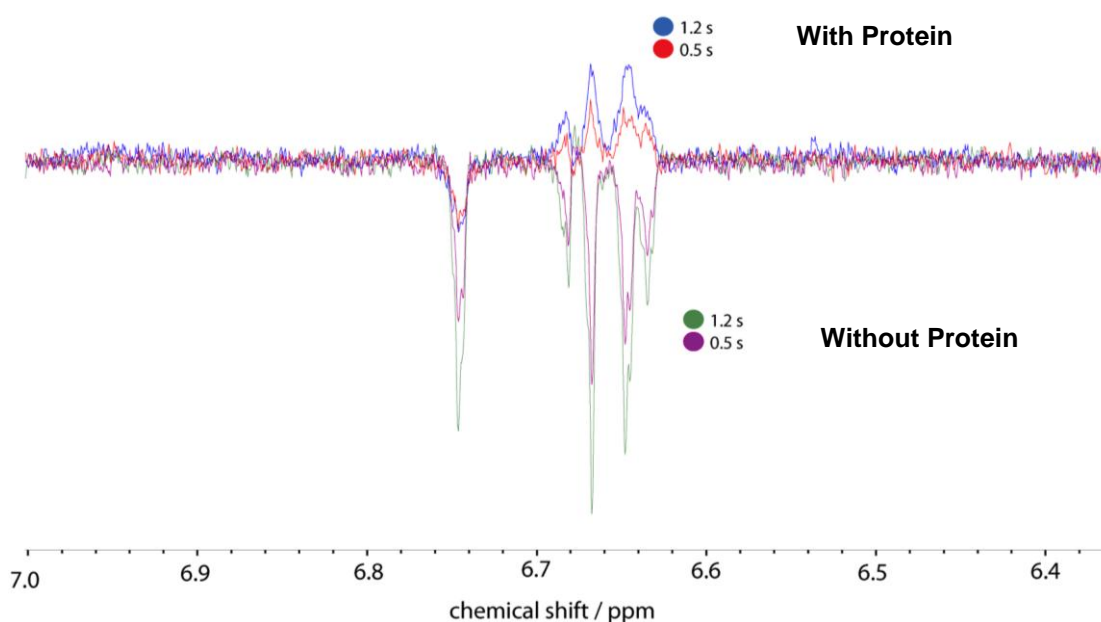
Figure 4.3: An example of both a LOGSY and a control spectrum for a fragment ligand bound to Hsp90. Three proton resonances are shown. The difference between experiments allow a subtraction which then gives a resultant difference spectrum

Immediately visible on the above example spectrum shows that two peaks in the 'with protein' LOGSY spectrum are positive whereas the remainder are negative. Of course, this doesn't matter once the reference spectrum is taken into account, but is an interesting observation nonetheless. The second point is how adjusting the NOE mixing time alters the size of the subsequent signal. All signals become either more positive or less negative as the mixing time is increased. This phenomenon is well documented from the original ePHOGSY experiment(Dalvit et al., 2001) and suggests that this is a variable that we can examine as part of our analysis.

4.2 Methods

4.2.1 Protein production and purification

Human Hsp90 protein was provided as explained in chapter 3 section 3.2.1.

4.2.2 Fragment ligands

The identity of the fragment ligands used in this chapter is the same as in chapter 3.
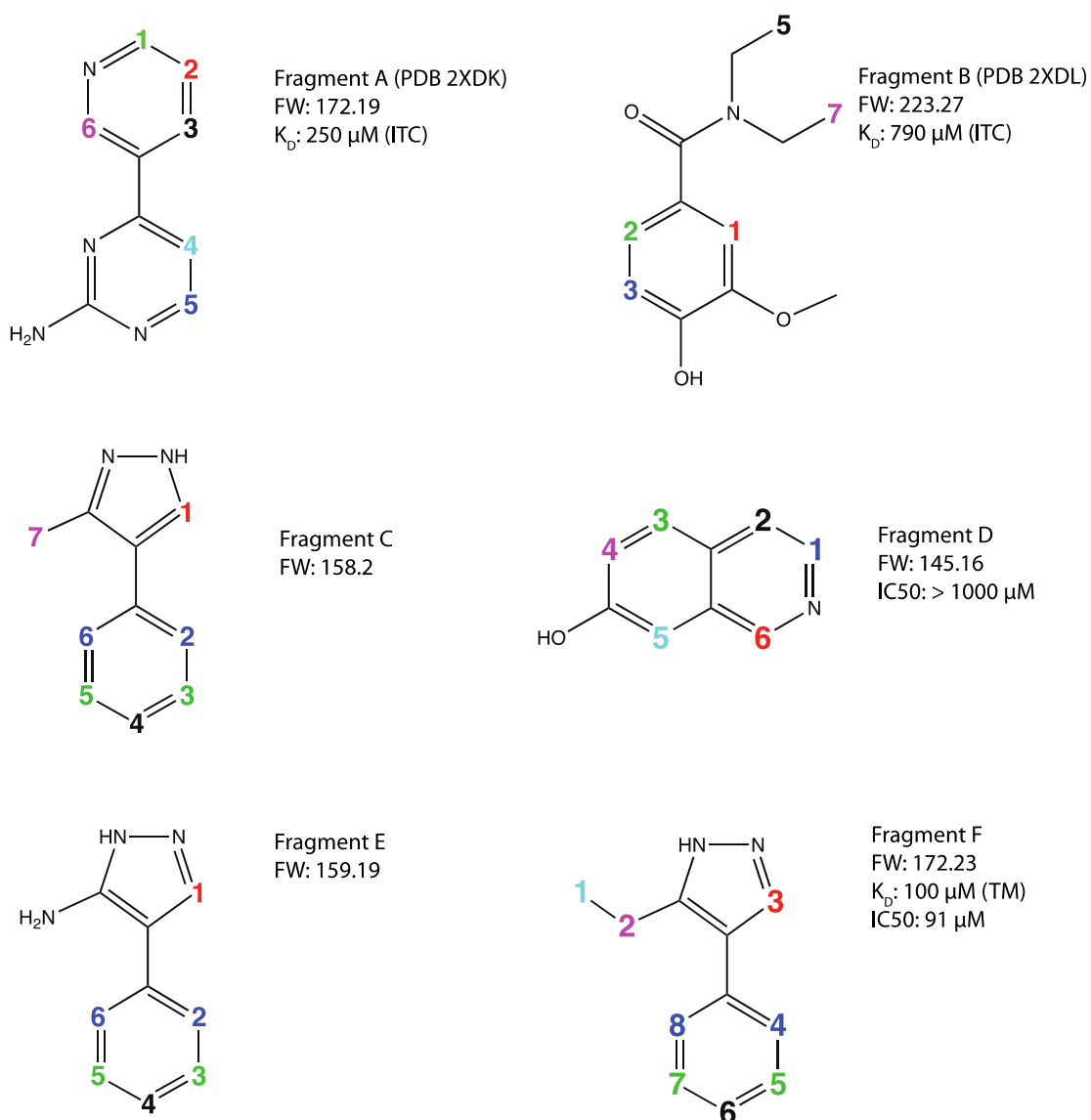
Figure 4.4: Fragment ligands were provided as freeze-dried compounds that were subsequently diluted into 100 mM DMSO stocks. Numbers denote protons or proton groups. Fragments A and B are available as PDB structures at rscb.org

4.2.3 NMR Experimental Setup

4.2.3.1 Sample Preparation

The samples examined by LOGSY NMR were the same as were used for quantitative STD analysis. These were prepared as 12 μM Hsp90 protein and 1.2 mM fragment ligand (DMSO final 2%) in 20 mM Tris, 100 mM NaCl, 1 mM DTT and 15% D_2O at pH 7.2. The ratio of ligand to protein for all NMR experiments was always 100:1, unless otherwise specified. All experiments were carried out at 5 °C in order to optimise the efficiency of binding and achieve improved signal-to-noise

4.2.3.2 LOGSY

LOGSY experiments were performed at 500 MHz using a Bruker DRX500 spectrometer equipped with a TXI cryoprobe. LOGSY experiments were carried out using the ePHOGSY sequence of Dalvit et al.(Dalvit et al., 2000) incorporating a CPMG period of 10 ms. Experiments were performed over 512 scans (plus 8 dummy scans) and spectra acquired with a TD of 16384 and a spectral width of 12 ppm.

[1]H spectra were referenced to 3-(Trimethylsilyl) propanoic acid (TSP). Data was processed and analysed using Bruker Topspin 3.2. LOGSY difference spectra were generated by subtraction of LOGSY spectra from companion reference spectra, and signals were quantified by integration of each resolvable peak where no overlaps were present.

4.2.4 Varying the NOE mixing period and calculation of initial rates

As explained previously, it has been observed that increasing signal is achieved by increasing the NOE mixing period, which can be attributed to the fact that WaterLOGSY experiments constructively use all magnetisation transfer processes to maximize magnetisation transfer to ligand. As a result it was decided to attempt to measure the integrals for all protons across a range of LOGSY experiments with increasing NOE mixing periods (0.3, 0.5, 0.8, 1.0 and 1.2 s).

From this we expected to observe LOGSY build up, therefore data was processed in a similar manner to STD data. LOGSY differences as absolute integrals (as opposed to an STD amplification factor) were plotted against the NOE mixing time (as opposed to saturation time), and curves fit to the same equations as previously used to calculate the initial rate of STD build up (see section 3.2.4.2):

$$LOGSY_{Diff} = LOGSY_{DiffMax}(1 - e^{-k_{LOGSY}t}) \qquad \text{(equation 10)}$$

Where 'LOGSY difference' signals were substituted in place of STD amplification factor and NOE mixing time substituted for saturation time.

It was decided to use integrals rather than intensity from peak height due to the line broadening that can be associated with a binding event, which would have led to inaccuracies in the subtraction event. With STD experiments peak heights are suitable to measure since it is the same physical sample that is used to generate both 'on' and 'off' resonance spectra.

4.2.5 Treatment of methyl, methylene and symmetrical protons of the ligand

As we must again deal with cases wherein individual chemical shifts encode the data of more than one proton, concessions need to be made in our treatment of the data. Whereas assessing quantitative STD data against actual structural restraints in the previous chapter enabled us to split processed rate values in proportion with distances derived from the structure, here we have no such information to guide our analysis.

As a result, here we have simply divided by the number of protons in the group. So a theoretical rate of "9" for a methyl group would be processed as a rate of "3" for each proton.

4.3 Results

4.3.1 Quantitative LOGSY for fragment A
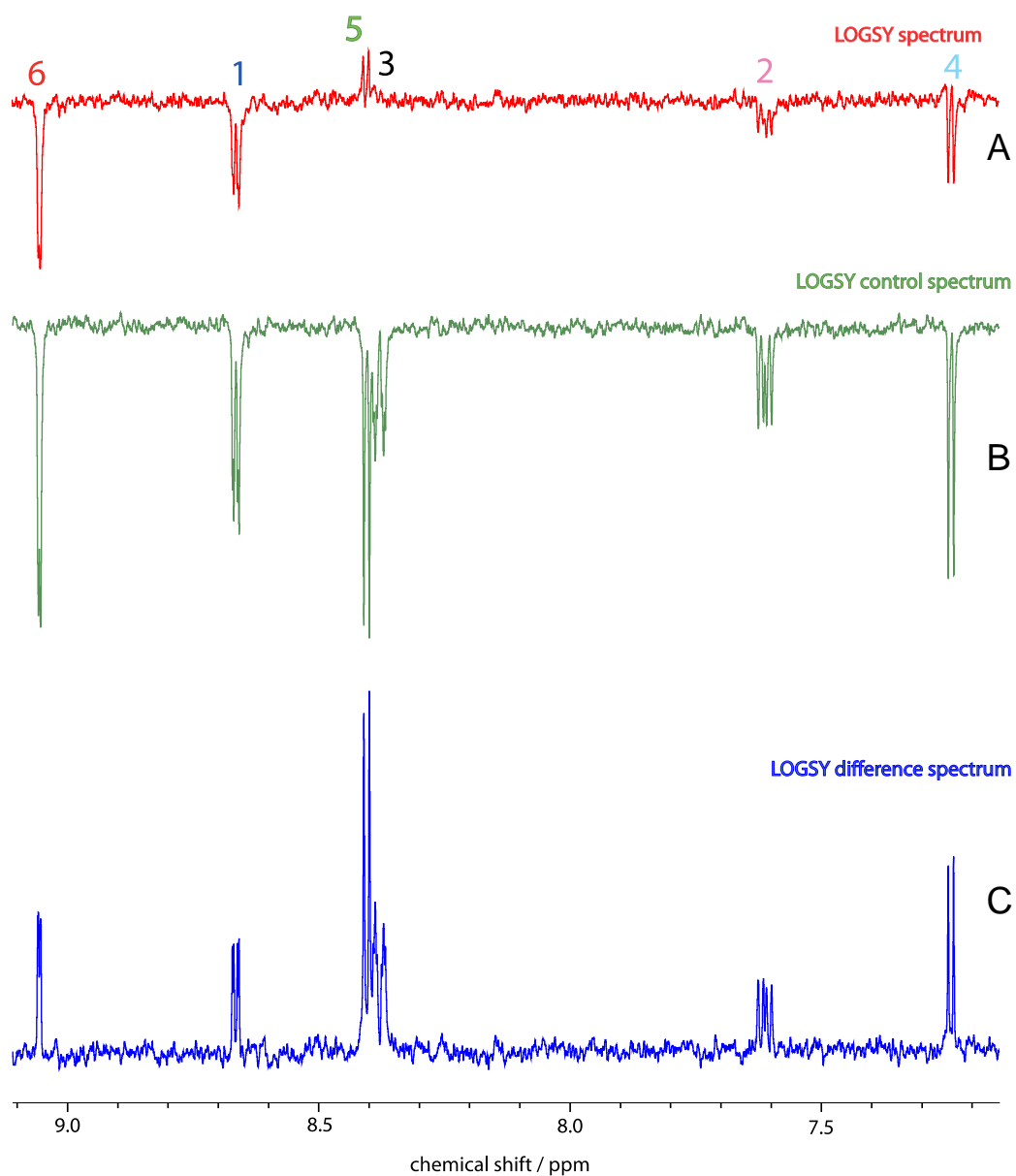
Figure 4.5: LOGSY (A), control (B) and LOGSY difference (C) spectra for Fragment A, acquired with an NOE mixing period of 1 second

Fragment A LOGSY spectra in fig. 4.5 shows positive LOGSY signals in the presence of Hsp90 (A) before subtraction for protons 5 and 3, but is negative for the remainder. The difference spectrum shows all protons positive with varying intensities. Acquisition of the above spectra at varying mixing times allows for production of buildup curves in fig. 4.6A.

Protons 5 and 3 can be clearly seen to have both the largest LOGSY signals in the difference spectrum as well as the steepest initial rates. This is different to the equivalent STD data.
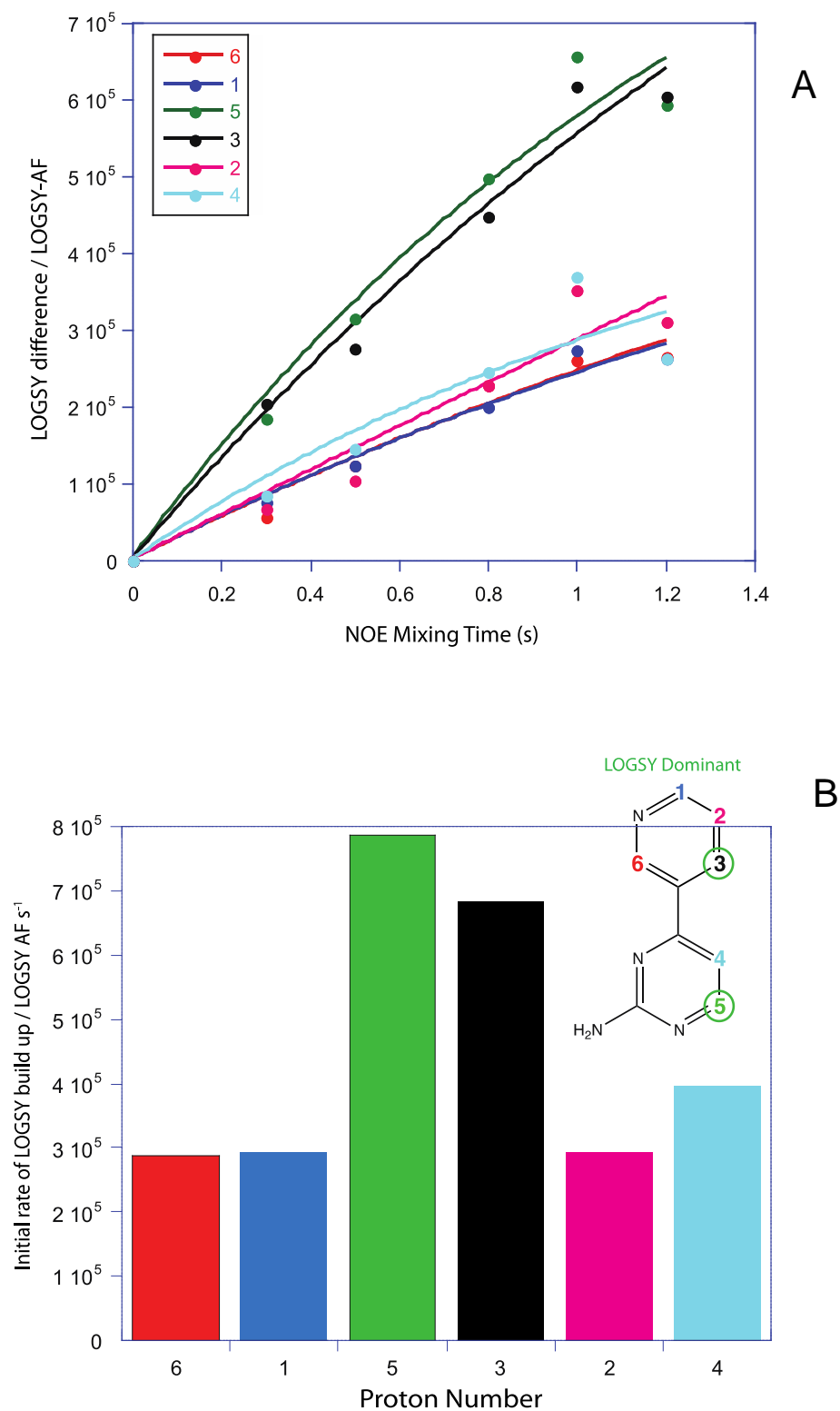
Figure 4.6: (A) LOGSY buildup curves for protons of fragment A, and (B) initial rate values of LOGSY buildup derived from (A)

4.3.2 Quantitative LOGSY for fragment B
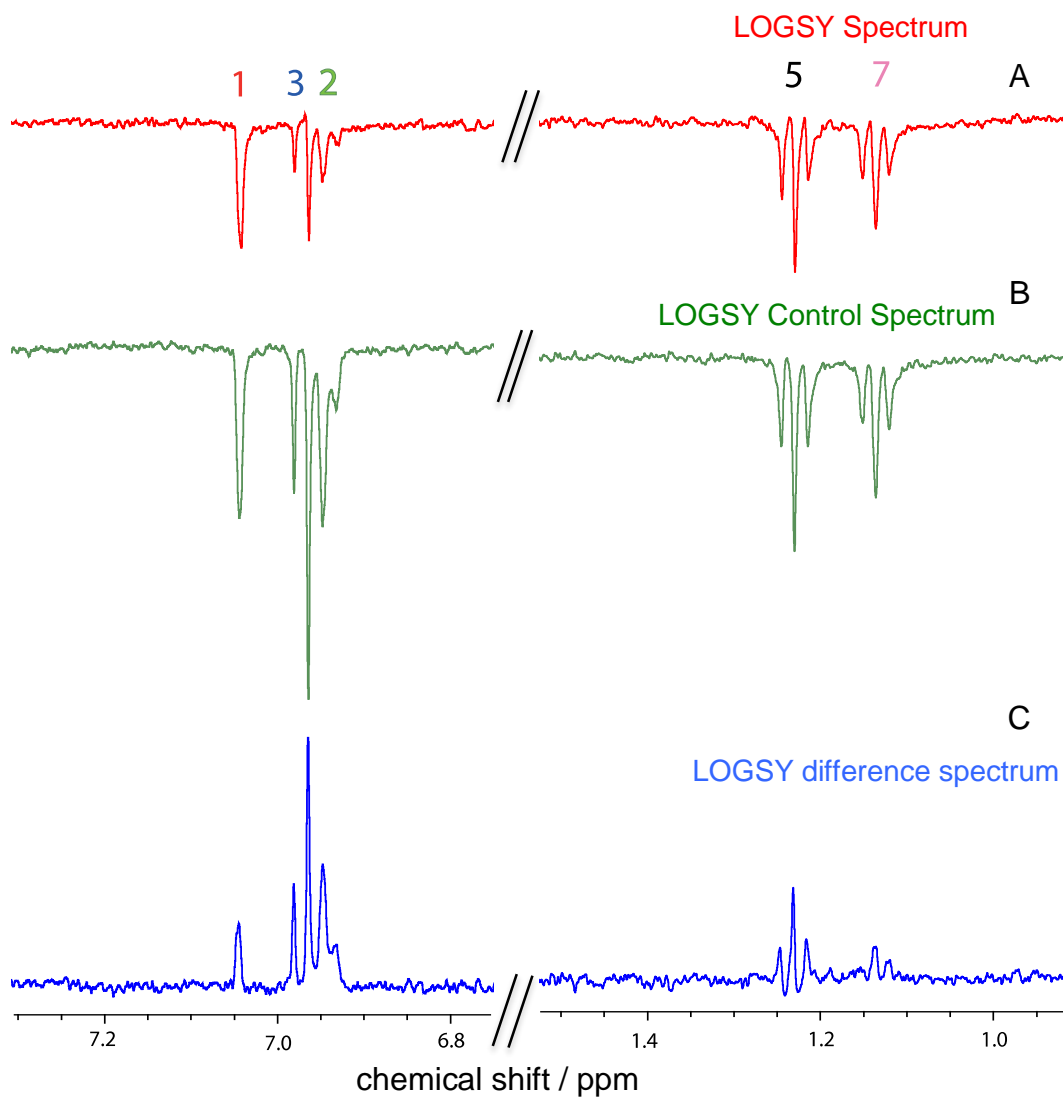
Figure 4.7: LOGSY (A), **control (B) and LOGSY difference (C) spectra for Fragment B acquired with an NOE mixing period of 1 second**

LOGSY spectra for fragment B in fig. 4.7 shows exclusively negative LOGSY signals in the presence of Hsp90 before subtraction. After subtraction of controls the difference spectrum shows all protons positive with varying intensities. Acquisition of the above spectra at varying mixing times allows for production of buildup curves in fig. 4.8

Proton 1 can be clearly seen to have the shallowest rate of LOGSY buildup in fig. 4.8. In contrast protons 3 and 2 possess steep initial rates of LOGSY buildup. Methyl protons 5 and 7 also possess steep initial rates of LOGSY buildup, but this takes into account multiple protons as well as a 'wobbly' build up curve. Again it is worth noting that the similarity in build up rate for these could be due to amide bond rotamer exchange.
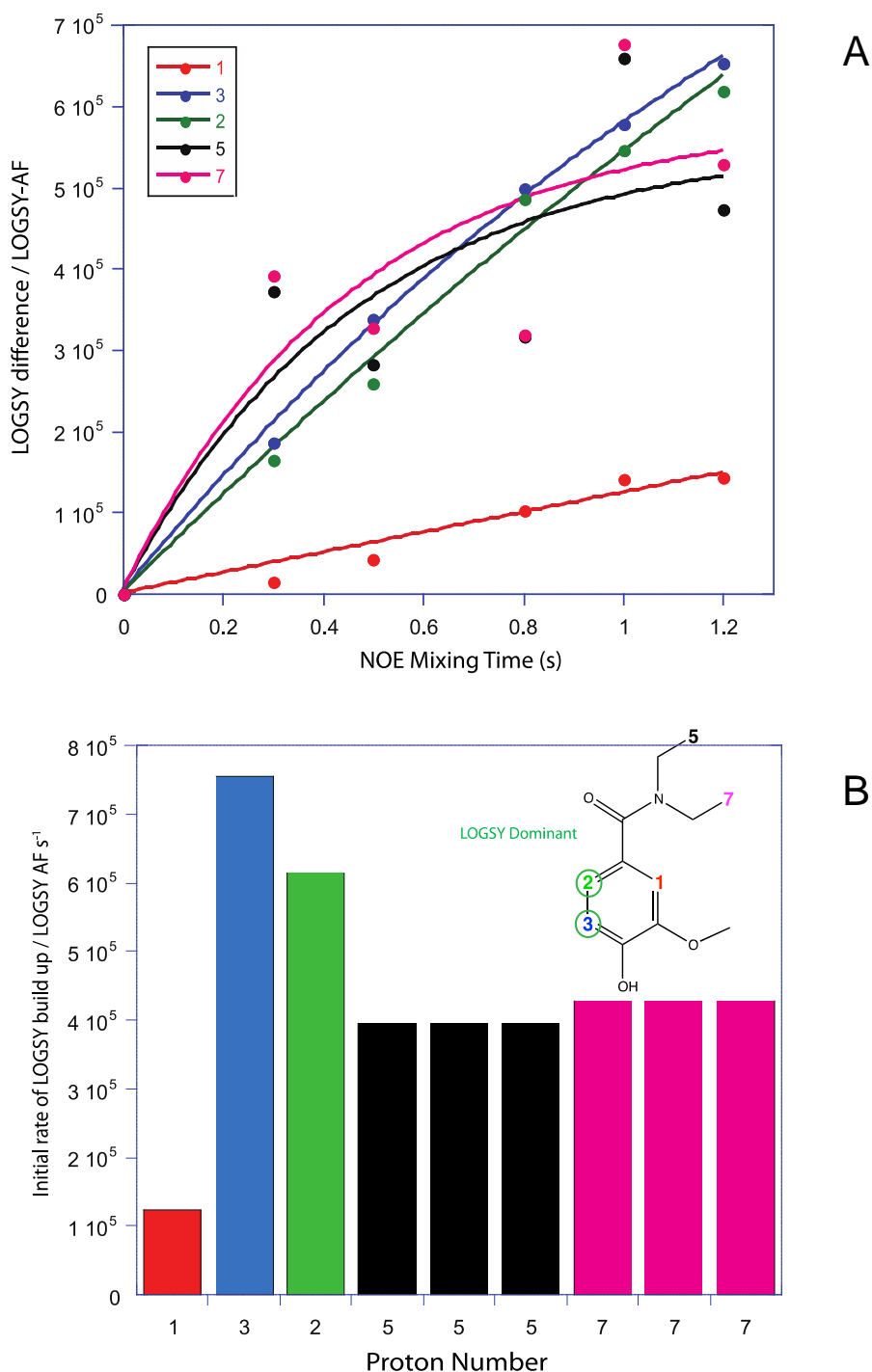
Figure 4.8: (A) LOGSY buildup curves for protons of fragment B, and (B) initial rate values of LOGSY buildup derived from (A)

4.3.3 Quantitative LOGSY for fragment C
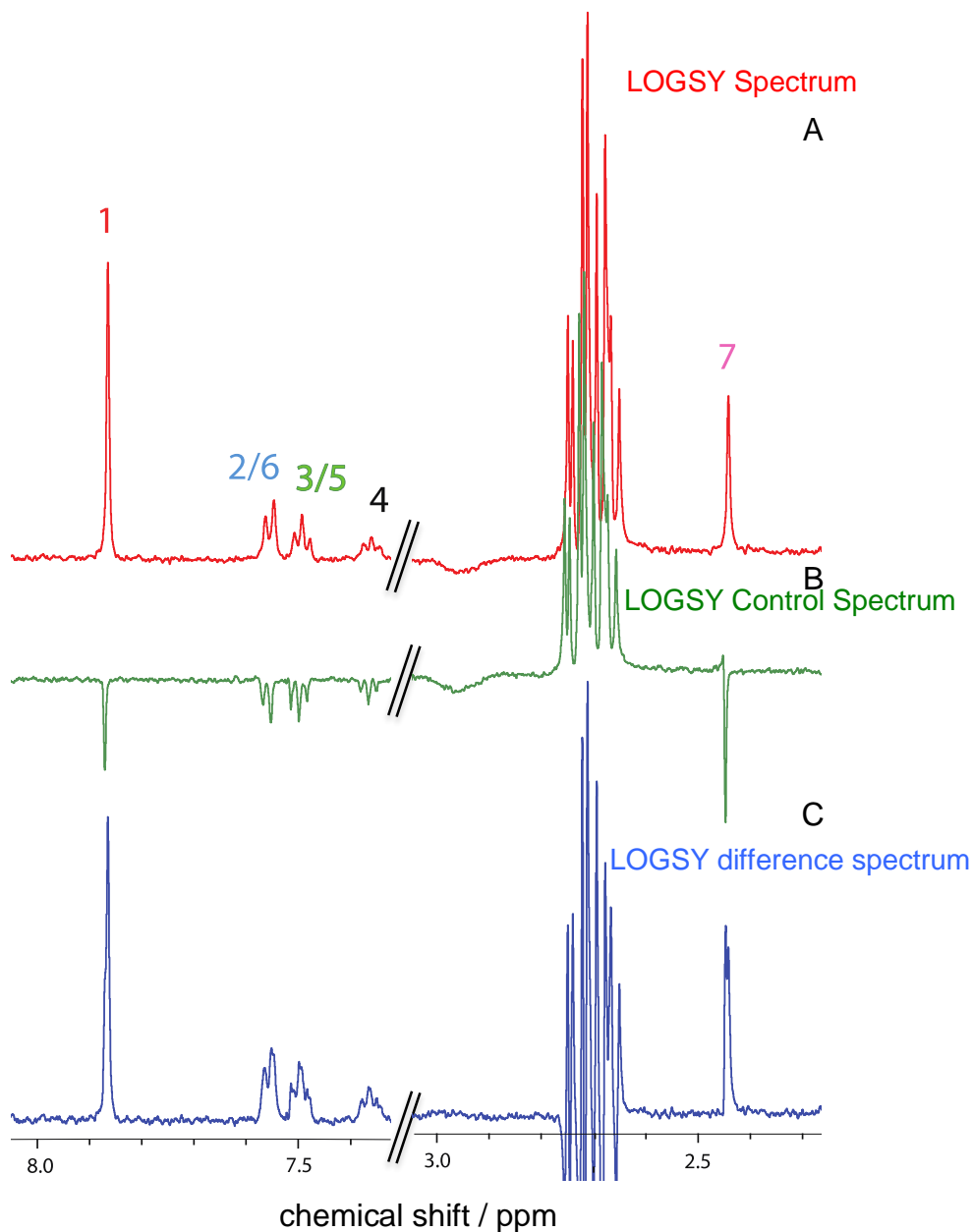
Figure 4.9: LOGSY, control and LOGSY difference spectra for Fragment C acquired with an NOE mixing period of 1 second

Fragment C exhibits different LOGSY spectra to that of fragment B, with all signals appearing positive in (A) before the controls are taken into account. These signals are accentuated once the signals from control spectra are taken subtracted, with proton 1 appearing noticeably stronger. LOGSY buildup curves are shown in fig. 4.10.

Initial rates derived from the LOGSY buildup curves in fig. 4.10A are illustrated in a bar chart in figure 4.10b. As expected proton 1 shows the steepest rate of LOGSY buildup.
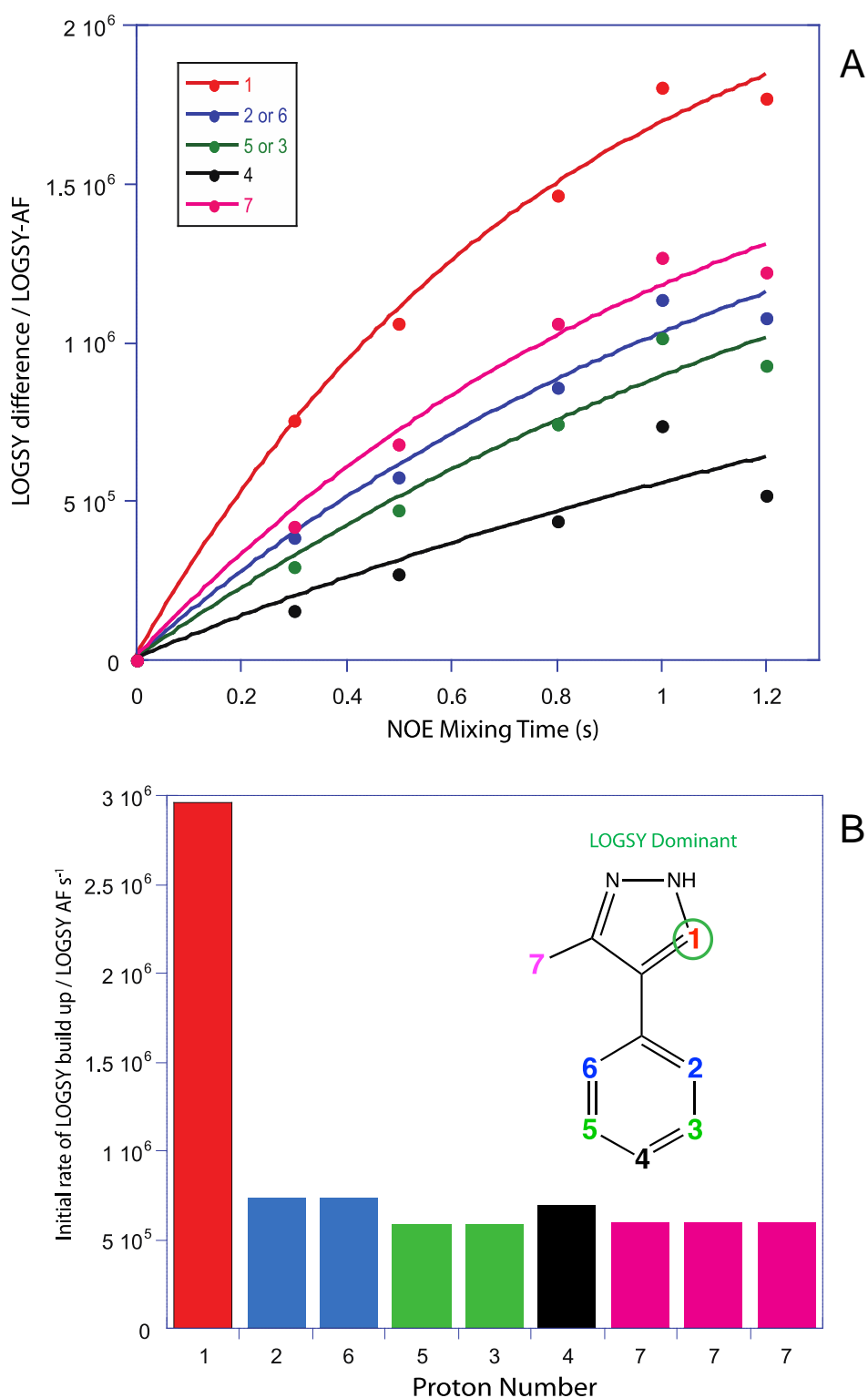
Figure 4.10: (A) LOGSY buildup curves for protons of fragment C, and (B) initial rate values of LOGSY buildup derived from (A)

4.3.4 Quantitative LOGSY for fragment D
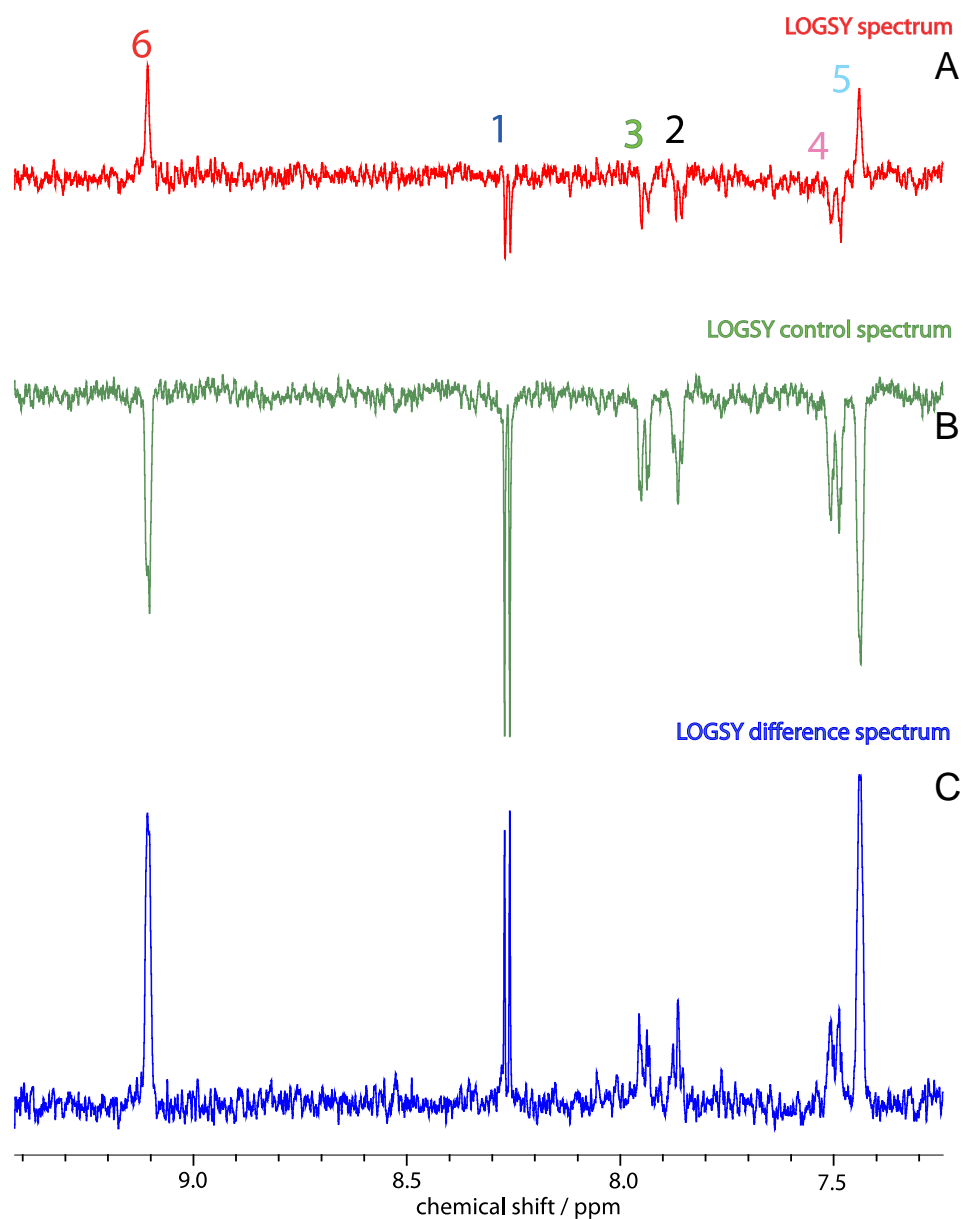
Figure 4.11: LOGSY (A), control (B) and LOGSY difference (C) spectra for Fragment D acquired with an NOE mixing period of 1 second

As with fragment A, fragment D exhibits a mixture of signals in fig. 4.11. Signals for protons 5 and 6 appear positive before subtraction of controls, whereas all appear positive after subtraction. Initial rates of LOGSY buildup for all protons of the fragment by acquisition of multiple spectra at differing mixing times is shown in fig. 4.12.

As expected, proton 5 and 6 shown much steeper initial rates of LOGSY buildup than protons 1-4, which all showed negative LOGSY signals before subtraction of controls.
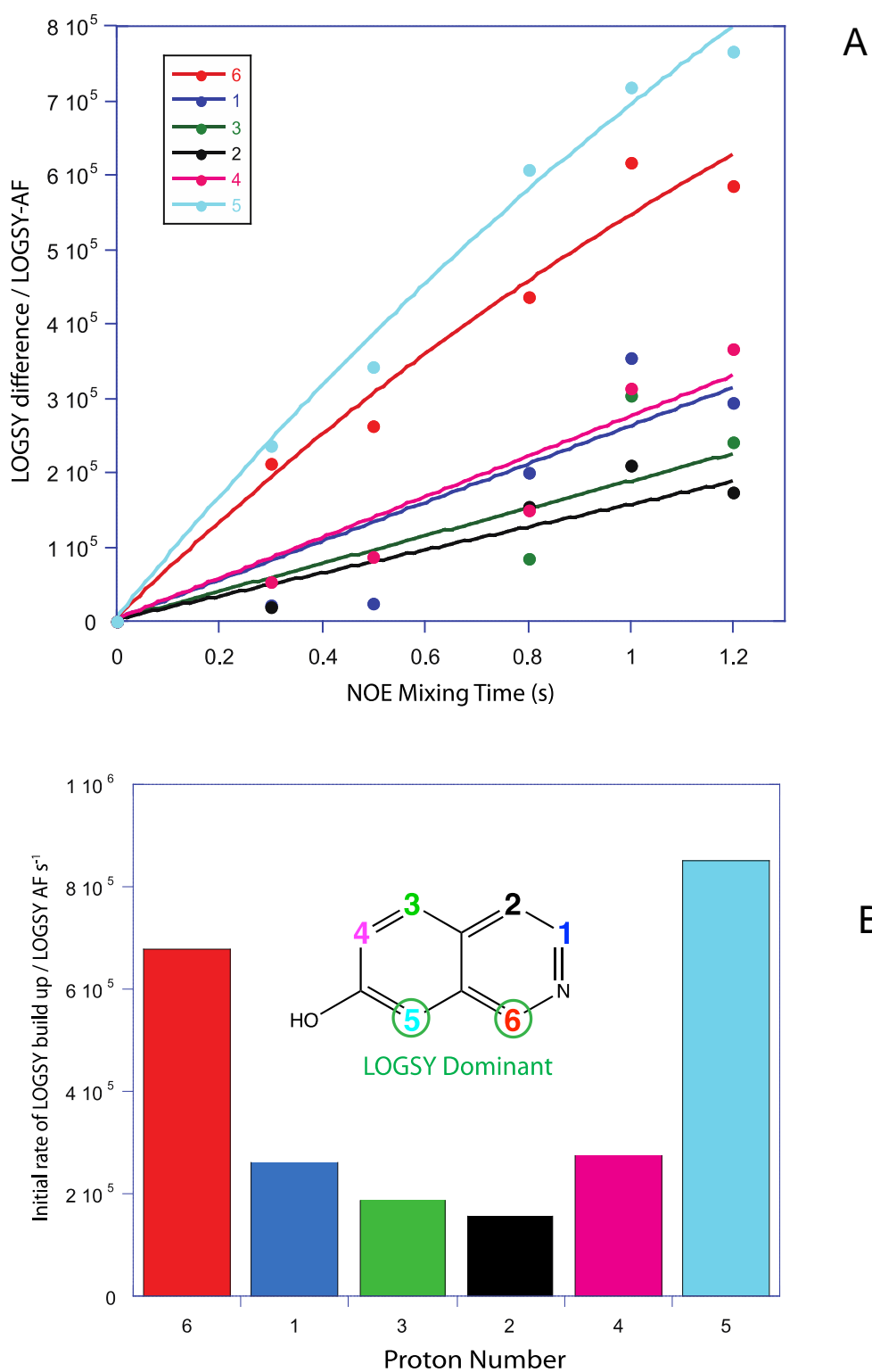
Figure 4.12: (A) LOGSY buildup curves for protons of fragment D, and (B) initial rate values of LOGSY buildup derived from (A)

4.3.5 Quantitative LOGSY for fragment E
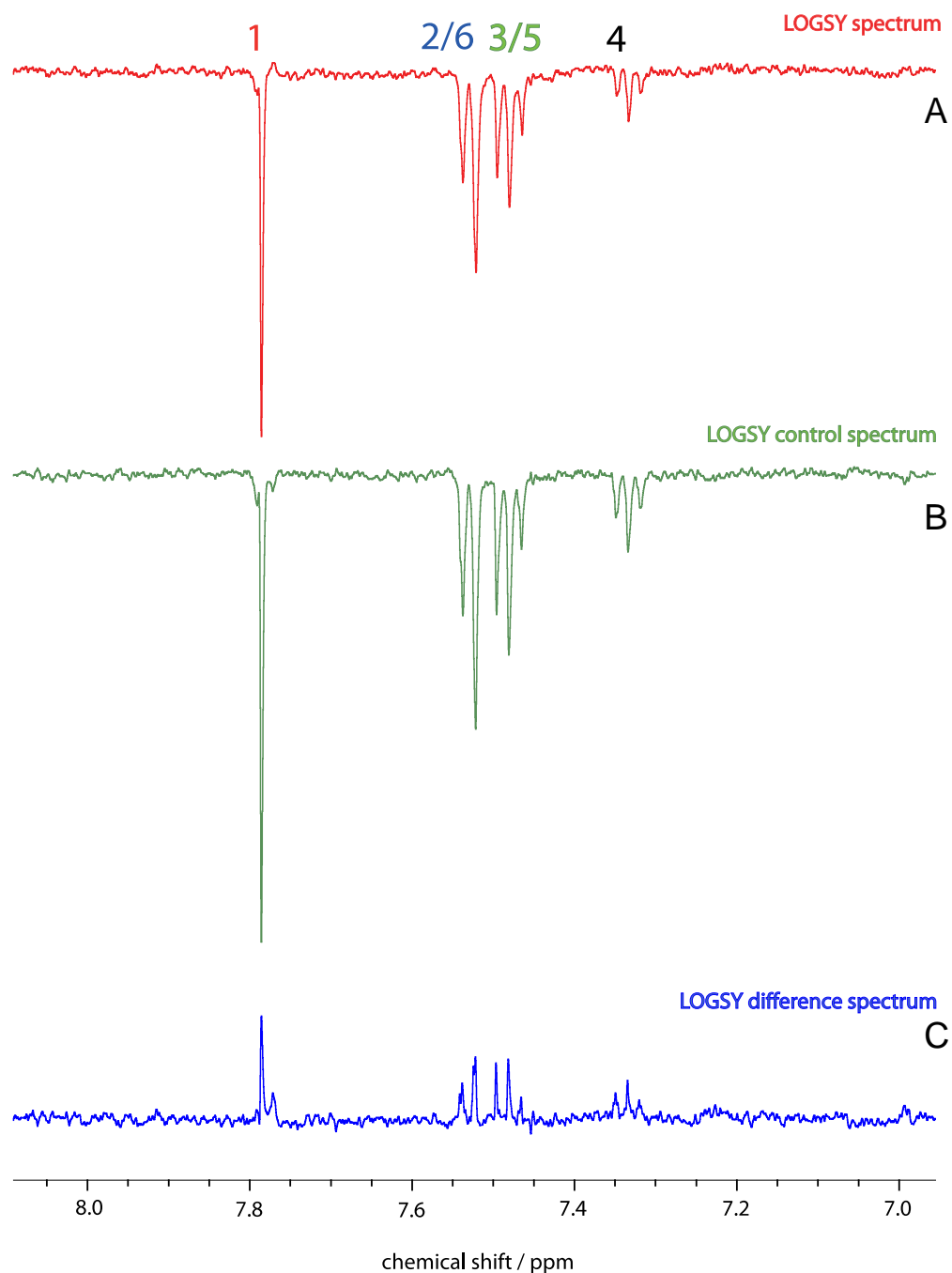
Figure 4.13: LOGSY (A), control (B) and LOGSY difference (C) spectra for Fragment E acquired with an NOE mixing period of 1 second

Similar to fragment B, all LOGSY signals appear negative in the LOGSY spectrum (fig. 4.13A), whereas all appear positive after subtraction of controls. Again, the left-most signal at 7.8 ppm appears to be of the greatest intensity. LOGSY build up curves were constructed in fig. 4.14.

Build up curves for fragment E in the presence of Hsp90 shows that the proton at position 1 has the steepest rate of LOGSY buildup. This is similar to fragment C in that the proton on the pyrazole group shows the greatest LOGSY signal.
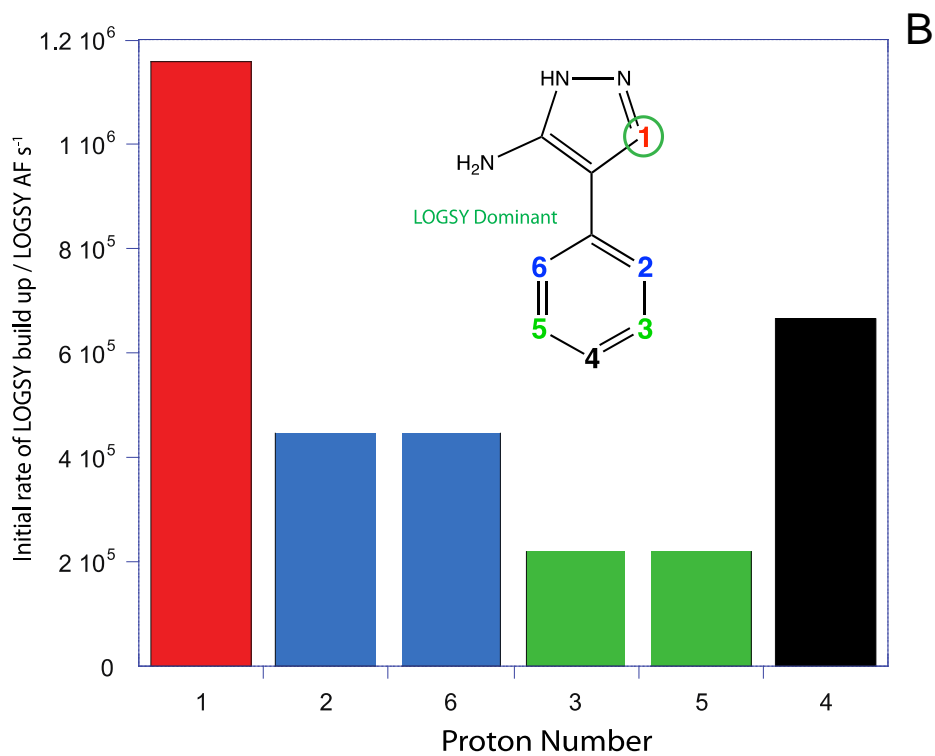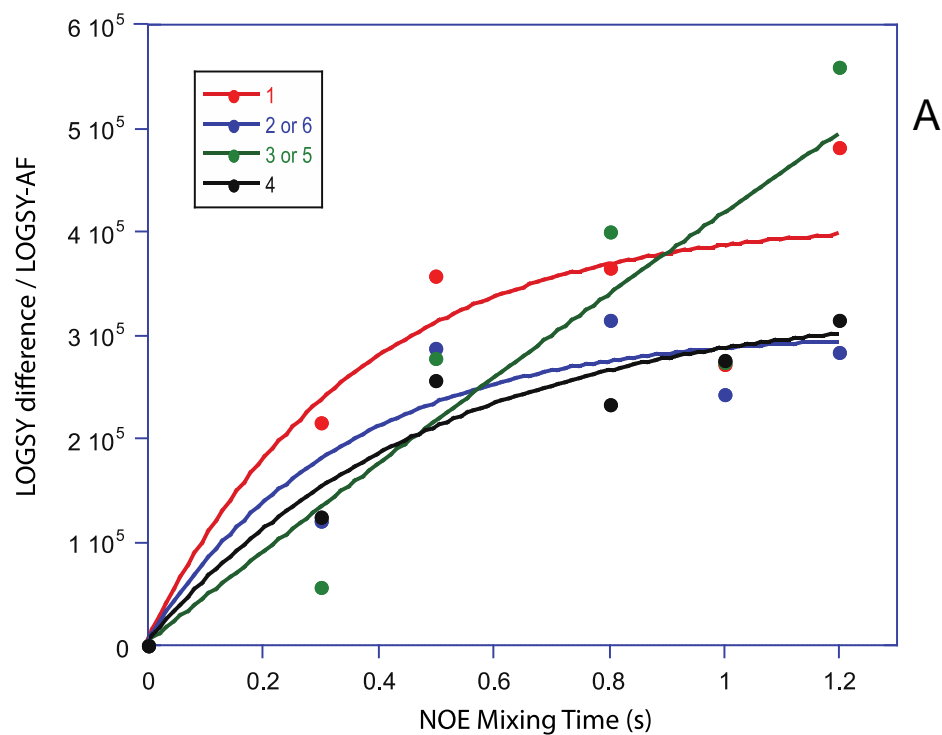
Figure 4.14: (A) LOGSY buildup curves for protons of fragment E, and (B) initial rate values of LOGSY buildup derived from (A)

4.3.6 Quantitative LOGSY for fragment F
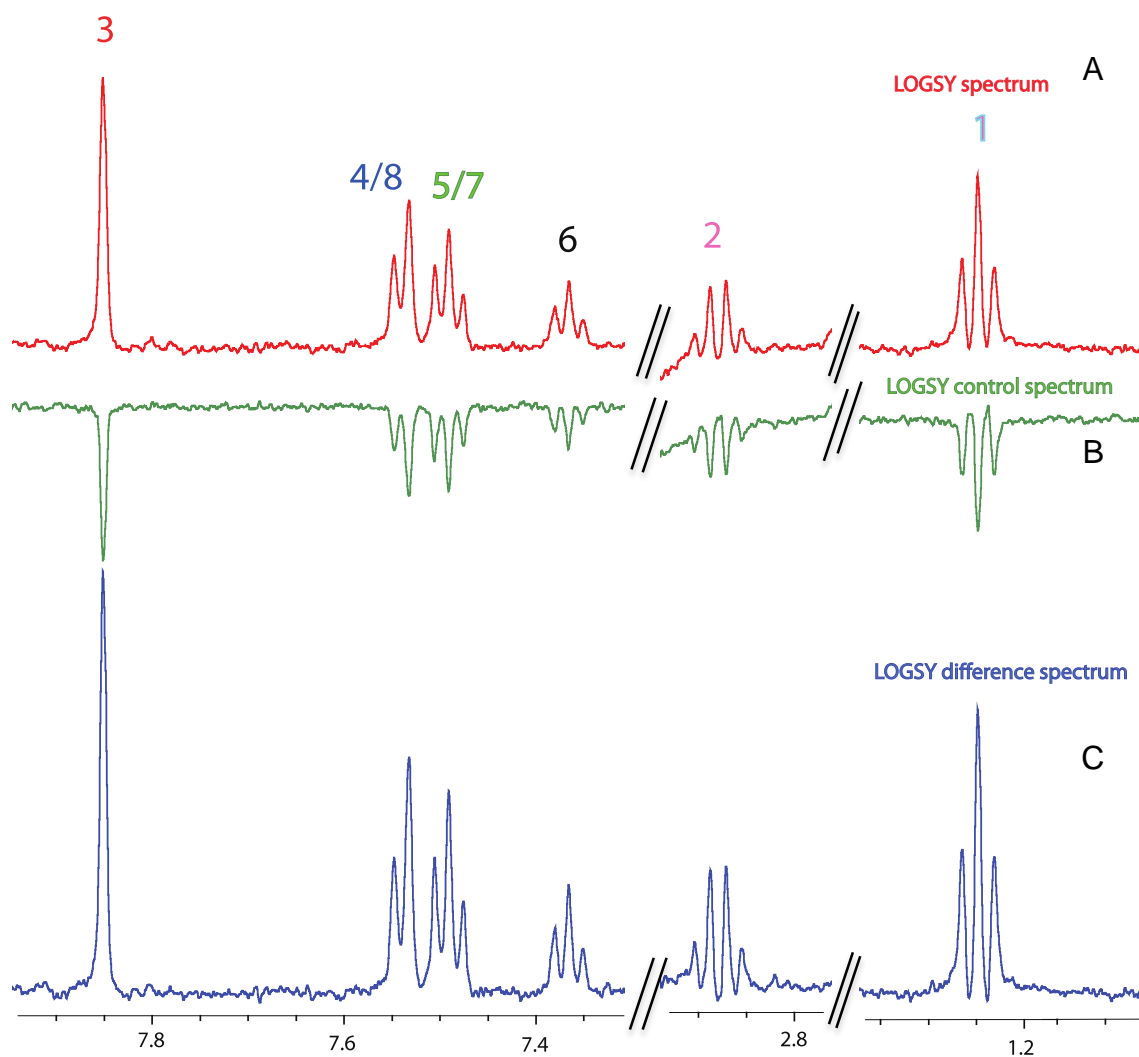
Figure 4.15: LOGSY (A), control (B) and LOGSY difference (C) spectra for Fragment F acquired with an NOE mixing period of 1 second

LOGSY spectra for fragment F in the presence of Hsp90 is entirely positive, signals which are accentuated following subtraction of control spectra. Six protons are observable with that of proton 3 providing the largest signal. LOGSY build up curves produced by acquisition of spectra at different NOE mixing times are extremely smooth and shown in fig. 4.16.

LOGSY build up curves for fragment F in the presence of Hsp90 show proton 3 as the standout LOGSY dominant signal, as determined by initial rate. This is tempered by the fact that this signal is caused by three equivalent protons of the methyl group. This aside, proton 3 exhibits the steepest initial rate.
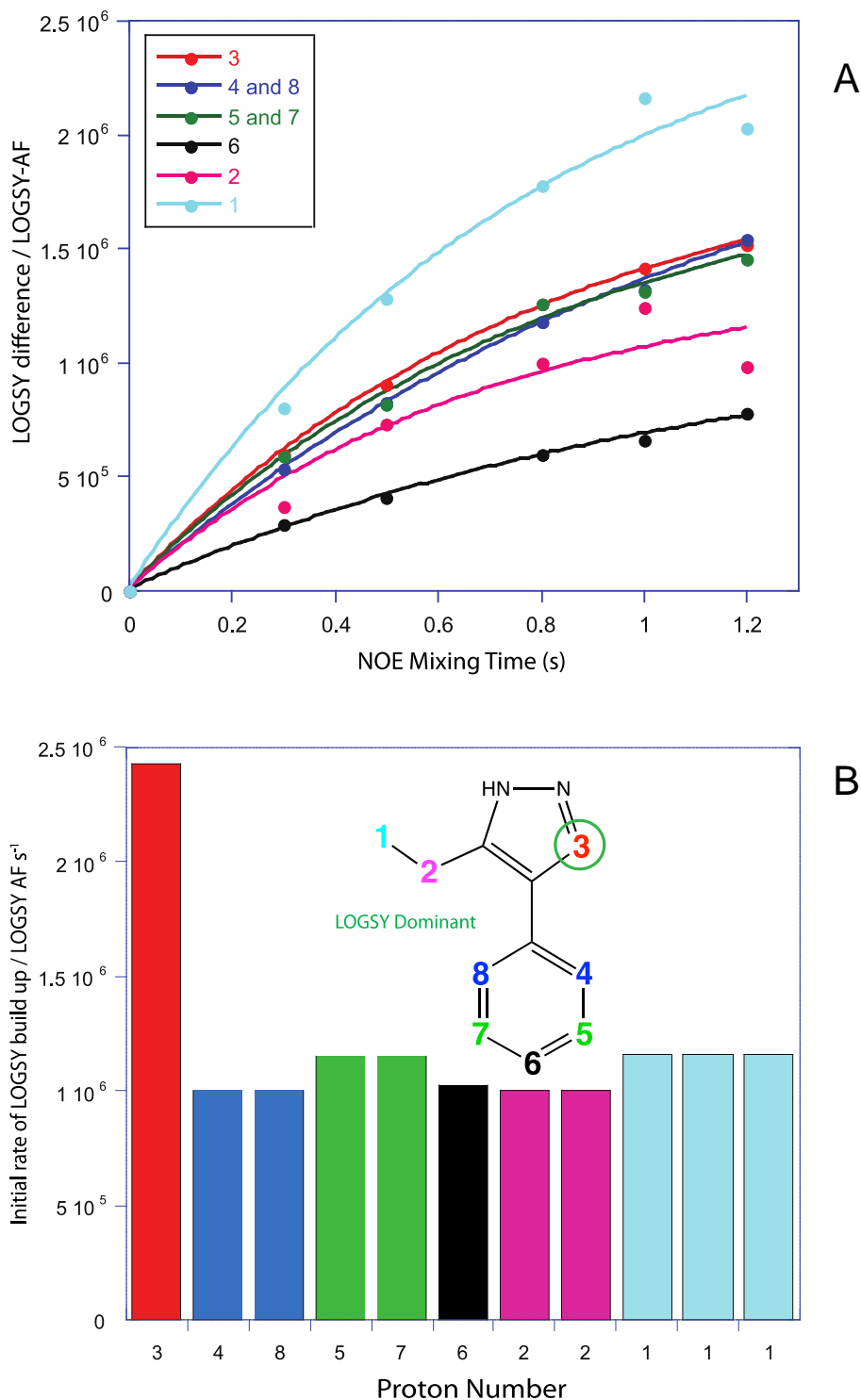
Figure 4.16: (A) LOGSY buildup curves for protons of fragment F, and (B) initial rate values of LOGSY buildup derived from (A)

4.4 Discussion

4.4.1 Initial observations of quantifying data from LOGSY spectra

The first point to observe from the creation of LOGSY difference spectra, created as a subtraction of the integrals from two different samples, one with both protein and ligand and the other just ligand, is that in each case a valid, positively phased spectrum is produced. It is also clear that these spectra are arrived at from variable component spectra.

For example fragments C and F both produce completely positive LOGSY spectra simply from the 'with protein' sample without accounting for the reference spectra. This is a useful property for positive binding fragments, as they would be observed from a fragment screen without the need for a reference. However, this is not necessarily typical of fragment ligands examined here. Fragments B and E, whose LOGSY spectra exhibit only negative peaks, exemplify this, but they produce a characteristic difference spectrum once the reference has been taken into account. Fragments A and D, on the other hand, display a mixture of both positive and negative peaks. What this means is unclear at this point and shall be probed further in the discussion chapter.

Increasing the NOE period for the LOGSY experiment has enabled the tentative plotting of buildup curves (see figs. 4.6A, 4.8A, 4.10A, 4.12A, 4.14A and 4.16A). Initial rates derived herein are the subject of focus for this chapter and will be treated as a value to determine whether or not a certain proton or group of protons is 'LOGSY dominant'. That is to say, stand out clearly above values of other parts of the ligand.

4.4.2 Protons of greatest LOGSY enhancements

Identification of individual protons that received the greatest LOGSY enhancement (as measured by crude initial rate) provided trends in the data. For each case, protons that were LOGSY-dominant were distinct from those that were determined to be 'STD-dominant'.
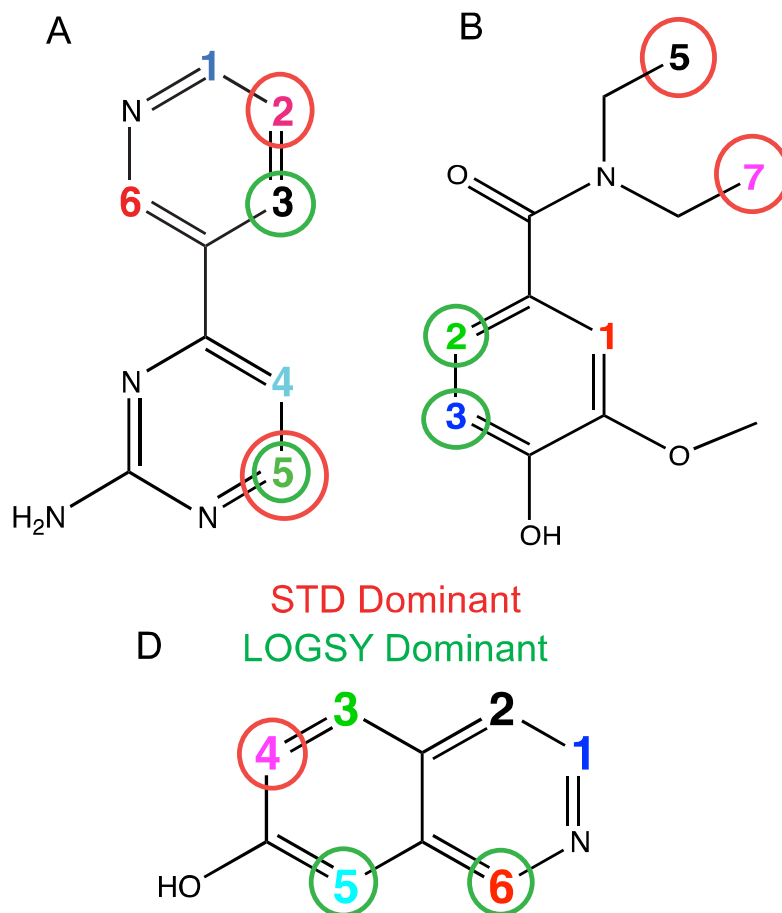
Figure 4.17: Fragments A, B and D. Most significant STD (circled red) and LOGSY (circled green) enhancements are shown, being defined as those protons that exhibit the steepest initial rate in STD and LOGSY experiments

Apart from proton 5 of fragment A, a distinct and different set of protons that are 'LOGSY-dominant' compared to those that are 'STD dominant'. This is the first clear sign that the quantitative STD and LOGSY experiments inform on different interaction processes regarding each individual protein-ligand complex.

4.4.3 Potential for binding mode clustering

Chapter three mentioned the possibility of grouping similar fragments of the same chemotype, on the basis of similar STD buildup patterns. For fragments C, E and F this relied upon the relatively strong STD received by the proton at the tip of the phenyl ring.

Supporting this concept of binding mode clustering is the LOGSY data of the remaining fragments as can be seen from the enhancements below.
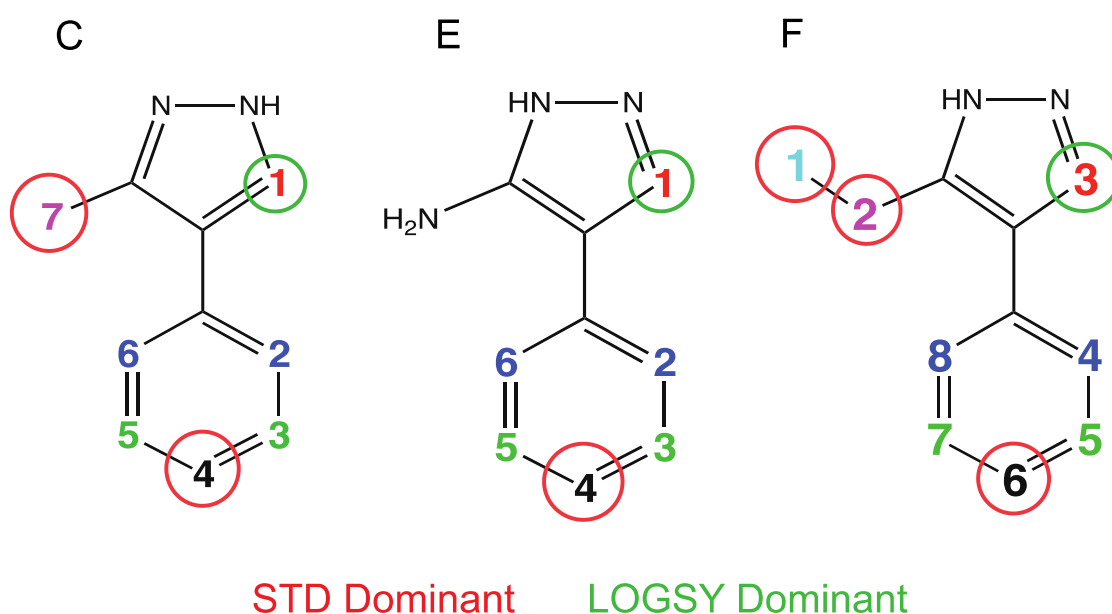
Figure 4.18: Fragments C, E and F. Most significant STD (circled red) and LOGSY (circled green) enhancements are shown, being defined as those protons that exhibit the steepest initial rate in STD and LOGSY experiments

The single proton of the pyrazole ring (protons coloured red in each fragment in fig. 4.18) is in each instance the clearest signal with the greatest rate of LOGSY buildup. Not only are the LOGSY-dominant protons distinct from the STD dominant protons, the same pattern exists across fragments within a particular chemotype.

4.4.4 Conserved, bound water molecules

The nucleotide binding site of Hsp90 is well characterised. The apo-structure of Hsp90 contains a series of ordered water molecules inside the pocket, and on binding of ADP, hydrogen bonds are formed with three of the conserved waters(Prodromou et al., 1997). Two of these water molecules remain conserved in the crystal structures for every fragment under analysis in this chapter. These are shown below for fragments A and D.
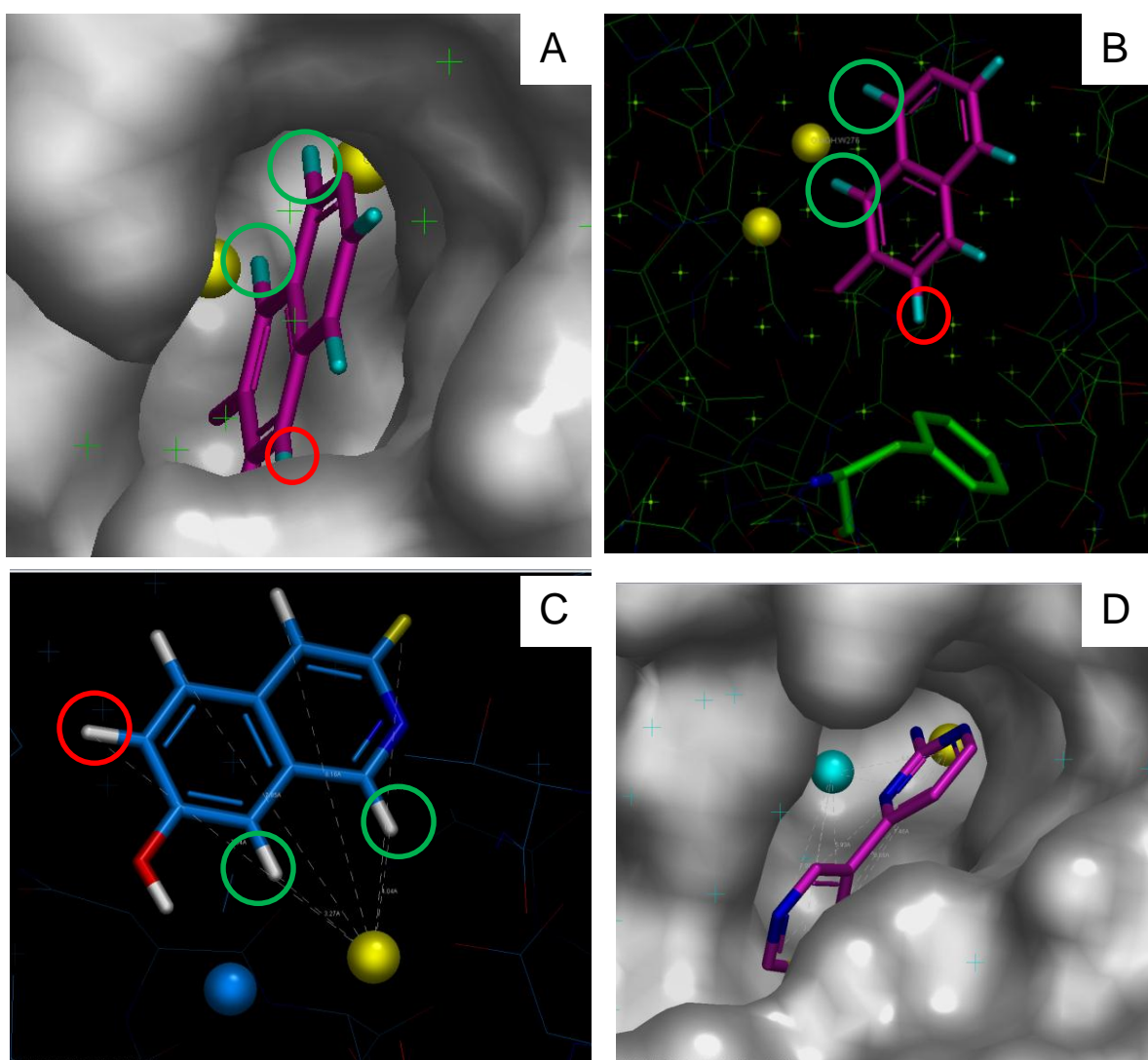
Figure 4.19: (A) Structure of fragment D bound to Hsp90 with two conserved water molecules buried at the bottom of the cleft visible behind. (B) The same as (A) but with the protein surface switched off, and the STD-dominant F138 switched on. (C) Another viewpoint of that shown in (B), and (D) the protein surface structure of bound fragment A. STD (red) and LOGSY (green) dominant protons are highlighted in (A), (B) and (C).

149

Fig. 4.19 A shows the position of the two key conserved water molecules at the base of the binding cleft. Highlighted are both the LOGSY and the STD dominant protons. As figs. 4.19 b and c also illustrate; not only are the LOGSY dominant protons distinct to the STD dominant ones, they are also positioned closest to the bound water molecules.
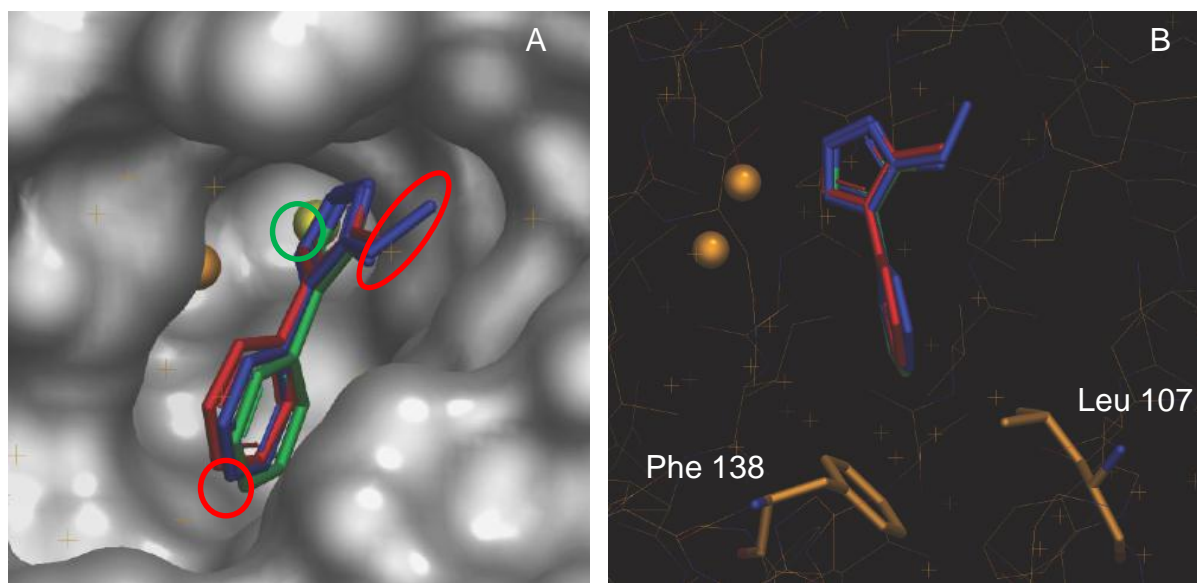
Figure 4.20: Bound-ligand overlays for compounds C, E and F. The conserved water molecules at the bottom of the binding cleft are visible. In (A) the protein surface is switched on, whilst in (B) the surface has been switched off and the side chains of the two major STD-donating residues switched on.

It is **exactly** the same situation for all the other fragments, as is made clear in figure 4.21. This is perhaps least surprising for the three pyrazole fragments given that they all bind with the same mode, as can be seen below in fig. 4.20.

It is clear that the proximity to the bound water is correlated with a larger LOGSY signal, at least in our experiments looking at these six fragments binding to Hsp90. In fig. 4.21 all 6 fragments including the three pyrazoles are shown as their bound crystal forms in relation to the conserved water molecules. These viewpoints how that regions of greatest LOGSY enhancement are orientated closer towards the water molecules.
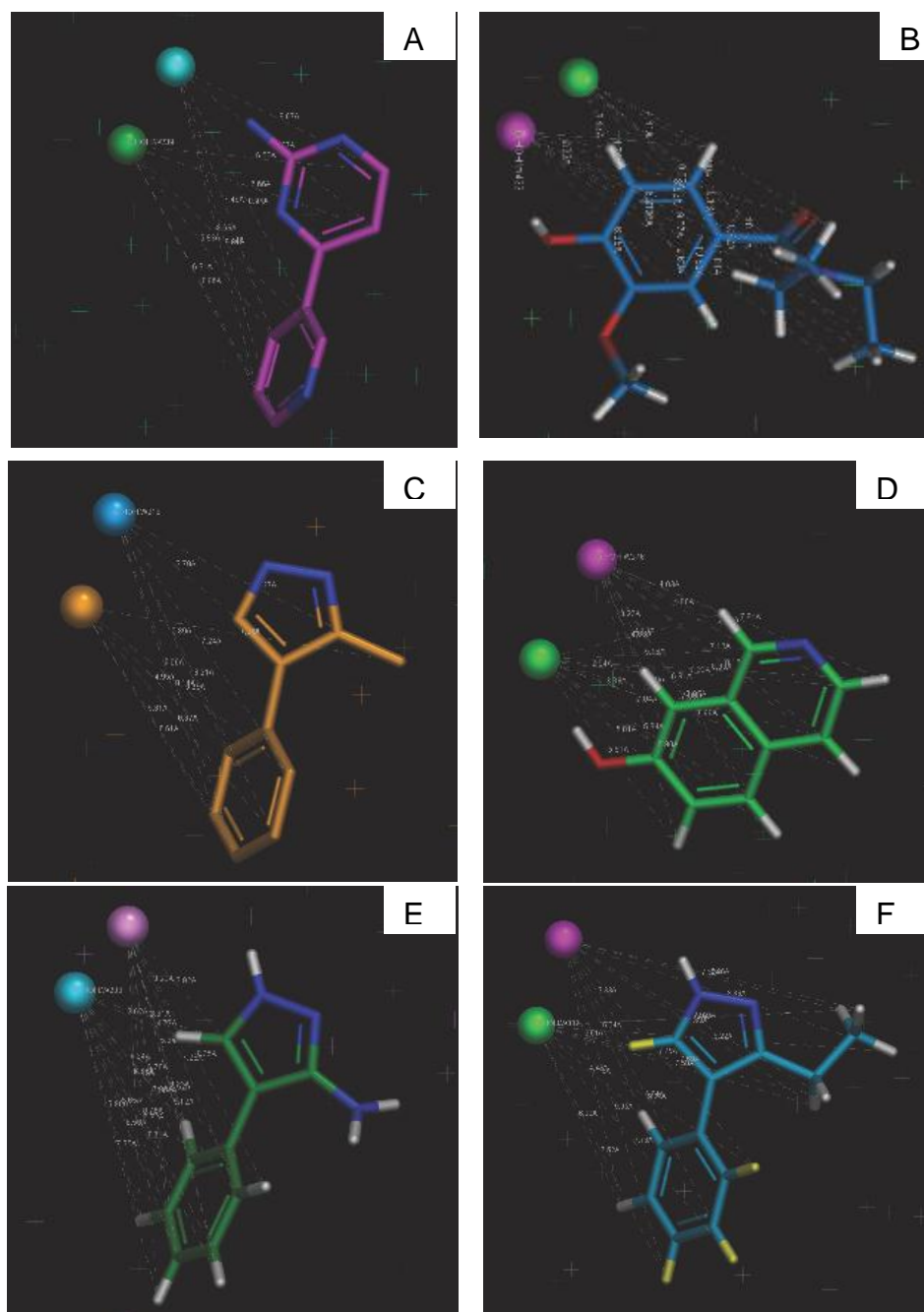
Figure 4.21: Crystal structures of Fragments A – F bound to Hsp90. In each case the model is shown with protein removed whilst two conserved water molecules remain present. In each figure the illustrative intermolecular distances (< 6 Å) between bound water and ligand protons are shown as white lines

It is suspected that measurement of the intermolecular proton-proton distances between water and ligand may provide a more quantitative assessment of our hypothesis. However in practice this is impossible, since hydrogen atoms cannot be accurately added to the oxygen of the waters in the structure in the absence of electron density or stereochemistry.

4.4.5 Validity of quantifying LOGSY data

Within this chapter, the method of quantification could be described as experimental. Whilst there is no doubt that running consecutive LOGSY experiments for two samples that contain protein and no protein – and then subsequently subtracting the integrals of one from the other – is valid, the subsequent quantification leaves room for doubt. Following this the integral of the difference signal was plotted against the NOE mixing time n order to generate a LOGSY buildup curves. All available data were simply fitted to the same equations that were used for analysing STD data. The resulting build up curves all have significant errors associated with them if using the method from chapter three.
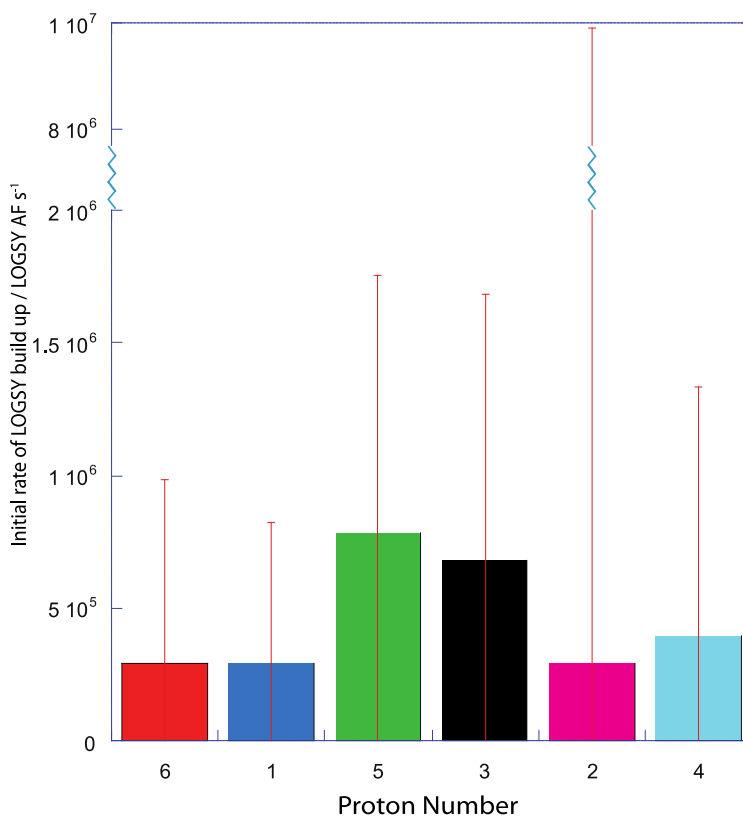
Figure 4.22: Initial rate of LOGSY build up values for fragment A as per fig. 4.7b. Y axis truncated in order to include associated error bars in calculating each initial rate

This is a reflection of the fact that LOGSY data is fitted to equations that are not optimal. Nonetheless, despite a significant error, the initial rates provide a qualitative observation. Unlike quantitative STD where errors were minimal, LOGSY analysis is not concerned with correlating experimental data and precise atomic-resolution data of crystal structure side

chains. Rather, LOGSY quantification allows a qualitative selection of protons that are LOGSY dominant.

Another point to observe is that running a single experiment for a fixed NOE period is all that is required. Unlike the STD analysis where build up curves routinely crossed each other, necessitating the acquisition of a rate or a T_1-adjusted STD value, the ranking order of protons (in terms of LOGSY difference signal) is the same when taken at any single fixed NOE mixing period. With the exception of fragment E, those protons identified as having the greatest LOGSY enhancements at the NOE mixing period of 0.3 s are also the same as those ranked in first place at 1.2 s. Perhaps this renders the calculation of a full rate unnecessary, which could in fact be beneficial in terms of throughput and efficiency. If the required information can be extracted from one experiment rather than five, it makes sense to only run one experiment.

Another point to make is that we have, as with the quantitative STD chapter, taken the liberty to split the experimental values in proportion with the protons of the group, where more than one proton is represented by one chemical shift. It is questionable as to whether dividing a rate by 3 for a methyl group or 2 for a methylene/symmetrical group is the best way to treat the data, but on reflection, it is the most equitable treatment.

For fragments A, B, C, D and F the majority of protons experience a reduced LOGSY intensity in experiments where the NOE mixing period has been increased from 1.0 to 1.2 seconds. This tallies with previous observations in which it was observed that increasing the NOE mixing period increased LOGSY signal up to a point, after which it became reduced(Dalvit et al., 2001), as shown in fig. 4.23.
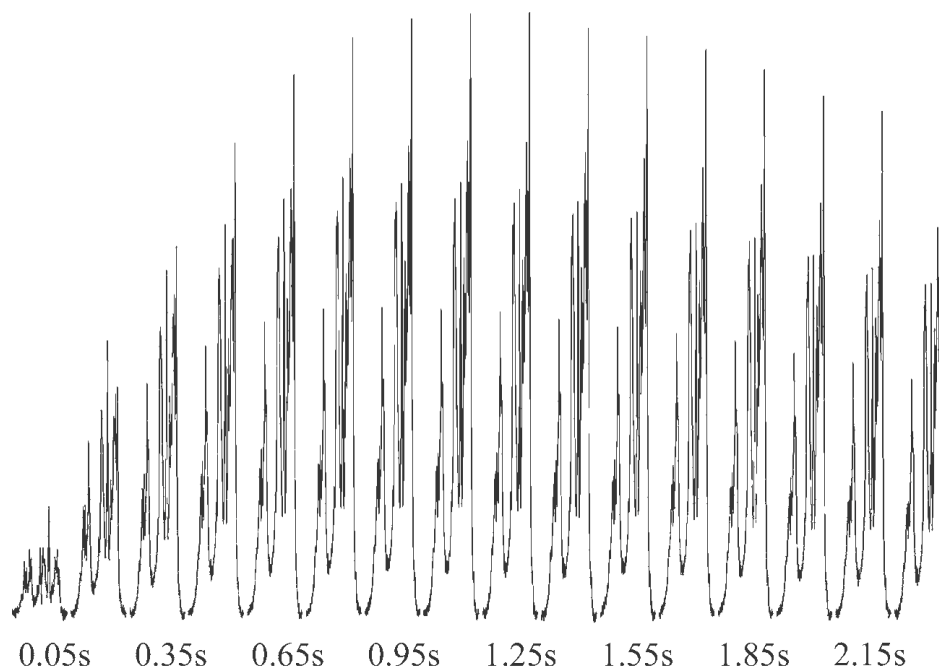
Figure 4.23: NOE-ePHOGSY spectra for HSA with increasing mixing time. The entire spectrum is displayed for each time. Figure taken from Dalvit et al.(Dalvit et al., 2001)

Referring to fig. 4.23, perhaps it is not optimal to look at build up over a range of mixing times up to 1.2 seconds, as the long, slow decay of LOGSY signal has already begun by this point. This is no doubt a factor in why fitting the quantitative LOGSY data to STD build up curves is associated with such a large error. If indeed one mixing period is sufficient to rank protons in order of LOGSY enhancements, experience in this thesis suggests that a mixing period of 1 second is optimal.

4.4.6 Conclusions and the differences between this analysis and SALMON

In this chapter we have determined that the LOGSY experiment may tentatively be used to produce LOGSY build up curves that give a series of initial rate values, much like their STD equivalents. We also determined that these initial rates are associated with a large degree of

error, and that for the purposes of our analysis acquiring data over one mixing period (1 s) is probably sufficient.

The significant finding is that not only are the protons deemed to be 'LOGSY dominant' found to be consistently different to those that are 'STD-dominant', but we have also determined that they are always positioned closest to conserved, bound water molecules in the Hsp90 binding site. On this basis, it is proposed that this provides a rationale for a simple, easy quantitative LOGSY experiment that can help inform on ligand binding mode orientation, so long as water-mediated interactions in the site of importance can be confirmed.

The SALMON methodology(Ludwig et al., 2008) that arrived with similar conclusions to this analysis relied on simply testing one NOE mixing period, whereas we have at least probed a range of mixing periods. A more crucial weakness than this however is that SALMON is simply interested in the sign of the LOGSY signal, and does not bother to quantify any of the effects. It even completely disregards those signals that do not change sign between LOGSY and control samples, emphasizing the need to produce a difference spectrum. Our analysis proposes that all protons of the ligand provide vital information that can assist in orientating the ligand towards the bound water.

Furthermore it is suggested that the bound face and the 'depth in the cleft' are more significant than the particular position of bound water. Our results suggest that the LOGSY dominant signals are strictly orientated toward the conserved water, but at the same time do not necessarily contradict the conclusions of SALMON, that this is due to these parts of the ligand being less solvent-exposed.

Chapter 5

Quantitative STD and LOGSY NMR spectroscopy with Ras and fragment ligands

5.1 Introduction

This chapter takes the principles of the previous two chapters and applies them to a different protein, that of the oncogenic protein Ras. In applying the insights derived from Hsp90 to Ras, it should be possible to verify our approaches by examining whether the evidence either corroborates or contradicts. Ras is sufficiently different to Hsp90 so as to provide another compelling test case.

5.1.1 Ras

Ras is a well-known GTP-binding protein that acts as a nucleotide-dependent switch for a number of principal growth signalling pathways in the cell(Schubbert et al., 2007, Vetter and Wittinghofer, 2001). Ras responds to extracellular signals and is converted from a GDP-bound form to a GTP-bound form, aided by guanine nucleotide exchange factors (GEFs), in particular SOS1. Ras^{GTP} is the active form involved in direct interactions with downstream effector molecules such as PI3K and Raf (figure 5.1).
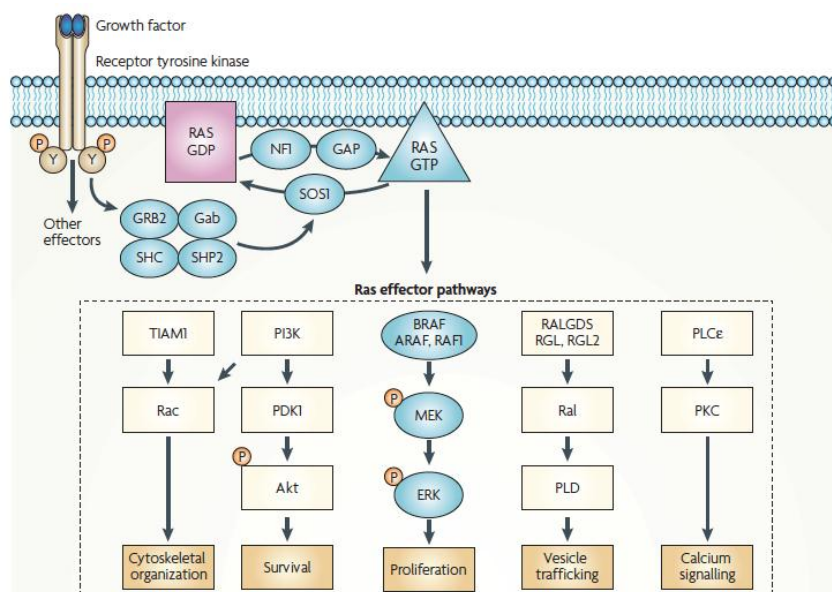
Figure 5.1: The Ras signalling pathway highlighted with proteins affected by mutations in cancer. Growth factor binding to extracellular cell receptors causes activation of receptor complexes, which include adaptors such as SHC, GRB2 and Gab. These proteins recruit SHP2 and SOS1, increasing Ras–GTP levels by catalysing nucleotide exchange on Ras. The GAP NF1 binds to Ras–GTP and accelerates the conversion of Ras–GTP to Ras–GDP, thus terminating signalling. Figure taken from (Schubbert et al., 2007)

Germline mutations affecting components of the Ras–Raf–MEK–ERK pathway are known to underpin developmental disorders, such as Noonan syndrome and Costello syndrome. Studies suggest that strength and duration of signalling through the Ras–Raf–MEK–ERK pathway regulates various developmental processes. Further structural, biochemical and functional analyses of these mutant proteins will extend our understanding of Ras signalling in development and cancer, hence the interest in Ras as a therapeutic target. (Schubbert et al., 2007)

The gene for Ras is frequently mutated, and is implicated in over 20% of human cancers(Schubbert et al., 2007). Mutated Ras exists in a prolonged GTP-bound state, which enables enhanced Ras-dependent signalling and consequently cancer cell survival and growth(Schubbert et al., 2007, Vetter and Wittinghofer, 2001).

Mutations in Ras are generally associated with poor outcomes and prognoses, and as such Ras has long been considered a critical oncogenic target for drug discovery. This chapter applies the concepts explored in this thesis thus far and tests them out on this most pivotal of cellular oncoproteins.

5.1.2 A realm of untapped potential

Despite its critical importance, Ras remains an impregnable protein for small-molecule inhibitors, even 30 years since its discovery. Ras binds to guanine nucleotides with a picomolar affinity – nucleotides that are also present at high concentrations in the cell – making the design of conventional competitive inhibitors to the nucleotide binding site very tough. Some small molecules have been reported in the past as having activity against Ras, but these are largely with unknown

mechanisms of action and are also in the absence of key structural information(Taveras et al., 1997).

In a more recent development, a covalent inhibitor to KRas (another GTPase member of the Ras superfamily) has been developed(Ostrem et al., 2013), targeting a novel binding pocket in the G12C mutant via a disulphide bond. Crystal structures of the compound – replete with covalent warhead – binding to KRas identified the novel pocket. Furthermore, the compound selectively altered the affinity of Ras for GTP, not GDP. Such selectivity is essential in ensuring non-mutated protein is left unscathed.

Covalent inhibitors to KRasG12C are one thing, but a site more amenable to a starting point for FBDD is clearly far more relevant for this quantitative STD and LOGSY analysis of fragments. For that reason, we need to go back a couple of years.

5.1.3 A Ras Binding Site for FBDD

Despite the difficulty presented by the Ras family of proteins to traditional methods of drug discovery, a small-molecule binding pocket has recently been identified(Maurer et al., 2012). The group from Genentech carried out a fragment screen with a 3,300 compound library using STD NMR and HSQC fingerprinting, and found 25 compounds that produced the same chemical shift perturbations (CSPs) that consistently mapped onto a site on KRas. These were V8, L56, D57, T74 and G75.
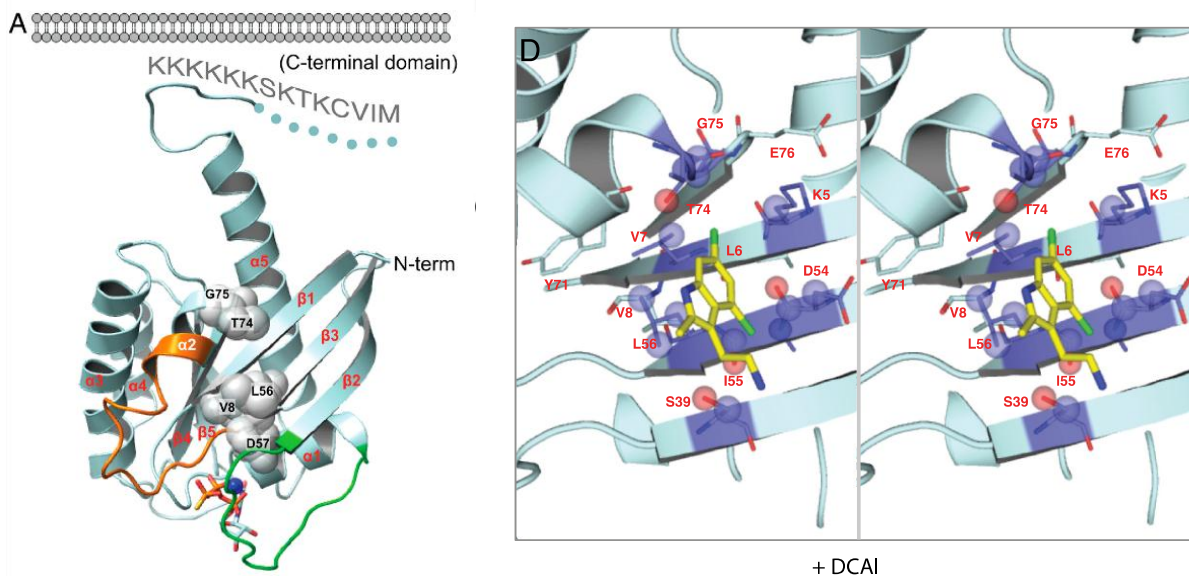
Figure 5.2: (A) Structure of KRas bound to GTP. Large spheres display amino acids that displayed consistent CSPs in the NMR screen. (B) Ligand DCAI bound to KRas. Amino acid residues of Ras that directly interact with DCAI are shown. Spheres indicate atoms that are within 4 Å. Figure adapted from (Maurer et al., 2012)

Fig. 5.2 highlights the small-molecule binding site is between the α2 helix and the β-sheet β1- β3. Other residues surrounding the pocket that also display CSP in HSQC fingerprints include K5, L6, V7, S39, D54, I55, L56 and T74. From this point forwards this binding site shall be referred to as the 'first site' of Ras.

The site itself was shown to measure 7 x 7 Å at the opening and have a depth of 5 Å(Maurer et al., 2012). This is large enough to accommodate a ligand benzyl (in addition to a chloryl) group, and as such makes it an amenable system for the fragment ligands under observation in this chapter. It is also noteworthy how much shallower this is than the nucleotide binding site of Hsp90 - 15 Å – that underwent analysis in the previous chapters. The Ras binding site is significantly less cavernous and more 'groove-like' compared to a protein such as Hsp90, but STD and LOGSY

are still expected to function perfectly well. Any differences in the implications of quantifying ligand-observed NMR data between the two proteins will serve as an interesting comparison for a later discussion.

5.1.4 Previous STD and LOGSY on Ras

STD NMR has been tentatively used to identify an epitope of a sugar-derived inhibitor to Ras(Peri et al., 2006). Here a single spectrum was used to determine that benzyl and phenylhydroxylamine moieties constituted a major interaction surface between 4 ligands and Ras.
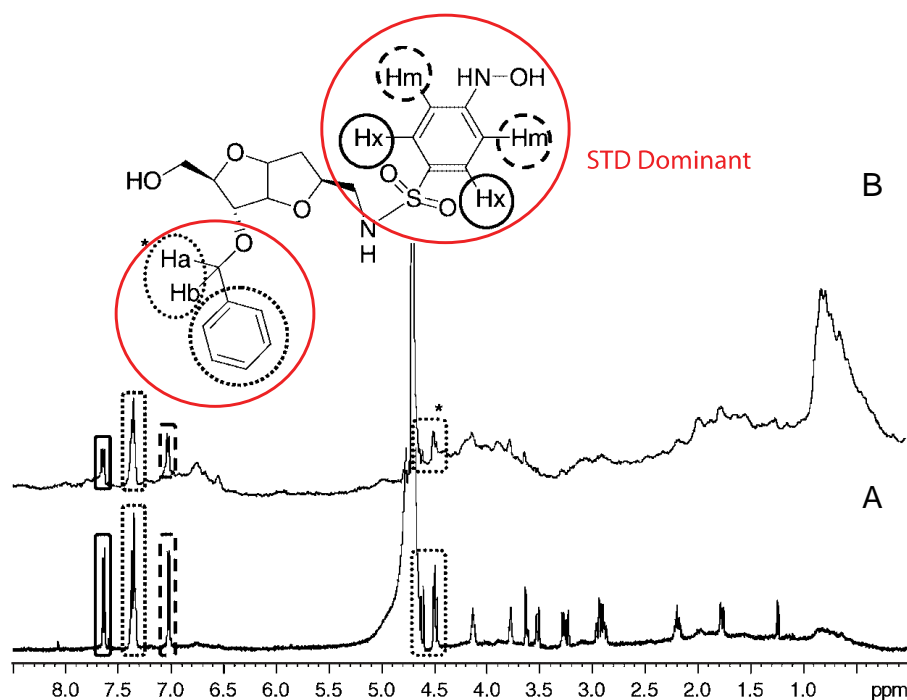
Figure 5.3: (A) ^{1}H NMR spectrum of compound 5 and Ras-GDP and (B) the equivalent STD spectrum. Spectrum acquired with a saturation time of two seconds, on a sample with a ligand ratio of 20:1. Figure adapted from Peri F, at al(Peri et al., 2006)

Aside from the fact that this is a single spectrum acquired at a single, fixed saturation time – thus ignoring the effect of longitudinal relaxation – the insight gleaned from this sort of analysis is limited. To say that two large functional groups at either end of

a compound are involved in major interactions with a long groove-like binding site is not sufficient.

Another more recent piece of work(Duppe et al., 2014) looked at the GTP-binding protein Rheb – a member of the Ras superfamily – focusing on targeting (or 'masking') the c-terminal CAAX-box. This is involved in membrane insertion and is critical for the normal functioning and subsequent downstream processes of Rheb. The group targeted the CAAX-box with a peptidomimetic 'receptor' and used STD NMR once again as a confirmation that their 'receptor' bound to Rheb. Again, a single STD spectrum was deemed sufficient to assert "the lipophilic CH2 groups of Pro, Lys, and AC5C show strong STD signals, indicating large nonpolar association areas". Again, a fairly vague and not so insightful statement.

There is little reported in the literature of quantitative STD against the Ras target, and certainly nothing quantitative with fragments ligands. This chapter takes a fully quantitative approach using a set of fragment ligands to Ras, in conjunction with a full set of proprietary structures. In addition, a 'second' binding site is probed in the absence of structural data.

5.2 Materials and Methods

5.2.1 Protein production and purification

Purified HRasG12V was provided by Astex Pharmaceuticals, after having been expressed and purified. HRasG12V was cloned into the pET28 vector and was subsequently expressed in BL21 (DE3). The protein was purified using a Ni^{2+} affinity column, thrombin tag-cleaved, and then purified by gel filtration.

The amino acid sequence for HRasG12V protein as encoded by the plasmid is as follows:

GSHMTEYKLVVVGAVGVGKSALTIQLIQNHFVDEYDPTIEDSYRK
QVVIDGETCLLDILDTAGQEEYSAMRDQYMRTGEGFLCVFAINNT
KSFEDIHQYREQIKRVKDSDDVPMVLVGNKCDLAARTVESRQAQ
DLARSYGIPYIETSAKTRQGVEDAFYTLVREIRQH

5.2.2 Identification of the protein by Mass Spectrometry

In order to confirm the identity of the HRasG12V construct the protein was tested by electrospray time-of-flight (ESI-TOF) mass spectrometry at Astex Pharmaceuticals using an Agilent 1200 LC and a Bruker MicroTOF mass spectrometer internally calibrated using Agilent low concentration Tunemix.

5.2.3 Fragment ligands to Ras

5.2.3.1 Single fragments binding to the first Ras binding site

Astex Pharmaceuticals provided a range of known fragment ligand hits for the first Ras binding site. Under investigation in this chapter is an initial set of fragment ligands H – L to investigate binding to Ras individually
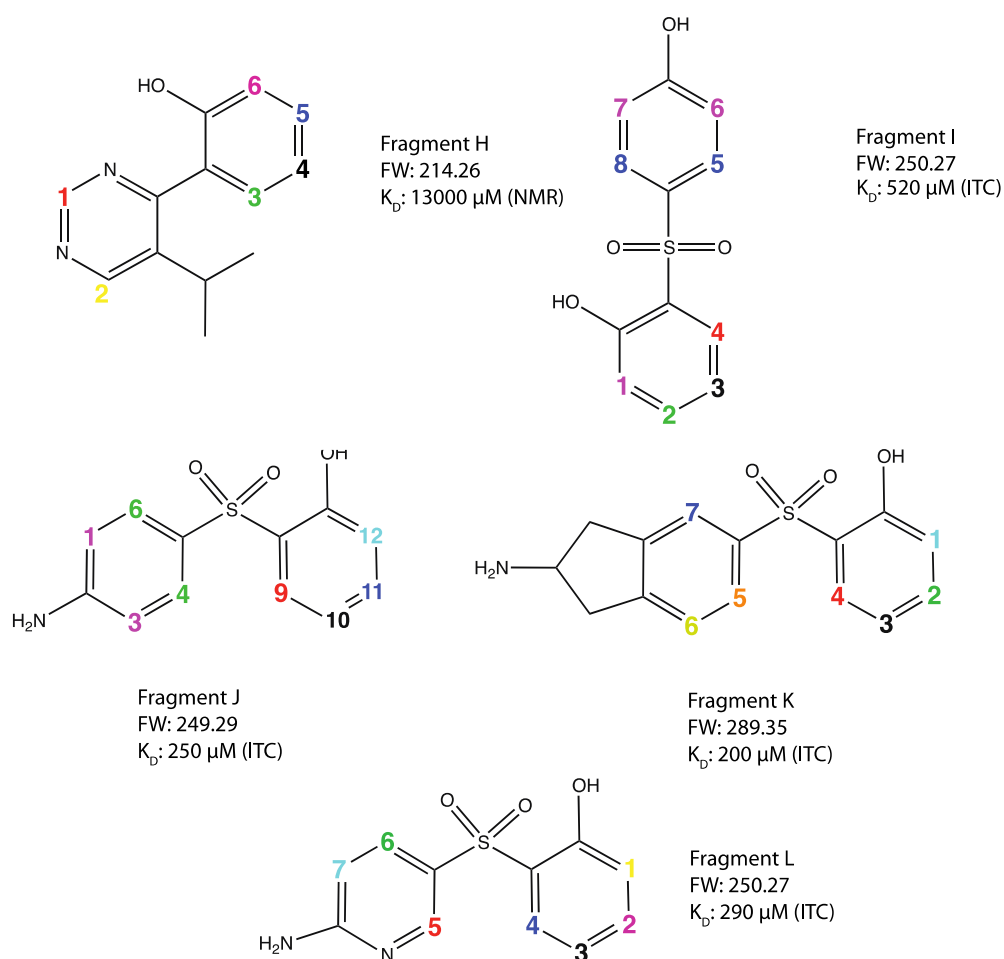
Figure 5.4: Fragment ligands H – L. Fragments were provided as freeze-dried compounds subsequently diluted into DMSO stocks of 100 mM. Coloured numbers denote protons or proton groups

5.2.3.2 Fragments binding to the second site in Ras, after saturation of the first site

In addition to the 5 ligands under investigation binding to the first binding site in Ras, it was subsequently decided to investigate two ligands that bound to the second site.
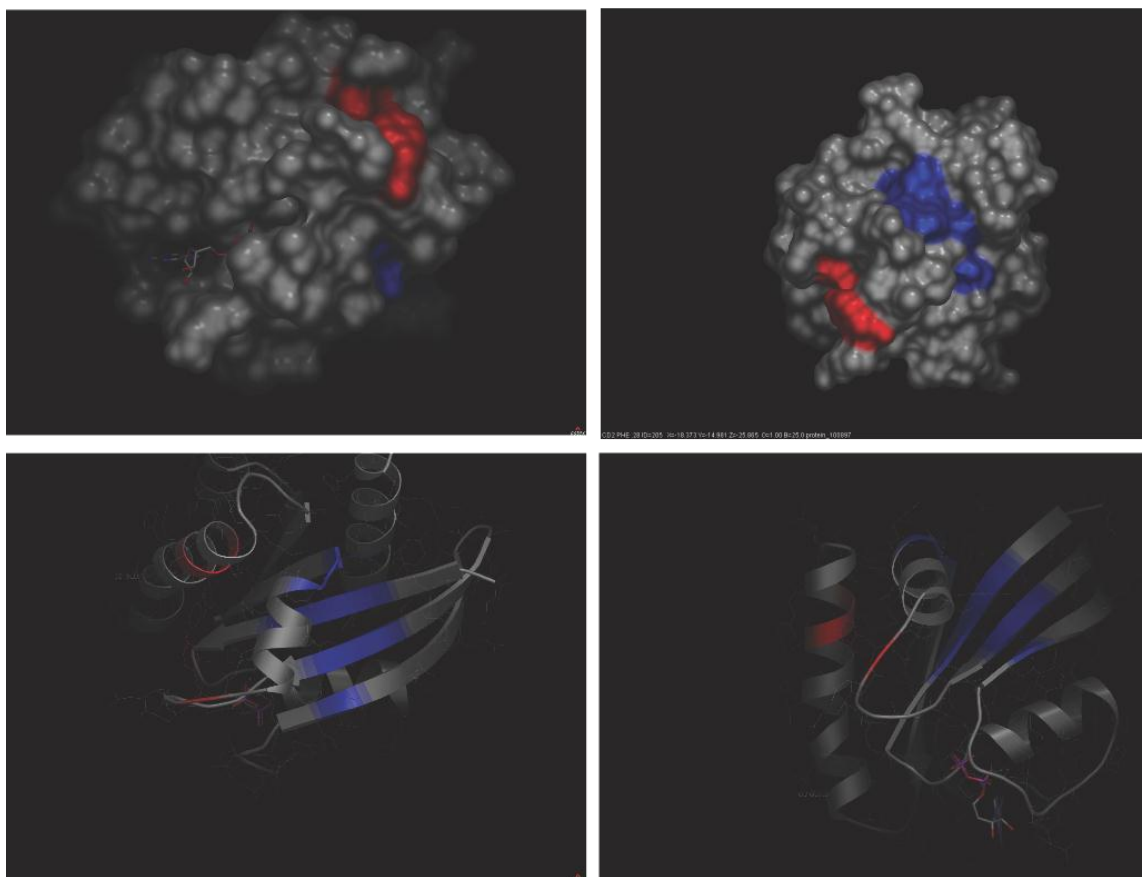
Figure 5.5: Binding sites on the Ras protein. Different viewpoints and surfaces are shown. The 'first site' is highlighted in blue – as introduced earlier on - whereas the suspected 'second site' is highlighted in red, comprising amino acid residues Y64, Q99 and I100

In order to facilitate investigations into the second site, fragments M and N are relatively tight-binding fragments used to saturate the first site, and then either of the weak binding fragments are then added in excess. It is the signals of the weak-binding fragment in the second site that we measure.
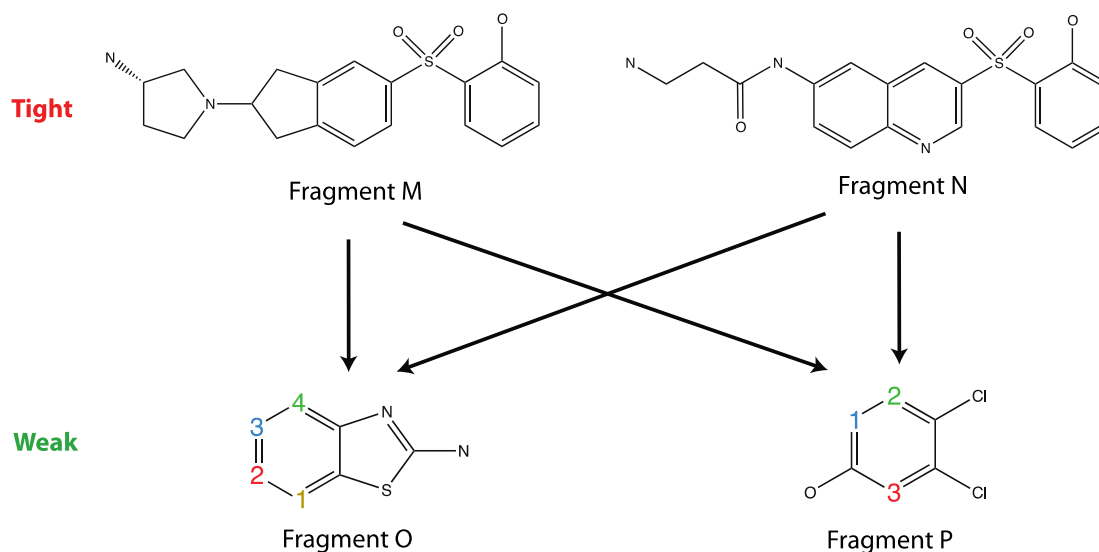
Figure 5.6: Four further fragments. Fragment M or N is used to saturate the first site, and fragment O or P is present in excess as a weak-binding fragment to the second site. This provides four combinations: M+O, M+P, N+O and N+P.

5.2.4 NMR experimental setup

5.2.4.1 Sample preparation

Samples for STD and LOGSY were prepared as 12 μM Ras protein and 1.2 mM fragment ligand (final DMSO concentration of 2%) in 20 mM Tris, 100 mM NaCl 1 mM DTT and 15% D_2O at pH 7.2. For all experiments the ratio of ligand to protein was 100:1, unless specified otherwise. All experiments were carried out at 5 °C. In addition, for LOGSY experiments an extra, identical sample for each fragment was made up but without the protein.

An exception to this sample setup is made for the two-site binding experiments. In this instance fragment O or P is present as usual at a 100 times excess to the protein (5 mM to 50 μM in this case) but in addition if saturating with fragment M in the first site this was present at 500 μM and if saturating with fragment N this was present at 200 μM. The relatively tight first-site binders are present at roughly 20 times the

value of their K_D (25 μM and 10 μM for M and N respectively) to ensure roughly 90% occupancy of the first site. STD and LOGSY NMR spectra for 2-site binding experiments are listed in appendix C.

5.2.4.2 STD NMR

As in chapter 3, STD NMR experiments were performed at 500 MHz using a Bruker DRX500 spectrometer equipped with a TXI cryoprobe using a standard Bruker STD sequence. STD NMR datasets were obtained over 128 scans (64 scans 'on' and 64 scans 'off saturation) with a 40 ms Gaussian shaped pulse (positioned at -3 ppm) and a delay of 7 seconds. Water suppression was achieved using a standard Bruker 3-9-19 WATERGATE sequence. Datasets were processed and analysed using Bruker Topspin 3.2 and the absolute intensities (peak heights) were quantified using MestReNova (Mnova). Intensities were used to calculate STD amplification (STD_{AF}) from STD difference spectra $[I_{STD} = (I - I_0)]$ and the control spectra (I_0) as has been previously described using the equation(Meyer and Peters, 2003):

$$STD_{AF} = \left(\frac{I_{STD}}{I_0}\right) \times Ligand\ Excess \qquad \text{(Equation 6)}$$

Repeating the same STD experiment for a range of saturation times - between 0.5 and 5 seconds – enables the calculation of initial rates as laid out previously(Begley et al., 2010). Buildup curves for all individual protons were fit to equation 7 by plotting STD_{AF} against saturation time (t) using KaleidaGraph software:

$$STD_{AF} = STD_{AFMax}(1 - e^{-k_{STD}t}) \qquad \text{(Equation 7)}$$

The initial rate (STD_{Fit}) is then determined by multiplying together the two KaleidaGraph output values for k_{STD} and STD_{AFMax}, as this product is the first derivative of equation 7:

$$STD_{Fit} = k_{STD}(STD_{AFMax}) \qquad \text{(Equation 8)}$$

The initial rate (STD_{FIT}) is again then calculated by multiplying with k_{STD}.

5.2.4.3 Inversion Recovery for Longitudinal Relaxation Time constant (T_1)

Inversion recovery experiments were performed using a Bruker AV3 600 MHz NMR spectrometer equipped with a QCI-F cryoprobe. Datasets were processed and analysed with Bruker Topspin 3.2. For each individual sample a series of 15 consecutive experiments were set up, with delay times (τ) each of 0.2, 0.4, 0.6, 0.8, 1, 1.2, 1.4, 1.6, 1.8, 2, 2.2, 2.4, 2.6, 2.8 and 3 seconds. Each delay time results in a differing integral value (a broad range from negative to positive), which when plotted against delay time allows the data to be fit to equation 9 using KaleidaGraph:

$$M_t = M_0(1 - 2e^{-\frac{\tau}{T1}}) \qquad \text{(Equation 9)}$$

The equation is then solved for T_1, or given by KaleidaGraph.

As before calculating the T_1 values allows for the second prong of this analysis, analyzing STD considering relaxation of the ligand (GEM-CRL)(Kemper et al., 2010). This depends upon acquiring a single set of STD values at a fixed saturation time, and then dividing each value by the T_1 for each proton. This normalises the data and corrects for differences in longitudinal relaxation. As part of this analysis all

comparisons and association between experimental data and the binding site structure will include both initial rates and T_1-adjusted data.

5.2.4.4 LOGSY NMR

As in chapter 4, LOGSY experiments were performed at 500 MHz using a Bruker DRX500 spectrometer equipped with a TXI cryoprobe. LOGSY experiments were carried out using the ePHOGSY sequence of Dalvit et al(Dalvit et al., 2000), incorporating a CPMG period of 10 ms. Experiments were performed over 512 scans and spectra acquired with 16384 points and a spectral width of 12 ppm. ^{1}H spectra were referenced to 3-(Trimethylsilyl) propanoic acid (TSP). Data was processed and analysed using Bruker Topspin 3.2. LOGSY difference spectra were generated by subtraction of LOGSY spectra from companion reference spectra, and signals were quantified by integration of each resolvable peak.

LOGSY experiments were repeated for a range of NOE mixing periods (0.3, 0.5, 0.8, 1.0 and 1.2.s). The integral for each peak observed in a LOGSY difference spectrum was recorded at each mixing time and used to construct a LOGSY buildup curve. Curves were fit to the same equations as for STD buildup curves detailed in this chapter.

5.2.5 Correlation of Experimental STD NMR data with Ras structural data

As in previous chapters, experimentally determined initial rates were correlated against distance restraints taken from the appropriate bound crystal structure PDB files (not in public domain). Every inter-proton distance (r) between each ligand

proton and every protein side chain of the crystal structure (providing it's within 6Å) was then processed as $\frac{1}{r^6}$. This lends greater weight to the saturation transfer pathways that are in close proximity. These were summated for each individual ligand proton to give an overall value for the sum of distances that might contribute saturation transfer.

5.2.6 Computational docking of fragments into Ras

Fragment ligands were computationally docked into the Ras protein with GOLD (Verdonk et al., 2003), and ranked using the Goldscore scoring function(Verdonk et al., 2003). GOLD and Goldscore docks and then ranks various protein-ligand binding poses according to fitness. Goldscore is optimised for ligand binding position and takes into account hydrogen bonding energy, van der Waals energy, and ligand torsion strain. For this analysis the top 9 ranked poses were recorded for analysis.

5.3 Results

5.3.1 Identification of the HRas G12V protein by Mass Spectrometry
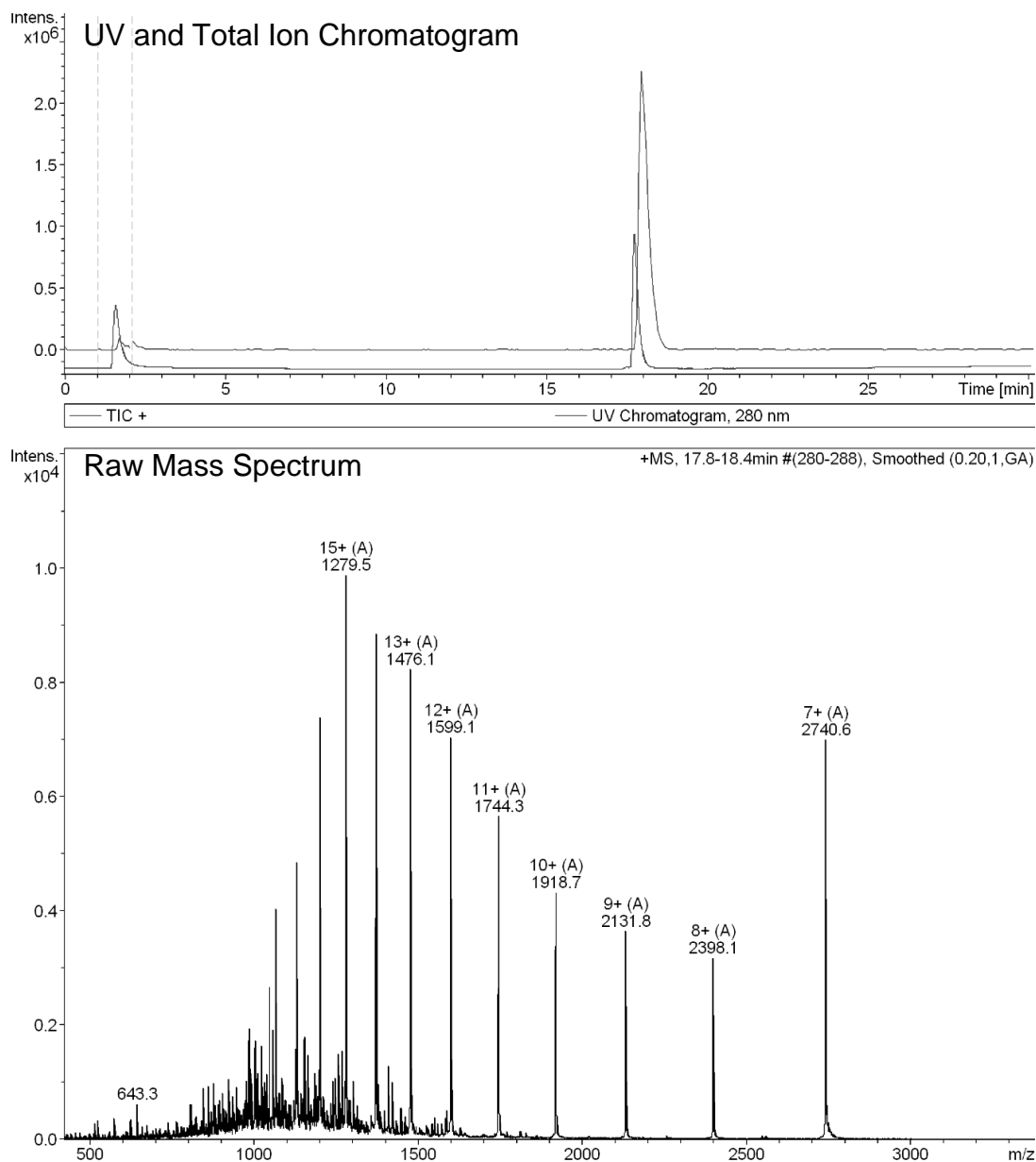
Figure 5.7: LC-MS and accompanying spectra for HRas

The UV chromatogram output from the LC-MS yielded a single significant peak containing a single protein species with an elution time of 18 minutes. The distribution of charged species in the spectrum is consistent with the singly charged species (as shown in figs. 5.7 and 5.8). The final mass of 19176 Da is the correct mass that would be expected for the HRasG12V construct.
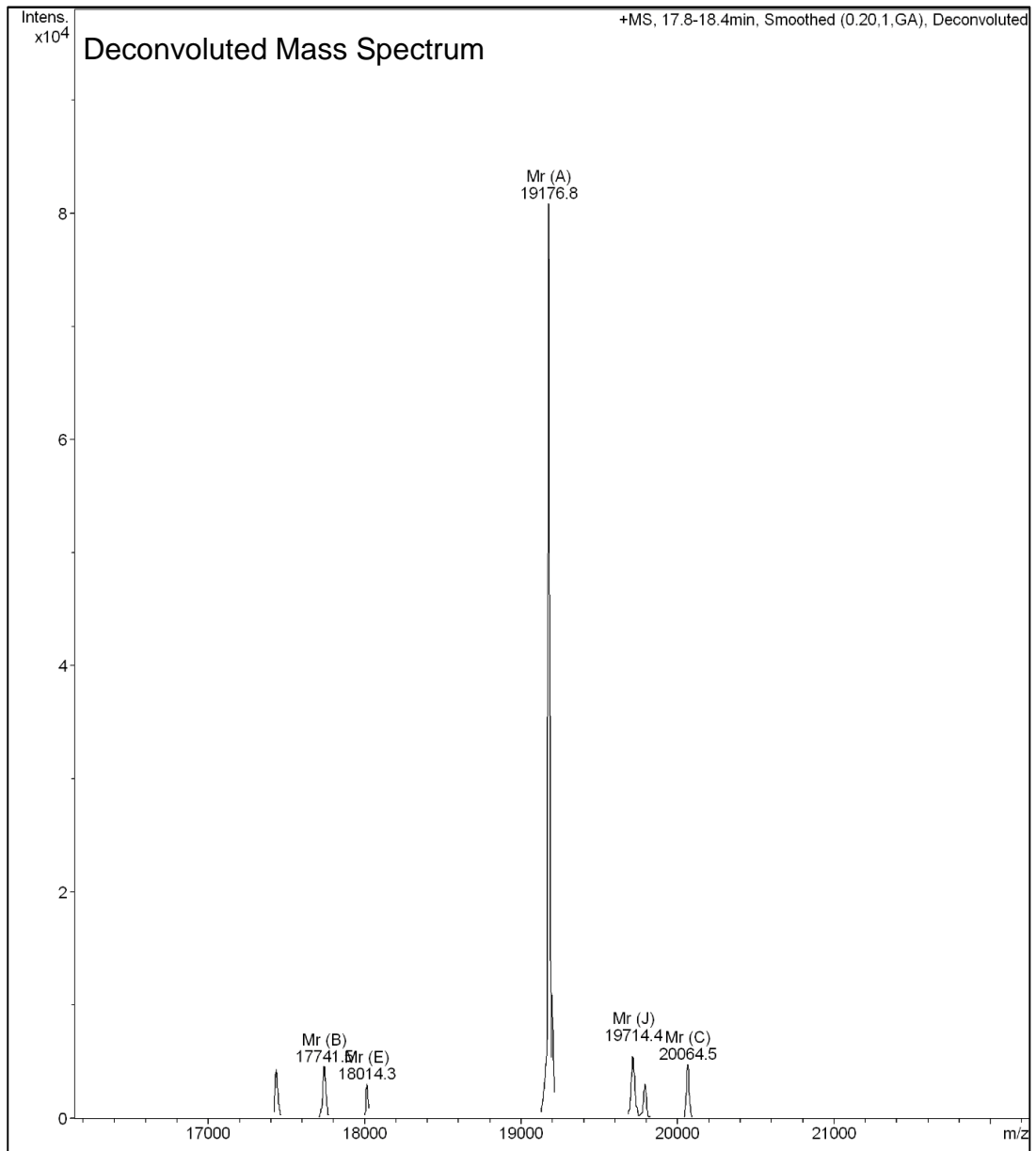
Figure 5.8: Deconvoluted mass spectrum of HRasG12V, with the sequence data below

GSHMTEYKLVVVGAVGVGKSALTIQLIQNHFVDEYDPTIEDSYRKQVVID
GETCLLDILDTAGQEEYSAMRDQYMRTGEGFLCVFAINNTKSFEDIHQY
REQIKRVKDSDDVPMVLVGNKCDLAARTVESRQAQDLARSYGIPYIETS
AKTRQGVEDAFYTLVREIRQH

5.3.2 Quantitative STD

5.3.2.1 Fragment H
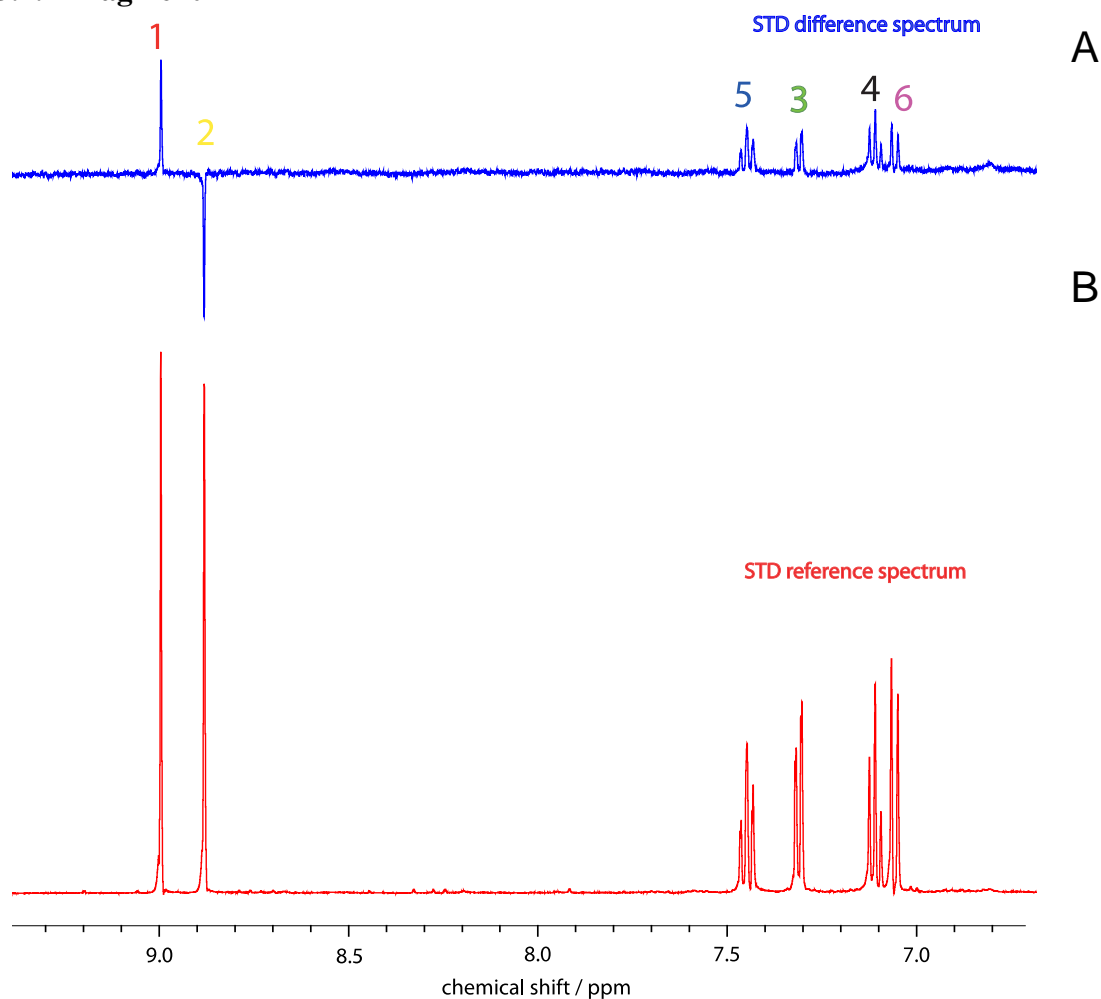
Figure 5.9: STD (A) and STD reference spectra (B) for fragment H, acquired at a saturation time of 5 seconds in this example

Fragment H STD spectra in fig. 5.9 show positive STD signals in the presence of Ras for all protons of the ligand except for the signal at ~8.9 ppm. The associated build up curves for this data is shown in fig. 5.10A, with the subsequent positive correlation with intermolecular structure in 5.10B. Protons 4 and 5 dominate the STD signal whereas proton 1 has the weakest STD build up, and this is reflected in the structure correlation. Isopropyl protons were not considered for analysis due to the impossibility of interpreting 6 protons through one chemical shift.
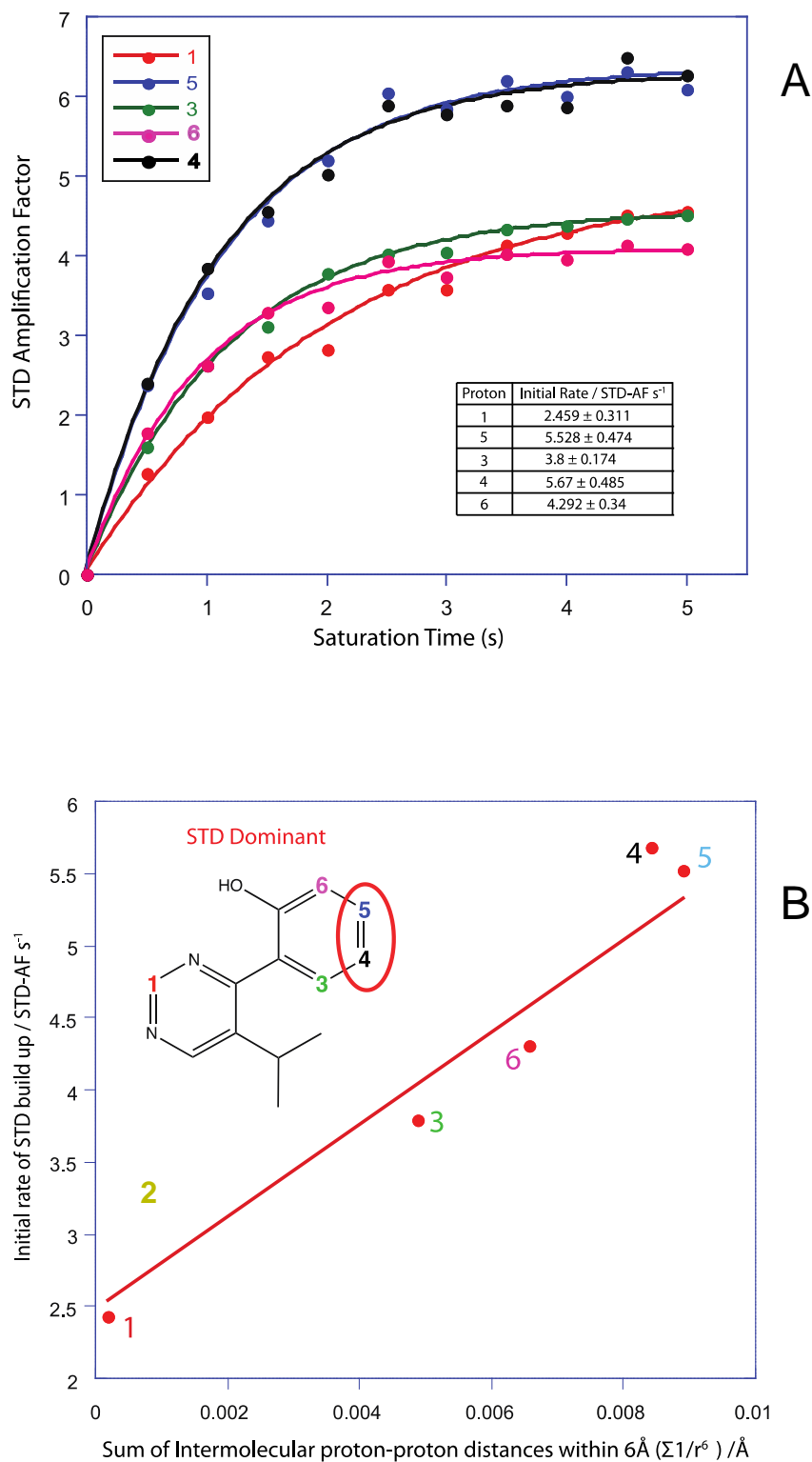
Figure 5.10: (A) STD build up curves for fragment H with associated initial rates and errors, and (B) these initial rates plotted against the sum of the intermolecular proton-proton distances derived from the crystal structure

Inversion recovery data for fragment H in fig. 5.11A allows us to modulate single-point STD values and correlate these values with structural restraints. An equally good, if not better correlation with intermolecular proton-proton distances is observed.

Proton	$T_1(s)$	Error
1	2.3776	0.0062
2	1.3044	0.0048
5	1.2843	0.0038
3	1.3902	0.0055
4	1.2089	0.0079
6	1.2835	0.0036
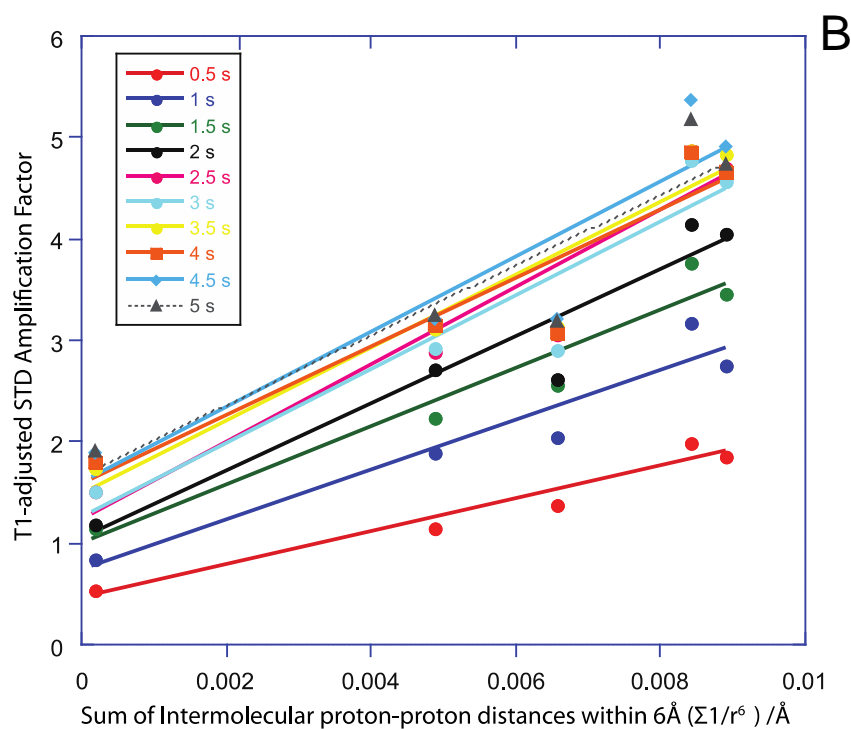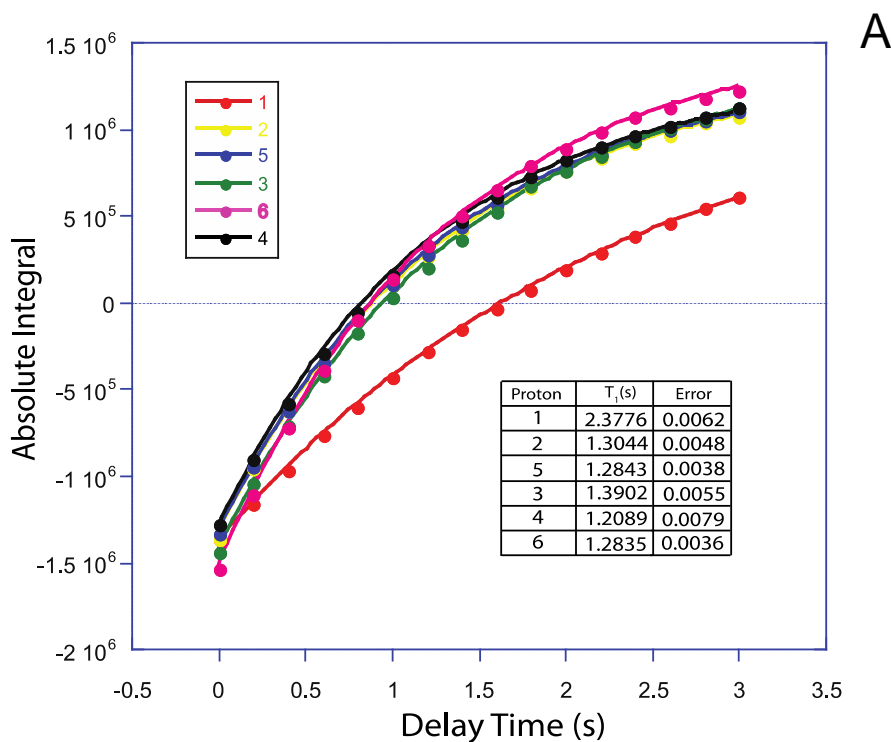
Figure 5.11: (A) Inversion recovery curves for fragment H with associated T_1 values, and (B) STD amplification factors modulated by T_1 plotted against the sum of structural restraints, for each saturation time.

5.3.2.2 Fragment I
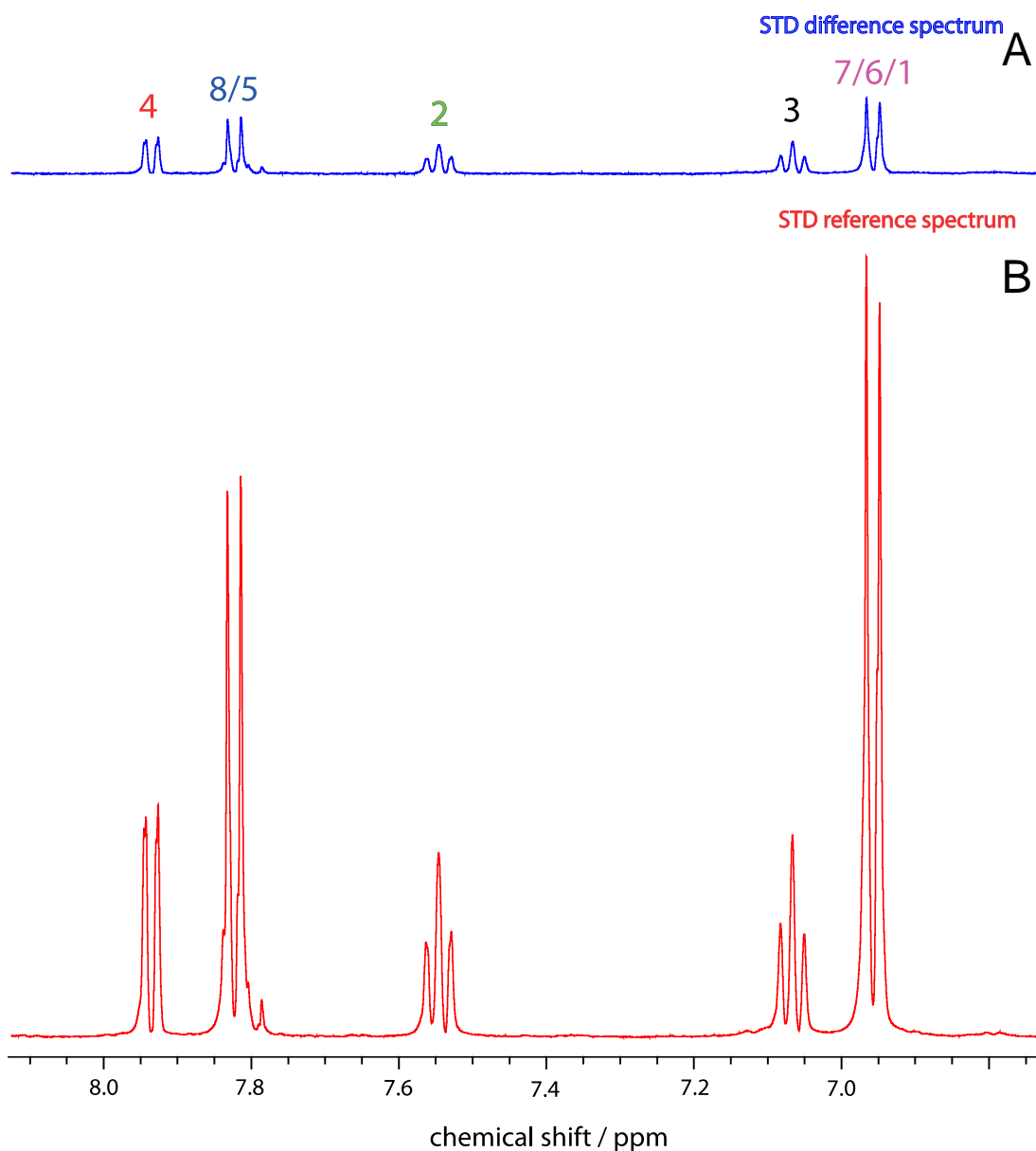
Figure 5.12: STD (A) and STD reference spectra (B) for fragment I, acquired at a saturation time of 5 seconds in this example

Fragment I STD spectra in fig. 5.12 shows positive STD signals in the presence of Ras for all protons of the ligand. The associated build up curves for this data is shown in fig. 5.13A, with the subsequent positive correlation with intermolecular structure in 5.13B. Protons 2 and 3 show the strongest STD signal, and this is reflected in the structure correlation where this half of the sulfone clearly receives a greater number of intermolecular pathway contributions for STD transfer.
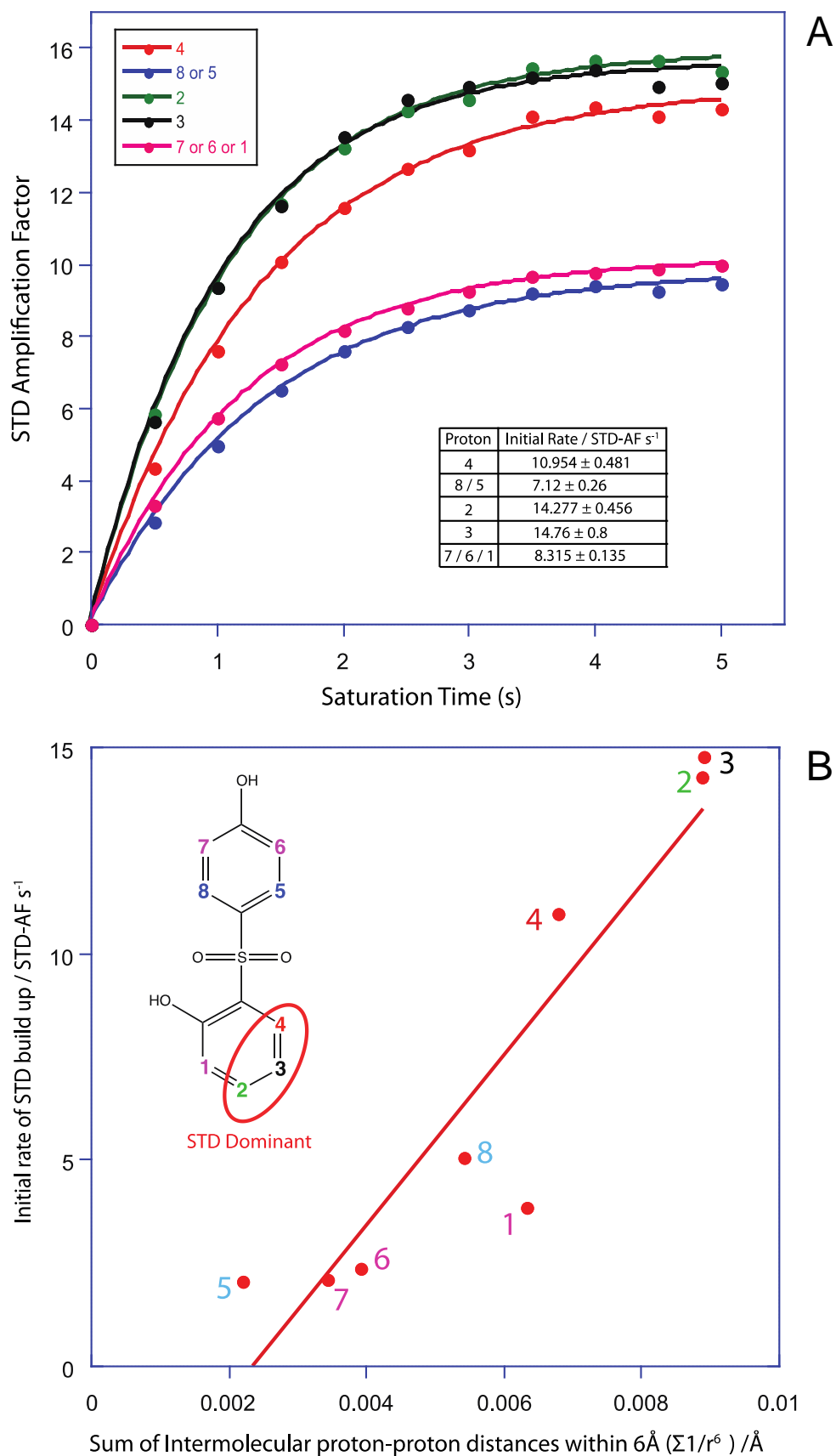
Figure 5.13: (A) STD build up curves for fragment I with associated initial rates and errors, and (B) these initial rates plotted against the sum of the intermolecular proton-proton distances derived from the crystal structure

There are good correlations between T_1-adjusted STD values and intermolecular proton-proton contacts that can be observed, as shown in fig. 5.14B.

Proton	T_1(s)	Error
4	1.7585	0.0056
8/5	1.6716	0.0042
2	1.3313	0.0045
3	1.2909	0.0085
7/6/1	1.4187	0.0032
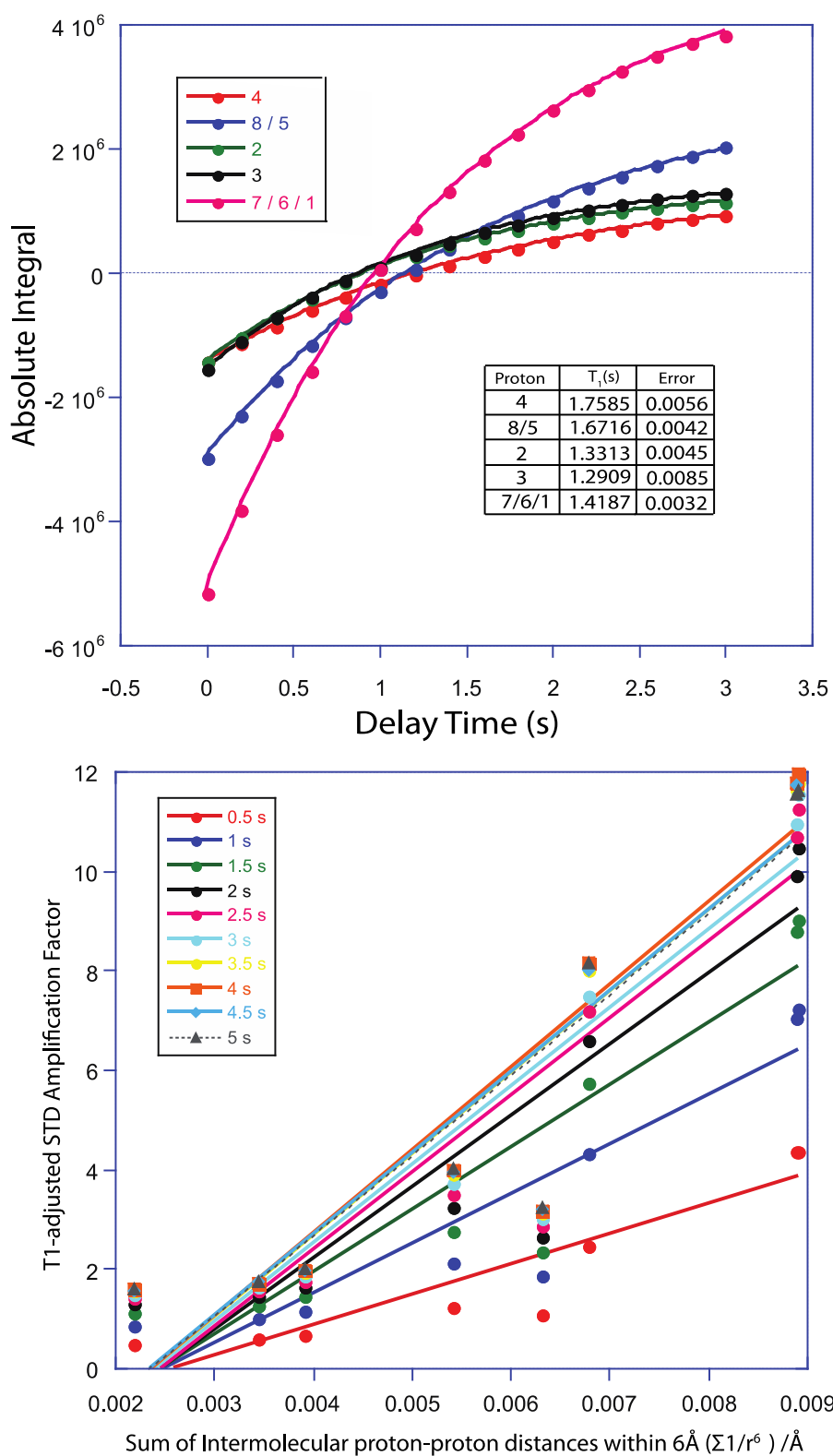
Figure 5.14: (A) Inversion recovery curves for fragment I with associated T_1 values, and (B) STD amplification factors modulated by T_1 plotted against the sum of structural restraints, for each saturation time.

5.3.2.3 Fragment J
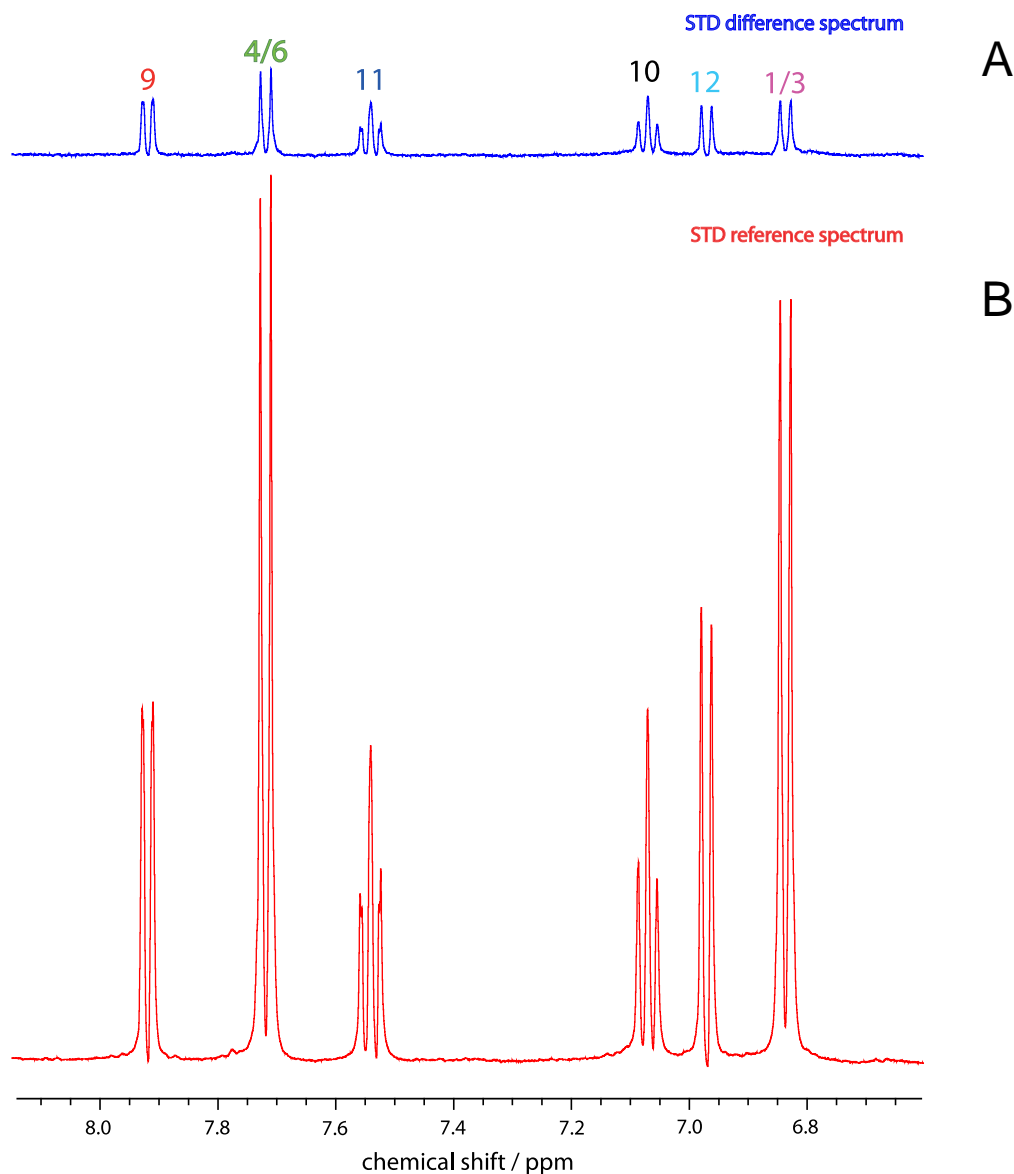
Figure 5.15: STD (A) and STD reference spectra (B) for fragment J, acquired at a saturation time of 5 seconds in this example

Fragment J STD spectra in fig. 5.15 shows positive STD signals in the presence of Ras for all protons of the ligand. Protons 10 and 11 show the greatest STD signal in fig. 5.15, and this is shown in the structure correlation where this half of the sulfone is clearly in receipt of a greater number of possible intermolecular pathway contributions for STD transfer. The 4 protons of the phenylamine group are clearly in receipt of less STD signal, and this is reflected by the structure.
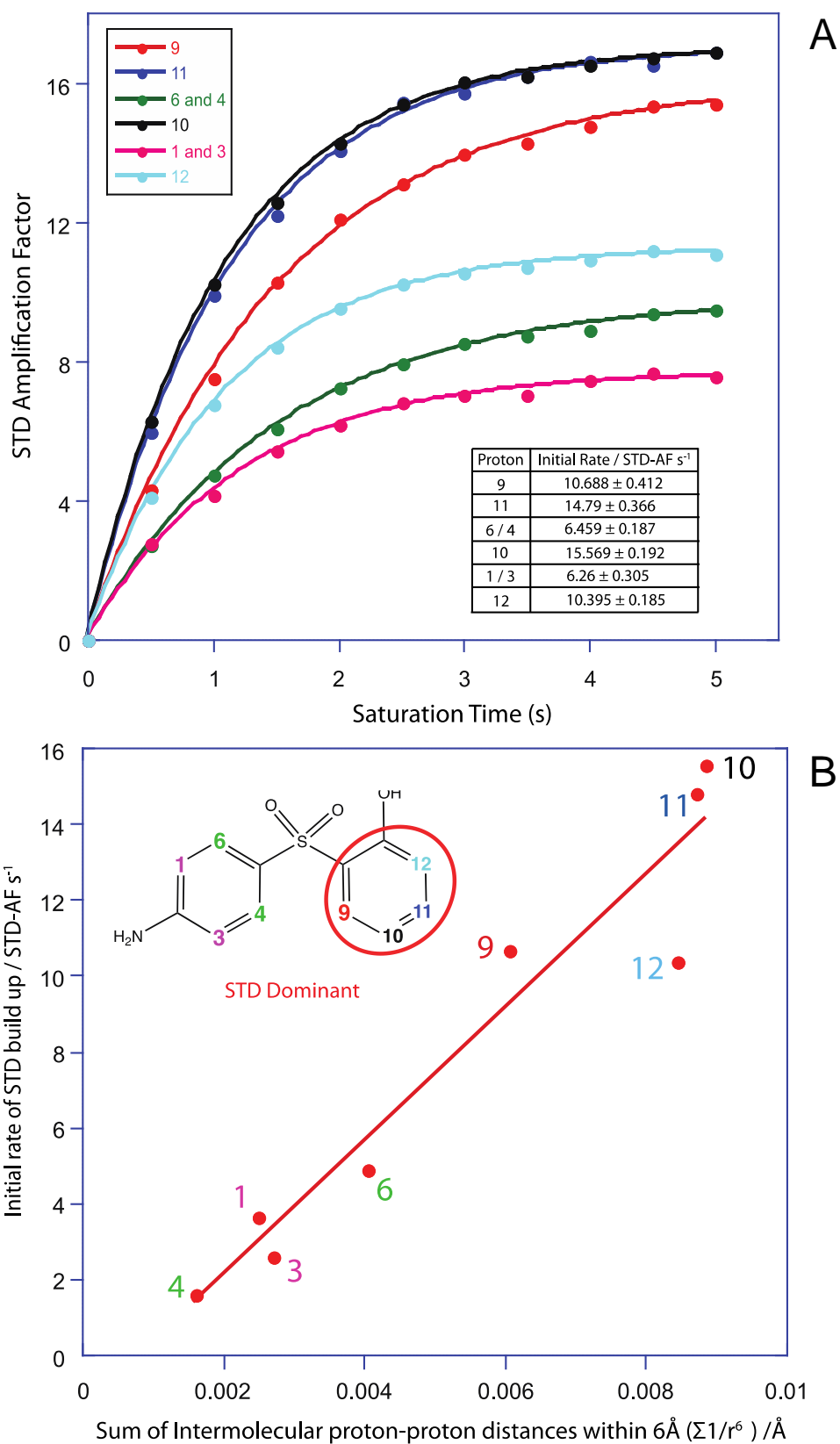
Figure 5.16: (A) STD build up curves for fragment J with associated initial rates and errors, and (B) these initial rates plotted against the sum of the intermolecular proton-proton distances derived from the crystal structure

Proton	T_1(s)	Error
9	1.7807	0.0038
4/6	1.7039	0.0032
11	1.3421	0.0039
10	1.3167	0.0086
12	1.3447	0.0053
1/3	1.4043	0.002
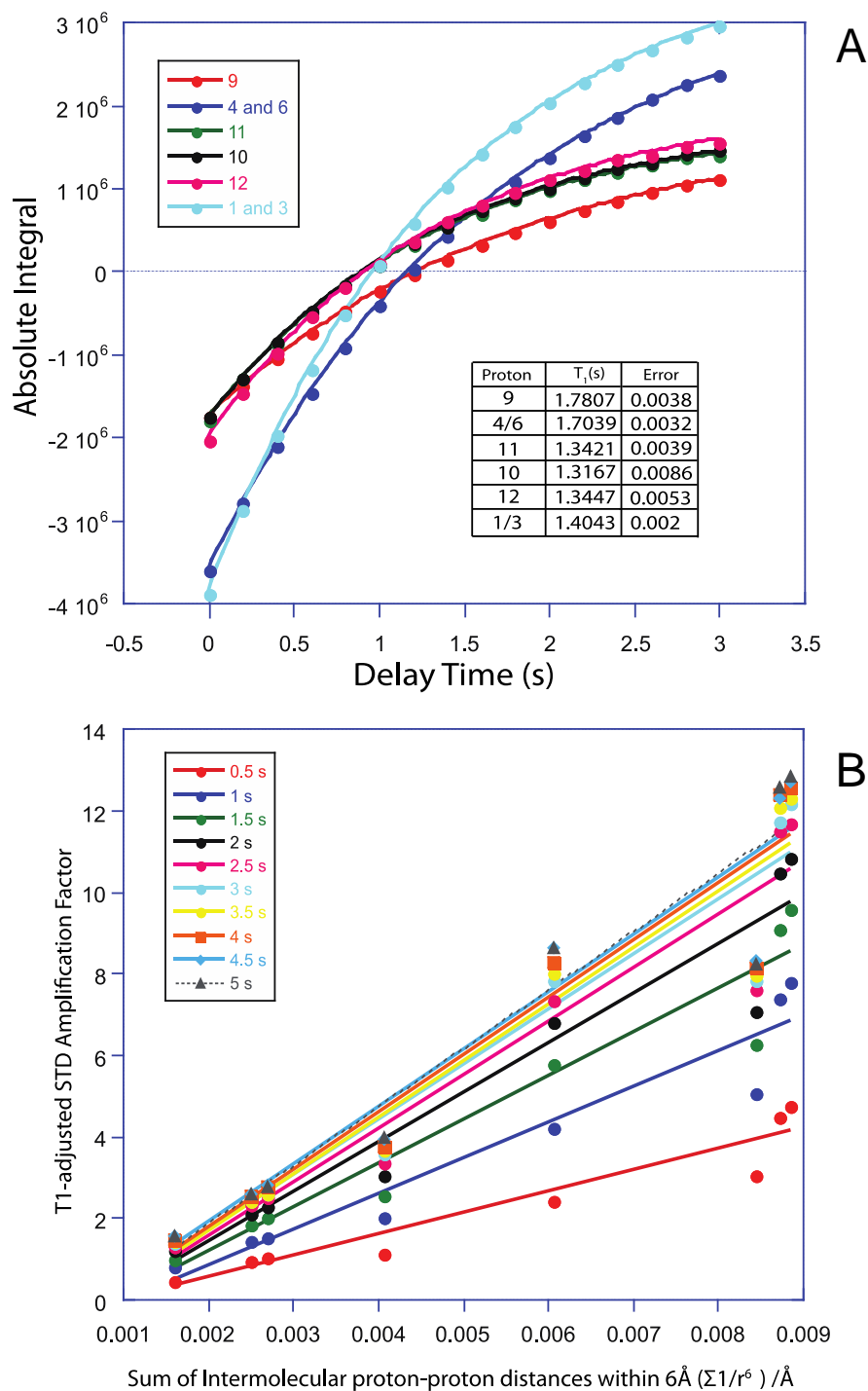
Figure 5.17: (A) Inversion recovery curves for fragment J with associated T_1 values, and (B) STD amplification factors modulated by T_1 plotted against the sum of structural restraints, for each saturation time.

Inversion recovery data for fragment J in fig. 5.17A allows us to modulate single-point STD values and correlate these values with structural restraints. An equally good correlation with intermolecular proton-proton distances is observed.

5.3.2.4 Fragment K
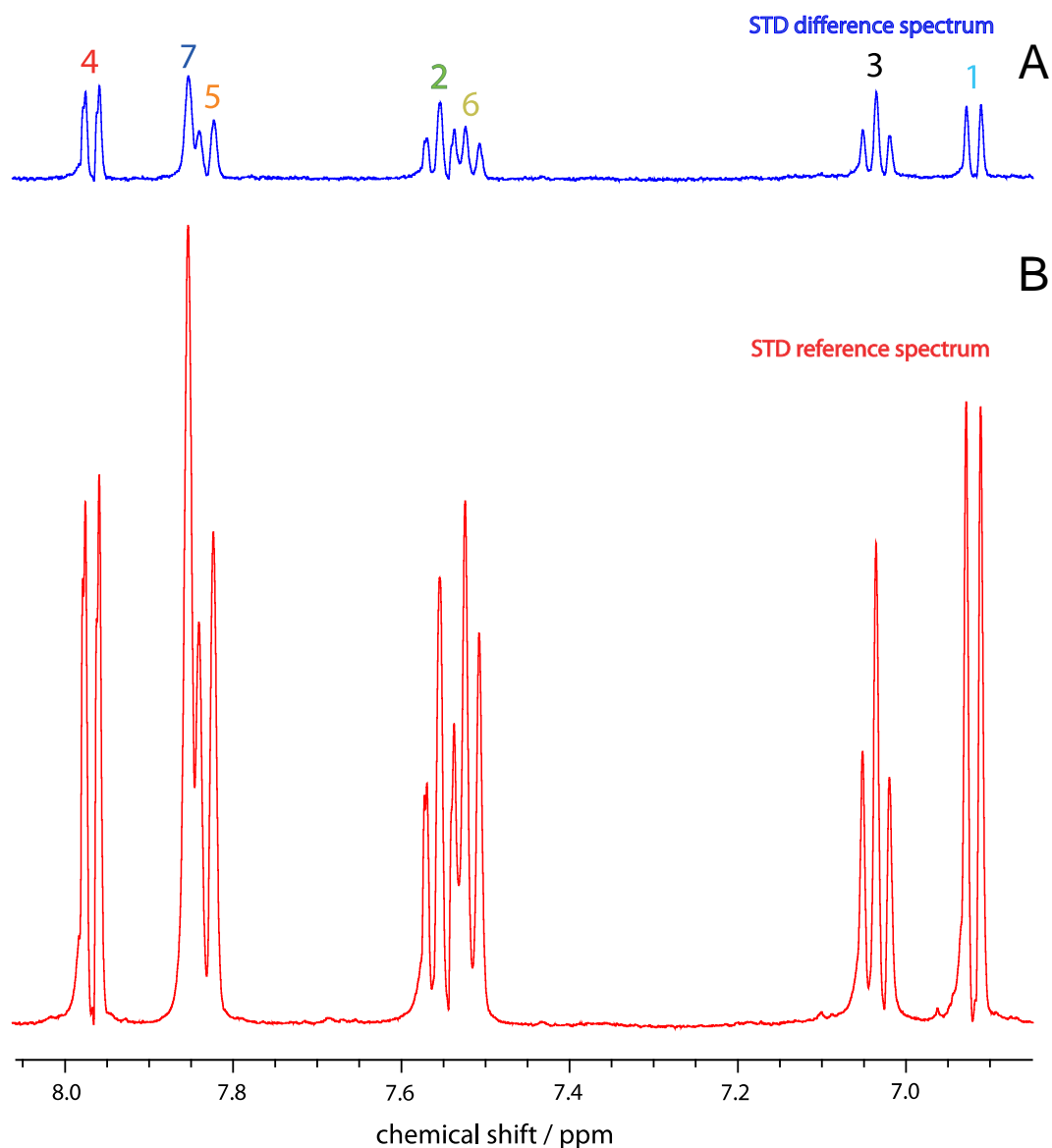
Figure 5.18: STD (A) and STD reference spectra (B) for fragment K, acquired at a saturation time of 5 seconds in this example

Fragment K STD spectra in fig. 5.18 shows positive STD signals in the presence of Ras for all protons of the ligand. The associated build up curves for this data is shown in fig. 5.19A, with the subsequent positive correlation with intermolecular structure in fig 5.19B. Protons 2 and 3 dominate the STD signal, and this is reflected in the structure correlation where this half of the sulfone clearly receives a greater number of intermolecular pathway contributions for STD transfer.
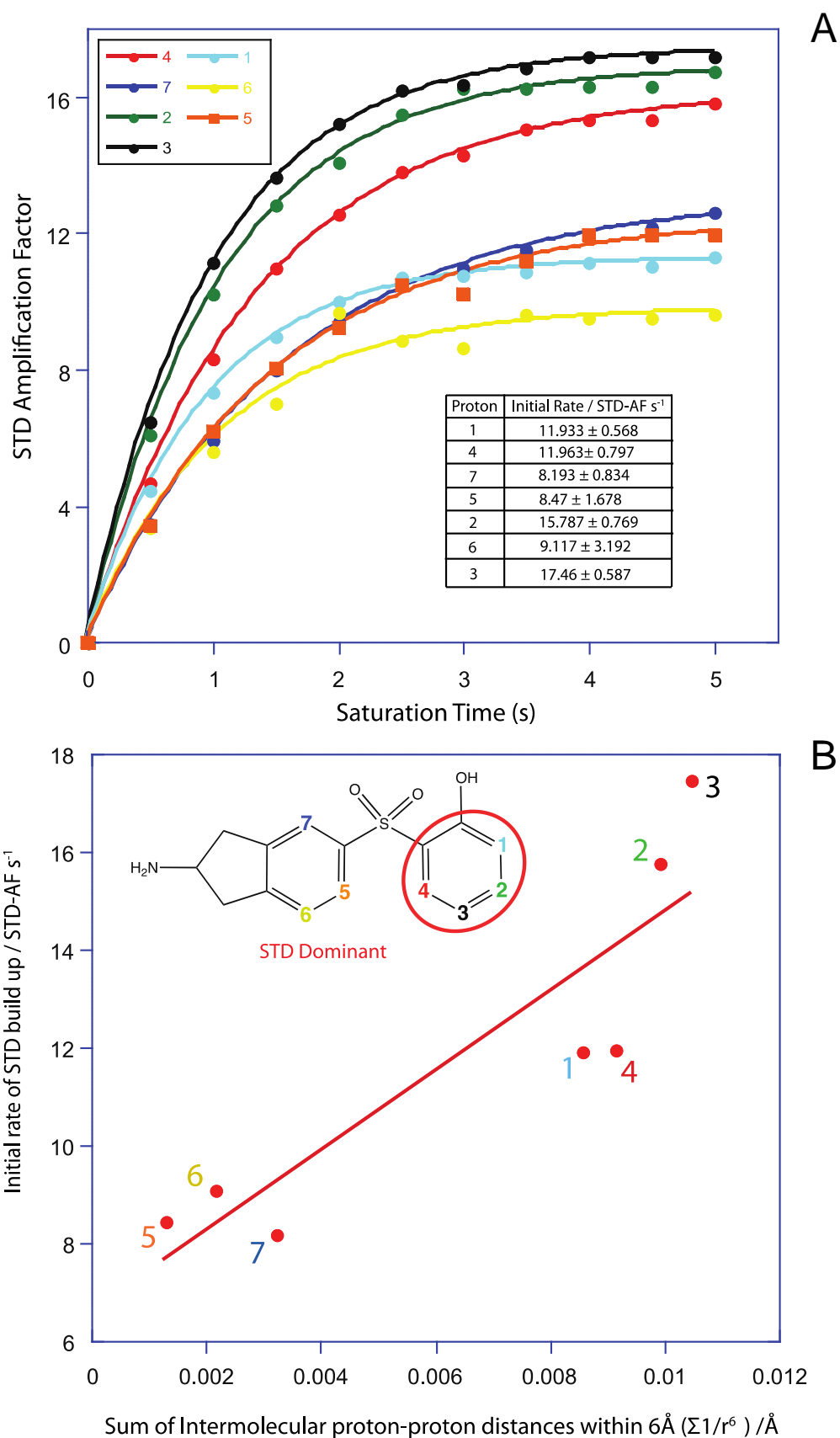
Figure 5.19: (A) STD build up curves for fragment K with associated initial rates and errors, and (B) these initial rates plotted against the sum of the intermolecular proton-proton distances derived from the crystal structure

5.3.2.5 Fragment L
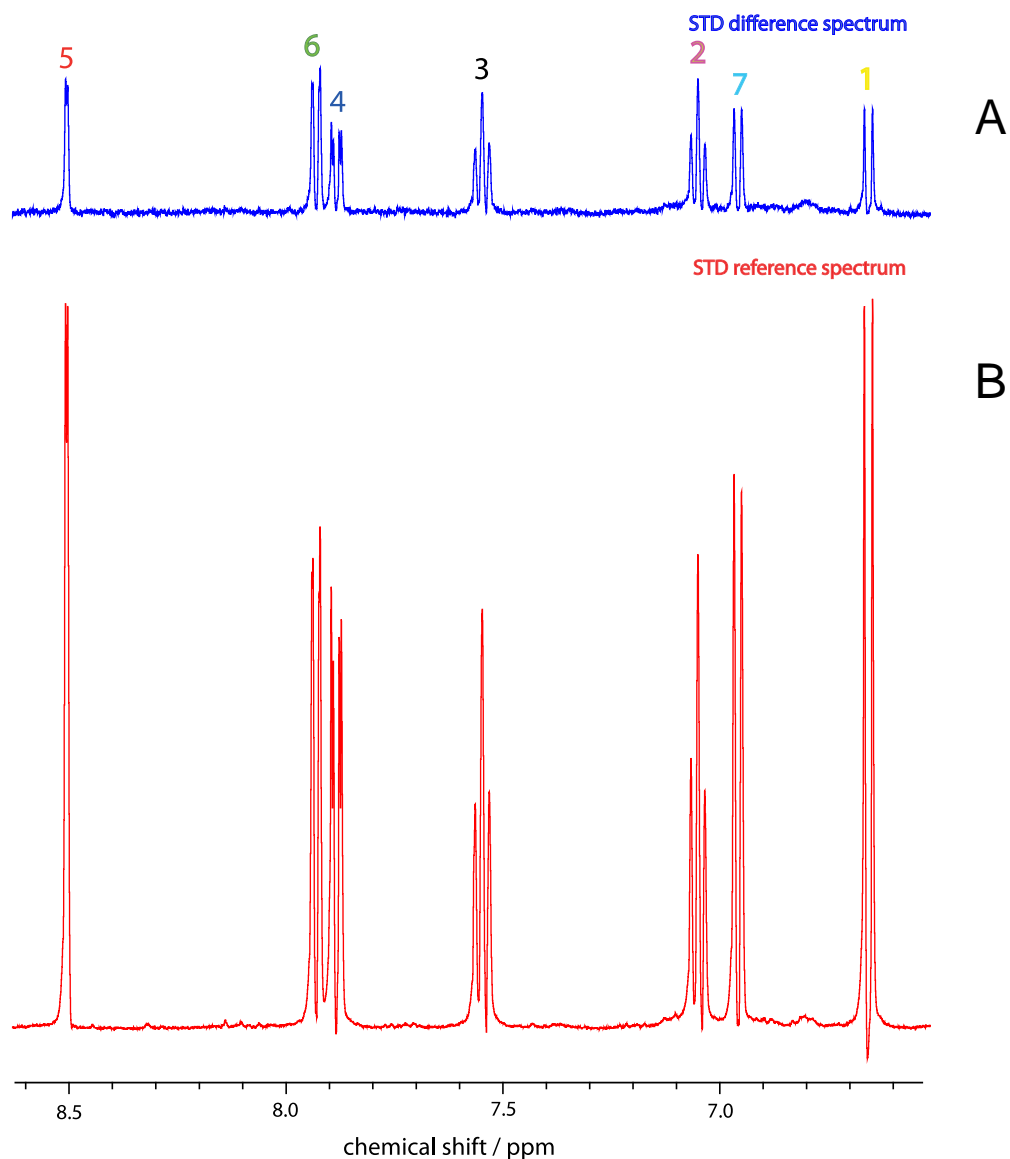
Figure 5.20: STD (A) and STD reference spectra (B) for fragment L, acquired at a saturation time of 5 seconds in this example

Fragment L STD spectra in fig. 5.20 show positive STD signals in the presence of Ras for all protons of the ligand. Proton 3 dominates the STD signal according to build ups in fig. 5.21, whilst the remainder of the phenolic ring is fairly STD dominant, and this is reflected in the structure correlation where this half of the fragment clearly receives a greater number of intermolecular pathway contributions for STD transfer.

The 3 protons of the phenylamine group are clearly less STD dominant, and this is reflected by the structure
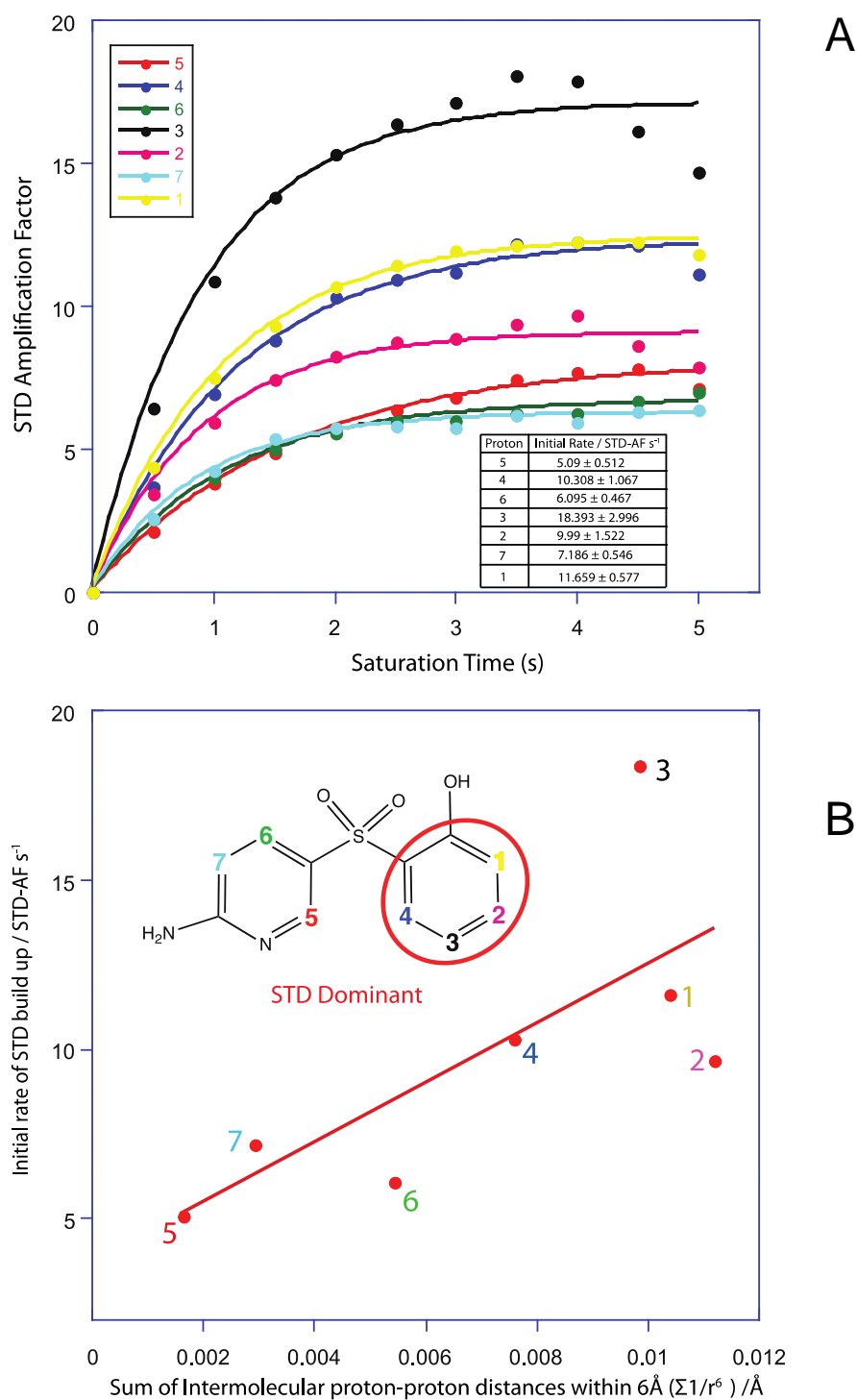
Figure 5.21: (A) STD build up curves for fragment L with associated initial rates and errors, and (B) these initial rates plotted against the sum of the intermolecular proton-proton distances derived from the crystal structure

Proton	$T_1(s)$	Error
5	2.5083	0.0076
6	1.7825	0.0052
4	1.7264	0.0052
3	1.327	0.0047
2	1.3121	0.01
7	1.3406	0.0054
1	1.373	0.0044
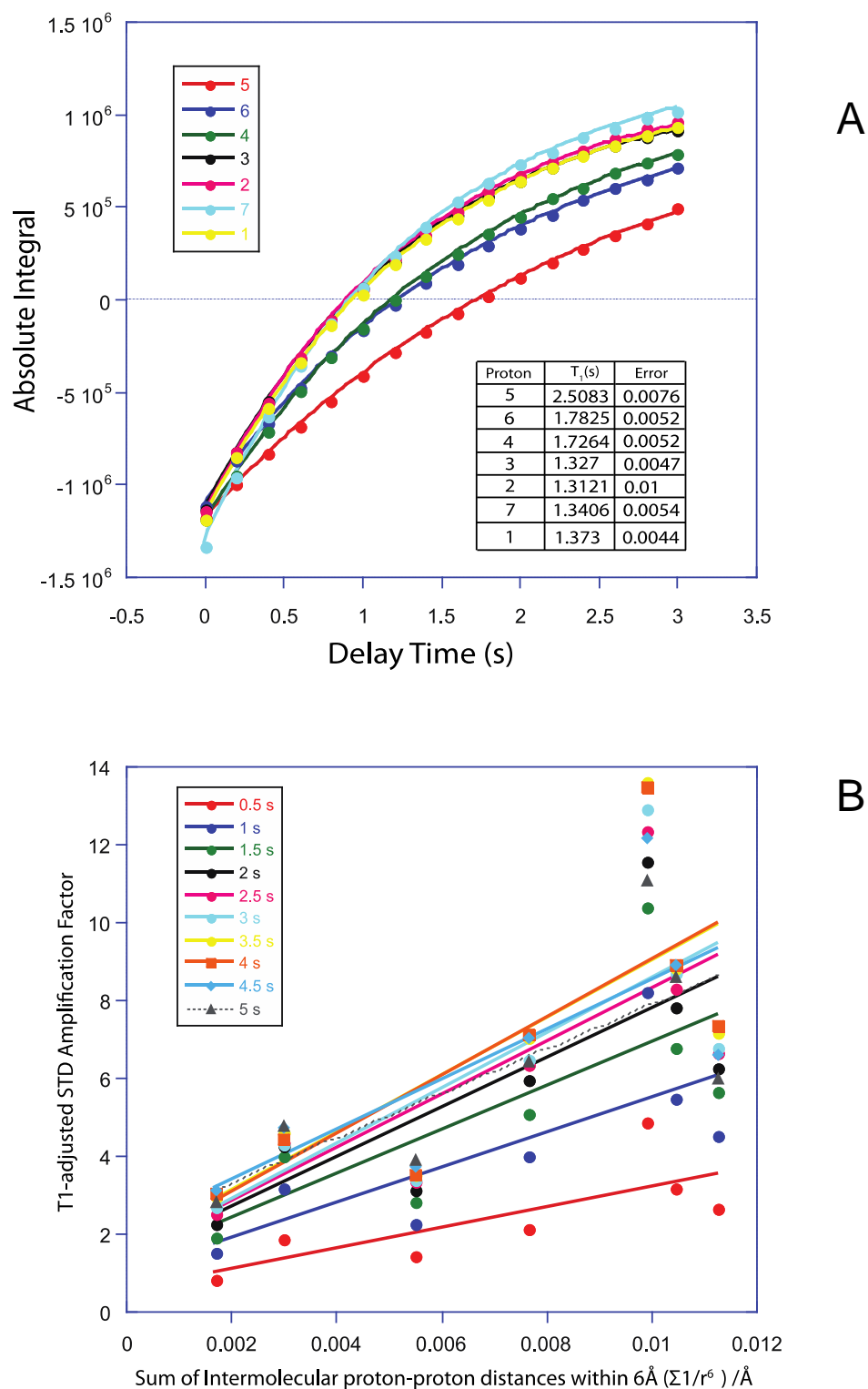
Figure 5.22: (A) Inversion recovery curves for fragment L with associated T1 values, and (B) STD amplification factors modulated by T1 plotted against the sum of structural restraints, for each saturation time.

Inversion recovery of fragment L in fig. 5.22A allows us to modulate single-point

STD values and correlate these values with structural restraints.

5.3.3 Quantitative LOGSY

5.3.3.1 Fragment H
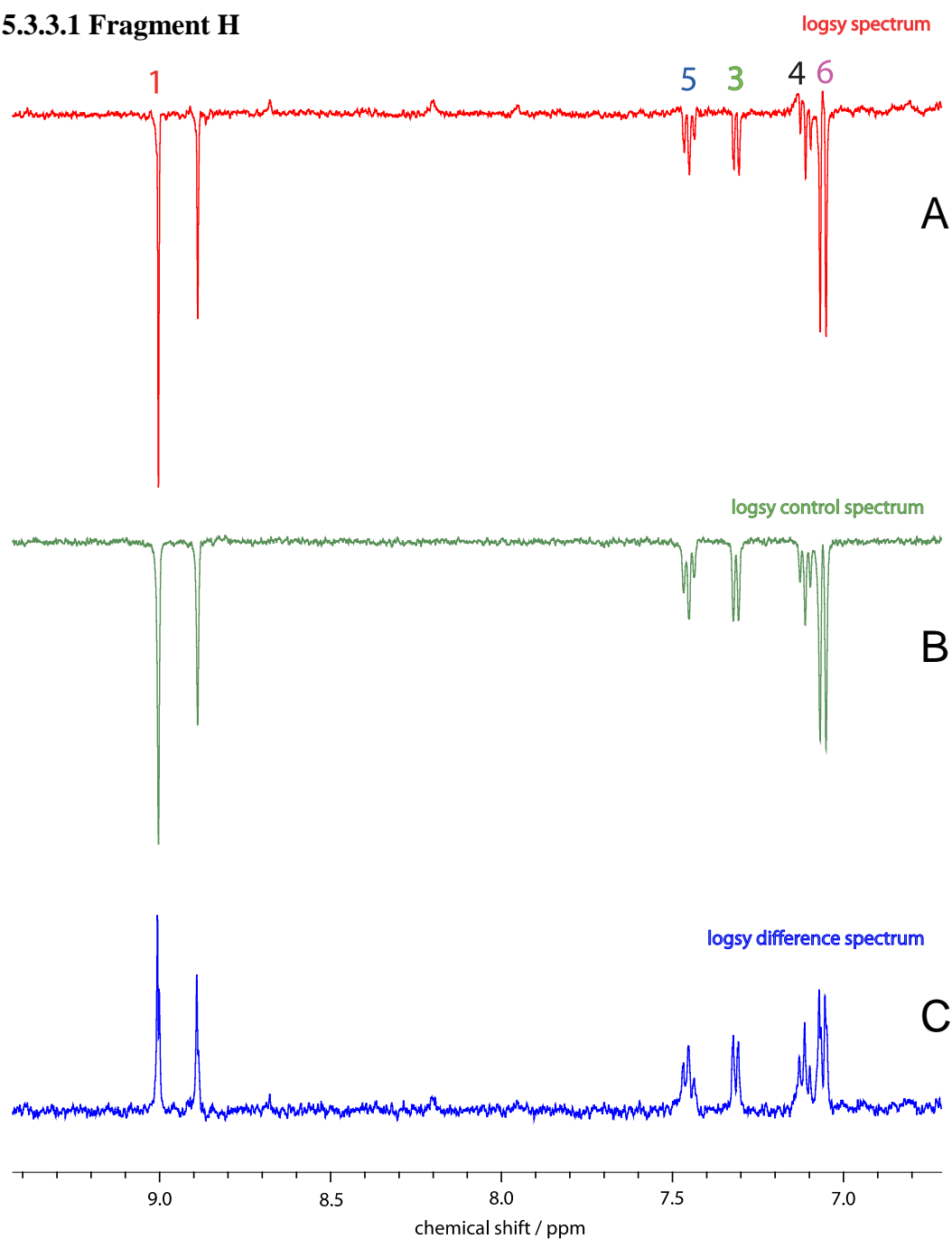
Figure 5.23: LOGSY (A), control (B) and difference (C) spectra for fragment H binding to Ras

Negative LOGSY signals for all protons of fragment H become positive once the reference is taken into account in fig. 5.23c. Fig. 5.24 shows how proton 6 is the signal with the greatest 'LOGSY enhancement' in terms of signal integral in the LOGSY difference spectrum.
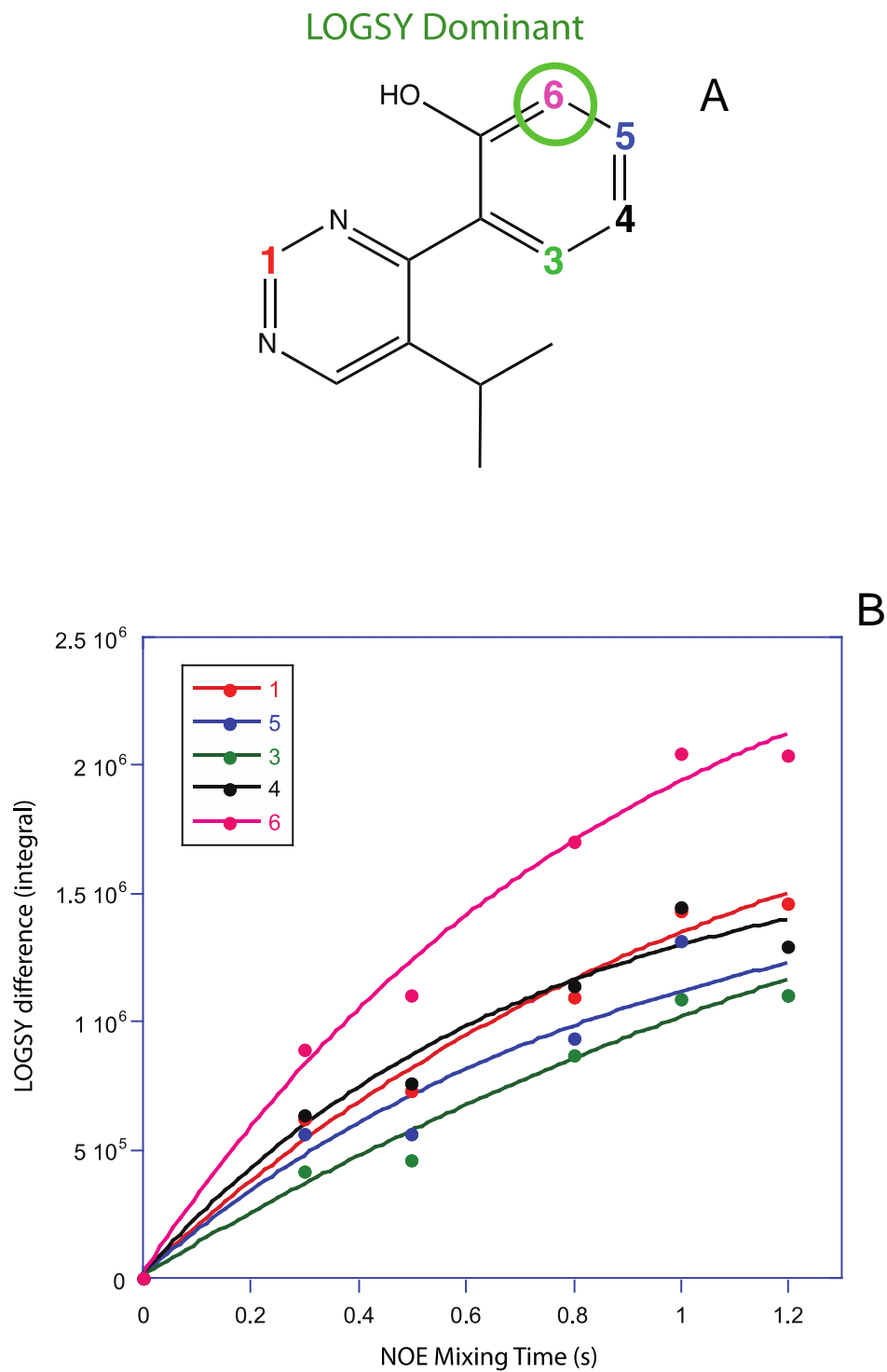
Figure 5.24: (A) Fragment H displayed with the highlighted region of LOGSY dominance, and (B) the LOGSY build up curves for quantitative LOGSY data of this fragment in the presence of Ras

5.3.3.2 Fragment I
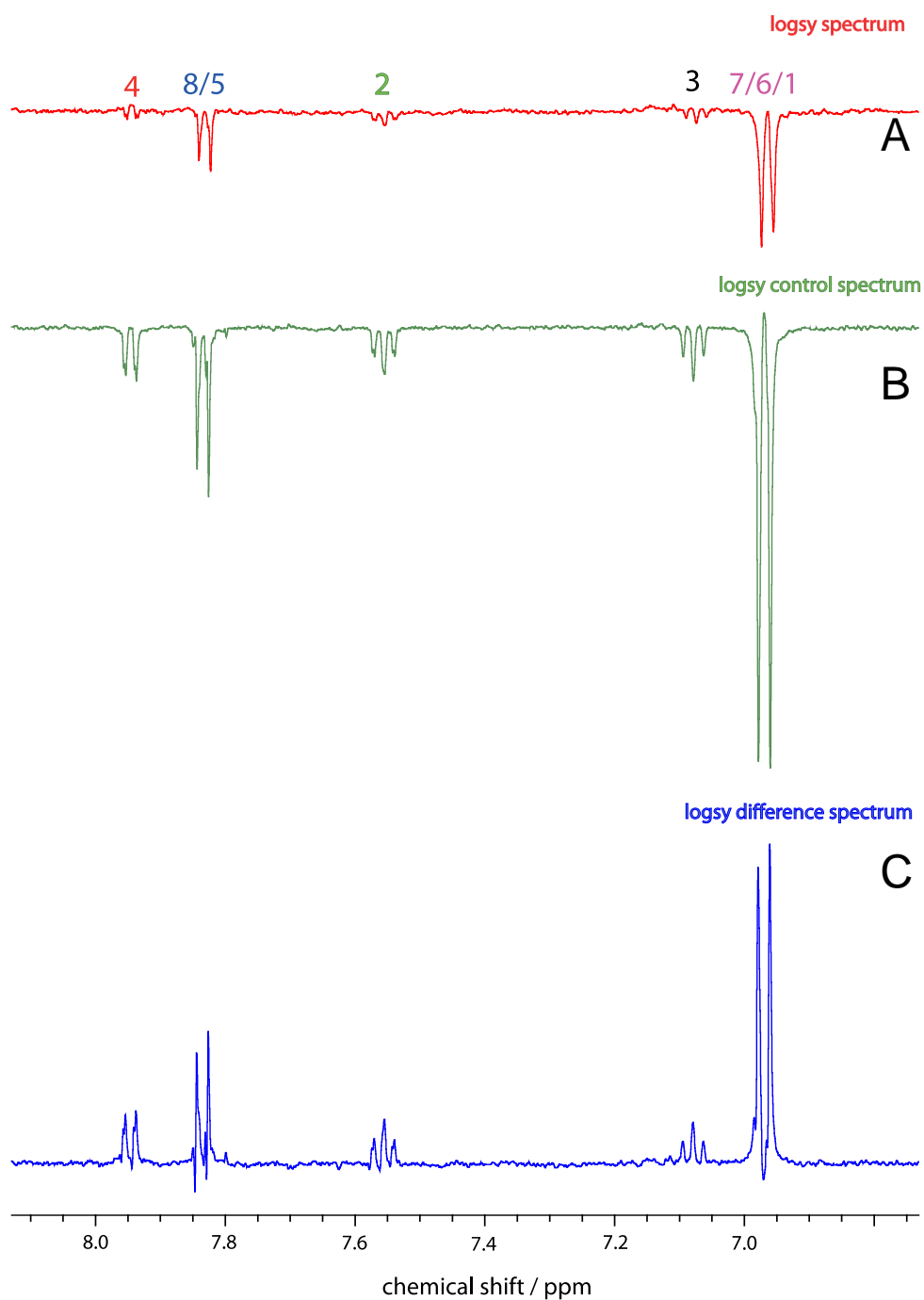
Figure 5.25: LOGSY (A), control (B), and difference (C) spectra for fragment I binding to Ras

Small negative LOGSY signals for all protons of fragment I become positive once the reference is taken into account in fig. 5.25. Fig. 5.26 shows how the signal for protons 1, 6 and 7 has the greatest LOGSY enhancement. However, it may be difficult to

conclude too much from this as 3 overlapping protons appearing at the same frequency obscures any valid interpretation
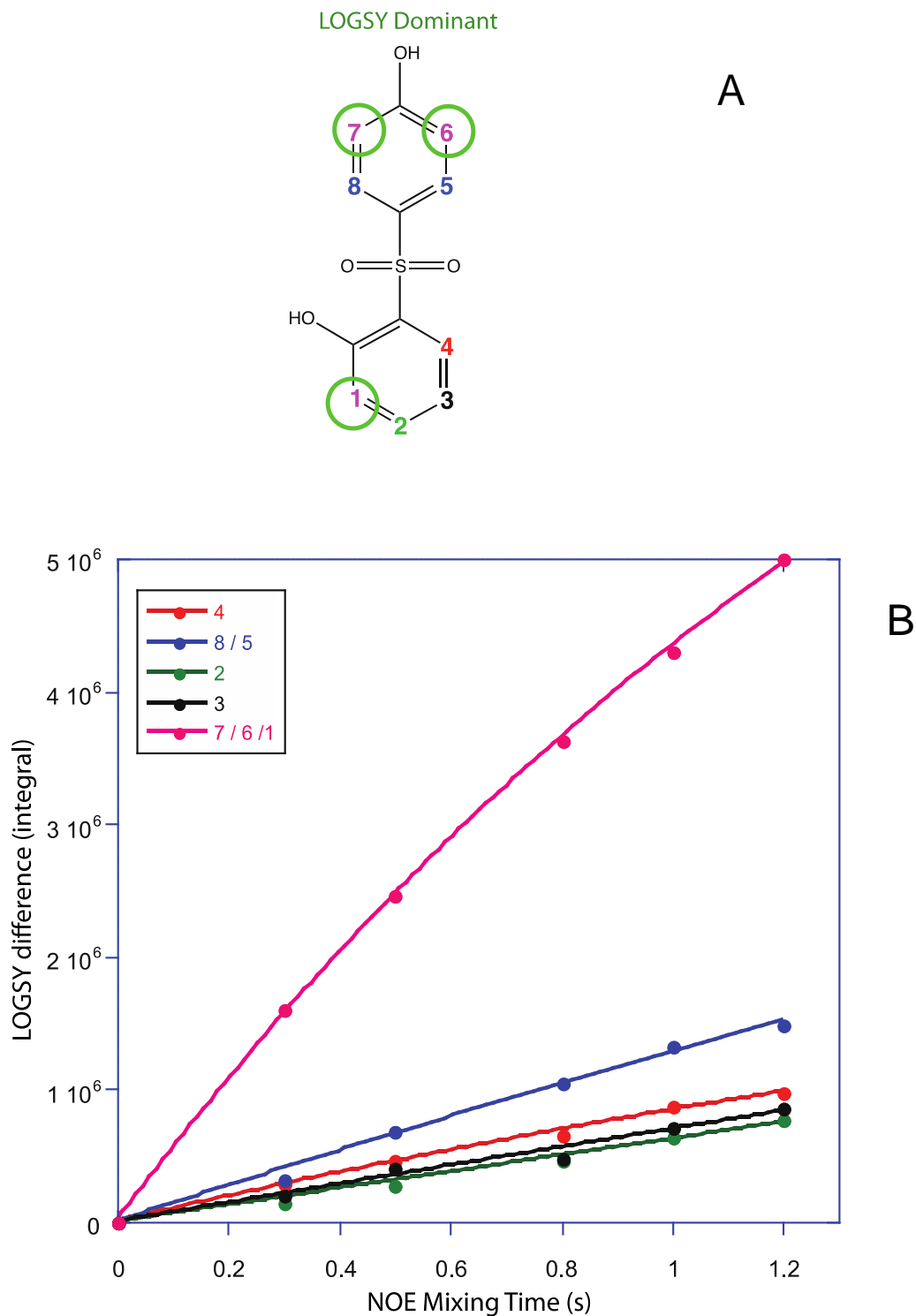
Figure 5.26: (A) Fragment I displayed with the highlighted regions of LOGSY dominance, and (B) the LOGSY build up curves for quantitative LOGSY data in the presence of Ras

5.3.3.3 Fragment J
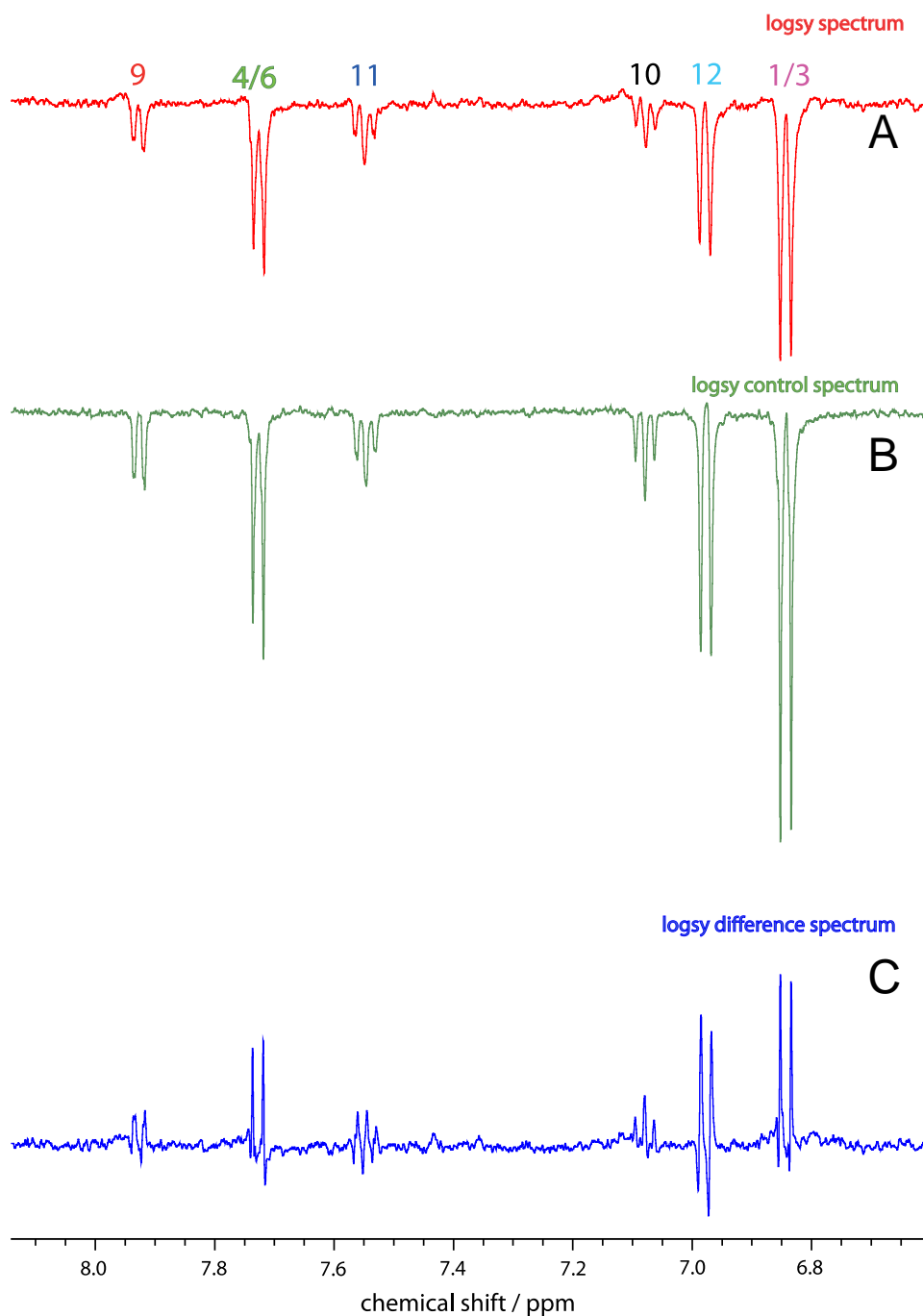
Figure 5.27: LOGSY (A), control (B), and difference (C) spectra for fragment J binding to Ras

Again, negative LOGSY signals produce a completely positive LOGSY difference spectrum for fragment J in the presence of Ras once the reference is taken into

account. Protons 1 and 3 of the phenylamine ring have the greatest LOGSY enhancement.
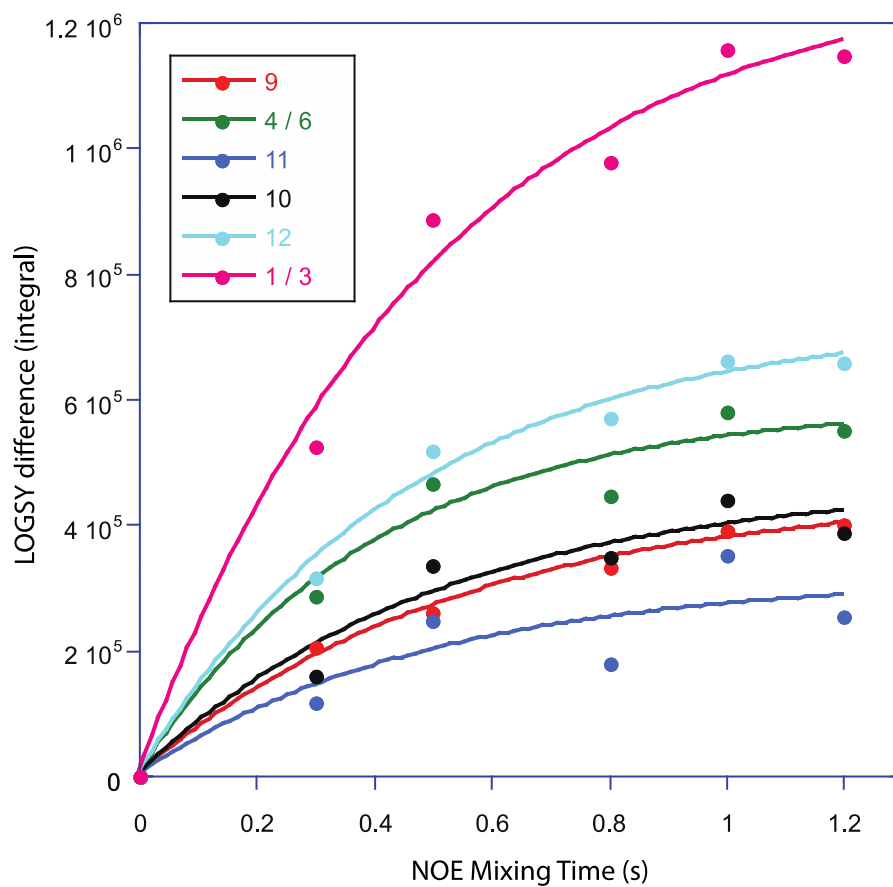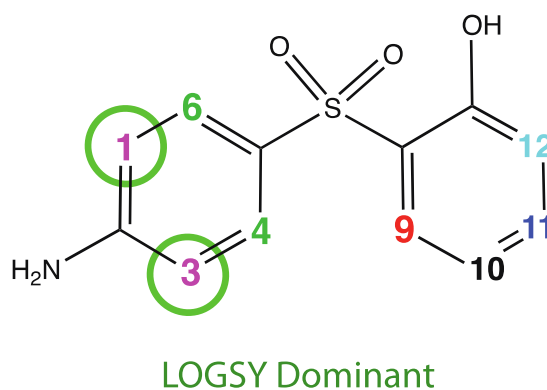
Figure 5.28: (A) Fragment J displayed with the highlighted region of LOGSY dominance, and (B) the LOGSY build up curves for quantitative LOGSY data of this fragment in the presence of Ras

5.3.3.4 Fragment K
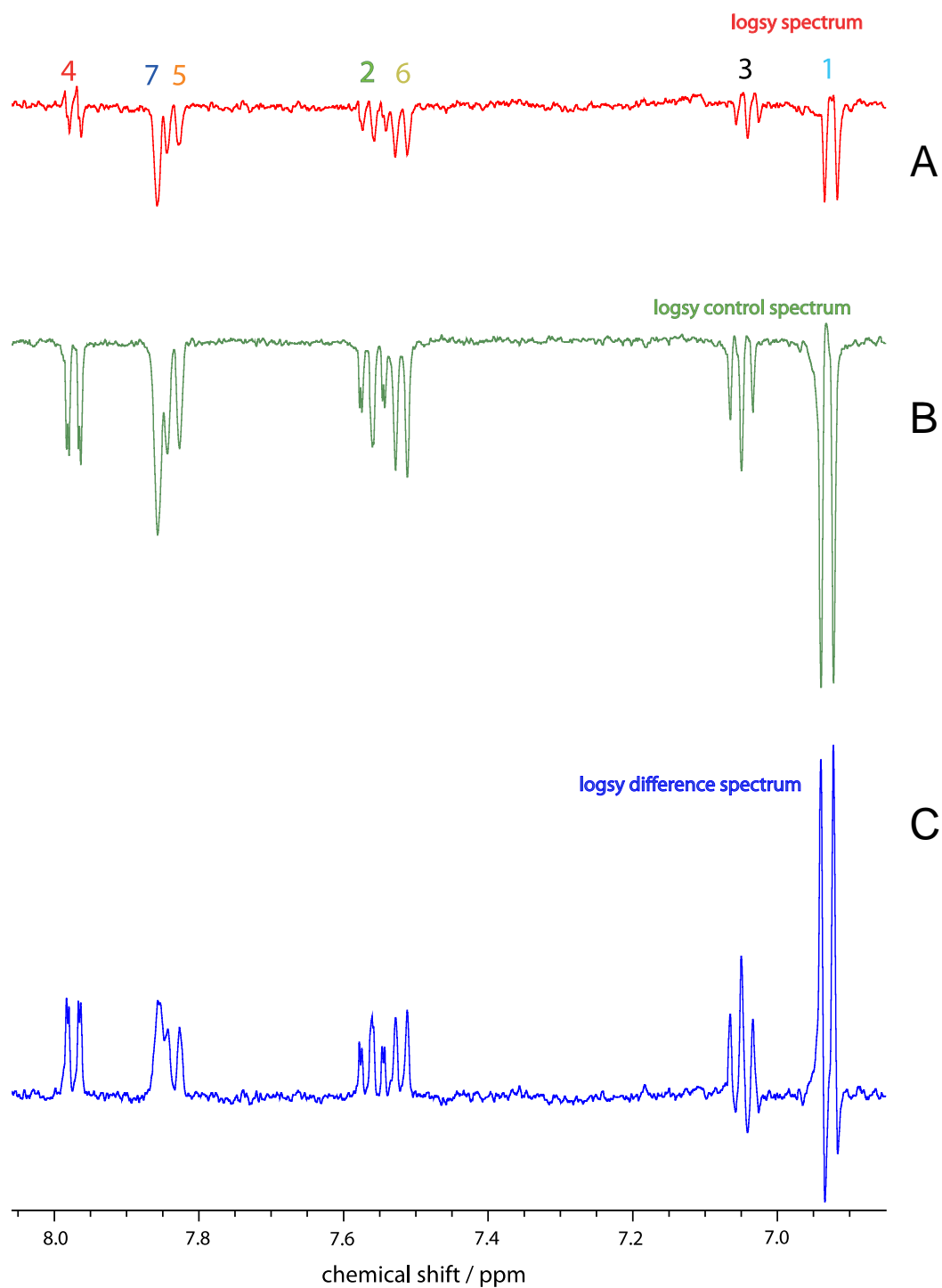
Figure 5.29: LOGSY (A), control (B), and difference (C) spectra for fragment K binding to Ras

Negative LOGSY signals in (A) again produce a positive LOGSY difference spectrum in (C) for fragment K. Proton 1 of the phenol ring receives the greatest LOGSY enhancement.

This can be observed in the LOGSY build up curve.
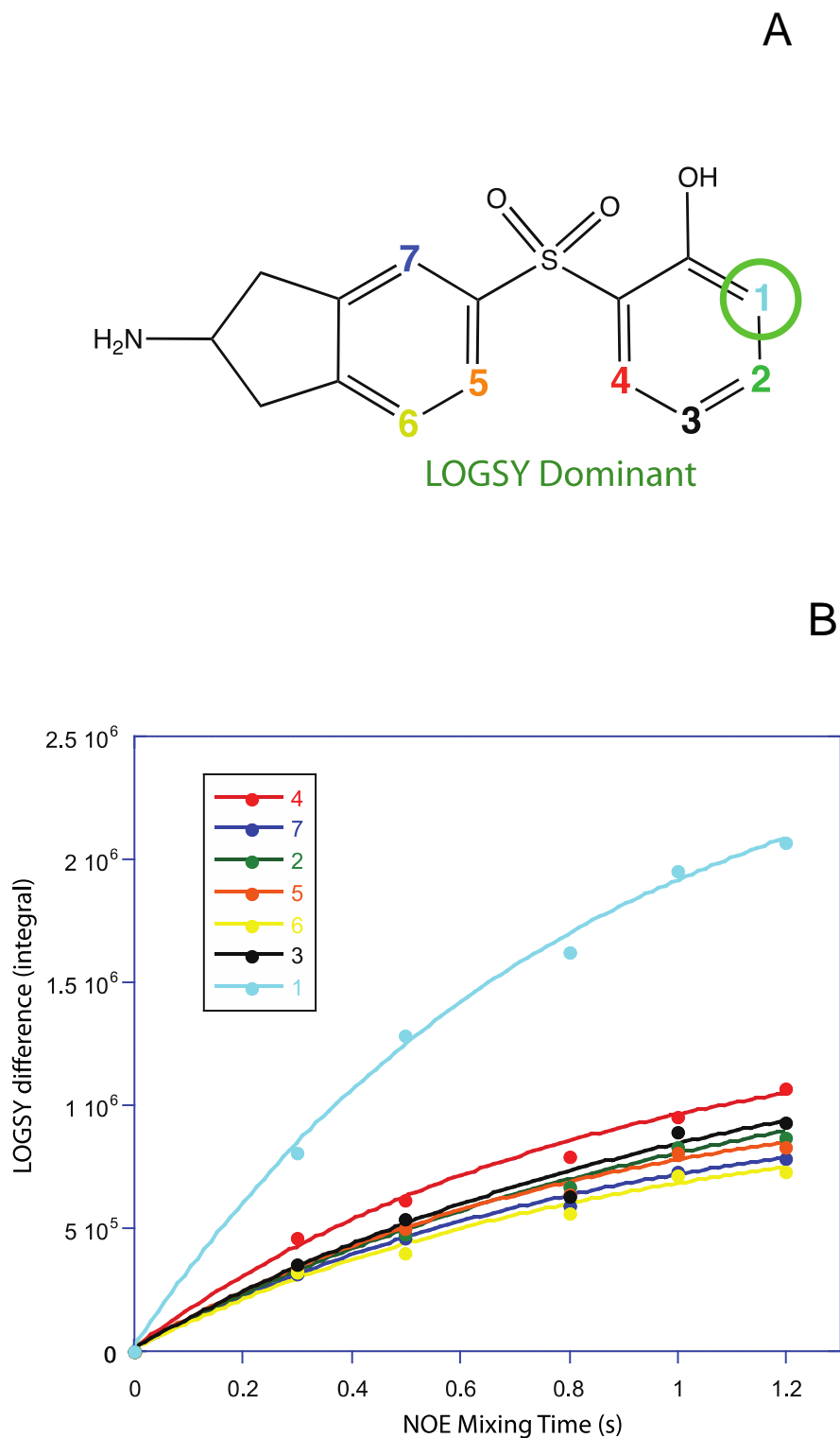
Figure 5.30: (A) Fragment K displayed with the highlighted region of LOGSY dominance, and (B) the LOGSY build up curves for quantitative LOGSY data of this fragment in the presence of Ras

5.3.3.5 Fragment L
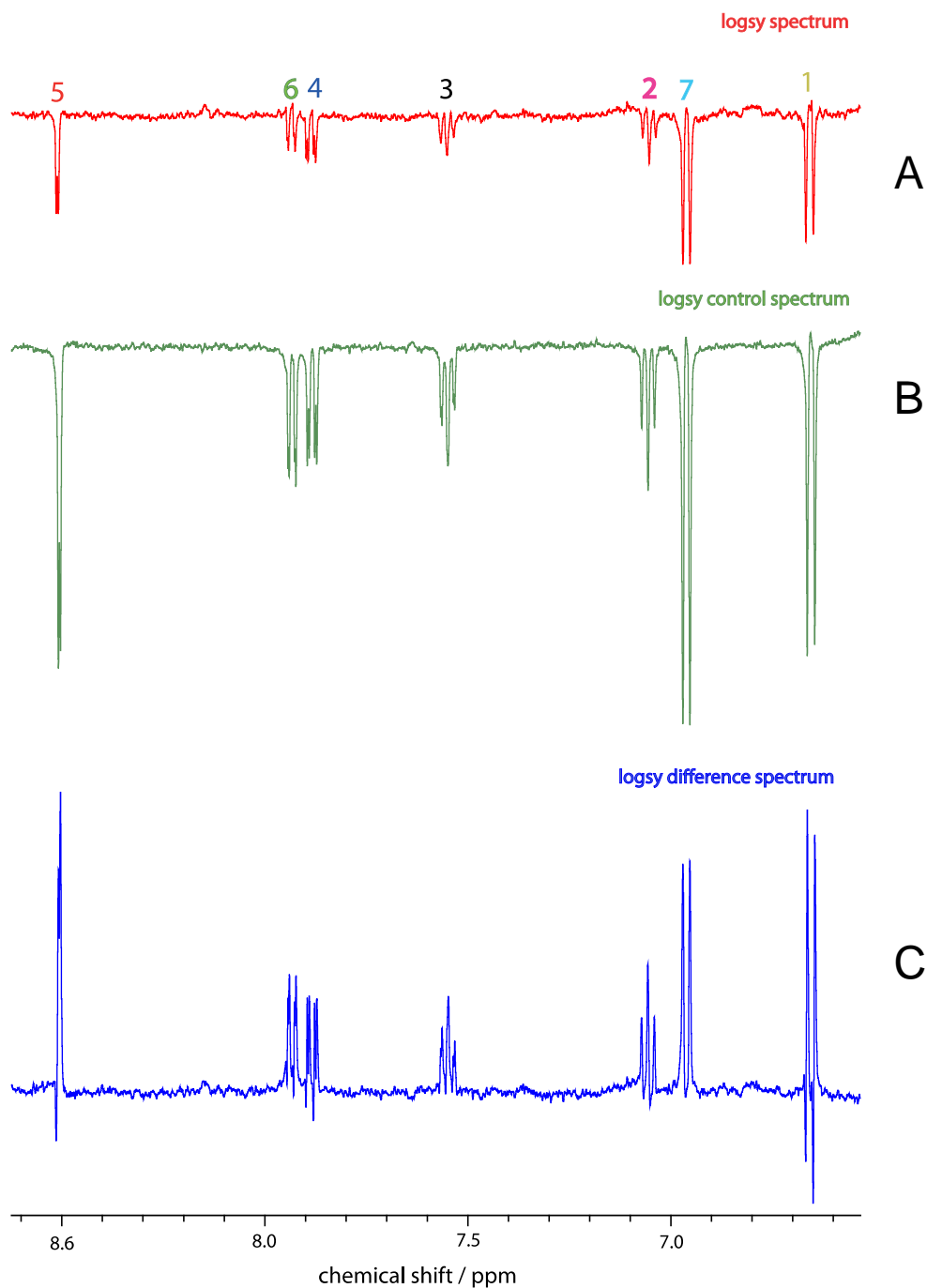
Figure 5.31: LOGSY (A), control (B), and difference (C) spectra for fragment L binding to Ras

Following the trends for all of the other sulfone fragments, a positive LOGSY spectrum for all signals of fragment L in the presence of Ras is produced from component spectra.

In this instance a full LOGSY build up curve was not possible, but taking the LOGSY difference value based on a single NOE mixing period offers up proton 1 as the dominant signal, which would tally with other similar fragments within the chemotype.
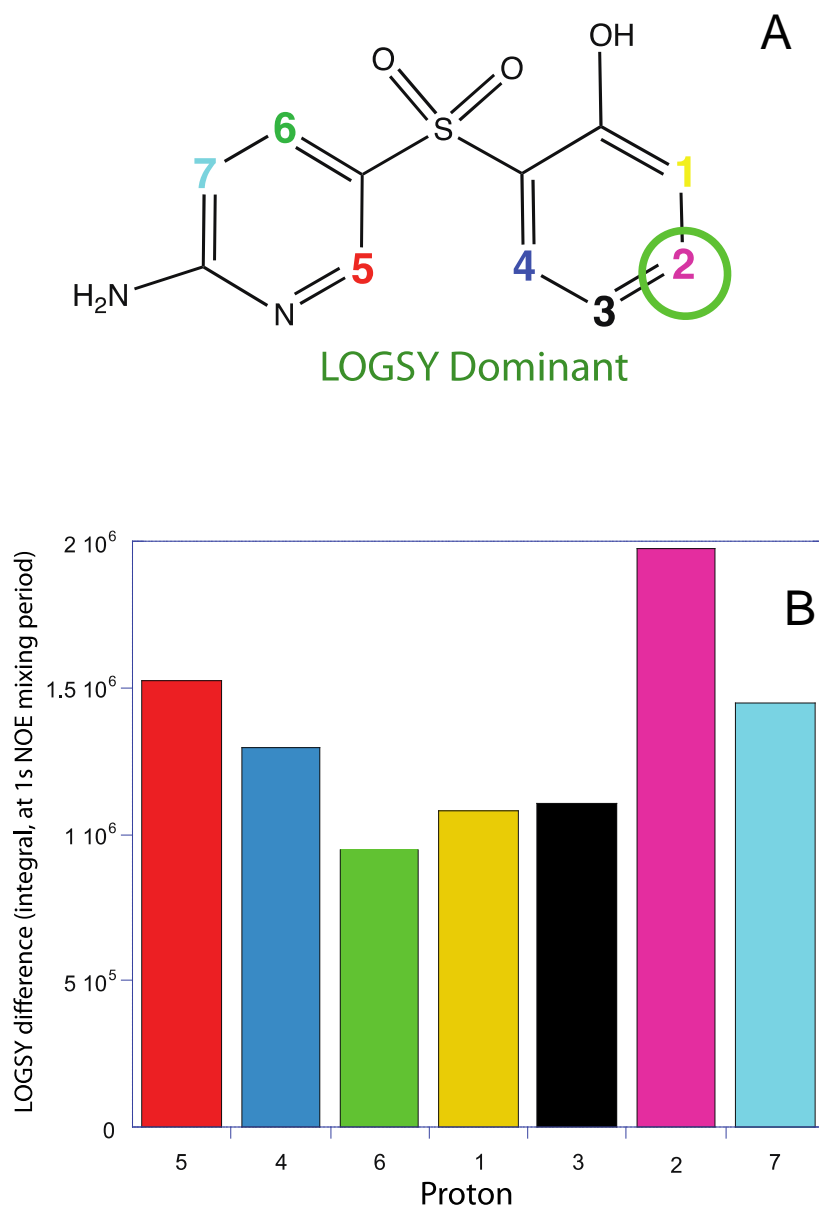
Figure 5.32: (A) Fragment L displayed with the highlighted region of LOGSY dominance, and (B) the LOGSY difference integrals (at 1s NOE mixing period) of this fragment in the presence of Ras

5.3.4 Two-site binding

5.3.4.1 Fragment M (500 µM) + O (5 mM)
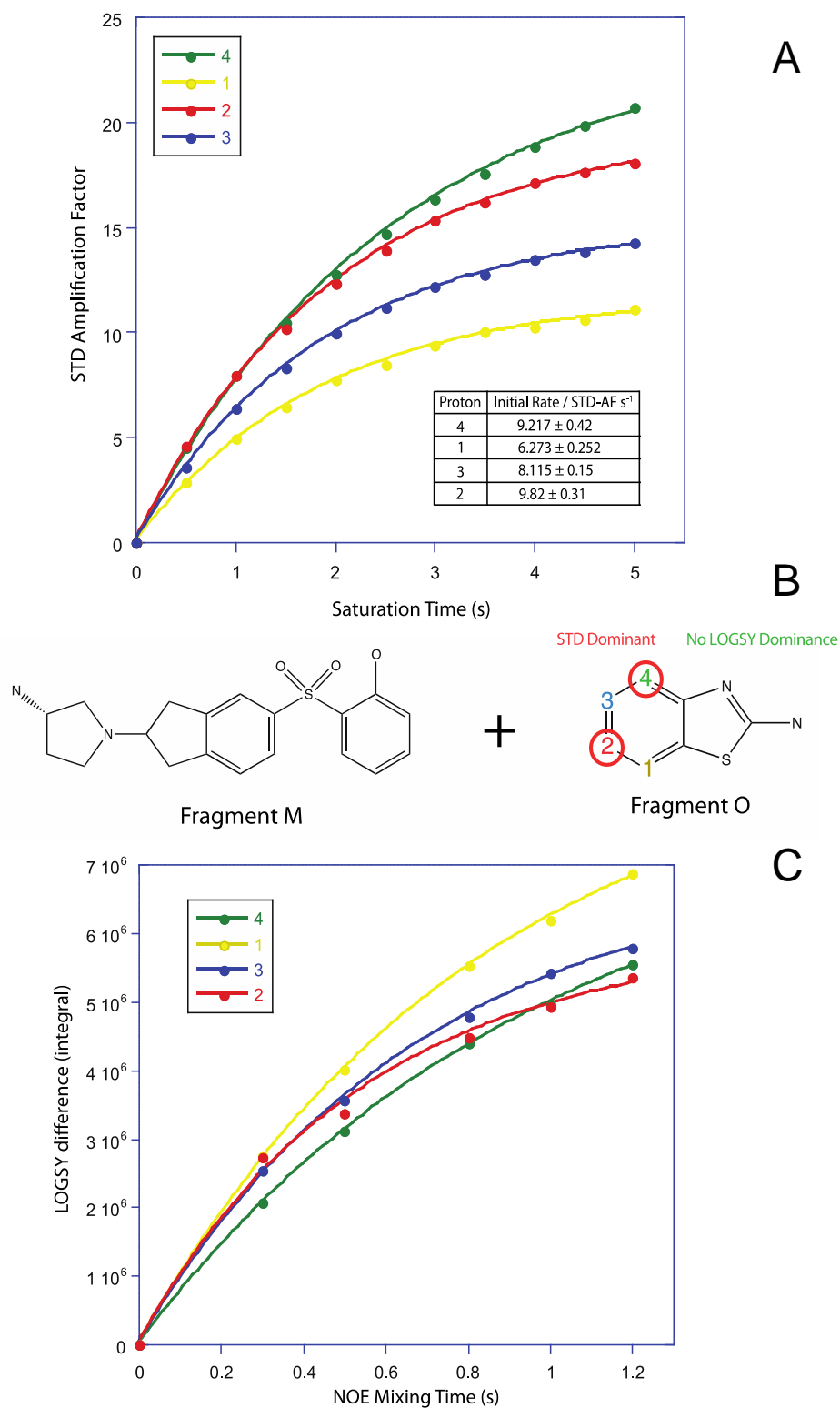
Figure 5.33: NMR data for fragment O bound to the Ras 2nd site, after saturation of the first site with fragment M. (A) STD build up curves and (B) LOGSY build up curves highlight protons 2 and 4 as STD dominant, with no LOGSY dominant protons (C)

5.3.4.2 Fragment M (500 µM) + P (5 mM)

Proton	Initial Rate / STD-AF s^{-1}
2	10.17 ± 1.289
1	12.96 ± 0.89
3	14.247 ± 0.9
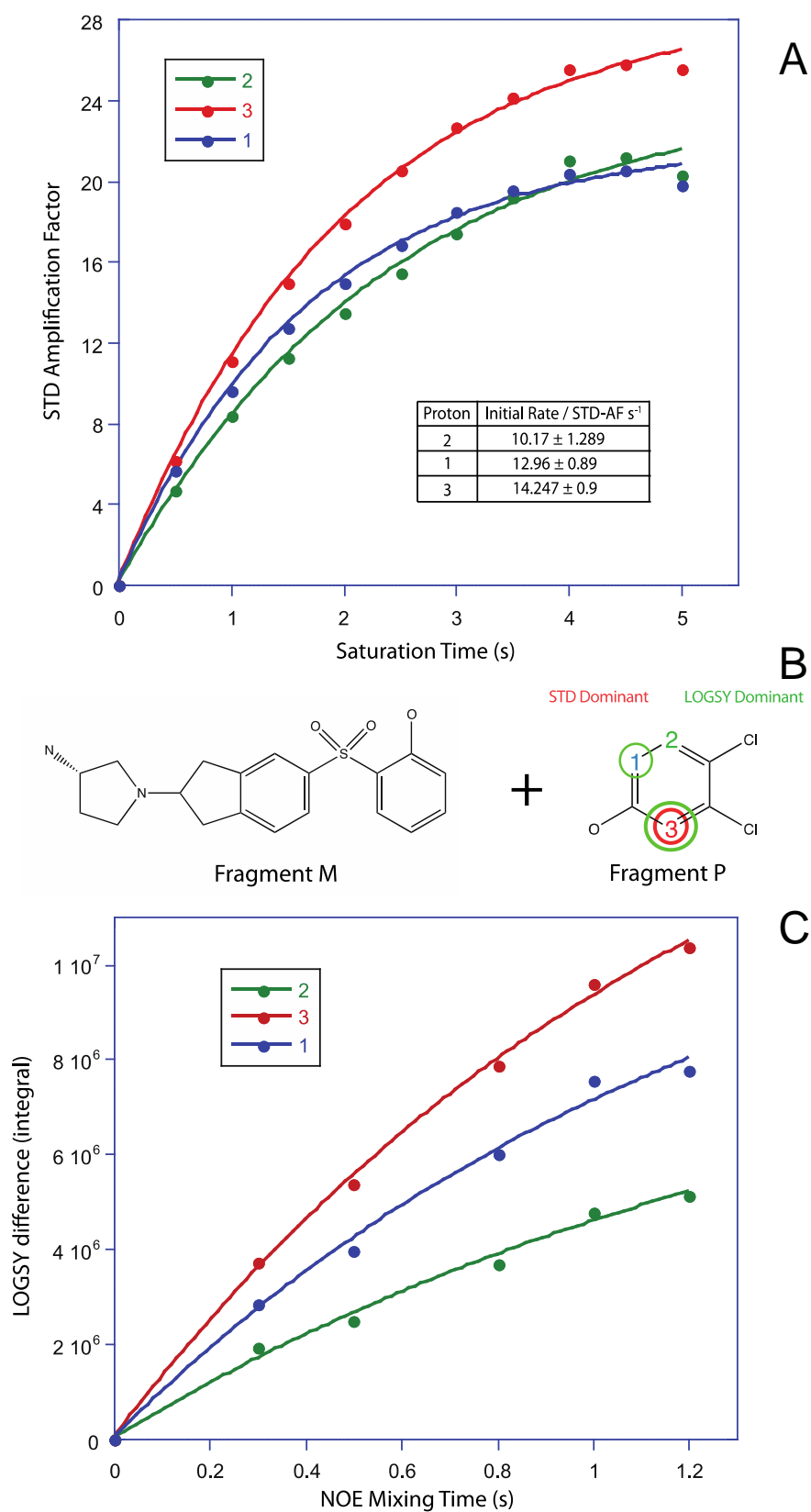
Figure 5.34: NMR data for fragment P bound to the Ras 2nd site, after saturation of the first site with fragment M. (A) STD build up curves and (B) LOGSY build up curves highlight protons 1 and 3 as STD dominant, with proton 3 also in receipt of the greatest degree of LOGSY enhancement (C)

199

5.3.4.3 Fragment N (200 µM) + O (5 mM)
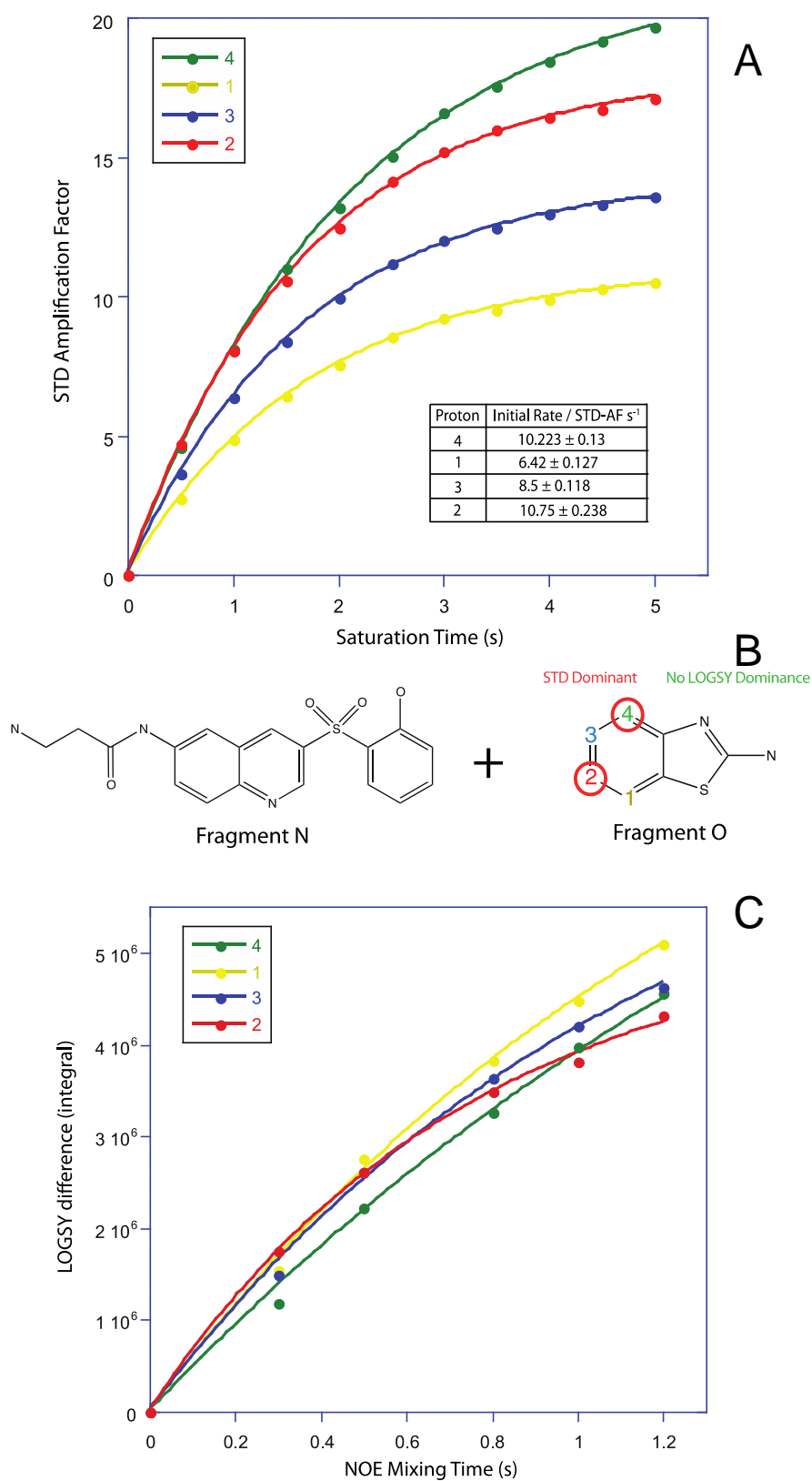
Figure 5.35: NMR data for fragment O bound to the Ras 2nd site, after saturation of the first site with fragment N. (A) STD build up curves and (B) LOGSY build up curves highlight protons 2 and 4 as STD dominant, with no proton in receipt of any significant LOGSY enhancement (C)

5.3.4.4 Fragment N (200 μM) + P (5 mM)

Proton	Initial Rate / STD-AF s⁻¹
2	15.673 ± 0.815
1	18.87 ± 1.329
3	17.42 ± 1.14
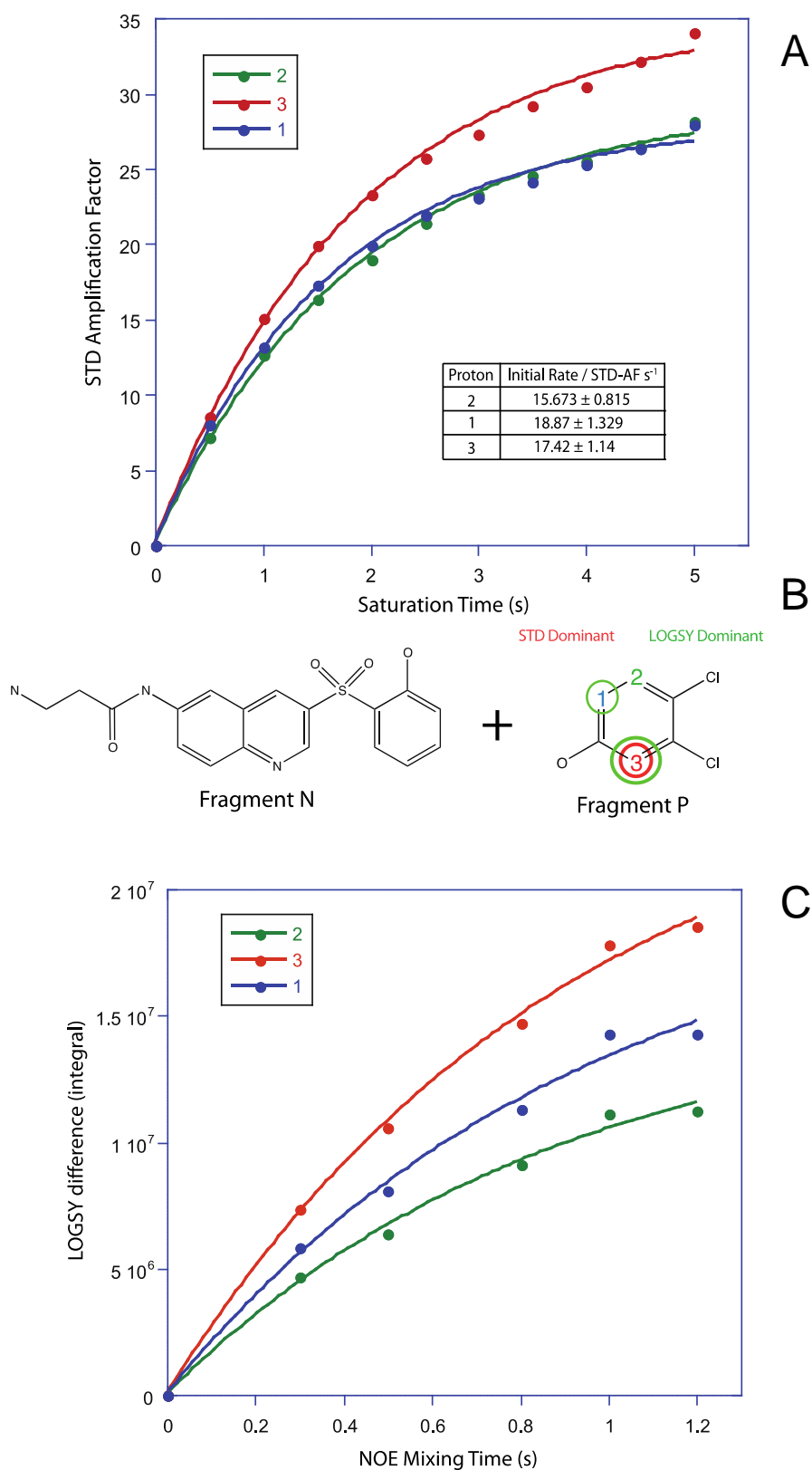
Figure 5.36: NMR data for fragment P bound to the Ras 2ⁿᵈ site, after saturation of the first site with fragment N. (A) STD build up curves and (B) LOGSY build up curves highlight protons 1 and 3 as STD dominant, with proton 3 also in receipt of the greatest degree of LOGSY enhancement (C)

5.3.5 Computational docking of fragment ligands into Ras – Top 9 ranked poses

As mentioned previously, each fragment ligand was individually docked into Hsp90 using GOLD. For this analysis the top 9 ranked poses were taken and shown below. This was done in order to compare with the binding modes present in the crystal structure, and consequently to examine how useful employing quantitative STD and LOGSY alongside computational techniques could prove to be.

5.3.5.1 Fragment H
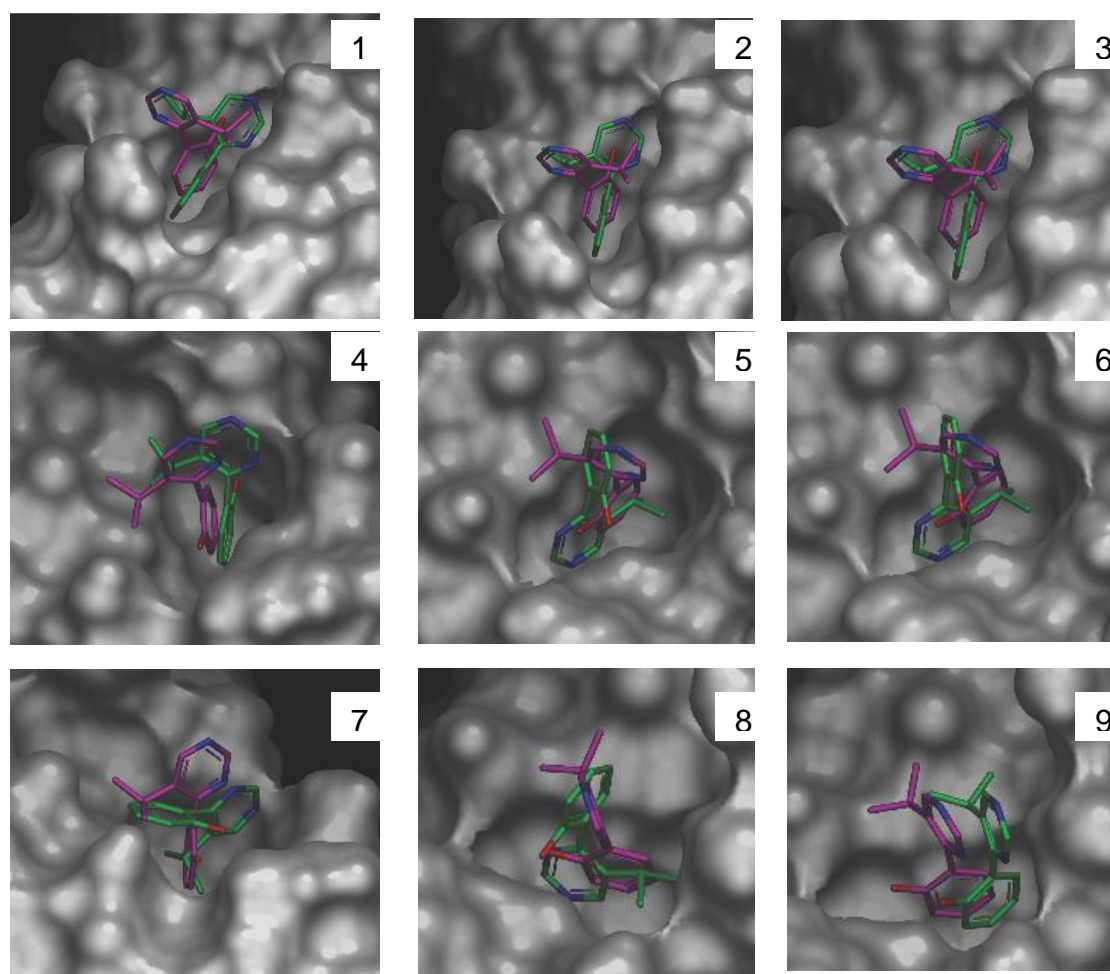
Figure 5.37: Top 9 ranked poses for fragment H binding to Ras. Correct binding mode from crystal structure (magenta) is overlaid with the numbered docking pose (green). Fitness of all ranked poses is as shown in the table

	Rank	1	2	3	4	5	6	7	8	9
H	Fitness	40.29	39.75	39.29	38.26	37.34	36.62	36.07	35.74	34.59

Poses 1 – 3 show solutions in which the phenol group is correctly orientated, but with the aminopyrimidine and isopropyl groups facing the opposite direction. Poses ranked 5, 6, 7 and 8 orientate the fragment with the phenol group out of the pocket, which goes against the crystal structure as well as the other poses. Pose 4 appears to be most correct.

5.3.5.2 Fragment I
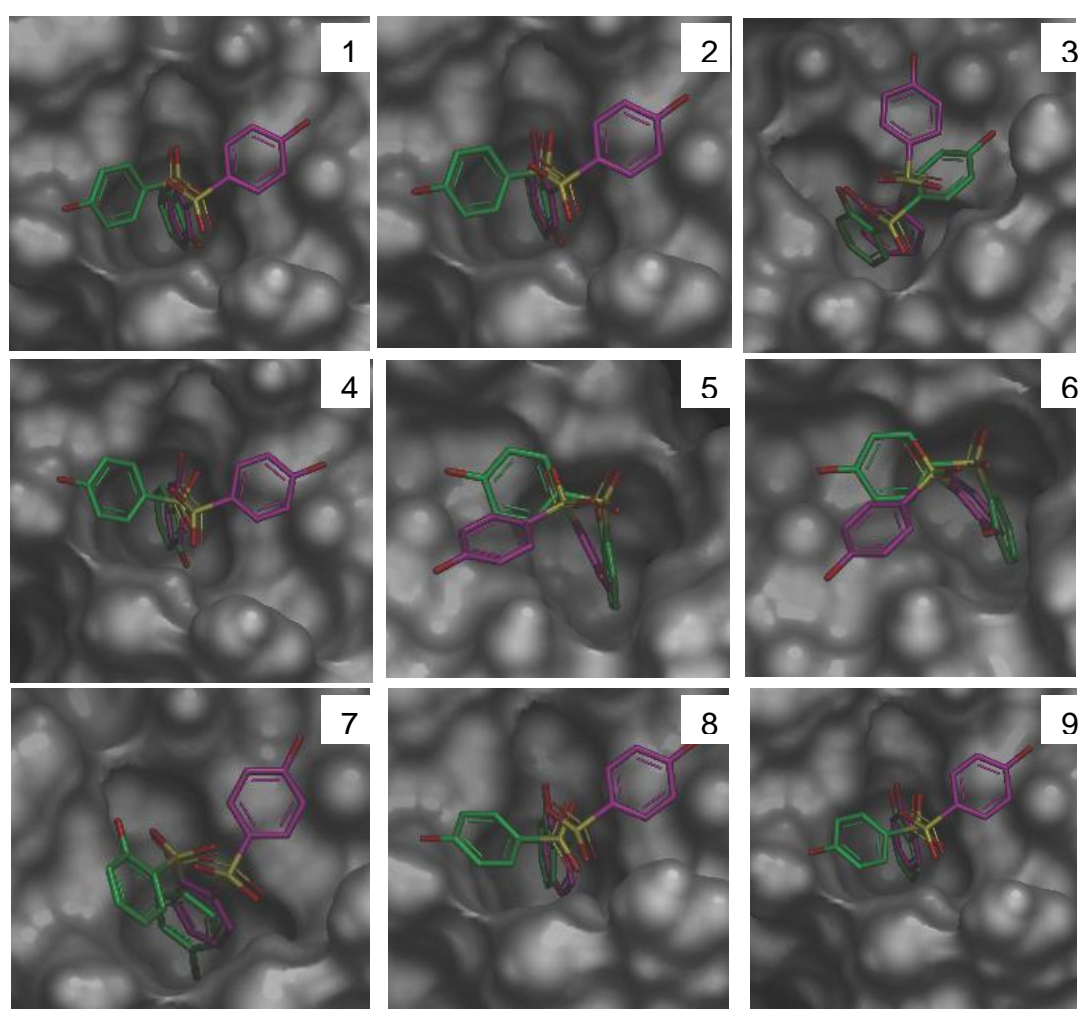
Figure 5.38: Top 9 ranked poses for fragment I binding to Ras. Correct binding mode from crystal structure (magenta) is overlaid with the numbered docking pose (green).

	Rank	1	2	3	4	5	6	7	8	9
I	Fitness	41.54	41.35	40.12	39.82	39.67	39.56	38.24	38.17	38.13

All poses bar number 7 show solutions in which the correct phenol group is orientated most deeply in the binding cleft (ortho), and with the other phenol group facing outwards (para). Poses ranked 1, 2, 4, 8 and 9, whilst orientated correctly, point the para phenol group 180° in the wrong direction, compared to the crystal structure. Poses 3, 5 and 6 appear to be closest to the correct solution.

5.3.5.3 Fragment J
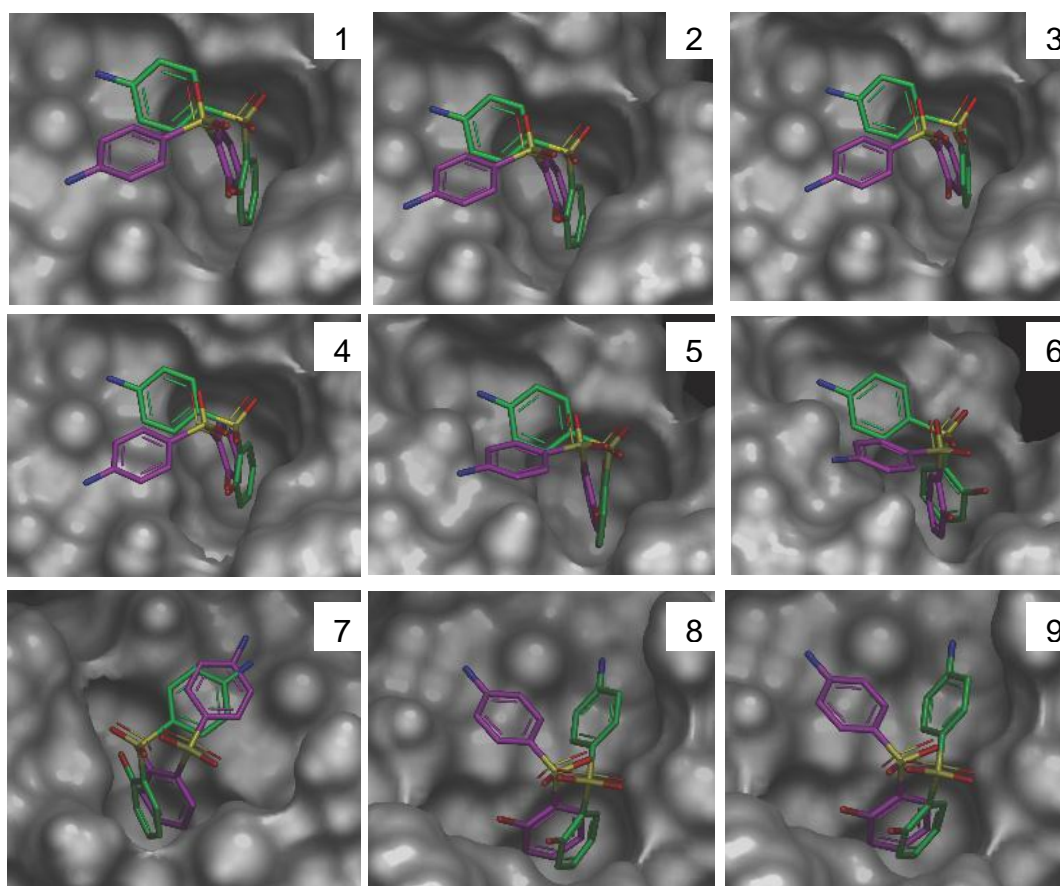
Figure 5.39: Top 9 ranked poses for fragment J binding to Ras. Correct binding mode from crystal structure (magenta) is overlaid with the numbered docking pose (green).

	Rank	1	2	3	4	5	6	7	8	9
J	Fitness	41.63	41.43	39.65	39.25	39.22	39.07	38.9	38.83	38.8

All poses correctly position the phenol group in the binding site with the aminobenzene portion of the fragment pointing outwards. In this instance all poses are fairly similar to that found in the crystal structure.

5.3.5.4 Fragment K
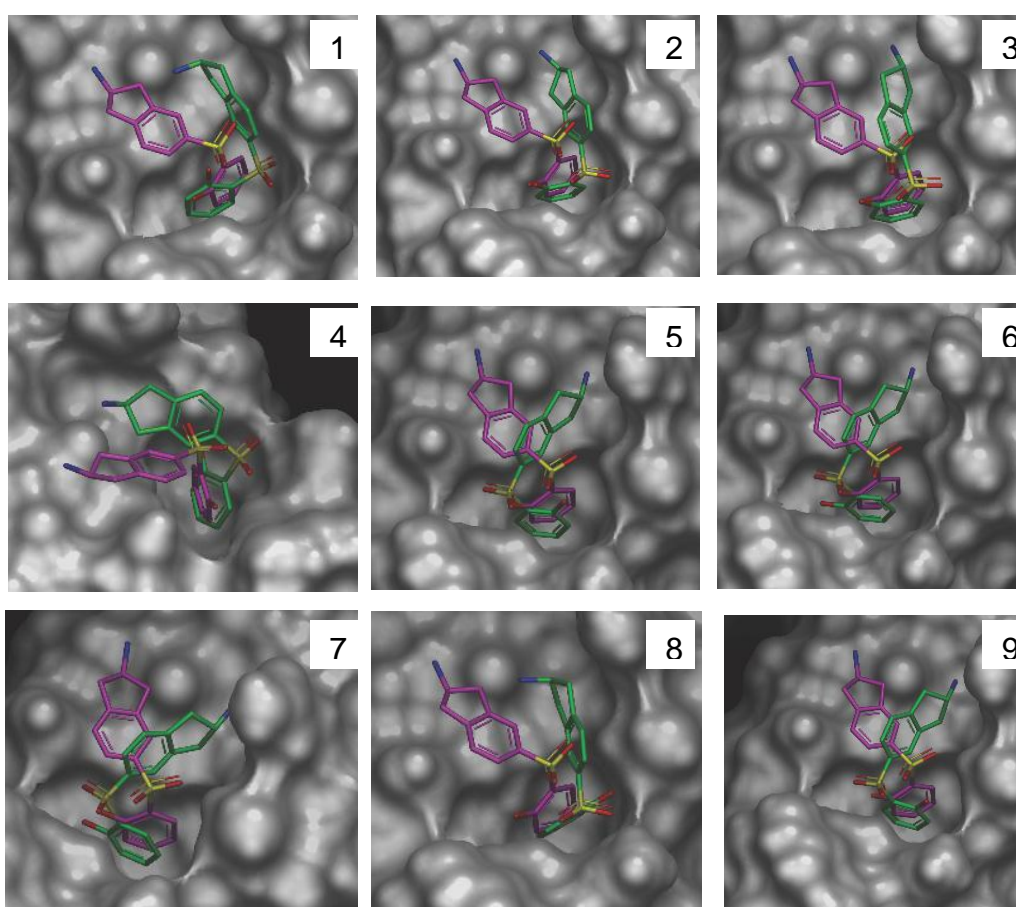
Figure 5.40: Top 9 ranked poses for fragment K binding to Ras. Correct binding mode from crystal structure (magenta) is overlaid with the numbered docking pose (green).

	Rank	1	2	3	4	5	6	7	8	9
K	Fitness	43.56	41.39	41.09	40.61	40.32	39.48	39.06	39.05	39.01

Once again the phenol group is orientated correctly in the binding site in all poses. There is little variation in binding mode between all nine poses.

5.3.5.5 Fragment L
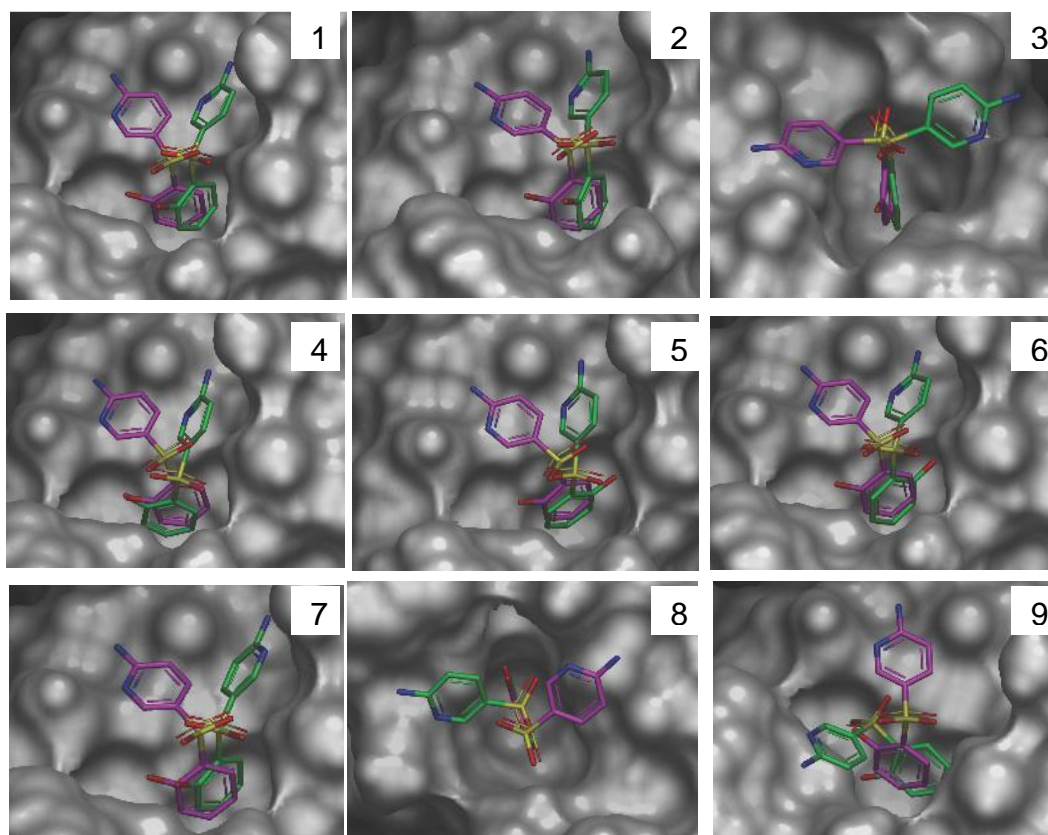
Figure 5.41: Top 9 ranked poses for fragment L binding to Ras. Correct binding mode from crystal structure (magenta) is overlaid with the numbered docking pose (green).

	Rank	1	2	3	4	5	6	7	8	9
L	Fitness	42.35	41.66	40.64	40.29	40.27	39.76	39.57	39.47	37.28

Once more, the phenol group is correctly positioned in the binding site, however in poses 3, 5 and 6 the group is orientated incorrectly by 180°, despite the para proton of the group still being in the correct position in all poses. Poses 1, 2 and 4 are close approximations of the bound mode represented in the crystal structure, although the aminopyridine group still does not perfectly overlay in any model.

5.4 Discussion

5.4.1 Initial comments on the experimental setup

Generally speaking, the experimental setup investigated in this chapter is at least equally reliable, if not more reliable than the setup for Hsp90. Although there is a small difference in molecular weight in favour of Hsp90, the fragment ligands here present a more convincing case. In this chapter fragments H − L are all largely aromatic, with separate, well-defined chemical shifts for each proton environment, due to the presence of heteroatoms acting as symmetry breakers. Furthermore, with no CH_3 or CH_2 groups to consider, no leap of faith regarding multiple protons through a single chemical shift is required to interpolate experimental data to fit structural data. In addition, there are more protons to consider for each fragment, lending validity to any correlations. More, reliable data points to consider in our correlations should lend significant weight to any findings herein.

5.4.2 Initial observations of quantitative STD in the presence of Ras

In general, all fragment ligands provide a series of smooth, well-fitting STD build up curves. Resulting initial rates derived from these build ups are accompanied with minimal error.

Fragment H is identified as being 'STD-dominant' at proton 5 and 4 of the phenolic ring. A reasonable correlation with the sum of the intermolecular proton-proton distances is observed, with proton 1 clearly in receipt of the least STD. The fragment I STD pattern shows a very good correlation with the structure. That said, it is also the case that in fragment I one chemical shift frequency provides the data for three protons: 1, 7 and 6. In this instance the data has been split according to the rules of

interpolation laid out in previous chapters, however it is worth noting that the STD intensities for protons 2 and 3 are so much stronger than the others in terms of STD intensity; this should have little bearing on any conclusions. The quantitative STD data for fragment J is unanimous in defining the whole of the phenolic ring – protons 9 – 12 - as STD dominant, in comparison to the phenylamine group which is firmly declared as being STD inferior. A very smooth correlation between the structure and experimental data is observed here.

Fragment K once again provides a series of strong STD build up curves, with the phenolic ring of protons 1 – 4 dominating the STD signal. The STD data and structure are again well correlated. And finally, fragment L produced a series of decent build up curves, although the final 2 points of the data for each curve do show a slight decline. Once again, protons 1 – 4 of the phenolic ring are STD dominant, whilst the remainder of the compound is inferior in terms of STD signal.

It is evident that the correlation between initial rate and the sum of the intermolecular proton-proton contacts is very good. This is clear across all five of the fragments under investigation in this chapter, binding to Ras. This implies that our STD analyses are valid across different protein targets, and as such the findings and subsequent conclusions are applicable in a general sense.

5.4.3 Potential for binding mode clustering

Whilst fragments I to L are all of the same chemotype, fragment H has many similarities to this group despite not possessing a sulfonyl group. All fragments contain a phenolic ring on one portion of the molecule. Protons that were determined to be in greatest receipt of saturation transfer difference signal are highlighted red.
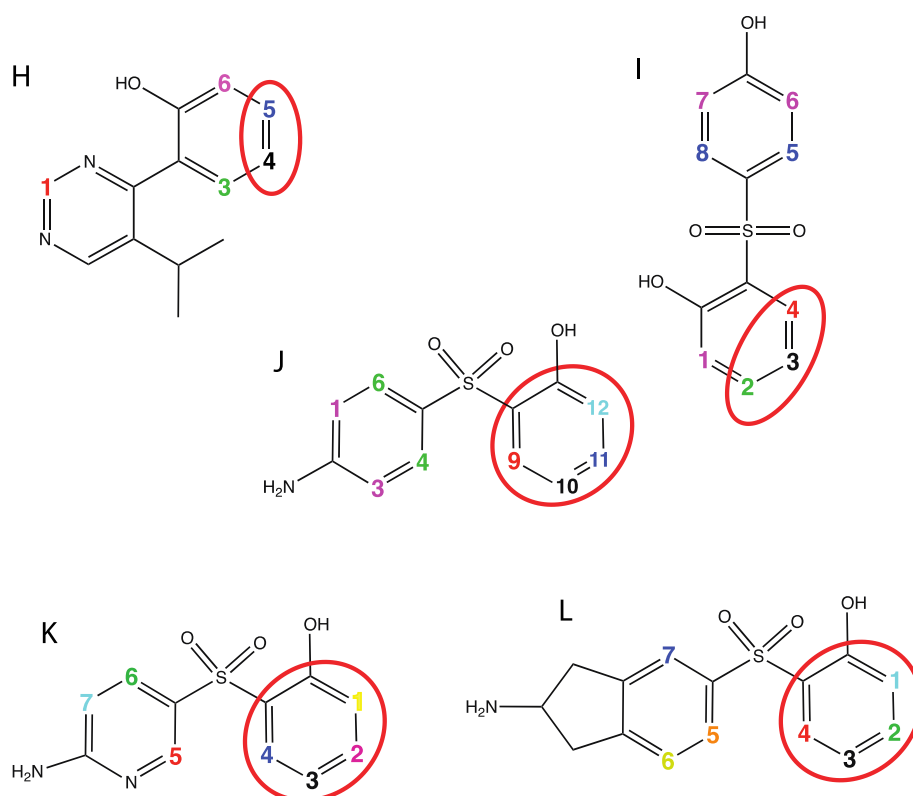
Figure 5.42: Examining the 5 fragment ligands together. STD-dominant regions for each fragment in the presence of Ras are circled red

In all instances it is the phenolic group that is STD dominant. For fragments H and I this isn't the case for the whole of the ring, whereas it is the case for fragments J – L. In this sense it seems safe to suggest that binding mode clustering taking into account quantitative STD data is equally as valid when applied to Ras as it is for Hsp90.

5.4.4 The intriguing case of fragment H

Fragment H has interesting STD properties that lead very neatly into a discussion on the Ras binding site. Aside from the usual good correlation between initial rate of STD build up, there is also the presence of an extra peak at ~8.9 ppm. The peak at this chemical shift represents the proton as shown by proton 2 in fig. 5.43.
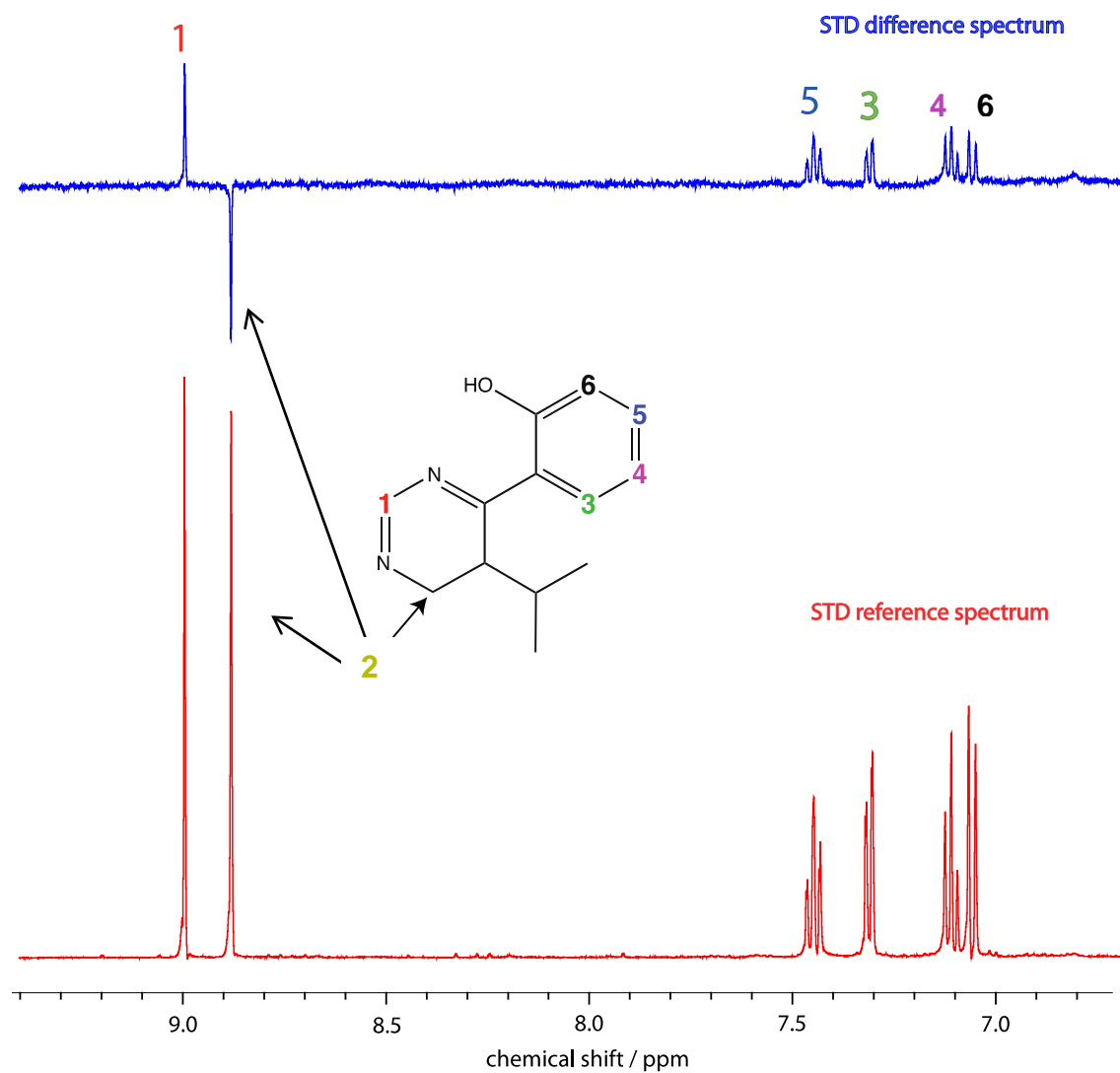
Figure 5.43: STD spectra for Fragment H. The peak at ~8.9 ppm represents the proton at position 2.

What can be clearly observed is how this peak appears negative in the processed STD difference spectrum. This is a phenomenon I never observed before. Typically, even if a ligand doesn't bind to a protein, a negative result simply appears amongst the noise with zero intensity. Consequently, the negative build up curve that was produced by this data was excluded from the analysis in fig. 5.10. This result could be caused by a positive NOE between the isopropyl protons and the proton at position 2, causing inversion of the STD signal. Furthermore, fragment H binds with an extraordinarily weak K_D of 13 mM, which really is testing the upper limit of STD applicability.

Closer inspection of the binding site provides a potential explanation for this puzzling result. Only two protons of the protein are within 6 Å of proton 2. Of those, one is the gamma proton of Serine 39 - which apart from being distant would be excluded from analysis being an exchangeable – and the other is the beta proton of serine 39, which resides 5.88 Å away. It's fair to say that this particular proton of the ligand is unusually distant from the binding site, especially for a small fragment. Closer examination of the binding site reveals a little more.

5.4.5 Closer examination of the binding site

As was alluded in the introduction(Maurer et al., 2012), the Ras binding site is a different type of 'beast' altogether to that of Hsp90. With a depth of 5 Å, the binding site does not allow much room for rotation. It is sufficiently large to accommodate a benzyl and a chloryl
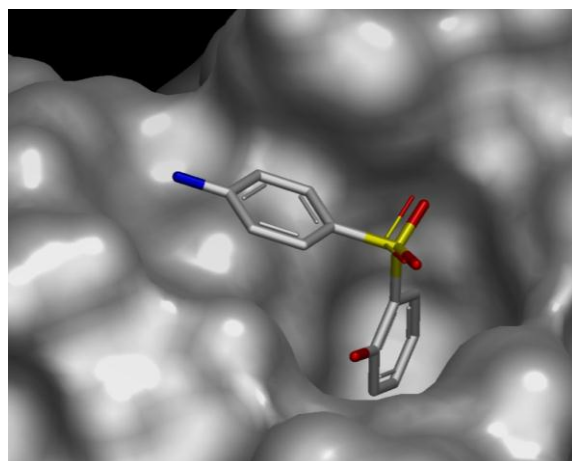
Figure 5.44: Crystal structure for fragment J bound to Ras. The phenolic group in greatest receipt of STD is clearly buried deepest.

211

group(Maurer et al., 2012), and so it is fair to assume that the phenol group present in all fragments examined here is accommodated. As such, with such limited chemical space to sample, figuring out a potential binding mode becomes much more trivial.

For all fragments examined here with a phenol group, this is easy. As fragment J shows in fig. 5.44, the phenolic moiety is the half of the fragment that is buried in the cleft. This information can be easily determined from the quantitative STD data on its own, in a qualitative sense, and this notion is bolstered when considering the identical binding mode of all other fragment ligands under consideration in this chapter, as shown by the overlays in fig. 5.45.
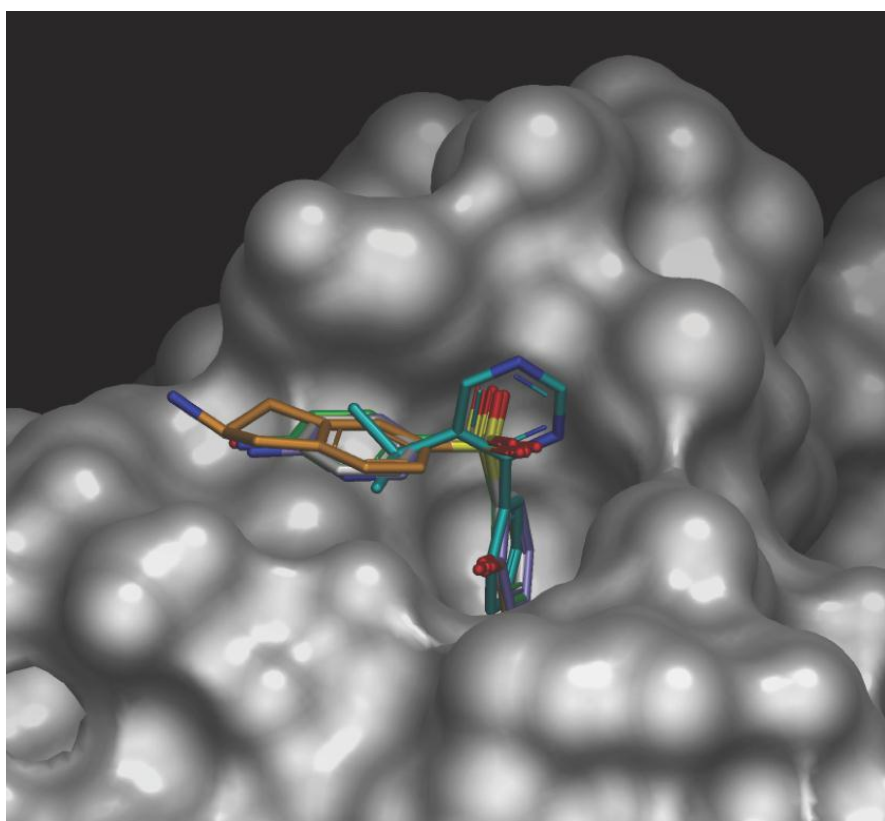
Figure 5.45: Overlays of the bound structures for fragments H – L. A common, conserved binding mode can be observed

Although there are several fewer intermolecular proton-proton distances to measure in the periphery for the halves of the fragments that are not part of the phenolic group, there are still enough to aid with distinguishing the binding mode more precisely than

this binary choice. The quantitative STD method clearly works on Ras, and good correlations are observed between experimental STD and the sum of the structural restraints, however this protein-ligand setup seems to be answering a slightly different question to that of the Hsp90 case.

5.4.6 Initial observations of quantitative LOGSY of 5 fragment ligands in the presence of Ras

Quantitative LOGSY is – at least on first glance – significantly harder to interpret. Generally speaking the data looks reasonable. A series of buildup curves can be generated from good quality LOGSY spectra, although it is worth noting that in all instances the component LOGSY spectrum (with protein) possesses exclusively negative signals before subtraction, rather than inversion of the signal that would indicate a significant LOGSY transfer.

Data for fragment H suggests that proton 6 of the phenol group has the greatest LOGSY buildup. Fragment I is tougher to assess due to a splitting of a gradient representing 3 protons. However, whichever way you look at it, protons 1, 6 and 7 are LOGSY dominant, and these are opposing ends of the fragment. Protons 1, 3 and 12 are LOGSY dominant in fragment J, whereas proton 1 in both fragments K and L is in receipt of the greatest LOGSY NOE transfer. Patterns are not instantly clear. Protons that we define as LOGSY dominant come from multiple parts of a fragment, and differ wildly between fragments of a chemotype.

It is worth mentioning at this point that in all Astex repository crystal structures with any fragment, on no occasion were conserved water molecules observed in the

binding pocket. This is perhaps to be expected given that the binding site is so small. In terms of the hypothesis I put forward in the previous chapter, this protein would clearly be unsuitable for testing such a claim. However, all is not lost.

Fragments K highlights the proton next to the hydroxyl group as being LOGSY dominant. Further to this, the protons highlighted by fragment J and I all exclusively reside next to hydroxyl or amine groups.

In the absence of conserved, bound water molecules in the binding site, there appears to be a relationship between the proximity of a proton in a ligand to an exchangeable group that determines the magnitude of a signal. This has been observed in other screening projects for protons adjacent to exchangeable groups by the Astex screening team.

5.4.7 How insightful is STD and LOGSY in conjunction with docking poses?

Docking poses were generated by GOLD in section 5.3.5 and ranked according to the Goldscore function. Clear limitations exist for docking programs such as GOLD, for instance it is known that using ensembles of protein structures increases performance(Korb et al., 2012), as does acquisition of more than ten poses. In addition other scoring functions such as ChemPLP, ASP and Chemscore may be employed. These all place greater emphasis on a different combination of factors including hydrogen bonding, Van der Waals and repulsive terms, ΔG, hydrophobic contact areas, and databases of known structures.

The poses generated in this analysis are certainly varied in nature. In most cases the general binding mode is roughly approximated by GOLD, however in certain instances it get it completely wrong. For example poses $5 - 8$ for fragment H are severely wrong to the extent that our STD analysis could very quickly and easily eliminate these from consideration.

Other more subtle discrepancies between crystal structure and binding mode pose, such as an aminopyridine ring being shifted 4 Å as for fragment L, are less likely to be flagged up by our quantitative analysis as clearly being incorrect, and so may well be beyond our remit. This analysis does however suggest a definite role for quantitative STD analysis as part of assessment with a computational approach. This is likely to be of much more use, and have wider applicability for situations wherein a crystal structure cannot be solved for a protein-ligand complex.

5.4.8 Examination of fragments binding in the 'second site'

Unlike all analysis of the first Ras binding site thus far, the suspected 'second site' is very much speculative. Whereas for the first site it was possible to refer back to myriad crystal structures, here we are working blind. Nonetheless there are some interesting observations.

The rationale here was to saturate the first site with one of two known fragment hits – fragments M and N, shown in fig. 5.46 – at a concentration sufficiently greater than their dissociation constants, and then to saturate the second binding site with one of two proposed fragment hits to the second site, at a significantly higher concentration than the first site binder. This gave 4 different combinations to analyse: M+O, M+P, N+O and N+P.
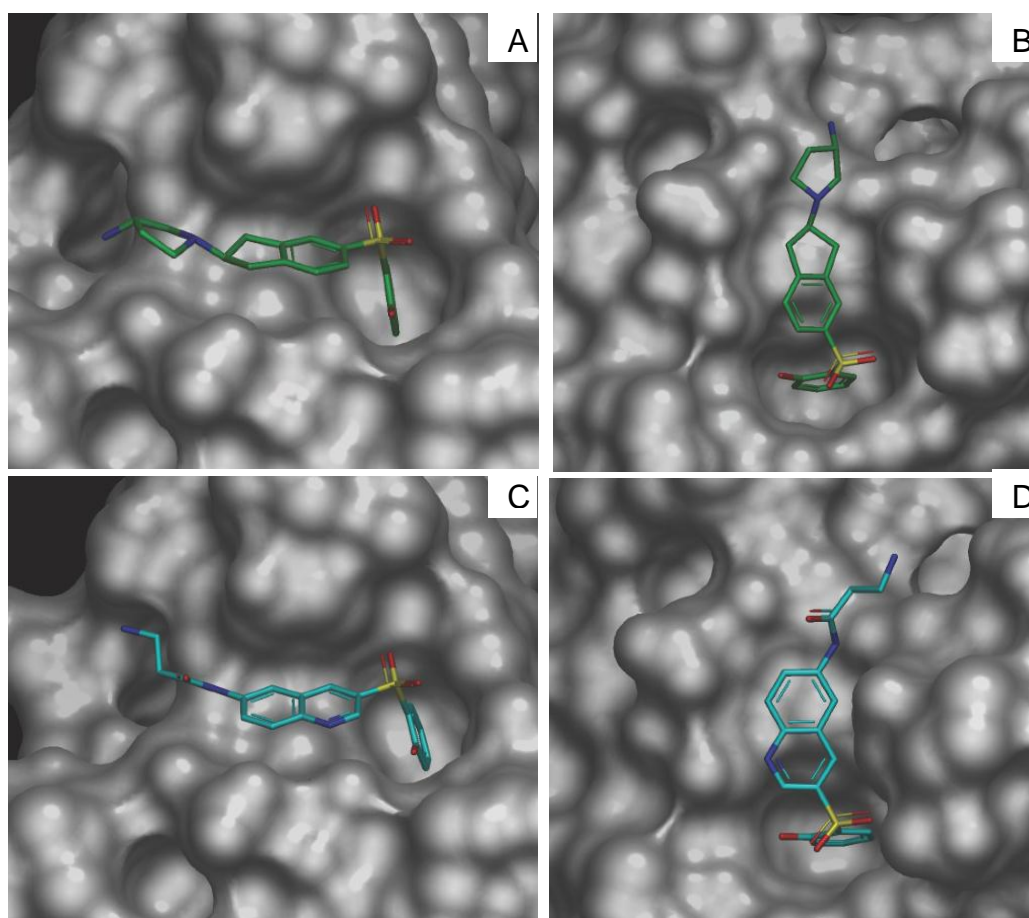
Figure 5.46: A) and B) show two views of fragment M bound to Ras whereas C) and D) show two viewpoints of fragment N in the same orientations

Before proceeding to discuss this any further, what is clear is that it does not matter whether it is fragment M or fragment N that's used for saturating the first binding site.

All STD and LOGSY data acquired is very similar for either fragment irrespective of which compound was used for the initial saturation. This is clear from the results but also clear from the bound crystal structures of fragments M and N in the 'first' binding site.

In terms of the experimental results, fragment O possesses four protons and from this two protons – 2 and 4 – are deemed STD dominant. In terms of the LOGSY buildup curves, no single rate of any proton stands out. Both of these observations hold whether fragment M or N is used to saturate the first site.

Fragment P is smaller with only three protons to test. Proton 3 is deemed to be in receipt of slightly greater STD than the other two protons. In terms of LOGSY, in this instance there is more of a hierarchy; proton 3 is dominant, followed by proton 1 and then proton 2. Again, the data proves that the fragment used to saturate the first site is irrelevant.

The data itself is robust with smooth, clear, buildup curves made possible from the data. The data for fragment O suggests that two protons from one end are STD dominant, and Fragment P suggests one proton is STD dominant. Without protons to sample from two different ends of a fragment – as with fragments H to L - there is no clear trend, or enough data points to suggest a binding mode from STD data alone. LOGSY data for both fragments is once again unclear, at least on first glance. However, the fact that there is no LOGSY dominance exhibited in fragment O, but there is in fragment P, is instructive; there are no exchangeable protons present in the fragment O, but there are in fragment P. In the absence of exchangeable protons in

fragment O there is no LOGSY dominance, whereas fragment P displays a pattern of LOGSY dominance for its three protons in line with each proton's relative proximity to the hydroxyl group.

On this evidence, second site binding corroborates our assertions made on the basis of the first site Ras-fragment binding, and this does provide a genuine opportunity to perhaps speculate as to the nature of the second site. Given the effect of proximity to exchangeable protons, with this ligand-observed NMR data we can safely assert that the second binding site possesses no bound water much like the first site. Furthermore in the absence of structural data for the second site, quantitative STD - in combination with binding mode poses from a docking algorithm – may be the most fruitful avenue to pursue.

Generally speaking, we have seen compelling evidence to suggest that quantitative STD and LOGSY are both techniques that may be applied to Ras and a series of fragment ligands. STD data corroborates all the principles observed with Hsp90, whereas LOGSY suggests that in the absence of bound, conserved water molecules in a binding site it is the proximity to exchangeable proton groups that is the dominant factor.

Chapter 6

Discussion

This chapter brings together the findings from the constituent chapters of this thesis, summarizes them, and places them into context. Over the course of this thesis we have determined that ligand-observed NMR methodologies are useful, powerful, convenient, and most importantly, full of potential. A number of fundamental biological questions, many of which will arise in the decades to come, will surely benefit from the rational implementation of the techniques and methods explored in this thesis.

6.1 Quantitative STD

On balance - based on what we have discovered with Hsp90 and Ras – both initial STD rates, as well as T_1-adjusted STD data can be said to give fairly positive correlations with distance restraints derived from crystal structures of the fragments bound to their proteins. This has been demonstrated for eleven fragment ligands in total, against two different proteins.

In theory, an initial rate based on 10 experimental points, fit to a strict equation, should provide a reliable value for a gradient. However based on our data, simply taking an STD amplification factor value and dividing through by an experimentally determined T_1 is equally as good in the majority of cases. This extends the applicability of quantitative STD as total experimental time is dramatically reduced if a rate need not be worked out. One STD experiment run for 20 minutes, along with a set of inversion recovery experiments (10 minutes maximum) could provide the same fundamental information as a rate based on 3h 20 minutes of NMR time.

We have shown that precise three-dimensional protein structures of bound ligands may be well correlated with STD NMR data derived from simple 1D NMR experiments, to a degree not previously shown before.

6.2 LOGSY

In this thesis quantitative LOGSY has proven itself to be a remarkable tool, to an extent completely unexpected. Investigations with Hsp90 showed that there was a direct correlation between the magnitude of a LOGSY signal and the proximity of that particular proton to bound water in the binding site. This promises to be an extremely useful NMR-based tool for investigating interactions between ligands and proteins where conserved, bound water is implicated.

Investigations with Ras showed that in the absence of bound water in the binding site, quantitative LOGSY could no longer inform upon binding orientation. Where no bound water is present, the proximity of a proton to an exchangeable group tends to dominate.

Although we were able to fit LOGSY difference data (based on the integral difference between two samples) to the same equations as were used to construct STD build up curves, in order to generate initial rates, they did not fit these equations perfectly and the subsequent fits were associated with very large errors. Furthermore, the lack of crossover of LOGSY build up curves (in contrast to STD build up curves) implies that differences in longitudinal relaxation appear to have little influence on the data. As a result it appears that once again, LOGSY data acquired from a single point encodes at least as much information as an experimentally derived rate. This has major benefits in terms of streamlining and extends

how broadly the method may be implemented: only two LOGSY experiments are required (with protein and without) run with 512 scans (2 x 22 minutes).

The absence of a sign change without taking into account a control spectrum (as is the case for all fragment ligands to Ras) would, according to the principles of the SALMON (Ludwig et al., 2008) methodology, imply a complete lack of binding between all of our ligands and Ras, something which is patently untrue as evidenced by positive STD data and the fact that these are all validated 'hits' for Ras. This goes to underline the importance of measuring the LOGSY signal magnitude for all signals, as well as running control spectra.

6.3 A comparison of proteins

STD and LOGSY analyses in this thesis focused on fragments binding to two proteins: Hsp90 and Ras. Whilst we have been able to show that quantitative STD is suited to studying fragments binding to both proteins, some differences in the results obtained with both proteins did make themselves apparent.

Differences in the nature of the binding sites – deep, cavernous Hsp90 versus the small and shallow 'groove-like' Ras – meant that STD informed upon different pieces of information. The quantitative approach undoubtedly works in terms of the correlations we were able to achieve with both proteins, but in qualitative terms STD on Ras can easily tell us which half of the fragment is orientated to point away from the binding site. However in a nucleotide-binding site such as found in Hsp90 it is unlikely for a small fragment to noticeably protrude from the site as it would for Ras. In a case such as this the precise relationship between the

sum of the side chain contributions is likely to be more important, and so a full analysis as we have shown is invaluable.

Both proteins prove that both techniques are clearly applicable to different types of proteins, but it is clear that quantitative LOGSY is likely to be far more useful for informing upon water-mediated interactions in a binding site.

6.4 In combination with docking simulations

One of the most promising ways in which we thought quantitative STD may be useful is in conjunction with suggested binding modes created with docking software. This was attempted in chapter 5 with the fragment ligands to Ras. Broadly speaking the mixture of binding poses generated by GOLD, in relation to the actual binding mode, were not universally correct and in many cases completely contradicted the crystal structure.
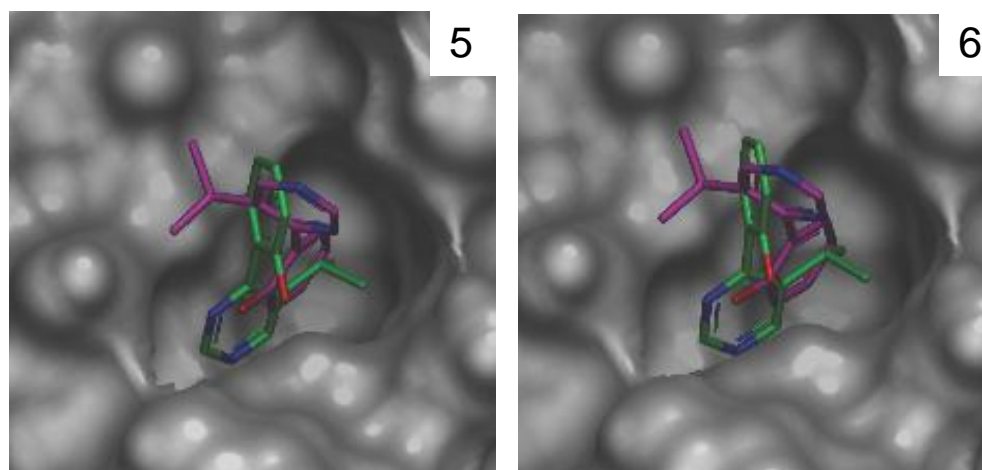
Figure 6.1: Binding poses ranked 5 and 6 (green) for fragment H binding to Ras. In both of these poses the fragment is orientated upside down to that in the crystal structure (magenta)

An example is illustrated by binding modes 5 and 6 binding to Ras in figure 6.1. In both instances the binding mode is clearly incorrect; the phenol group is not directly in the

binding pocket, and protrudes from the top. In the absence of a crystal structure, our STD analyses would instantly be able to state that these modes would be unlikely (since the protons suggested by these poses at the base of the pocket receive minimal STD signal), and as a result they can be dismissed.

As the myriad docking poses generated by GOLD for all five fragments to Ras shows, quantitative STD should come in handy for dismissing a wide variety of poses. In the absence of crystal structure, this is extremely useful.

6.5 In a perfect world

In this thesis an ongoing theme has been a discussion of the advantages and limitations of certain fragments that make up this study. Just as an aside, it would be interesting to try and describe what a perfect fragment amenable to quantitative STD and LOGSY might look like. Drawing upon some of the inspirations acquired during this investigation, I've invented a compound that shall be called 'fragment Z'. The predicted ^{1}H 1D spectrum for this fragment is shown in figure 6.2.
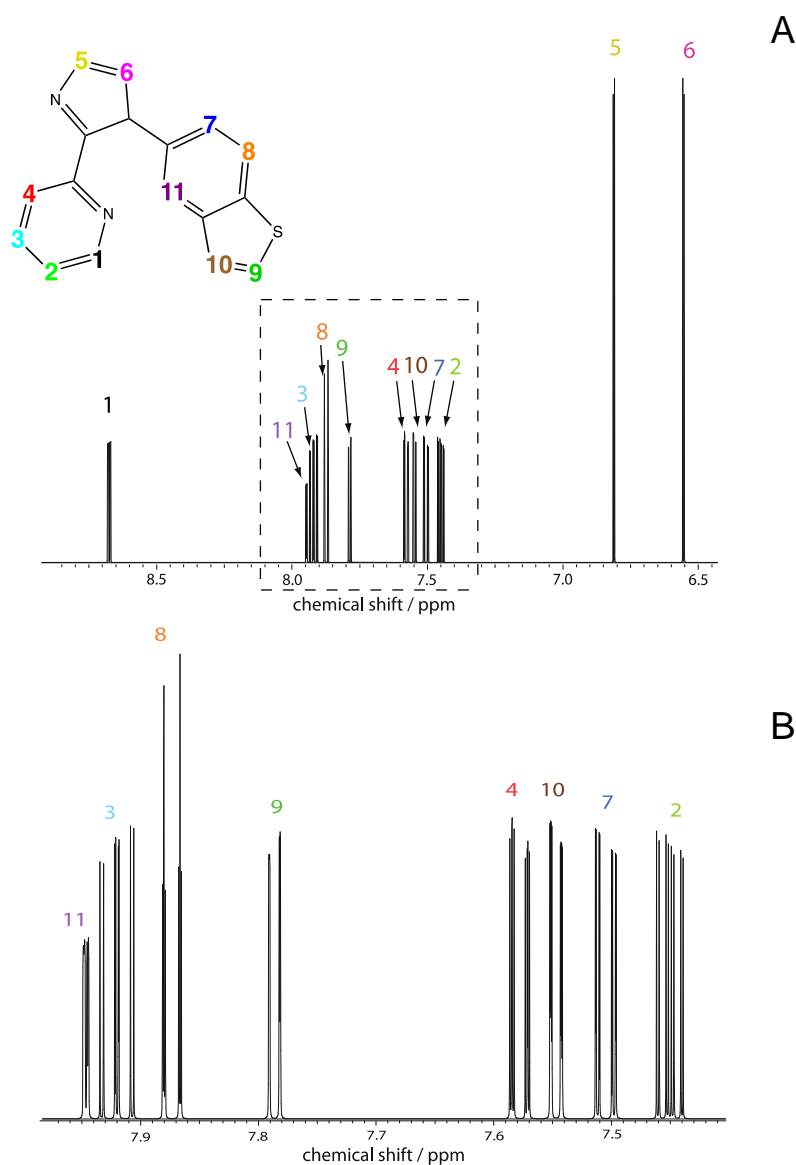
Figure 6.2: Predicted ^{1}H NMR spectra for fragment Z. (A) whole spectrum and (B) region between 7.4 – 8.8 ppm expanded. All 11 protons appear at distinct chemical shifts enabling easy unambiguous assignment of all protons of the fragment

Fragment Z would be ideal for a number of reasons. Firstly, it is comprised exclusively of a large number of aromatic protons. This has the advantages of ensuring all chemical shifts are well away from any solvent peaks or those of biological buffer components such as DTT, Tris or β-mercaptoethanol, meaning that no ligand information is lost. Significantly, these protons are also far from the position of application of the selective pulse, therefore fear of accidental excitation is even further alleviated, as explored in chapter 2. The other advantage of aromatic protons is that they are single protons. Processing data as one chemical shift per proton avoids the need to split any data according to multiple protons of a group i.e. methyl protons. A large number of protons ensures that any trends modelled with data is based on substantial evidence.

Fragment Z also possesses no symmetry, unlike several of the compounds in this investigation. The absence of symmetry is ensured by insertion of heteroatoms at key positions in the aromatic rings. Furthermore, there is no chance that the fragment might adopt different conformations which would remove a lot of valuable information i.e. chair/boat conformations that have axial and equatorial protons in both conformations.

Other ideal additional properties of a perfect fragment would include: no tautomerism, a dissociation constant of between 10 μm and 1 mM and good solubility in aqueous buffer. Of course, it is highly unlikely that fragments in an industrial fragment library will adhere to all of these conditions, but the more of them that a fragment satisfies, the more use quantitative STD and LOGSY will surely be.

6.6 Future experiments and the future of FBDD

In future it may be interesting to conduct LOGSY experiments with varying ratios of H_2O/D_2O (as well as different co-solvents such as methanol) and move gradually from a solution of pure water towards a sample of pure D_2O. It may be expected that an incremental reduction in the proportion of water molecules might cause an overall reduction in LOGSY signal, but it would be interesting to see whether the LOGSY signal to particular protons fell steadily, or whether there would be a discrete fall as bound water in the binding site was replaced.

Another interesting experiment would be to carry out quantitative STD and LOGSY with fragments on perdeuterated protein. Would a reduction in the 'proton-sink' provide increased precision in quantitative STD and LOGSY? Large scale implementation of fragment screening processes with perdeuterated protein is unlikely and implausible, but on a one-off basis this would answer an interesting question. Perdeuteration rarely produces proteins with 100% deuteration at every single proton position; so different deuteration levels might offer different saturation transfer pathways, which could enhance quantitative STD (and therefore minimise unwanted spin diffusion).

To take this project forward in a very direct sense, the methods refined in this thesis could be applied to a range of further proteins and ligands of different shapes and sizes. I expect this would corroborate the findings established thus far, but it would provide further justification and reassurance of the methods.

Based on observations in this thesis, I have reason to believe that quantitative ligand-

observed NMR could easily form a significant part of early stage FBDD methodology. Despite the increasing popularity of SPR as an initial screen, and despite the ease and high-throughput nature of crystallisation trials for validating hits, there is scope for ligand-observed NMR to remain as both the principal screening tool and a tool for validating hits by quantification.

It is clear from this thesis that the quantitative ligand-observed NMR techniques are likely to prove most useful in the absence of a crystal structure for a bound ligand. Despite advances in x-ray crystallography, it is still often the case that some proteins do not take particularly well to the crystallisation process. From the point of view of a pharmaceutical company interested in a new mutant of an interesting protein target, this can be infuriating, and in many cases this causes the termination of a screening programme entirely, irrespective of how theoretically solid and exciting pursuing such a target may be. This thesis suggests that this kind of thinking may be short-sighted, and provides justification for an alternative approach.

In combination with docking poses of ligands bound to the target protein using software such as GOLD (which will take the apo- crystal structure of the protein, the ligand, and possibly some NOE restraints directly), methods refined in this thesis show that it is plausible to gain a handle on protein-ligand binding mode via an alternative route. Some computational docking programmes already automatically directly incorporate 2D HSQC NMR data in order to aid the narrowing down of binding mode solutions (in the form of chemical shift perturbations), so perhaps if one was minded to do so, quantitative STD NMR intensities could be incorporated **prospectively** into GOLD as part of the computational method.

No doubt most pharmaceutical and biotechnology companies are likely to stay fixed in their ways, and unwilling to proceed in the absence of the 'gold standard' of the bound-ligand crystal structure. But others may take an alternative view, and decide that a risk is worth taking.

For just a small amount of extra effort, STD and LOGSY experiments could be run on hits, as single compounds, to assess if there are patterns of STD or LOGSY build up that are consistent with the binding mode of a particular chemotype (categorisation). This could help both as a function to narrow down the field of hits to put forward for x-ray screening, and aid with further characterization of binding complexes in the absence of a crystal structure.

References

ALBERT, D. H., TAPANG, P., MAGOC, T. J., PEASE, L. J., REUTER, D. R., WEI, R.-Q., LI, J., GUO, J., BOUSQUET, P. F. & GHOREISHI-HAACK, N. S. 2006. Preclinical activity of ABT-869, a multitargeted receptor tyrosine kinase inhibitor. *Mol Cancer Ther,* 5**,** 995-1006.

ALI, M. M., ROE, S. M., VAUGHAN, C. K., MEYER, P., PANARETOU, B., PIPER, P. W., PRODROMOU, C. & PEARL, L. H. 2006. Crystal structure of an Hsp90-nucleotide-p23/Sba1 closed chaperone complex. *Nature,* 440**,** 1013-7.

ANDERSON, W. A. & FREEMAN, R. 1962. Influence of a Second Radiofrequency Field on High‐Resolution Nuclear Magnetic Resonance Spectra. *J Chem Phys,* 37**,** 85-103.

ANGULO, J., ENRÍQUEZ‐NAVAS, P. M. & NIETO, P. M. 2010. Ligand–receptor binding affinities from saturation transfer difference (STD) NMR spectroscopy: the binding isotherm of STD initial growth rates. *Chem-Eur J,* 16**,** 7803-7812.

ANGULO, J. & NIETO, P. M. 2011. STD-NMR: application to transient interactions between biomolecules-a quantitative approach. *Eur Biophys J,* 40**,** 1357-69.

ANTONINI, L. V., PEREGRINA, J. R., ANGULO, J., MEDINA, M. & NIETO, P. M. 2014. A STD-NMR study of the interaction of the Anabaena ferredoxin-NADP+ reductase with the coenzyme. *Molecules,* 19**,** 672-85.

BARILE, E. & PELLECCHIA, M. 2014. NMR-based approaches for the identification and optimization of inhibitors of protein-protein interactions. *Chem Rev,* 114**,** 4749-63.

BARKER, J. J., BARKER, O., BOGGIO, R., CHAUHAN, V., CHENG, R. K. Y., CORDEN, V., COURTNEY, S. M., EDWARDS, N., FALQUE, V. M., FUSAR, F., GARDINER, M., HAMELIN, E. M. N., HESTERKAMP, T., ICHIHARA, O., JONES, R. S., MATHER, O., MERCURIO, C., MINUCCI, S., MONTALBETTI, C. A. G. N., MÜLLER, A., PATEL, D., PHILLIPS, B. G., VARASI, M., WHITTAKER, M., WINKLER, D. & YARNOLD, C. J. 2009. Fragment-based Identification of Hsp90 Inhibitors. *ChemMedChem,* 4**,** 963-966.

BEGLEY, D. W., ZHENG, S. & VARANI, G. 2010. Fragment-based discovery of novel thymidylate synthase leads by NMR screening and group epitope mapping. *Chem Biol Drug Des,* 76**,** 218-33.

BENIE, A. J., MOSER, R., BAUML, E., BLAAS, D. & PETERS, T. 2003. Virus-ligand interactions: identification and characterization of ligand binding by NMR spectroscopy. *JACS,* 125**,** 14-5.

BIET, T. & PETERS, T. 2001. Molecular Recognition of UDP‐Gal by β‐1, 4‐Galactosyltransferase T1. *Angew. Chemie,* 40**,** 4189-4192.

BUKAU, B., WEISSMAN, J. & HORWICH, A. 2006. Molecular chaperones and protein quality control. *Cell,* 125**,** 443-451.

CHAPMAN, P. B., HAUSCHILD, A., ROBERT, C., HAANEN, J. B., ASCIERTO, P., LARKIN, J., DUMMER, R., GARBE, C., TESTORI, A., MAIO, M., HOGG, D., LORIGAN, P., LEBBE, C., JOUARY, T., SCHADENDORF, D., RIBAS, A., O'DAY, S. J., SOSMAN, J. A., KIRKWOOD, J. M., EGGERMONT, A. M., DRENO, B., NOLOP, K., LI, J., NELSON, B., HOU, J., LEE, R. J., FLAHERTY, K. T., MCARTHUR, G. A. & GROUP, B.-S. 2011.

Improved survival with vemurafenib in melanoma with BRAF V600E mutation. *N Engl J Med,* 364, 2507-16.

CHEN, B., ZHONG, D. & MONTEIRO, A. 2006. Comparative genomics and evolution of the HSP90 family of genes across all kingdoms of organisms. *BMC Genomics,* 7, 156.

CONGREVE, M., CARR, R., MURRAY, C. & JHOTI, H. 2003. A 'rule of three' for fragment-based lead discovery? *Drug Discov Today,* 8, 876-7.

CUTTING, B., SHELKE, S. V., DRAGIC, Z., WAGNER, B., GATHJE, H., KELM, S. & ERNST, B. 2007. Sensitivity enhancement in saturation transfer difference (STD) experiments through optimized excitation schemes. *Magn Reson Chem,* 45, 720-4.

DALVIT, C., FOGLIATTO, G., STEWART, A., VERONESI, M. & STOCKMAN, B. 2001. WaterLOGSY as a method for primary NMR screening: practical aspects and range of applicability. *J Biomol NMR,* 21, 349-59.

DALVIT, C., PEVARELLO, P., TATO, M., VERONESI, M., VULPETTI, A. & SUNDSTROM, M. 2000. Identification of compounds with binding affinity to proteins via magnetization transfer from bulk water. *J Biomol NMR,* 18, 65-8.

DIAS, D. M. & CIULLI, A. NMR approaches in structure-based lead discovery: Recent developments and new frontiers for targeting multi-protein complexes. *Prog Biophys Mol Biol*, 116, 101-112

DICARA, D., RAPISARDA, C., SUTCLIFFE, J. L., VIOLETTE, S. M., WEINREB, P. H., HART, I. R., HOWARD, M. J. & MARSHALL, J. F. 2007. Structure-function analysis of Arg-Gly-Asp helix motifs in alpha v beta 6 integrin ligands. *J Biol Chem,* 282, 9657-65.

DOAK, B. C., MORTON, C. J., SIMPSON, J. S. & SCANLON, M. J. 2013. Design and Evaluation of the Performance of an NMR Screening Fragment Library. *Aust J Chem,* 66, 1465-1472.

FREEMAN, R. 1998. Shaped radiofrequency pulses in high resolution NMR. *Prog Nucl Magn Res Spectrosc,* 32, 59-106.

GESCHWINDNER, S., OLSSON, L. L., ALBERT, J. S., DEINUM, J., EDWARDS, P. D., DE BEER, T. & FOLMER, R. H. 2007. Discovery of a novel warhead against beta-secretase through fragment-based lead generation. *J Med Chem,* 50, 5903-11.

GOETZ, M. P., TOFT, D. O., AMES, M. M. & ERLICHMAN, C. 2003. The Hsp90 chaperone complex as a novel target for cancer therapy. *Ann Oncol,* 14, 1169-76.

HARATA, K., NAGAHORA, H. & JIGAMI, Y. 1995. X-ray structure of wheat germ agglutinin isolectin 3. *Acta Crystallogr D Biol Crystallogr,* 51, 1013-9.

HOWARD, S., BERDINI, V., BOULSTRIDGE, J. A., CARR, M. G., CROSS, D. M., CURRY, J., DEVINE, L. A., EARLY, T. R., FAZAL, L., GILL, A. L., HEATHCOTE, M., MAMAN, S., MATTHEWS, J. E., MCMENAMIN, R. L., NAVARRO, E. F., O'BRIEN, M. A., O'REILLY, M., REES, D. C., REULE, M., TISI, D., WILLIAMS, G., VINKOVIC, M. & WYATT, P. G. 2009. Fragment-based discovery of the pyrazol-4-yl urea (AT9283), a multitargeted kinase inhibitor with potent aurora kinase activity. *J Med Chem,* 52, 379-88.

JAYALAKSHMI, V. & KRISHNA, N. R. 2004. CORCEMA refinement of the bound ligand conformation within the protein binding pocket in reversibly forming weak complexes using STD-NMR intensities. *J Magn Reson,* 168, 36-45.

JENCKS, W. P. 1981. On the attribution and additivity of binding energies. *PNAS,* 78, 4046-50.

JHOTI, H., CLEASBY, A., VERDONK, M. & WILLIAMS, G. 2007. Fragment-based screening using X-ray crystallography and NMR spectroscopy. *Curr Opin Chem Biol,* 11, 485-93.

KEMPER, S., PATEL, M. K., ERREY, J. C., DAVIS, B. G., JONES, J. A. & CLARIDGE, T. D. 2010. Group epitope mapping considering relaxation of the ligand (GEM-CRL): including longitudinal relaxation rates in the analysis of saturation transfer difference (STD) experiments. *J Magn Reson,* 203, 1-10.

KRISHNA, N. R. & JAYALAKSHMI, V. 2006. Complete relaxation and conformational exchange matrix analysis of STD-NMR spectra of ligand–receptor complexes. *Prog Nucl Magn Res Spectrosc,* 49**,** 1-25.

LEE, Y., ZENG, H., MAZUR, A., WEGSTROTH, M., CARLOMAGNO, T., REESE, M., LEE, D., BECKER, S., GRIESINGER, C. & HILTY, C. 2012. Hyperpolarized binding pocket nuclear Overhauser effect for determination of competitive ligand binding. *Angew. Chem,* 51**,** 5179-82.

LEPRE, C. A., MOORE, J. M. & PENG, J. W. 2004. Theory and applications of NMR-based screening in pharmaceutical research. *Chem Rev,* 104**,** 3641-76.

LEY, N. B., ROWE, M. L., WILLIAMSON, R. A. & HOWARD, M. J. 2014. Optimising selective excitation pulses to maximise saturation transfer difference NMR spectroscopy. *RSC Adv,* 4**,** 7347-7351.

LIEPINSH, E. & OTTING, G. 1996. Proton exchange rates from amino acid side chains-- implications for image contrast. *Magn Reson Med,* 35**,** 30-42.

LUDWIG, C., MICHIELS, P. J. A., WU, X., KAVANAGH, K. L., PILKA, E., JANSSON, A., OPPERMANN, U. & GUNTHER, U. L. 2008. SALMON: Solvent accessibility, ligand binding, and mapping of ligand orientation by NMR Spectroscopy. *J. Med Chem,* 51**,** 1-3.

MAYER, M. & MEYER, B. 1999. Characterization of ligand binding by saturation transfer difference NMR spectroscopy. *Angew. Chemie,* 38**,** 1784-1788.

MAYER, M. & JAMES, T. L. 2004. NMR-based characterization of phenothiazines as a RNA binding scaffold. *JACS,* 126**,** 4453-60.

MAYER, M. & MEYER, B. 2001. Group Epitope Mapping by Saturation Transfer Difference NMR To Identify Segments of a Ligand in Direct Contact with a Protein Receptor. *JACS,* 123**,** 6108-6117.

MEDEK, A., HAJDUK, P. J., MACK, J. & FESIK, S. W. 2000. The use of differential chemical shifts for determining the binding site location and orientation of protein-bound ligands. *JACS,* 122**,** 1241-1242.

MEINECKE, R. & MEYER, B. 2001. Determination of the binding specificity of an integral membrane protein by saturation transfer difference NMR: RGD peptide ligands binding to integrin alphaIIbbeta3. *J Med Chem,* 44**,** 3059-65.

MEYER, B. & PETERS, T. 2003. NMR spectroscopy techniques for screening and identifying ligand binding to protein receptors. *Angew. Chem,* 42**,** 864-90.

MIRELMAN, D., GALUN, E., SHARON, N. & LOTAN, R. 1975. Inhibition of fungal growth by wheat germ agglutinin. *Nature,* 256**,** 414-6.

MOORE, J., ABDUL-MANAN, N., FEJZO, J., JACOBS, M., LEPRE, C., PENG, J. & XIE, X. 2004. Leveraging structural approaches: applications of NMR-based screening and X-ray crystallography for inhibitor design. *J Synchrotron Radiat,* 11**,** 97-100.

MOSER, C., LANG, S. A. & STOELTZING, O. 2009. Heat-shock protein 90 (Hsp90) as a molecular target for therapy of gastrointestinal cancer. *Anticancer Res,* 29**,** 2031-42.

MURRAY, C. W., CARR, M. G., CALLAGHAN, O., CHESSARI, G., CONGREVE, M., COWAN, S., COYLE, J. E., DOWNHAM, R., FIGUEROA, E., FREDERICKSON, M., GRAHAM, B., MCMENAMIN, R., O'BRIEN, M. A., PATEL, S., PHILLIPS, T. R., WILLIAMS, G., WOODHEAD, A. J. & WOOLFORD, A. J. 2010. Fragment-based drug discovery

applied to Hsp90. Discovery of two lead series with high ligand efficiency. *J Med Chem,* 53**,** 5942-55.

NAVRATILOVA, I. & HOPKINS, A. L. 2010. Fragment screening by surface plasmon resonance. *ACS Med Chem Lett,* 1**,** 44-8.

NEUHAUS, D. & WILLIAMSON, M. P. 1989. *The nuclear Overhauser effect in structural and conformational analysis*, VCH New York.

ORTS, J., GRIESINGER, C. & CARLOMAGNO, T. 2009. The INPHARMA technique for pharmacophore mapping: A theoretical guide to the method. *J Magn Reson,* 200**,** 64-73.

OTTING, G. & WUETHRICH, K. 1989. Studies of protein hydration in aqueous solution by direct NMR observation of individual protein-bound water molecules. *JACS,* 111**,** 1871-1875.

PEARL, L. H. & PRODROMOU, C. 2006. Structure and mechanism of the Hsp90 molecular chaperone machinery. *Annu Rev Biochem,* 75**,** 271-94.

PELLECCHIA, M., BERTINI, I., COWBURN, D., DALVIT, C., GIRALT, E., JAHNKE, W., JAMES, T. L., HOMANS, S. W., KESSLER, H., LUCHINAT, C., MEYER, B., OSCHKINAT, H., PENG, J., SCHWALBE, H. & SIEGAL, G. 2008. Perspectives on NMR in drug discovery: a technique comes of age. *Nat Rev Drug Discov,* 7**,** 738-45.

POORNIMA, C. S. & DEAN, P. M. 1995. Hydration in drug design. 3. Conserved water molecules at the ligand-binding sites of homologous proteins. *J Comput Aided Mol Des,* 9**,** 521-31.

PRODROMOU, C., ROE, S. M., O'BRIEN, R., LADBURY, J. E., PIPER, P. W. & PEARL, L. H. 1997. Identification and structural characterization of the ATP/ADP-binding site in the Hsp90 molecular chaperone. *Cell,* 90**,** 65-75.

RADEMACHER, C., KRISHNA, N. R., PALCIC, M., PARRA, F. & PETERS, T. 2008. NMR experiments reveal the molecular basis of receptor recognition by a calicivirus. *JACS,* 130**,** 3669-75.

SANCHEZ-PEDREGAL, V. M., REESE, M., MEILER, J., BLOMMERS, M. J., GRIESINGER, C. & CARLOMAGNO, T. 2005. The INPHARMA method: protein-mediated interligand NOEs for pharmacophore mapping. *Angew. Chem,* 44**,** 4172-5.

SCHULTE, T. W., AKINAGA, S., SOGA, S., SULLIVAN, W., STENSGARD, B., TOFT, D. & NECKERS, L. M. 1998. Antibiotic radicicol binds to the N-terminal domain of Hsp90 and shares important biologic activities with geldanamycin. *Cell stress chaperon,* 3**,** 100.

SCHWEFEL, D., MAIERHOFER, C., BECK, J. G., SEEBERGER, S., DIEDERICHS, K., MOLLER, H. M., WELTE, W. & WITTMANN, V. 2010. Structural basis of multivalent binding to wheat germ agglutinin. *JACS,* 132**,** 8704-19.

SCOTT, D. E., COYNE, A. G., HUDSON, S. A. & ABELL, C. 2012. Fragment-based approaches in drug discovery and chemical biology. *Biochemistry,* 51**,** 4990-5003.

SILLERUD, L. O. & LARSON, R. S. 2006. Nuclear magnetic resonance-based screening methods for drug discovery. *Methods Mol Biol,* 316**,** 227-89.

STOCKMAN, B. J. & DALVIT, C. 2002. NMR screening techniques in drug discovery and drug design. *Prog Nucl Magn Res Spectrosc,* 41**,** 187-231.

TANOLI, S. A., TANOLI, N. U., BONDANCIA, T. M., USMANI, S., KERSSEBAUM, R., FERREIRA, A. G., FERNANDES, J. B. & UL-HAQ, Z. 2013. Crude to leads: a triple-pronged direct NMR approach in coordination with docking simulation. *Analyst,* 138**,** 5137-45.

TSAI, J., LEE, J. T., WANG, W., ZHANG, J., CHO, H., MAMO, S., BREMER, R., GILLETTE, S., KONG, J., HAASS, N. K., SPROESSER, K., LI, L., SMALLEY, K. S. M., FONG, D., ZHU, Y.-L., MARIMUTHU, A., NGUYEN, H., LAM, B., LIU, J., CHEUNG, I., RICE, J., SUZUKI, Y., LUU, C., SETTACHATGUL, C., SHELLOOE, R., CANTWELL, J., KIM, S.-H., SCHLESSINGER, J., ZHANG, K. Y. J., WEST, B. L., POWELL, B., HABETS, G., ZHANG, C., IBRAHIM, P. N., HIRTH, P., ARTIS, D. R., HERLYN, M. & BOLLAG, G. 2008. Discovery of a selective inhibitor of oncogenic B-Raf kinase with potent antimelanoma activity. *PNAS,* 105**,** 3041-3046.

VERDONK, M. L. & REES, D. C. 2008. Group Efficiency: A Guideline for Hits-to-Leads Chemistry. *ChemMedChem,* 3**,** 1179-1180.

VILENCHIK, M., SOLIT, D., BASSO, A., HUEZO, H., LUCAS, B., HE, H., ROSEN, N., SPAMPINATO, C., MODRICH, P. & CHIOSIS, G. 2004. Targeting wide-range oncogenic transformation via PU24FCl, a specific inhibitor of tumor Hsp90. *Chem Biol,* 11**,** 787-97.

VIVAT HANNAH, V., ATMANENE, C., ZEYER, D., VAN DORSSELAER, A. & SANGLIER-CIANFERANI, S. 2010. Native MS: an 'ESI' way to support structure- and fragment-based drug discovery. *Future Med Chem,* 2**,** 35-50.

WAGSTAFF, J. L., VALLATH, S., MARSHALL, J. F., WILLIAMSON, R. A. & HOWARD, M. J. 2010. Two-dimensional heteronuclear saturation transfer difference NMR reveals detailed integrin alphavbeta6 protein-peptide interactions. *Chem Commun (Camb),* 46**,** 7533-5.

WIELENS, J., HEADEY, S. J., RHODES, D. I., MULDER, R. J., DOLEZAL, O., DEADMAN, J. J., NEWMAN, J., CHALMERS, D. K., PARKER, M. W., PEAT, T. S. & SCANLON, M. J. 2013. Parallel screening of low molecular weight fragment libraries: do differences in methodology affect hit identification? *J Biomol Screen,* 18**,** 147-59.

WILLIAMSON, M. P. 2013. Using chemical shift perturbation to characterise ligand binding. *Prog Nucl Magn Reson Spectrosc,* 73**,** 1-16.

WISHART, D. 2005. NMR spectroscopy and protein structure determination: applications to drug discovery and development. *Curr Pharm Biotechnol,* 6**,** 105-20.

WOODHEAD, A. J., ANGOVE, H., CARR, M. G., CHESSARI, G., CONGREVE, M., COYLE, J. E., COSME, J., GRAHAM, B., DAY, P. J., DOWNHAM, R., FAZAL, L., FELTELL, R., FIGUEROA, E., FREDERICKSON, M., LEWIS, J., MCMENAMIN, R., MURRAY, C. W., O'BRIEN, M. A., PARRA, L., PATEL, S., PHILLIPS, T., REES, D. C., RICH, S., SMITH, D. M., TREWARTHA, G., VINKOVIC, M., WILLIAMS, B. & WOOLFORD, A. J. A. 2010. Discovery of (2,4-Dihydroxy-5-isopropylphenyl)-[5-(4-methylpiperazin-1-ylmethyl)-1,3-dihydroisoindol-2-yl]methanone (AT13387), a Novel Inhibitor of the Molecular Chaperone Hsp90 by Fragment Based Drug Design. *J Med Chem,* 53**,** 5956-5969.

WORKMAN, P., BURROWS, F., NECKERS, L. E. N. & ROSEN, N. 2007. Drugging the cancer chaperone HSP90. *Ann N Y Acad Sci,* 1113**,** 202-216.

WRIGHT, C. S. 1980. Crystallographic elucidation of the saccharide binding mode in wheat germ agglutinin and its biological significance. *J Mol Biol,* 141**,** 267-91.

WRIGHT, C. S. 1989. Comparison of the refined crystal structures of two wheat germ isolectins. *J Mol Biol,* 209**,** 475-87.

WRIGHT, C. S. & KELLOGG, G. E. 1996. Differences in hydropathic properties of ligand binding at four independent sites in wheat germ agglutinin-oligosaccharide crystal complexes. *Protein Sci,* 5**,** 1466-76.

WYATT, P. G., WOODHEAD, A. J., BERDINI, V., BOULSTRIDGE, J. A., CARR, M. G., CROSS, D. M., DAVIS, D. J., DEVINE, L. A., EARLY, T. R. & FELTELL, R. E. 2008. Identification of N-(4-Piperidinyl)-4-(2, 6-dichlorobenzoylamino)-1 H-pyrazole-3-carboxamide (AT7519), a Novel Cyclin Dependent Kinase Inhibitor Using Fragment-Based X-Ray Crystallography and Structure Based Drug Design†. *J Med Chem,* 51**,** 4986-4999.

Appendix A

This appendix is an attachment of the publication, published in January 2014, which forms the basis of chapter two.

RSC Advances

COMMUNICATION

Optimising selective excitation pulses to maximise saturation transfer difference NMR spectroscopy†

Nathan B. Ley, Michelle L. Rowe, Richard A. Williamson and Mark J. Howard*

A simple method is presented that optimizes the STD NMR Gaussian pulse to deliver significant increases in STD amplification factors with minimal perturbation of the ligand. This approach is practically demonstrated using the wheat-germ agglutinin/N-acetyl-D-glucosamine protein–ligand system.

Saturation transfer difference (STD) NMR is a popular method for identifying small ligand molecules that interact with a particular protein of interest[1-6] and is used extensively to identify chemical fragments that bind to target biomolecules in drug discovery.[7-14] However, more recently STD NMR has been used to investigate the binding mode of samples containing a single ligand from the outset or as a secondary screen and it is important to obtain optimum results for such experiments.[15-18] ^{1}H STD NMR is initiated by the saturation of protein magnetization that is created using a specific shaped excitation pulse (Fig. 1).

Although the shaped excitation pulse initially saturates a small proportion of ^{1}H, typically upfield methyl protons, this saturation disperses across the protein quickly via spin-diffusion to saturate many protons. [1]H nuclei of any ligand interacting with the protein will also experience this saturation as it is transferred from protein to ligand. Any magnetization transferred to the ligand before it dissociates from the protein can be measured in a ^{1}H NMR ligand spectrum as the difference between two NMR datasets; one where the protein is saturated (on or I) and the other when it is not (off or I_o). The difference spectrum I_{STD} is simply defined as $(I-I_o)$. To compensate for indirect saturation effects, 'on' saturation is achieved by placing the pulse within the protein proton spectral envelope (ca. 0 ppm) and 'off' saturation is achieved by placing the same pulse distant from this envelope (ca. 30 ppm). It is worth noting that for STD NMR involving cells or virus-like particles, the 'off'

School of Biosciences, University of Kent, Canterbury CT2 7NJ, UK. E-mail: m.j. howard@kent.ac.uk; Tel: +44 (0)1227 3274730
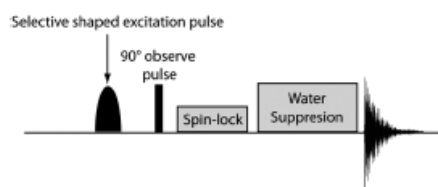
Fig. 1 ^{1}H STD NMR pulse sequence highlighting the shaped excitation pulse that drives saturation of the protein. Pulse sequence regions responsible for spin-locking (to reducing protein background signal) and water suppression are also shown.

saturation position has to be much further up- or downfield (ca. ±300 ppm) to prevent accidental excitation during the 'off' condition brought about by the very large molecular weight of these systems.[19] Indirect effects are further minimized by interleaving 'on' and 'off' experiments and the data split into their respective spectra after acquisition. The saturation of the protein is typically achieved by repeatedly pulsing a shaped excitation pulse that is typically 20 to 50 milliseconds in length over a period of 1 to 10 seconds. The pulse is shaped in nature (e.g. Gaussian[20] or E-burp[21]) to further limit its excitation profile and prevent accidental excitation of ligand. Gaussian or E-burp pulses are preferred to hard pulses for STD NMR because of the virtual absence of side-lobes and low excitation levels at large offsets from the pulse.[3,20,21] It is crucial that saturation pulses are applied to provide efficient saturation of the protein without accidental excitation of ligand protons that can distort results.

We communicate here that Gaussian shaped excitation pulses can be shorter than 50 ms and rationally placed to minimise direct ligand excitation. This approach provides maximal saturation of the protein to deliver optimal STD amplification factors from any difference spectra obtained. This optimisation is demonstrated using the Gaussian pulse, as this is currently the most commonly used shaped-pulse for STD in both academia and industry. However, the approach describe herein could equally be applied to E-burp or other pulse

schemes. Optimising any STD shaped-pulse will dramatically improve the sensitivity of STD NMR data and we can demonstrate +10-fold increases in amplification factor for the Gaussian pulse scheme. The demonstration datasets presented were obtained using a known STD NMR system of wheat-germ agglutinin (WGA) protein from *Triticum vulgaris*, with an *N*-acetyl-D-glucosamine (GlcNAc) ligand.[4] All components were purchased from Sigma-Aldrich. Samples were prepared using 20 μM WGA, 1 mM GlcNAc in deuterium oxide corrected to pH 7.4 in a buffer of 10 mM sodium phosphate and 10 mM sodium chloride. 1 mM raffinose was used in addition to GlcNAc and WGA as a negative STD control for Fig. 2 but was omitted from all other experiments. All NMR experiments were run at 283 K using a Bruker AV3 600 MHz NMR spectrometer equipped with a QCI-F cryoprobe. Datasets were processed and analysed using Bruker Topspin 3.0 and ^{1}H spectra were referenced to 4,4-dimethyl-4-silapentane-1-sulphonic acid (DSS). Shaped pulses were generated and optimized using Bruker Shape Tool. STD NMR datasets were obtained over 512 scans (256 scans 'on' and 256 scans 'off' saturation) with 2.5, 5, 10, 25 or 50 ms Gaussian shaped pulses and variable 'on' saturation positions but with 'off' saturation set to −30 ppm in all experiments. The GlcNAc methyl proton absolute intensity was obtained using MestReNova (Mnova) and used to calculate the STD amplification factor (STD$_{amp}$) from STD difference spectra [$I_{STD} = (I − I_o)$] and STD control spectra (I_o) as previously described using the equation:[3]

$$STD_{amp} = (I_{STD}/I_0) \times \text{ligand excess.}$$

Fig. 2 shows the STD NMR difference spectra for WGA/GlcNAc where the methyl protons of GlcNAc (at 1.8 ppm relative
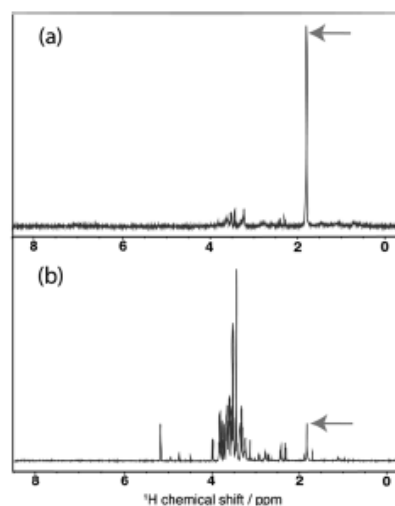
to DSS) provide a simple but robust system to monitor the effect of changing the Gaussian pulse length and 'on' saturation position for a constant saturation period of 2 seconds.

Fig. 3 demonstrates the effect on STD amplification factor when altering the on-resonance position with respect to the upfield methyl GlcNAc resonance and shortening the length of the Gaussian pulse. Our analysis concentrates on data using 2.5, 5 and 10 ms Gaussian pulses in preference to longer 20 and 50 ms pulses that have been used in many studies (*e.g.* see ref. 3, 15, 22–27). Inspection of Fig. 3 suggests that 2.5 ms Gaussian pulse placed at −1.8 ppm (1080 Hz) upfield from the ligand resonance provides the optimum STD result with an amplification factor 7 times greater than a 5 ms pulse and 19 times greater than a 10 ms pulse. This is not surprising and it has been noted previously that STD difference spectra display a high-dependence on the power level of the shaped pulse.[21] The 2.5 ms Gaussian pulse surpasses 5 ms and 10 ms pulses over the entire on-resonance range in Fig. 3 and the measured amplification factor when using this pulse increases dramatically when it is applied with an offset below 2.8 ppm (1680 Hz) upfield from the GlcNAc methyl resonance.

The increase observed by the 2.5 ms Gaussian pulse could be attributed to either accidental excitation of the free-ligand or excitation of the bound ligand resonance. The latter case is extremely unlikely because the GlcNAc/WGA system does not demonstrate large ligand shifts upon binding. The interpretation of accidental excitation with small on-resonances offsets for a 2.5 ms Gaussian pulse can be tested in two ways. First, by obtaining practical NMR Gaussian excitation profiles (Fig. 4) from a 2 seconds comb of 2.5 ms and 5.0 ms pulses. Second, by measuring a 'virtual' STD amplification factor for GlcNAc methyl resonances in the absence of the protein WGA for a range of on-resonances offsets. The second process would detect excitation of the ligand by a Gaussian pulse for a particular offset (Fig. 5). This accidental excitation would manifest as a non-zero STD$_{amp}$ value because STD 'I' and 'I_o' experiments should yield the same result in the absence of

Fig. 2 ^{1}H STD NMR difference (a) and control (b) spectrum obtained over 256 scans using a 10 ms Gaussian pulse for WGA/GlcNAc/Raffinose. The GlcNAc ^{1}H methyl resonance that is referred in the text is highlighted with the grey arrow.
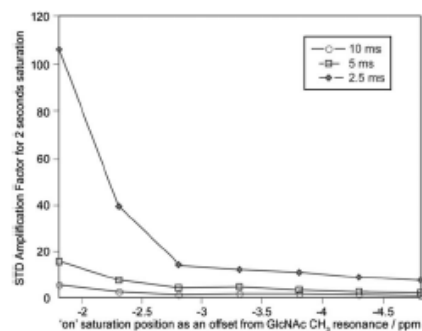
Fig. 3 GlcNAc methyl ^{1}H STD amplification factor in the presence of WGA for 2.5, 5 and 10 ms Gaussian pulses over a range of 'on' saturation points. The 'on' resonance position is shown as a ppm offset (600 MHz ^{1}H) from the ligand resonance; *e.g.* an offset of −1.8 ppm is at 0 ppm. NMR spectra associated with these data are shown in ESI† Fig. S1−3.
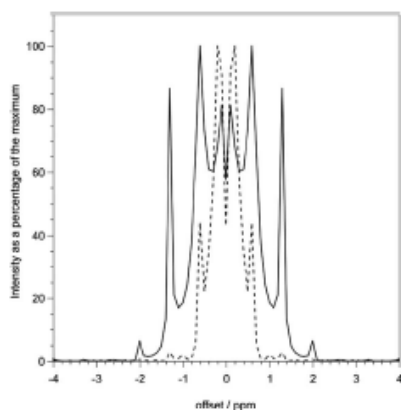
Fig. 4 Excitation profiles of 2.5 ms (solid line) and 5 ms (dotted line) Gaussian pulses delivered continually as a train of pulses for 2 s at 14.1 T (600 MHz ^{1}H). Each profile was acquired by measuring the intensity of the ^{1}HDO resonance in deuterium oxide (D_2O) with a 0.1 ppm resolution between data points over a ±4 ppm offset window.

Fig. 5 ^{1}H STD NMR amplification factor using a 2.5 ms Gaussian pulse over a range of 'on' saturation points for 1 mM GlcNAc control with no WGA protein present in the sample. ESI† Fig. S5 shows the GlcNAc methyl STD difference.

approach to providing saturation for STD is to loop the pulse continually without any inter-pulse delay over the saturation period. Therefore, a 2 seconds saturation period would then use 400 5 ms pulses or 800 2.5 ms pulses. Measuring the residual ^{1}H resonance (HDO) in ^{2}H$_2$O provides a single resonance with a narrow half peak height below 0.003 ppm (2 Hz). This minimises potential measurement discrepancies caused by B_1 inhomogeneity that can distort the efficiency of composite pulses. Profiles were created by sweeping the carrier frequency in a pulse-acquire experiment containing the shaped pulse of interest and measuring the signal intensity from the residual ^{1}H resonance.

Fig. 4 demonstrates the expected result of shortening the Gaussian pulse length to create a wider excitation profile. In addition, Fig. 4 illustrates the profile obtained from a 2 seconds train of pulses is significantly different from a single Gaussian pulse as shown in ESI† Fig. S4. The pulse train profiles confirm a 2 ppm offset is sufficient for a 5 ms Gaussian pulse but a 2.5 ms Gaussian pulse should be placed at least 2.5 ppm from the nearest resonance to prevent accidental excitation. Referring to Fig. 3 suggests STD performed with a 5 ms Gaussian pulse rather than a 10 ms pulse provides *ca.* 3-fold increase in STD$_{amp}$ for a 2.0 ppm offset. Equally, Fig. 3 also informs that STD experiments using a 2.5 ms Gaussian pulse in preference to 10 ms provides *ca.* 15-fold increase in STD$_{amp}$ when using a 2.5 ppm offset. These data confirm the merit of using shorter Gaussian pulses that are optimally positioned with respect to the closest ligand resonance.

The effect of significant sidebands that occur away from the pulse centre was investigated using a control experiment where no WGA protein was added to the sample (Fig. 5). Any significant sideband was defined for where the intensity was greater 1% of the maximum; this dictates the farthest significant side band for the 2.5 ms Gaussian pulse at ± 2.0 ppm. Fig. 5 displays the STD$_{amp}$ results of a control experiment without protein where STD signal must be due to excitation of the ligand by the 2.5 ms Gaussian shaped pulse in the on-resonance position. The STD$_{amp}$ values fall to zero when the 2.5 ms pulse is placed at offsets greater than or equal to 1.8 ppm and Fig. 4 confirms the 1.8 ppm position as providing a 'valley' in the excitation profile in between two excitation bands at offsets of 2.0 ppm and 1.4 ppm. Interestingly, despite 2.5 ms Gaussian excitation sideband at 1.4 ppm delivering over 85% of the maximum excitation intensity, the equivalent point provided a modest STD$_{amp}$ of less than 10 in Fig. 5. In contrast, the sideband at 0.6 ppm that defines the 100% profile intensity point is responsible for a much higher control STD$_{amp}$. This suggests that although Gaussian side bands are present in pulse trains, their influence on saturation and creating accidental excitation in STD could be limited. Furthermore, the excitation sideband at 2.0 ppm appears not to provide any control amplification value at the same location in Fig. 5 and suggests this small sideband does not significantly excite the ligand resonance. The 1.8 ppm and 2.0 ppm offsets in Fig. 4 correlate to 1.5% and 6.4% of the maximum excitation for a 2.5 ms Gaussian pulse train. As both of these offsets provide zero STD$_{amp}$ in the control experiment (Fig. 5), they must be below the lower excitation limit where

protein. As $I_{STD} = (I - I_o)$, the difference spectrum should be blank and yield an STD$_{amp}$ value of zero. If a difference spectrum with signals is obtained, this is because $I_{STD} > 0$, therefore $I \neq I_o$ and as no protein is present to facilitate saturation transfer, the $I \neq I_o$ scenario has to be due to excitation by the on-resonance pulse. Ultimately, Fig. 5 demonstrates both correct ($I_{STD} = 0$) and incorrect ($I_{STD} \neq 0$) results for this negative control experiment. The combination of Fig. 4 and 5 will allow us to identify offset values at which the excitation profile creates accidental excitation. This also provides the identification of a maximum allowable percentage excitation that would not create a false-positive spectrum.

Although spectrometer software enables users to evaluate shaped pulses for excitation and width, it was considered prudent to obtain practically obtained excitation profiles for 2 seconds trains of 2.5 ms and 5 ms Gaussian pulses. These profiles were produced using identical pulse trains that created the STD NMR data shown in Fig. 1–3 and 5. The standard

false-positive STD data could occur in a 256-scan STD NMR experiment.

The 'on' saturation shaped pulse is usually positioned around 0 ppm to excite protons of upshifted methyl groups within the protein. The efficiency of protons excitation will clearly influence saturation of the protein and transfer to the ligand. Optimal positioning of the shaped excitation pulse with respect to protein methyl protons will boost efficiency. Fig. 3 demonstrates this effect through the observed increase in STD amplification factor as the shaped-pulse offset is reduced. Therefore, the protein target used in STD NMR experiments has an influence on the optimization of the shape pulse and when methyl protons are significantly upshifted they can be excited for saturation by a shaped pulse with a larger offset. This effect is further accentuated for larger proteins with greater numbers of methyl groups and additional dipolar line broadening to extend the protein excitation envelope. Therefore, Fig. 3 is specific to the WGA/GlcNAc system and STD optimisation should be considered for any new target-protein ligand system, particularly if using quantitative STD NMR.[16,26] STD optimisation curves, as in Fig. 3, provide cursory identification of direct on-resonance ligand excitation as a significant increase in observed STD amplification factor. However, a control STD curve, such as that shown in Fig. 5, provides the ultimate assessment and confirms the offsets where excitation is avoided when protein is absent. In our WGA/GlcNAc system, Fig. 5 also confirms that an offset of −1.8 ppm from the ligand reference is safe for 256 scan STD experiments. It is important to reiterate the scan dependence on this information and it is crucial that scan number is identical when creating curves equivalent to Fig. 3 and 5.

Conclusions

Our 14.1 T based study concluded that for 256-scan 'on' saturation STD experiments, a 2.5 ms Gaussian pulse can be placed as near as −1.8 ppm upfield from the closest ligand ^{1}H resonance to provide a 19-fold improvement in STD_{amp} compared to a 10 ms Gaussian pulse train. However, 5 ms Gaussian pulse still delivers a 3-fold improvement over the 10 ms pulse should the user want to exercise caution. The overall message is that Gaussian pulses within a 2 seconds pulse train can be shortened to provide significant enhancements in STD NMR. This approach would be beneficial when optimising STD NMR for single ligand/target systems or when applying quantitative analysis.

^{1}H STD NMR can be optimized by using short Gaussian shaped pulses that are rationally placed at relatively short offset distances from the closest ligand resonance. Our example measured ligand STD_{amp} values over a range of offsets for the ligand in the presence and absence of protein to identify the optimum offset condition. The increased efficiency in saturating the protein was due to a wider-targeted Gaussian pulse that excites a larger population of upshifted methyl groups in the protein. This does suggest that the widespread use of 20 and 50 ms Gaussian pulses in STD NMR to be disadvantageous and the application of shorter pulses can be evaluated easily using the methods described. The shaped pulse length is an

experimental parameter that can be easily modified within modern spectrometers and the power level adjustment required is easily obtained using spectrometer manufacturer software tools within the acquisition software. This approach need not be limited to Gaussian pulses and our method could be utilized with any STD shaped pulse configuration (e.g. E-BURP 90° pulses).

Acknowledgements

Notes and references

1 M. Mayer and B. Meyer, J. Am. Chem. Soc., 2001, 123, 6108–6117.

2 M. Mayer and B. Meyer, Angew. Chem., Int. Ed., 1999, 38, 1784–1788.

3 B. Meyer and T. Peters, Angew. Chem., Int. Ed. Engl., 2003, 42, 864–890.

4 M. Mayer and B. Meyer, Angew. Chem., Int. Ed., 1999, 38, 1784–1788.

5 J. L. Wagstaff, S. L. Taylor and M. J. Howard, Mol. Biosyst., 2013, 9, 571–577.

6 T. Biet and T. Peters, Angew. Chem., Int. Ed., 2001, 40, 4189–4192.

7 B. J. Stockman and C. Dalvit, Prog. Nucl. Magn. Reson. Spectrosc., 2002, 41, 187–231.

8 H. Jhoti, A. Cleasby, M. Verdonk and G. Williams, Curr. Opin. Chem. Biol., 2007, 11, 485–493.

9 C. A. Lepre, J. M. Moore and J. W. Peng, Chem. Rev., 2004, 104, 3641–3675.

10 J. Moore, N. Abdul-Manan, J. Fejzo, M. Jacobs, C. Lepre, J. Peng and X. L. Xie, J. Synchrotron Radiat., 2004, 11, 97–100.

11 M. Pellecchia, I. Bertini, D. Cowburn, C. Dalvit, E. Giralt, W. Jahnke, T. L. James, S. W. Homans, H. Kessler, C. Luchinat, B. Meyer, H. Oschkinat, J. Peng, H. Schwalbe and G. Siegal, Nat. Rev. Drug Discovery, 2008, 7, 738–745.

12 J. W. Peng, J. Moore and N. Abdul-Manan, Prog. Nucl. Magn. Reson. Spectrosc., 2004, 44, 225–256.

13 L. O. Sillerud and R. S. Larson, Methods Mol. Biol., 2006, 316, 227–289.

14 D. Wishart, Curr. Pharm. Biotechnol., 2005, 6, 105–120.

15 D. Dicara, C. Rapisarda, J. L. Sutcliffe, S. M. Violette, P. H. Weinreb, I. R. Hart, M. J. Howard and J. F. Marshall, J. Biol. Chem., 2007, 282, 9657–9665.

16 S. Kemper, M. K. Patel, J. C. Errey, B. G. Davis, J. A. Jones and T. D. Claridge, J. Magn. Reson., 2010, 203, 1–10.

17 J. L. Wagstaff, S. Vallath, J. F. Marshall, R. A. Williamson and M. J. Howard, Chem. Commun., 2010, 46, 7533–7535.

18 D. W. Begley, S. X. Zheng and G. Varani, Chem. Biol. Drug Des., 2010, 76, 218–233.

19 C. Rademacher, N. R. Krishna, M. Palcic, F. Parra and T. Peters, J. Am. Chem. Soc., 2008, 130, 3669–3675.

20 R. Freeman, *Prog. Nucl. Magn. Reson. Spectrosc.*, 1998, **32**, 59–106.

21 B. Cutting, S. V. Shelke, Z. Dragic, B. Wagner, H. Gathje, S. Kelm and B. Ernst, *Magn. Reson. Chem.*, 2007, **45**, 720–724.

22 B. Meyer, J. Klein, M. Mayer, R. Meinecke, H. Moller, A. Neffe, O. Schuster, J. Wulfken, Y. Ding, O. Knaie, J. Labbe, M. M. Palcic, O. Hindsgaul, B. Wagner and B. Ernst, *Ernst Schering Res. Found. Workshop*, 2004, 149–167.

23 B. Meyer, T. Weimar and T. Peters, *Eur. J. Biochem.*, 1997, **246**, 705–709.

24 J. Angulo, P. M. Enriquez-Navas and P. M. Nieto, *Chem.-Eur. J.*, 2010, **16**, 7803–7812.

25 J. Angulo, B. Langpap, A. Blume, T. Biet, B. Meyer, N. R. Krishna, H. Peters, M. M. Palcic and T. Peters, *J. Am. Chem. Soc.*, 2006, **128**, 13529–13538.

26 J. Angulo and P. M. Nieto, *Eur. Biophys. J.*, 2011, **40**, 1357–1369.

27 J. Angulo, C. Rademacher, T. Biet, A. J. Benie, A. Blume, H. Peters, M. Palcic, F. Parra and T. Peters, *Methods Enzymol*, 2006, **416**, 12–30.

Appendix B

This table shows the proton numbers referred to in this thesis and their equivalent proton numbers in this appendix. In the following tables the identity of the recipient ligand proton is shown, along with the amino acid donor side chain, the distance (in Å), and in green, the distance written as $(1/\text{Å}^6)$. The sum of all values in green is written at the bottom of each table and is taken as the "distance" restraint against which experimental STD NMR data is correlated. Data for exchangeable donor protons is not included, and donor methyl groups are "sum averaged" as one distance.

Fragment

Hsp90

A

5	4	3	2	1	6
16	17	18	19	20	21

B

2	3	1	4	4	6	6	5	5	5	7	7	7
27	28	33	20	21	22	23	17	18	19	24	25	26

C

7	7	7	1	2	3	4	5	6
13	14	15	17	18	19	20	21	22

D

4	3	2	1	6	5
13	14	15	16	17	18

E

1	6	5	4	3	2
16	17	18	19	20	21

F

3	2	2	1	1	1	4	5	6	7	8
20	19	18	17	16	15	21	22	23	24	25

Ras

H

1	3	4	5	6
25	26	27	28	29

I

7	8	5	6	4	3	2	1
19	20	21	22	23	24	25	26

J

3	4	6	1	9	10	11	12
20	21	22	23	24	25	26	27

K

6	5	7	4	3	2	1
27	28	29	32	33	34	35

L

7	6	5	1	2	3	4
21	22	23	24	25	26	27

Proton numbers in the main thesis

Proton numbers in this appendix

Fragment A

		Recipient ligand proton	Donor Side Chain	Distance (Å)		Distance (1/Å^6)	
		XXX 1 X H16	ALA 55 A HB2	2.85		0.001866082	
		XXX 1 X H16	MET 98 A HG3	3.03		0.001292243	
exch		XXX 1 X H16	THR 184 A HG1	3.07		0.001194455	
		XXX 1 X H16	ALA 55 A HB1	3.09		0.001148812	
		XXX 1 X H16	GLY 97 A H	3.24		0.00086443	
	meth	XXX 1 X H16	ILE 96 A HG22	3.4	3.79	0.000647331	0.00033564
	meth	XXX 1 X H16	ILE 96 A HG23	3.6		0.000459394	
		XXX 1 X H16	GLY 97 A HA2	3.65		0.000422905	
		XXX 1 X H16	MET 98 A HG2	3.66		0.000416019	
		XXX 1 X H16	ALA 55 A HB3	3.98		0.000251595	
	meth	XXX 1 X H16	MET 98 A HE2	4	4.88	0.000244141	7.43467E-05
	meth	XXX 1 X H16	ILE 96 A HG21	4.38		0.00014163	
		XXX 1 X H16	ALA 55 A HA	4.4		0.000137811	
		XXX 1 X H16	ILE 96 A H	4.53		0.000115721	
		XXX 1 X H16	THR 184 A HB	4.57		0.000109775	
exch		XXX 1 X H16	THR 152 A HG1	4.79		8.27917E-05	
		XXX 1 X H16	MET 98 A HA	4.8		8.17622E-05	
		XXX 1 X H16	GLY 97 A HA3	4.83		7.87621E-05	
	meth	XXX 1 X H16	THR 184 A HG21	4.86		7.58896E-05	
		XXX 1 X H16	MET 98 A H	4.92		7.05033E-05	
	meth	XXX 1 X H16	MET 98 A HE3	5.12		5.55112E-05	
exch	meth	XXX 1 X H16	LYS 58 A HZ2	5.19		5.11677E-05	
		XXX 1 X H16	LYS 58 A HD2	5.25		4.77578E-05	
		XXX 1 X H16	MET 98 A HB2	5.3		4.51175E-05	
		XXX 1 X H16	ALA 55 A H	5.31		4.46101E-05	
		XXX 1 X H16	GLY 95 A HA3	5.33		4.36151E-05	
	meth	XXX 1 X H16	MET 98 A HE1	5.51		3.57347E-05	
		XXX 1 X H16	SER 52 A HA	5.66		3.0416E-05	
		XXX 1 X H16	ILE 96 A HB	5.67		3.00955E-05	
		XXX 1 X H16	MET 98 A HB3	5.69		2.94664E-05	
	meth	XXX 1 X H16	THR 184 A HG23	5.76		2.7382E-05	
		XXX 1 X H16	ASN 51 A HB3	5.79		2.65417E-05	
exch		XXX 1 X H16	ASN 106 A HD22	5.81		2.59982E-05	
		XXX 1 X H16	GLY 183 A HA2	5.85		2.49497E-05	
					SUM	0.008866004	0.007588978

		Recipient ligand proton	Donor Side Chain	Distance (Å)		Distance (1/Å^6)	
		XXX 1 X H17	MET 98 A HG2	2.85		0.001866082	
		XXX 1 X H17	MET 98 A HG3	3		0.001371742	
	meth	XXX 1 X H17	MET 98 A HE2	3.48	4.23	0.000563021	0.000174565
exch		XXX 1 X H17	ASN 106 A HD22	3.62		0.000444374	
exch		XXX 1 X H17	ASN 106 A HD21	4.33		0.00015173	
		XXX 1 X H17	ALA 55 A HB2	4.38		0.00014163	
exch		XXX 1 X H17	THR 184 A HG1	4.42		0.000134112	
	meth	XXX 1 X H17	MET 98 A HE1	4.51		0.000118834	
exch	meth	XXX 1 X H17	LYS 58 A HZ2	4.66	5.3	9.76528E-05	4.51175E-05
	meth	XXX 1 X H17	MET 98 A HE3	4.7		9.27711E-05	
		XXX 1 X H17	ASP 102 A HB3	4.96		6.71599E-05	
		XXX 1 X H17	MET 98 A HA	5.07		5.88779E-05	
		XXX 1 X H17	ASN 106 A HB2	5.09		5.75034E-05	
		XXX 1 X H17	MET 98 A HB3	5.1		5.68302E-05	
		XXX 1 X H17	ASN 106 A HB3	5.11		5.61661E-05	
		XXX 1 X H17	MET 98 A HB2	5.18		5.17632E-05	
		XXX 1 X H17	ASN 51 A HB3	5.22		4.94284E-05	
		XXX 1 X H17	ALA 55 A HB1	5.24		4.83072E-05	
	meth	XXX 1 X H17	ILE 96 A HG23	5.26	5.42	4.72156E-05	3.94461E-05
	meth	XXX 1 X H17	ILE 96 A HG22	5.28		4.61526E-05	
	meth	XXX 1 X H17	THR 184 A HG21	5.34		4.31273E-05	
exch	meth	XXX 1 X H17	LYS 58 A HZ3	5.51		3.57347E-05	
		XXX 1 X H17	GLY 97 A HA2	5.66		3.0416E-05	
		XXX 1 X H17	GLY 97 A H	5.69		2.94664E-05	
	meth	XXX 1 X H17	ILE 96 A HG21	5.72		2.85512E-05	
exch	meth	XXX 1 X H17	LYS 58 A HZ1	5.74		2.79595E-05	
		XXX 1 X H17	ALA 55 A HA	5.78		2.68184E-05	
		XXX 1 X H17	ALA 55 A HB3	5.81		2.59982E-05	
		XXX 1 X H17	LYS 58 A HD2	5.84		2.52071E-05	
exch		XXX 1 X H17	THR 152 A HG1	5.96		2.23112E-05	
		XXX 1 X H17	MET 98 A H	5.97		2.20879E-05	
					SUM	0.004925158	0.004244614

	Recipient ligand proton	Donor Side Chain	Distance (Å)		Distance (1/Å^6)	
meth	XXX 1 X H18	MET 98 A HE1	3.27	3.82	0.000817925	0.000323515
meth	XXX 1 X H18	LEU 107 A HD21	3.34	4.27	0.000720313	0.000164981
exch	XXX 1 X H18	ASN 51 A HD22	3.49		0.000553411	
meth	XXX 1 X H18	MET 98 A HE2	3.52		0.000525707	
	XXX 1 X H18	PHE 138 A HD1	3.53		0.000516835	
meth	XXX 1 X H18	LEU 107 A HD11	3.97	4.89	0.000255421	7.34385E-05
meth	XXX 1 X H18	THR 184 A HG21	4.19	5.00	0.000184806	6.42566E-05
	XXX 1 X H18	PHE 138 A HE1	4.19		0.000184806	
	XXX 1 X H18	PHE 138 A HB2	4.26		0.000167318	
	XXX 1 X H18	ASN 51 A HB3	4.27		0.000164981	
	XXX 1 X H18	LEU 107 A HG	4.38		0.00014163	
exch	XXX 1 X H18	ASN 51 A HD21	4.41		0.000135947	
meth	XXX 1 X H18	VAL 150 A HG11	4.51	5.23	0.000118834	4.88641E-05
meth	XXX 1 X H18	LEU 107 A HD23	4.58		0.000108345	
meth	XXX 1 X H18	MET 98 A HE3	4.66		9.76528E-05	
meth	XXX 1 X H18	VAL 186 A HG21	4.74	4.96	8.81718E-05	6.71599E-05
meth	XXX 1 X H18	VAL 150 A HG21	4.77		8.48965E-05	
meth	XXX 1 X H18	VAL 186 A HG22	4.82		7.97476E-05	
meth	XXX 1 X H18	LEU 107 A HD22	4.89		7.31386E-05	
	XXX 1 X H18	ASN 51 A HB2	4.98		6.55577E-05	
meth	XXX 1 X H18	VAL 150 A HG13	5.21		5.00004E-05	
	XXX 1 X H18	ASN 106 A HB3	5.3		4.51175E-05	
meth	XXX 1 X H18	VAL 186 A HG23	5.32		4.41093E-05	
meth	XXX 1 X H18	LEU 107 A HD13	5.34		4.31273E-05	
meth	XXX 1 X H18	LEU 107 A HD12	5.35		4.26459E-05	
meth	XXX 1 X H18	THR 184 A HG22	5.39		4.07819E-05	
meth	XXX 1 X H18	THR 184 A HG23	5.41		3.98856E-05	
	XXX 1 X H18	PHE 138 A HB3	5.44		3.85839E-05	
meth	XXX 1 X H18	VAL 150 A HG22	5.44		3.85839E-05	
exch	XXX 1 X H18	THR 184 A HG1	5.49		3.6523E-05	
meth	XXX 1 X H18	LEU 48 A HD22	5.49		3.6523E-05	
	XXX 1 X H18	ASN 106 A HB2	5.56		3.38494E-05	
	XXX 1 X H18	MET 98 A HG3	5.58		3.3128E-05	
	XXX 1 X H18	PHE 138 A HZ	5.7		2.91575E-05	
meth	XXX 1 X H18	LEU 48 A HD23	5.75		2.7669E-05	
	XXX 1 X H18	PHE 138 A HA	5.8		2.62683E-05	
exch	XXX 1 X H18	ASN 106 A HD22	5.95		2.25371E-05	
meth	XXX 1 X H18	VAL 150 A HG12	5.97		2.20879E-05	
				SUM	0.004987604	0.002189446

	Recipient ligand proton	Donor Side Chain	Distance (Å)		Distance (1/Å^6)	
meth	XXX 1 X H19	LEU 107 A HD21	1.96	2.61	0.017638578	0.003163421
meth	XXX 1 X H19	LEU 107 A HD23	2.57		0.003470574	
	XXX 1 X H19	PHE 138 A HB2	2.62		0.003091664	
	XXX 1 X H19	PHE 138 A HD1	3.09		0.001148812	
	XXX 1 X H19	PHE 138 A HB3	3.28		0.000803077	
meth	XXX 1 X H19	LEU 107 A HD22	3.3		0.000774313	
	XXX 1 X H19	LEU 107 A HG	3.59		0.000467125	
	XXX 1 X H19	PHE 138 A HD2	3.91		0.000279859	
exch	XXX 1 X H19	ASN 51 A HD22	3.95		0.00026328	
meth	XXX 1 X H19	LEU 107 A HD11	4.07	4.73	0.000220006	8.96747E-05
exch	XXX 1 X H19	ASN 51 A HD21	4.09		0.000213629	
	XXX 1 X H19	PHE 138 A HE1	4.2		0.000182181	
	XXX 1 X H19	ASN 106 A HB3	4.41		0.000135947	
	XXX 1 X H19	LEU 107 A HA	4.5		0.000120427	
	XXX 1 X H19	PHE 138 A HA	4.7		9.27711E-05	
meth	XXX 1 X H19	MET 98 A HE1	4.76		8.59722E-05	
	XXX 1 X H19	PHE 138 A HE2	4.84		7.77907E-05	
meth	XXX 1 X H19	LEU 107 A HD13	4.87		7.49594E-05	
	XXX 1 X H19	PHE 138 A HZ	4.96		6.71599E-05	
	XXX 1 X H19	PHE 138 A H	4.97		6.63532E-05	
	XXX 1 X H19	ASN 106 A HB2	5.01		6.32373E-05	
meth	XXX 1 X H19	LEU 107 A HD12	5.24		4.83072E-05	
meth	XXX 1 X H19	VAL 150 A HG21	5.25		4.77578E-05	
	XXX 1 X H19	LEU 107 A HB3	5.32		4.41093E-05	
meth	XXX 1 X H19	MET 98 A HE2	5.54		3.45893E-05	
	XXX 1 X H19	LEU 107 A HB2	5.64		3.10689E-05	
	XXX 1 X H19	ASN 51 A HB3	5.72		2.85512E-05	
meth	XXX 1 X H19	VAL 150 A HG11	5.88		2.41956E-05	
meth	XXX 1 X H19	LEU 48 A HD23	5.92		2.32311E-05	
				SUM	0.029142617	0.009863555

	Recipient ligand proton	Donor Side Chain	Distance (Å)		Distance (1/Å^6)	
	XXX 1 X H20	ASN 106 A HB3	3.03		0.001292243	
	XXX 1 X H20	PHE 138 A HB2	3.41		0.000636024	
meth	XXX 1 X H20	LEU 107 A HD23	3.43	4.06	0.000614095	0.00022438
	XXX 1 X H20	PHE 138 A HB3	3.62		0.000444374	
meth	XXX 1 X H20	LEU 107 A HD21	3.89		0.000288604	
	XXX 1 X H20	ASN 106 A HB2	4.28		0.000162681	
exch	XXX 1 X H20	ASN 51 A HD21	4.32		0.00015385	
	XXX 1 X H20	ASN 106 A HA	4.38		0.00014163	
	XXX 1 X H20	LEU 107 A HG	4.45		0.000128777	
	XXX 1 X H20	LEU 107 A HA	4.47		0.000125359	
	XXX 1 X H20	PHE 138 A H	4.71		9.15956E-05	
meth	XXX 1 X H20	LEU 107 A HD22	4.85		7.68333E-05	
exch	XXX 1 X H20	ASN 51 A HD22	4.89		7.31386E-05	
	XXX 1 X H20	PHE 138 A HD2	4.94		6.88079E-05	
	XXX 1 X H20	LYS 112 A HE3	5		0.000064	
	XXX 1 X H20	PHE 138 A HD1	5.18		5.17632E-05	
	XXX 1 X H20	TYR 139 A HE2	5.28		4.61526E-05	
	XXX 1 X H20	VAL 136 A HA	5.39		4.07819E-05	
exch	XXX 1 X H20	TYR 139 A HH	5.44		3.85839E-05	
exch	XXX 1 X H20	ASN 106 A HD22	5.51		3.57347E-05	
	XXX 1 X H20	LEU 107 A H	5.6		3.24244E-05	
	XXX 1 X H20	PHE 138 A HA	5.68		2.9779E-05	
meth	XXX 1 X H20	LEU 107 A HD11	5.93		2.2997E-05	
				SUM	0.004358923	0.003580774

		Recipient ligand proton	Donor Side Chain	Distance (Å)	Distance (1/Å^6)	
exch		XXX 1 X H21	ASN 106 A HD22	3.94	0.000267315	
		XXX 1 X H21	ASN 106 A HB3	3.97	0.000255421	
exch		XXX 1 X H21	ASN 106 A HD21	4.4	0.000137811	
		XXX 1 X H21	ASN 51 A HB3	4.45	0.000128777	
exch	meth	XXX 1 X H21	LYS 58 A HZ2	4.49	0.000122046	
		XXX 1 X H21	ASN 106 A HB2	4.78	8.38364E-05	
exch	meth	XXX 1 X H21	LYS 58 A HZ1	4.98	6.55577E-05	
exch		XXX 1 X H21	ASN 51 A HD22	5.07	5.88779E-05	
		XXX 1 X H21	MET 98 A HG2	5.09	5.75034E-05	
exch		XXX 1 X H21	ASN 51 A HD21	5.12	5.55112E-05	
	meth	XXX 1 X H21	MET 98 A HE2	5.33	4.36151E-05	
		XXX 1 X H21	ASN 51 A HA	5.34	4.31273E-05	
exch	meth	XXX 1 X H21	LYS 58 A HZ3	5.37	4.17018E-05	
		XXX 1 X H21	MET 98 A HG3	5.53	3.49663E-05	
		XXX 1 X H21	ALA 55 A HB2	5.57	3.34864E-05	
	meth	XXX 1 X H21	MET 98 A HE1	5.82	2.57313E-05	
		XXX 1 X H21	ASP 54 A HB2	5.83	2.54676E-05	
		XXX 1 X H21	ASN 51 A HB2	5.89	2.39501E-05	
				SUM	0.000755883	0.000686536

Fragment B

		Recipient ligand proton	Donor Side Chain	Distance (Å)		Distance (1/Å^6)	
exch	meth	XXX 1 X H17	LYS 58 A HZ2	2.99	3.53	0.0013995	0.000513916
		XXX 1 X H17	GLY 108 A HA3	3.16		0.001004332	
exch	meth	XXX 1 X H17	LYS 58 A HZ3	3.59		0.000467125	
		XXX 1 X H17	MET 98 A HG2	3.67		0.000409264	
exch	meth	XXX 1 X H17	LYS 58 A HZ1	4.02		0.000236943	
		XXX 1 X H17	MET 98 A HG3	4.29		0.000160419	
		XXX 1 X H17	GLY 108 A HA2	4.38		0.00014163	
		XXX 1 X H17	LYS 58 A HD2	4.41		0.000135947	
		XXX 1 X H17	ASP 102 A HB3	4.87		7.49594E-05	
	meth	XXX 1 X H17	ILE 96 A HG21	4.92	4.98	7.05033E-05	6.55577E-05
	meth	XXX 1 X H17	ILE 96 A HG23	4.92		7.05033E-05	
		XXX 1 X H17	LYS 58 A HD3	5.03		6.17436E-05	
	meth	XXX 1 X H17	ILE 96 A HG22	5.1		5.68302E-05	
		XXX 1 X H17	ALA 55 A HB2	5.22		4.94284E-05	
		XXX 1 X H17	LYS 58 A HE3	5.24		4.83072E-05	
		XXX 1 X H17	MET 98 A HA	5.39		4.07819E-05	
		XXX 1 X H17	ALA 55 A HA	5.54		3.45893E-05	
		XXX 1 X H17	LYS 58 A HE2	5.63		3.14014E-05	
		XXX 1 X H17	GLY 108 A H	5.69		2.94664E-05	
		XXX 1 X H17	ALA 55 A HB1	5.96		2.23112E-05	
		XXX 1 X H17	MET 98 A HB3	5.97		2.20879E-05	
					SUM	0.002464506	0.002332227

		Recipient ligand proton	Donor Side Chain	Distance (Å)		Distance (1/Å^6)	
		XXX 1 X H18	MET 98 A HG2	2.34		0.006091228	
		XXX 1 X H18	GLY 108 A HA3	2.81		0.002031244	
		XXX 1 X H18	MET 98 A HG3	2.9		0.001681171	
		XXX 1 X H18	ASP 102 A HB3	3.92		0.000275603	
		XXX 1 X H18	GLY 108 A HA2	4.2		0.000182181	
	meth	XXX 1 X H18	MET 98 A HE1	4.49	4.73	0.000122046	8.92962E-05
	meth	XXX 1 X H18	MET 98 A HE2	4.49		0.000122046	
		XXX 1 X H18	MET 98 A HA	4.61		0.000104182	
		XXX 1 X H18	MET 98 A HB3	4.61		0.000104182	
exch	meth	XXX 1 X H18	LYS 58 A HZ2	4.71		9.15956E-05	
		XXX 1 X H18	GLY 108 A H	4.87		7.49594E-05	
		XXX 1 X H18	LEU 107 A HA	4.91		7.13692E-05	
		XXX 1 X H18	MET 98 A HB2	4.93		6.96496E-05	
		XXX 1 X H18	LEU 107 A HB3	5.02		6.24853E-05	
		XXX 1 X H18	ASP 102 A HB2	5.05		6.02909E-05	
	meth	XXX 1 X H18	MET 98 A HE3	5.21		5.00004E-05	
exch		XXX 1 X H18	THR 184 A HG1	5.25		4.77578E-05	
	meth	XXX 1 X H18	ILE 96 A HG23	5.35	5.62	4.26459E-05	3.17382E-05
exch	meth	XXX 1 X H18	LYS 58 A HZ3	5.36		4.21707E-05	
		XXX 1 X H18	ALA 55 A HB2	5.38		4.12388E-05	
	meth	XXX 1 X H18	ILE 96 A HG22	5.68		2.9779E-05	
exch	meth	XXX 1 X H18	LYS 58 A HZ1	5.76		2.7382E-05	
	meth	XXX 1 X H18	ILE 96 A HG21	5.83		2.54676E-05	
		XXX 1 X H18	THR 109 A H	5.85		2.49497E-05	
		XXX 1 X H18	LYS 58 A HD2	5.86		2.46953E-05	
	meth	XXX 1 X H18	THR 109 A HG23	5.92		2.32311E-05	
		XXX 1 X H18	LEU 107 A HB2	5.94		2.27657E-05	
					SUM	0.011337412	0.011043231

		Recipient ligand proton	Donor Side Chain	Distance (Å)		Distance (1/Å^6)	
		XXX 1 X H19	MET 98 A HG2	2.28		0.00711854	
		XXX 1 X H19	MET 98 A HG3	3.12		0.001084108	
		XXX 1 X H19	GLY 108 A HA3	3.51		0.000534758	
		XXX 1 X H19	MET 98 A HA	3.64		0.000429924	
		XXX 1 X H19	ASP 102 A HB3	3.7		0.000389753	
	meth	XXX 1 X H19	ILE 96 A HG23	4.21	4.59	0.0001796	0.000106936
exch	meth	XXX 1 X H19	LYS 58 A HZ2	4.36		0.000145573	
		XXX 1 X H19	MET 98 A HB3	4.45		0.000128777	
		XXX 1 X H19	GLY 108 A HA2	4.47		0.000125359	
		XXX 1 X H19	ASP 102 A HB2	4.55		0.000112702	
exch	meth	XXX 1 X H19	LYS 58 A HZ3	4.58		0.000108345	
	meth	XXX 1 X H19	ILE 96 A HG21	4.66		9.76528E-05	
	meth	XXX 1 X H19	ILE 96 A HG22	4.9		7.22476E-05	
		XXX 1 X H19	MET 98 A HB2	4.99		6.47734E-05	
		XXX 1 X H19	HIS 154 A HD2	5.08		5.81859E-05	
		XXX 1 X H19	THR 99 A H	5.13		5.48651E-05	
		XXX 1 X H19	LYS 58 A HD2	5.18		5.17632E-05	
	meth	XXX 1 X H19	MET 98 A HE2	5.32		4.41093E-05	
exch	meth	XXX 1 X H19	LYS 58 A HZ1	5.4		4.03309E-05	
		XXX 1 X H19	LYS 58 A HD3	5.56		3.38494E-05	
		XXX 1 X H19	MET 98 A H	5.57		3.34864E-05	
		XXX 1 X H19	GLY 108 A H	5.58		3.3128E-05	
		XXX 1 X H19	ASP 102 A HA	5.72		2.85512E-05	
		XXX 1 X H19	ALA 55 A HB2	5.74		2.79595E-05	
	meth	XXX 1 X H19	MET 98 A HE1	5.76		2.7382E-05	
		XXX 1 X H19	GLY 97 A HA2	5.8		2.62683E-05	
exch		XXX 1 X H19	THR 184 A HG1	5.88		2.41956E-05	
		XXX 1 X H19	GLY 97 A H	5.88		2.41956E-05	
		XXX 1 X H19	LEU 107 A HA	6		2.14335E-05	
					SUM	0.010803373	0.010489316

		Recipient ligand proton	Donor Side Chain	Distance (Å)		Distance (1/Å^6)	
	meth	XXX 1 X H20	ILE 96 A HG22	2.86	3.02	0.001827275	0.00131813
	meth	XXX 1 X H20	ILE 96 A HG23	3.06		0.001218068	
	meth	XXX 1 X H20	ILE 96 A HG21	3.14		0.001043331	
		XXX 1 X H20	LYS 58 A HD2	3.22		0.000897149	
exch	meth	XXX 1 X H20	LYS 58 A HZ2	3.32		0.000746744	
		XXX 1 X H20	ALA 55 A HB2	3.34		0.000720313	
		XXX 1 X H20	ALA 55 A HA	3.54		0.000508137	
		XXX 1 X H20	ALA 55 A HB1	3.73		0.000371319	
exch	meth	XXX 1 X H20	LYS 58 A HZ3	4.09		0.000213629	
		XXX 1 X H20	MET 98 A HG3	4.12		0.000204464	
		XXX 1 X H20	LYS 58 A HD3	4.2		0.000182181	
		XXX 1 X H20	MET 98 A HG2	4.25		0.000169694	
		XXX 1 X H20	GLY 97 A H	4.59		0.000106936	
exch	meth	XXX 1 X H20	LYS 58 A HZ1	4.75		8.70639E-05	
		XXX 1 X H20	ALA 55 A HB3	4.79		8.27917E-05	
		XXX 1 X H20	LYS 58 A HB2	4.82		7.97476E-05	
		XXX 1 X H20	ILE 96 A H	4.83		7.87621E-05	
		XXX 1 X H20	LYS 58 A HE3	4.92		7.05033E-05	
		XXX 1 X H20	ILE 96 A HB	5.03		6.17436E-05	
		XXX 1 X H20	ALA 55 A H	5.16		5.29788E-05	
		XXX 1 X H20	MET 98 A HA	5.25		4.77578E-05	
	meth	XXX 1 X H20	ILE 96 A HD13	5.28		4.61526E-05	
		XXX 1 X H20	GLY 97 A HA2	5.35		4.26459E-05	
		XXX 1 X H20	LYS 58 A HG3	5.37		4.17018E-05	
		XXX 1 X H20	GLY 108 A HA3	5.38		4.12388E-05	
		XXX 1 X H20	LYS 58 A HB3	5.46		3.77437E-05	
		XXX 1 X H20	ILE 96 A HG12	5.48		3.69247E-05	
exch		XXX 1 X H20	THR 184 A HG1	5.48		3.69247E-05	
		XXX 1 X H20	LYS 58 A HE2	5.51		3.57347E-05	
		XXX 1 X H20	HIS 154 A HD2	5.72		2.85512E-05	
	meth	XXX 1 X H20	MET 98 A HE2	5.95		2.25371E-05	
		XXX 1 X H20	ASP 54 A HB3	5.98		2.18672E-05	
					SUM	0.008078249	0.005239016

	XXX 1 X H21	MET 98 A HG3	2.48		0.004298233	
	XXX 1 X H21	MET 98 A HG2	2.96		0.00148679	
meth	XXX 1 X H21	ILE 96 A HG23	2.98	3.39	0.001427915	0.000654999
meth	XXX 1 X H21	ILE 96 A HG22	3.35		0.000707508	
	XXX 1 X H21	GLY 97 A H	3.75		0.000359594	
	XXX 1 X H21	MET 98 A HA	3.81		0.000326927	
meth	XXX 1 X H21	ILE 96 A HG21	3.85		0.000307069	
	XXX 1 X H21	ALA 55 A HB2	3.88		0.000293096	
	XXX 1 X H21	GLY 97 A HA2	3.88		0.000293096	
	XXX 1 X H21	ALA 55 A HB1	4.01		0.00024051	
exch	XXX 1 X H21	THR 184 A HG1	4.08		0.00021679	
meth	XXX 1 X H21	MET 98 A HE2	4.41	5.08	0.000135947	5.81859E-05
	XXX 1 X H21	MET 98 A H	4.59		0.000106936	
	XXX 1 X H21	MET 98 A HB2	4.74		8.81718E-05	
	XXX 1 X H21	ALA 55 A HA	4.75		8.70639E-05	
	XXX 1 X H21	GLY 97 A HA3	4.8		8.17622E-05	
	XXX 1 X H21	HIS 154 A HD2	4.85		7.68333E-05	
	XXX 1 X H21	LYS 58 A HD2	4.86		7.58896E-05	
	XXX 1 X H21	MET 98 A HB3	4.94		6.88079E-05	
exch meth	XXX 1 X H21	LYS 58 A HZ2	4.96		6.71599E-05	
	XXX 1 X H21	ILE 96 A H	5		0.000064	
meth	XXX 1 X H21	MET 98 A HE1	5.08		5.81859E-05	
	XXX 1 X H21	ALA 55 A HB3	5.17		5.23669E-05	
	XXX 1 X H21	GLY 108 A HA3	5.35		4.26459E-05	
exch	XXX 1 X H21	THR 152 A HG1	5.37		4.17018E-05	
	XXX 1 X H21	ASP 102 A HB3	5.4		4.03309E-05	
	XXX 1 X H21	ILE 96 A HG12	5.4		4.03309E-05	
	XXX 1 X H21	ILE 96 A HB	5.5		3.61263E-05	
exch meth	XXX 1 X H21	LYS 58 A HZ3	5.56		3.38494E-05	
	XXX 1 X H21	LYS 58 A HD3	5.67		3.00955E-05	
meth	XXX 1 X H21	MET 98 A HE3	5.75		2.7669E-05	
	XXX 1 X H21	THR 184 A HB	5.77		2.70985E-05	
meth	XXX 1 X H21	THR 184 A HG21	5.83		2.54676E-05	
	XXX 1 X H21	ASP 102 A HB2	5.92		2.32311E-05	
meth	XXX 1 X H21	ILE 96 A HD13	5.92		2.32311E-05	
	XXX 1 X H21	THR 99 A H	5.96		2.23112E-05	
				SUM	0.010975239	0.008975433

		Recipient ligand proton	Donor Side Chain	Distance (Å)	Distance (1/Å^6)
		XXX 1 X H22	ASN 51 A HB3	2.99	0.0013995
		XXX 1 X H22	ALA 55 A HB2	3.34	0.000720313
		XXX 1 X H22	ASN 51 A HA	4.17	0.000190188
		XXX 1 X H22	ALA 55 A H	4.33	0.00015173
		XXX 1 X H22	ASP 54 A HB2	4.36	0.000145573
		XXX 1 X H22	ASN 51 A HB2	4.49	0.000122046
		XXX 1 X H22	ALA 55 A HB3	4.66	9.76528E-05
		XXX 1 X H22	ALA 55 A HB1	4.81	8.07476E-05
		XXX 1 X H22	ALA 55 A HA	4.87	7.49594E-05
exch		XXX 1 X H22	ASN 51 A HD22	4.98	6.55577E-05
exch	meth	XXX 1 X H22	LYS 58 A HZ2	5.05	6.02909E-05
		XXX 1 X H22	SER 52 A HA	5.06	5.95795E-05
		XXX 1 X H22	ASP 54 A HB3	5.13	5.48651E-05
	meth	XXX 1 X H22	MET 98 A HE1	5.18	5.17632E-05
		XXX 1 X H22	MET 98 A HG3	5.28	4.61526E-05
exch		XXX 1 X H22	THR 184 A HG1	5.36	4.21707E-05
	meth	XXX 1 X H22	THR 184 A HG21	5.51	3.57347E-05
		XXX 1 X H22	SER 52 A H	5.64	3.10689E-05
exch		XXX 1 X H22	ASN 51 A HD21	5.67	3.00955E-05
		XXX 1 X H22	GLY 108 A HA3	5.67	3.00955E-05
		XXX 1 X H22	MET 98 A HG2	5.72	2.85512E-05
	meth	XXX 1 X H22	MET 98 A HE2	5.75	2.7669E-05
		XXX 1 X H22	LYS 58 A HD2	5.77	2.70985E-05
	meth	XXX 1 X H22	ILE 96 A HG22	5.89	2.39501E-05
		XXX 1 X H22	ASP 54 A H	5.93	2.2997E-05
			SUM	0.003422235	0.003283118

		Recipient ligand proton	Donor Side Chain	Distance (Å)	Distance (1/Å^6)
exch	meth	XXX 1 X H23	LYS 58 A HZ2	3.98	0.000251595
		XXX 1 X H23	GLY 108 A HA3	4.02	0.000236943
		XXX 1 X H23	ALA 55 A HB2	4.32	0.00015385
		XXX 1 X H23	ASN 51 A HB3	4.49	0.000122046
		XXX 1 X H23	MET 98 A HG2	4.75	8.70639E-05
		XXX 1 X H23	MET 98 A HG3	4.8	8.17622E-05
exch	meth	XXX 1 X H23	LYS 58 A HZ1	5.01	6.32373E-05
exch	meth	XXX 1 X H23	LYS 58 A HZ3	5.17	5.23669E-05
		XXX 1 X H23	ASP 54 A HB2	5.23	4.88641E-05
	meth	XXX 1 X H23	THR 109 A HG22	5.27	4.66806E-05
		XXX 1 X H23	LYS 58 A HD2	5.29	4.56316E-05
	meth	XXX 1 X H23	MET 98 A HE1	5.31	4.46101E-05
		XXX 1 X H23	ALA 55 A HA	5.33	4.36151E-05
	meth	XXX 1 X H23	THR 109 A HG23	5.39	4.07819E-05
		XXX 1 X H23	ASN 51 A HA	5.46	3.77437E-05
		XXX 1 X H23	ALA 55 A H	5.5	3.61263E-05
		XXX 1 X H23	GLY 108 A HA2	5.54	3.45893E-05
		XXX 1 X H23	ASP 54 A HB3	5.55	3.4217E-05
		XXX 1 X H23	ALA 55 A HB1	5.58	3.3128E-05
		XXX 1 X H23	LEU 107 A HB3	5.65	3.07404E-05
		XXX 1 X H23	LYS 58 A HE3	5.74	2.79595E-05
	meth	XXX 1 X H23	MET 98 A HE2	5.78	2.68184E-05
		XXX 1 X H23	ALA 55 A HB3	5.85	2.49497E-05
	meth	XXX 1 X H23	ILE 96 A HG22	5.86	2.46953E-05
exch		XXX 1 X H23	THR 184 A HG1	5.92	2.32311E-05
				SUM	0.001262815 0.001079229

		Recipient ligand proton	Donor Side Chain	Distance (Å)		Distance (1/Å^6)	
exch	meth	XXX 1 X H24	LYS 58 A HZ2	2.15		0.010124399	
		XXX 1 X H24	LYS 58 A HD2	3.26		0.000833095	
exch	meth	XXX 1 X H24	LYS 58 A HZ1	3.32		0.000746744	
		XXX 1 X H24	LYS 58 A HE3	3.5		0.000543991	
exch	meth	XXX 1 X H24	LYS 58 A HZ3	3.56		0.000491247	
		XXX 1 X H24	ALA 55 A HA	3.81		0.000326927	
		XXX 1 X H24	ALA 55 A HB2	3.87		0.000297669	
		XXX 1 X H24	ASP 54 A HB3	3.88		0.000293096	
		XXX 1 X H24	ASP 54 A HB2	4.11		0.000207467	
		XXX 1 X H24	ALA 55 A H	4.47		0.000125359	
		XXX 1 X H24	LYS 58 A HD3	4.48		0.000123689	
		XXX 1 X H24	LYS 58 A HE2	4.57		0.000109775	
		XXX 1 X H24	LYS 58 A HG3	4.8		8.17622E-05	
	meth	XXX 1 X H24	ILE 96 A HG22	4.84	5.12	7.77907E-05	5.57285E-05
		XXX 1 X H24	ALA 55 A HB1	4.97		6.63532E-05	
	meth	XXX 1 X H24	ILE 96 A HG21	5.01		6.32373E-05	
		XXX 1 X H24	ALA 55 A HB3	5.33		4.36151E-05	
		XXX 1 X H24	GLY 108 A HA3	5.34		4.31273E-05	
		XXX 1 X H24	LYS 58 A HB2	5.43		3.90123E-05	
		XXX 1 X H24	ASN 51 A HB3	5.49		3.6523E-05	
	meth	XXX 1 X H24	ILE 96 A HG23	5.5		3.61263E-05	
		XXX 1 X H24	ASN 51 A HA	5.53		3.49663E-05	
		XXX 1 X H24	LYS 58 A HG2	5.69		2.94664E-05	
		XXX 1 X H24	ASP 54 A HA	5.9		2.37076E-05	
		XXX 1 X H24	MET 98 A HG2	5.99		2.16491E-05	
					SUM	0.003458404	0.003336978

		Recipient ligand proton	Donor Side Chain	Distance (Å)		Distance (1/Å^6)	
		XXX 1 X H25	ALA 55 A HB2	2.13		0.010708346	
		XXX 1 X H25	ALA 55 A HA	2.36		0.005787993	
		XXX 1 X H25	ALA 55 A H	3.1		0.001126756	
		XXX 1 X H25	LYS 58 A HD2	3.2		0.000931323	
		XXX 1 X H25	ALA 55 A HB1	3.24		0.00086443	
exch	meth	XXX 1 X H25	LYS 58 A HZ2	3.42		0.000624947	
		XXX 1 X H25	ALA 55 A HB3	3.58		0.000475009	
	meth	XXX 1 X H25	ILE 96 A HG22	3.69	4.25	0.000396134	0.000170495
		XXX 1 X H25	ASP 54 A HB2	3.83		0.000316816	
		XXX 1 X H25	ASP 54 A HB3	3.95		0.00026328	
		XXX 1 X H25	LYS 58 A HE3	4.23		0.000174565	
	meth	XXX 1 X H25	ILE 96 A HG21	4.37		0.000143586	
		XXX 1 X H25	LYS 58 A HG3	4.57		0.000109775	
		XXX 1 X H25	LYS 58 A HB2	4.63		0.000101511	
	meth	XXX 1 X H25	ILE 96 A HG23	4.68		9.51754E-05	
		XXX 1 X H25	LYS 58 A HD3	4.68		9.51754E-05	
exch	meth	XXX 1 X H25	LYS 58 A HZ3	4.69		9.39643E-05	
exch	meth	XXX 1 X H25	LYS 58 A HZ1	4.75		8.70639E-05	
		XXX 1 X H25	ILE 96 A H	5.03		6.17436E-05	
		XXX 1 X H25	ASN 51 A HB3	5.16		5.29788E-05	
		XXX 1 X H25	LEU 56 A H	5.17		5.23669E-05	
		XXX 1 X H25	ASN 51 A HA	5.32		4.41093E-05	
		XXX 1 X H25	LYS 58 A HE2	5.38		4.12388E-05	
		XXX 1 X H25	ASP 54 A HA	5.38		4.12388E-05	
		XXX 1 X H25	ASP 54 A H	5.4		4.03309E-05	
		XXX 1 X H25	SER 52 A HA	5.44		3.85839E-05	
		XXX 1 X H25	LYS 58 A H	5.5		3.61263E-05	
		XXX 1 X H25	GLY 97 A H	5.52		3.53481E-05	
		XXX 1 X H25	ILE 96 A HB	5.69		2.94664E-05	
		XXX 1 X H25	LYS 58 A HB3	5.71		2.88525E-05	
		XXX 1 X H25	LYS 58 A HG2	5.72		2.85512E-05	
		XXX 1 X H25	MET 98 A HG3	5.74		2.79595E-05	
		XXX 1 X H25	GLY 95 A HA3	5.78		2.68184E-05	
					SUM	0.022175587	0.021711187

		Recipient ligand proton	Donor Side Chain	Distance (Å)	Distance (1/Å^6)
		XXX 1 X H26	ASP 54 A HB2	2.6	0.003237128
		XXX 1 X H26	ASP 54 A HB3	2.96	0.00148679
		XXX 1 X H26	ALA 55 A H	3.19	0.000948977
		XXX 1 X H26	ALA 55 A HB2	3.25	0.000848594
		XXX 1 X H26	ALA 55 A HA	3.65	0.000422905
exch	meth	XXX 1 X H26	LYS 58 A HZ2	3.76	0.000353894
		XXX 1 X H26	ASN 51 A HA	3.84	0.000311898
		XXX 1 X H26	ASN 51 A HB3	4.06	0.000223277
		XXX 1 X H26	LYS 58 A HD2	4.3	0.000158194
		XXX 1 X H26	LYS 58 A HE3	4.36	0.000145573
		XXX 1 X H26	ALA 55 A HB3	4.49	0.000122046
		XXX 1 X H26	ASP 54 A H	4.6	0.000105549
		XXX 1 X H26	ALA 55 A HB1	4.68	9.51754E-05
exch	meth	XXX 1 X H26	LYS 58 A HZ1	4.76	8.59722E-05
		XXX 1 X H26	ASP 54 A HA	4.87	7.49594E-05
exch	meth	XXX 1 X H26	LYS 58 A HZ3	5.21	5.00004E-05
		XXX 1 X H26	LYS 58 A HG3	5.23	4.88641E-05
		XXX 1 X H26	SER 52 A HA	5.42	3.94461E-05
	meth	XXX 1 X H26	ILE 96 A HG22	5.46	3.77437E-05
		XXX 1 X H26	ASN 51 A HB2	5.46	3.77437E-05
		XXX 1 X H26	LYS 58 A HE2	5.74	2.79595E-05
		XXX 1 X H26	LYS 58 A HD3	5.74	2.79595E-05
		XXX 1 X H26	LEU 56 A H	5.78	2.68184E-05
		XXX 1 X H26	LYS 58 A HB2	5.93	2.2997E-05
				SUM	0.008450598 0.008412854

	Recipient ligand proton	Donor Side Chain	Distance (Å)		Distance (1/Å^6)		
	XXX 1 X H27	SER 52 A HA	2.68		0.002698928		
	XXX 1 X H27	ALA 55 A HB2	2.87		0.001789405		
	XXX 1 X H27	THR 184 A HB	2.92		0.001613255		
	XXX 1 X H27	ALA 55 A HB3	2.95		0.001517288		
exch	XXX 1 X H27	SER 52 A HG	3.59		0.000467125		
	XXX 1 X H27	ALA 55 A HB1	3.62		0.000444374		
exch	XXX 1 X H27	THR 184 A HG1	3.65		0.000422905		
meth	XXX 1 X H27	THR 184 A HG21	3.69	4.36	0.000396134	0.000145573	
	XXX 1 X H27	ASN 51 A HB3	4.09		0.000213629		
	XXX 1 X H27	ALA 55 A H	4.28		0.000162681		
meth	XXX 1 X H27	THR 184 A HG22	4.36		0.000145573		
	XXX 1 X H27	SER 52 A H	4.45		0.000128777		
	XXX 1 X H27	ASN 51 A HB2	4.64		0.000100206		
	XXX 1 X H27	SER 52 A HB3	4.77		8.48965E-05		
	XXX 1 X H27	THR 184 A H	4.9		7.22476E-05		
	XXX 1 X H27	GLY 95 A HA3	4.92		7.05033E-05		
	XXX 1 X H27	ASP 93 A HB3	4.98		6.55577E-05		
meth	XXX 1 X H27	THR 184 A HG23	5.03		6.17436E-05		
	XXX 1 X H27	GLY 97 A H	5.14		5.42277E-05		
	XXX 1 X H27	ALA 55 A HA	5.17		5.23669E-05		
	XXX 1 X H27	ASP 93 A HB2	5.18		5.17632E-05		
meth	XXX 1 X H27	MET 98 A HE1	5.21		5.00004E-05		
	XXX 1 X H27	SER 52 A HB2	5.27		4.66806E-05		
	XXX 1 X H27	GLY 95 A H	5.29		4.56316E-05		
meth	XXX 1 X H27	MET 98 A HE2	5.36		4.21707E-05		
	XXX 1 X H27	GLY 97 A HA2	5.4		4.03309E-05		
	XXX 1 X H27	ASN 51 A HA	5.52		3.53481E-05		
	XXX 1 X H27	LEU 56 A H	5.55		3.4217E-05		
	XXX 1 X H27	THR 184 A HA	5.7		2.91575E-05		
	XXX 1 X H27	MET 98 A HG3	5.72		2.85512E-05		
	XXX 1 X H27	ASP 93 A H	5.74		2.79595E-05		
meth	XXX 1 X H27	VAL 186 A HG23	5.77		2.70985E-05		
	XXX 1 X H27	ILE 96 A H	5.82		2.57313E-05		
	XXX 1 X H27	LEU 56 A HG	5.85		2.49497E-05		
meth	XXX 1 X H27	ILE 96 A HG22	5.89		2.39501E-05		
	XXX 1 X H27	ASP 54 A HB2	5.96		2.23112E-05		
				SUM	0.010227643	0.009626546	

	Recipient ligand proton	Donor Side Chain	Distance (Å)		Distance (1/Å^6)	
exch	XXX 1 X H28	SER 52 A HG	2.63		0.003021799	
	XXX 1 X H28	SER 52 A HA	2.89		0.001716378	
	XXX 1 X H28	ASN 51 A HB2	3.11		0.001105192	
	XXX 1 X H28	SER 52 A H	3.19		0.000948977	
	XXX 1 X H28	ASN 51 A HB3	3.39		0.000658873	
	XXX 1 X H28	THR 184 A HB	3.92		0.000275603	
meth	XXX 1 X H28	THR 184 A HG21	3.92	4.4	0.000275603	0.000129941
meth	XXX 1 X H28	THR 184 A HG22	4.11		0.000207467	
	XXX 1 X H28	SER 52 A HB2	4.25		0.000169694	
meth	XXX 1 X H28	VAL 186 A HG23	4.26	4.6	0.000167318	0.000104636
meth	XXX 1 X H28	VAL 186 A HG21	4.3		0.000158194	
	XXX 1 X H28	SER 52 A HB3	4.36		0.000145573	
exch	XXX 1 X H28	ASN 51 A HD22	4.52		0.000117265	
	XXX 1 X H28	LEU 48 A HA	4.77		8.48965E-05	
	XXX 1 X H28	ASP 93 A HB3	4.86		7.58896E-05	
	XXX 1 X H28	LEU 48 A HB3	4.95		6.79781E-05	
	XXX 1 X H28	ALA 55 A HB3	4.96		6.71599E-05	
meth	XXX 1 X H28	ILE 91 A HG22	5.02		6.24853E-05	
	XXX 1 X H28	ALA 55 A HB2	5.03		6.17436E-05	
	XXX 1 X H28	ASN 51 A H	5.04		6.10122E-05	
	XXX 1 X H28	ASN 51 A HA	5.12		5.55112E-05	
exch	XXX 1 X H28	THR 184 A HG1	5.13		5.48651E-05	
meth	XXX 1 X H28	LEU 48 A HD22	5.18		5.17632E-05	
meth	XXX 1 X H28	VAL 186 A HG22	5.26		4.72156E-05	
meth	XXX 1 X H28	THR 184 A HG23	5.3		4.51175E-05	
meth	XXX 1 X H28	ILE 91 A HG21	5.31		4.46101E-05	
	XXX 1 X H28	ALA 55 A H	5.63		3.14014E-05	
meth	XXX 1 X H28	LEU 48 A HD23	5.65		3.07404E-05	
	XXX 1 X H28	ASP 93 A H	5.65		3.07404E-05	
	XXX 1 X H28	ILE 49 A HA	5.69		2.94664E-05	
	XXX 1 X H28	SER 53 A H	5.69		2.94664E-05	
	XXX 1 X H28	VAL 186 A HB	5.7		2.91575E-05	
	XXX 1 X H28	ASP 93 A HB2	5.73		2.82535E-05	
meth	XXX 1 X H28	MET 98 A HE1	5.75		2.7669E-05	
	XXX 1 X H28	ILE 91 A HB	5.84		2.52071E-05	
exch	XXX 1 X H28	ASN 51 A HD21	5.93		2.2997E-05	
	XXX 1 X H28	ALA 55 A HB1	5.96		2.23112E-05	
SUM					0.006838668	0.005955062

	Recipient ligand proton	Donor Side Chain	Distance (Å)		Distance (1/Å^6)	
meth	XXX 1 X H33	MET 98 A HE1	2.59	3.4	0.003312847	0.000647331
meth	XXX 1 X H33	MET 98 A HE2	3.56		0.000491247	
	XXX 1 X H33	LEU 107 A HB3	3.63		0.000437079	
meth	XXX 1 X H33	THR 184 A HG21	3.86		0.000302326	
	XXX 1 X H33	MET 98 A HG3	3.87		0.000297669	
meth	XXX 1 X H33	MET 98 A HE3	4.05		0.000226605	
exch	XXX 1 X H33	THR 184 A HG1	4.12		0.000204464	
	XXX 1 X H33	ASN 51 A HB3	4.25		0.000169694	
	XXX 1 X H33	MET 98 A HG2	4.37		0.000143586	
	XXX 1 X H33	LEU 107 A HB2	4.71		9.15956E-05	
	XXX 1 X H33	GLY 108 A HA3	4.95		6.79781E-05	
exch	XXX 1 X H33	ASN 51 A HD22	4.97		6.63532E-05	
	XXX 1 X H33	LEU 107 A HA	5.03		6.17436E-05	
meth	XXX 1 X H33	LEU 107 A HD23	5.04		6.10122E-05	
meth	XXX 1 X H33	THR 184 A HG23	5.14		5.42277E-05	
	XXX 1 X H33	ALA 55 A HB2	5.14		5.42277E-05	
meth	XXX 1 X H33	LEU 107 A HD22	5.32		4.41093E-05	
	XXX 1 X H33	THR 184 A HB	5.33		4.36151E-05	
meth	XXX 1 X H33	THR 184 A HG22	5.38		4.12388E-05	
	XXX 1 X H33	ASN 51 A HB2	5.42		3.94461E-05	
meth	XXX 1 X H33	VAL 150 A HG11	5.43		3.90123E-05	
	XXX 1 X H33	PHE 138 A HB2	5.47		3.73316E-05	
	XXX 1 X H33	MET 98 A HB2	5.56		3.38494E-05	
meth	XXX 1 X H33	THR 109 A HG23	5.56		3.38494E-05	
	XXX 1 X H33	PHE 138 A HD1	5.84		2.52071E-05	
exch	XXX 1 X H33	ASN 51 A HD21	5.85		2.49497E-05	
meth	XXX 1 X H33	LEU 103 A HD23	5.86		2.46953E-05	
	XXX 1 X H33	MET 98 A HB3	5.95		2.25371E-05	
exch	XXX 1 X H33	THR 152 A HG1	5.97		2.20879E-05	
				SUM	0.006156731	0.002172891

Fragment c

	Recipient ligand proton	Donor Side Chain	Distance (Å)	Distance (1/Å^6)		
	XXX 1 X H13	MET 98 A HG3	3.26	0.000833095		
	XXX 1 X H13	MET 98 A HG2	3.32	0.000746744		
methyl	XXX 1 X H13	MET 98 A HE2	3.34	0.000720313	4.11	0.000207467
methyl	XXX 1 X H13	ALA 55 A HB2	4.03	0.000233437	4.81	8.07476E-05
exch	XXX 1 X H13	THR 184 A HG1	4.25	0.000169694		
methyl	XXX 1 X H13	MET 98 A HE1	4.32	0.00015385		
methyl	XXX 1 X H13	MET 98 A HE3	4.67	9.64048E-05		
	XXX 1 X H13	ASN 51 A HB3	4.77	8.48965E-05		
methyl	XXX 1 X H13	ALA 55 A HB1	4.97	6.63532E-05		
methyl	XXX 1 X H13	THR 184 A HG21	5.06	5.95795E-05		
methyl	XXX 1 X H13	ILE 96 A HG23	5.13	5.48651E-05	5.296666667	4.52881E-05
exch	XXX 1 X H13	ASN 106 A HD22	5.15	5.3599E-05		
methyl	XXX 1 X H13	ILE 96 A HG22	5.2	5.05801E-05		
methyl	XXX 1 X H13	ALA 55 A HB3	5.43	3.90123E-05		
	XXX 1 X H13	MET 98 A HB2	5.46	3.77437E-05		
	XXX 1 X H13	MET 98 A HB3	5.49	3.6523E-05		
methyl	XXX 1 X H13	ILE 96 A HG21	5.56	3.38494E-05		
	XXX 1 X H13	GLY 97 A H	5.58	3.3128E-05		
methyl	XXX 1 X H13	LEU 107 A HD21	5.6	3.24244E-05		
	XXX 1 X H13	ALA 55 A HA	5.62	3.17382E-05		
	XXX 1 X H13	MET 98 A HA	5.63	3.14014E-05		
	XXX 1 X H13	GLY 97 A HA2	5.65	3.07404E-05		
	XXX 1 X H13	ASP 102 A HB3	5.7	2.91575E-05		
	XXX 1 X H13	THR 184 A HB	5.72	2.85512E-05		
	XXX 1 X H13	ASN 106 A HB2	5.72	2.85512E-05		
	XXX 1 X H13	ASN 106 A HB3	5.88	2.41956E-05		
exch	XXX 1 X H13	THR 152 A HG1	5.9	2.37076E-05		
	XXX 1 X H13	LYS 58 A HD2	5.97	2.20879E-05		
	XXX 1 X H13	ALA 55 A H	5.98	2.18672E-05		
				SUM		0.002413502

	Recipient ligand proton	Donor Side Chain	Distance (Å)	Distance (1/Å^6)		
	XXX 1 X H14	MET 98 A HG3	2.23	0.008131503		
	XXX 1 X H14	MET 98 A HG2	2.81	0.002031244		
exch	XXX 1 X H14	THR 184 A HG1	3.05	0.001242227		
methyl	XXX 1 X H14	MET 98 A HE2	3.11	0.001105192	3.96	0.000259316
methyl	XXX 1 X H14	ALA 55 A HB2	3.68	0.000402636	4.203333333	0.000181316
methyl	XXX 1 X H14	ILE 96 A HG23	3.83	0.000316816	4.203333333	0.000181316
	XXX 1 X H14	GLY 97 A HA2	3.9	0.000284192		
	XXX 1 X H14	GLY 97 A H	3.9	0.000284192		
methyl	XXX 1 X H14	ALA 55 A HB1	4.06	0.000223277		
methyl	XXX 1 X H14	ILE 96 A HG22	4.11	0.000207467		
methyl	XXX 1 X H14	MET 98 A HE3	4.26	0.000167318		
	XXX 1 X H14	MET 98 A HA	4.51	0.000118834		
methyl	XXX 1 X H14	MET 98 A HE1	4.51	0.000118834		
exch	XXX 1 X H14	THR 152 A HG1	4.54	0.0001142		
	XXX 1 X H14	MET 98 A HB2	4.61	0.000104182		
	XXX 1 X H14	MET 98 A H	4.63	0.000101511		
methyl	XXX 1 X H14	THR 184 A HG21	4.65	9.89196E-05		
methyl	XXX 1 X H14	ILE 96 A HG21	4.67	9.64048E-05		
	XXX 1 X H14	THR 184 A HB	4.83	7.87621E-05		
methyl	XXX 1 X H14	ALA 55 A HB3	4.87	7.49594E-05		
	XXX 1 X H14	MET 98 A HB3	4.9	7.22476E-05		
	XXX 1 X H14	GLY 97 A HA3	5.11	5.61661E-05		
	XXX 1 X H14	ALA 55 A HA	5.25	4.77578E-05		
	XXX 1 X H14	ILE 96 A H	5.47	3.73316E-05		
methyl	XXX 1 X H14	THR 184 A HG23	5.52	3.53481E-05		
	XXX 1 X H14	ASP 102 A HB3	5.62	3.17382E-05		
	XXX 1 X H14	LYS 58 A HD2	5.86	2.46953E-05		
	XXX 1 X H14	ASN 51 A HB3	5.91	2.34679E-05		
exch	XXX 1 X H14	ASN 106 A HD22	5.94	2.27657E-05		
	XXX 1 X H14	THR 152 A HB	5.94	2.27657E-05		
				SUM		0.01207254

	Recipient ligand proton	Donor Side Chain	Distance (Å)	Distance (1/Å^6)		
methyl	XXX 1 X H15	ALA 55 A HB2	2.45	0.004623847	3.243333333	0.000859113
methyl	XXX 1 X H15	ALA 55 A HB1	3.33	0.000733389		
methyl	XXX 1 X H15	ILE 96 A HG22	3.58	0.000475009	3.86	0.000302326
	XXX 1 X H15	ALA 55 A HA	3.87	0.000297669		
methyl	XXX 1 X H15	ILE 96 A HG23	3.88	0.000293096		
	XXX 1 X H15	MET 98 A HG3	3.93	0.000271422		
methyl	XXX 1 X H15	ALA 55 A HB3	3.95	0.00026328		
	XXX 1 X H15	MET 98 A HG2	4.07	0.000220006		
methyl	XXX 1 X H15	ILE 96 A HG21	4.12	0.000204464		
exch	XXX 1 X H15	THR 184 A HG1	4.37	0.000143586		
	XXX 1 X H15	GLY 97 A H	4.47	0.000125359		
	XXX 1 X H15	LYS 58 A HD2	4.53	0.000115721		
methyl	XXX 1 X H15	MET 98 A HE2	4.54	0.0001142	5.406666667	4.00334E-05
	XXX 1 X H15	ALA 55 A H	4.57	0.000109775		
exch methyl	XXX 1 X H15	LYS 58 A HZ3	4.99	6.47734E-05		
	XXX 1 X H15	ASN 51 A HB3	5	0.000064		
	XXX 1 X H15	ILE 96 A H	5.12	5.55112E-05		
	XXX 1 X H15	GLY 97 A HA2	5.19	5.11677E-05		
	XXX 1 X H15	LYS 58 A HE2	5.36	4.21707E-05		
	XXX 1 X H15	ASP 54 A HB2	5.52	3.53481E-05		
	XXX 1 X H15	SER 52 A HA	5.58	3.3128E-05		
	XXX 1 X H15	THR 184 A HB	5.62	3.17382E-05		
methyl	XXX 1 X H15	THR 184 A HG21	5.71	2.88525E-05		
	XXX 1 X H15	LYS 58 A HD3	5.73	2.82535E-05		
methyl	XXX 1 X H15	MET 98 A HE1	5.81	2.59982E-05		
	XXX 1 X H15	ASP 54 A HB3	5.82	2.57313E-05		
	XXX 1 X H15	MET 98 A HA	5.83	2.54676E-05		
	XXX 1 X H15	ILE 96 A HB	5.87	2.4444E-05		
methyl	XXX 1 X H15	MET 98 A HE3	5.87	2.4444E-05		
	XXX 1 X H15	GLY 95 A HA3	5.87	2.4444E-05		
	XXX 1 X H15	ASN 51 A HA	5.91	2.34679E-05		
	XXX 1 X H15	LYS 58 A HB2	5.96	2.23112E-05		
				SUM		0.002828608

	Recipient ligand proton	Donor Side Chain	Distance (Å)	Distance (1/Å^6)		
	XXX 1 X H17	ASN 51 A HB3	3.26	0.000833095		
methyl	XXX 1 X H17	THR 184 A HG21	3.33	0.000733389	4.02	0.000236943
	XXX 1 X H17	ASN 51 A HB2	3.42	0.000624947		
methyl	XXX 1 X H17	VAL 186 A HG21	3.51	0.000534758	3.783333333	0.000340998
methyl	XXX 1 X H17	VAL 186 A HG23	3.59	0.000467125		
exch	XXX 1 X H17	SER 52 A HG	3.6	0.000459394		
	XXX 1 X H17	THR 184 A HB	3.76	0.000353894		
methyl	XXX 1 X H17	THR 184 A HG22	3.89	0.000288604		
	XXX 1 X H17	SER 52 A HA	3.99	0.000247835		
	XXX 1 X H17	SER 52 A H	4.19	0.000184806		
methyl	XXX 1 X H17	VAL 186 A HG22	4.25	0.000169694		
exch	XXX 1 X H17	ASN 51 A HD22	4.47	0.000125359		
exch	XXX 1 X H17	THR 184 A HG1	4.53	0.000115721		
methyl	XXX 1 X H17	MET 98 A HE2	4.8	8.17622E-05		
methyl	XXX 1 X H17	THR 184 A HG23	4.84	7.77907E-05		
	XXX 1 X H17	LEU 48 A HA	5.04	6.10122E-05		
	XXX 1 X H17	LEU 48 A HB3	5.25	4.77578E-05		
methyl	XXX 1 X H17	LEU 48 A HD22	5.27	4.66806E-05		
methyl	XXX 1 X H17	ALA 55 A HB2	5.27	4.66806E-05		
	XXX 1 X H17	ASN 51 A HA	5.37	4.17018E-05		
	XXX 1 X H17	VAL 186 A HB	5.37	4.17018E-05		
	XXX 1 X H17	SER 52 A HB3	5.45	3.81611E-05		
methyl	XXX 1 X H17	MET 98 A HE1	5.47	3.73316E-05		
methyl	XXX 1 X H17	ALA 55 A HB3	5.47	3.73316E-05		
	XXX 1 X H17	SER 52 A HB2	5.5	3.61263E-05		
methyl	XXX 1 X H17	VAL 150 A HG13	5.51	3.57347E-05		
	XXX 1 X H17	ASN 51 A H	5.56	3.38494E-05		
	XXX 1 X H17	PHE 138 A HD1	5.64	3.10689E-05		
methyl	XXX 1 X H17	ILE 91 A HG22	5.66	3.0416E-05		
methyl	XXX 1 X H17	LEU 48 A HD23	5.74	2.79595E-05		
methyl	XXX 1 X H17	VAL 150 A HG11	5.81	2.59982E-05		
exch	XXX 1 X H17	ASN 51 A HD21	5.81	2.59982E-05		
methyl	XXX 1 X H17	ILE 91 A HG21	5.82	2.57313E-05		
	XXX 1 X H17	VAL 186 A H	5.87	2.4444E-05		
	XXX 1 X H17	ASP 93 A HB3	5.89	2.39501E-05		
methyl	XXX 1 X H17	VAL 186 A HG11	5.9	2.37076E-05		
	XXX 1 X H17	ILE 91 A HB	5.94	2.27657E-05		
				SUM		0.00392553

266

		Recipient ligand proton	Donor Side Chain	Distance (Å)	Distance (1/Å^6)
		XXX 1 X H18	ASN 51 A HB3	2.69	0.002639285
		XXX 1 X H18	ASN 51 A HA	4.1	0.000210522
		XXX 1 X H18	ASN 51 A HB2	4.18	0.000187475
exch		XXX 1 X H18	ASN 51 A HD22	4.39	0.000139705
exch		XXX 1 X H18	ASN 51 A HD21	4.65	9.89196E-05
	methyl	XXX 1 X H18	ALA 55 A HB2	4.69	9.39643E-05
	methyl	XXX 1 X H18	MET 98 A HE2	5.03	6.17436E-05
		XXX 1 X H18	ASP 54 A HB2	5.13	5.48651E-05
	methyl	XXX 1 X H18	LEU 107 A HD21	5.3	4.51175E-05
	methyl	XXX 1 X H18	MET 98 A HE1	5.55	3.4217E-05
		XXX 1 X H18	PHE 138 A HB2	5.61	3.20791E-05
		XXX 1 X H18	ALA 55 A H	5.63	3.14014E-05
		XXX 1 X H18	MET 98 A HG3	5.8	2.62683E-05
		XXX 1 X H18	MET 98 A HG2	5.81	2.59982E-05
		XXX 1 X H18	ASP 54 A HB3	5.9	2.37076E-05
		XXX 1 X H18	ASN 51 A H	5.9	2.37076E-05
	methyl	XXX 1 X H18	ALA 55 A HB3	5.94	2.27657E-05
exch	methyl	XXX 1 X H18	LYS 58 A HZ3	5.95	2.25371E-05
		XXX 1 X H18	SER 52 A HA	5.97	2.20879E-05
		XXX 1 X H18	SER 52 A H	5.98	2.18672E-05
		XXX 1 X H18	ASN 106 A HB3	5.99	2.16491E-05
			SUM		0.003320913

	Recipient ligand proton	Donor Side Chain	Distance (Å)	Distance (1/Å^6)		
exch	XXX 1 X H19	ASN 51 A HD21	3.78	0.000342807		
	XXX 1 X H19	PHE 138 A HB2	3.93	0.000271422		
methyl	XXX 1 X H19	LEU 107 A HD21	4.08	0.00021679	4.566666667	0.000110256
	XXX 1 X H19	ASN 51 A HB3	4.12	0.000204464		
exch	XXX 1 X H19	ASN 51 A HD22	4.17	0.000190188		
methyl	XXX 1 X H19	LEU 107 A HD23	4.56	0.000111227		
	XXX 1 X H19	ASN 106 A HB3	4.68	9.51754E-05		
	XXX 1 X H19	PHE 138 A HB3	4.81	8.07476E-05		
methyl	XXX 1 X H19	LEU 107 A HD22	5.06	5.95795E-05		
	XXX 1 X H19	ASN 51 A HB2	5.17	5.23669E-05		
	XXX 1 X H19	PHE 138 A H	5.26	4.72156E-05		
	XXX 1 X H19	ASN 51 A HA	5.39	4.07819E-05		
	XXX 1 X H19	ASN 106 A HB2	5.53	3.49663E-05		
	XXX 1 X H19	PHE 138 A HD1	5.66	3.0416E-05		
	XXX 1 X H19	PHE 138 A HA	5.88	2.41956E-05		
		SUM				0.000992007

	Recipient ligand proton	Donor Side Chain	Distance (Å)	Distance (1/Å^6)		
methyl	XXX 1 X H20	LEU 107 A HD21	2.35	0.005937352	2.743333333	0.002346003
	XXX 1 X H20	PHE 138 A HB2	2.44	0.00473872		
methyl	XXX 1 X H20	LEU 107 A HD22	2.85	0.001866082		
methyl	XXX 1 X H20	LEU 107 A HD23	3.03	0.001292243		
	XXX 1 X H20	PHE 138 A HB3	3.08	0.001171374		
	XXX 1 X H20	PHE 138 A HD1	3.91	0.000279859		
	XXX 1 X H20	PHE 138 A HD2	3.95	0.00026328		
exch	XXX 1 X H20	ASN 51 A HD21	4.1	0.000210522		
exch	XXX 1 X H20	ASN 51 A HD22	4.27	0.000164981		
methyl	XXX 1 X H20	LEU 107 A HD11	4.49	0.000122046	4.986666667	6.50336E-05
	XXX 1 X H20	PHE 138 A H	4.55	0.000112702		
	XXX 1 X H20	LEU 107 A HA	4.6	0.000105549		
	XXX 1 X H20	LEU 107 A HG	4.66	9.76528E-05		
	XXX 1 X H20	PHE 138 A HA	4.68	9.51754E-05		
methyl	XXX 1 X H20	LEU 107 A HD13	4.74	8.81718E-05		
	XXX 1 X H20	ASN 106 A HB3	5.12	5.55112E-05		
	XXX 1 X H20	PHE 138 A HE1	5.24	4.83072E-05		
	XXX 1 X H20	PHE 138 A HE2	5.29	4.56316E-05		
	XXX 1 X H20	ASN 51 A HB3	5.37	4.17018E-05		
methyl	XXX 1 X H20	MET 98 A HE1	5.38	4.12388E-05		
	XXX 1 X H20	LEU 107 A HB3	5.49	3.6523E-05		
	XXX 1 X H20	ASN 106 A HB2	5.67	3.00955E-05		
methyl	XXX 1 X H20	LEU 107 A HD12	5.73	2.82535E-05		
	XXX 1 X H20	TYR 139 A HE2	5.8	2.62683E-05		
	XXX 1 X H20	PHE 138 A HZ	5.82	2.57313E-05		
exch	XXX 1 X H20	TYR 139 A HH	5.89	2.39501E-05		
	XXX 1 X H20	ASN 51 A HB2	5.96	2.23112E-05		
				SUM		0.009607429

	Recipient ligand proton	Donor Side Chain	Distance (Å)	Distance (1/Å^6)		
methyl	XXX 1 X H21	LEU 107 A HD21	2.38	0.005502224	3.086666667	0.001156276
methyl	XXX 1 X H21	LEU 107 A HD11	2.86	0.001827275	3.526666667	0.000519773
	XXX 1 X H21	PHE 138 A HD1	2.98	0.001427915		
methyl	XXX 1 X H21	LEU 107 A HD22	3.02	0.00131813		
	XXX 1 X H21	PHE 138 A HE1	3.34	0.000720313		
methyl	XXX 1 X H21	LEU 107 A HD13	3.38	0.000670656		
	XXX 1 X H21	PHE 138 A HB2	3.54	0.000508137		
methyl	XXX 1 X H21	VAL 150 A HG21	3.71	0.000383492	4.49	0.000122046
methyl	XXX 1 X H21	LEU 107 A HD23	3.86	0.000302326		
methyl	XXX 1 X H21	MET 98 A HE1	3.92	0.000275603	4.743333333	8.78007E-05
	XXX 1 X H21	PHE 138 A HZ	4.21	0.0001796		
methyl	XXX 1 X H21	VAL 150 A HG11	4.24	0.00017211	5.036666667	6.12549E-05
	XXX 1 X H21	LEU 107 A HG	4.25	0.000169694		
methyl	XXX 1 X H21	LEU 107 A HD12	4.34	0.000149645		
	XXX 1 X H21	PHE 138 A HB3	4.42	0.000134112		
	XXX 1 X H21	PHE 138 A HD2	4.44	0.000130528		
methyl	XXX 1 X H21	VAL 186 A HG22	4.59	0.000106936	4.97	6.63532E-05
methyl	XXX 1 X H21	VAL 150 A HG22	4.59	0.000106936		
exch	XXX 1 X H21	ASN 51 A HD22	4.6	0.000105549		
methyl	XXX 1 X H21	VAL 186 A HG21	4.69	9.39643E-05		
	XXX 1 X H21	PHE 138 A HE2	4.7	9.27711E-05		
methyl	XXX 1 X H21	MET 98 A HE2	4.83	7.87621E-05		
methyl	XXX 1 X H21	VAL 150 A HG13	5.06	5.95795E-05		
	XXX 1 X H21	PHE 138 A HA	5.12	5.55112E-05		
	XXX 1 X H21	LEU 107 A HB3	5.12	5.55112E-05		
methyl	XXX 1 X H21	VAL 150 A HG23	5.17	5.23669E-05		
exch	XXX 1 X H21	ASN 51 A HD21	5.18	5.17632E-05		
methyl	XXX 1 X H21	THR 184 A HG21	5.3	4.51175E-05		
methyl	XXX 1 X H21	LEU 48 A HD22	5.38	4.12388E-05	5.66	3.0416E-05
	XXX 1 X H21	LEU 107 A HA	5.38	4.12388E-05		
methyl	XXX 1 X H21	MET 98 A HE3	5.48	3.69247E-05		
	XXX 1 X H21	ASN 51 A HB3	5.57	3.34864E-05		
methyl	XXX 1 X H21	VAL 186 A HG13	5.62	3.17382E-05		
methyl	XXX 1 X H21	VAL 186 A HG23	5.63	3.14014E-05		
	XXX 1 X H21	VAL 150 A HB	5.64	3.10689E-05		
methyl	XXX 1 X H21	LEU 48 A HD23	5.67	3.00955E-05		
methyl	XXX 1 X H21	VAL 186 A HG11	5.68	2.9779E-05		
methyl	XXX 1 X H21	VAL 150 A HG12	5.81	2.59982E-05		
	XXX 1 X H21	LEU 107 A HB2	5.82	2.57313E-05		
methyl	XXX 1 X H21	LEU 103 A HD23	5.84	2.52071E-05		
methyl	XXX 1 X H21	LEU 48 A HD21	5.93	2.2997E-05		
	XXX 1 X H21	ASN 51 A HB2	5.94	2.27657E-05		
		SUM				0.005672302

Recipient ligand proton	Donor Side Chain	Distance (Å)	Distance (1/Å^6)		
methyl	XXX 1 X H22	THR 184 A HG21	2.93	0.001580499	3.71	0.000383492
methyl	XXX 1 X H22	MET 98 A HE1	3.08	0.001171374	3.533333333	0.000513916
methyl	XXX 1 X H22	MET 98 A HE2	3.23	0.000880613		
methyl	XXX 1 X H22	VAL 186 A HG22	3.42	0.000624947	3.623333333	0.000441927
methyl	XXX 1 X H22	VAL 150 A HG11	3.46	0.000582832	4.01	0.00024051
methyl	XXX 1 X H22	VAL 186 A HG21	3.53	0.000516835		
methyl	XXX 1 X H22	VAL 150 A HG13	3.82	0.000321825		
methyl	XXX 1 X H22	LEU 107 A HD11	3.86	0.000302326	4.763333333	8.56119E-05
methyl	XXX 1 X H22	VAL 186 A HG23	3.92	0.000275603		
methyl	XXX 1 X H22	THR 184 A HG22	4	0.000244141		
methyl	XXX 1 X H22	LEU 107 A HD21	4.13	0.000201511	5.033333333	6.14987E-05
methyl	XXX 1 X H22	THR 184 A HG23	4.2	0.000182181		
methyl	XXX 1 X H22	VAL 150 A HG21	4.2	0.000182181	4.786666667	8.31383E-05
methyl	XXX 1 X H22	MET 98 A HE3	4.29	0.000160419		
	XXX 1 X H22	PHE 138 A HD1	4.36	0.000145573		
	XXX 1 X H22	PHE 138 A HE1	4.5	0.000120427		
methyl	XXX 1 X H22	VAL 150 A HG22	4.52	0.000117265		
	XXX 1 X H22	ASN 51 A HB3	4.62	0.000102837		
exch	XXX 1 X H22	THR 184 A HG1	4.63	0.000101511		
methyl	XXX 1 X H22	VAL 150 A HG12	4.75	8.70639E-05		
exch	XXX 1 X H22	ASN 51 A HD22	4.8	8.17622E-05		
	XXX 1 X H22	THR 184 A HB	4.88	7.40425E-05		
methyl	XXX 1 X H22	LEU 107 A HD13	5.04	6.10122E-05		
	XXX 1 X H22	ASN 51 A HB2	5.1	5.68302E-05		
methyl	XXX 1 X H22	LEU 107 A HD22	5.27	4.66806E-05		
	XXX 1 X H22	PHE 138 A HB2	5.34	4.31273E-05		
methyl	XXX 1 X H22	LEU 107 A HD12	5.39	4.07819E-05		
	XXX 1 X H22	LEU 107 A HG	5.4	4.03309E-05		
methyl	XXX 1 X H22	LEU 48 A HD22	5.45	3.81611E-05		
methyl	XXX 1 X H22	VAL 186 A HG13	5.47	3.73316E-05		
methyl	XXX 1 X H22	VAL 186 A HG11	5.5	3.61263E-05		
	XXX 1 X H22	VAL 150 A HB	5.58	3.3128E-05		
	XXX 1 X H22	MET 98 A HG3	5.59	3.2774E-05		
methyl	XXX 1 X H22	VAL 150 A HG23	5.64	3.10689E-05		
methyl	XXX 1 X H22	LEU 107 A HD23	5.7	2.91575E-05		
	XXX 1 X H22	VAL 186 A HB	5.8	2.62683E-05		
	XXX 1 X H22	VAL 186 A HA	5.83	2.54676E-05		
exch	XXX 1 X H22	ASN 51 A HD21	5.85	2.49497E-05		
	XXX 1 X H22	PHE 138 A HZ	5.93	2.2997E-05		
methyl	XXX 1 X H22	LEU 103 A HD23	5.96	2.23112E-05		
			SUM			0.002533897

Fragment D

	Recipient ligand proton	Donor Side Chain	Distance (Å)	Distance (1/Å^6)		
	XXX 1 X H13	PHE 138 A HB2	2.37	0.005642998		
	XXX 1 X H13	PHE 138 A HD1	2.78	0.002166363		
exch	XXX 1 X H13	ASN 51 A HD22	2.78	0.002166363		
exch	XXX 1 X H13	ASN 51 A HD21	3.41	0.000636024		
	XXX 1 X H13	PHE 138 A HB3	3.69	0.000396134		
meth	XXX 1 X H13	LEU 107 A HD22	3.72	0.000377348	4.46	0.000127055
	XXX 1 X H13	ASN 51 A HB3	3.74	0.000365402		
	XXX 1 X H13	LEU 107 A HB3	3.84	0.000311898		
	XXX 1 X H13	PHE 138 A HA	4.12	0.000204464		
	XXX 1 X H13	LEU 107 A HB2	4.12	0.000204464		
meth	XXX 1 X H13	LEU 107 A HD23	4.42	0.000134112		
	XXX 1 X H13	ASN 51 A HB2	4.47	0.000125359		
	XXX 1 X H13	PHE 138 A HE1	4.5			
meth	XXX 1 X H13	MET 98 A HE1	4.67	9.64048E-05		
	XXX 1 X H13	PHE 138 A H	4.7	9.27711E-05		
meth	XXX 1 X H13	LEU 48 A HD23	4.72	9.04374E-05	4.983333333	6.52951E-05
meth	XXX 1 X H13	VAL 186 A HG21	4.78	8.38364E-05	5.273333333	4.65038E-05
meth	XXX 1 X H13	THR 109 A HG21	4.85	7.68333E-05	4.963333333	6.68897E-05
meth	XXX 1 X H13	THR 109 A HG23	4.86	7.58896E-05		
meth	XXX 1 X H13	LEU 48 A HD22	4.87	7.49594E-05		
	XXX 1 X H13	PHE 138 A HD2	4.93	6.96496E-05		
meth	XXX 1 X H13	LEU 107 A HD13	5.14			
meth	XXX 1 X H13	THR 109 A HG22	5.18	5.17632E-05		
meth	XXX 1 X H13	LEU 107 A HD21	5.24	4.83072E-05		
meth	XXX 1 X H13	VAL 186 A HG22	5.25	4.77578E-05		
meth	XXX 1 X H13	LEU 48 A HD21	5.36	4.21707E-05		
meth	XXX 1 X H13	THR 184 A HG21	5.41	3.98856E-05		
meth	XXX 1 X H13	VAL 150 A HG21	5.57			
	XXX 1 X H13	LEU 48 A HA	5.59	3.2774E-05		
meth	XXX 1 X H13	VAL 150 A HG11	5.71			
meth	XXX 1 X H13	VAL 186 A HG23	5.79	2.65417E-05		
	XXX 1 X H13	PHE 138 A HZ	5.86	2.46953E-05		
	XXX 1 X H13	ASN 51 A HA	5.9	2.37076E-05		
	XXX 1 X H13	LEU 107 A HG	5.92	2.32311E-05		
meth	XXX 1 X H13	MET 98 A HE3	5.96	2.23112E-05		
			SUM	0.009989653		

	Recipient ligand proton	Donor Side Chain	Distance (Å)	Distance (1/Å^6)		
	XXX 1 X H14	LEU 107 A HB3	2.72	0.002469372		
	XXX 1 X H14	LEU 107 A HB2	3.44	0.000603461		
meth	XXX 1 X H14	MET 98 A HE1	3.61	0.000451811	4.413333333	0.000135332
meth	XXX 1 X H14	THR 109 A HG23	3.91	0.000279859	4.33	0.00015173
meth	XXX 1 X H14	LEU 107 A HD22	4.21	0.0001796	4.646666667	9.93461E-05
meth	XXX 1 X H14	LEU 107 A HD23	4.23	0.000174565		
	XXX 1 X H14	PHE 138 A HB2	4.38	0.00014163		
meth	XXX 1 X H14	THR 109 A HG22	4.42	0.000134112		
	XXX 1 X H14	ASN 51 A HB3	4.49	0.000122046		
	XXX 1 X H14	LEU 107 A HA	4.51	0.000118834		
meth	XXX 1 X H14	THR 109 A HG21	4.66	9.76528E-05		
	XXX 1 X H14	GLY 108 A HA3	4.72	9.04374E-05		
exch	XXX 1 X H14	ASN 51 A HD22	4.77	8.48965E-05		
meth	XXX 1 X H14	MET 98 A HE2	4.79	8.27917E-05		
meth	XXX 1 X H14	MET 98 A HE3	4.84	7.77907E-05		
	XXX 1 X H14	MET 98 A HG3	4.85	7.68333E-05		
	XXX 1 X H14	MET 98 A HG2	4.96	6.71599E-05		
	XXX 1 X H14	PHE 138 A HD1	5.09	5.75034E-05		
meth	XXX 1 X H14	THR 184 A HG21	5.2	5.05801E-05		
exch	XXX 1 X H14	ASN 51 A HD21	5.22	4.94284E-05		
	XXX 1 X H14	LEU 107 A HG	5.25	4.77578E-05		
	XXX 1 X H14	PHE 138 A HB3	5.31	4.46101E-05		
meth	XXX 1 X H14	LEU 107 A HD13	5.42			
meth	XXX 1 X H14	LEU 107 A HD21	5.5	3.61263E-05		
	XXX 1 X H14	GLY 108 A H	5.57	3.34864E-05		
	XXX 1 X H14	THR 109 A H	5.61	3.20791E-05		
meth	XXX 1 X H14	VAL 150 A HG11	5.63			
exch	XXX 1 X H14	THR 184 A HG1	5.76	2.7382E-05		
	XXX 1 X H14	ASN 51 A HB2	5.77	2.70985E-05		
			SUM	0.004318717		

	Recipient ligand proton	Donor Side Chain	Distance (Å)	Distance (1/Å^6)		
	XXX 1 X H15	MET 98 A HG3	2.79	0.00212019		
	XXX 1 X H15	MET 98 A HG2	2.93	0.001580499		
meth	XXX 1 X H15	MET 98 A HE1	3.5	0.000543991	3.956666667	0.000260629
meth	XXX 1 X H15	MET 98 A HE2	3.81	0.000326927		
	XXX 1 X H15	GLY 108 A HA3	3.87	0.000297669		
	XXX 1 X H15	LEU 107 A HB3	4.11	0.000207467		
exch	XXX 1 X H15	THR 184 A HG1	4.49	0.000122046		
meth	XXX 1 X H15	MET 98 A HE3	4.56	0.000111227		
meth	XXX 1 X H15	ALA 55 A HB2	4.71			
	XXX 1 X H15	LEU 107 A HA	4.84	7.77907E-05		
	XXX 1 X H15	MET 98 A HB2	4.87	7.49594E-05		
meth	XXX 1 X H15	LYS 58 A HZ2	4.94	6.88079E-05	5.533333333	3.48401E-05
	XXX 1 X H15	MET 98 A HB3	4.95	6.79781E-05		
meth	XXX 1 X H15	THR 184 A HG21	5.07	5.88779E-05		
	XXX 1 X H15	ASP 102 A HB3	5.17	5.23669E-05		
	XXX 1 X H15	MET 98 A HA	5.19	5.11677E-05		
	XXX 1 X H15	LEU 107 A HB2	5.2	5.05801E-05		
	XXX 1 X H15	GLY 108 A HA2	5.37	4.17018E-05		
meth	XXX 1 X H15	THR 109 A HG23	5.4			
	XXX 1 X H15	GLY 108 A H	5.47	3.73316E-05		
	XXX 1 X H15	ASN 51 A HB3	5.52	3.53481E-05		
meth	XXX 1 X H15	LEU 107 A HD23	5.53			
meth	XXX 1 X H15	ALA 55 A HB1	5.58			
meth	XXX 1 X H15	ILE 96 A HG23	5.71			
meth	XXX 1 X H15	THR 109 A HG22	5.78			
meth	XXX 1 X H15	LYS 58 A HZ1	5.79	2.65417E-05		
	XXX 1 X H15	GLY 97 A HA2	5.82	2.57313E-05		
exch	XXX 1 X H15	THR 152 A HG1	5.85	2.49497E-05		
meth	XXX 1 X H15	LYS 58 A HZ3	5.87	2.4444E-05		
meth	XXX 1 X H15	ILE 96 A HG22	5.93			
			SUM	0.005016251		

	Recipient ligand proton	Donor Side Chain	Distance (Å)	Distance (1/Å^6)		
	XXX 1 X H16	MET 98 A HG3	2.4	0.005232781		
	XXX 1 X H16	MET 98 A HG2	3.2	0.000931323		
meth	XXX 1 X H16	ALA 55 A HB2	3.38	0.000670656	3.873333333	0.000296136
exch	XXX 1 X H16	THR 184 A HG1	3.48	0.000563021		
meth	XXX 1 X H16	ILE 96 A HG23	3.52	0.000525707	3.916666667	0.000277013
meth	XXX 1 X H16	ALA 55 A HB1	3.64	0.000429924		
	XXX 1 X H16	GLY 97 A H	3.71	0.000383492		
meth	XXX 1 X H16	ILE 96 A HG22	3.76	0.000353894		
	XXX 1 X H16	GLY 97 A HA2	3.85	0.000307069		
meth	XXX 1 X H16	MET 98 A HE2	3.97	0.000255421	4.586666667	0.000107403
	XXX 1 X H16	MET 98 A HA	4.29	0.000160419		
meth	XXX 1 X H16	MET 98 A HE1	4.45	0.000128777		
meth	XXX 1 X H16	ILE 96 A HG21	4.47	0.000125359		
meth	XXX 1 X H16	ALA 55 A HB3	4.6	0.000105549		
meth	XXX 1 X H16	LYS 58 A HZ2	4.65	9.89196E-05	5.4	4.03309E-05
	XXX 1 X H16	MET 98 A HB2	4.7	9.27711E-05		
	XXX 1 X H16	MET 98 A H	4.74	8.81718E-05		
	XXX 1 X H16	ALA 55 A HA	4.76	8.59722E-05		
exch	XXX 1 X H16	THR 152 A HG1	4.83	7.87621E-05		
	XXX 1 X H16	GLY 97 A HA3	4.93	6.96496E-05		
meth	XXX 1 X H16	THR 184 A HG21	5.09	5.75034E-05		
	XXX 1 X H16	MET 98 A HB3	5.1	5.68302E-05		
	XXX 1 X H16	ILE 96 A H	5.11	5.61661E-05		
	XXX 1 X H16	THR 184 A HB	5.12	5.55112E-05		
	XXX 1 X H16	LYS 58 A HD2	5.17	5.23669E-05		
meth	XXX 1 X H16	MET 98 A HE3	5.34	4.31273E-05		
	XXX 1 X H16	GLY 108 A HA3	5.47	3.73316E-05		
	XXX 1 X H16	HIS 154 A HD2	5.54	3.45893E-05		
meth	XXX 1 X H16	LYS 58 A HZ3	5.61	3.20791E-05		
	XXX 1 X H16	ALA 55 A H	5.78	2.68184E-05		
	XXX 1 X H16	GLY 95 A HA3	5.86	2.46953E-05		
	XXX 1 X H16	ASP 102 A HB3	5.92	2.32311E-05		
	XXX 1 X H16	ILE 96 A HB	5.94	2.27657E-05		
meth	XXX 1 X H16	LYS 58 A HZ1	5.94	2.27657E-05		
			SUM	0.008462837		

	Recipient ligand proton	Donor Side Chain	Distance (Å)	Distance (1/Å^6)		
	XXX 1 X H17	THR 184 A HB	2.52	0.003904782		
	XXX 1 X H17	SER 52 A HA	3.06	0.001218068		
meth	XXX 1 X H17	ALA 55 A HB3	3.22	0.000897149	3.43	0.000614095
exch	XXX 1 X H17	THR 184 A HG1	3.24	0.00086443		
meth	XXX 1 X H17	THR 184 A HG21	3.31	0.000760382	3.966666667	0.000256712
meth	XXX 1 X H17	ALA 55 A HB2	3.32	0.000746744		
exch	XXX 1 X H17	SER 52 A HG	3.48	0.000563021		
meth	XXX 1 X H17	ALA 55 A HB1	3.75	0.000359594		
meth	XXX 1 X H17	THR 184 A HG22	3.96	0.000259316		
	XXX 1 X H17	ASN 51 A HB3	4.5	0.000120427		
meth	XXX 1 X H17	THR 184 A HG23	4.63	0.000101511		
	XXX 1 X H17	THR 184 A H	4.66	9.76528E-05		
	XXX 1 X H17	SER 52 A H	4.83	7.87621E-05		
	XXX 1 X H17	ASP 93 A HB3	4.85	7.68333E-05		
	XXX 1 X H17	ALA 55 A H	4.85	7.68333E-05		
	XXX 1 X H17	SER 52 A HB3	4.87	7.49594E-05		
	XXX 1 X H17	GLY 95 A HA3	4.9	7.22476E-05		
meth	XXX 1 X H17	MET 98 A HE1	4.95	6.79781E-05		
	XXX 1 X H17	GLY 97 A H	4.99	6.47734E-05		
	XXX 1 X H17	ASP 93 A HB2	5.15	5.3599E-05		
meth	XXX 1 X H17	MET 98 A HE2	5.16	5.29788E-05		
	XXX 1 X H17	GLY 95 A H	5.17	5.23669E-05		
	XXX 1 X H17	GLY 97 A HA2	5.18	5.17632E-05		
meth	XXX 1 X H17	VAL 186 A HG23	5.18	5.17632E-05		
	XXX 1 X H17	ASN 51 A HB2	5.23	4.88641E-05		
	XXX 1 X H17	THR 184 A HA	5.33	4.36151E-05		
	XXX 1 X H17	ASP 93 A H	5.44	3.85839E-05		
	XXX 1 X H17	SER 52 A HB2	5.48	3.69247E-05		
	XXX 1 X H17	MET 98 A HG3	5.51	3.57347E-05		
exch	XXX 1 X H17	THR 152 A HG1	5.55	3.4217E-05		
	XXX 1 X H17	ALA 55 A HA	5.59	3.2774E-05		
	XXX 1 X H17	GLY 183 A HA2	5.69	2.94664E-05		
meth	XXX 1 X H17	VAL 186 A HG21	5.7	2.91575E-05		
	XXX 1 X H17	LEU 56 A H	5.92	2.32311E-05		
	XXX 1 X H17	ILE 96 A H	5.95	2.25371E-05		
meth	XXX 1 X H17	ILE 96 A HG22	5.98	2.18672E-05		
			SUM	0.007125605		

	Recipient ligand proton	Donor Side Chain	Distance (Å)	Distance (1/Å^6)		
	XXX 1 X H18	ASN 51 A HB3	3.16	0.001004332		
exch	XXX 1 X H18	SER 52 A HG	3.25	0.000848594		
	XXX 1 X H18	ASN 51 A HB2	3.43	0.000614095		
meth	XXX 1 X H18	THR 184 A HG21	3.46	0.000582832	4.083333333	0.00021573
	XXX 1 X H18	SER 52 A HA	3.62	0.000444374		
meth	XXX 1 X H18	VAL 186 A HG21	3.62	0.000444374	3.913333333	0.000278432
meth	XXX 1 X H18	VAL 186 A HG23	3.67	0.000409264		
meth	XXX 1 X H18	THR 184 A HG22	3.87	0.000297669		
	XXX 1 X H18	THR 184 A HB	3.88	0.000293096		
	XXX 1 X H18	SER 52 A H	3.88	0.000293096		
exch	XXX 1 X H18	ASN 51 A HD22	4.28	0.000162681		
meth	XXX 1 X H18	VAL 186 A HG22	4.45	0.000128777		
exch	XXX 1 X H18	THR 184 A HG1	4.8	8.17622E-05		
meth	XXX 1 X H18	LEU 48 A HD22	4.91	7.13692E-05		
meth	XXX 1 X H18	THR 184 A HG23	4.92	7.05033E-05		
	XXX 1 X H18	LEU 48 A HA	4.97	6.63532E-05		
meth	XXX 1 X H18	MET 98 A HE1	5.04	6.10122E-05		
	XXX 1 X H18	SER 52 A HB2	5.05	6.02909E-05		
	XXX 1 X H18	SER 52 A HB3	5.09	5.75034E-05		
meth	XXX 1 X H18	ALA 55 A HB2	5.13	5.48651E-05		
meth	XXX 1 X H18	ALA 55 A HB3	5.17	5.23669E-05		
	XXX 1 X H18	LEU 48 A HB3	5.19	5.11677E-05		
	XXX 1 X H18	PHE 138 A HD1	5.27	4.66806E-05		
	XXX 1 X H18	ILE 91 A HG22	5.27	4.66806E-05		
	XXX 1 X H18	ASN 51 A HA	5.29	4.56316E-05		
	XXX 1 X H18	VAL 186 A HB	5.36	4.21707E-05		
meth	XXX 1 X H18	LEU 48 A HD23	5.44	3.85839E-05		
	XXX 1 X H18	ILE 91 A HG21	5.45	3.81611E-05		
	XXX 1 X H18	ASP 93 A HB3	5.54	3.45893E-05		
	XXX 1 X H18	ASN 51 A H	5.58	3.3128E-05		
exch	XXX 1 X H18	ASN 51 A HD21	5.69	2.94664E-05		
meth	XXX 1 X H18	VAL 150 A HG13	5.82	2.57313E-05		
	XXX 1 X H18	ILE 91 A HB	5.83	2.54676E-05		
	XXX 1 X H18	VAL 186 A H	5.85	2.49497E-05		
meth	XXX 1 X H18	MET 98 A HE2	5.91	2.34679E-05		
meth	XXX 1 X H18	VAL 186 A HG11	5.99	2.16491E-05		
			SUM	0.003715929		

Fragment E

	Recipient ligand proton	Donor Side Chain	Distance (Å)		Distance (1/Å^6)	
meth	XXX 1 X H16	THR 184 A HG21	2.95	3.65	0.001517288	0.000422905
	XXX 1 X H16	ASN 51 A HB3	3.32		0.000746744	
	XXX 1 X H16	THR 184 A HB	3.47		0.000572827	
meth	XXX 1 X H16	VAL 186 A HG23	3.5	3.7033333	0.000543991	0.000387653
	XXX 1 X H16	ASN 51 A HB2	3.51		0.000534758	
meth	XXX 1 X H16	THR 184 A HG22	3.54		0.000508137	
meth	XXX 1 X H16	VAL 186 A HG21	3.54		0.000508137	
exch	XXX 1 X H16	SER 52 A HG	3.69		0.000396134	
	XXX 1 X H16	SER 52 A HA	4.02		0.000236943	
meth	XXX 1 X H16	VAL 186 A HG22	4.07		0.000220006	
exch	XXX 1 X H16	THR 184 A HG1	4.15		0.000195754	
	XXX 1 X H16	SER 52 A H	4.2		0.000182181	
meth	XXX 1 X H16	THR 184 A HG23	4.46		0.000127055	
exch	XXX 1 X H16	ASN 51 A HD22	4.49		0.000122046	
meth	XXX 1 X H16	MET 98 A HE2	4.58	5.1333333	0.000108345	5.46516E-05
meth	XXX 1 X H16	VAL 150 A HG13	4.93		6.96496E-05	
meth	XXX 1 X H16	MET 98 A HE1	4.94		6.88079E-05	
	XXX 1 X H16	LEU 48 A HA	5.09		5.75034E-05	
meth	XXX 1 X H16	LEU 48 A HD22	5.34		4.31273E-05	
	XXX 1 X H16	LEU 48 A HB3	5.43		3.90123E-05	
meth	XXX 1 X H16	VAL 150 A HG11	5.44		3.85839E-05	
	XXX 1 X H16	VAL 186 A HB	5.44		3.85839E-05	
	XXX 1 X H16	ASN 51 A HA	5.46		3.77437E-05	
	XXX 1 X H16	ALA 55 A HB2	5.48		3.69247E-05	
	XXX 1 X H16	SER 52 A HB2	5.51		3.57347E-05	
	XXX 1 X H16	SER 52 A HB3	5.58		3.3128E-05	
	XXX 1 X H16	ASN 51 A H	5.59		3.2774E-05	
meth	XXX 1 X H16	ILE 91 A HG22	5.62		3.17382E-05	
	XXX 1 X H16	VAL 186 A H	5.77		2.70985E-05	
	XXX 1 X H16	ALA 55 A HB3	5.79		2.65417E-05	
exch	XXX 1 X H16	ASN 51 A HD21	5.85		2.49497E-05	
	XXX 1 X H16	ASP 93 A HB3	5.86		2.46953E-05	
meth	XXX 1 X H16	ILE 91 A HG21	5.88		2.41956E-05	
meth	XXX 1 X H16	MET 98 A HE3	5.88		2.41956E-05	
	XXX 1 X H16	THR 184 A HA	5.94		2.27657E-05	
	XXX 1 X H16	PHE 138 A HD1	5.95		2.25371E-05	
meth	XXX 1 X H16	LEU 48 A HD23	5.95		2.25371E-05	
meth	XXX 1 X H16	VAL 186 A HG11	5.95		2.25371E-05	
				SUM		0.003573705

		Recipient ligand proton	Donor Side Chain	Distance (Å)		Distance (1/Å^6)	
		XXX 1 X H17	ASN 51 A HB3	2.91		0.001646805	
exch		XXX 1 X H17	ASN 51 A HD22	4.09		0.000213629	
		XXX 1 X H17	ASN 51 A HB2	4.29		0.000160419	
exch		XXX 1 X H17	ASN 51 A HD21	4.33		0.00015173	
	meth	XXX 1 X H17	LEU 107 A HD11	4.34	5.15	0.000149645	5.3599E-05
		XXX 1 X H17	ASN 51 A HA	4.46		0.000127055	
	meth	XXX 1 X H17	MET 98 A HE2	4.56	5	0.000111227	0.000064
	meth	XXX 1 X H17	MET 98 A HE1	4.65		9.89196E-05	
		XXX 1 X H17	PHE 138 A HB2	5.13		5.48651E-05	
		XXX 1 X H17	MET 98 A HG3	5.3		4.51175E-05	
	meth	XXX 1 X H17	LEU 107 A HD12	5.31		4.46101E-05	
		XXX 1 X H17	MET 98 A HG2	5.42		3.94461E-05	
		XXX 1 X H17	ALA 55 A HB2	5.53		3.49663E-05	
	meth	XXX 1 X H17	LEU 107 A HD21	5.6		3.24244E-05	
	meth	XXX 1 X H17	THR 184 A HG21	5.64		3.10689E-05	
		XXX 1 X H17	ASP 54 A HB2	5.7		2.91575E-05	
		XXX 1 X H17	LEU 107 A HG	5.78		2.68184E-05	
	meth	XXX 1 X H17	MET 98 A HE3	5.79		2.65417E-05	
	meth	XXX 1 X H17	LEU 107 A HD13	5.8		2.62683E-05	
exch		XXX 1 X H17	THR 184 A HG1	5.86		2.46953E-05	
			SUM			0.002282248	

279

		Recipient ligand proton	Donor Side Chain	Distance (Å)		Distance (1/Å^6)	
		XXX 1 X H18	PHE 138 A HB2	3.29		0.000788542	
	meth	XXX 1 X H18	LEU 107 A HD11	3.37	4.06	0.000682685	0.000223277
exch		XXX 1 X H18	ASN 51 A HD21	3.72		0.000377348	
		XXX 1 X H18	LEU 107 A HG	3.91		0.000279859	
	meth	XXX 1 X H18	LEU 107 A HD12	3.93		0.000271422	
exch		XXX 1 X H18	ASN 51 A HD22	4.03		0.000233437	
		XXX 1 X H18	PHE 138 A HB3	4.14		0.000198609	
		XXX 1 X H18	ASN 51 A HB3	4.5		0.000120427	
	meth	XXX 1 X H18	LEU 107 A HD21	4.56	5.316666667	0.000111227	4.42755E-05
	meth	XXX 1 X H18	LEU 107 A HD13	4.88		7.40425E-05	
		XXX 1 X H18	PHE 138 A HD1	4.94		6.88079E-05	
		XXX 1 X H18	PHE 138 A H	5.05		6.02909E-05	
		XXX 1 X H18	PHE 138 A HD2	5.24		4.83072E-05	
	meth	XXX 1 X H18	MET 98 A HE1	5.24		4.83072E-05	
		XXX 1 X H18	ASN 106 A HB3	5.27		4.66806E-05	
		XXX 1 X H18	ASN 106 A HB2	5.34		4.31273E-05	
		XXX 1 X H18	ASN 51 A HB2	5.4		4.03309E-05	
		XXX 1 X H18	LEU 107 A HA	5.41		3.98856E-05	
		XXX 1 X H18	PHE 138 A HA	5.46		3.77437E-05	
	meth	XXX 1 X H18	LEU 107 A HD23	5.59		3.2774E-05	
	meth	XXX 1 X H18	LEU 107 A HD22	5.8		2.62683E-05	
	meth	XXX 1 X H18	MET 98 A HE2	5.84		2.52071E-05	
		XXX 1 X H18	ASN 51 A HA	5.97		2.20879E-05	
			SUM				0.002087458

280

	Recipient ligand proton	Donor Side Chain	Distance (Å)		Distance (1/Å^6)	
	XXX 1 X H19	LEU 107 A HG	2.59		0.003312847	
	XXX 1 X H19	PHE 138 A HB2	2.61		0.003163421	
meth	XXX 1 X H19	LEU 107 A HD21	2.95	3.65	0.001517288	0.000422905
	XXX 1 X H19	PHE 138 A HB3	3.24		0.00086443	
meth	XXX 1 X H19	LEU 107 A HD11	3.25	3.95	0.000848594	0.00026328
	XXX 1 X H19	PHE 138 A HD1	3.28		0.000803077	
	XXX 1 X H19	PHE 138 A HD2	3.41		0.000636024	
meth	XXX 1 X H19	LEU 107 A HD23	3.64		0.000429924	
meth	XXX 1 X H19	LEU 107 A HD12	4.02		0.000236943	
	XXX 1 X H19	PHE 138 A HE1	4.2		0.000182181	
	XXX 1 X H19	PHE 138 A HE2	4.28		0.000162681	
exch	XXX 1 X H19	ASN 51 A HD22	4.29		0.000160419	
exch	XXX 1 X H19	ASN 51 A HD21	4.35		0.000147593	
meth	XXX 1 X H19	LEU 107 A HD22	4.36		0.000145573	
meth	XXX 1 X H19	VAL 150 A HG21	4.51	5.33	0.000118834	4.36151E-05
meth	XXX 1 X H19	LEU 107 A HD13	4.58		0.000108345	
	XXX 1 X H19	PHE 138 A HA	4.63		0.000101511	
	XXX 1 X H19	PHE 138 A HZ	4.64		0.000100206	
	XXX 1 X H19	LEU 107 A HA	4.71		9.15956E-05	
	XXX 1 X H19	LEU 107 A HB3	4.84		7.77907E-05	
meth	XXX 1 X H19	MET 98 A HE1	4.97		6.63532E-05	
	XXX 1 X H19	PHE 138 A H	5.03		6.17436E-05	
meth	XXX 1 X H19	VAL 150 A HG11	5.07		5.88779E-05	
	XXX 1 X H19	LEU 107 A HB2	5.34		4.31273E-05	
meth	XXX 1 X H19	VAL 150 A HG22	5.54		3.45893E-05	
	XXX 1 X H19	ASN 51 A HB3	5.68		2.9779E-05	
meth	XXX 1 X H19	LEU 48 A HD22	5.84		2.52071E-05	
meth	XXX 1 X H19	LEU 48 A HD23	5.88		2.41956E-05	
meth	XXX 1 X H19	VAL 150 A HG23	5.94		2.27657E-05	
			SUM			0.010360215

Flag	Recipient ligand proton	Donor Side Chain	Distance (Å)		Distance (1/Å^6)	
meth	XXX 1 X H20	VAL 150 A HG21	2.58	3.283333333	0.003390641	0.000798197
meth	XXX 1 X H20	LEU 107 A HD21	2.64	3.453333333	0.002953768	0.000589616
	XXX 1 X H20	PHE 138 A HE1	2.87		0.001789405	
	XXX 1 X H20	PHE 138 A HD1	3.13		0.001063491	
meth	XXX 1 X H20	VAL 150 A HG11	3.15	3.856666667	0.001023615	0.000303898
meth	XXX 1 X H20	VAL 150 A HG22	3.24		0.00086443	
meth	XXX 1 X H20	LEU 107 A HD23	3.57		0.000483048	
meth	XXX 1 X H20	VAL 186 A HG22	3.72	4.183333333	0.000377348	0.00018658
meth	XXX 1 X H20	VAL 150 A HG13	3.75		0.000359594	
	XXX 1 X H20	PHE 138 A HZ	3.84		0.000311898	
meth	XXX 1 X H20	VAL 186 A HG21	3.93		0.000271422	
meth	XXX 1 X H20	MET 98 A HE1	3.97	4.86	0.000255421	7.58896E-05
meth	XXX 1 X H20	VAL 150 A HG23	4.03		0.000233437	
	XXX 1 X H20	LEU 107 A HG	4.05		0.000226605	
meth	XXX 1 X H20	LEU 107 A HD22	4.15		0.000195754	
meth	XXX 1 X H20	LEU 107 A HD11	4.15	4.963333333	0.000195754	6.68897E-05
	XXX 1 X H20	PHE 138 A HB2	4.27		0.000164981	
	XXX 1 X H20	VAL 150 A HB	4.54		0.0001142	
exch	XXX 1 X H20	ASN 51 A HD22	4.6		0.000105549	
meth	XXX 1 X H20	VAL 186 A HG13	4.61	5.123333333	0.000104182	5.52948E-05
meth	XXX 1 X H20	VAL 150 A HG12	4.67		9.64048E-05	
	XXX 1 X H20	PHE 138 A HE2	4.75		8.70639E-05	
meth	XXX 1 X H20	VAL 186 A HG11	4.77		8.48965E-05	
meth	XXX 1 X H20	LEU 48 A HD22	4.77	5.253333333	8.48965E-05	4.75763E-05
meth	XXX 1 X H20	THR 184 A HG21	4.79	5.31	8.27917E-05	4.46101E-05
meth	XXX 1 X H20	VAL 186 A HG23	4.9		7.22476E-05	
	XXX 1 X H20	PHE 138 A HD2	4.92		7.05033E-05	
meth	XXX 1 X H20	MET 98 A HE2	5.13		5.48651E-05	
	XXX 1 X H20	PHE 138 A HB3	5.19		5.11677E-05	
meth	XXX 1 X H20	LEU 107 A HD13	5.29		4.56316E-05	
meth	XXX 1 X H20	VAL 148 A HG11	5.36		4.21707E-05	
exch	XXX 1 X H20	ASN 51 A HD21	5.38		4.12388E-05	
	XXX 1 X H20	VAL 150 A HA	5.4		4.03309E-05	
meth	XXX 1 X H20	LEU 107 A HD12	5.45		3.81611E-05	
meth	XXX 1 X H20	LEU 48 A HD23	5.46		3.77437E-05	
meth	XXX 1 X H20	MET 98 A HE3	5.48		3.69247E-05	
meth	XXX 1 X H20	THR 184 A HG22	5.49		3.6523E-05	
	XXX 1 X H20	PHE 138 A HA	5.52		3.53481E-05	
meth	XXX 1 X H20	LEU 48 A HD21	5.53		3.49663E-05	
meth	XXX 1 X H20	THR 184 A HG23	5.65		3.07404E-05	
	XXX 1 X H20	ASN 51 A HB3	5.68		2.9779E-05	
meth	XXX 1 X H20	VAL 148 A HG12	5.69		2.94664E-05	
	XXX 1 X H20	LEU 107 A HB3	5.72		2.85512E-05	
meth	XXX 1 X H20	LEU 103 A HD23	5.77		2.70985E-05	
	XXX 1 X H20	VAL 186 A HA	5.86		2.46953E-05	
	XXX 1 X H20	ASN 51 A HB2	5.91		2.34679E-05	
	XXX 1 X H20	TRP 162 A HE3	5.93		2.2997E-05	
meth	XXX 1 X H20	VAL 186 A HG12	5.99		2.16491E-05	
				SUM		0.006253035

	Recipient ligand proton	Donor Side Chain	Distance (Å)		Distance (1/Å^6)	
meth	XXX 1 X H21	THR 184 A HG21	2.55	3.26	0.003637131	0.000833095
meth	XXX 1 X H21	VAL 186 A HG22	3.05	3.283333333	0.001242227	0.000798197
meth	XXX 1 X H21	VAL 150 A HG13	3.06	3.453333333	0.001218068	0.000589616
meth	XXX 1 X H21	VAL 150 A HG11	3.12		0.001084108	
meth	XXX 1 X H21	MET 98 A HE1	3.13	3.716666667	0.001063491	0.000379383
meth	XXX 1 X H21	VAL 186 A HG21	3.23		0.000880613	
meth	XXX 1 X H21	THR 184 A HG22	3.44		0.000603461	
meth	XXX 1 X H21	VAL 186 A HG23	3.57		0.000483048	
meth	XXX 1 X H21	MET 98 A HE2	3.59		0.000467125	
meth	XXX 1 X H21	THR 184 A HG23	3.79		0.000337415	
meth	XXX 1 X H21	VAL 150 A HG22	4.01	4.45	0.00024051	0.000128777
meth	XXX 1 X H21	VAL 150 A HG21	4.03		0.000233437	
meth	XXX 1 X H21	LEU 107 A HD21	4.16	5.046666667	0.000192948	6.05302E-05
meth	XXX 1 X H21	VAL 150 A HG12	4.18		0.000187475	
exch	XXX 1 X H21	THR 184 A HG1	4.38		0.00014163	
meth	XXX 1 X H21	MET 98 A HE3	4.43		0.000132305	
	XXX 1 X H21	ASN 51 A HB3	4.52			0.000117265
	XXX 1 X H21	THR 184 A HB	4.55			0.000112702
exch	XXX 1 X H21	ASN 51 A HD22	4.65		9.89196E-05	
	XXX 1 X H21	PHE 138 A HE1	4.67			9.64048E-05
	XXX 1 X H21	PHE 138 A HD1	4.74			8.81718E-05
	XXX 1 X H21	ASN 51 A HB2	4.91			7.13692E-05
meth	XXX 1 X H21	LEU 107 A HD11	4.96		6.71599E-05	
meth	XXX 1 X H21	VAL 186 A HG13	5.15		5.3599E-05	
meth	XXX 1 X H21	LEU 48 A HD22	5.17		5.23669E-05	
meth	XXX 1 X H21	VAL 186 A HG11	5.21		5.00004E-05	
	XXX 1 X H21	VAL 150 A HB	5.23			4.88641E-05
meth	XXX 1 X H21	VAL 150 A HG23	5.31		4.46101E-05	
	XXX 1 X H21	VAL 150 A HA	5.32			4.41093E-05
	XXX 1 X H21	VAL 186 A HB	5.45			3.81611E-05
meth	XXX 1 X H21	LEU 107 A HD22	5.47		3.73316E-05	
	XXX 1 X H21	VAL 186 A HA	5.47			3.73316E-05
meth	XXX 1 X H21	LEU 107 A HD23	5.51		3.57347E-05	
	XXX 1 X H21	THR 152 A HB	5.56			3.38494E-05
	XXX 1 X H21	PHE 138 A HB2	5.8			2.62683E-05
exch	XXX 1 X H21	ASN 51 A HD21	5.81		2.59982E-05	
	XXX 1 X H21	LEU 107 A HG	5.86			2.46953E-05
exch	XXX 1 X H21	THR 152 A HG1	5.91		2.34679E-05	
meth	XXX 1 X H21	LEU 103 A HD21	5.93		2.2997E-05	
	XXX 1 X H21	LYS 185 A H	5.96			2.23112E-05
meth	XXX 1 X H21	LEU 48 A HD23	5.97		2.20879E-05	
			SUM			0.003551102

Fragment F

	Recipient ligand proton	Donor Side Chain	Distance (Å)		Distance (1/Å^6)		
	XXX 1 X H20	ASN 51 A HB3	3.01		0.001344625		
methyl	XXX 1 X H20	THR 184 A HG21	3.23	3.86	0.000302326	0.000906979	0.000302326
	XXX 1 X H20	ASN 51 A HB2	3.48		0.000563021		
methyl	XXX 1 X H20	THR 184 A HG22	3.66				
methyl	XXX 1 X H20	VAL 186 A HG21	3.71	3.896666667	0.000285654	0.000856962	0.000285654
methyl	XXX 1 X H20	VAL 186 A HG23	3.71				
exch	XXX 1 X H20	SER 52 A HG	3.73		0.000371319		
	XXX 1 X H20	THR 184 A HB	3.86		0.000302326		
	XXX 1 X H20	SER 52 A HA	4.11		0.000207467		
	XXX 1 X H20	SER 52 A H	4.17		0.000190188		
exch	XXX 1 X H20	ASN 51 A HD22	4.27		0.000164981		
methyl	XXX 1 X H20	VAL 186 A HG22	4.27		0.000164981		
exch	XXX 1 X H20	THR 184 A HG1	4.68		9.51754E-05		
methyl	XXX 1 X H20	THR 184 A HG23	4.69		9.39643E-05		
methyl	XXX 1 X H20	MET 98 A HE2	4.8		8.17622E-05		
	XXX 1 X H20	LEU 48 A HA	4.92		7.05033E-05		
	XXX 1 X H20	LEU 48 A HB3	5.21		5.00004E-05		
methyl	XXX 1 X H20	LEU 48 A HD22	5.26		4.72156E-05		
	XXX 1 X H20	ASN 51 A HA	5.27		4.66806E-05		
methyl	XXX 1 X H20	VAL 150 A HG13	5.33		4.36151E-05		
methyl	XXX 1 X H20	ALA 55 A HB2	5.35		4.26459E-05		
methyl	XXX 1 X H20	MET 98 A HE1	5.43		3.90123E-05		
	XXX 1 X H20	ASN 51 A H	5.53		3.49663E-05		
	XXX 1 X H20	SER 52 A HB3	5.56		3.38494E-05		
	XXX 1 X H20	PHE 138 A HD1	5.57		3.34864E-05		
	XXX 1 X H20	VAL 186 A HB	5.59		3.2774E-05		
exch	XXX 1 X H20	ASN 51 A HD21	5.59		3.2774E-05		
methyl	XXX 1 X H20	VAL 150 A HG11	5.61		3.20791E-05		
	XXX 1 X H20	SER 52 A HB2	5.61		3.20791E-05		
methyl	XXX 1 X H20	ALA 55 A HB3	5.63		3.14014E-05		
	XXX 1 X H20	VAL 186 A H	5.91		2.34679E-05		
methyl	XXX 1 X H20	LEU 48 A HD23	5.91		2.34679E-05		
methyl	XXX 1 X H20	ILE 91 A HG22	5.91		2.34679E-05		
			SUM		0.003553415		

	Recipient ligand proton	Donor Side Chain	Distance (Å)		Distance (1/Å^6)		
methyl	XXX 1 X H19	ALA 55 A HB2	3.32	4.21	0.0001796	0.000538801	0.0001796
	XXX 1 X H19	MET 98 A HG3	4.04		0.000229992		
methyl	XXX 1 X H19	MET 98 A HE2	4.13	5.003333333	6.37446E-05	0.000191234	6.37446E-05
	XXX 1 X H19	MET 98 A HG2	4.24		0.00017211		
methyl	XXX 1 X H19	ALA 55 A HB1	4.47		0.000125359		
	XXX 1 X H19	ASN 51 A HB3	4.55		0.000112702		
	XXX 1 X H19	ALA 55 A HA	4.67		9.64048E-05		
methyl	XXX 1 X H19	ILE 96 A HG22	4.69	4.966666667	6.66208E-05	0.000199862	6.66208E-05
exch	XXX 1 X H19	THR 184 A HG1	4.8		8.17622E-05		
methyl	XXX 1 X H19	ALA 55 A HB3	4.84		7.77907E-05		
methyl	XXX 1 X H19	ILE 96 A HG23	4.95		6.79781E-05		
	XXX 1 X H19	ALA 55 A H	4.98		6.55577E-05		
	XXX 1 X H19	LYS 58 A HD2	5.07		5.88779E-05		
methyl	XXX 1 X H19	LYS 58 A HZ3	5.09		5.75034E-05		
	XXX 1 X H19	ASP 54 A HB2	5.22		4.94284E-05		
methyl	XXX 1 X H19	ILE 96 A HG21	5.26		4.72156E-05		
methyl	XXX 1 X H19	MET 98 A HE1	5.31		4.46101E-05		
	XXX 1 X H19	ASN 51 A HA	5.36		4.21707E-05		
exch	XXX 1 X H19	ASN 106 A HD22	5.45		3.81611E-05		
methyl	XXX 1 X H19	THR 184 A HG21	5.55		3.4217E-05		
methyl	XXX 1 X H19	MET 98 A HE3	5.57		3.34864E-05		
	XXX 1 X H19	GLY 97 A H	5.58		3.3128E-05		
	XXX 1 X H19	LYS 58 A HE2	5.62		3.17382E-05		
	XXX 1 X H19	ASP 54 A HB3	5.65		3.07404E-05		
	XXX 1 X H19	GLY 97 A HA2	5.85		2.49497E-05		
	XXX 1 X H19	LYS 58 A HD3	5.89		2.39501E-05		
	XXX 1 X H19	THR 184 A HB	5.91		2.34679E-05		
	XXX 1 X H19	SER 52 A HA	5.92		2.32311E-05		
methyl	XXX 1 X H19	LEU 107 A HD21	5.96		2.23112E-05		
			SUM		0.001328414		

	Recipient ligand proton	Donor Side Chain	Distance (Å)		Distance (1/Å^6)		
methyl	XXX 1 X H18	MET 98 A HE2	2.45	3.303333333	0.000769636	0.002308909	0.000769636
	XXX 1 X H18	MET 98 A HG3	2.63		0.003021799		
	XXX 1 X H18	MET 98 A HG2	3.06		0.001218068		
methyl	XXX 1 X H18	MET 98 A HE1	3.62		0.000444374		
exch	XXX 1 X H18	THR 184 A HG1	3.82		0.000321825		
methyl	XXX 1 X H18	MET 98 A HE3	3.84		0.000311898		
methyl	XXX 1 X H18	THR 184 A HG21	4.49		0.000122046		
methyl	XXX 1 X H18	ALA 55 A HB2	4.52	5.26	4.72156E-05	0.000141647	4.72156E-05
methyl	XXX 1 X H18	LEU 107 A HD21	4.61	5.303333333	4.49476E-05	0.000134843	4.49476E-05
	XXX 1 X H18	MET 98 A HB2	4.81		8.07476E-05		
exch	XXX 1 X H18	ASN 106 A HD22	5.02		6.24853E-05		
	XXX 1 X H18	MET 98 A HB3	5.06		5.95795E-05		
	XXX 1 X H18	GLY 97 A HA2	5.16		5.29788E-05		
	XXX 1 X H18	ASN 51 A HB3	5.21		5.00004E-05		
exch	XXX 1 X H18	THR 152 A HG1	5.22		4.94284E-05		
	XXX 1 X H18	MET 98 A HA	5.23		4.88641E-05		
methyl	XXX 1 X H18	ILE 96 A HG23	5.37		4.17018E-05		
methyl	XXX 1 X H18	ALA 55 A HB1	5.37		4.17018E-05		
	XXX 1 X H18	THR 184 A HB	5.37		4.17018E-05		
methyl	XXX 1 X H18	LEU 107 A HD23	5.43		3.90123E-05		
	XXX 1 X H18	ASP 102 A HB3	5.51		3.57347E-05		
methyl	XXX 1 X H18	ILE 96 A HG22	5.53		3.49663E-05		
	XXX 1 X H18	GLY 97 A H	5.56		3.38494E-05		
methyl	XXX 1 X H18	THR 184 A HG23	5.63		3.14014E-05		
	XXX 1 X H18	ASN 106 A HB2	5.63		3.14014E-05		
	XXX 1 X H18	MET 98 A H	5.66		3.0416E-05		
	XXX 1 X H18	ASN 106 A HB3	5.84		2.52071E-05		
methyl	XXX 1 X H18	LEU 107 A HD22	5.87		2.4444E-05		
methyl	XXX 1 X H18	ALA 55 A HB3	5.89		2.39501E-05		
			SUM		0.005592147		

	Recipient ligand proton	Donor Side Chain	Distance (Å)		Distance (1/Å^6)		
	XXX 1 X H17	MET 98 A HG3	2.51		0.003999058		
	XXX 1 X H17	MET 98 A HG2	2.69		0.002639285		
methyl	XXX 1 X H17	ILE 96 A HG23	3	3.46	0.000582832	0.001748496	0.000582832
methyl	XXX 1 X H17	ILE 96 A HG22	3.51		0.000534758		
	XXX 1 X H17	MET 98 A HA	3.87		0.000297669		
methyl	XXX 1 X H17	ILE 96 A HG21	3.87		0.000297669		
	XXX 1 X H17	GLY 97 A H	3.93		0.000271422		
	XXX 1 X H17	GLY 97 A HA2	4.02		0.000236943		
methyl	XXX 1 X H17	ALA 55 A HB2	4.03	4.573333333	0.000109296	0.000327887	0.000109296
methyl	XXX 1 X H17	MET 98 A HE2	4.06	4.833333333	7.84367E-05	0.00023531	7.84367E-05
exch	XXX 1 X H17	THR 184 A HG1	4.17		0.000190188		
methyl	XXX 1 X H17	ALA 55 A HB1	4.3		0.000158194		
	XXX 1 X H17	MET 98 A H	4.68		9.51754E-05		
	XXX 1 X H17	MET 98 A HB2	4.75		8.70639E-05		
	XXX 1 X H17	MET 98 A HB3	4.86		7.58896E-05		
	XXX 1 X H17	ALA 55 A HA	4.89		7.31386E-05		
	XXX 1 X H17	GLY 97 A HA3	4.99		6.47734E-05		
methyl	XXX 1 X H17	MET 98 A HE3	5		0.000064		
	XXX 1 X H17	ASP 102 A HB3	5.06		5.95795E-05		
	XXX 1 X H17	LYS 58 A HD2	5.08		5.81859E-05		
	XXX 1 X H17	ILE 96 A H	5.22		4.94284E-05		
exch	XXX 1 X H17	THR 152 A HG1	5.24		4.83072E-05		
methyl	XXX 1 X H17	ALA 55 A HB3	5.39		4.07819E-05		
	XXX 1 X H17	LYS 58 A HD3	5.39		4.07819E-05		
	XXX 1 X H17	ILE 96 A HG13	5.44		3.85839E-05		
methyl	XXX 1 X H17	MET 98 A HE1	5.44		3.85839E-05		
exch	XXX 1 X H17	ASN 106 A HD22	5.46		3.77437E-05		
	XXX 1 X H17	ILE 96 A HG12	5.55		3.4217E-05		
	XXX 1 X H17	ILE 96 A HB	5.61		3.20791E-05		
methyl	XXX 1 X H17	THR 184 A HG21	5.84		2.52071E-05		
	XXX 1 X H17	THR 184 A HB	5.88		2.41956E-05		
	XXX 1 X H17	LYS 58 A HE2	5.9		2.37076E-05		
	XXX 1 X H17	ASP 102 A HB2	5.92		2.32311E-05		
			SUM		0.008994973		

	Recipient ligand proton	Donor Side Chain	Distance (Å)		Distance (1/Å^6)		
methyl	XXX 1 X H16	ALA 55 A HB2	2.31	2.833333333	0.00193292	0.005798761	0.00193292
methyl	XXX 1 X H16	ALA 55 A HB1	2.58		0.003390641		
methyl	XXX 1 X H16	ILE 96 A HG22	2.62	3.063333333	0.001210137	0.00363041	0.001210137
methyl	XXX 1 X H16	ILE 96 A HG23	2.95		0.001517288		
	XXX 1 X H16	GLY 97 A H	3.24		0.00086443		
	XXX 1 X H16	ALA 55 A HA	3.48		0.000563021		
methyl	XXX 1 X H16	ALA 55 A HB3	3.61		0.000451811		
methyl	XXX 1 X H16	ILE 96 A HG21	3.62		0.000444374		
	XXX 1 X H16	MET 98 A HG3	3.82		0.000321825		
	XXX 1 X H16	ILE 96 A H	3.97		0.000255421		
exch	XXX 1 X H16	THR 184 A HG1	3.98		0.000251595		
	XXX 1 X H16	GLY 97 A HA2	4.03		0.000233437		
	XXX 1 X H16	MET 98 A HG2	4.4		0.000137811		
	XXX 1 X H16	LYS 58 A HD2	4.53		0.000115721		
	XXX 1 X H16	ALA 55 A H	4.65		9.89196E-05		
methyl	XXX 1 X H16	MET 98 A HE2	4.69		9.39643E-05		
	XXX 1 X H16	GLY 95 A HA3	4.8		8.17622E-05		
	XXX 1 X H16	ILE 96 A HB	4.89		7.31386E-05		
	XXX 1 X H16	THR 184 A HB	5.07		5.88779E-05		
	XXX 1 X H16	GLY 97 A HA3	5.14		5.42277E-05		
	XXX 1 X H16	LYS 58 A HD3	5.28		4.61526E-05		
	XXX 1 X H16	LYS 58 A HB2	5.35		4.26459E-05		
	XXX 1 X H16	MET 98 A HA	5.37		4.17018E-05		
exch	XXX 1 X H16	THR 152 A HG1	5.55		3.4217E-05		
	XXX 1 X H16	ILE 96 A HG13	5.56		3.38494E-05		
	XXX 1 X H16	MET 98 A H	5.58		3.3128E-05		
methyl	XXX 1 X H16	THR 184 A HG21	5.6		3.24244E-05		
	XXX 1 X H16	ILE 96 A HG12	5.61		3.20791E-05		
	XXX 1 X H16	SER 52 A HA	5.63		3.14014E-05		
	XXX 1 X H16	ILE 96 A HA	5.63		3.14014E-05		
methyl	XXX 1 X H16	LYS 58 A HZ3	5.65		3.07404E-05		
methyl	XXX 1 X H16	MET 98 A HE3	5.85		2.49497E-05		
	XXX 1 X H16	GLY 183 A HA2	5.9		2.37076E-05		
	XXX 1 X H16	LYS 58 A HE2	5.96		2.23112E-05		
	XXX 1 X H16	LEU 56 A H	5.96		2.23112E-05		
	XXX 1 X H16	ASP 54 A HB2	6		2.14335E-05		
			SUM		0.006383772		

	Recipient ligand proton	Donor Side Chain	Distance (Å)		Distance (1/Å^6)		
	XXX 1 X H15	MET 98 A HG3	2.4		0.005232781		
exch	XXX 1 X H15	THR 184 A HG1	2.47		0.004403706		
	XXX 1 X H15	GLY 97 A HA2	2.8		0.002075161		
	XXX 1 X H15	GLY 97 A H	3.06		0.001218068		
methyl	XXX 1 X H15	MET 98 A HE2	3.28	4.113333333	0.00020646	0.000619381	0.00020646
	XXX 1 X H15	MET 98 A HG2	3.48		0.000563021		
methyl	XXX 1 X H15	ILE 96 A HG23	3.67	4.14	0.000198609	0.000595826	0.000198609
methyl	XXX 1 X H15	ALA 55 A HB2	3.7	4.073333333	0.000218927	0.000656782	0.000218927
methyl	XXX 1 X H15	ALA 55 A HB1	3.78		0.000342807		
exch	XXX 1 X H15	THR 152 A HG1	3.83		0.000316816		
methyl	XXX 1 X H15	ILE 96 A HG22	3.92		0.000275603		
	XXX 1 X H15	MET 98 A H	4.1		0.000210522		
	XXX 1 X H15	THR 184 A HB	4.15		0.000195754		
	XXX 1 X H15	GLY 97 A HA3	4.15		0.000195754		
methyl	XXX 1 X H15	MET 98 A HE3	4.22		0.000177062		
methyl	XXX 1 X H15	THR 184 A HG21	4.35	5.033333333	6.14987E-05	0.000184496	6.14987E-05
	XXX 1 X H15	MET 98 A HA	4.4		0.000137811		
	XXX 1 X H15	MET 98 A HB2	4.5		0.000120427		
methyl	XXX 1 X H15	ALA 55 A HB3	4.74		8.81718E-05		
methyl	XXX 1 X H15	ILE 96 A HG21	4.83		7.87621E-05		
methyl	XXX 1 X H15	MET 98 A HE1	4.84		7.77907E-05		
	XXX 1 X H15	ILE 96 A H	4.91		7.13692E-05		
methyl	XXX 1 X H15	THR 184 A HG23	5.12		5.55112E-05		
	XXX 1 X H15	MET 98 A HB3	5.16		5.29788E-05		
	XXX 1 X H15	ALA 55 A HA	5.2		5.05801E-05		
	XXX 1 X H15	GLY 183 A HA2	5.36		4.21707E-05		
	XXX 1 X H15	GLY 95 A HA3	5.48		3.69247E-05		
	XXX 1 X H15	THR 152 A HB	5.59		3.2774E-05		
methyl	XXX 1 X H15	THR 184 A HG22	5.63		3.14014E-05		
	XXX 1 X H15	THR 184 A HA	5.68		2.9779E-05		
	XXX 1 X H15	THR 184 A H	5.8		2.62683E-05		
methyl	XXX 1 X H15	THR 152 A HG21	5.81		2.59982E-05		
	XXX 1 X H15	ILE 96 A HB	5.98		2.18672E-05		
	XXX 1 X H15	ILE 96 A HG13	5.99		2.16491E-05		
			SUM		0.011021155		

	Recipient ligand proton	Donor Side Chain	Distance (Å)		Distance (1/Å^6)		
methyl	XXX 1 X H21	THR 184 A HG21	2.88	3.58	0.000475009	0.001425027	0.000475009
methyl	XXX 1 X H21	MET 98 A HE1	3.37	3.773333333	0.000346457	0.00103937	0.000346457
methyl	XXX 1 X H21	VAL 150 A HG11	3.44	3.97	0.000255421	0.000766264	0.000255421
methyl	XXX 1 X H21	VAL 186 A HG22	3.44	3.66	0.000416019	0.001248058	0.000416019
methyl	XXX 1 X H21	MET 98 A HE2	3.49		0.000553411		
methyl	XXX 1 X H21	VAL 186 A HG21	3.6		0.000459394		
methyl	XXX 1 X H21	VAL 150 A HG13	3.75		0.000359594		
methyl	XXX 1 X H21	THR 184 A HG22	3.76		0.000353894		
methyl	XXX 1 X H21	LEU 107 A HD11	3.89	4.706666667	9.19855E-05	0.000275956	9.19855E-05
methyl	XXX 1 X H21	VAL 186 A HG23	3.94		0.000267315		
methyl	XXX 1 X H21	THR 184 A HG23	4.1		0.000210522		
methyl	XXX 1 X H21	LEU 107 A HD21	4.13	4.943333333	6.853E-05	0.00020559	6.853E-05
methyl	XXX 1 X H21	VAL 150 A HG21	4.14	4.713333333	9.12076E-05	0.000273623	9.12076E-05
	XXX 1 X H21	PHE 138 A HD1	4.3		0.000158194		
	XXX 1 X H21	ASN 51 A HB3	4.37		0.000143586		
exch	XXX 1 X H21	ASN 51 A HD22	4.43		0.000132305		
methyl	XXX 1 X H21	VAL 150 A HG22	4.43		0.000132305		
methyl	XXX 1 X H21	MET 98 A HE3	4.46		0.000127055		
	XXX 1 X H21	PHE 138 A HE1	4.53		0.000115721		
methyl	XXX 1 X H21	VAL 150 A HG12	4.72		9.04374E-05		
exch	XXX 1 X H21	THR 184 A HG1	4.74		8.81718E-05		
methyl	XXX 1 X H21	LEU 107 A HD13	4.82		7.97476E-05		
	XXX 1 X H21	THR 184 A HB	4.9		7.22476E-05		
	XXX 1 X H21	ASN 51 A HB2	5.01		6.32373E-05		
methyl	XXX 1 X H21	LEU 107 A HD22	5.01		6.32373E-05		
	XXX 1 X H21	PHE 138 A HB2	5.21		5.00004E-05		
methyl	XXX 1 X H21	LEU 48 A HD22	5.26		4.72156E-05		
methyl	XXX 1 X H21	LEU 107 A HD12	5.41		3.98856E-05		
methyl	XXX 1 X H21	VAL 186 A HG13	5.49		3.6523E-05		
exch	XXX 1 X H21	ASN 51 A HD21	5.49		3.6523E-05		
methyl	XXX 1 X H21	VAL 186 A HG11	5.53		3.49663E-05		
	XXX 1 X H21	VAL 150 A HB	5.54		3.45893E-05		
methyl	XXX 1 X H21	VAL 150 A HG23	5.57		3.34864E-05		
methyl	XXX 1 X H21	LEU 107 A HD23	5.69		2.94664E-05		
	XXX 1 X H21	LEU 107 A HG	5.78		2.68184E-05		
	XXX 1 X H21	VAL 186 A HB	5.82		2.57313E-05		
	XXX 1 X H21	VAL 186 A HA	5.85		2.49497E-05		
	XXX 1 X H21	MET 98 A HG3	5.89		2.39501E-05		
	XXX 1 X H21	VAL 150 A HA	5.97		2.20879E-05		
			SUM		0.002505742		

	Recipient ligand proton	Donor Side Chain	Distance (Å)	Distance	Distance (1/Å^6)		
methyl	XXX 1 X H22	LEU 107 A HD11	2.7	3.18	0.000967024	0.002901072	0.000967024
methyl	XXX 1 X H22	LEU 107 A HD13	2.85		0.001866082		
	XXX 1 X H22	PHE 138 A HD1	2.93		0.001580499		
methyl	XXX 1 X H22	LEU 107 A HD21	3.12	3.616666667	0.000446837	0.001340511	0.000446837
	XXX 1 X H22	PHE 138 A HE1	3.22		0.000897149		
methyl	XXX 1 X H22	LEU 107 A HD22	3.27		0.000817925		
methyl	XXX 1 X H22	VAL 150 A HG21	3.38	4.19	0.000184806	0.000554418	0.000184806
	XXX 1 X H22	PHE 138 A HB2	3.61		0.000451811		
methyl	XXX 1 X H22	VAL 150 A HG11	3.93	4.733333333	8.89196E-05	0.000266759	8.89196E-05
methyl	XXX 1 X H22	MET 98 A HE1	3.98	4.77	8.48965E-05	0.000254689	8.48965E-05
methyl	XXX 1 X H22	LEU 107 A HD12	3.99		0.000247835		
	XXX 1 X H22	PHE 138 A HZ	4.16		0.000192948		
methyl	XXX 1 X H22	VAL 150 A HG22	4.32		0.00015385		
exch	XXX 1 X H22	ASN 51 A HD22	4.37		0.000143586		
methyl	XXX 1 X H22	VAL 186 A HG22	4.4	4.81	8.07476E-05	0.000242243	8.07476E-05
methyl	XXX 1 X H22	LEU 107 A HD23	4.46		0.000127055		
	XXX 1 X H22	PHE 138 A HD2	4.49		0.000122046		
	XXX 1 X H22	PHE 138 A HB3	4.5		0.000120427		
methyl	XXX 1 X H22	VAL 186 A HG21	4.57		0.000109775		
	XXX 1 X H22	LEU 107 A HG	4.63		0.000101511		
	XXX 1 X H22	PHE 138 A HE2	4.69		9.39643E-05		
methyl	XXX 1 X H22	VAL 150 A HG13	4.76		8.59722E-05		
methyl	XXX 1 X H22	MET 98 A HE2	4.85		7.68333E-05		
methyl	XXX 1 X H22	VAL 150 A HG23	4.87		7.49594E-05		
exch	XXX 1 X H22	ASN 51 A HD21	4.98		6.55577E-05		
	XXX 1 X H22	LEU 107 A HB3	5.04		6.10122E-05		
methyl	XXX 1 X H22	THR 184 A HG21	5.12		5.55112E-05		
	XXX 1 X H22	PHE 138 A HA	5.13		5.48651E-05		
methyl	XXX 1 X H22	LEU 48 A HD22	5.14	5.603333333	3.23088E-05	9.69265E-05	3.23088E-05
	XXX 1 X H22	VAL 150 A HB	5.3		4.51175E-05		
methyl	XXX 1 X H22	VAL 186 A HG13	5.43		3.90123E-05		
	XXX 1 X H22	LEU 107 A HA	5.46		3.77437E-05		
methyl	XXX 1 X H22	VAL 186 A HG23	5.46		3.77437E-05		
methyl	XXX 1 X H22	MET 98 A HE3	5.48		3.69247E-05		
methyl	XXX 1 X H22	VAL 150 A HG12	5.51		3.57347E-05		
	XXX 1 X H22	ASN 51 A HB3	5.53		3.49663E-05		
methyl	XXX 1 X H22	VAL 186 A HG11	5.54		3.45893E-05		
methyl	XXX 1 X H22	LEU 48 A HD23	5.76		2.7382E-05		
methyl	XXX 1 X H22	VAL 148 A HG11	5.84		2.52071E-05		
methyl	XXX 1 X H22	LEU 103 A HD23	5.88		2.41956E-05		
	XXX 1 X H22	LEU 107 A HB2	5.89		2.39501E-05		
methyl	XXX 1 X H22	LEU 48 A HD21	5.91		2.34679E-05		
methyl	XXX 1 X H22	THR 184 A HG22	5.92		2.32311E-05		
	XXX 1 X H22	ASN 51 A HB2	5.97		2.20879E-05		
			SUM		0.005725638		

	Recipient ligand proton	Donor Side Chain	Distance (Å)		Distance (1/Å^6)		
methyl	XXX 1 X H23	LEU 107 A HD22	2.25	2.93	0.001580499	0.004741498	0.001580499
	XXX 1 X H23	PHE 138 A HB2	2.69		0.002639285		
methyl	XXX 1 X H23	LEU 107 A HD21	2.97		0.001457006		
	XXX 1 X H23	PHE 138 A HB3	3.16		0.001004332		
methyl	XXX 1 X H23	LEU 107 A HD23	3.57		0.000483048		
methyl	XXX 1 X H23	LEU 107 A HD13	3.69	4.263333333	0.000166535	0.000499604	0.000166535
	XXX 1 X H23	PHE 138 A HD2	3.73		0.000371319		
	XXX 1 X H23	PHE 138 A HD1	3.93		0.000271422		
methyl	XXX 1 X H23	LEU 107 A HD11	4.03		0.000233437		
exch	XXX 1 X H23	ASN 51 A HD21	4.08		0.00021679		
	XXX 1 X H23	LEU 107 A HA	4.2		0.000182181		
exch	XXX 1 X H23	ASN 51 A HD22	4.26		0.000167318		
	XXX 1 X H23	PHE 138 A H	4.83		7.87621E-05		
	XXX 1 X H23	LEU 107 A HG	4.84		7.77907E-05		
	XXX 1 X H23	LEU 107 A HB3	4.9		7.22476E-05		
	XXX 1 X H23	PHE 138 A HA	4.91		7.13692E-05		
	XXX 1 X H23	PHE 138 A HE2	4.94		6.88079E-05		
methyl	XXX 1 X H23	MET 98 A HE1	5.04		6.10122E-05		
methyl	XXX 1 X H23	LEU 107 A HD12	5.07		5.88779E-05		
	XXX 1 X H23	PHE 138 A HE1	5.08		5.81859E-05		
	XXX 1 X H23	ASN 106 A HB3	5.09		5.75034E-05		
	XXX 1 X H23	PHE 138 A HZ	5.52		3.53481E-05		
methyl	XXX 1 X H23	VAL 150 A HG21	5.59		3.2774E-05		
	XXX 1 X H23	ASN 51 A HB3	5.64		3.10689E-05		
	XXX 1 X H23	ASN 106 A HB2	5.65		3.07404E-05		
	XXX 1 X H23	TYR 139 A HE2	5.66		3.0416E-05		
exch	XXX 1 X H23	TYR 139 A HH	5.67		3.00955E-05		
	XXX 1 X H23	LEU 107 A HB2	5.73		2.82535E-05		
methyl	XXX 1 X H23	MET 98 A HE2	5.78		2.68184E-05		
	XXX 1 X H23	LEU 107 A H	5.89		2.39501E-05		
			SUM		0.006880017		

	Recipient ligand proton	Donor Side Chain	Distance (Å)		Distance (1/Å^6)		
methyl	XXX 1 X H24	LEU 107 A HD22	3.75	3.98	0.000251595	0.000754784	0.000251595
exch	XXX 1 X H24	ASN 51 A HD21	3.76		0.000353894		
methyl	XXX 1 X H24	LEU 107 A HD21	3.91		0.000279859		
	XXX 1 X H24	PHE 138 A HB2	3.96		0.000259316		
exch	XXX 1 X H24	ASN 51 A HD22	4.22		0.000177062		
	XXX 1 X H24	ASN 106 A HB3	4.23		0.000174565		
methyl	XXX 1 X H24	LEU 107 A HD23	4.28		0.000162681		
	XXX 1 X H24	ASN 51 A HB3	4.63		0.000101511		
	XXX 1 X H24	PHE 138 A HB3	4.65		9.89196E-05		
	XXX 1 X H24	ASN 106 A HB2	5.13		5.48651E-05		
	XXX 1 X H24	PHE 138 A H	5.38		4.12388E-05		
exch	XXX 1 X H24	ASN 106 A HD22	5.5		3.61263E-05		
methyl	XXX 1 X H24	MET 98 A HE1	5.51		3.57347E-05		
	XXX 1 X H24	ASN 51 A HB2	5.62		3.17382E-05		
	XXX 1 X H24	LEU 107 A HA	5.65		3.07404E-05		
methyl	XXX 1 X H24	MET 98 A HE2	5.66		3.0416E-05		
	XXX 1 X H24	PHE 138 A HD1	5.68		2.9779E-05		
methyl	XXX 1 X H24	LEU 107 A HD11	5.75		2.7669E-05		
	XXX 1 X H24	ASN 51 A HA	5.8		2.62683E-05		
methyl	XXX 1 X H24	LEU 107 A HD13	5.85		2.49497E-05		
	XXX 1 X H24	PHE 138 A HD2	5.93		2.2997E-05		
			SUM		0.001123533		

293

	Recipient ligand proton	Donor Side Chain	Distance (Å)		Distance (1/Å^6)		
	XXX 1 X H25	ASN 51 A HB3	3.15		0.001023615		
exch	XXX 1 X H25	ASN 51 A HD22	4.29		0.000160419		
	XXX 1 X H25	ASN 51 A HA	4.37		0.000143586		
exch	XXX 1 X H25	ASN 51 A HD21	4.42		0.000134112		
methyl	XXX 1 X H25	MET 98 A HE2	4.55		0.000112702		
	XXX 1 X H25	ASN 51 A HB2	4.58		0.000108345		
methyl	XXX 1 X H25	LEU 107 A HD21	4.77	5.23	4.88641E-05	0.000146592	4.88641E-05
methyl	XXX 1 X H25	MET 98 A HE1	5.1		5.68302E-05		
methyl	XXX 1 X H25	ALA 55 A HB2	5.11		5.61661E-05		
methyl	XXX 1 X H25	LEU 107 A HD22	5.36		4.21707E-05		
	XXX 1 X H25	ASP 54 A HB2	5.45		3.81611E-05		
	XXX 1 X H25	PHE 138 A HB2	5.47		3.73316E-05		
	XXX 1 X H25	MET 98 A HG3	5.55		3.4217E-05		
methyl	XXX 1 X H25	LEU 107 A HD23	5.56		3.38494E-05		
	XXX 1 X H25	ASN 106 A HB3	5.57		3.34864E-05		
	XXX 1 X H25	MET 98 A HG2	5.7		2.91575E-05		
exch	XXX 1 X H25	ASN 106 A HD22	5.71		2.88525E-05		
methyl	XXX 1 X H25	THR 184 A HG21	5.75		2.7669E-05		
		SUM			0.001496763		

Fragment H

	Recipient ligand proton	Donor Side Chain	Distance (Å)		Distance (1/Å^6)	
meth	XXX 1 X H25	THR 74 A HG21	3.97	4.913333333	0.000255421	7.10792E-05
exch	XXX 1 X H25	THR 74 A HG1	4.07			
	XXX 1 X H25	THR 74 A HB	4.77		8.48965E-05	
meth	XXX 1 X H25	THR 74 A HG22	5.32		4.41093E-05	
meth	XXX 1 X H25	THR 74 A HG23	5.45		3.81611E-05	
	XXX 1 X H25	LYS 5 A HG2	5.92		2.32311E-05	
			SUM			0.000179207

	Recipient ligand proton	Donor Side Chain	Distance (Å)		Distance (1/Å^6)	
exch	XXX 1 X H26	THR 74 A HG1	2.33			
	XXX 1 X H26	TYR 71 A HA	2.69		0.002639285	
	XXX 1 X H26	TYR 71 A HB3	3.6		0.000459394	
	XXX 1 X H26	TYR 71 A HB2	3.75		0.000359594	
meth	XXX 1 X H26	LEU 56 A HD22	3.87	4.676666667	0.000297669	9.55832E-05
	XXX 1 X H26	THR 74 A HB	3.95		0.00026328	
	XXX 1 X H26	GLY 75 A H	4.31		0.000156004	
	XXX 1 X H26	LEU 56 A HB2	4.51		0.000118834	
	XXX 1 X H26	TYR 71 A H	4.61		0.000104182	
meth	XXX 1 X H26	THR 74 A HG21	4.65	5.16	9.89196E-05	5.29788E-05
	XXX 1 X H26	GLY 75 A HA2	4.75		8.70639E-05	
meth	XXX 1 X H26	VAL 7 A HG22	4.81	5.326666667	8.07476E-05	4.37791E-05
meth	XXX 1 X H26	LEU 56 A HD23	4.85		7.68333E-05	
	XXX 1 X H26	THR 74 A H	4.87		7.49594E-05	
	XXX 1 X H26	LYS 5 A HG2	4.88		7.40425E-05	
	XXX 1 X H26	LYS 5 A HB3	4.91		7.13692E-05	
	XXX 1 X H26	GLY 75 A HA3	5.12		5.55112E-05	
meth	XXX 1 X H26	THR 74 A HG23	5.14		5.42277E-05	
	XXX 1 X H26	LEU 56 A HB3	5.24		4.83072E-05	
meth	XXX 1 X H26	LEU 56 A HD21	5.31		4.46101E-05	
	XXX 1 X H26	GLN 70 A HB3	5.35		4.26459E-05	
meth	XXX 1 X H26	LEU 56 A HD13	5.41		3.98856E-05	
meth	XXX 1 X H26	VAL 7 A HG21	5.44		3.85839E-05	
	XXX 1 X H26	LYS 5 A HG3	5.54		3.45893E-05	
meth	XXX 1 X H26	THR 74 A HG22	5.69		2.94664E-05	
meth	XXX 1 X H26	VAL 7 A HG23	5.73		2.82535E-05	
	XXX 1 X H26	THR 74 A HA	5.74		2.79595E-05	
	XXX 1 X H26	TYR 71 A HD2	5.88		2.41956E-05	
				SUM		0.004873444

	Recipient ligand proton	Donor Side Chain	Distance (Å)		Distance (1/Å^6)	
meth	XXX 1 X H27	VAL 7 A HG22	2.63	3.15	0.003021799	0.001023615
	XXX 1 X H27	TYR 71 A HB2	2.87		0.001789405	
	XXX 1 X H27	GLY 75 A HA2	3.14		0.001043331	
	XXX 1 X H27	TYR 71 A HA	3.2		0.000931323	
	XXX 1 X H27	GLY 75 A HA3	3.38		0.000670656	
meth	XXX 1 X H27	VAL 7 A HG21	3.39		0.000658873	
meth	XXX 1 X H27	VAL 7 A HG23	3.43		0.000614095	
	XXX 1 X H27	GLY 75 A H	3.57		0.000483048	
	XXX 1 X H27	TYR 71 A HB3	3.67		0.000409264	
	XXX 1 X H27	LYS 5 A HB3	3.73		0.000371319	
meth	XXX 1 X H27	LEU 56 A HD22	3.76	4.306666667	0.000353894	0.00015673
	XXX 1 X H27	LEU 56 A HB2	3.79		0.000337415	
	XXX 1 X H27	LEU 56 A HB3	3.9		0.000284192	
exch	XXX 1 X H27	THR 74 A HG1	3.94			
meth	XXX 1 X H27	LEU 56 A HD23	4.03		0.000233437	
	XXX 1 X H27	LYS 5 A HG2	4.77		8.48965E-05	
meth	XXX 1 X H27	VAL 7 A HG13	4.82		7.97476E-05	
	XXX 1 X H27	THR 74 A HB	4.82		7.97476E-05	
	XXX 1 X H27	LEU 56 A H	4.87		7.49594E-05	
	XXX 1 X H27	VAL 7 A HA	4.89		7.31386E-05	
	XXX 1 X H27	TYR 71 A HD1	5.01		6.32373E-05	
meth	XXX 1 X H27	LEU 56 A HD21	5.13		5.48651E-05	
	XXX 1 X H27	LYS 5 A HG3	5.16		5.29788E-05	
	XXX 1 X H27	LYS 5 A HB2	5.16		5.29788E-05	
meth	XXX 1 X H27	VAL 7 A HG11	5.18		5.17632E-05	
	XXX 1 X H27	GLU 76 A H	5.18		5.17632E-05	
	XXX 1 X H27	THR 74 A H	5.28		4.61526E-05	
	XXX 1 X H27	TYR 71 A H	5.31		4.46101E-05	
	XXX 1 X H27	VAL 7 A HB	5.35		4.26459E-05	
	XXX 1 X H27	LYS 5 A HA	5.44		3.85839E-05	
	XXX 1 X H27	MET 72 A HA	5.47		3.73316E-05	
	XXX 1 X H27	LEU 6 A H	5.51		3.57347E-05	
meth	XXX 1 X H27	LEU 56 A HD13	5.62		3.17382E-05	
	XXX 1 X H27	MET 72 A H	5.69		2.94664E-05	
	XXX 1 X H27	LEU 56 A HG	5.74		2.79595E-05	
	XXX 1 X H27	PHE 78 A HE2	5.82		2.57313E-05	
	XXX 1 X H27	VAL 7 A H	5.83		2.54676E-05	
	XXX 1 X H27	LEU 6 A HA	6		2.14335E-05	
				SUM		0.008409116

	Recipient ligand proton	Donor Side Chain	Distance (Å)		Distance (1/Å^6)	
meth	XXX 1 X H28	VAL 7 A HG22	2.76	3.446666667	0.002262276	0.000596492
	XXX 1 X H28	LEU 56 A H	2.84		0.001905855	
	XXX 1 X H28	LEU 56 A HB2	2.93		0.001580499	
	XXX 1 X H28	LEU 56 A HB3	3.03		0.001292243	
meth	XXX 1 X H28	VAL 7 A HG23	3.42		0.000624947	
	XXX 1 X H28	LYS 5 A HB3	3.47		0.000572827	
	XXX 1 X H28	LEU 6 A H	3.6		0.000459394	
	XXX 1 X H28	VAL 7 A HA	3.76		0.000353894	
	XXX 1 X H28	ILE 55 A HA	3.93		0.000271422	
	XXX 1 X H28	GLY 75 A HA2	4.01		0.00024051	
	XXX 1 X H28	LYS 5 A HA	4.05		0.000226605	
meth	XXX 1 X H28	VAL 7 A HG21	4.16		0.000192948	
meth	XXX 1 X H28	LEU 56 A HD22	4.35	4.84	7.77907E-05	7.77907E-05
	XXX 1 X H28	TYR 71 A HB2	4.44		0.000130528	
	XXX 1 X H28	LYS 5 A HG3	4.48		0.000123689	
meth	XXX 1 X H28	LEU 56 A HD23	4.49		0.000122046	
	XXX 1 X H28	GLY 75 A HA3	4.59		0.000106936	
	XXX 1 X H28	LEU 56 A HA	4.63		0.000101511	
	XXX 1 X H28	LEU 6 A HA	4.64		0.000100206	
	XXX 1 X H28	VAL 7 A H	4.77		8.48965E-05	
meth	XXX 1 X H28	VAL 7 A HG13	4.79	5.473333333	8.27917E-05	3.71953E-05
	XXX 1 X H28	LYS 5 A HG2	4.82		7.97476E-05	
	XXX 1 X H28	LYS 5 A HB2	5		0.000064	
	XXX 1 X H28	LEU 6 A HB2	5.1		5.68302E-05	
	XXX 1 X H28	ASP 54 A HB3	5.18		5.17632E-05	
	XXX 1 X H28	TYR 71 A HB3	5.23		4.88641E-05	
	XXX 1 X H28	VAL 7 A HB	5.23		4.88641E-05	
	XXX 1 X H28	GLU 76 A H	5.28		4.61526E-05	
	XXX 1 X H28	LEU 56 A HG	5.32		4.41093E-05	
meth	XXX 1 X H28	LEU 56 A HD13	5.36		4.21707E-05	
	XXX 1 X H28	TYR 71 A HA	5.42		3.94461E-05	
	XXX 1 X H28	GLY 75 A H	5.51		3.57347E-05	
	XXX 1 X H28	ILE 55 A H	5.59		3.2774E-05	
meth	XXX 1 X H28	VAL 7 A HG11	5.64		3.10689E-05	
meth	XXX 1 X H28	LEU 56 A HD21	5.68		2.9779E-05	
	XXX 1 X H28	SER 39 A HB2	5.68		2.9779E-05	
meth	XXX 1 X H28	ILE 55 A HG23	5.74		2.79595E-05	
	XXX 1 X H28	VAL 8 A H	5.84		2.52071E-05	
	XXX 1 X H28	LEU 6 A HB3	5.85		2.49497E-05	
exch	XXX 1 X H28	THR 74 A HG1	5.9			
meth	XXX 1 X H28	LEU 56 A HD12	5.91		2.34679E-05	
meth	XXX 1 X H28	ILE 55 A HG22	5.94		2.27657E-05	
	XXX 1 X H28	SER 39 A HB3	5.96		2.23112E-05	
meth	XXX 1 X H28	VAL 7 A HG12	5.99		2.16491E-05	
				SUM		0.008913026

	Recipient ligand proton	Donor Side Chain	Distance (Å)		Distance (1/Å^6)
	XXX 1 X H29	LEU 56 A HB2	2.96		0.00148679
	XXX 1 X H29	LEU 56 A H	2.97		0.001457006
	XXX 1 X H29	ILE 55 A HA	3.44		0.000603461
	XXX 1 X H29	SER 39 A HB2	3.62		0.000444374
	XXX 1 X H29	LEU 56 A HB3	3.91		0.000279859
	XXX 1 X H29	LEU 56 A HA	3.92		0.000275603
	XXX 1 X H29	ILE 55 A H	3.94		0.000267315
	XXX 1 X H29	ASP 54 A HB3	4.08		0.00021679
	XXX 1 X H29	LEU 6 A H	4.14		0.000198609
	XXX 1 X H29	LYS 5 A HG3	4.18		0.000187475
	XXX 1 X H29	LYS 5 A HA	4.25		0.000169694
	XXX 1 X H29	SER 39 A HB3	4.3		0.000158194
	XXX 1 X H29	ASP 54 A HA	4.42		0.000134112
	XXX 1 X H29	LYS 5 A HB3	4.52		0.000117265
	XXX 1 X H29	SER 39 A HA	4.78		8.38364E-05
	XXX 1 X H29	TYR 40 A H	4.79		8.27917E-05
meth	XXX 1 X H29	LEU 56 A HD13	4.84		7.77907E-05
meth	XXX 1 X H29	LEU 56 A HD22	4.95		6.79781E-05
meth	XXX 1 X H29	VAL 7 A HG22	4.95		6.79781E-05
	XXX 1 X H29	LYS 5 A HG2	4.98		6.55577E-05
	XXX 1 X H29	ASP 54 A HB2	5.07		5.88779E-05
exch	XXX 1 X H29	SER 39 A HG	5.25		
	XXX 1 X H29	VAL 7 A HA	5.34		4.31273E-05
meth	XXX 1 X H29	LEU 56 A HD12	5.37		4.17018E-05
	XXX 1 X H29	ASP 54 A H	5.44		3.85839E-05
	XXX 1 X H29	ILE 55 A HB	5.49		3.6523E-05
meth	XXX 1 X H29	LEU 56 A HD23	5.6		3.24244E-05
meth	XXX 1 X H29	ILE 55 A HG22	5.62		3.17382E-05
	XXX 1 X H29	LEU 6 A HB2	5.62		3.17382E-05
meth	XXX 1 X H29	VAL 7 A HG23	5.72		2.85512E-05
	XXX 1 X H29	LEU 56 A HG	5.73		2.82535E-05
meth	XXX 1 X H29	ILE 55 A HG23	5.76		2.7382E-05
	XXX 1 X H29	ILE 55 A HG12	5.86		2.46953E-05
	XXX 1 X H29	ILE 55 A HG13	5.9		2.37076E-05
	XXX 1 X H29	LYS 5 A HB2	5.91		2.34679E-05
	XXX 1 X H29	GLY 75 A HA2	5.94		2.27657E-05
			SUM		0.00656047

Fragment I

	Recipient ligand proton	Donor Side Chain	Distance (Å)		Distance (1/Å^6)	
meth	XXX 1 X H19	LEU 56 A HD11	2.99	3.423333333	0.0013995	0.000621305
meth	XXX 1 X H19	LEU 56 A HD13	3.11		0.001105192	
	XXX 1 X H19	TYR 71 A HE1	3.22		0.000897149	
	XXX 1 X H19	TYR 71 A HD1	3.36		0.000694967	
meth	XXX 1 X H19	LEU 56 A HD21	3.77	4.27	0.000348299	0.000164981
	XXX 1 X H19	GLU 37 A HG2	3.82		0.000321825	
meth	XXX 1 X H19	LEU 56 A HD22	3.91		0.000279859	
meth	XXX 1 X H19	LEU 56 A HD12	4.17		0.000190188	
	XXX 1 X H19	TYR 71 A HB3	4.24		0.00017211	
	XXX 1 X H19	TYR 71 A HH	4.81		8.07476E-05	
	XXX 1 X H19	TYR 71 A HE2	4.81		8.07476E-05	
	XXX 1 X H19	GLU 37 A HG3	4.88		7.40425E-05	
	XXX 1 X H19	TYR 71 A HD2	4.89		7.31386E-05	
	XXX 1 X H19	ASP 38 A HA	5		0.000064	
	XXX 1 X H19	TYR 71 A HB2	5.04		6.10122E-05	
	XXX 1 X H19	LEU 56 A HG	5.09		5.75034E-05	
meth	XXX 1 X H19	LEU 56 A HD23	5.13		5.48651E-05	
	XXX 1 X H19	LEU 56 A HB2	5.37		4.17018E-05	
	XXX 1 X H19	SER 39 A HB3	5.38		4.12388E-05	
	XXX 1 X H19	GLU 37 A HB3	5.75		2.7669E-05	
	XXX 1 X H19	TYR 71 A HA	5.8		2.62683E-05	
	XXX 1 X H19	SER 39 A H	5.84		2.52071E-05	
				SUM		0.003444866

	Recipient ligand proton	Donor Side Chain	Distance (Å)		Distance (1/Å^6)	
	XXX 1 X H20	TYR 71 A HB3	2.79		0.00212019	
meth	XXX 1 X H20	LEU 56 A HD22	3	3.713333333	0.001371742	0.000381431
	XXX 1 X H20	TYR 71 A HD2	3.22		0.000897149	
meth	XXX 1 X H20	LEU 56 A HD13	3.41	4.113333333	0.000636024	0.00020646
	XXX 1 X H20	TYR 71 A HD1	3.56		0.000491247	
meth	XXX 1 X H20	LEU 56 A HD21	3.66		0.000416019	
	XXX 1 X H20	TYR 71 A HA	3.79		0.000337415	
	XXX 1 X H20	TYR 71 A HE2	3.98		0.000251595	
meth	XXX 1 X H20	LEU 56 A HD11	4		0.000244141	
	XXX 1 X H20	TYR 71 A HB2	4.02		0.000236943	
	XXX 1 X H20	TYR 71 A HE1	4.25		0.000169694	
meth	XXX 1 X H20	LEU 56 A HD23	4.48		0.000123689	
	XXX 1 X H20	LEU 56 A HB2	4.71		9.15956E-05	
meth	XXX 1 X H20	LEU 56 A HD12	4.93		6.96496E-05	
exch	XXX 1 X H20	TYR 71 A HH	5.05		6.02909E-05	
meth	XXX 1 X H20	THR 74 A HG21	5.14	5.283333333	5.42277E-05	4.59782E-05
meth	XXX 1 X H20	THR 74 A HG23	5.16		5.29788E-05	
	XXX 1 X H20	TYR 71 A H	5.3		4.51175E-05	
	XXX 1 X H20	SER 39 A HB3	5.32		4.41093E-05	
	XXX 1 X H20	LEU 56 A HG	5.33		4.36151E-05	
meth	XXX 1 X H20	THR 74 A HG22	5.55		0.000034217	
	XXX 1 X H20	LEU 56 A HB3	5.6		3.24244E-05	
	XXX 1 X H20	GLU 37 A HG2	5.86		2.46953E-05	
		SUM				0.00541966

		Recipient ligand proton	Donor Side Chain	Distance (Å)		Distance (1/Å^6)	
exch		XXX 1 X H21	SER 39 A HG	2.49		0.004195695	
		XXX 1 X H21	SER 39 A HB3	2.95		0.001517288	
		XXX 1 X H21	SER 39 A HB2	3.87		0.000297669	
	meth	XXX 1 X H21	LEU 56 A HD13	4.04	4.9	0.000229992	7.22476E-05
		XXX 1 X H21	SER 39 A H	4.51		0.000118834	
		XXX 1 X H21	LEU 56 A HB2	4.86		7.58896E-05	
	meth	XXX 1 X H21	LEU 56 A HD12	5.22		4.94284E-05	
exch	meth	XXX 1 X H21	LYS 5 A HZ2	5.22		4.94284E-05	
		XXX 1 X H21	SER 39 A HA	5.23		4.88641E-05	
	meth	XXX 1 X H21	LEU 56 A HD22	5.35		4.26459E-05	
	meth	XXX 1 X H21	LEU 56 A HD11	5.44		3.85839E-05	
exch	meth	XXX 1 X H21	LYS 5 A HZ3	5.46		3.77437E-05	
		XXX 1 X H21	LEU 56 A HA	5.74		2.79595E-05	
		XXX 1 X H21	ASP 38 A HA	5.79		2.65417E-05	
exch	meth	XXX 1 X H21	LYS 5 A HZ1	5.85		2.49497E-05	
					SUM		0.002185293

	Recipient ligand proton	Donor Side Chain	Distance (Å)		Distance (1/Å^6)	
	XXX 1 X H22	SER 39 A H	2.9		0.001681171	
exch	XXX 1 X H22	SER 39 A HG	2.95		0.001517288	
	XXX 1 X H22	SER 39 A HB3	3.04		0.001266947	
	XXX 1 X H22	ASP 38 A HA	3.71		0.000383492	
meth	XXX 1 X H22	LEU 56 A HD13	3.78	4.34	0.000342807	0.000149645
	XXX 1 X H22	SER 39 A HB2	4.27		0.000164981	
meth	XXX 1 X H22	LEU 56 A HD12	4.5		0.000120427	
	XXX 1 X H22	SER 39 A HA	4.68		9.51754E-05	
meth	XXX 1 X H22	LEU 56 A HD11	4.74		8.81718E-05	
	XXX 1 X H22	LEU 56 A HB2	5.49		3.6523E-05	
	XXX 1 X H22	LEU 56 A HA	5.61		3.20791E-05	
	XXX 1 X H22	GLU 37 A HG2	5.75		2.7669E-05	
	XXX 1 X H22	ASP 38 A HB3	5.85		2.49497E-05	
	XXX 1 X H22	ASP 38 A HB2	5.87		2.4444E-05	
meth	XXX 1 X H22	LEU 56 A HD22	5.91		2.34679E-05	
	XXX 1 X H22	ASP 38 A H	5.99		2.16491E-05	
				SUM	0.004333954	0.003908725

		Recipient ligand proton	Donor Side Chain	Distance (Å)		Distance (1/Å^6)	
	meth	XXX 1 X H23	THR 74 A HG23	2.05	2.733333333	0.013473389	0.002397974
		XXX 1 X H23	TYR 71 A HA	2.92		0.001613255	
	meth	XXX 1 X H23	THR 74 A HG21	2.95		0.001517288	
		XXX 1 X H23	TYR 71 A HB3	3.17		0.000985472	
	meth	XXX 1 X H23	THR 74 A HG22	3.2		0.000931323	
	meth	XXX 1 X H23	LEU 56 A HD22	3.31	4.093333333	0.000760382	0.000212587
		XXX 1 X H23	GLY 75 A H	4.24		0.00017211	
	meth	XXX 1 X H23	LEU 56 A HD23	4.25		0.000169694	
		XXX 1 X H23	TYR 71 A HD2	4.26		0.000167318	
		XXX 1 X H23	LEU 56 A HB2	4.34		0.000149645	
	meth	XXX 1 X H23	VAL 7 A HG22	4.36	4.79	0.000145573	8.27917E-05
		XXX 1 X H23	THR 74 A H	4.41		0.000135947	
		XXX 1 X H23	LYS 5 A HD3	4.45		0.000128777	
		XXX 1 X H23	TYR 71 A HB2	4.54		0.0001142	
	exch	XXX 1 X H23	THR 74 A HG1	4.57		0.000109775	
	meth	XXX 1 X H23	LEU 56 A HD21	4.72		9.04374E-05	
	meth	XXX 1 X H23	VAL 7 A HG21	4.74		8.81718E-05	
		XXX 1 X H23	GLY 75 A HA2	4.74		8.81718E-05	
		XXX 1 X H23	THR 74 A HB	4.79		8.27917E-05	
		XXX 1 X H23	LEU 56 A HB3	4.8		8.17622E-05	
exch	meth	XXX 1 X H23	LYS 5 A HZ2	4.8		8.17622E-05	
	meth	XXX 1 X H23	LEU 56 A HD13	5.06		5.95795E-05	
		XXX 1 X H23	GLY 75 A HA3	5.09		5.75034E-05	
		XXX 1 X H23	LYS 5 A HB3	5.15		5.3599E-05	
		XXX 1 X H23	MET 72 A HA	5.21		5.00004E-05	
	meth	XXX 1 X H23	VAL 7 A HG23	5.27		4.66806E-05	
		XXX 1 X H23	MET 72 A H	5.34		4.31273E-05	
		XXX 1 X H23	TYR 71 A H	5.43		3.90123E-05	
		XXX 1 X H23	THR 74 A HA	5.58		3.3128E-05	
		XXX 1 X H23	LYS 5 A HD2	5.77		2.70985E-05	
exch	meth	XXX 1 X H23	LYS 5 A HZ3	5.81		2.59982E-05	
		XXX 1 X H23	TYR 71 A HD1	5.87		2.4444E-05	
		XXX 1 X H23	LYS 5 A HG2	5.94		2.27657E-05	
	meth	XXX 1 X H23	VAL 7 A HG13	5.94		2.27657E-05	
		XXX 1 X H23	LEU 56 A HG	5.96		2.23112E-05	
					SUM		0.006785791

	Recipient	Donor	Distance (Å)	Distance	Distance (1/d⁶)	
meth	XXX 1 X H24	VAL 7 A HG22	2.42	2.746666667	0.004978607	0.002328972
meth	XXX 1 X H24	VAL 7 A HG21	2.81		0.002031244	
	XXX 1 X H24	GLY 75 A HA2	2.85		0.001866082	
meth	XXX 1 X H24	VAL 7 A HG23	3.01		0.001344625	
	XXX 1 X H24	GLY 75 A HA3	3.08		0.001171374	
meth	XXX 1 X H24	THR 74 A HG23	3.13	4.06	0.001063491	0.000223277
	XXX 1 X H24	GLY 75 A H	3.16		0.001004332	
	XXX 1 X H24	LYS 5 A HB3	3.8		0.000332123	
meth	XXX 1 X H24	LEU 56 A HD22	3.84	4.326666667	0.000311898	0.000152433
	XXX 1 X H24	LEU 56 A HB3	3.92		0.000275603	
meth	XXX 1 X H24	LEU 56 A HD23	3.99		0.000247835	
	XXX 1 X H24	LEU 56 A HB2	4.11		0.000207467	
	XXX 1 X H24	LYS 5 A HD3	4.32		0.00015385	
	XXX 1 X H24	MET 72 A HA	4.41		0.000135947	
	XXX 1 X H24	TYR 71 A HB3	4.43		0.000132305	
meth	XXX 1 X H24	THR 74 A HG22	4.45		0.000128777	
	XXX 1 X H24	TYR 71 A HA	4.58		0.000108345	
meth	XXX 1 X H24	THR 74 A HG21	4.6		0.000105549	
meth	XXX 1 X H24	VAL 7 A HG13	4.62	5.063333333	0.000102837	5.93446E-05
exch	XXX 1 X H24	THR 74 A HG1	4.73		8.92962E-05	
	XXX 1 X H24	THR 74 A H	4.74		8.81718E-05	
meth	XXX 1 X H24	VAL 7 A HG11	4.76		8.59722E-05	
	XXX 1 X H24	VAL 7 A HA	4.86		7.58896E-05	
	XXX 1 X H24	VAL 7 A HB	4.94		6.88079E-05	
	XXX 1 X H24	GLU 76 A H	5.06		5.95795E-05	
	XXX 1 X H24	LYS 5 A HB2	5.1		5.68302E-05	
meth	XXX 1 X H24	LEU 56 A HD21	5.15		5.3599E-05	
	XXX 1 X H24	LEU 56 A H	5.18		5.17632E-05	
	XXX 1 X H24	LYS 5 A HG2	5.37		4.17018E-05	
	XXX 1 X H24	LYS 5 A HD2	5.4		4.03309E-05	
	XXX 1 X H24	PHE 78 A HE1	5.5		3.61263E-05	
	XXX 1 X H24	THR 74 A HA	5.55		3.4217E-05	
	XXX 1 X H24	TYR 71 A HB2	5.56		3.38494E-05	
exch meth	XXX 1 X H24	LYS 5 A HZ2	5.61		3.20791E-05	
	XXX 1 X H24	MET 72 A H	5.66		3.0416E-05	
	XXX 1 X H24	VAL 7 A H	5.66		3.0416E-05	
	XXX 1 X H24	THR 74 A HB	5.67		3.00955E-05	
	XXX 1 X H24	LYS 5 A HA	5.71		2.88525E-05	
	XXX 1 X H24	LEU 56 A HG	5.74		2.79595E-05	
	XXX 1 X H24	LEU 6 A H	5.75		2.7669E-05	
meth	XXX 1 X H24	LEU 56 A HD13	5.81		2.59982E-05	
meth	XXX 1 X H24	VAL 7 A HG12	5.81		2.59982E-05	
	XXX 1 X H24	PHE 78 A HZ	5.82		2.57313E-05	
				SUM		0.008914131

	Recipient ligand proton	Donor Side Chain	Distance (Å)		Distance (1/Å^6)	
meth	XXX 1 X H25	VAL 7 A HG22	2.56	3.073333333	0.003552714	0.001186703
	XXX 1 X H25	LYS 5 A HB3	2.78		0.002166363	
meth	XXX 1 X H25	VAL 7 A HG23	2.92		0.001613255	
	XXX 1 X H25	GLY 75 A HA2	3.26		0.000833095	
	XXX 1 X H25	LEU 56 A HB3	3.37		0.000682685	
	XXX 1 X H25	LEU 56 A H	3.44		0.000603461	
	XXX 1 X H25	LEU 56 A HB2	3.53		0.000516835	
	XXX 1 X H25	LEU 6 A H	3.53		0.000516835	
meth	XXX 1 X H25	VAL 7 A HG21	3.74		0.000365402	
	XXX 1 X H25	LYS 5 A HA	3.82		0.000321825	
	XXX 1 X H25	VAL 7 A HA	3.93		0.000271422	
	XXX 1 X H25	GLY 75 A HA3	3.97		0.000255421	
	XXX 1 X H25	LYS 5 A HG2	4.15		0.000195754	
	XXX 1 X H25	LYS 5 A HD3	4.22		0.000177062	
	XXX 1 X H25	LYS 5 A HB2	4.28		0.000162681	
	XXX 1 X H25	LEU 6 A HA	4.38		0.00014163	
	XXX 1 X H25	ILE 55 A HA	4.48		0.000123689	
	XXX 1 X H25	VAL 7 A H	4.56		0.000111227	
	XXX 1 X H25	GLU 76 A H	4.66		9.76528E-05	
meth	XXX 1 X H25	LEU 56 A HD22	4.73		8.92962E-05	
meth	XXX 1 X H25	LEU 56 A HD23	4.79		8.27917E-05	
meth	XXX 1 X H25	VAL 7 A HG13	4.89		7.31386E-05	
	XXX 1 X H25	GLY 75 A H	4.96		6.71599E-05	
	XXX 1 X H25	VAL 7 A HB	4.98		6.55577E-05	
meth	XXX 1 X H25	THR 74 A HG23	5.01		6.32373E-05	
	XXX 1 X H25	LEU 56 A HA	5.24		4.83072E-05	
	XXX 1 X H25	LEU 6 A HB2	5.26		4.72156E-05	
	XXX 1 X H25	LYS 5 A HD2	5.27		4.66806E-05	
	XXX 1 X H25	LYS 5 A HG3	5.28		4.61526E-05	
	XXX 1 X H25	ASP 54 A HB3	5.38		4.12388E-05	
meth	XXX 1 X H25	VAL 7 A HG11	5.52		3.53481E-05	
exch meth	XXX 1 X H25	LYS 5 A HZ2	5.58		3.3128E-05	
	XXX 1 X H25	GLY 77 A H	5.64		3.10689E-05	
exch meth	XXX 1 X H25	LYS 5 A HZ3	5.69		2.94664E-05	
	XXX 1 X H25	LEU 56 A HG	5.71		2.88525E-05	
exch	XXX 1 X H25	THR 74 A HG1	5.72		2.85512E-05	
	XXX 1 X H25	LYS 5 A H	5.72		2.85512E-05	
	XXX 1 X H25	LEU 6 A HB3	5.86		2.46953E-05	
meth	XXX 1 X H25	LEU 56 A HD13	5.87		2.4444E-05	
	XXX 1 X H25	SER 39 A HB2	5.91		2.34679E-05	
	XXX 1 X H25	SER 39 A HB3	5.92		2.32311E-05	
				SUM	0.008886521	

		Recipient ligand proton	Donor Side Chain	Distance (Å)		Distance (1/Å^6)	
		XXX 1 X H26	LEU 56 A HB2	3.14		0.001043331	
		XXX 1 X H26	LEU 56 A H	3.22		0.000897149	
		XXX 1 X H26	LYS 5 A HG2	3.45		0.000593042	
		XXX 1 X H26	LYS 5 A HB3	3.61		0.000451811	
		XXX 1 X H26	LYS 5 A HA	3.66		0.000416019	
		XXX 1 X H26	LEU 6 A H	3.78		0.000342807	
		XXX 1 X H26	SER 39 A HB2	3.8		0.000332123	
		XXX 1 X H26	ILE 55 A HA	3.83		0.000316816	
		XXX 1 X H26	LEU 56 A HB3	3.87		0.000297669	
		XXX 1 X H26	ASP 54 A HB3	3.95		0.00026328	
		XXX 1 X H26	SER 39 A HB3	4.14		0.000198609	
		XXX 1 X H26	LYS 5 A HD3	4.25		0.000169694	
		XXX 1 X H26	LEU 56 A HA	4.37		0.000143586	
		XXX 1 X H26	ILE 55 A H	4.38		0.00014163	
exch	meth	XXX 1 X H26	LYS 5 A HZ3	4.43		0.000132305	
	meth	XXX 1 X H26	VAL 7 A HG22	4.53	5.203333333	0.000115721	5.0386E-05
		XXX 1 X H26	ASP 54 A HA	4.68		9.51754E-05	
exch	meth	XXX 1 X H26	LYS 5 A HZ2	4.72		9.04374E-05	
		XXX 1 X H26	LYS 5 A HG3	4.94		6.88079E-05	
		XXX 1 X H26	ASP 54 A HB2	4.95		6.79781E-05	
		XXX 1 X H26	LYS 5 A HB2	5.05		6.02909E-05	
exch		XXX 1 X H26	SER 39 A HG	5.06		5.95795E-05	
	meth	XXX 1 X H26	LEU 56 A HD22	5.12		5.55112E-05	
		XXX 1 X H26	SER 39 A HA	5.15		5.3599E-05	
	meth	XXX 1 X H26	VAL 7 A HG23	5.18		5.17632E-05	
	meth	XXX 1 X H26	LEU 56 A HD13	5.2		5.05801E-05	
		XXX 1 X H26	ASP 54 A H	5.24		4.83072E-05	
		XXX 1 X H26	GLY 75 A HA2	5.25		4.77578E-05	
		XXX 1 X H26	VAL 7 A HA	5.27		4.66806E-05	
		XXX 1 X H26	LYS 5 A HD2	5.52		3.53481E-05	
		XXX 1 X H26	LEU 6 A HB2	5.62		3.17382E-05	
		XXX 1 X H26	TYR 40 A H	5.63		3.14014E-05	
	meth	XXX 1 X H26	LEU 56 A HD23	5.68		2.9779E-05	
exch	meth	XXX 1 X H26	LYS 5 A HZ1	5.74		2.79595E-05	
		XXX 1 X H26	LEU 6 A HA	5.76		2.7382E-05	
	meth	XXX 1 X H26	LEU 56 A HD12	5.79		2.65417E-05	
		XXX 1 X H26	LYS 5 A HE2	5.88		2.41956E-05	
		XXX 1 X H26	LEU 56 A HG	5.9		2.37076E-05	
	meth	XXX 1 X H26	VAL 7 A HG21	5.9		2.37076E-05	
	meth	XXX 1 X H26	THR 74 A HG23	5.9		2.37076E-05	
						0.006320321	

Fragment J

	Recipient ligand proton	Donor Side Chain	Distance (Å)		Distance (1/Å^6)	
exch	XXX 1 X H20	SER 39 A HG	2.76			
	XXX 1 X H20	SER 39 A HB3	3.12		0.001084108	
	XXX 1 X H20	SER 39 A H	3.15		0.001023615	
meth	XXX 1 X H20	LEU 56 A HD13	4.09	4.543333333		0.000113698
	XXX 1 X H20	ASP 38 A HA	4.18		0.000187475	
	XXX 1 X H20	SER 39 A HB2	4.25		0.000169694	
meth	XXX 1 X H20	LEU 56 A HD12	4.68			
meth	XXX 1 X H20	LEU 56 A HD11	4.86			
	XXX 1 X H20	SER 39 A HA	4.87		7.49594E-05	
	XXX 1 X H20	LEU 56 A HB2	5.92		2.32311E-05	
	XXX 1 X H20	LEU 56 A HA	5.95		2.25371E-05	
				SUM		0.002699317

	Recipient ligand proton	Donor Side Chain	Distance (Å)		Distance (1/Å^6)	
exch	XXX 1 X H21	SER 39 A HG	2.63			
	XXX 1 X H21	SER 39 A HB3	3.14		0.001043331	
	XXX 1 X H21	SER 39 A HB2	4		0.000244141	
meth	XXX 1 X H21	LEU 56 A HD13	4.19	4.986666667		6.50336E-05
	XXX 1 X H21	SER 39 A H	4.77		8.48965E-05	
	XXX 1 X H21	LYS 5 A HE3	5.25		4.77578E-05	
	XXX 1 X H21	LEU 56 A HB2	5.26		4.72156E-05	
meth	XXX 1 X H21	LEU 56 A HD12	5.28			
	XXX 1 X H21	SER 39 A HA	5.43		3.90123E-05	
meth	XXX 1 X H21	LEU 56 A HD22	5.46			
meth	XXX 1 X H21	LEU 56 A HD11	5.49			
meth	XXX 1 X H21	LYS 5 A HZ1	5.82			
	XXX 1 X H21	LYS 5 A HE2	5.87		2.4444E-05	
				SUM		0.001595831

309

	Recipient ligand proton	Donor Side Chain	Distance (Å)		Distance (1/Å^6)	
meth	XXX 1 X H22	LEU 56 A HD22	2.98	3.676666667		0.000404832
	XXX 1 X H22	TYR 71 A HD1	3.12		0.001084108	
meth	XXX 1 X H22	LEU 56 A HD13	3.3	4.003333333		0.000242923
	XXX 1 X H22	TYR 71 A HB3	3.35		0.000707508	
	XXX 1 X H22	TYR 71 A HE1	3.45		0.000593042	
meth	XXX 1 X H22	LEU 56 A HD21	3.62			
	XXX 1 X H22	TYR 71 A HD2	3.84		0.000311898	
meth	XXX 1 X H22	LEU 56 A HD11	3.9			
	XXX 1 X H22	TYR 71 A HE2	4.21		0.0001796	
	XXX 1 X H22	TYR 71 A HA	4.22		0.000177062	
meth	XXX 1 X H22	LEU 56 A HD23	4.43			
	XXX 1 X H22	TYR 71 A HB2	4.46		0.000127055	
exch	XXX 1 X H22	TYR 71 A HH	4.74			
	XXX 1 X H22	LEU 56 A HB2	4.75		8.70639E-05	
meth	XXX 1 X H22	LEU 56 A HD12	4.81			
	XXX 1 X H22	SER 39 A HB3	5.3		4.51175E-05	
	XXX 1 X H22	LEU 56 A HG	5.35		4.26459E-05	
	XXX 1 X H22	LEU 56 A HB3	5.7		2.91575E-05	
	XXX 1 X H22	TYR 71 A H	5.79		2.65417E-05	
exch	XXX 1 X H22	THR 74 A HG1	5.83			
				SUM		0.004058554

	Recipient ligand proton	Donor Side Chain	Distance (Å)		Distance (1/Å^6)	
meth	XXX 1 X H23	LEU 56 A HD11	2.95	3.416666667		0.000628614
meth	XXX 1 X H23	LEU 56 A HD13	3.16			
	XXX 1 X H23	TYR 71 A HE2	3.37		0.000682685	
meth	XXX 1 X H23	LEU 56 A HD21	3.74	4.25		0.000169694
	XXX 1 X H23	TYR 71 A HD2	3.85		0.000307069	
exch	XXX 1 X H23	TYR 71 A HH	3.86			
meth	XXX 1 X H23	LEU 56 A HD22	3.9			
meth	XXX 1 X H23	LEU 56 A HD12	4.14			
	XXX 1 X H23	TYR 71 A HE1	4.44		0.000130528	
	XXX 1 X H23	GLU 37 A HB3	4.5		0.000120427	
	XXX 1 X H23	TYR 71 A HB3	4.81		8.07476E-05	
	XXX 1 X H23	TYR 71 A HD1	4.92		7.05033E-05	
	XXX 1 X H23	ASP 38 A HA	4.97		6.63532E-05	
meth	XXX 1 X H23	LEU 56 A HD23	5.11			
	XXX 1 X H23	LEU 56 A HG	5.13		5.48651E-05	
	XXX 1 X H23	SER 39 A HB3	5.29		4.56316E-05	
	XXX 1 X H23	LEU 56 A HB2	5.47		3.73316E-05	
	XXX 1 X H23	TYR 71 A HB2	5.54		3.45893E-05	
	XXX 1 X H23	GLU 37 A HB2	5.59		3.2774E-05	
	XXX 1 X H23	SER 39 A H	5.64		3.10689E-05	
				SUM		0.002492882

	Recipient ligand proton	Donor Side Chain	Distance (Å)		Distance (1/Å^6)	
	XXX 1 X H24	THR 74 A HB	2.96		0.00148679	
	XXX 1 X H24	TYR 71 A HA	2.99		0.0013995	
	XXX 1 X H24	TYR 71 A HB3	3.12		0.001084108	
meth	XXX 1 X H24	LEU 56 A HD22	3.39	4.156666667		0.000193878
	XXX 1 X H24	TYR 71 A HD1	3.69		0.000396134	
exch	XXX 1 X H24	THR 74 A HG1	3.8			
	XXX 1 X H24	GLY 75 A H	4.15		0.000195754	
	XXX 1 X H24	LYS 5 A HG2	4.23		0.000174565	
meth	XXX 1 X H24	LEU 56 A HD23	4.31			
	XXX 1 X H24	LEU 56 A HB2	4.4		0.000137811	
meth	XXX 1 X H24	THR 74 A HG21	4.5	4.993333333		6.45144E-05
	XXX 1 X H24	TYR 71 A HB2	4.55		0.000112702	
meth	XXX 1 X H24	VAL 7 A HG22	4.65	5.173333333		5.21648E-05
	XXX 1 X H24	THR 74 A H	4.67		9.64048E-05	
	XXX 1 X H24	GLY 75 A HA2	4.71		9.15956E-05	
meth	XXX 1 X H24	LEU 56 A HD21	4.77			
	XXX 1 X H24	LYS 5 A HE2	4.9		7.22476E-05	
meth	XXX 1 X H24	LEU 56 A HD13	4.92			
	XXX 1 X H24	LEU 56 A HB3	5.01		6.32373E-05	
	XXX 1 X H24	GLY 75 A HA3	5.02		6.24853E-05	
	XXX 1 X H24	LYS 5 A HG3	5.04		6.10122E-05	
meth	XXX 1 X H24	VAL 7 A HG21	5.14			
	XXX 1 X H24	LYS 5 A HE3	5.16		5.29788E-05	
meth	XXX 1 X H24	THR 74 A HG22	5.17			
	XXX 1 X H24	THR 74 A HA	5.26		4.72156E-05	
meth	XXX 1 X H24	THR 74 A HG23	5.31			
	XXX 1 X H24	TYR 71 A H	5.45		3.81611E-05	
	XXX 1 X H24	MET 72 A HA	5.47		3.73316E-05	
	XXX 1 X H24	TYR 71 A HE1	5.49		3.6523E-05	
	XXX 1 X H24	MET 72 A H	5.52		3.53481E-05	
	XXX 1 X H24	LYS 5 A HB3	5.52		3.53481E-05	
	XXX 1 X H24	TYR 71 A HD2	5.71		2.88525E-05	
meth	XXX 1 X H24	VAL 7 A HG23	5.73			
meth	XXX 1 X H24	LEU 56 A HD11	5.98			
				SUM		0.006056663

	Recipient ligand proton	Donor Side Chain	Distance (Å)		Distance (1/Å^6)	
meth	XXX 1 X H25	VAL 7 A HG22	2.56	3.023333333		0.001309435
	XXX 1 X H25	GLY 75 A HA2	2.82		0.001988407	
	XXX 1 X H25	GLY 75 A HA3	3.02		0.00131813	
meth	XXX 1 X H25	VAL 7 A HG21	3.07			
	XXX 1 X H25	GLY 75 A H	3.08		0.001171374	
meth	XXX 1 X H25	VAL 7 A HG23	3.44			
	XXX 1 X H25	LYS 5 A HG2	3.77		0.000348299	
	XXX 1 X H25	THR 74 A HB	3.79		0.000337415	
meth	XXX 1 X H25	LEU 56 A HD22	3.82	4.303333333		0.00015746
	XXX 1 X H25	TYR 71 A HB3	3.95		0.00026328	
meth	XXX 1 X H25	LEU 56 A HD23	3.97			
	XXX 1 X H25	LEU 56 A HB2	4.01		0.00024051	
	XXX 1 X H25	LEU 56 A HB3	4.02		0.000236943	
	XXX 1 X H25	LYS 5 A HB3	4.13		0.000201511	
	XXX 1 X H25	TYR 71 A HA	4.33		0.00015173	
	XXX 1 X H25	MET 72 A HA	4.33		0.00015173	
	XXX 1 X H25	LYS 5 A HG3	4.44		0.000130528	
meth	XXX 1 X H25	VAL 7 A HG13	4.62	5.096666667		5.70535E-05
meth	XXX 1 X H25	VAL 7 A HG11	4.8			
	XXX 1 X H25	THR 74 A H	4.93		6.96496E-05	
	XXX 1 X H25	VAL 7 A HA	5.02		6.24853E-05	
	XXX 1 X H25	GLU 76 A H	5.02		6.24853E-05	
meth	XXX 1 X H25	LEU 56 A HD21	5.12			
	XXX 1 X H25	VAL 7 A HB	5.18		5.17632E-05	
exch	XXX 1 X H25	THR 74 A HG1	5.2			
	XXX 1 X H25	TYR 71 A HB2	5.21		5.00004E-05	
	XXX 1 X H25	LEU 56 A H	5.22		4.94284E-05	
	XXX 1 X H25	THR 74 A HA	5.39		4.07819E-05	
	XXX 1 X H25	PHE 78 A HZ	5.44		3.85839E-05	
	XXX 1 X H25	MET 72 A H	5.46		3.77437E-05	
	XXX 1 X H25	LYS 5 A HE2	5.54		3.45893E-05	
	XXX 1 X H25	LYS 5 A HB2	5.54		3.45893E-05	
	XXX 1 X H25	LYS 5 A HE3	5.55		3.4217E-05	
meth	XXX 1 X H25	LEU 56 A HD13	5.59			
	XXX 1 X H25	LYS 5 A HA	5.61		3.20791E-05	
	XXX 1 X H25	TYR 71 A HD1	5.66		3.0416E-05	
	XXX 1 X H25	PHE 78 A HE2	5.68		2.9779E-05	
	XXX 1 X H25	LEU 6 A H	5.74		2.79595E-05	
	XXX 1 X H25	LEU 56 A HG	5.8		2.62683E-05	
meth	XXX 1 X H25	VAL 7 A HG12	5.87			
	XXX 1 X H25	VAL 7 A H	5.95		2.25371E-05	
	XXX 1 X H25	MET 72 A HG2	5.97		2.20879E-05	
meth	XXX 1 X H25	THR 74 A HG21	5.97			
	XXX 1 X H25	GLU 76 A HG3	5.99		2.16491E-05	
		SUM				0.0088429

313

	Recipient ligand proton	Donor Side Chain	Distance (Å)		Distance (1/Å^6)	
meth	XXX 1 X H26	VAL 7 A HG22	2.43	3.096666667		0.001134053
meth	XXX 1 X H26	VAL 7 A HG23	3.12			
	XXX 1 X H26	GLY 75 A HA2	3.22		0.000897149	
	XXX 1 X H26	LYS 5 A HG3	3.31		0.000760382	
	XXX 1 X H26	LEU 56 A HB2	3.32		0.000746744	
	XXX 1 X H26	LEU 56 A HB3	3.36		0.000694967	
	XXX 1 X H26	LEU 56 A H	3.4		0.000647331	
	XXX 1 X H26	LYS 5 A HB3	3.43		0.000614095	
	XXX 1 X H26	LYS 5 A HG2	3.5		0.000543991	
	XXX 1 X H26	LEU 6 A H	3.53		0.000516835	
meth	XXX 1 X H26	VAL 7 A HG21	3.74			
	XXX 1 X H26	LYS 5 A HA	3.83		0.000316816	
	XXX 1 X H26	VAL 7 A HA	3.92		0.000275603	
	XXX 1 X H26	GLY 75 A HA3	3.93		0.000271422	
	XXX 1 X H26	LEU 6 A HA	4.36		0.000145573	
	XXX 1 X H26	ILE 55 A HA	4.41		0.000135947	
meth	XXX 1 X H26	LEU 56 A HD22	4.6	5.08		5.81859E-05
	XXX 1 X H26	GLU 76 A H	4.66		9.76528E-05	
	XXX 1 X H26	VAL 7 A H	4.69		9.39643E-05	
meth	XXX 1 X H26	LEU 56 A HD23	4.7			
meth	XXX 1 X H26	VAL 7 A HG13	4.71	5.326666667		4.37791E-05
	XXX 1 X H26	LYS 5 A HB2	4.79		8.27917E-05	
	XXX 1 X H26	GLY 75 A H	4.9		7.22476E-05	
	XXX 1 X H26	LYS 5 A HE3	4.98		6.55577E-05	
	XXX 1 X H26	VAL 7 A HB	5.01		6.32373E-05	
	XXX 1 X H26	LEU 6 A HB2	5.18		5.17632E-05	
	XXX 1 X H26	LEU 56 A HA	5.19		5.11677E-05	
	XXX 1 X H26	THR 74 A HB	5.38		4.12388E-05	
meth	XXX 1 X H26	VAL 7 A HG11	5.38			
	XXX 1 X H26	ASP 54 A HB3	5.4		4.03309E-05	
	XXX 1 X H26	LYS 5 A HE2	5.55		3.4217E-05	
meth	XXX 1 X H26	LEU 56 A HD13	5.59			
	XXX 1 X H26	GLY 77 A H	5.59		3.2774E-05	
	XXX 1 X H26	LYS 5 A HD2	5.62		3.17382E-05	
	XXX 1 X H26	LEU 56 A HG	5.68		2.9779E-05	
	XXX 1 X H26	LYS 5 A HD3	5.74		2.79595E-05	
	XXX 1 X H26	TYR 71 A HB3	5.79		2.65417E-05	
	XXX 1 X H26	LYS 5 A H	5.79		2.65417E-05	
	XXX 1 X H26	LEU 6 A HB3	5.8		2.62683E-05	
	XXX 1 X H26	GLU 76 A HG3	5.86		2.46953E-05	
meth	XXX 1 X H26	VAL 7 A HG12	5.89			
meth	XXX 1 X H26	LEU 56 A HD21	5.94			
				SUM		0.008723339

	Recipient ligand proton	Donor Side Chain	Distance (Å)		Distance (1/Å^6)	
	XXX 1 X H27	LYS 5 A HG3	2.81		0.002031244	
	XXX 1 X H27	LEU 56 A HB2	3.04		0.001266947	
	XXX 1 X H27	LEU 56 A H	3.15		0.001023615	
	XXX 1 X H27	LYS 5 A HA	3.59		0.000467125	
	XXX 1 X H27	ILE 55 A HA	3.68		0.000402636	
	XXX 1 X H27	LEU 6 A H	3.7		0.000389753	
	XXX 1 X H27	LYS 5 A HG2	3.74		0.000365402	
	XXX 1 X H27	LYS 5 A HE3	3.81		0.000326927	
	XXX 1 X H27	ASP 54 A HB3	3.86		0.000302326	
	XXX 1 X H27	LEU 56 A HB3	3.93		0.000271422	
	XXX 1 X H27	SER 39 A HB2	4.08		0.00021679	
	XXX 1 X H27	SER 39 A HB3	4.27		0.000164981	
	XXX 1 X H27	LEU 56 A HA	4.34		0.000149645	
	XXX 1 X H27	ILE 55 A H	4.39		0.000139705	
	XXX 1 X H27	LYS 5 A HB3	4.46		0.000127055	
meth	XXX 1 X H27	VAL 7 A HG22	4.52	5.286666667		4.58045E-05
	XXX 1 X H27	ASP 54 A HA	4.67		9.64048E-05	
	XXX 1 X H27	LYS 5 A HE2	4.92		7.05033E-05	
meth	XXX 1 X H27	LEU 56 A HD13	4.94			6.88079E-05
	XXX 1 X H27	LYS 5 A HD2	4.96		6.71599E-05	
meth	XXX 1 X H27	LEU 56 A HD22	4.97			
	XXX 1 X H27	ASP 54 A HB2	5.02		6.24853E-05	
	XXX 1 X H27	ASP 54 A H	5.1		5.68302E-05	
	XXX 1 X H27	SER 39 A HA	5.21		5.00004E-05	
	XXX 1 X H27	GLY 75 A HA2	5.21		5.00004E-05	
	XXX 1 X H27	VAL 7 A HA	5.22		4.94284E-05	
	XXX 1 X H27	LYS 5 A HB2	5.28		4.61526E-05	
meth	XXX 1 X H27	VAL 7 A HG23	5.37			
exch	XXX 1 X H27	SER 39 A HG	5.38			
	XXX 1 X H27	LEU 6 A HB2	5.44		3.85839E-05	
	XXX 1 X H27	TYR 40 A H	5.48		3.69247E-05	
meth	XXX 1 X H27	LEU 56 A HD12	5.53			
	XXX 1 X H27	LYS 5 A HD3	5.55		3.4217E-05	
meth	XXX 1 X H27	LEU 56 A HD23	5.6			
	XXX 1 X H27	LEU 6 A HA	5.67		3.00955E-05	
meth	XXX 1 X H27	LYS 5 A HZ2	5.77			
	XXX 1 X H27	LEU 56 A HG	5.87		2.4444E-05	
	XXX 1 X H27	ILE 55 A HB	5.96		2.23112E-05	
meth	XXX 1 X H27	VAL 7 A HG21	5.97			
meth	XXX 1 X H27	LYS 5 A HZ1	5.97			
	XXX 1 X H27	ILE 55 A HG13	5.98		2.18672E-05	
			SUM			0.008517594

Fragment K

		Recipient ligand proton	Donor Side Chain	Distance (Å)	Distance (1/Å^6)
exch		XXX 1 X H27	SER 39 A HG	2.81	0.002031244
		XXX 1 X H27	SER 39 A HB3	2.97	0.001457006
		XXX 1 X H27	SER 39 A H	3.68	0.000402636
		XXX 1 X H27	SER 39 A HB2	4.16	0.000192948
	meth	XXX 1 X H27	LEU 56 A HD23	4.96	6.71599E-05
		XXX 1 X H27	SER 39 A HA	5.23	4.88641E-05
		XXX 1 X H27	ASP 38 A HA	5.29	4.56316E-05
	meth	XXX 1 X H27	LEU 56 A HD22	5.71	2.88525E-05
exch	meth	XXX 1 X H27	LYS 5 A HZ2	5.79	2.65417E-05
		XXX 1 X H27	ARG 41 A HD2	5.93	2.2997E-05
exch	meth	XXX 1 X H27	LYS 5 A HZ3	5.96	2.23112E-05
				SUM	0.002170083

		Recipient ligand proton	Donor Side Chain	Distance (Å)		Distance (1/Å^6)
exch		XXX 1 X H28	SER 39 A HG	3.25		0.000848594
		XXX 1 X H28	SER 39 A HB3	3.34		0.000720313
exch	meth	XXX 1 X H28	LYS 5 A HZ2	3.47		0.000572827
exch	meth	XXX 1 X H28	LYS 5 A HZ3	3.84		0.000311898
		XXX 1 X H28	SER 39 A HB2	4.07		0.000220006
exch	meth	XXX 1 X H28	LYS 5 A HZ1	4.22		0.000177062
	meth	XXX 1 X H28	LEU 56 A HD23	4.93		6.96496E-05
		XXX 1 X H28	SER 39 A H	5.23		4.88641E-05
		XXX 1 X H28	LEU 56 A HB2	5.5		3.61263E-05
		XXX 1 X H28	ARG 41 A HD2	5.54		3.45893E-05
		XXX 1 X H28	LYS 5 A HD3	5.56		3.38494E-05
		XXX 1 X H28	LYS 5 A HD2	5.59		3.2774E-05
		XXX 1 X H28	LYS 5 A HE3	5.72		2.85512E-05
		XXX 1 X H28	SER 39 A HA	5.76		2.7382E-05
	meth	XXX 1 X H28	THR 74 A HG21	5.78		2.68184E-05
					SUM	0.001278923

		Recipient ligand proton	Donor Side Chain	Distance (Å)		Distance (1/Å^6)	
meth		XXX 1 X H29	LEU 56 A HD23	3.12	3.886666667	0.001084108	0.000290092
meth		XXX 1 X H29	LEU 56 A HD12	3.35	4.1	0.000707508	0.000210522
		XXX 1 X H29	TYR 71 A HD1	3.37		0.000682685	
		XXX 1 X H29	TYR 71 A HB3	3.45		0.000593042	
		XXX 1 X H29	TYR 71 A HE1	3.72		0.000377348	
meth		XXX 1 X H29	LEU 56 A HD21	3.89		0.000288604	
		XXX 1 X H29	TYR 71 A HD2	3.9		0.000284192	
meth		XXX 1 X H29	LEU 56 A HD11	4.06		0.000223277	
		XXX 1 X H29	TYR 71 A HE2	4.21		0.0001796	
		XXX 1 X H29	TYR 71 A HA	4.28		0.000162681	
		XXX 1 X H29	TYR 71 A HB2	4.58		0.000108345	
		XXX 1 X H29	LEU 56 A HB2	4.63		0.000101511	
meth		XXX 1 X H29	LEU 56 A HD22	4.65		9.89196E-05	
exch		XXX 1 X H29	TYR 71 A HH	4.81		8.07476E-05	
meth		XXX 1 X H29	LEU 56 A HD13	4.89		7.31386E-05	
		XXX 1 X H29	SER 39 A HB3	4.91		7.13692E-05	
		XXX 1 X H29	LEU 56 A HG	5.43		3.90123E-05	
		XXX 1 X H29	TYR 71 A H	5.64		3.10689E-05	
exch	meth	XXX 1 X H29	LYS 5 A HZ2	5.65		3.07404E-05	
		XXX 1 X H29	LEU 56 A HB3	5.71		2.88525E-05	
		XXX 1 X H29	THR 74 A HB	5.79		2.65417E-05	
meth		XXX 1 X H29	THR 74 A HG21	5.8		2.62683E-05	
					SUM		0.003213132

		Recipient ligand proton	Donor Side Chain	Distance (Å)		Distance (1/Å^6)	
		XXX 1 X H32	THR 74 A HB	2.59		0.003312847	
		XXX 1 X H32	TYR 71 A HA	2.9		0.001681171	
		XXX 1 X H32	TYR 71 A HB3	2.91		0.001646805	
	meth	XXX 1 X H32	THR 74 A HG21	3.23	3.646666667	0.000880613	0.00042523
	meth	XXX 1 X H32	LEU 56 A HD12	3.27		0.000817925	
	meth	XXX 1 X H32	THR 74 A HG22	3.27		0.000817925	
		XXX 1 X H32	GLY 75 A H	3.79		0.000337415	
		XXX 1 X H32	LYS 5 A HD2	4		0.000244141	
		XXX 1 X H32	TYR 71 A HD1	4.14		0.000198609	
		XXX 1 X H32	LEU 56 A HB2	4.18		0.000187475	
	meth	XXX 1 X H32	LEU 56 A HD13	4.27		0.000164981	
		XXX 1 X H32	TYR 71 A HB2	4.33		0.00015173	
	meth	XXX 1 X H32	VAL 7 A HG22	4.37	4.83	0.000143586	7.87621E-05
exch		XXX 1 X H32	THR 74 A HG1	4.4		0.000137811	
exch	meth	XXX 1 X H32	LYS 5 A HZ2	4.42	5.266666667	0.000134112	4.68581E-05
	meth	XXX 1 X H32	THR 74 A HG23	4.44		0.000130528	
		XXX 1 X H32	THR 74 A H	4.49		0.000122046	
		XXX 1 X H32	GLY 75 A HA2	4.57		0.000109775	
		XXX 1 X H32	LEU 56 A HB3	4.72		9.04374E-05	
	meth	XXX 1 X H32	LEU 56 A HD11	4.73		8.92962E-05	
	meth	XXX 1 X H32	VAL 7 A HG21	4.82		7.97476E-05	
	meth	XXX 1 X H32	LEU 56 A HD23	4.88		7.40425E-05	
		XXX 1 X H32	GLY 75 A HA3	4.88		7.40425E-05	
		XXX 1 X H32	LYS 5 A HB3	4.89		7.31386E-05	
		XXX 1 X H32	LYS 5 A HE3	4.9		7.22476E-05	
		XXX 1 X H32	MET 72 A HA	5.25		4.77578E-05	
		XXX 1 X H32	THR 74 A HA	5.26		4.72156E-05	
	meth	XXX 1 X H32	VAL 7 A HG23	5.3		4.51175E-05	
		XXX 1 X H32	LYS 5 A HD3	5.33		4.36151E-05	
		XXX 1 X H32	TYR 71 A H	5.35		4.26459E-05	
		XXX 1 X H32	MET 72 A H	5.44		3.85839E-05	
		XXX 1 X H32	TYR 71 A HD2	5.6		3.24244E-05	
exch	meth	XXX 1 X H32	LYS 5 A HZ3	5.63		3.14014E-05	
exch	meth	XXX 1 X H32	LYS 5 A HZ1	5.75		2.7669E-05	
		XXX 1 X H32	LEU 56 A HG	5.87		2.4444E-05	
	meth	XXX 1 X H32	LEU 56 A HD21	5.88		2.41956E-05	
	meth	XXX 1 X H32	VAL 7 A HG13	5.97		2.20879E-05	
		XXX 1 X H32	LYS 5 A HG3	5.99		2.16491E-05	
					SUM	0.009151065	

	Recipient ligand proton	Donor Side Chain	Distance (Å)		Distance (1/Å^6)	
meth	XXX 1 X H33	VAL 7 A HG22	2.3	2.713333333	0.006755119	0.002506
meth	XXX 1 X H33	VAL 7 A HG21	2.84		0.001905855	
	XXX 1 X H33	GLY 75 A HA2	2.85		0.001866082	
meth	XXX 1 X H33	VAL 7 A HG23	3		0.001371742	
	XXX 1 X H33	GLY 75 A H	3.03		0.001292243	
	XXX 1 X H33	GLY 75 A HA3	3.05		0.001242227	
meth	XXX 1 X H33	LEU 56 A HD12	3.63	4.136666667	0.000437079	0.000199571
	XXX 1 X H33	LEU 56 A HB3	3.65		0.000422905	
	XXX 1 X H33	LYS 5 A HB3	3.72		0.000377348	
	XXX 1 X H33	THR 74 A HB	3.72		0.000377348	
	XXX 1 X H33	LEU 56 A HB2	3.79		0.000337415	
meth	XXX 1 X H33	LEU 56 A HD13	3.81		0.000326927	
meth	XXX 1 X H33	THR 74 A HG22	3.84	4.616666667	0.000311898	0.000103283
	XXX 1 X H33	LYS 5 A HD2	3.92		0.000275603	
	XXX 1 X H33	TYR 71 A HB3	3.97		0.000255421	
	XXX 1 X H33	MET 72 A HA	4.48		0.000123689	
meth	XXX 1 X H33	VAL 7 A HG13	4.49	4.976666667	0.000122046	6.58216E-05
	XXX 1 X H33	TYR 71 A HA	4.54		0.0001142	
meth	XXX 1 X H33	THR 74 A HG21	4.66		9.76528E-05	
meth	XXX 1 X H33	VAL 7 A HG11	4.72		9.04374E-05	
	XXX 1 X H33	VAL 7 A HA	4.74		8.81718E-05	
	XXX 1 X H33	LEU 56 A H	4.86		7.58896E-05	
	XXX 1 X H33	VAL 7 A HB	4.91		7.13692E-05	
	XXX 1 X H33	GLU 76 A H	4.94		6.88079E-05	
	XXX 1 X H33	THR 74 A H	4.96		6.71599E-05	
meth	XXX 1 X H33	LEU 56 A HD11	4.97		6.63532E-05	
	XXX 1 X H33	LYS 5 A HB2	5.02		6.24853E-05	
	XXX 1 X H33	TYR 71 A HB2	5.16		5.29788E-05	
	XXX 1 X H33	LYS 5 A HD3	5.2		5.05801E-05	
meth	XXX 1 X H33	THR 74 A HG23	5.35		4.26459E-05	
	XXX 1 X H33	PHE 78 A HE2	5.37		4.17018E-05	
	XXX 1 X H33	LEU 56 A HG	5.45		3.81611E-05	
	XXX 1 X H33	LEU 6 A H	5.46		3.77437E-05	
	XXX 1 X H33	LYS 5 A HA	5.47		3.73316E-05	
	XXX 1 X H33	VAL 7 A H	5.49		3.6523E-05	
meth	XXX 1 X H33	LEU 56 A HD23	5.5		3.61263E-05	
meth	XXX 1 X H33	LYS 5 A HZ2	5.59		3.2774E-05	
	XXX 1 X H33	LYS 5 A HE3	5.61		3.20791E-05	
	XXX 1 X H33	THR 74 A HA	5.65		3.07404E-05	
	XXX 1 X H33	LYS 5 A HG3	5.67		3.00955E-05	
meth	XXX 1 X H33	VAL 7 A HG12	5.72		2.85512E-05	
	XXX 1 X H33	PHE 78 A HZ	5.76		2.7382E-05	
	XXX 1 X H33	MET 72 A H	5.78		2.68184E-05	
	XXX 1 X H33	THR 74 A HG1	5.82		2.57313E-05	
	XXX 1 X H33	LEU 6 A HA	5.85		2.49497E-05	
				SUM		0.010460127

		Recipient ligand proton	Donor Side Chain	Distance (Å)		Distance (1/Å^6)	
	meth	XXX 1 X H34	VAL 7 A HG22	2.58	3.153333333	0.003390641	0.00101714
		XXX 1 X H34	LYS 5 A HB3	2.98		0.001427915	
	meth	XXX 1 X H34	VAL 7 A HG23	3.03		0.001292243	
		XXX 1 X H34	LEU 56 A H	3.1		0.001126756	
		XXX 1 X H34	LEU 56 A HB3	3.15		0.001023615	
		XXX 1 X H34	LEU 56 A HB2	3.26		0.000833095	
		XXX 1 X H34	LEU 6 A H	3.3		0.000774313	
		XXX 1 X H34	GLY 75 A HA2	3.45		0.000593042	
		XXX 1 X H34	LYS 5 A HD2	3.52		0.000525707	
		XXX 1 X H34	LYS 5 A HA	3.72		0.000377348	
		XXX 1 X H34	VAL 7 A HA	3.81		0.000326927	
	meth	XXX 1 X H34	VAL 7 A HG21	3.85		0.000307069	
		XXX 1 X H34	ILE 55 A HA	4.13		0.000201511	
		XXX 1 X H34	GLY 75 A HA3	4.16		0.000192948	
		XXX 1 X H34	LYS 5 A HD3	4.18		0.000187475	
		XXX 1 X H34	LEU 6 A HA	4.31		0.000156004	
		XXX 1 X H34	LYS 5 A HB2	4.43		0.000132305	
		XXX 1 X H34	VAL 7 A H	4.47		0.000125359	
	meth	XXX 1 X H34	LEU 56 A HD12	4.63	5.096666667	0.000101511	5.70535E-05
	meth	XXX 1 X H34	LEU 56 A HD13	4.72		9.04374E-05	
		XXX 1 X H34	GLU 76 A H	4.77		8.48965E-05	
	meth	XXX 1 X H34	VAL 7 A HG13	4.79	5.41	8.27917E-05	3.98856E-05
	meth	XXX 1 X H34	THR 74 A HG22	4.9		7.22476E-05	
		XXX 1 X H34	GLY 75 A H	4.94		6.88079E-05	
		XXX 1 X H34	LEU 6 A HB2	4.96		6.71599E-05	
		XXX 1 X H34	LEU 56 A HA	4.96		6.71599E-05	
		XXX 1 X H34	VAL 7 A HB	5		0.000064	
		XXX 1 X H34	ASP 54 A HB3	5.13		5.48651E-05	
		XXX 1 X H34	LYS 5 A HG2	5.31		4.46101E-05	
		XXX 1 X H34	LYS 5 A HG3	5.33		4.36151E-05	
		XXX 1 X H34	LEU 56 A HG	5.47		3.73316E-05	
	meth	XXX 1 X H34	VAL 7 A HG11	5.51		3.57347E-05	
exch	meth	XXX 1 X H34	LYS 5 A HZ2	5.59		3.2774E-05	
		XXX 1 X H34	LEU 6 A HB3	5.63		3.14014E-05	
	meth	XXX 1 X H34	LEU 56 A HD23	5.64		3.10689E-05	
		XXX 1 X H34	THR 74 A HB	5.66		3.0416E-05	
		XXX 1 X H34	GLY 77 A H	5.67		3.00955E-05	
		XXX 1 X H34	LYS 5 A HE3	5.75		2.7669E-05	
		XXX 1 X H34	SER 39 A HB2	5.77		2.70985E-05	
		XXX 1 X H34	ILE 55 A H	5.81		2.59982E-05	
		XXX 1 X H34	TYR 71 A HB3	5.83		2.54676E-05	
		XXX 1 X H34	LYS 5 A H	5.84		2.52071E-05	
	meth	XXX 1 X H34	THR 74 A HG21	5.84		2.52071E-05	
	meth	XXX 1 X H34	ILE 55 A HG23	5.92		2.32311E-05	
	meth	XXX 1 X H34	VAL 7 A HG12	5.93		2.2997E-05	
	meth	XXX 1 X H34	LEU 56 A HD11	5.94		2.27657E-05	
		XXX 1 X H34	LEU 6 A HG	5.94		2.27657E-05	
exch	meth	XXX 1 X H34	LYS 5 A HZ3	5.95		2.25371E-05	
		XXX 1 X H34	VAL 8 A H	5.97		2.20879E-05	
					SUM		0.009919052

321

		Recipient ligand proton	Donor Side Chain	Distance (Å)		Distance (1/Å^6)	
		XXX 1 X H35	LYS 5 A HD3	3.04		0.001266947	
		XXX 1 X H35	LYS 5 A HD2	3.16		0.001004332	
		XXX 1 X H35	LEU 56 A HB2	3.16		0.001004332	
		XXX 1 X H35	LEU 56 A H	3.17		0.000985472	
		XXX 1 X H35	LYS 5 A HA	3.55		0.000499609	
		XXX 1 X H35	ASP 54 A HB3	3.61		0.000451811	
		XXX 1 X H35	ILE 55 A HA	3.63		0.000437079	
		XXX 1 X H35	LEU 6 A H	3.65		0.000422905	
		XXX 1 X H35	SER 39 A HB2	3.74		0.000365402	
		XXX 1 X H35	LYS 5 A HB3	3.75		0.000359594	
		XXX 1 X H35	LEU 56 A HB3	3.94		0.000267315	
		XXX 1 X H35	ILE 55 A H	4.17		0.000190188	
		XXX 1 X H35	LEU 56 A HA	4.31		0.000156004	
exch	meth	XXX 1 X H35	LYS 5 A HZ3	4.37	4.786666667	0.000143586	8.31383E-05
exch	meth	XXX 1 X H35	LYS 5 A HZ2	4.42		0.000134112	
		XXX 1 X H35	ASP 54 A HA	4.52		0.000117265	
		XXX 1 X H35	SER 39 A HB3	4.53		0.000115721	
	meth	XXX 1 X H35	VAL 7 A HG22	4.67		9.64048E-05	
		XXX 1 X H35	ASP 54 A HB2	4.78		8.38364E-05	
		XXX 1 X H35	LYS 5 A HG2	4.88		7.40425E-05	
		XXX 1 X H35	SER 39 A HA	5		0.000064	
		XXX 1 X H35	ASP 54 A H	5.02		6.24853E-05	
	meth	XXX 1 X H35	LEU 56 A HD23	5.19		5.11677E-05	
		XXX 1 X H35	LYS 5 A HB2	5.19		5.11677E-05	
		XXX 1 X H35	LYS 5 A HE3	5.22		4.94284E-05	
	meth	XXX 1 X H35	LEU 56 A HD12	5.24		4.83072E-05	
		XXX 1 X H35	VAL 7 A HA	5.32		4.41093E-05	
		XXX 1 X H35	LYS 5 A HG3	5.33		4.36151E-05	
	meth	XXX 1 X H35	VAL 7 A HG23	5.34		4.31273E-05	
		XXX 1 X H35	GLY 75 A HA2	5.34		4.31273E-05	
		XXX 1 X H35	LYS 5 A HE2	5.34		4.31273E-05	
exch		XXX 1 X H35	SER 39 A HG	5.35		4.26459E-05	
		XXX 1 X H35	LEU 6 A HB2	5.41		3.98856E-05	
	meth	XXX 1 X H35	THR 74 A HG22	5.42		3.94461E-05	
		XXX 1 X H35	TYR 40 A H	5.53		3.49663E-05	
exch	meth	XXX 1 X H35	LYS 5 A HZ1	5.57		3.34864E-05	
	meth	XXX 1 X H35	LEU 56 A HD22	5.74		2.79595E-05	
		XXX 1 X H35	LEU 6 A HA	5.77		2.70985E-05	
		XXX 1 X H35	ILE 55 A HB	5.81		2.59982E-05	
	meth	XXX 1 X H35	LEU 56 A HD13	5.81		2.59982E-05	
		XXX 1 X H35	ILE 55 A HG13	5.87		2.4444E-05	
		XXX 1 X H35	LEU 56 A HG	5.9		2.37076E-05	
		XXX 1 X H35	ARG 41 A HG3	5.95		2.25371E-05	
	meth	XXX 1 X H35	THR 74 A HG21	5.96		2.23112E-05	
	meth	XXX 1 X H35	ILE 55 A HG23	5.99		2.16491E-05	
					SUM		0.008568098

Fragment L

	Recipient ligand proton	Donor Side Chain	Distance (Å)		Distance (1/Å^6)	
meth	XXX 1 X H21	LEU 56 B HD11	2.99	3.416666667		0.000628614
meth	XXX 1 X H21	LEU 56 B HD13	3.14		0.001043331	
	XXX 1 X H21	TYR 71 B HE2	3.34		0.000720313	
	XXX 1 X H21	TYR 71 B HD2	3.54		0.000508137	
meth	XXX 1 X H21	LEU 56 B HD21	3.88	4.36		0.000145573
	XXX 1 X H21	GLU 37 B HG2	3.97		0.000255421	
meth	XXX 1 X H21	LEU 56 B HD22	3.98		0.000251595	
meth	XXX 1 X H21	LEU 56 B HD12	4.12		0.000204464	
exch	XXX 1 X H21	TYR 71 B HH	4.15		0.000195754	
exch	XXX 1 X H21	ARG 68 B HH12	4.28		0.000162681	
	XXX 1 X H21	TYR 71 B HB3	4.4		0.000137811	
	XXX 1 X H21	TYR 71 B HE1	4.81		8.07476E-05	
	XXX 1 X H21	TYR 71 B HD1	4.96		6.71599E-05	
	XXX 1 X H21	ASP 38 B HA	5.01		6.32373E-05	
	XXX 1 X H21	GLU 37 B HG3	5.05		6.02909E-05	
exch	XXX 1 X H21	ARG 68 B HH11	5.1		5.68302E-05	
	XXX 1 X H21	SER 39 B HB3	5.18		5.17632E-05	
meth	XXX 1 X H21	LEU 56 B HD23	5.22		4.94284E-05	
	XXX 1 X H21	LEU 56 B HG	5.22		4.94284E-05	
	XXX 1 X H21	TYR 71 B HB2	5.28		4.61526E-05	
exch	XXX 1 X H21	ARG 68 B HH22	5.42		3.94461E-05	
	XXX 1 X H21	LEU 56 B HB2	5.49		3.6523E-05	
	XXX 1 X H21	SER 39 B H	5.52		3.53481E-05	
	XXX 1 X H21	GLU 37 B HB3	5.67		3.00955E-05	
exch	XXX 1 X H21	SER 39 B HG	5.73		2.82535E-05	
	XXX 1 X H21	TYR 71 B HA	5.87		2.4444E-05	
				SUM		0.00294106

	Recipient ligand proton	Donor Side Chain	Distance (Å)		Distance (1/Å^6)	
	XXX 1 X H22	TYR 71 B HB3	2.82		0.001988407	
meth	XXX 1 X H22	LEU 56 B HD22	3.08	3.776666667		0.000344626
	XXX 1 X H22	TYR 71 B HD1	3.18		0.000967024	
meth	XXX 1 X H22	LEU 56 B HD13	3.37	4.073333333		0.000218927
	XXX 1 X H22	TYR 71 B HD2	3.5		0.000543991	
meth	XXX 1 X H22	LEU 56 B HD21	3.72		0.000377348	
	XXX 1 X H22	TYR 71 B HA	3.73		0.000371319	
	XXX 1 X H22	TYR 71 B HE1	3.9		0.000284192	
meth	XXX 1 X H22	LEU 56 B HD11	3.97		0.000255421	
	XXX 1 X H22	TYR 71 B HB2	4.04		0.000229992	
	XXX 1 X H22	TYR 71 B HE2	4.18		0.000187475	
meth	XXX 1 X H22	LEU 56 B HD23	4.53		0.000115721	
	XXX 1 X H22	LEU 56 B HB2	4.83		7.87621E-05	
meth	XXX 1 X H22	LEU 56 B HD12	4.88		7.40425E-05	
exch	XXX 1 X H22	TYR 71 B HH	4.98		6.55577E-05	
	XXX 1 X H22	TYR 71 B H	5.21		5.00004E-05	
	XXX 1 X H22	SER 39 B HB3	5.27		4.66806E-05	
exch	XXX 1 X H22	ARG 68 B HH12	5.42		3.94461E-05	
	XXX 1 X H22	LEU 56 B HG	5.47		3.73316E-05	
	XXX 1 X H22	THR 74 B HB	5.55		3.4217E-05	
exch	XXX 1 X H22	SER 39 B HG	5.79		2.65417E-05	
	XXX 1 X H22	LEU 56 B HB3	5.86		2.46953E-05	
meth	XXX 1 X H22	MET 72 B HE2	5.87		2.4444E-05	
exch	XXX 1 X H22	GLN 70 B HE21	5.89		2.39501E-05	
	XXX 1 X H22	GLU 37 B HG2	5.89		2.39501E-05	
				SUM		0.00543159

		Recipient ligand proton	Donor Side Chain	Distance (Å)		Distance (1/Å^6)	
exch		XXX 1 X H23	SER 39 B HG	2.26		0.007504977	
		XXX 1 X H23	SER 39 B HB3	3.15		0.001023615	
		XXX 1 X H23	SER 39 B HB2	3.79		0.000337415	
	meth	XXX 1 X H23	LEU 56 B HD13	4.18	4.986666667		6.50336E-05
		XXX 1 X H23	SER 39 B H	4.8		8.17622E-05	
		XXX 1 X H23	LEU 56 B HB2	5.19		5.11677E-05	
	meth	XXX 1 X H23	LEU 56 B HD12	5.27		4.66806E-05	
		XXX 1 X H23	SER 39 B HA	5.37		4.17018E-05	
	meth	XXX 1 X H23	LEU 56 B HD22	5.41		3.98856E-05	
	meth	XXX 1 X H23	LEU 56 B HD11	5.51		3.57347E-05	
		XXX 1 X H23	LEU 56 B HA	5.8		2.62683E-05	
exch	meth	XXX 1 X H23	LYS 5 B HZ3	5.89		2.39501E-05	
		XXX 1 X H23	LYS 5 B HD2	5.89		2.39501E-05	
					SUM		0.001650914

	Recipient ligand proton	Donor Side Chain	Distance (Å)		Distance (1/Å^6)	
	XXX 1 X H24	THR 74 B HB	2.41		0.005103848	
	XXX 1 X H24	TYR 71 B HA	2.78		0.002166363	
	XXX 1 X H24	TYR 71 B HB3	3.21		0.00091405	
meth	XXX 1 X H24	THR 74 B HG21	3.41	3.803333333		0.00033038
meth	XXX 1 X H24	LEU 56 B HD22	3.42	4.176666667		0.000188374
meth	XXX 1 X H24	THR 74 B HG22	3.44		0.000603461	
	XXX 1 X H24	GLY 75 B H	3.94		0.000267315	
exch	XXX 1 X H24	THR 74 B HG1	4.25		0.000169694	
	XXX 1 X H24	TYR 71 B HD1	4.28		0.000162681	
meth	XXX 1 X H24	LEU 56 B HD23	4.3		0.000158194	
	XXX 1 X H24	LEU 56 B HB2	4.34		0.000149645	
	XXX 1 X H24	THR 74 B H	4.38		0.00014163	
meth	XXX 1 X H24	VAL 7 B HG22	4.47	4.786666667		8.31383E-05
	XXX 1 X H24	TYR 71 B HB2	4.52		0.000117265	
	XXX 1 X H24	GLY 75 B HA2	4.53		0.000115721	
meth	XXX 1 X H24	THR 74 B HG23	4.56		0.000111227	
	XXX 1 X H24	LYS 5 B HD2	4.63		0.000101511	
	XXX 1 X H24	LYS 5 B HB3	4.77		8.48965E-05	
meth	XXX 1 X H24	VAL 7 B HG21	4.77		8.48965E-05	
meth	XXX 1 X H24	LEU 56 B HD21	4.81		8.07476E-05	
	XXX 1 X H24	GLY 75 B HA3	4.91		7.13692E-05	
	XXX 1 X H24	MET 72 B HA	4.92		7.05033E-05	
meth	XXX 1 X H24	LEU 56 B HD13	4.97		6.63532E-05	
	XXX 1 X H24	LEU 56 B HB3	5.07		5.88779E-05	
	XXX 1 X H24	THR 74 B HA	5.1		5.68302E-05	
meth	XXX 1 X H24	VAL 7 B HG23	5.12		5.55112E-05	
meth	XXX 1 X H24	MET 72 B HE2	5.17		5.23669E-05	
	XXX 1 X H24	MET 72 B H	5.24		4.83072E-05	
	XXX 1 X H24	TYR 71 B H	5.31		4.46101E-05	
	XXX 1 X H24	LYS 5 B HD3	5.46		3.77437E-05	
	XXX 1 X H24	LYS 5 B HG3	5.75		2.7669E-05	
	XXX 1 X H24	TYR 71 B HD2	5.85		2.49497E-05	
	XXX 1 X H24	GLN 70 B HG2	5.92		2.32311E-05	
		SUM				0.010390909

	Recipient ligand proton	Donor Side Chain	Distance (Å)		Distance (1/Å^6)	
	XXX 1 X H25	GLY 75 B HA2	2.59		0.003312847	
meth	XXX 1 X H25	VAL 7 B HG22	2.62	2.79		0.00212019
meth	XXX 1 X H25	VAL 7 B HG23	2.87		0.001789405	
meth	XXX 1 X H25	VAL 7 B HG21	2.88		0.001752448	
	XXX 1 X H25	GLY 75 B HA3	3.01		0.001344625	
	XXX 1 X H25	GLY 75 B H	3.07		0.001194455	
	XXX 1 X H25	LYS 5 B HB3	3.47		0.000572827	
	XXX 1 X H25	THR 74 B HB	3.49		0.000553411	
meth	XXX 1 X H25	THR 74 B HG22	3.72	4.496666667		0.000120964
meth	XXX 1 X H25	LEU 56 B HD22	3.9	4.386666667		0.000140343
	XXX 1 X H25	LEU 56 B HB2	3.92		0.000275603	
meth	XXX 1 X H25	LEU 56 B HD23	4.04		0.000229992	
	XXX 1 X H25	LEU 56 B HB3	4.08		0.00021679	
	XXX 1 X H25	MET 72 B HA	4.36		0.000145573	
	XXX 1 X H25	TYR 71 B HB3	4.54		0.0001142	
meth	XXX 1 X H25	THR 74 B HG21	4.57		0.000109775	
	XXX 1 X H25	TYR 71 B HA	4.62		0.000102837	
	XXX 1 X H25	LYS 5 B HD2	4.65		9.89196E-05	
	XXX 1 X H25	LYS 5 B HB2	4.71		9.15956E-05	
	XXX 1 X H25	GLU 76 B H	4.78		8.38364E-05	
meth	XXX 1 X H25	MET 72 B HE2	4.91		7.13692E-05	
	XXX 1 X H25	THR 74 B H	4.94		6.88079E-05	
	XXX 1 X H25	VAL 7 B HB	4.97		6.63532E-05	
	XXX 1 X H25	VAL 7 B HA	4.97		6.63532E-05	
	XXX 1 X H25	LYS 5 B HD3	4.97		6.63532E-05	
meth	XXX 1 X H25	VAL 7 B HG13	5.01		6.32373E-05	
	XXX 1 X H25	LEU 56 B H	5.04		6.10122E-05	
meth	XXX 1 X H25	VAL 7 B HG11	5.06		5.95795E-05	
meth	XXX 1 X H25	THR 74 B HG23	5.2		5.05801E-05	
meth	XXX 1 X H25	LEU 56 B HD21	5.22		4.94284E-05	
	XXX 1 X H25	LYS 5 B HA	5.23		4.88641E-05	
	XXX 1 X H25	LYS 5 B HG3	5.28		4.61526E-05	
	XXX 1 X H25	THR 74 B HA	5.32		4.41093E-05	
	XXX 1 X H25	LEU 6 B H	5.48		3.69247E-05	
exch	XXX 1 X H25	THR 74 B HG1	5.62		3.17382E-05	
meth	XXX 1 X H25	LEU 56 B HD13	5.62		3.17382E-05	
	XXX 1 X H25	PHE 78 B HZ	5.65		3.07404E-05	
	XXX 1 X H25	PHE 78 B HE2	5.65		3.07404E-05	
meth	XXX 1 X H25	MET 72 B HE1	5.68		2.9779E-05	
	XXX 1 X H25	TYR 71 B HB2	5.69		2.94664E-05	
	XXX 1 X H25	VAL 7 B H	5.72		2.85512E-05	
	XXX 1 X H25	MET 72 B H	5.8		2.62683E-05	
	XXX 1 X H25	LEU 6 B HA	5.81		2.59982E-05	
	XXX 1 X H25	LEU 56 B HG	5.82		2.57313E-05	
	SUM					0.011191441

	Recipient ligand proton	Donor Side Chain	Distance (Å)		Distance (1/Å^6)	
meth	XXX 1 X H26	VAL 7 B HG22	2.75	3.106666667		0.001112326
meth	XXX 1 X H26	VAL 7 B HG23	2.79		0.00212019	
	XXX 1 X H26	LYS 5 B HB3	2.82		0.001988407	
	XXX 1 X H26	GLY 75 B HA2	3.26		0.000833095	
	XXX 1 X H26	LEU 56 B H	3.29		0.000788542	
	XXX 1 X H26	LEU 6 B H	3.3		0.000774313	
	XXX 1 X H26	LEU 56 B HB2	3.32		0.000746744	
	XXX 1 X H26	LYS 5 B HA	3.5		0.000543991	
	XXX 1 X H26	LEU 56 B HB3	3.53		0.000516835	
meth	XXX 1 X H26	VAL 7 B HG21	3.78		0.000342807	
	XXX 1 X H26	LYS 5 B HD3	3.8		0.000332123	
	XXX 1 X H26	VAL 7 B HA	3.99		0.000247835	
	XXX 1 X H26	GLY 75 B HA3	4.18		0.000187475	
	XXX 1 X H26	LYS 5 B HB2	4.2		0.000182181	
	XXX 1 X H26	ILE 55 B HA	4.22		0.000177062	
	XXX 1 X H26	LYS 5 B HD2	4.25		0.000169694	
	XXX 1 X H26	LEU 6 B HA	4.25		0.000169694	
	XXX 1 X H26	GLU 76 B H	4.59		0.000106936	
meth	XXX 1 X H26	THR 74 B HG22	4.62		0.000102837	
	XXX 1 X H26	VAL 7 B H	4.63		0.000101511	
meth	XXX 1 X H26	LEU 56 B HD22	4.73	5.16		5.29788E-05
meth	XXX 1 X H26	LEU 56 B HD23	4.86		7.58896E-05	
	XXX 1 X H26	VAL 7 B HB	4.95		6.79781E-05	
	XXX 1 X H26	GLY 75 B H	5.03		6.17436E-05	
	XXX 1 X H26	ASP 54 B HB3	5.04		6.10122E-05	
	XXX 1 X H26	LEU 6 B HB2	5.05		6.02909E-05	
	XXX 1 X H26	LYS 5 B HG3	5.08		5.81859E-05	
	XXX 1 X H26	LEU 56 B HA	5.11		5.61661E-05	
meth	XXX 1 X H26	VAL 7 B HG13	5.17		5.23669E-05	
	XXX 1 X H26	THR 74 B HB	5.37		4.17018E-05	
	XXX 1 X H26	LYS 5 B HG2	5.38		4.12388E-05	
	XXX 1 X H26	LYS 5 B H	5.58		3.3128E-05	
meth	XXX 1 X H26	THR 74 B HG21	5.59		3.2774E-05	
meth	XXX 1 X H26	LEU 56 B HD13	5.64		3.10689E-05	
	XXX 1 X H26	GLY 77 B H	5.64		3.10689E-05	
meth	XXX 1 X H26	VAL 7 B HG11	5.7		2.91575E-05	
	XXX 1 X H26	LEU 6 B HB3	5.71		2.88525E-05	
	XXX 1 X H26	LEU 56 B HG	5.76		2.7382E-05	
	XXX 1 X H26	LEU 6 B HG	5.81		2.59982E-05	
	XXX 1 X H26	SER 39 B HB3	5.82		2.57313E-05	
meth	XXX 1 X H26	LEU 6 B HD23	5.89		2.39501E-05	
	XXX 1 X H26	LYS 5 B HE2	5.91		2.34679E-05	
	XXX 1 X H26	ILE 55 B H	5.94		2.27657E-05	
				SUM		0.009834064

		Recipient ligand proton	Donor Side Chain	Distance (Å)		Distance (1/Å^6)	
		XXX 1 X H27	LYS 5 B HD3	3.03		0.001292243	
		XXX 1 X H27	LEU 56 B HB2	3.19		0.000948977	
		XXX 1 X H27	LEU 56 B H	3.2		0.000931323	
		XXX 1 X H27	LYS 5 B HA	3.51		0.000534758	
		XXX 1 X H27	ASP 54 B HB3	3.56		0.000491247	
		XXX 1 X H27	ILE 55 B HA	3.64		0.000429924	
		XXX 1 X H27	LEU 6 B H	3.67		0.000409264	
		XXX 1 X H27	LYS 5 B HD2	3.75		0.000359594	
		XXX 1 X H27	LYS 5 B HB3	3.82		0.000321825	
		XXX 1 X H27	SER 39 B HB2	3.97		0.000255421	
		XXX 1 X H27	SER 39 B HB3	4.06		0.000223277	
		XXX 1 X H27	LEU 56 B HB3	4.16		0.000192948	
		XXX 1 X H27	ILE 55 B H	4.26		0.000167318	
		XXX 1 X H27	LEU 56 B HA	4.3		0.000158194	
		XXX 1 X H27	ASP 54 B HA	4.57		0.000109775	
		XXX 1 X H27	LYS 5 B HE2	4.59		0.000106936	
	meth	XXX 1 X H27	VAL 7 B HG22	4.62	5.19		5.11677E-05
		XXX 1 X H27	ASP 54 B HB2	4.77		8.48965E-05	
	meth	XXX 1 X H27	LEU 56 B HD13	5		0.000064	
		XXX 1 X H27	ASP 54 B H	5.02		6.24853E-05	
	meth	XXX 1 X H27	VAL 7 B HG23	5.04		6.10122E-05	
	meth	XXX 1 X H27	LEU 56 B HD22	5.1		5.68302E-05	
	meth	XXX 1 X H27	THR 74 B HG22	5.18		5.17632E-05	
		XXX 1 X H27	SER 39 B HA	5.19		5.11677E-05	
exch		XXX 1 X H27	SER 39 B HG	5.2		5.05801E-05	
		XXX 1 X H27	LYS 5 B HB2	5.26		4.72156E-05	
		XXX 1 X H27	VAL 7 B HA	5.32		4.41093E-05	
		XXX 1 X H27	GLY 75 B HA2	5.35		4.26459E-05	
		XXX 1 X H27	LYS 5 B HG3	5.38		4.12388E-05	
		XXX 1 X H27	LYS 5 B HG2	5.39		4.07819E-05	
		XXX 1 X H27	TYR 40 B H	5.4		4.03309E-05	
exch	meth	XXX 1 X H27	LYS 5 B HZ3	5.47		3.73316E-05	
		XXX 1 X H27	LYS 5 B HE3	5.48		3.69247E-05	
		XXX 1 X H27	LEU 6 B HB2	5.48		3.69247E-05	
	meth	XXX 1 X H27	LEU 56 B HD12	5.61		3.20791E-05	
	meth	XXX 1 X H27	THR 74 B HG21	5.69		2.94664E-05	
		XXX 1 X H27	LEU 6 B HA	5.73		2.82535E-05	
	meth	XXX 1 X H27	LEU 56 B HD23	5.76		2.7382E-05	
		XXX 1 X H27	ILE 55 B HG13	5.84		2.52071E-05	
		XXX 1 X H27	ILE 55 B HB	5.85		2.49497E-05	
	meth	XXX 1 X H27	VAL 7 B HG21	5.91		2.34679E-05	
					SUM	0.007591323	

Appendix C

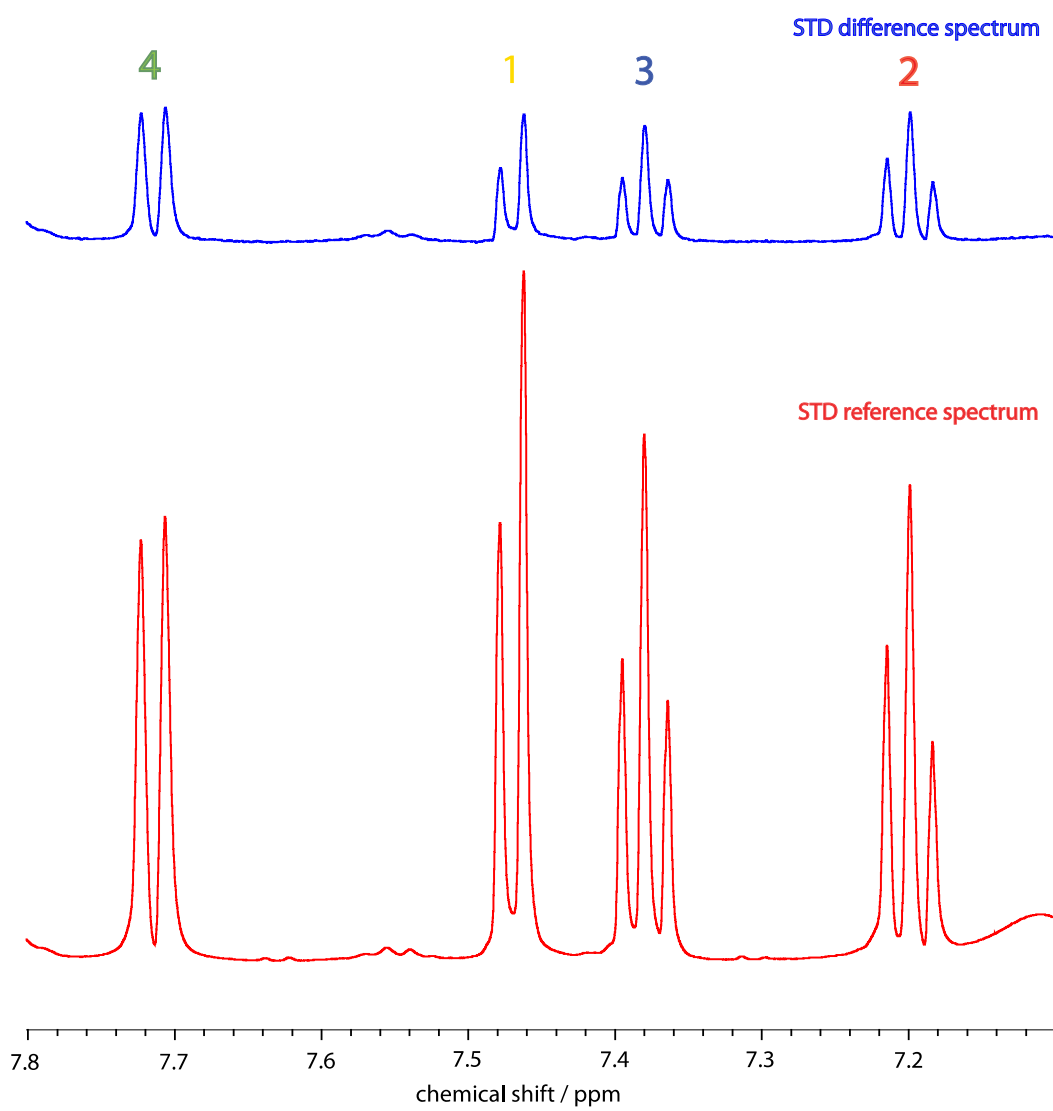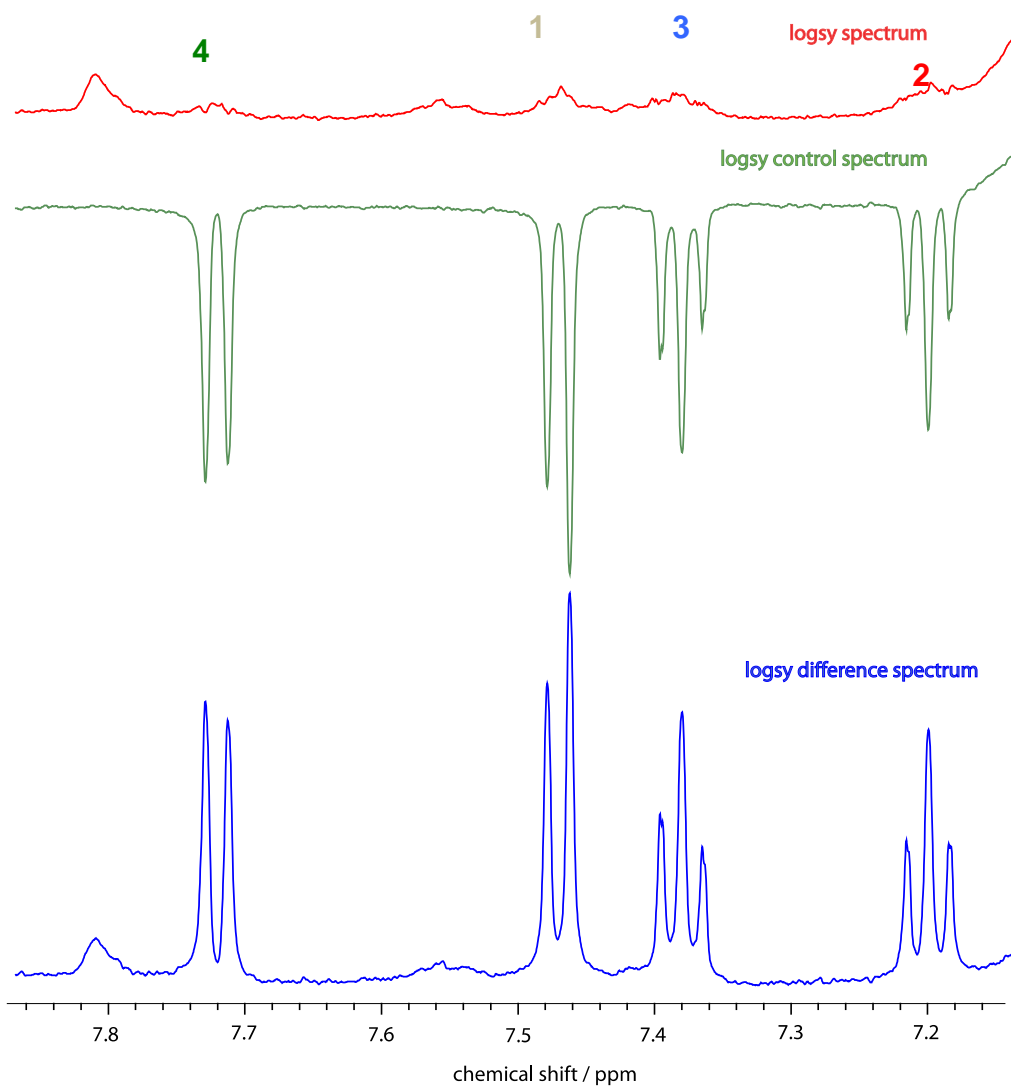Exemplary STD and LOGSY spectra for section 5.3.4.1, Fragment M (500 µM) + O (5 mM)
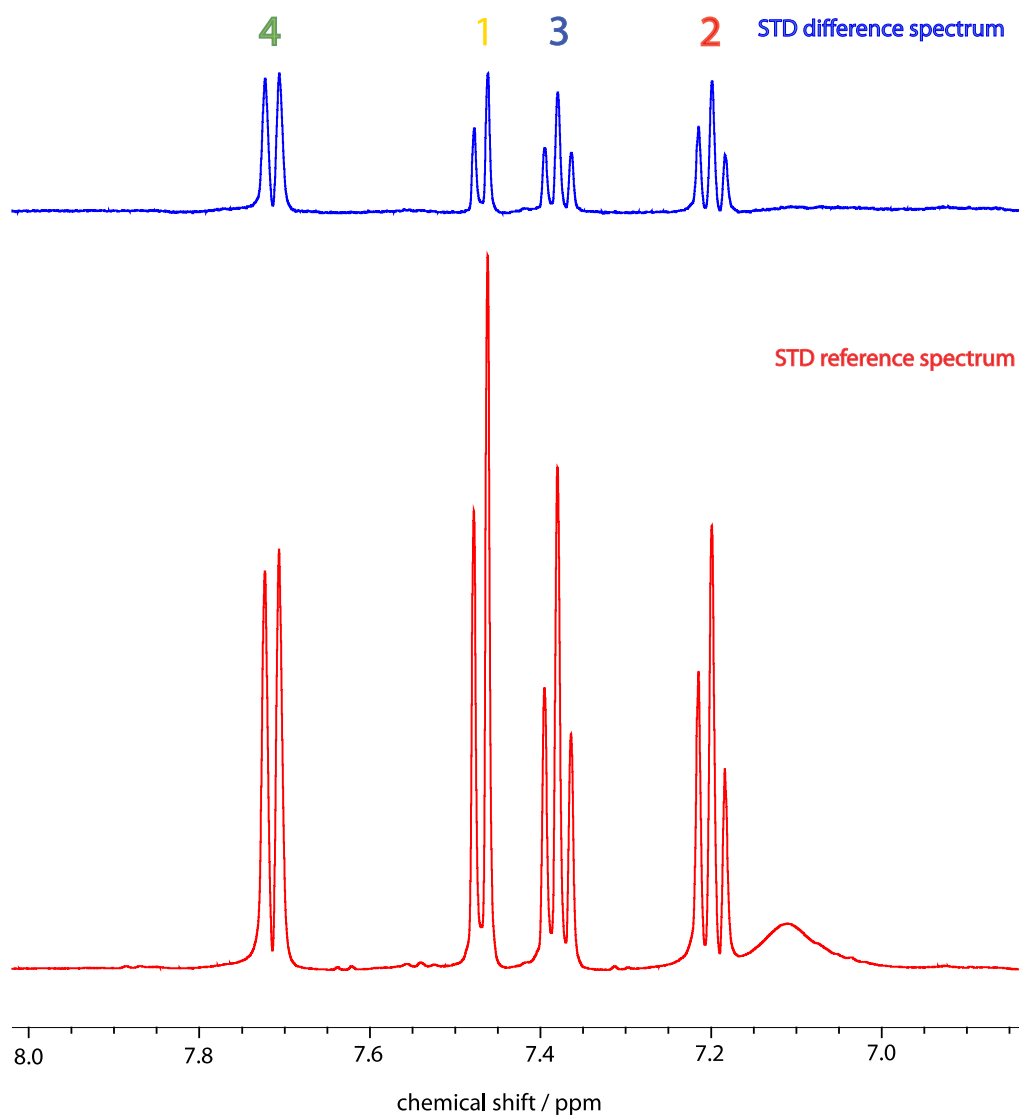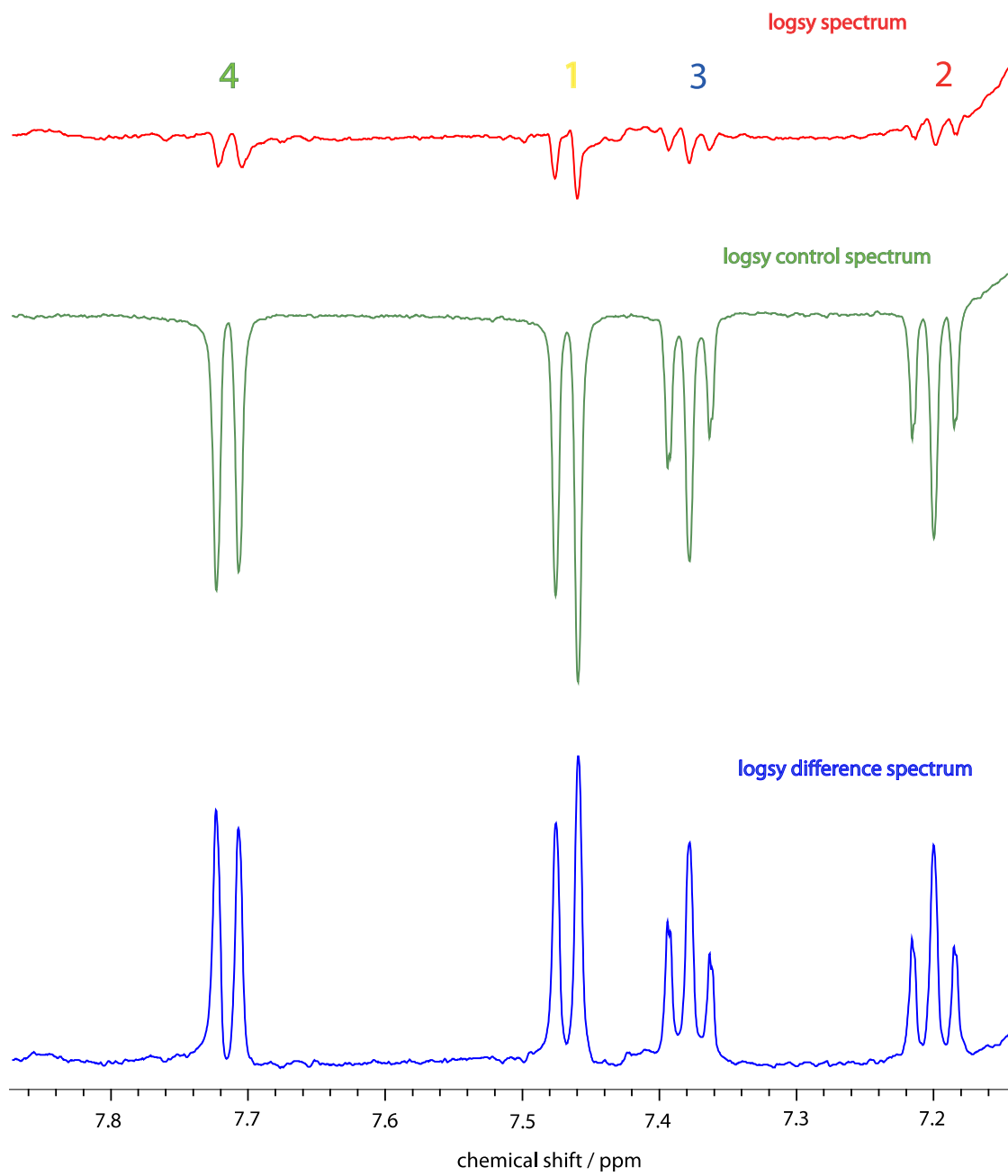
Exemplary STD and LOGSY spectra for section 5.3.4.2 Fragment M (500 µM) + P (5 mM)
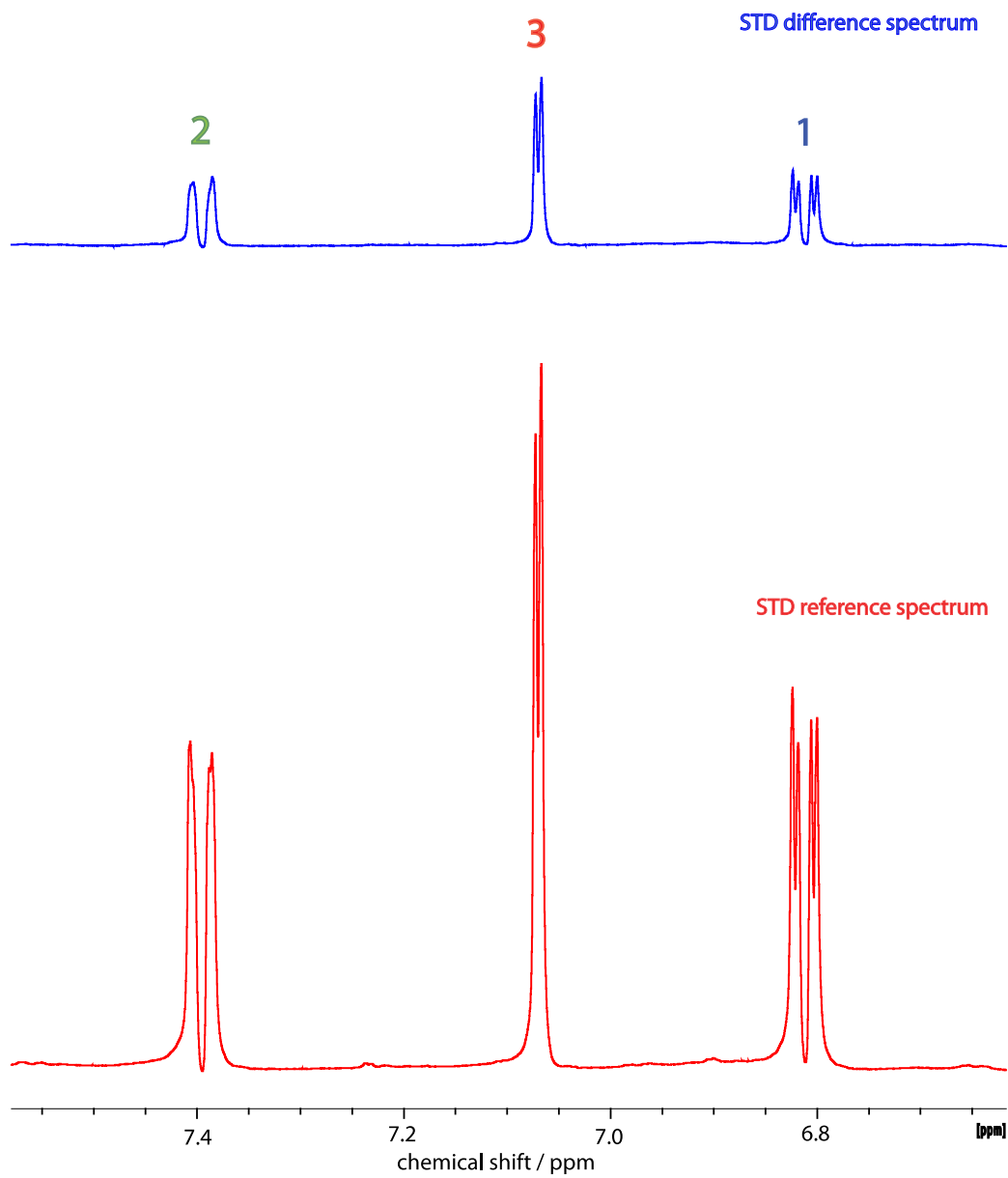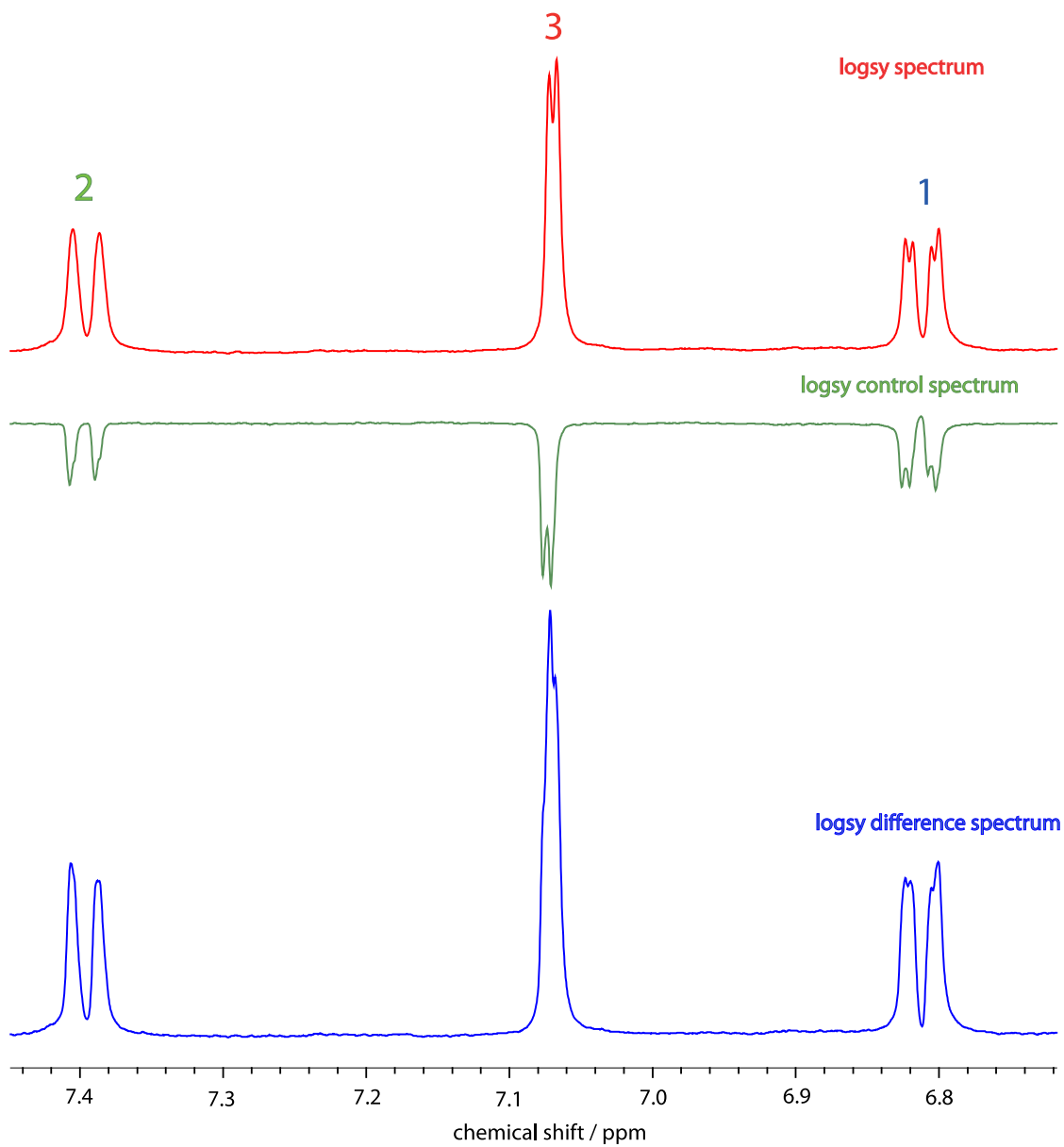
Exemplary STD and LOGSY spectra for 5.3.4.3 Fragment N (200 μM) + O (5 mM)

Exemplary STD and LOGSY spectra for 5.3.4.4 Fragment N (200 μM) + P (5 mM)